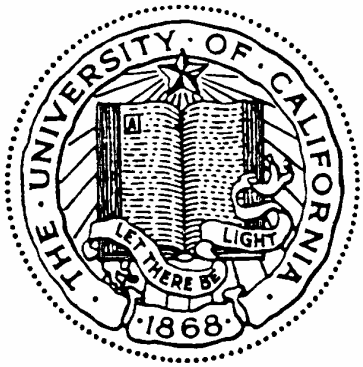

STRUCTURAL SYSTEMS
RESEARCH PROJECT

Report No.
SSRP–25/01

EXPERIMENTAL INVESTIGATION OF DEVELOPMENT LENGTH REQUIRED FOR LARGE-DIAMETER HEADED REINFORCING BARS IN TENSION

by

NAVEED ASGHARPOUR
RAHUL RAMAN
P. BENSON SHING

Final Report Submitted to the California Department of Transportation under Contract No. 65A1051

November 2025

Department of Structural Engineering
University of California San Diego
La Jolla, California 92093-0085

University of California, San Diego
Department of Structural Engineering
Structural Systems Research Project
Report No. SSRP–25/01

Experimental Investigation of Development Length Required for Large-Diameter Headed Reinforcing Bars in Tension

by

Naveed Asgharpour

Graduate Student Researcher

Rahul Raman

Post-Doctoral Researcher

P. Benson Shing

Professor of Structural Engineering

Final Report Submitted to the California Department of Transportation
under Contract No. 65A1051

Department of Structural Engineering
University of California San Diego
La Jolla, California 92093-0085
November 2025

Technical Report Documentation Page

1. Report No.	2. Government Accession No.	3. Recipient's Catalog No.
CA 25-4026		

4. Title and Subtitle	5. Report Date
Experimental Investigation of Development Length Required for Large-Diameter Headed Reinforcing Bars in Tension	11/10/2025
	6. Performing Organization Code

7. Author(s)	8. Performing Organization Report No.
Naveed Asgharpour, Rahul Raman, and P. Benson Shing	UCSD/SSRP-25/01

9. Performing Organization Name and Address	10. Work Unit No. (TRAIS)
Department of Structural Engineering University of California San Diego 9500 Gilman Drive, Mail Code 0085 La Jolla, California 92093-0085	11. Contract or Grant No. 65A1051

12. Sponsoring Agency Name and Address	13. Type of Report and Period Covered
California Department of Transportation Division of Engineering Services 1801 30th St., MS #9-2/5I Sacramento, California 95816	Final Report 14. Sponsoring Agency Code

15. Supplementary Notes

Prepared in cooperation with the State of California Department of Transportation.

16. Abstract

The study presented in this report was to investigate the anchorage capacities of No. 14 and No. 18 headed bars, including the influence of the embedment length, concrete strength, head size, parallel tie reinforcement, and bar group on the anchorage strength, and evaluate the applicability of the development length requirements for No. 11 or smaller headed bars in ACI 318-19 and the 10th Edition of AASHTO LRFD Bridge Design Specifications to larger diameter bars. Thirteen bar anchorage tests were conducted. Eleven of these had single bars and two had double side-by-side bars. Heads with net bearing areas of $4A_b$ and $9A_b$, were considered. The target compressive strengths of the concrete used were 4,000, 6,000, and 8,000 psi. The specimens had bar embedment lengths equal to 70% or 100% of the minimum according to ACI 318-19. The test results show that the anchorage failure of a headed bar is normally initiated by concrete breakout but eventually governed by bar pullout when the bearing strength of the concrete at the T head has been weakened by the opening of breakout cracks. The bar force at which concrete breakout occurs is approximately proportional to the square of the embedment length, rather than the embedment length to the power of 1.5 as specified in ACI 318 for embedded anchor bolts. After the occurrence of breakout cracks, parallel tie reinforcement can play a significant role in providing the necessary anchorage capacity. The specimens that satisfied the development length formula in ACI 318-19 performed satisfactorily. Two specimens that satisfied the AASHTO formula and had a head size of $9A_b$ had anchorage failures. This indicates that the AASHTO formula over-estimates the influence of the head size. The unified formula in AASHTO considers only the bond strength and the bearing resistance at the T head, and does not explicitly account for concrete breakout. It can be perceived that if anchorage failure is initiated by concrete breakout, the size of the T head will not have a significant influence on the anchorage resistance, as supported by the data in this study and other prior studies on smaller diameter bars, which have shown that the use of a head size greater than $4A_b$ will not necessarily improve the anchorage capacity and the benefit is small at best. Even though the ACI formula appears to be safe for the large-diameter bars, it is more conservative for No. 18 bars than No. 14 bars, probably due to the fact that the development length is proportional to the bar diameter to the power of 1.5. A rational method has been proposed in this study to determine the development lengths for headed bars and the required parallel tie reinforcement. It is based on the anchor bolt provisions in ACI 318, which have been improved to account for the influence of the bar embedment length and the contribution of the parallel tie reinforcement in an accurate and rational manner.

17. Key Words	18. Distribution Statement
Bridges, reinforced concrete, development length, large-diameter bars, headed bars, No. 14 bars, No. 18 bars, anchorage strength, breakout failure, pullout failure	No restrictions. This document is available to the public through the National Technical Information Service, Springfield, Virginia 22161.

19. Security Classification (of this report)	20. Security Classification (of this page)	21. No. of Pages	22. Price
Unclassified	Unclassified	380	

DISCLAIMER

This document is disseminated in the interest of information exchange. The contents of this report reflect the views of the authors who are responsible for the facts and accuracy of the data presented herein. The contents do not necessarily reflect the official views or policies of the State of California or the Federal Highway Administration. This publication does not constitute a standard, specification or regulation. This report does not constitute an endorsement by the California Department of Transportation of any product described herein.

For individuals with sensory disabilities, this document is available in Braille, large print, audiocassette, or compact disk. To obtain a copy of this document in one of these alternate formats, please contact: the Division of Research and Innovation, MS-83, California Department of Transportation, P.O. Box 942873, Sacramento, CA 94273-0001.

ACKNOWLEDGMENTS

This study was supported by the California Department of Transportation (Caltrans) under Contract No. 65A1051. Dr. Foued Zayati was the project manager. The authors are most grateful for his support throughout the project. The authors would also like to acknowledge the dedication and professionalism of the engineering staff, Michael Sanders, Joel Fullerton, and Michael Dyson, of the Powell Structural Engineering Laboratories in specimen construction, instrumentation, and the preparation and execution of the laboratory experiments. The assistance of the undergraduate engineering aids, Zackary Kamibayashiyama and Reed Gallagher, in the construction and instrumentation of the test specimens are also appreciated.

ABSTRACT

The study presented in this report was to investigate the anchorage capacities of No. 14 and No. 18 headed bars, including the influence of the embedment length, concrete strength, head size, parallel tie reinforcement, and bar group on the anchorage strength, and evaluate the applicability of the development length requirements for No. 11 or smaller headed bars in ACI 318-19 and the 10th Edition of AASHTO LRFD Bridge Design Specifications to larger diameter bars. Thirteen bar anchorage tests were conducted. Eleven of these had single bars and two had double side-by-side bars. Heads with net bearing areas of $4A_b$ and $9A_b$, were considered. The target compressive strengths of the concrete used were 4,000, 6,000, and 8,000 psi. The specimens had bar embedment lengths equal to 70% or 100% of the minimum according to ACI 318-19. The test results show that the anchorage failure of a headed bar is normally initiated by concrete breakout but eventually governed by bar pullout when the bearing strength of the concrete at the T head has been weakened by the opening of breakout cracks. The bar force at which concrete breakout occurs is approximately proportional to the square of the embedment length, rather than the embedment length to the power of 1.5 as specified in ACI 318 for embedded anchor bolts. After the occurrence of breakout cracks, parallel tie reinforcement can play a significant role in providing the necessary anchorage capacity. The specimens that satisfied the development length formula in ACI 318-19 performed satisfactorily. Two specimens that satisfied the AASHTO formula and had a head size of $9A_b$ had anchorage failures. This indicates that the AASHTO formula over-estimates the influence of the head size. The unified formula in AASHTO considers only the bond strength and the bearing resistance at the T head, and does not explicitly account for concrete breakout. It can be perceived that if anchorage failure is initiated by concrete breakout, the size of the T head will not have a significant influence on the anchorage resistance, as supported by the data in this study and other prior studies on smaller diameter bars, which have shown that the use of a head size greater than $4A_b$ will not necessarily improve the anchorage capacity and the benefit is small at best. Even though the ACI formula appears to be safe for the large-diameter bars, it is more conservative for No. 18 bars than No. 14 bars, probably due to the fact that the development length is proportional to the bar diameter to the power of 1.5. A rational method has been proposed in this study to determine the development lengths for headed bars and the required parallel tie reinforcement. It is based on the anchor bolt provisions in ACI 318, which have been improved to account for the influence of the bar embedment length and the contribution of the parallel tie reinforcement in an accurate and rational manner.

Table of Contents

Disclaimer.....**i**

Acknowledgments.....**iii**

Abstract.....**v**

Table of Contents.....**vii**

Chapter 1 Introduction.....**1-1**

1.1 Background.....1-1

1.2 Objectives and Scope.....1-2

1.3 Organization of the Report.....1-3

Chapter 2 Literature Review.....**2-1**

2.1 Experimental Research on Anchorage Capacity of Headed Bars.....2-2

2.1.1 Summary.....2-13

2.2 Anchorage Capacity and Development Length Formulas for Headed Bars.....2-14

2.2.1 De Vries et al. (1999).....2-15

2.2.2 Ghimire et al. (2018).....2-16

2.2.3 Zaborac and Bayrak (2022).....2-17

2.2.4 Development Length Formula in ACI 318-14/11/08.....2-19

2.2.5 Development Length Formula in ACI 318-19.....2-20

2.2.6 AASHTO LRFD Bridge Design Specifications.....2-21

2.2.7 Bar Development Lengths Specified in Caltrans MTD 20-21.....2-23

2.2.8 Anchorage Capacity of Headed Anchor Bolts Specified in ACI 318-19.....2-24

2.3 Comparison of Development Length Formulas.....2-26

Chapter 3 Development Length Test Program.....**3-1**

3.1 Specimen Configurations and Test Matrix.....3-1

3.2 Specimen Design.....3-4

3.3 Specimen Construction.....3-15

3.4 Material Properties.....3-16

3.5 Test Setup.....3-18

3.6 Instrumentation.....3-22

3.7 Test Procedure.....3-23

Chapter 4 Experimental Observations and Results.....4-1

4.1 Summary of Test Results.....4-1

4.2 Specimen 1.....4-4

4.2.1 General Observations.....4-4

4.2.2 Test Results.....4-7

4.3 Specimen 2.....4-11

4.3.1 General Observations.....4-11

4.3.2 Test Results.....4-13

4.4 Specimen 3.....4-19

4.4.1 General Observations 4-19

4.4.2 Test Results.....4-20

4.5 Specimen 4.....4-25

4.5.1 General Observations.....4-25

4.5.2 Test Results.....4-30

4.6 Specimen 5.....4-34

4.6.1 General Observations.....4-34

4.6.2 Test Results.....4-37

4.7 Specimen 6.....4-41

4.7.1 General Observations.....4-41

4.7.2 Test Results.....4-43

4.8 Specimen 7.....4-48

4.8.1 General Observations.....4-48

4.8.2 Test Results....4-51
4.9 Specimen 8....4-55
4.9.1 General Observations....4-55
4.9.2 Test Results....4-57
4.10 Specimen 9....4-64
4.10.1 General Observations....4-64
4.10.2 Test Results....4-66
4.11 Specimen 10....4-73
4.11.1 General Observations....4-73
4.11.2 Test Results....4-75
4.12 Specimen 11....4-79
4.12.1 General Observations....4-79
4.12.2 Test Results....4-80
4.13 Specimen 12....4-84
4.13.1 General Observations....4-84
4.13.2 Test Results....4-87
4.14 Specimen 13....4-92
4.14.1 General Observations....4-92
4.14.2 Test Results....4-95
Chapter 5 Analysis of Experimental Data....5-1
5.1 Anchorage Strength of Headed Bars....5-1
5.2 Anchorage Forces Developed in Test Specimens....5-2
5.2.1 Specimen 1....5-2
5.2.2 Specimen 2....5-6
5.2.3 Specimen 3....5-10
5.2.4 Specimen 4....5-13

5.2.5 Specimen 5.....5-16
5.2.6 Specimen 6.....5-19
5.2.7 Specimen 7.....5-22
5.2.8 Specimen 8.....5-25
5.2.9 Specimen 9.....5-31
5.2.10 Specimen 10.....5-37
5.2.11 Specimen 11.....5-40
5.2.12 Specimen 12.....5-43
5.2.13 Specimen 13.....5-47
Chapter 6 Tension Development of Headed Bars.....6-1
6.1 Calculation of Anchorage Strength of Headed Bars.....6-1
6.1.1 Breakout Resistance.....6-2
6.1.2 Bar Pullout Strength.....6-9
6.2 Determination of Development Lengths.....6-14
Chapter 7 Summary and Conclusions.....7-1
7.1 Summary.....7-1
7.2 Conclusions.....7-1
References.....R-1
Appendix A: Design of RC Beam Specimens.....A-1
Appendix B: Material Properties of Stirrup Samples.....B-1
Appendix C: Drawings of Steel Load Beam.....C-1
Appendix D: Strain Gauge Layouts & Force-Strain Curves.....D-1
D.1 Specimen 1.....D.1
D.2 Specimen 2.....D.8
D.3 Specimen 3.....D.19
D.4 Specimen 4.....D.27

D.5 Specimen 5.....D.35
D.6 Specimen 6.....D.44
D.7 Specimen 7.....D.54
D.8 Specimen 8.....D.63
D.9 Specimen 9.....D.78
D.10 Specimen 10.....D.90
D.11 Specimen 11.....D.98
D.12 Specimen 12.....D.106
D.13 Specimen 13.....D.117

Chapter 1 Introduction

1.1 Background

Large-diameter RC bridge columns and piles often have No. 11 or larger bars as longitudinal reinforcement. These bars extend into the bent cap and footing connected to the column with an embedment length that is sufficient to develop the tension capacity of the bars in the plastic hinge regions of the column in the event of a major earthquake. Compared to bars that have straight ends or are ended with standard hooks, headed bars allow a significant reduction of the required development length. A shorter development length allows a smaller height for the cap beams and footings. Compared to bars with 90-degree hooks, the use of headed bars can significantly reduce congestion in the joint regions, improving the constructability, the quality of concrete placement, and the cost efficiency in construction.

A study by Papadopoulos et al. (2015) on column-to-slab joints in slab bridges has shown that No. 9 and No. 10, Grade 60, headed bars can have a development length as low as $11d_b$ for concrete that has a compression strength of 4,500 psi. The bars considered in that study had full-size heads with a net bearing area of $9A_b$. Based on that study, Caltrans MTD 20-21 (Caltrans 2016a) specifies a minimum development length of $11d_b$ for headed bars connecting columns or extended piles to deck slabs in slab bridges provided the joint reinforcement meets the detailing requirements in Caltrans MTD 20-7 (Caltrans 2016b). For headed bars anchored in column-to-bent cap and column-to-footing joints, MTD 20-21 specifies a minimum development length of $19d_b$, which is largely based on the development length requirements in ACI 318-14 (ACI 2014) for No. 11 or smaller bars. Currently, Caltrans permits only full-size heads that have a net bearing area of $9A_b$, while ACI 318 only requires a net bearing area not less than $4A_b$. The use of larger heads may cause constructability issues by increasing congestion in the joint regions.

The development length requirements for headed bars in ACI 318 limit the bar size to No. 11 or smaller because of the lack of experimental data to support the use of larger-diameter bars. The development length formula in ACI 318-19 is based on experimental data from No. 11 and smaller bars and the work of Shao et al. (2016) and Ghimire et al. (2017). A unified formula has been introduced in the 10th Edition of AASHTO LRFD Bridge Design Specifications (AASHTO 2024) for the

tension development of straight, hooked, and headed bars. It is based on the work of Zaborac and Bayrak (2022). Again, for headed bars, the AASHTO specifications allow only No. 11 or smaller bars.

Little data is available on the anchorage capacity of No. 14 and No. 18 headed bars. Stoker et al. (1974) conducted 18 pullout tests on No. 11, 14, and 18, Grade-60, headed bars. The variables considered in their study included the embedment length, the concrete cover, and the concrete strength. The embedment length considered ranged from $11d_b$ to $37d_b$. The concrete specimens had reinforcement details representative of those in the cap beams of a box-girder bridge designed according to the current specifications. Four of the specimens had a group of 4 No. 11 bars, while the rest had single bars. Six of the specimens developed concrete failure in the anchorage region, and three had bar fractures. The rest had the tests stopped when the loading reached 90 to 95% of the guaranteed tensile strength of the bars. The study showed that an embedment length of $16d_b$ was sufficient to develop the guaranteed tensile strength (90 ksi) of a #18 headed bar that had a concrete cover of $3.3d_b$, while an embedment length of $11d_b$ would result in anchorage failure. The study provided no data for embedment lengths between these two limits.

1.2 Objectives and Scope

The main aims of the study reported here are to investigate experimentally the anchorage capacities of No. 14 and No. 18 headed bars, including the influence of the embedment length, concrete strength, head size, parallel tie reinforcement, and bar group on the anchorage strength, evaluate the applicability of the development length requirements for No. 11 or smaller headed bars in ACI 318-19 (ACI 2019) and the 10th Edition of AASHTO LRFD Bridge Design Specifications (AASHTO 2024) to larger diameter bars, and develop a rational method and recommendations for determining development lengths required for headed bars of any diameters and the reinforcement required for the joint regions.

In this study, bar anchorage tests were conducted on No. 14 and No. 18 headed bars, which were anchored in RC beams that were reinforced with longitudinal bars and rectangular stirrups that had the size and spacing representative of those used in the cap beams of bridge structures. A total of thirteen specimens were tested, of which eleven had single bars and two had double side-by-side bars. The influence of the head size, namely, heads with net bearing areas of $4A_b$ and $9A_b$, on the anchorage capacity was investigated. The target compressive strengths of the concrete used were 4,000, 6,000, and 8,000 psi. The specimens had bar embedment lengths equal to 70% or 100% of

the minimum according to the ACI 318-19 formula intended for smaller bars. The strains in the headed bars and stirrups were measured with strain gauges. The test data and observations were used to determine the load resisting mechanisms developed in the bar anchorage regions and support the development of design recommendations that can be used for the No. 14 and No. 18 bars.

1.3 Organization of the Report

Chapter 2 of the report presents a summary of past studies on the tension development of headed bars, the specifications in ACI 318 and AASHTO for determining the development lengths for No. 11 and smaller bars, and the anchor bolt provisions in ACI 318, which are relevant to the anchorage of headed bars.

Chapter 3 describes the experimental program carried out in this study, including the design of the test specimens, specimen reinforcement details, specimen construction, the properties of the materials used, test setup, loading method, and instrumentation.

Chapter 4 presents the test observations and results.

Chapter 5 presents a detailed analysis of the test data, which quantifies the load resisting mechanisms developed in the bar anchorage regions, and specifically the concrete breakout resistance and the bar pullout resistance.

Chapter 6 presents the method and recommendations proposed in this study for determining the development lengths for headed bars as well as the quantity of stirrups required for the joint regions, along with supporting test data.

Chapter 7 provides a summary of the findings and the conclusions from this study as well as recommendations for future work.

Chapter 2 Literature Review

Headed reinforcing bars can have T heads of different shapes, sizes, and ways of connecting to the bar. ASTM A970 Standard Specification (ASTM 2018) specifies the material, manufacturing, and quality control requirements for headed bars. The heads can be formed by integral hot forging; or be machined from bar stock or cut from plate and connected to the bar by welding or threading. The head can be screwed onto the threaded end of the bar directly or onto an externally threaded coupling sleeve cold-swagged onto the bar (Shao et al. 2016). The head can also be secured with nuts. For the case of a welded head, the reinforcing bar must conform to ASTM A706. ACI 318-19 (ACI 2019) specifies that the head dimension, and the size of obstruction and bar deformation interruptions introduced in the manufacturing process shall conform to Annex A1 of ASTM A970 for Class HA heads, which shall have the net bearing area be no less than four times the nominal cross-sectional area of the bar.

Papadopoulos et al. (2015) provided a succinct summary of past research on the anchorage capacity of headed bars and the development length requirements for the bars. Since then, a significant amount of experimental data on the anchorage capacity of headed bars has been acquired (Shao et al. 2016, Ghimire et al. 2019a, 2019b), and a new development length formula for headed bars has been adopted in ACI 318-19 based on the work of Ghimire et al. (2019b). Furthermore, a unified development length formula for headed, hooked, and straight reinforcing bars has been in the 10th Edition of AASHTO LRDF Bridge Design Specifications (AASHTO 2024) based on the work of Zaborac and Bayrak (2022). All these formulas are limited to headed bars not larger than No. 11. In the following sections, the literature review provided by Papadopoulos et al. (2015) has been expanded to include findings from the new studies, and the development length formulas adopted in the current and earlier editions of ACI 318 and the 10th Edition of AASHTO are compared.

In addition, the development length requirements recommended in Caltrans MTD 20-21 (Caltrans 2016a) for headed bars and the relevant provisions for headed anchor bolts in ACI 318 are discussed.

2.1 Experimental Research on Anchorage Capacity of Headed Bars

The pullout resistance of a headed bar is provided by the bearing of the concrete on the T head and the bond between the bar and the surrounding concrete, which is largely attributed to the bearing resistance developed at the bar ribs, as shown in Figure 2.1. A number of experimental studies were conducted to evaluate the anchorage capacity of headed bars. Studies have shown that the anchorage failure of a headed bar can be governed by one of the following four mechanisms: (1) side-face blowout failure of concrete, which may occur when the bar is close to the edge of a concrete slab or block; (2) concrete breakout failure, which may occur when the embedment length is shallow; (3) bearing failure at the T head; and (4) punch-though failure, which may occur when the bar is in compression and the head has a shallow concrete cover on its exterior surface. The first three mechanisms are associated with bars in tension and are very similar to those observed for headed anchor bolts in tension (Eligehausen et al. 2006). Side-blowout failure is characterized by the spalling of the concrete cover on the surface parallel and adjacent to the bar, as shown in Figure 2.2. Breakout failure is characterized by the formation of a cone-shaped concrete breakout, as shown in Figure 2.3. A bar with a short embedment length but an adequate lateral concrete cover may exhibit this type of failure. Bearing failure at the T head can be characterized by the lateral splitting and/or crushing of the concrete in front of the head, as shown in Figure 2.4. Punch-through failure may occur when the bar is in compression and there is not enough concrete cover over the exterior face of the head to resist the punching force, resulting in the cracking and spalling of the concrete cover, as shown in Figure 2.5.

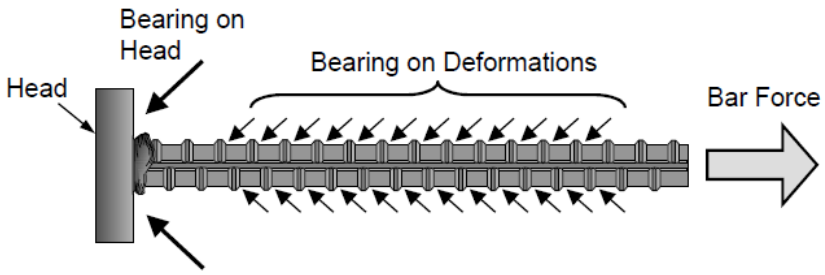

Figure 2.1: Pullout resistance of a headed bar (Thompson et al. 2002)

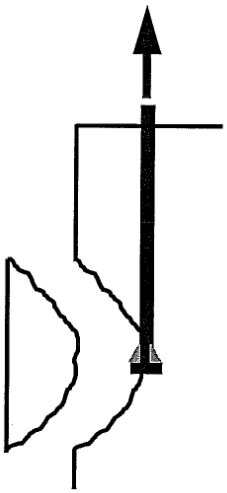

Figure 2.2: Side-blowout failure (De Vries et al. 1996)

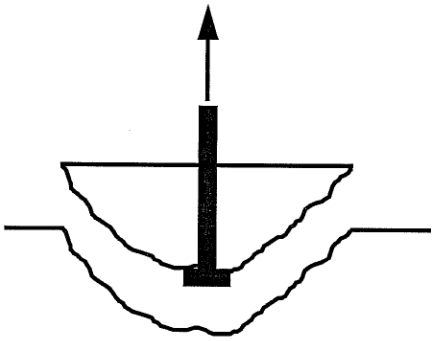

Figure 2.3: Concrete breakout failure (De Vries et al. 1996)

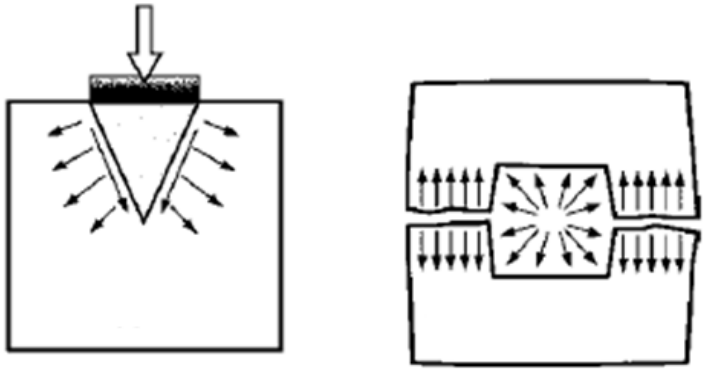

(a) Side view (b) Top view

Figure 2.4: Bearing failure (Thompson et al. 2002)

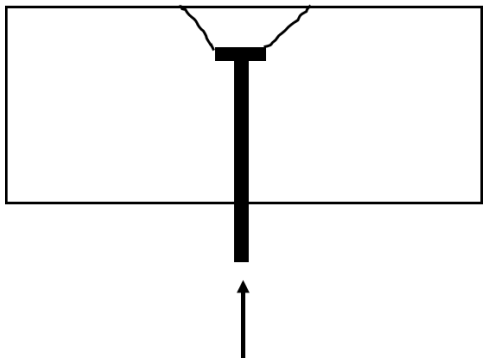

Figure 2.5: Punch-through failure

De Vries (1996) conducted more than 140 pullout tests to evaluate the anchorage performance of headed bars with variables including the embedment length (distance from the bearing surface of the T head to the concrete surface), bonded length (which may be less than or equal to the embedment length), concrete strength, transverse reinforcement, head geometry, and edge distance of bars. Eighteen of these tests (De Vries et al. 1999) were conducted with shallow embedment lengths varying from $1.8d_b$ to $11.5d_b$. Some of the bars had a small edge distance of 2 in. The bar sizes were No. 6, 8, and 11. The ratio of the net bearing area of the head to the nominal cross-sectional area of the bar varied from 4.7 to 10.0. Some of the concrete specimens had transverse reinforcement perpendicular to the bars. The bars in each concrete block were spaced

sufficiently far apart to avoid the overlap of the failure surfaces. Of the 18 specimens, 3 had bar fracture while the rest had anchorage failure. Two of the specimens with bar fracture had an embedment length of $5.7d_b$ and a concrete compressive strength of 12,000 psi, while the third had twice as much embedment length and a concrete strength of 4,000 psi. These three specimens had the bar located at least 18 in. from the closest edge of the slab. Furthermore, the bars did not have bonding with the concrete. Therefore, the anchorage capacity was entirely provided by the bearing of the concrete against the T head. For the other specimens, the failure mechanism was concrete breakout (with cone-shaped fracture) as shown in Figure 2.6. Their results showed that an embedment length as short as $11.5d_b$ could be sufficient to develop the full tensile capacity of a headed bar embedded in 4,000 psi concrete without breakout failure. Furthermore, they observed that the bond stress between the bar and the surrounding concrete slightly increased the anchorage capacity, and that the transverse reinforcement and the ratio of the head area to the bar area did not affect the anchorage capacity.

Figure 2.6: Concrete breakout failure in a shallow embedment test (De Vries et al. 1999)

Bashandy (1996) conducted 32 pullout tests to study the anchorage performance of headed bars in exterior beam-to-column joints. Each specimen had two headed reinforcing bars (mimicking the longitudinal bars extending from the beam) anchored in the RC column. The variables included the bar size (No. 8 and No. 11), the embedment length ($6d_b$ to $13d_b$), the side cover, the ratio of the gross head area to the nominal bar area (3 to 8.1), and the presence or absence of confining reinforcement parallel to the bars in the joint. The compressive strength of the concrete in the specimens was between 3,000 psi and 5,800 psi. The yield strength of the headed bars was approximately 80 ksi. During the tests, the bars did not yield and the load capacity was governed by anchorage failure. Eighteen specimens had side-blowout failure, as shown in Figure 2.7. The remaining fourteen had anchorage failure related to the shear failure in the joint region. His study showed that the side concrete cover, embedment length, and confining reinforcement were the primary factors affecting the anchorage capacity. Increasing the thickness of the side cover or the amount of confining reinforcement increased the anchorage capacity. Bar diameters did not have significant influence on the anchorage capacity. Cyclic tension loading and unloading up to 80% of the ultimate anchorage strength did not affect the anchorage capacity.

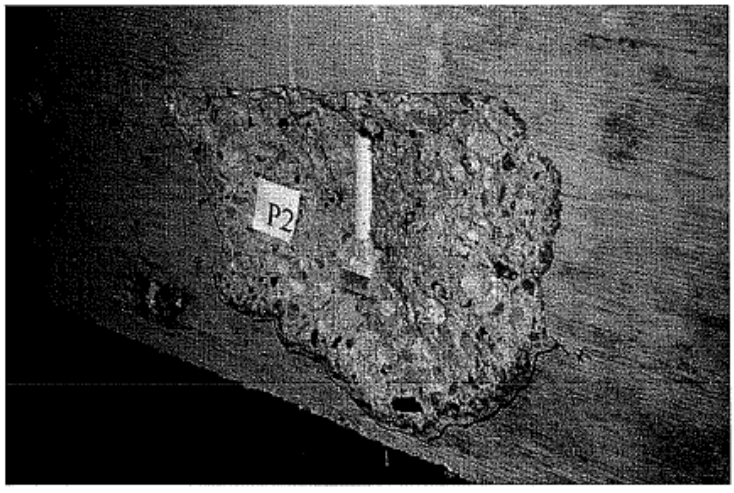

Figure 2.7: Side-blowout failure in a beam-to-column joint test (Bashandy 1996)

Wright and McCabe (1997) conducted "beam-end" tests to examine the anchorage capacity of headed bars. The bars in the beam-end specimens had limited side concrete cover. They considered only Grade 75, No. 8, bars with an embedment length of 12 in. ($12d_b$) and concrete strengths between 4,500 and 5,000 psi. The variables investigated were the side concrete cover ($2d_b$ and $3d_b$), the bonded length of the bars, and the quantity and spacing of transverse reinforcement. The bars yielded in some of the tests, but none of the specimens was loaded to bar fracture. They observed that with a concrete cover of $2d_b$, the presence of transverse reinforcement enhanced the anchorage capacity of a bar. However, with a cover of $3d_b$, the effect of transverse reinforcement was not noticeable. Interestingly, they also showed that the addition of a PVC tube to avoid the bonding of the bar with the surrounding concrete reduced concrete cracking and increased the anchorage capacity. However, this could be related to the fact that the specimens had side-blowout failure.

Thompson et al. (2005a and 2005b) studied the anchorage capacity of headed bars terminated at the end of a beam. They idealized the load transfer mechanism in that region with a strut-&-tie model, and bar anchorage was considered to be located in a compression-compression-tension (CCT) node of the model. They tested 64 CCT node specimens. They observed that the anchorage failure in CCT nodes was characterized by the crushing of concrete in front of the bar ribs and lateral splitting. They postulated that the anchorage capacity of a headed bar in a CCT node was contributed by the bearing capacity of the concrete at the T head and the bond force between the bar and the concrete. However, because the bond resistance would have passed the peak value before the peak bearing capacity would develop, they suggested that a reduced bond strength should be considered in calculating the anchorage capacity. They also studied experimentally the behavior of lap splices with headed bars (Thompson et al. 2006a). Based on their experimental data,

they have proposed formulas to calculate the reduced bond strength and the bearing capacity of concrete against a T head in CCT nodes and lap splices (Thompson et al. 2006b). They further concluded that the formulas were also applicable to headed bars with deep embedment and beam-to-column joints. However, their model does not account for the breakout failure of concrete.

Kang et al. (2010) studied the performance of bars with small heads ($2.7A_b$) in exterior beam-to-column joints. Twelve pullout tests were conducted on No. 6 bars with a yield strength of 67 ksi. Both circular and square heads were investigated. The bars were embedded in concrete blocks with a compressive strength of 5,000 psi over a length of $10d_b$, and were subjected to monotonic tensile loading as well as cyclic loading and unloading. All the bars yielded and experienced strain hardening. The specimens failed with the splitting of the concrete and local concrete crushing in front of the head. The anchorage strength was not significantly affected by the difference in the head geometry and the cyclic history. Furthermore, two exterior beam-to-column joint assemblies were tested under cyclic loading. One assembly had headed bars for the longitudinal reinforcement in the beam, and the other had hooked bars. Both had an embedment length of $15d_b$ in the beam-to-column joint. While the specimen with headed bars performed satisfactorily, the hooked bars had anchorage failure which triggered the failure of the joint.

Papadopoulos et al. (2015) conducted a study to determine the development length required for headed bars anchored in slab-to-column joints of slab bridges. Three slab-single column assemblies were tested. The headed longitudinal bars from the columns were anchored in the slabs with embedment lengths of 8.7 d_b , 9.8 d_b , and 11 d_b , respectively. The sizes of the longitudinal bars were No. 9 in Specimen 1, and No. 10 in Specimens 2 and 3. The bars had circular heads with the net bearing area equal to 9 times the nominal bar area. The bars were Grade 60 and the concrete had a targeted compressible strength of 5,000 psi. The slab-to-column joints were reinforced with the

detailing requirements that were later incorporated in the 2016 update of MTD 20-7 (Caltrans 2016b). The tests have shown that bar embedment lengths of $8.7d_b$ and $9.8d_b$ with 5,000 psi concrete were sufficient to develop the ultimate moment capacity of the columns but resulted in moderate to severe punching cracks in the concrete cover above the T heads caused by the bars in compression, as shown in Figure 2.8, while an embedment length of $11d_b$ with 4,500 psi concrete resulted in only mild punching cracks. Based on this study, Caltrans (MTD 20-21, 2016a) has recommended a minimum development length of $11d_b$ for headed column/pile extension bars embedded in slab-to-column joints of slab bridges, and required that the net bearing area of the head be at least 9 times the nominal cross-sectional area of the bar. The recommendation is based on the understanding that the expected compressive strength of the concrete used in typical bridge structures is not less than 4,000 psi.

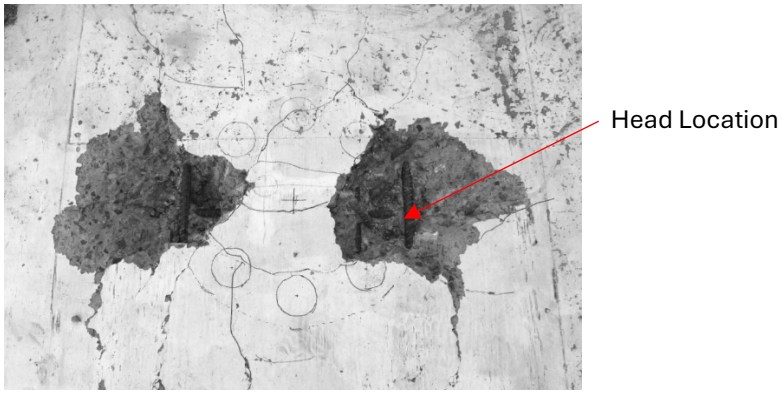

Figure 2.8: Punching cracks on slab surface (Papadopoulos et al. 2015)

Shao et al. (2016) carried out an extensive experimental study to identify factors that could influence the anchorage capacity of headed bars and to provide data for developing a development length formula that would be applicable to high-strength bars and concrete. In their study, 233 specimens were tested. There were four types of specimens. Two hundred and two of the specimens were to simulate the anchorage conditions in exterior beam-to-column joints, similar to those tested

by Bashandy (1996), ten were beam specimens, similar to those tested by Thompson et al. (2005a, 2005b), fifteen were specimens with shallow embedment (each containing one to three bars), and six were specimens with lap splices, similar to those tested by Thompson et al. (2006a).The bar sizes considered were No. 5, 6, 8, and 11. Different types of T heads were considered, with the ratio of the net bearing area to the nominal bar area ranging from 3.8 to 14.9. The headed bars were all Grade 120, while the compressive strength of the concrete ranged from 3,960 to 16,030 psi. Additional parameters investigated included the amount of confining reinforcement, the number of headed bars in a specimen, the spacing between the T heads, and the embedment length. One hundred ninety-six of the beam-to-column joint specimens exhibited anchorage failure. Most of them had breakout failure, while some had side-face blowout failure, with the failure patterns shown in Figure 2.9. Test results from the beam-to-column joint specimens are summarized in the papers by Ghimire et al. (2019a and 2019b). The study has shown that the development length formula in ACI 318-14 (ACI 2014) and its earlier editions does not accurately account for the effect of the concrete compressive strength and the spacing of headed bars in a joint. It has been found that the anchorage capacity of headed bars is more closely correlated to $\sqrt[4]{f_c'}$ than $\sqrt{f_c'}$, the latter of which has been adopted in ACI 318. The study has also found that the anchorage strength of headed bars in a beam-to-column joint is proportional to the amount of confining reinforcement per bar in the joint region parallel to the headed bars being developed. The data have shown that the anchorage strength will decrease with the decrease of the bar spacing when the center-to-center bar spacing is less than 8 d_b. For the case of No. 5 headed bars with confining reinforcement in the joint region, the head size showed some influence on the anchorage strength. Nevertheless, this influence was negligible for No. 8 and 11 bars with or without confining steel. For the No. 5 bars, the head size showed a beneficial influence only when the ratio of the net bearing area to the nominal bar area was greater than 9.5.

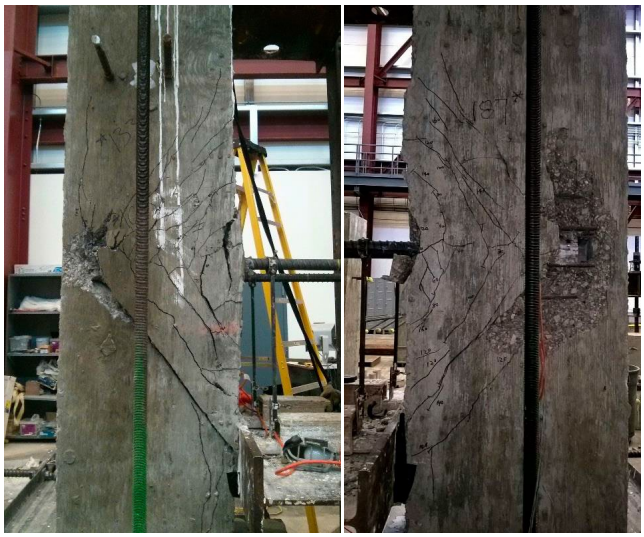

Breakout Failure Side-Face Blowout Failure

Figure 2.9: Breakout and side-face blowout failures (Shao et al. 2016)

Ghimire et al. (2018) tested 32 No. 8 headed bars anchored in concrete specimens simulating the reinforcement details in column-to-foundation joints. The ratio of the net bearing area of the head to the nominal bar area ranged from 4 to 15. The embedment lengths varied from 6 d_b to 8.5 d_b . The compressive strength of the concrete was between 4,200 and 8,620 psi, and the headed bars were Grade 120. All the specimens had breakout failure. The tests have shown that reinforcement perpendicular to the headed bar in the slab has negligible influence on the anchorage capacity. Similar to the observations of Shao et al. (2016), the tests have shown little influence of the head size on the anchorage strength.

All the aforementioned experimental studies had bar sizes not greater than No. 11. The only experimental data available for larger diameter headed bars were from the 18 pullout tests conducted by Stoker et al. (1974) on No. 11, 14, and 18, Grade 60, headed bars. The variables considered in their study included the embedment length, the side concrete cover, and the concrete strength. The embedment length considered for the headed bars varied from 11d_b to 37d_b. The bonding between the bars and the concrete was released over a portion of the embedment length.

The ratio of the net bearing area of the head to the nominal bar area was 13 for the No. 18 bars, and 15 for the No. 11 and 14 bars. The compressive strengths of the concrete varied from 3,550 psi to 5,400 psi. The concrete specimens had reinforcement details representative of those in the cap beam of a box-girder bridge designed according to the specifications in that time period. Five of the specimens had 4 No. 11 bars tested as a group, while the rest had single bars. The heads in the bar groups were staggered along the height. Six of the specimens developed concrete failure in the anchorage region, and three had bar failure. One test had anchorage device failure. The rest had the tests stopped when the loading reached 90 to 95% of the guaranteed tensile strength of the bars. The study showed that for the #18 headed bars that had a concrete cover of $3.3d_b$ and a concrete strength of 4,820 psi, an embedment length of $16d_b$ was sufficient to develop the guaranteed bar tensile strength of 90 ksi, while an embedment length of $10.6d_b$ with a concrete strength of 3,550 psi could develop a maximum tensile stress of 69 ksi. There were no data for embedment lengths between these two values. Their results also showed that bar groups had a weaker anchorage than single bars. For a group of four #11 headed bars, with a concrete cover of $5.3d_b$ and a clear bar spacing of $1.5d_b$, concrete failure occurred in the anchorage region even with an embedment length of $27.7d_b$ and a concrete strength of 5,210 psi. Furthermore, the bar group tests showed that increasing the embedment length did not increase the anchorage capacity. This unusual observation could be related to the specimen design and loading scheme used in the tests. In contrast to the typical cone-shaped breakout failure observed in the other test programs discussed previously, all the specimens tested in this study developed a crack pattern that consisted of a main longitudinal crack at the center of the concrete block crossed by horizontal transverse cracks. This could be attributed to the loading scheme that subjected the concrete blocks to tension and the small cross-sectional dimensions of the blocks, which had relatively light reinforcement. As a result, the

anchorage capacity was limited by the tensile resistance of the blocks rather than the concrete breakout observed in other studies. Because of this, this study did not provide conclusive results.

2.1.1 Summary

Experimental data currently available on the anchorage capacity of headed reinforcing bars are exclusively on No. 11 and smaller bars. Only limited number of bar anchorage tests were conducted on No. 14 and 18 headed bars, and data from these tests are somewhat inconclusive because of the limited number of specimens, as well as the loading condition and the small dimensions of the anchoring reinforced concrete blocks used in the specimens, which did not reflect the conditions in an actual joint. It is also notable that the majority of the tests had anchorage failure rather than bar fracture.

Key observations from the anchorage tests on No. 11 and smaller headed bars are summarized as follows.

1. Similar to that observed for headed anchor bolts, the anchorage failure of headed bars under tension is typically governed by one of two possible modes, namely, breakout or side-face blowout failure. Bearing failure was mainly observed at T heads anchored at the end of a beam specimen.
2. With 4,000 psi concrete, an embedment length of 11db appears to be sufficient to develop the full tensile strength of a Grade 60 headed bar well-centered in the concrete specimen.
3. Except for the case of headed bars anchored at the end of a beam, where bearing failure was observed, the ratio of the net bearing area of the head to the nominal bar diameter does not appear to affect the anchorage capacity when the ratio does not exceed 9.5.

4. The study by Shao et al. (2016) has shown that that the anchorage capacity of headed bars is more closely correlated to $\sqrt[4]{f_c'}$ than $\sqrt{f_c'}$.
5. Transverse reinforcement (perpendicular to headed bars) in the bar anchorage region does not appear to improve the anchorage strength, but confining reinforcement in a beam-to-column joint parallel to the headed bars being developed can increase the anchorage strength, and the increase is proportional to the amount of transverse reinforcement per bar.
6. Tests have shown that when the anchorage capacity of a headed bar is reached (at impending anchorage failure), the T head will be fully engaged to resist tension, and the bond force along the bar will diminish.
7. Cyclic tension loading and unloading up to 80% of the ultimate anchorage capacity does not appear to affect the anchorage strength.
8. Shear cracking in a beam-to-column joint can significantly lower the anchorage strength of a headed bar.
9. Increasing side concrete cover can prevent side-face blowout failure and thus increase the anchorage capacity.

2.2 Anchorage Capacity and Development Length Formulas for Headed Bars

This section discusses methods proposed to calculate the anchorage capacity of headed bars in several key studies, the development length formulas adopted in ACI 318-19 and its earlier editions, and the new formula introduced in the 10th Edition of AASHTO LRFD Bridge Design Specifications. Furthermore, current recommendations of Caltrans for the development of headed bars are summarized, and the formula in ACI 318 for calculating the anchorage capacity of headed anchor bolts is presented. The latter is relevant to headed bars because other than the lack of bond strength, headed anchor bolts exhibit similar anchorage mechanisms.

2.2.1 De Vries et al. (1999)

De Vries et al. (1999) adopted the concrete capacity design (CCD) method, originally proposed by Fuchs et al. (1995) and Eligehausen and Balogh (1995) for headed anchor bolts embedded in concrete, to calculate the anchorage capacity of headed bars in plain concrete. They validated the method with their test data from shallow-embedment pullout tests. For a single headed bar embedded with a distance of at least 1.5 times the embedment length from the edge of the concrete member, which will allow a full cone-shaped breakout failure, they adopted the following equation for calculating the anchorage strength P_n.

$$P_n = 21.2 h_d^{1.5} \sqrt{f_c'} \tag{2.1}$$

in which h_d is the embedment length and f_c' is the specified concrete strength, with all units in pounds and inches. This formula was derived with the assumption that the concrete breakout cone has the shape of an inverted pyramidal frustrum and the top face of the frustrum has dimensions of $3h_d$ by $3h_d$. For a group of anchored bars with the center-to-center spacing less than three times the embedment length, the failure surfaces of individual bars will intersect, resulting in a total anchorage capacity less than the sum of the capacities of the individual anchors. The size of the failure cone of an individual bar can also be reduced if the bar is placed with a distance less than 1.5 times the embedment length from the edge. To account for the group and edge placement effects, they modified Equation (2.1) as follows.

$$P_n = \Psi \frac{A_n}{9 h_d^2} 21.2 h_d^{1.5} \sqrt{f_c'} \tag{2.2}$$

in which A_n is the total available area of the top concrete breakout surface and Ψ is a factor to account for the disturbance to the assumed radial stress pattern caused by the reduced edge distance.

$$\Psi = 0.7 + 0.3\frac{C_1}{1.5h_d} \leq 1 \tag{2.3}$$

where C_1 is the minimum edge distance.

Equation (2.2) does not account for the effect of the reinforcement in the concrete member on the capacity of the anchors and does not accurately reflect the loading conditions in a beam-to-column or slab-to-column joint, in which part of the concrete section developing the moment resistance will be subjected to compression. If the compression develops in a region close to the tension bars, it will interfere with the development of the cone-shaped breakout failure. De Vries et al. also recommended that the distance of 1.5 h_d that defines the top area of the assumed failure cone in Equation (2.2) be measured from the perimeter of the head rather than the center of the bar to account for the fact that the size of a T head in a bar is much larger than the head in an anchor bolt, and therefore the size of a T head will have a higher impact on the anchorage resistance. When P_n in Equation (2.2) is replaced by the tensile strength of the bar, an expression for the required tension development length can be obtained by a simple rearrangement of the terms in the equation.

2.2.2 Ghimire et al. (2018)

Based on the experimental data of Shao et al. (2016) and others, Ghimire et al. (2018) proposed the following formula to calculate the development length of headed bars in tension.

$$l_{dt} = \left(\frac{f_y \psi_e \psi_{cs} \psi_o}{400 f_c'^{0.25}}\right) d_b^{1.5} \geq 8.0 d_b \text{ or } 6 \text{ in.} \tag{2.4}$$

in which l_{dt} is the development length in inches, f_y is the specified yield strength of the bar in psi, ψ_e is the modification factor for the surface treatment of the bar, ψ_{cs} is the modification factor for confining reinforcement and bar spacing, ψ_o is the modification factor for bar location, d_b is the nominal bar diameter in inches, and f_c' is the specified concrete compressive strength in psi. The formula is applicable to headed bars with a yield strength up to 120,000 psi and concrete with a compressive strength up to 16,000 psi. The factor ψ_e is 1.2 for epoxy-coated or zinc and epoxy dual-coated bars and 1.0 otherwise. The value of the factor ψ_{cs} depends on the ratio of the cross-sectional area of the confining reinforcement parallel to l_{dt} to the total cross-sectional area of the headed bars being developed, or the center-to-center spacing of the headed bars. The bar location factor ψ_o is 1.0 for headed bars located inside the column core of a beam-to-column joint with a clear concrete cover equal to or greater than 2.5 in., or in other locations with a minimum clear cover equal to or greater than 8 d_b; it is equal to 1.25 otherwise.

2.2.3 Zaborac and Bayrak (2022)

Based on the unified approach adopted in fib model code 2010 (fib 2013), Zoborac and Bayrak (2022) proposed the following formula to calculate the anchorage capacity of bars in tension with different anchorage conditions, which include bars with straight ends, bars with 90-degree hooks, and headed bars (with units in kips and inches).

$$f_{su} = 4.74\left(\frac{\sqrt{l_e}}{d_b}\right)\left(\frac{c_b\left(1-\beta_t\right)+1.67 n_s k_{tr}}{\sqrt{c_b}}\right)\sqrt[4]{f_c'}+\frac{F_h}{A_b} \le 1.53\left(\frac{l_e}{d_b}\right)1.5\sqrt{f_c'}+\frac{F_h}{A_b} \tag{2.5}$$

in which f_{su} is the anchorage strength in terms of bar stress, l_e is the embedment length, β_t is the ratio of the transverse stress (negative for compression) across the splitting plane to the concrete tensile strength and is limited to the range of $-1 \le \beta_t \le 0$, $n_s = E_s / E_c$, c_b is the concrete cover

parameter, k_{tr} is the transverse reinforcement index, and F_h is the resisting force developed by a 90-degree hook or T head (with a value of zero for a straight bar). The definitions of c_b and k_{tr} are similar to those used in the ACI 318-19 formula for the development length of straight reinforcing bars in tension. The resisting force by a T head is calculated with the following formula.

$$F_h = A_h \nu f_c' \cos^2 \theta_c \tag{2.6}$$

in which A_h is the net bearing area of the head, θ_c is the compression field angle which is assumed to be 45°, and ν is the concrete strength efficiency factor which is to be calculated with the following expression.

$$0.45 \le \nu = 0.85 - \frac{f_c'}{138} \le 0.65 \tag{2.7}$$

Equation (2.5) considers the contributions of both the bond strength and the bearing resistance of the T head to the anchorage strength, and that the average bond strength for a headed bar is the same as that for a straight bar. However, test data have shown that the bond resistance in a headed bar tends to diminish significantly before reaching the anchorage capacity and it does not contribute to the anchorage capacity as significantly as the T head. This stems from the fact that the development length of a headed bar is much shorter than that of a straight bar and therefore, significant plastic deformation can develop over the entire development length of a headed bar, resulting in significantly reduced average bond strength. Furthermore, Equation (2.6) accounts for the positive effect of the confining reinforcement perpendicular to the headed bar. However, test data have shown that the effect of the perpendicular reinforcement is small and negligible.

2.2.4 Development Length Formula in ACI 318-14/11/08

ACI 318-14 (as well as its two earlier editions) has the following formula to calculate the development length required for headed bars in tension.

$$l_{dt} = \text{ longest of } \left(\frac{0.016 f_y \psi_e}{\sqrt{f_c'}} \right) d_b, \ 8d_b, \text{ and } 6 \text{ in.} \tag{2.8}$$

in which ψ_e is 1.2 for epoxy-coated reinforcement and 1.0 otherwise, f_y is the nominal yield strength of the reinforcing bar, d_b is the bar diameter, and f_c' is the specified compressive strength of concrete, with all units in pounds and inches.

It is stated in the code that the use of Equation (2.8) shall be subjected to the following conditions:

1. Bar size shall not exceed No. 11 (due to the lack of experimental data on larger bars).
2. $f_y \le 60{,}000$ psi .
3. Minimum net bearing area of the head = $4A_b$.
4. Minimum clear concrete cover = $2d_b$.
5. Minimum clear spacing of bars = $4d_b$.

It is stated in the commentary section of the code that Equation (2.8) was developed with due consideration of the anchor bolt provisions in the code and the bearing strength, with reference to the work of Thompson et al. (2005a and 2005b). Nevertheless, the formula is empirical and does not explicitly account for the breakout, side-face blowout, or bearing failure mechanism observed in tests. The formula does not account for the influence of the head size aside from the requirement that the net bearing area of the head shall not be less than $4A_b$.

2.2.5 Development Length Formula in ACI 318-19

ACI 318-19 has a new development length formula for headed bars in tension based on the work of Ghimire et al. (2018). The formula is shown in Equation (2.9).

$$l_{dt} = \text{ longest of } \left(\frac{f_y \psi_e \psi_p \psi_o \psi_c}{75\sqrt{f_c'}} \right) d_b^{1.5},\ 8d_b, \text{ and } 6 \text{ in.} \tag{2.9}$$

The units in the formula are pounds and inches, and the values of the modification factors are to be determined as follows. The surface condition factor ψ_e is 1.2 for an epoxy-coated or zinc and epoxy dual-coated bar, and 1.0 otherwise. The factor ψ_p is 1.0 if the total cross-sectional area of parallel tie reinforcement located within $8d_b$ of the center line of the headed bars towards the middle of the joint is not less than 30% of the total cross-sectional area of the headed bars being developed, or if the minimum center-to-center spacing of the headed bars is not less than 6 times the nominal bar diameter; otherwise, it is equal to 1.6. The location factor ψ_o is 1.0 if the headed bars terminate inside a column core with the side cover to the bar not less than 2.5 in., or if they do not terminate inside a column core, the side cover is not less than 6 times the nominal bar diameter; otherwise, it is 1.25. The value of the concrete strength factor is calculated with the following equation.

$$\begin{aligned} \psi_c &= \frac{f_c'}{15{,}000} + 0.6 \quad \text{for } f_c' < 6{,}000 \text{ psi} \\ &= 1.0 \quad \text{for } f_c' \geq 6{,}000 \text{ psi} \end{aligned} \tag{2.10}$$

The use of Equation (2.8) shall be subjected to the following conditions:

1. Bar size shall not exceed No. 11.
2. Minimum net bearing area of the head = $4A_b$.
3. Minimum clear concrete cover = $2d_b$.

4. Minimum center-to-center spacing of bars = $3d_b$.

2.2.6 AASHTO LRFD Bridge Design Specifications

A unified formula has been introduced in the 10th Edition of AASHTO LRFD Bridge Design Specifications (AASHTO 2024) to calculate the development lengths of bars in tension with different end conditions. The formula is based on the work of Zaborac and Bayrak (2022), and is shown in Equation (2.11), with units in kips and inches.

$$l_{dt} = \text{ longest of } \left[0.17 d_b \left(\frac{\lambda_{er} f_y - \dfrac{F_h}{A_b}}{1.97 \lambda f_c'^{0.25}} \right)^2 \right] \times \left(\lambda_{rl} \times \lambda_{cf} \times \lambda_{rc} \right),\ 8d_b, \text{ and } 6 \text{ in.} \tag{2.11}$$

in which

$F_h = 0.5 A_{ht} \upsilon f_c'$ for a headed bar, where A_{ht} is the net bearing area of the head and υ is the concrete efficiency factor, which is calculated with the following expression: $0.45 \le \upsilon = 0.85 - f_c'/20 \le 0.65$;

λ_{er} = excess reinforcement factor (required total cross-sectional area of reinforcement being developed divided by the area provided);

λ = concrete weight modification factor (it is 1.0 for normal weight concrete);

λ_{rl} = reinforcement location factor (it is 1.3 if more than 12 in. of fresh concrete is cast below the bar; otherwise, it is 1.0);

λ_{cf} = coating factor (it is 1.0 if the bar has no epoxy coating or zinc and epoxy dual-coating);

λ_{rc} = reinforcement confinement factor calculated as follows:

$$0.3 \le \lambda_{rc} = \frac{d_b c_b}{\left(c_b\left(1-\beta_t\right)+1.67 n_s k_{tr}\right)^2} \le 1.0$$

where

c_b = smaller of the distance from the center of the bar being developed to the nearest concrete surface or one-half the center-to-center spacing of the bars being developed;

$n_s = E_s / E_c$ (ratio of the modulus of elasticity of steel to that of concrete);

β_t = ratio of unfactored compressive stress due to permanent loads transverse to the plane of splitting to the modulus of rupture, and its value shall be within the following range: $-1 \le \beta_t \le 0$ (compressive stress is negative);

$k_{tr} = A_{tr} / (sn)$, where A_{tr} = total cross-sectional area of tie bars crossing the splitting plane within spacing *s*, *n* = number of bars being developed along the splitting plane, and *s* = spacing of the tie bars along the development length.

For headed bars anchored within beam-to-column joints, it is permissible to reduce the development length calculated with Equation (2.11) by 20% if the total area of parallel tie reinforcement located within $8d_b$ from the center line of the headed bar towards the center of the beam-to-column joint is not less than 30% of the total area of the headed bars.

The use of Equation (2.11) shall be subjected to the following conditions.

1. Bar size shall not exceed No. 11 for headed bars (and No. 18 for bars with other end conditions).

2. Headed bars shall conform to ASTM A970 and satisfy dimension requirements for Class HA heads in Annex 1 of ASTM A970.
3. $f_c' \leq 15{,}000$ psi for normal weight concrete.
4. Minimum net bearing area of the head = $4A_b$.
5. Minimum clear cover to head = $2d_b$.
6. Minimum center-to-center spacing of bars = $3d_b$.

2.2.7 Bar Development Lengths Specified in Caltrans MTD 20-21 (December 2016)

Caltrans MTD 20-21 (Caltrans 2016a) has specifications on development lengths required for straight, hooked, and headed bars used in bridge structures, as shown in Figure 2.10. For headed bars, it requires a full-size head that has a net bearing area of $9A_b$. The values shown in the figure are based on past experimental studies conducted on bridge structural assemblies.

Table 1. Bar Development Lengths

Development length l_d = (table value) x bar diameter (d_b)

C or S	Longitudinal/Main bars in:	Embedded into/ Extended within	STRAIGHT	HOOK	HEADED[1] (Full size)	INSTRUCTIONS
S	Columns	Bent caps and footings	24	19	18[2]	Extend to bottom of top deck reinf. (avoid prestress ducts, etc.)
	Walls	Bent caps, footings	24	19	18[3]	-
	Pile Extensions and walls	Slab bridge	24	19	11[4]	Touch bottom of top steel in slab
C	Bent Caps	Bent caps	24	19	14	-
C	Footings	Footings	24	19	14	-
C	In-span hinges	In-span hinges	24	19	14	-

C = Capacity Protected
S = Seismic Critical

[1] *Interim development length based on committee decision using conservative values.*
[2] *Extend to top reinforcement in cap.*
[3] *Extend to bottom reinforcement in footing.*
[4] *Lower bound value based on tests (Papadopoulis, 2015)*

Figure 2.10: Bar development length table from Caltrans MTD 20-21

2.2.8 Anchorage Capacity of Headed Anchor Bolts Specified in ACI 318-19

The anchorage resistance mechanisms of a cast-in headed anchor bolt in tension resemble those of a headed reinforcing bar expect that an anchor bolt has a smooth surface and thus does not develop bond resistance. According to ACI 318-19 (ACI 2019), the anchorage capacity of a headed anchor bolt in tension can be governed by the concrete breakout strength or the pullout strength. The concrete breakout failure of a headed bar has been discussed in Section 2.1. The pullout strength of a headed anchor bolt is provided by the bearing resistance of the head, while that of a headed bar is provided by the bearing as well as bond resistance as shown in some studies discussed in Section 2.1. However, it should be noted that the term pullout failure was used generally in some past studies to mean the anchorage failure of headed bars regardless of the mechanism.

Section 17.6.2 of ACI 318-19 provides the following formula to calculate the concrete breakout strength of a single cast-in headed anchor bolt.

$$N_{cb} = \frac{A_{Nc}}{A_{Nco}} \psi_{ed,N} \psi_{c,N} N_b \tag{2.12}$$

For an anchor group, the formula has an additional modification factor as follows:

$$N_{cb} = \frac{A_{Nc}}{A_{Nco}} \psi_{ec,N} \psi_{ed,N} \psi_{c,N} N_b \tag{2.13}$$

where N_b is the concrete breakout strength of a single anchor that is well centered in a concrete member so that a full breakout cone can be developed and is calculated with the following formula.

$$N_b = 24\sqrt{f_c'} h_{ef}^{1.5} \tag{2.14}$$

in which h_{ef} is the effective embedment length of the anchor bolt, and all units are in pounds and inches. For light-weight concrete, a reduction factor λ_a is applied to the value of N_b calculated with the above expression. The formula proposed by De Vries et al. (1999) to calculate the concrete breakout strength of a headed bar, as discussed in Section 2.2.1, is based on the anchor bolt formulas shown above. As discussed in Section 2.2.1, the formulas are based on the assumption that the shape of the full concrete breakout cone of an anchor that is placed in a concrete member with a distance from any edge greater than $1.5h_{ef}$ can be represented by an inverted pyramidal frustrum and the top face of the frustrum has dimensions of $3h_{ef}$ x $3h_{ef}$. The variable A_{Nco} in Equations (2.12) and (2.13) is equal to $9h_{ef}^2$, which is the area of the top face of the frustrum, while A_{Nc} is the total actual area of the top face projected by the failure frustrum(s) of a single anchor or an anchor group when the minimum edge distance of an anchor is less than $1.5h_{ef}$ or the center-to-center spacing of the anchors in a group is less than $3h_{ef}$.

The modification factor $\psi_{ec,N}$ is to account for the eccentricity of the resultant load applied to an anchor group. The factor $\psi_{ed,N}$ is to account for the edge effect when the minimum edge distance is less than $1.5h_{ef}$. The factor ψ_c is to account for the influence of cracking in anchor regions at service load levels.

ACI 318-19 provides the following formula to calculate the nominal pullout strength of a single cast-in headed anchor bolt.

$$N_{pn} = 8\psi_{c,P} A_{brg} f_c' \tag{2.15}$$

in which A_{brg} is the net bearing area of the head, and $\psi_{c,P}$ is equal to 1.0 if the anchor is located in a region where concrete cracking is expected at service load levels and equal to 1.4 otherwise. All units are in pounds and inches. It is stated in the commentary of ACI 318-10 that N_{pn} corresponds to the force at which concrete crushing will occur at the head and does not necessarily represent the force required to pull the anchor completely out of the concrete. It should be noted that the bearing capacity of the head given by Equation (2.15) is significantly higher than that assumed in Equation (2.11), the development length formula proposed for ASSHTO.

2.3 Comparison of Development Length Formulas

The tension development length formulas for headed bars in ACI 318-14, ACI 319-19, and AASHTO LRFD Bridge Design Specifications are compared by considering the development lengths required for bars with different diameters and concrete with different compressive strengths. All these formulas are limited to No. 11 and smaller bars. The formula in AASHTO considers the influence of the head size, while the ACI formulas do not. All three require that the net bearing area of the T head be at least $4A_b$.

Even though the ACI and AASHTO formulas are not intended for bars larger than No. 11 due to the lack of supporting experimental data, this comparison study considers No. 8, 11, 14 and 18 bars to examine the differences in the development lengths calculated with these formulas as the bar size increases and to determine a suitable baseline formula that can be used as a starting point for the experimental study to be conducted on No. 14 and 18 bars in this project. Two head sizes are considered. One has the net bearing area equal to $4A_b$ and the other has the bearing area equal to $9A_b$. The compressive strengths of the concrete considered are 4,000, 8,000, and 12,000 psi. The bars are Grade 60 with no surface coating. The following embedment conditions are assumed:

- There is no excessive headed bar reinforcement to resist flexure.
- Side concrete cover to the anchored bars is at least 6d_b.
- Total cross-sectional area of parallel tie reinforcement within $8d_b$ of the center line of the headed bars is not less than 30% of the total cross-sectional area of the headed bars being developed.
- No confinement reinforcement transverse to the anchored bars.

Based on the above conditions, the values of the modification factors for the different formulas are shown in the table below.

Table 2.1: Development length modification factors

ACI 318-19		ACI 318-14		AASHTO	
ψ_e	1	ψ_e	1	λ_{er}	1
ψ_p	1	-	-	λ	1
ψ_o	1	-	-	λ_{rl}	1
ψ_c	see Note 1	-	-	λ_{cf}	1
-	-	-	-	λ_{rc}	0.3

Note 1: $\psi_c = f_c'/15{,}000 + 0.6 \le 1.0$.
Note 2: For the AASHTO formula, the 0.8 reduction factor is applied for meeting the parallel tie requirement.

Figure 2.11 shows the development lengths normalized by the respective bar diameters calculated with the different formulas for No. 8, 11, 14 and 18 bars. It can be seen that the normalized development length calculated with the ACI 318-19 formula increases with the bar size, while that with the other two formulas remain constant. This is because the other two formulas have the development length proportional to the bar diameter, d_b, while ACI 318-19 has the development length proportional to $d_b^{1.5}$. For the head size of 4A_b, the development lengths required by AASHTO and ACI 318-14 are very close to each other. With 4,000 psi concrete, ACI 318-19 requires a

significantly shorter development length for No. 8 bars compared to the other two but a comparable development length for No. 18 bars. With 8,000 and 12,000 psi concrete, ACI 318-19 requires a significantly longer development length for No. 18 bars. According to the AASHTO formula, increasing the head size from $4A_b$ to $9A_b$ can result in a significant reduction of the development length, except for 12,000 psi concrete, with which the development length is governed by the lower limit of $8d_b$ for both cases. The AASHTO formula appears to be quite sensitive to the head size. For the head size of $9A_b$, it is also very sensitive to the concrete strength. This is reasonable if the anchorage capacity is governed by the pullout failure (due to the crushing of concrete at the bearing face of the head), but it is questionable if the anchorage capacity is governed by the concrete breakout failure. This also appears to be inconsistent with the experimental data discussed previously.

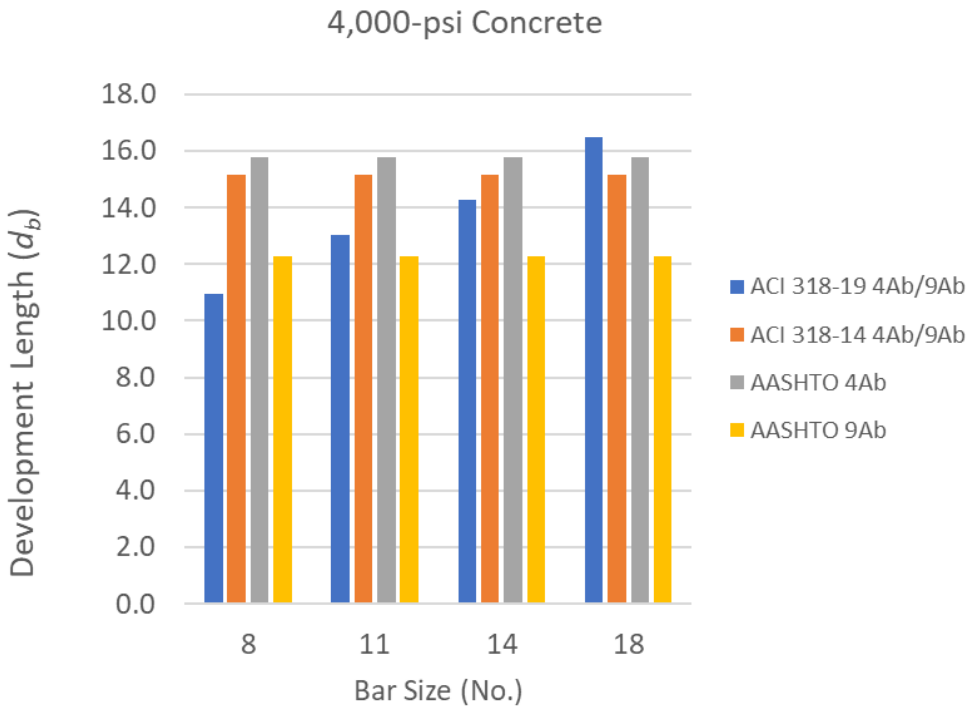

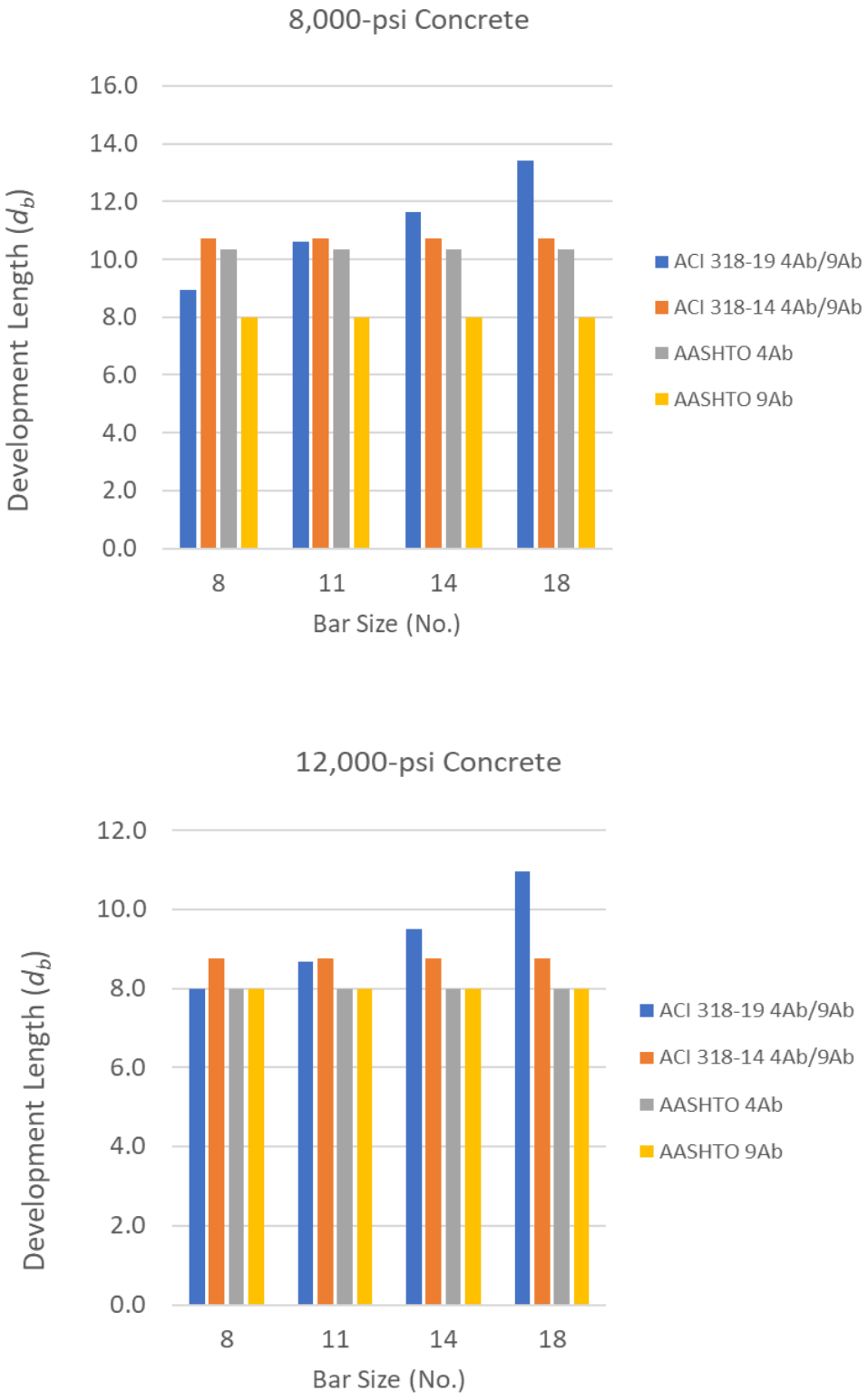

Figure 2.11: Comparison of development lengths calculated with different formulas

Chapter 3 Development Length Test Program

3.1 Specimen Configurations and Test Matrix

Thirteen specimens were tested to evaluate the anchorage capacity of headed bars embedded in reinforced concrete (RC) beams. As shown in Figure 3.1, each test specimen consisted of an RC beam that had either one headed bar or two side-by-side headed bars embedded perpendicular to the beam. With the two ends of the RC beam restrained, the bar(s) was subjected to a gradually increasing pull force up to a point at which anchorage failure or bar fracture occurred, or the bar was close to imminent fracture.

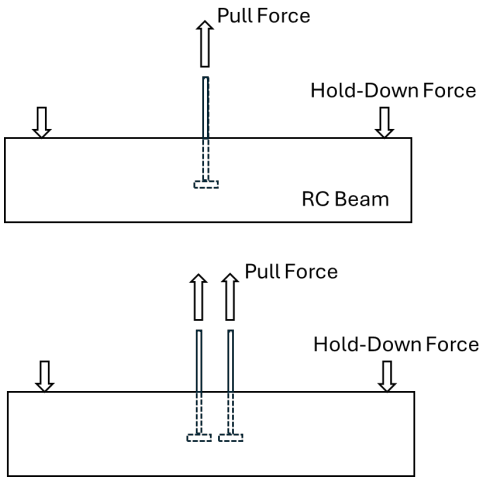

Figure 3.1: Specimen configurations

As will be discussed later, the pull tests were designed to mimic the anchorage condition of a longitudinal bar extending from a bridge column into a cap beam. However, compared to an actual beam-to-column joint, the design details of the specimens were simplified since the investigation would focus on the anchorage capacity of a single bar and a pair of bars rather than multiple anchored bars in a typical beam-to-column joint. This would allow a better understanding of the influence of different design parameters on the anchorage capacity of a headed bar and a

quantitative evaluation of the tension development length requirements in current codes. To be on the conservative side and also partly compensate for the aforementioned simplification, the headed bars in the specimens had a less favorable edge distance condition than those in an actual beam-to-column joint. In each specimen, the headed bar(s) had the edge distances on both sides close to the minimum found in a typical cap beam, while the bars in an actual cap beam will have the minimum edge distance on one side only and a much larger edge distance on the other side. Furthermore, the compressive stress induced by the bending of the column section in part of the joint region was not replicated in the loading condition for the tests. The compressive stress in an actual joint could enhance the concrete breakout resistance.

The sizes of the headed bars considered were No. 14 and No. 18. The bars were embedded in the beams with a length equal to either 100% or 70% of the minimum tension development length required in ACI 318-19. Two head sizes were considered. One had the net bearing area equal to $4A_b$ and the other had the bearing area equal to $9A_b$, where A_b is the nominal cross-sectional area of the bar. The target compressive strengths of the concrete were 4,000, 6,000, and 8,000 psi for the respective specimens.

As shown in Table 3.1, a total of 13 specimens were tested. As will be discussed later, the design details of the beams met the conditions in ACI 318-19 that would permit both the parallel tie reinforcement modification factor, ψ_p, and the location modification factor, ψ_o, in the development length formula be equal to 1. In Table 3.1, the bar embedment lengths are also compared to the minimum required by the AASHTO LRFD Bridge Design Specifications (AASHTO 2024). It should be mentioned that the development length formulas for headed bars in both the ACI and AASHTO specifications are limited to No. 11 or smaller headed bars. These formulas are considered in this study to check if one or both could be applied to No. 14 and 18 bars with different head sizes. The

formula in AASHTO is a unified formula for straight, hooked, and headed bars. For No. 11 or smaller bars, the development length can be reduced by a factor of 0.80 if the parallel tie reinforcement provided meets the requirement as that specified in ACI for ψ_p = 1, as stated in Section 5.10.8.2.7 of the AASHTO Specifications. For consistency in comparison with ACI, this reduction factor is retained for the No. 14 and 18 bars.

Table 3.1: Test matrix

Spec.	Bar Size	Head Size	No. of Bars	Stirrups	$\frac{\bar{A}_{tt}}{A_{hs}}$	Embedment Length			Breakout Cone Length[1] (in.)	$\tilde{A}_{tt}$ (in.^{2})	Specified Concrete Strength (ksi)
						% of ACI 318-19	% of AASHTO	in. (d_b)			
1	#14	$4A_b$	1	2#5@12"	0.55	70	63	16.75 (9.9)	50.3	2.48	4,000
2	#14	$4A_b$	1	2#5@12"	0.55	100	90	24 (14.2)	72.0	**3.72**	4,000
3	#14	$9A_b$	1	2#5@12"	0.55	70	81	16.75 (9.9)	50.3	2.48	4,000
4	#14	$4A_b$	1	2#5@12"	0.55	71	80	14 (8.3)	42.0	2.48	8,000
5	#14	$4A_b$	1	2#4@12"	0.36	71	80	14 (8.3)	42.0	1.60	8,000
6	#14	$4A_b$	1	2#5@12"	0.55	102	114	20 (11.8)	60.0	**3.72**	8,000
7	#14	$9A_b$	1	2#5@12"	0.55	71	104	14 (8.3)	42.0	2.48	8,000
8	#14	$4A_b$	2	4#5@12"	0.83	100	90	24 (14.2)	80.0	**8.68**	4,000
9	#14	$9A_b$	2	4#5@12"	0.83	100	115	24 (14.2)	80.0	**8.68**	4,000
10	#14	$4A_b$	1	2#5@12"	0.55	70	77	16 (9.5)	48.0	2.48	6,000
11	#14	$9A_b$	1	2#5@12"	0.55	70	108	16 (9.5)	48.0	2.48	6,000
12	#18	$4A_b$	1	2#6@12"	0.88	70	73	26 (11.5)	78.0	5.28	4,000
13	#18	$4A_b$	1	2#6@12"	0.88	99	104	37 (16.4)	111.0	**8.80**	4,000

Note: A_b is the cross-sectional area of one headed bar; $\bar{A}_{tt}$ is the total cross-sectional area of parallel tie reinforcement (stirrups) within $8d_b$ from headed bar(s), where d_b is the nominal diameter of a headed bar; $\tilde{A}_{tt}$ is the total cross-sectional area of parallel tie reinforcement in expected breakout crack region based on the assumed breakout cone length; A_{hs} is the total cross-sectional area of headed bar(s).

[1]Breakout cone length is assumed to be 3 times the embedment length of the headed bar.

[2]Total cross-sectional area of parallel tie reinforcement (stirrups) crossing breakout cracks.

3.2 Specimen Design

As will be discussed in Section 3.5, each test beam was held down to the strong floor in the laboratory with a steel beam and post-tensioning rods at each end. The headed bar(s) was centered between the two steel hold-down beams. The clear distance between the steel beams was selected to be long enough not to interfere with the potential concrete breakout area on the top face of the concrete beam. Similar to that observed for the breakout failure of anchor bolts, the breakout block was assumed to have the shape of an inverted pyramidal frustum, with the length of the top face measured from the center of the bar in each direction equal to 1.5 times the embedded length of the bar, as assumed in ACI 318-19 for the breakout failure of headed anchor bolts.

The width of each beam was selected to provide a side cover of about $7\,d_b$ on each side of the headed bar, measured from the center of the bar, where d_b is the nominal diameter of the headed bar. This was slightly greater than the minimum side cover of $6\,d_b$ specified in ACI 318-19 as the condition for the modification factor ψ_o in the development length formula to be equal to 1, and was representative of the edge distance of a bar closest to the edge of a beam-to-column joint in a typical bridge that has large cap beams.

The depths of the RC beams were selected to accommodate the embedment lengths of the headed bars and to provide the flexural strength required to resist the applied pull force. The beams were reinforced with top and bottom longitudinal bars and stirrups. The beam depth and the amount of the longitudinal reinforcement were to meet the design criteria that the flexural compressive stress in the concrete and the stress in the tension steel induced by the pull force applied to the headed bars would be within the elastic limits. This was based on the consideration that cap beams in a bridge structure are capacity protected. For the stress analysis, it was assumed that the RC beam

had the two ends fixed and the span length was equal to the clear distance between the hold-down beams. Beams with the same headed bar size had the same width, depth, and longitudinal reinforcement whether they had one or two headed bars. The design was governed by the most severe loading condition that two headed bars were pulled simultaneously, with the maximum compressive stress developed in the concrete limited to no more than 50% of the smallest target compressive strength of 4,000 psi and the tensile stress in the longitudinal bars to be no more than 50% of the nominal yield strength.

The RC beams had rectangular ties as stirrups. The spacing of the ties was 12 in. on center, which is representative of those in the beam-to-column joint region of a cap beam. The size of the ties was selected based on the following considerations. First, the cross-sectional area of the ties should be sufficient to meet the shear demand in the tests. Second, the tie area would satisfy the ACI requirement that the total cross-sectional area of the parallel tie reinforcement, $\overline{A}_{tt}$, within 8 d_b from the center line of the headed bars shall exceed 0.3 A_{hs}, where A_{hs} is the total cross-sectional area of the headed bars being developed, so that the development length modification factor ψ_p can be equal to 1. In this study, the ties on both sides of a headed bar were counted. In the AASHTO specifications, the required development length can be reduced by a factor of 0.8 if the above parallel tie condition is met. It should also be stated that the total area of vertical stirrups that serve as shear reinforcement in a beam-to-column joint of a bent cap has to be no less than 20% of the total area of column longitudinal reinforcement anchored in the joint, according to the Seismic Design Criteria of Caltrans (Caltrans 2019). Furthermore, as discussed in Chapter 2, the most common cause of anchorage failure of headed bars was concrete breakout. Once breakout cracks occur, the parallel ties crossing the inclined breakout cracks will contribute to the breakout resistance. Hence, the total cross-sectional area of parallel ties crossing the cracks is an important parameter. Therefore, the

third consideration is that the specimens that had an embedment length equal to 100% of the minimum required by ACI 318-19, would have the ratios of the total area of the cross ties in the breakout region to the total cross-sectional area of the headed bar(s) being developed close to each other as possible. For calculating the total tie area in the breakout region, the projected length of the breakout cone at the top face of the beam was assumed to be 3 times the embedment length of the bar as discussed in Chapter 2. The lengths of the breakout cones calculated for the different embedment lengths in the specimens are shown in Table 3.1. For specimens that had a reduced embedment length, the tie size remained the same as that for the corresponding specimen that had a fully developed bar so that only one parameter was varied at a time and the test results could be meaningfully compared.

Based on the above considerations, single No. 5 rectangular ties at 12-in. spacing were selected to serve as stirrups for the specimens that had one No. 14 headed bar. This results in $\overline{A}_{tt} / A_{hs}$ = 0.55 as shown in Table 3.1. For the specimens that had one No. 14 headed bar with 100% embedment, the selected stirrups had a total tie area of 3.72 in.^{2} within the breakout region as shown in Table 3.1, which corresponds to a tie-to-bar area ratio of 1.65. For the specimens with two No. 14 headed bars, double No. 5 rectangular ties at 12-in. spacing were selected. This corresponds to a total tie area of 8.68 in.^{2} within the breakout region, as shown in Table 3.1, and a tie-to-bar area ratio of 1.93. For the specimens with one No. 18 headed bar, single No. 6 rectangular ties at 12-in. spacing were selected. Hence, for the specimen with a fully developed No. 18 bar, the total tie area within the breakout region was 8.80 in.^{2} and the tie-to-bar area ratio was 2.20. It should be noted that the actual tie area within the breakout region varies with the embedment length of the headed bar as shown in Table 3.1.

The design calculations and strength check for the beams are shown in Appendix A. The reinforcing steel in the beams was Grade 60. The headed bars met ASTM A706 standard as well as the requirements for Class HA head dimensions in Annex 1 of ASTM A970. They were manufactured by HRC-USA, with the product numbers shown in Table 3.2 and pictures shown in Figure 3.2.

Table 3.2: Types of headed bars used in the tests

Bar Size	Head Size	Bar Type	Comments
#14	4 A_b	HRC 555	Caltrans Pre-approved
#14	9 A_b	HRC 220 (Type 150)	Caltrans Pre-approved
#18	4 A_b	HRC 551	Threaded Installation

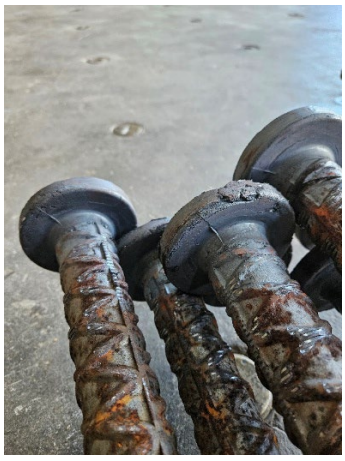

No. 14 Bar with $4A_b$ Head Size

No. 14 Bar with $9A_b$ Head Size

No. 18 Bar with $4A_b$ Head Size (Courtesy of HRC-USA)

Figure 3.2: Headed bars used in the study

The RC beams in Specimens 1 to 11, which had No. 14 headed bars, had the same dimensions. The length of the beams was 150 in., which provided a clear distance of 90 in. between

the two steel hold-down beams as will be shown in Section 3.5. This distance was deemed sufficient not to interfere with the potential concrete breakout region. The width of the beams was 26 in., which provided a side cover of $7.7d_b$, where d_b, is the diameter of the headed bar. The depth of the beams was 42 inches. Each beam had 4 No. 11 longitudinal reinforcing bars at the top and 4 No. 11 longitudinal bars at the bottom. In addition, there were 4 No. 8 longitudinal reinforcing bars added at intermediate levels to make the steel cage sturdier. The reinforcement details of Specimens 1 to 7, 10, and 11, which had one headed bar, are shown in Figure 3.3 through Figure 3.6. Except for Specimen 5, these specimens had No. 5 stirrups spaced at 12 in. on center along the entire length. For Specimen 5, the four set of stirrups closest to the headed bar were No. 4 in order to study the influence of the stirrup area on the concrete breakout strength. The reinforcement details of Specimens 8 and 9, which had two parallel headed bars, are shown in Figure 3.7 through Figure 3.10. These two specimens had two sets of No. 5 stirrups spaced at 12 in. on center to match the increased headed bar area.

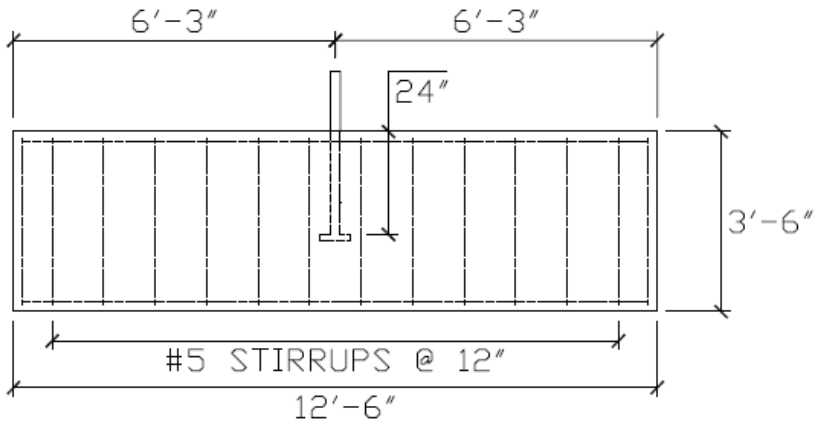

Figure 3.3: Elevation view of Specimen 2 (Specimens 1, 3 to 7, 10, and 11 had the same design except for the bar embedment length and that the four sets of stirrups closest to the headed bar in Specimen 5 were No. 4)

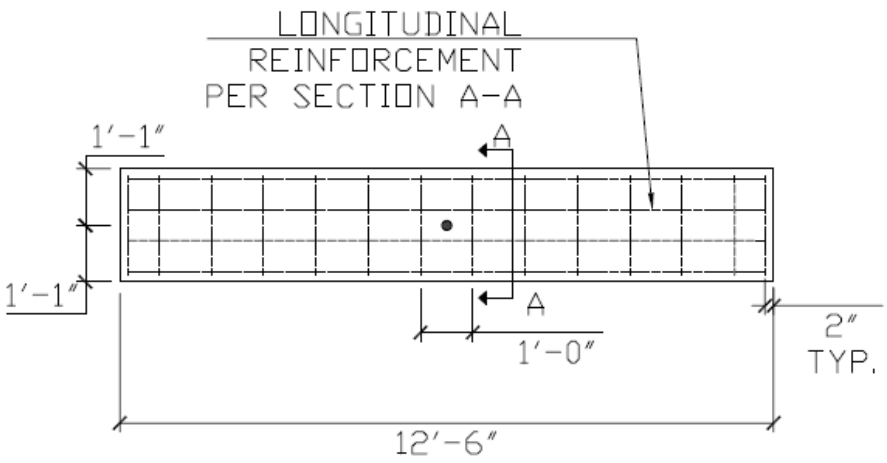

Figure 3.4: Plan view of Specimen 2 (Specimens 1, 3 to 7, 10, and 11 had the same design)

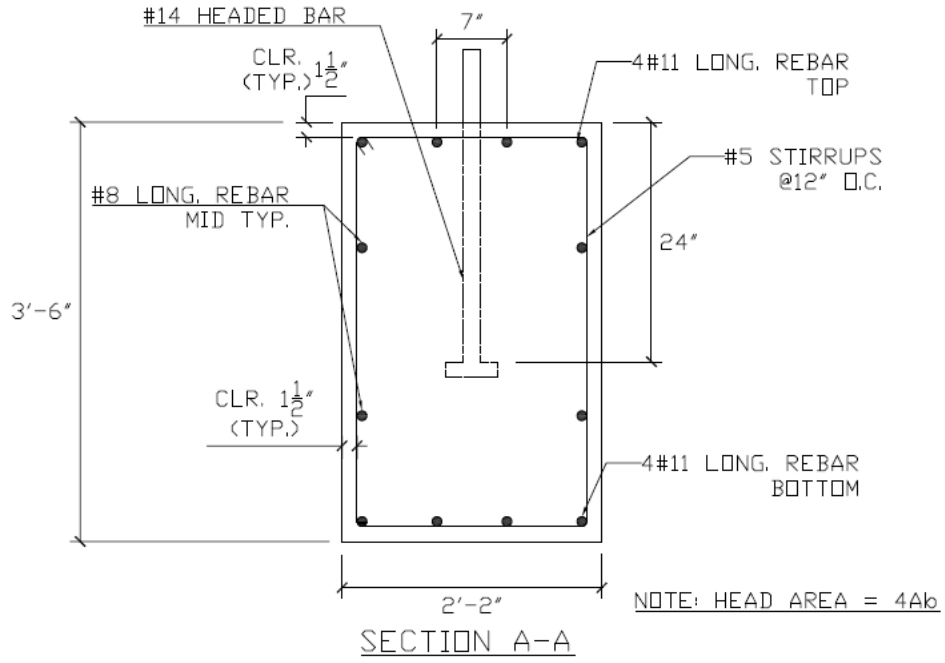

Figure 3.5: Cross-section view of Specimen 2 (Specimens 1, 3 to 7, 10, and 11 had the same design except for the bar embedment length, the head size, and that the four sets of stirrups closest to the headed bar in Specimen 5 were No. 4)

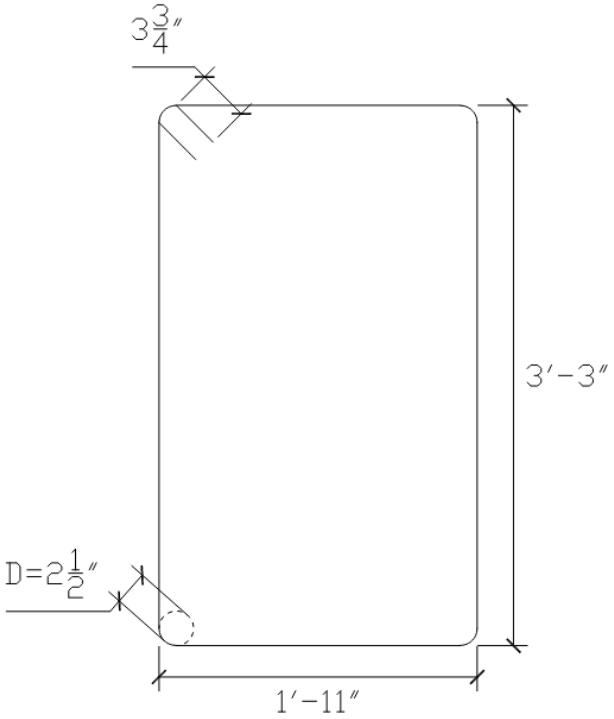

Figure 3.6: Dimensions of No. 5 stirrups for Specimens 1 to 7, 10, and 11

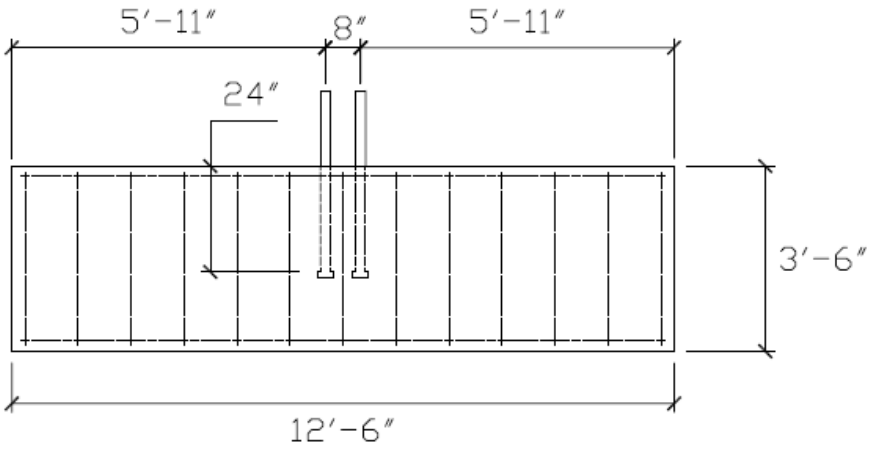

Figure 3.7: Elevation view of Specimens 8 and 9 (Specimen 8 had a smaller head than Specimen 9)

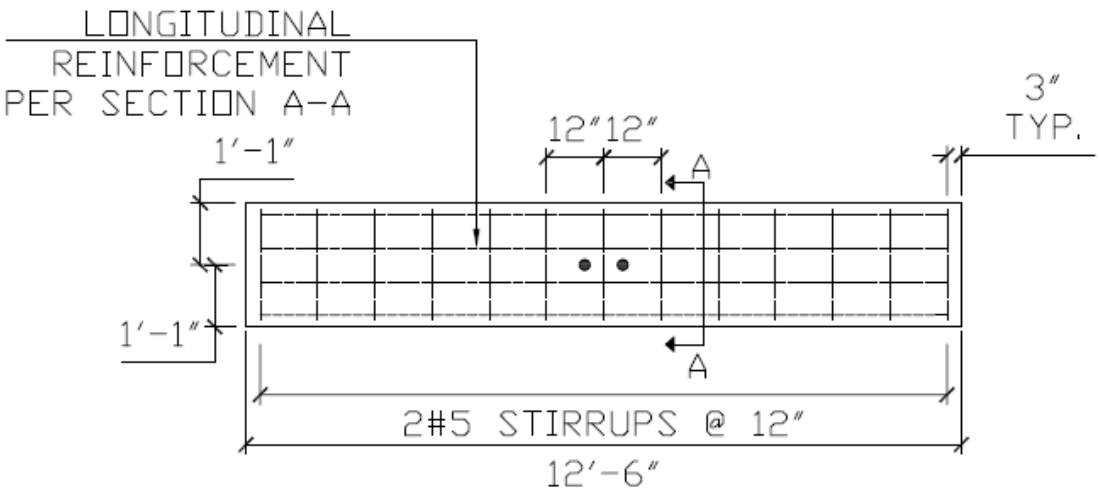

Figure 3.8: Plan view of Specimens 8 and 9

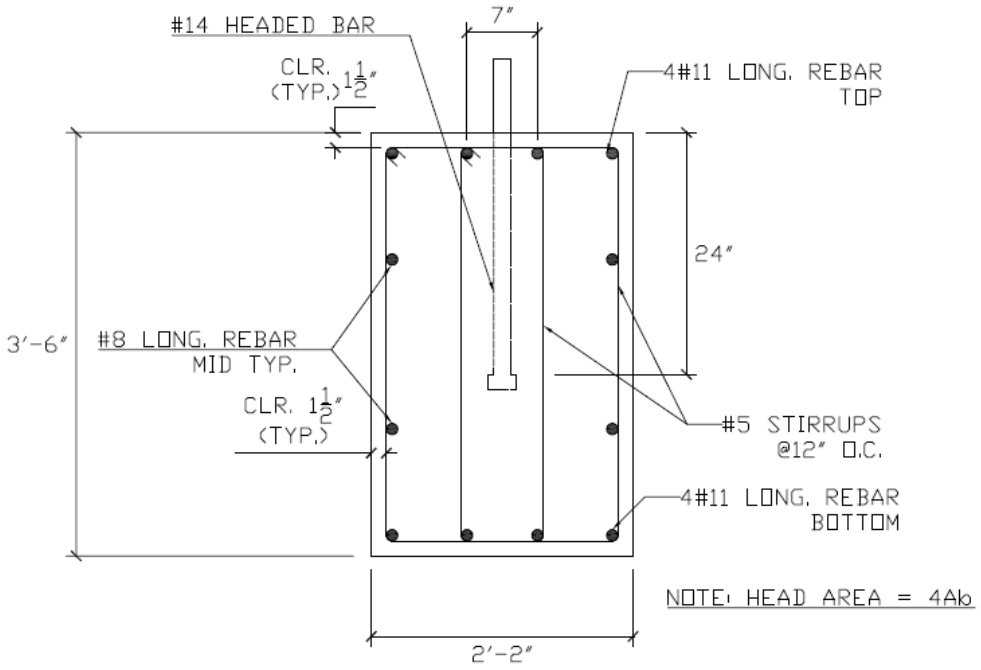

Figure 3.9: Cross-section view of Specimens 8 and 9 (Note: Specimen 9 had a head area of 9A_b)

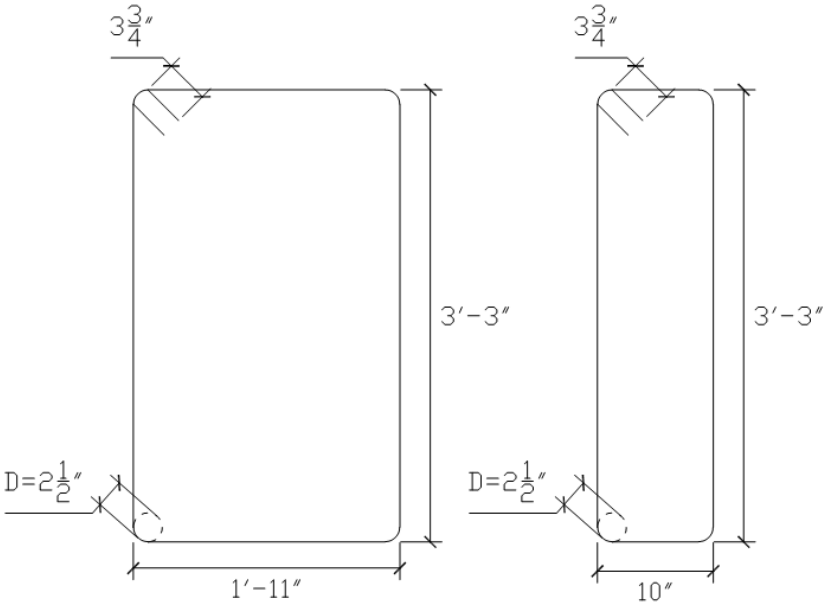

Figure 3.10: Dimensions of stirrups for Specimens 8 and 9

Specimens 12 and 13 had one No. 18 headed bar. The bearing area of the T head was $4A_b$. The dimensions and reinforcement details of the beams in these specimens are shown in Figure 3.11 through Figure 3.14. The length of the beams was 198 in., which provided a clear distance of 138 in. between the two steel hold-down beams to avoid interference with potential breakout cracks. The width of the beams was 35 in., which provides a side cover of $7.8d_b$. The depth of the beams was 48 inches. Each beam had 8 No. 11 longitudinal reinforcing bars at the top and 8 No. 11 longitudinal bars at the bottom, and No. 6 stirrups spaced at 12 in. on center. In addition, there were 6 No. 8 longitudinal reinforcing bars added at intermediate levels to make the steel cage sturdier.

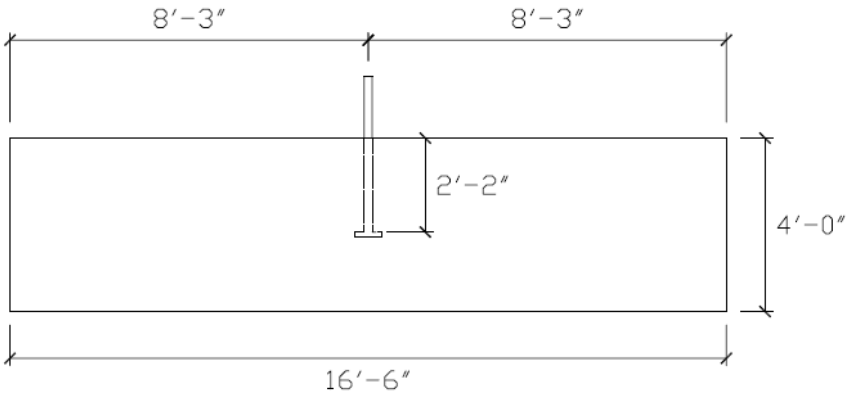

Figure 3.11: Elevation view of Specimen 12 (Specimen 13 had the same design but had a bar embedment length of 3’-1”)

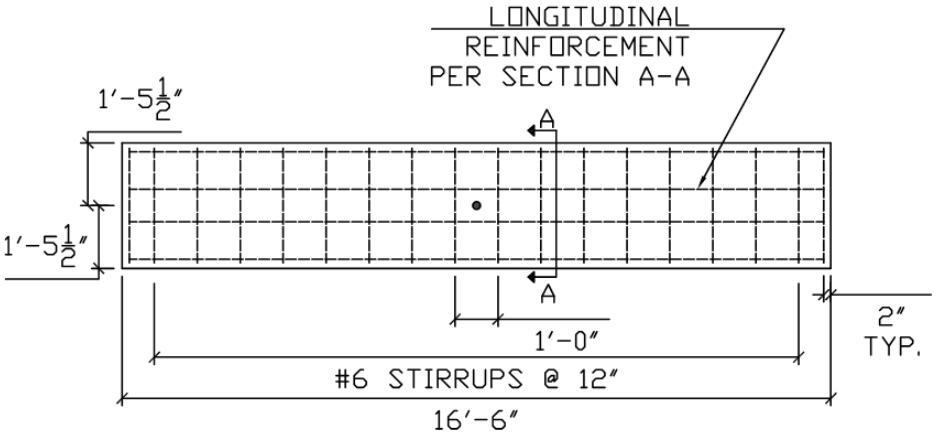

Figure 3.12: Plan view of Specimens 12 and 13

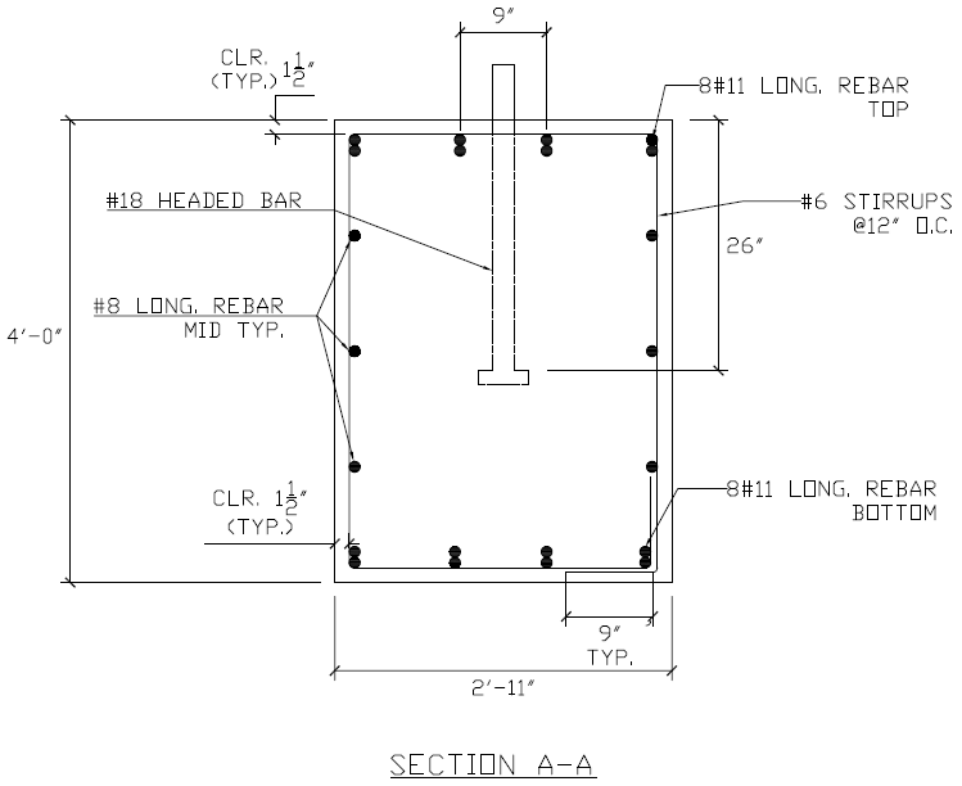

Figure 3.13: Cross-section view of Specimen 12 (Specimen 13 had the same design but had a bar embedment length of 3’-1”)

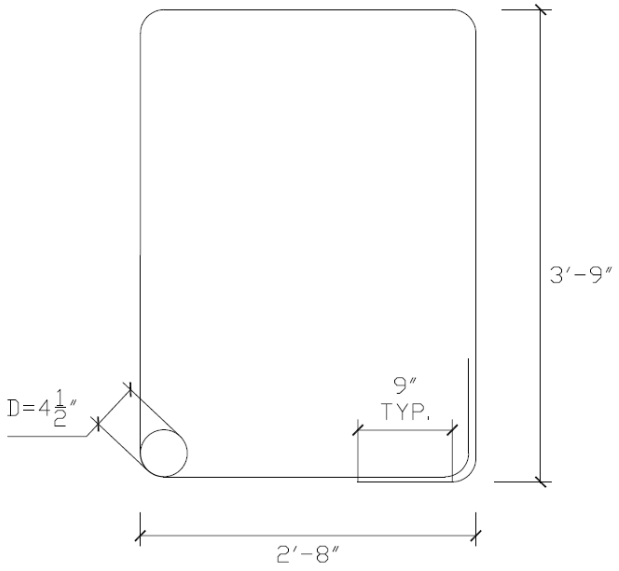

Figure 3.14: Dimensions of stirrups for Specimens 12 and 13

3.3 Specimen Construction

The specimens were constructed in the laboratory. Figure 3.15 shows the assembled steel cage for Specimen 1, and Figure 3.16 shows the steel cage inside the form and the assembly with the headed bar secured in place before concrete placement. Pull tests were conducted on the headed bars when the concrete reached their respective target compressive strengths. Six-in.-by-twelve-in. concrete cylinder samples were collected during the concrete pours, and they were tested on the 7th, 14th, 21st, and 28th days after casting, as well as on the day of the anchorage test.

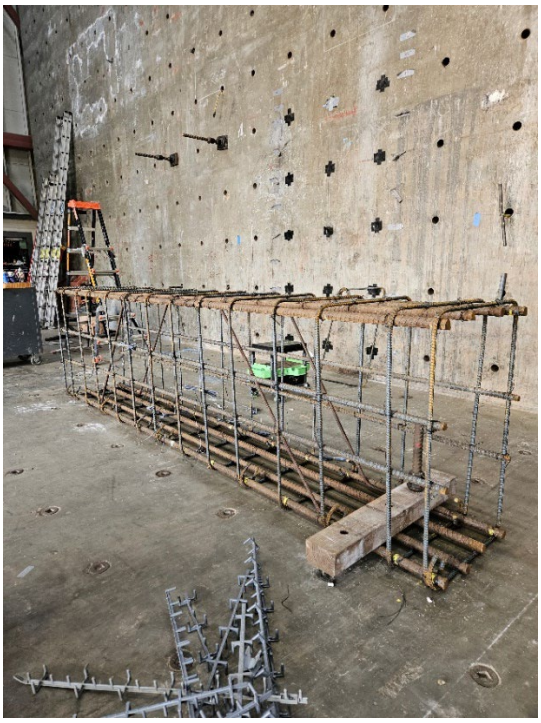

Figure 3.15: Steel cage for Specimen 1

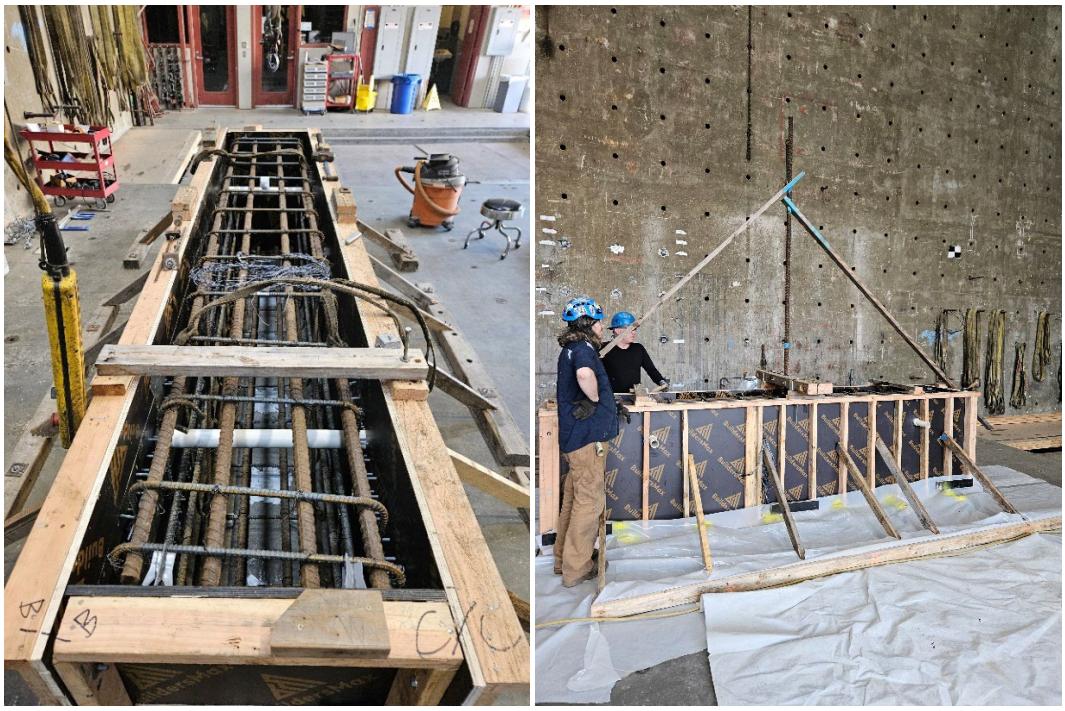

Figure 3.16: Steel cage inside the form; assembly ready for casting

3.4 Material Properties

The average compressive strengths of the concrete obtained from the cylinder samples on the 7th, 14th, 21st, and 28th days after casting, and on the day of the anchorage test, which might or might not occur on the 28th day, are shown in Table 3.3.

The average yield and tensile strengths obtained from rebar samples for the stirrups are shown in Table 3.4. The stress-strain curves for the steel are shown in Appendix B. The stress-strain relations for the headed bars were obtained in the anchorage tests based on the applied tensile force and the strain measured by the strain gage attached to the bar above the top surface of the beam.

Table 3.3: Compressive strengths of concrete for the specimens

Beam Specimen	Average Concrete Compressive Strength, f_c' (ksi)				
	7th Day	14th Day	21st Day	28th Day	Day of Anchorage Test
1	2.63	3.38	3.43	4.12	4.12 (28th Day)
2	2.49	3.33	3.63	3.89	3.89 (28th Day)
3	2.49	3.33	3.63	3.89	4.13 (43rd Day)
4	7.27	8.00	8.47	8.63	8.00 (14th day)
5	7.27	8.00	8.47	8.63	8.00 (14th day)
6	7.62	8.58 (13th)	No Data	No Data	8.58 (13th day)
7	7.62	8.58 (13th)	No Data	No Data	8.58 (13th day)
8	2.76	4.07 (19th)	4.35	No Data	4.35 (20th Day)
9	2.76	4.07 (19th)	4.35	No Data	4.35 (21st Day)
10	3.37	4.39	4.96	No Data	5.43 (51st Day)
11	3.37	4.39	4.96	No Data	5.43 (51st Day)
12	No Data	3.69	3.94	No Data	3.94 (21st Day)
13	2.40 (6th)	3.31	3.84	4.21	4.21 (28th Day)

Table 3.4: Yield and tensile strengths of stirrups for the specimens

Specimen	Stirrups	Average Yield Strength (ksi)	Average Tensile Strength (ksi)
1	#5	65.4	106.6
2	#5	65.6	91.5
3	#5	65.6	91.5
4	#5	66.2	92.5
5	#5	66.2	92.5
	#4	66.5	94.9
6	#5	65.9	90.7
7	#5	65.9	90.7
8	#5	65.3	92.7
9	#5	65.3	92.7
10	#5	60.6	90.6
11	#5	60.6	90.6
12	#6	63.2	90.0
13	#6	63.2	90.0

3.5 Test Setup

Schematics of the test setup for the specimens that had one No. 14 headed bar are shown in Figure 3.17 through Figure 3.19. Pictures of test setups are shown in Figure 3.20. The concrete beam specimen sat on the strong floor in the laboratory and was held down by a steel beam at each end, which was restrained by 4 post-tensioning rods. The headed bar passed through a steel load beam and a 300-kip center-hole hydraulic jack. The steel load beam spanned across the beam specimen and was simply supported by two concrete blocks. It served as a reaction beam for the center-hole jack. Above the center-hole jack, the headed bar was secured by a set of grips or a rebar coupler. During a test, the center-hole jack exerted a tension force on the headed bar by pushing against the grips (or coupler) while reacting against the steel load beam. The design of the steel load beam for the tests is discussed in Appendix C. As shown in Figure 3.19, the clear distance between the hold-down beams was 90 inches. In most of the tests, a steel restraining system consisting of an HSS beam and a set of high-strength rods was used to keep the broken end of the headed bar in place should bar fracture occurred. The restraining system is not shown in the schematics but shown in the picture in Figure 3.20(b).

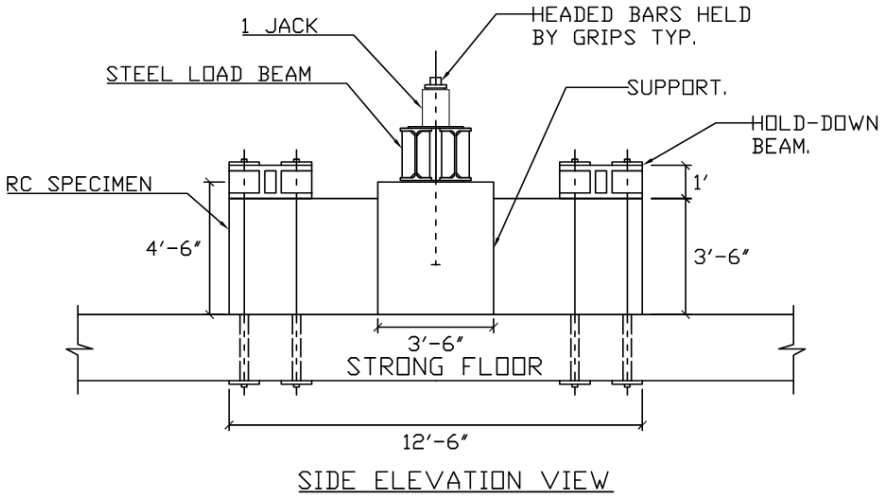

Figure 3.17: Side elevation view of test setup for specimens with one No. 14 headed bar

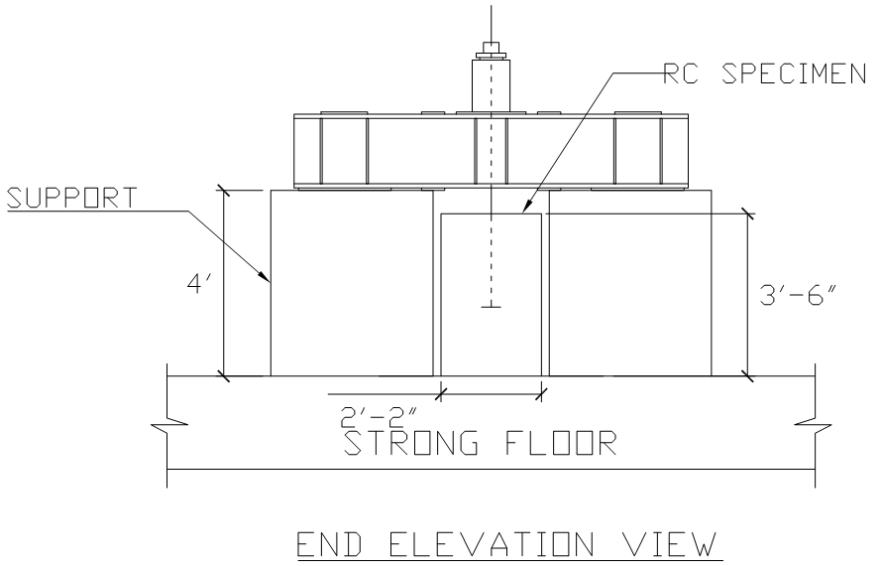

Figure 3.18: End elevation view of test setup for specimens with one No. 14 headed bar

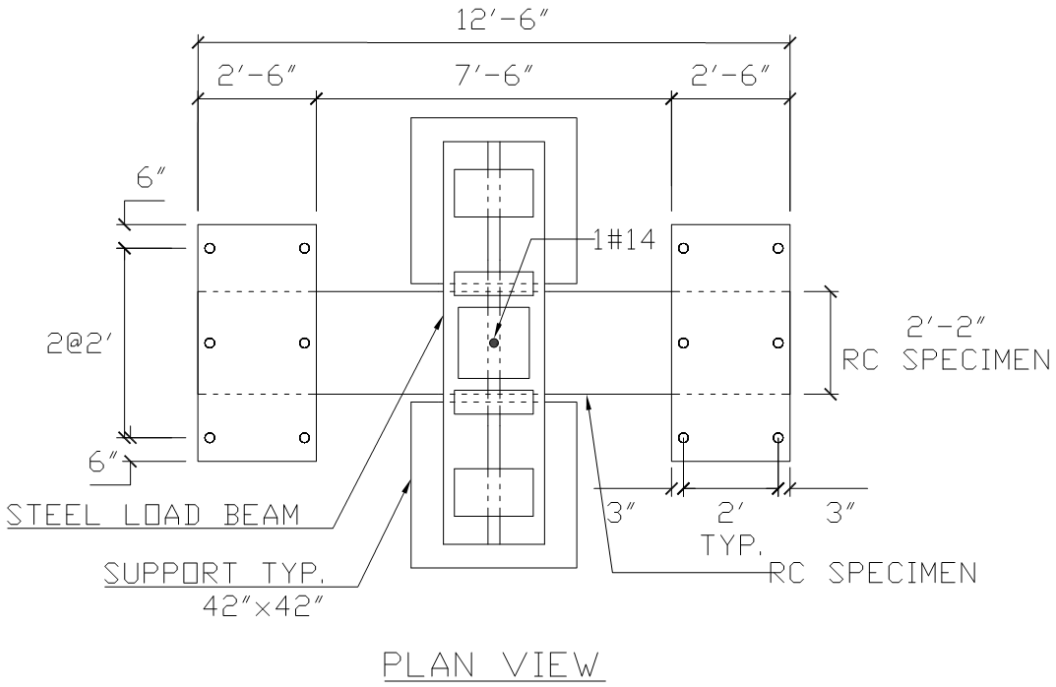

Figure 3.19: Plan view of test setup for specimens with one No. 14 headed bar

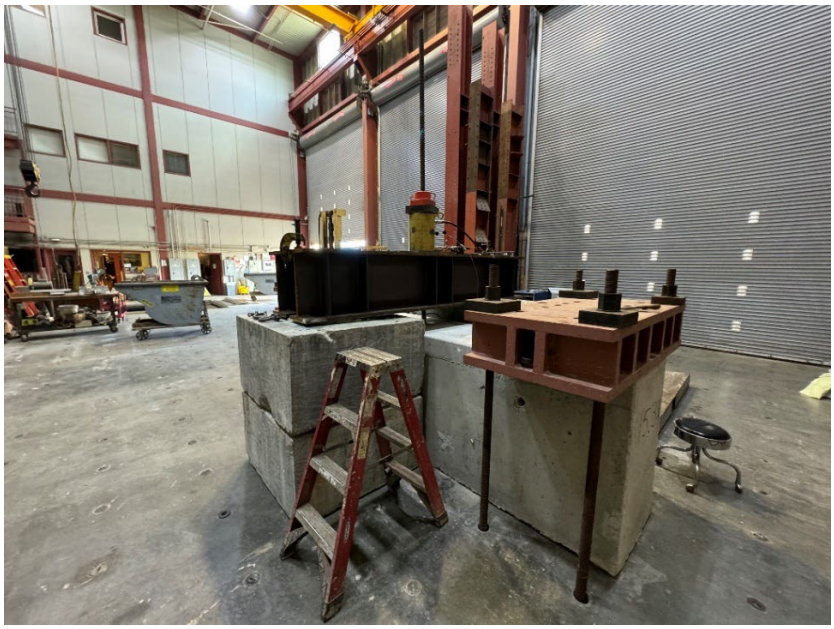

(a) Specimen 1

(b) Specimen 3

Figure 3.20: Test setup for specimens with one No. 14 headed bar

For testing specimens with one No. 18 headed bar, two 300-kip center-hole jacks were used to provide the required load capacity. Hence, instead of having the steel load beam directly resting on two concrete blocks and the bar threaded through the loading jack, a center-hole jack was placed between each end of the steel load beam and the supporting concrete block to exert a pull force on the bar by pushing against the load beam. For testing the anchorage capacity of two side-by-side No. 14 headed bars, the test setup was modified to allow two headed bars to be pulled at the same time. To this end, the steel load beam was placed parallel to the concrete beam specimen and was simply supported by two steel beams that were pushed by four 300-kip center-hole jacks, as shown in Figure 3.21.

Figure 3.21: Test setup for specimens with two No. 14 headed bars

3.6 Instrumentation

The specimens had strain gauges installed on the headed bars and the stirrups that were within the expected concrete breakout region. The tensile strains measured along the embedment length of a headed bar were used to estimate the bond stress along the bar and the bearing stress developed at the bar head. Figure 3.22 through Figure 3.24 show the locations and nomenclature of the strain gauges in Specimen 1. The gauges on the stirrups were located close to potential crack planes that could develop during concrete breakout failure. The strain gauge plans for the other specimens are shown in Appendix D together with the strain data collected. The pressure in the hydraulic jack(s) was measured to calculate the load applied to the headed bar(s).

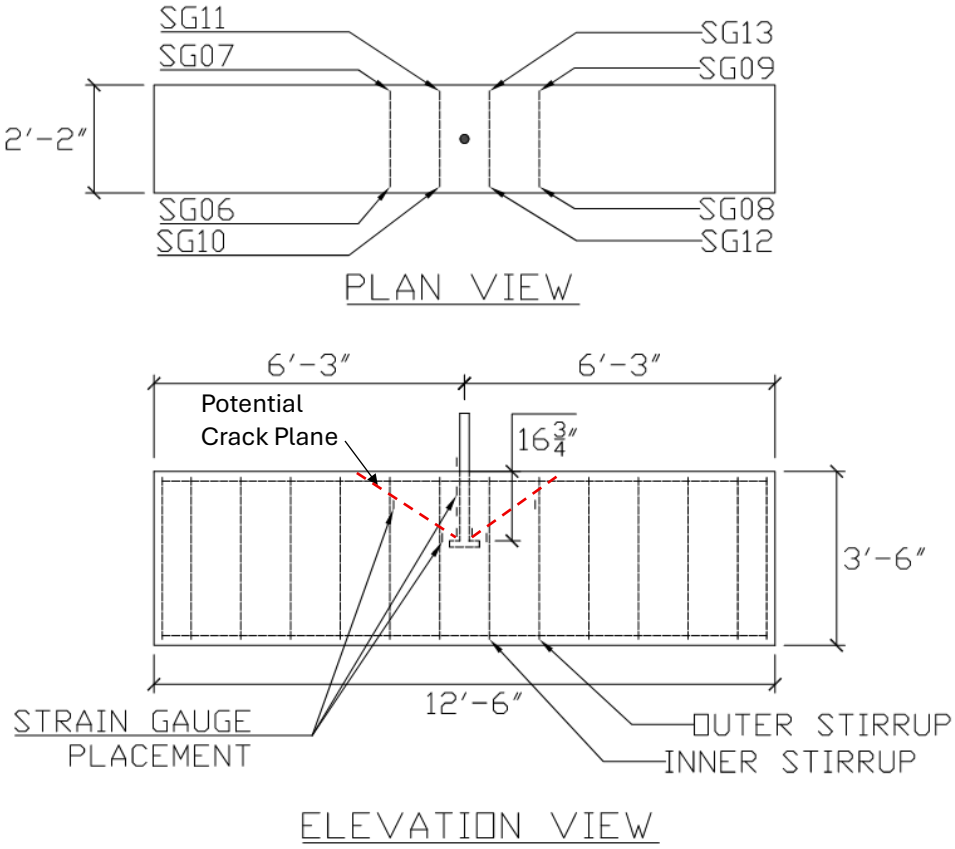

Figure 3.22: Locations of strain gauges in Specimen 1

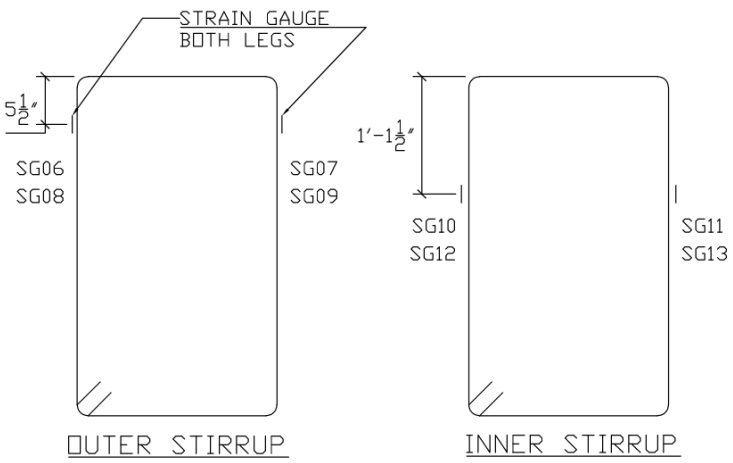

Figure 3.23: Locations of stirrup strain gauges and their nomenclature for Specimen 1

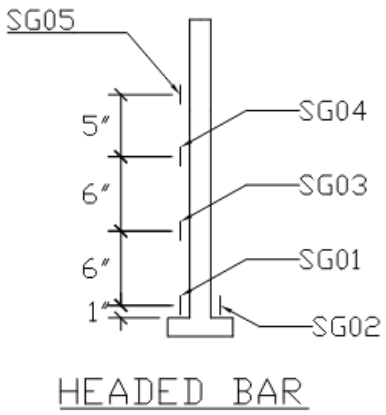

Figure 3.24: Locations of headed bar strain gauges and their nomenclature for Specimen 1

3.7 Test Procedure

During each anchorage test, the pressure in the hydraulic jack(s) was increased slowly with a motorized pump, which was controlled manually, until either the headed bar reached its tensile strength or fractured, or the bar anchorage failed. The strain data and the pressure in the hydraulic jack(s) were recorded with a data-acquisition system.

Chapter 4 Experimental Observations and Results

4.1 Summary of Test Results

A total of thirteen specimens were tested. The specimen characteristics and test results are summarized in Table 4.1. Eight of the specimens had embedment lengths equal to 70% of the minimum required by ACI 318-19 (ACI 2019) based on the target compressive strength of the concrete, while the actual length ratios based on the concrete cylinder strength obtained on the day of the anchorage test vary from 70 to 74%. Of these eight specimens, six had anchorage failures and two did not. The remaining five specimens had embedment lengths equal to 100% of the minimum required by ACI 31-19 based on the target compressive strength of the concrete, while the actual ratios vary from 99 to 105% based on the measured concrete strength. None of these specimens had anchorage failure. Nine specimens had a head size of $4A_b$ and four had a head size of $9A_b$. The benefits of a larger head are not consistent as shown in the test results. The comparison of Specimens 1 and 3 as well as Specimens 4 and 7 shows that a larger head resulted in higher anchorage resistance even though Specimen 7 still had an anchorage failure. Nevertheless, Specimens 10 and 11 did not show the benefits of a larger head. It is understandable that the size of the head had little influence if anchorage failure is dominated by concrete breakout. Most importantly, the test results that the AASHTO specification (AASHTO 2024) tends to overestimate the anchorage strength provided by a larger head. Specimens 7 and 11, which had a head size of $9A_b$, had embedment lengths equal to 74 and 70% of that required by ACI, which does not consider the head size. Nevertheless, they met the AASHTO development length requirement, which accounts for the larger head size of $9A_b$. Both specimens had anchorage failures. Furthermore, it should be noted that these two specimens had concrete strengths significantly above 4,000 psi, which also contributed to the overestimation of the bearing resistance of the head in the AASHTO formula.

All the specimens, except for Specimen 13, had concrete breakout cracks. In general, specimens that had a higher quantity of stirrups (tie reinforcement parallel to the anchored bars) performed better in terms of the anchorage capacity and the severity of the breakout cracks. As will be shown later, Specimen 13, which had $\overline{A}_{tt} / A_{hs}$ = 0.88 and $\tilde{A}_{tt} / A_{hs}$ = 2.2, performed the best in that it did not exhibit any concrete breakout cracks, while Specimen 5, which had $\overline{A}_{tt} / A_{hs}$ = 0.36 and $\tilde{A}_{tt} / A_{hs}$ = 0.71, had the most severe breakout cracks. However, as will be discussed in Chapter 6, the good performance of Specimen 13 can be largely attributed to its long embedment length rather than the tie reinforcement, which was hardly engaged in the test. Furthermore, all the specimens, except Specimen 3, that had $\tilde{A}_{tt} / A_{hs}$ = 1.10 or less had anchorage failures, while those that had $\tilde{A}_{tt} / A_{hs}$ = 1.32 or greater did not. It should be noted that that the value of $\tilde{A}_{tt} / A_{hs}$ is approximately proportional to the size of the breakout cone and thereby the embedment length of the headed bar(s). Hence, it plays an instrumental role in prohibiting the opening of concrete breakout cracks and subsequent anchorage failure. Specimens with two side-by-side headed bars performed as satisfactory as those with a single bar.

Based on the test results, the development length requirement in ACI 318-19 appears to be adequate for No. 14 and 18 headed bars that have a head size of at least $4A_b$, while the AASHTO requirement does not appear to be adequate for bars that have a head size of $9A_b$ because it tends to overestimate the resistance provided by the head, especially when the concrete strength is relatively high. Furthermore, the quantity of parallel ties within the potential concrete breakout region has a significant influence on the anchorage capacity and the severity of concrete cracking. The test results and failure modes for the specimens are discussed in detail in the following sections.

Table 4.1: Specimen characteristics and summary of test results

Spec.	Bar Size	Head Size	No. of Bars	Stirrups	$\frac{\bar{A}_{tt}}{A_{hs}}$	Embedment Length			Breakout Cone Length[3] (in.)	$\frac{\tilde{A}_{tt}}{A_{hs}}$	Concrete Cylinder Strength[4] (ksi)	Anchorage Failure (Y or N)
						% of ACI 318-19[2]	% of AASHTO[2]	in. (d_b)				
1	#14	$4A_b$	1	2#5@12"	0.55	70	64	16.75 (9.9)	50.3	1.10	4,120	Y
2	#14	$4A_b$	1	2#5@12"	0.55	99	88	24 (14.2)	72.0	1.65	3,890	N
3	#14	$9A_b$	1	2#5@12"	0.55	70	83	16.75 (9.9)	50.3	1.10	4,130	N
4	#14	$4A_b$	1	2#5@12"	0.55	71	80	14 (8.3)	42.0	1.10	8,000	Y
5	#14	$4A_b$	1	2#4@12"	0.36	71	80	14 (8.3)	42.0	0.71	8,000	Y
6	#14	$4A_b$	1	2#5@12"	0.55	105	120	20 (11.8)	60.0	1.65	8,580	N
7[1]	#14	9Ab	1	2#5@12"	0.55	74	104	14 (8.3)	42.0	1.10	8,580	Y
8	#14	$4A_b$	2	4#5@12"	0.83	101	95	24 (14.2)	80.0	1.93	4,350	N
9	#14	$9A_b$	2	4#5@12"	0.83	101	124	24 (14.2)	80.0	1.93	4,350	N
10	#14	$4A_b$	1	2#5@12"	0.55	70	73	16 (9.5)	48.0	1.10	5,430	Y
11[1]	#14	$9A_b$	1	2#5@12"	0.55	70	99	16 (9.5)	48.0	1.10	5,430	Y
12	#18	$4A_b$	1	2#6@12"	0.88	70	72	26 (11.5)	78.0	1.32	3,940	N
13	#18	$4A_b$	1	2#6@12"	0.88	101	107	37 (16.4)	111.0	2.20	4,210	N

[1]Anchorage failure in spite of meeting the AASHTO requirement.
[2]Based on actual concrete cylinder strength obtained on the day of the anchorage test.
[3]Breakout cone length is assumed to be 3 times the embedment length of the headed bar.
[4]Obtained on the day of the anchorage test.
Note: A_b is the cross-sectional area of one headed bar; $\bar{A}_{tt}$ is the total cross-sectional area of parallel tie reinforcement within $8d_b$ from headed bar(s), where d_b is the nominal diameter of a headed bar; $\tilde{A}_{tt}$ is the total cross-sectional area of parallel tie reinforcement in expected breakout crack region based on the assumed breakout cone length; A_{hs} is the total cross-sectional area of headed bar(s).

4.2 Specimen 1

4.2.1 General Observations

Specimen 1 had the target concrete strength of 4,000 psi. The headed bar in the specimen had an embedment length of 16.75 in., which was equal to 70% of the minimum development length required by ACI 318-19. As the pull force applied to the bar reached 179 kips, the bar had anchorage failure. The strain gauge data, which will be presented later, show that even though bar fracture did not occur, the tensile force developed in the headed bar exceeded the yield strength and the bar experienced significant inelastic deformation.

The damage in the concrete beam is shown in Figure 4.1. The first cracks observed in the test had the shape of a breakout cone. As the headed bar was pulled further, cracks developed at the top of the beam and the cracked concrete pieces were lifted as the bar was being pulled out, as shown in the pictures in Figure 4.1(a) and (b). As shown in Figure 4.1(c), there was severe concrete crushing in the vicinity of the headed bar. The cone-shaped cracks did not open much in comparison to the cracks near the top. As shown in Figure 4.2, the depth of the cone-shaped crack was measured to be about 14 in. on one face and 13 in. on the other face of the beam. The average depth of the cone was 13.5 in., as shown in the schematic diagram in Figure 4.2(c). It was less than the bar embedment length of 16.75 in. measured from the top face of the head. The average angle of the inclined breakout cracks was about 33 degrees, which was close to that observed in the breakout failure of headed anchor bolts, which is discussed in ACI 318-19. However, since the inclined breakout cracks developed in the beam did not open widely as the bar continued to move up under the applied force, the final failure mechanism of the bar anchorage seems to be caused by bar slip and the crushing of the concrete above the bearing face of the T head. It was possible that the occurrence of the breakout cracks weakened the bearing resistance of the concrete above the T head.

(a) Cracking at the top of the beam

(b) After the test

(c) After removing cracked concrete pieces at the top

Figure 4.1: Damage in the concrete beam of Specimen 1

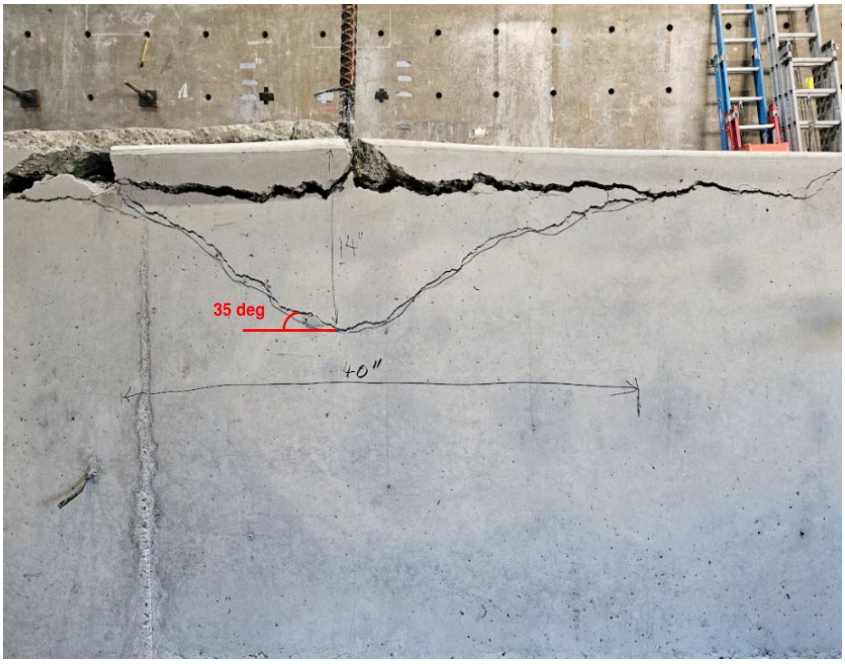

(a) Side Face 1

(b) Side Face 2

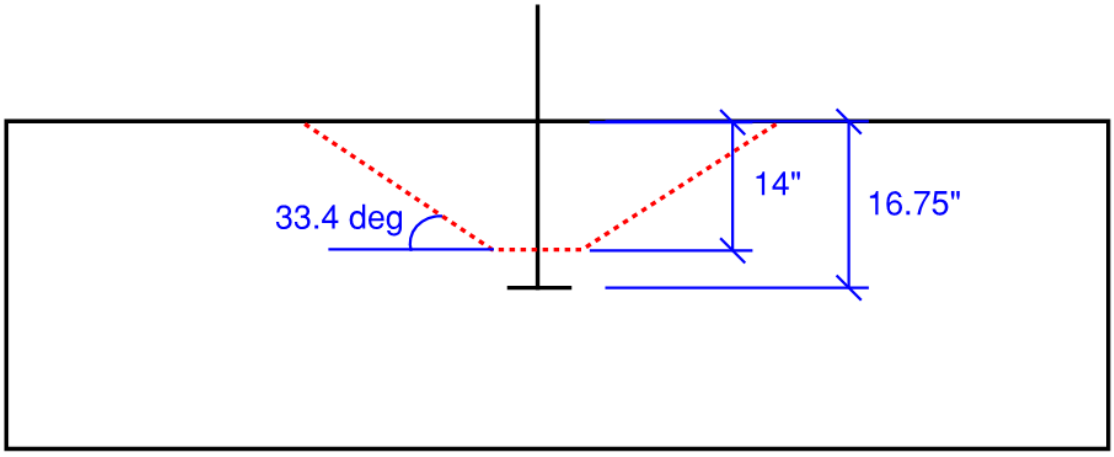

(c) Schematic of breakout cracks (average of both faces)

Figure 4.2: Breakout cracks in Specimen 1

4.2.2 Test Results

Figure 4.3 shows the pull force applied to the headed bar plotted against time. The ultimate load reached was 179 kips. This was less than the expected ultimate strength but greater than the

yield strength of the No. 14 headed bar. The yield strength of the bar was around 160 kips, as can be identified from the load-vs.-strain data for the bar presented in Figures D.6 and D.7 in Appendix D.

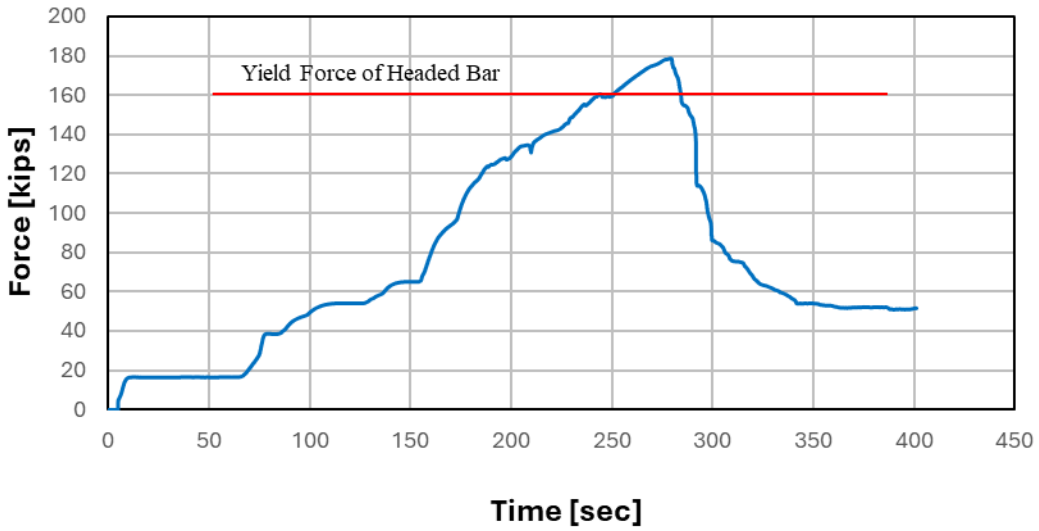

Figure 4.3: Pull force applied to the headed bar versus time for Specimen 1

Figure 4.4 shows the tensile strains developed at different locations along the headed bar over time, while Figure 4.5 shows the tensile strains in the stirrups. They were measured by strain gauges, whose locations are shown in Figures D.1 and D.2 in Appendix D.

It can be observed from Figure 4.4 that the tensile strains in the headed bar increased gradually as the pull force applied to the bar (shown in Figure 4.3) increased. Gauges SG04 and SG05, which were close to the top face of the beam, registered much higher strains than the other gauges. Gauge SG04 was located 3.75 in. below the top face of the beam, while SG05 was 1.25 in. above the top face. The strains registered by these two gauges jumped suddenly when the applied pull force reached 160 kips, indicating the yielding of the bar. The No. 14 headed bar had a nominal cross-sectional area of 2.25 square inches. Hence, the yield stress of the bar is estimated to be 71.1 ksi, with the yield strain equal to 0.00245. The fact that SG05 registered a much lower peak strain than SG04 could be attributed to the bending of the bar.

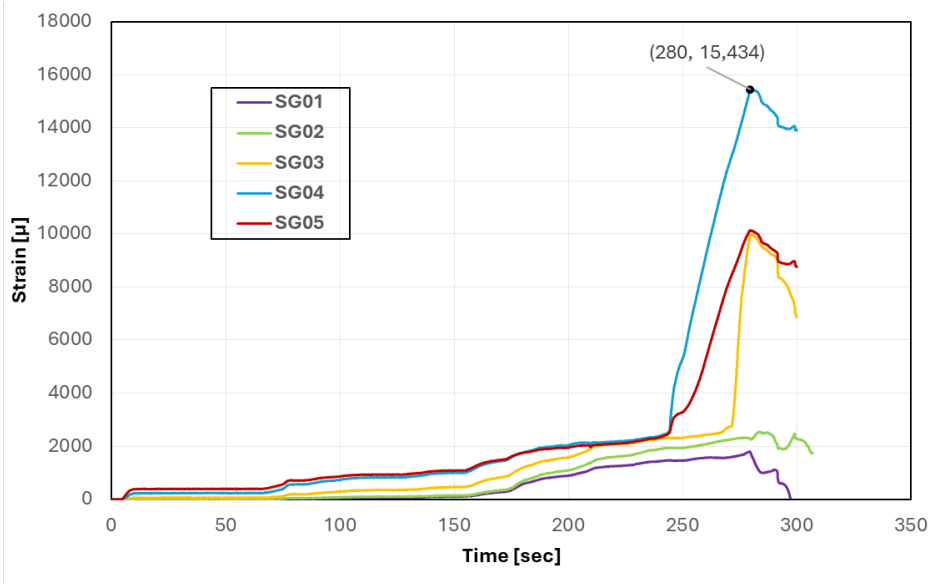

Figure 4.4: Strains along headed bar versus time for Specimen 1

Yielding of the headed bar at the location of SG03 occurred a little later than that shown by the gauges (SG04 and SG05) above. Gauges SG01 and SG02 were located 1 in. above the bearing surface of the T head. They registered the lowest strains. When the pull force reached the maximum value, the strain registered by SG02 was 0.0023, which was slightly below the yield strain of 0.0025, while the average strain from the two gauges was 0.0021. This indicates that the bond between the bar and the concrete contributed to the pullout resistance.

Each of the four sets of stirrups adjacent to the headed bar had 2 strain gauges (with one on each leg) as shown in Figure D.2 in Appendix D. However, 3 of the gauges on the stirrups did not function during the test. The strains registered by the functioning gauges are plotted in Figure 4.5. Gauges SG06, SG07, and SG08 were on the outer stirrups, while SG10 and SG12 were on the inner stirrups (closest to the headed bar). As shown in Table 3.4, The yield strength of the stirrups was 65.4 ksi, which corresponded to a yield strain of 0.0023. As shown in the figure, when the applied force reached the maximum value, the inner stirrups developed very high tensile strains, which far exceeded the yield strain, while the maximum strain in the outer stirrups barely reached the yield

value. The strains in the inner stirrups started to increase rapidly after 200 sec., at which the pull force applied was 129 kips (see Figure 4.3). This was due to the initiation of concrete breakout cracks.

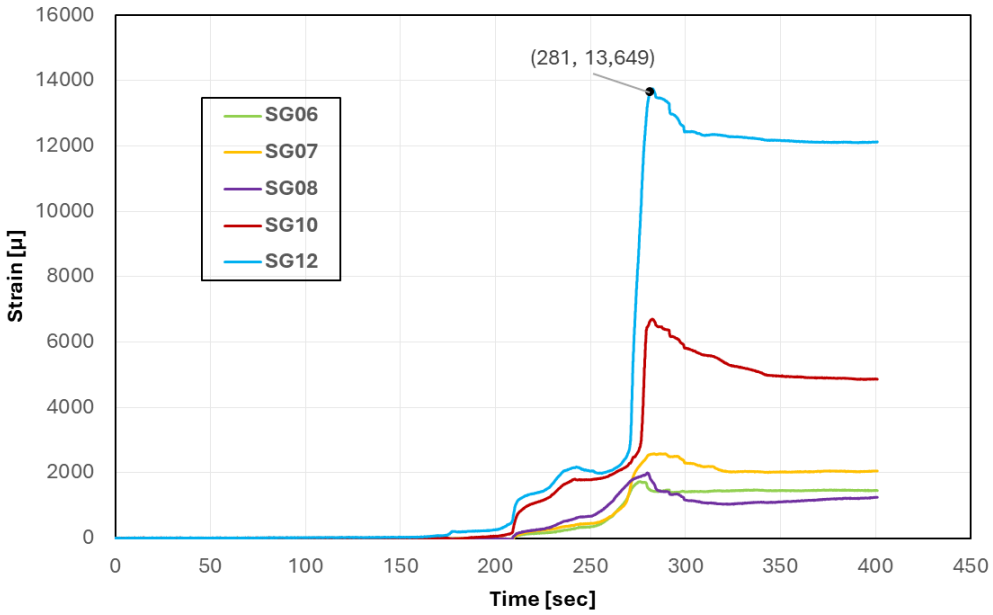

Figure 4.5: Strains in stirrups versus time for Specimen 1

Strains developed in the headed bar and stirrups at time instants of interest (i.e., when major strain increments occurred) are shown in Table 4.2. The table shows that the strains developed in the stirrups were negligible when the applied force was at 65 kips (which was 41% of the yield force of the headed bar). At this force level, there was practically no cracking in the concrete beam and the tensile strain developed in the headed bar near the T head was only 1/10 of that developed near the top face of the beam, indicating that the bearing force against the T head was very small and most of the applied force was carried by the bond along the bar.

When the applied force was increased to 129 kips, the tensile strain developed near the T head was a little less than 50% of the bar strain near the top face of the beam. At this point, the tensile strains in the stirrups were still very small. When the applied force increased to 133 kips, the tensile strains in the inner stirrup started to increase rapidly, and at 158 kips, the strain in an inner stirrup

almost reached the yield strain. When the applied load reached the maximum resistance of 179 kips, the tensile strains in the inner stirrups way exceeded the yield value and the strain in one outer stirrup barely reached the yield value. At that stage, the average tensile strain in the bar near the T head was 0.00205, which was slightly below the yield value. Based on that strain value, the anchorage resistance provided by the bar head was 134 kips. The remaining 45 kips of the applied force had to be provided by the bond stress along the bar.

Table 4.2: Strains in headed bar and stirrups at different load levels for Specimen 1

Time (sec)	Force Applied (kips)	SG01 (μstr)	SG02 (μstr)	SG03 (μstr)	SG04 (μstr)	SG05 (μstr)	SG06 (μstr)	SG07 (μstr)	SG08 (μstr)	SG10 (μstr)	SG12 (μstr)
150	65	106	152	473	1003	1085	0	0	0	6	35
175	104	352	419	954	1588	1620	0	0	0	0	104
200	129	898	1098	1571	2039	1942	0	0	0	64	267
210	133	1132	1396	1925	2107	2000	35	63	76	468	887
243	160	1467	1931	2324	2467	2432	314	421	628	1780	2172
275	177	1656	2306	6846	13993	9256	1712	2162	1858	2643	8419
279	179	1791	2313	9746	15280	10098	1706	2434	1945	5992	12620

4.3 Specimen 2

4.3.1 General Observations

For Specimen 2, the target concrete strength was 4,000 psi and the headed bar had an embedment length of 24 in., which was equal to the minimum development length required by ACI 318-19. The specimen was tested three times, with the headed bar loaded, unloaded, and reloaded, due to the slip of the bar in the rebar grips. The maximum load reached in the first two tests was 225 kips, which corresponds to a tensile stress of 100 ksi. This force was close to the ultimate strength of the bar as indicated by the force-vs.-strain curves presented in Figure D.20 in Appendix D. In the third test, the rebar grips were replaced by a rebar coupler, and the headed bar fractured at a load that was slightly less than 210 kips. Breakout cracks developed during the first test. Figure 4.6 shows the

breakout crack pattern developed in the specimen at the end of the tests. The maximum depth of the cone-shaped breakout crack was measured to be 24 in. on one face of the beam and 24.5 in. on the other face. On each face, an additional horizontal crack formed at 7 in. above the lowermost point of the cone-shaped breakout crack. The average angle of the inclined cracks was around 38 degrees. The cracks on the side faces did not open much during the test. However, extensive cracks developed at the top face of the beam around the bar and the cracked concrete was lifted as the bar was pulled, as shown in Figure 4.7. This can be attributed to the plastic elongation and slip of the bar.

(a) Side Face 1

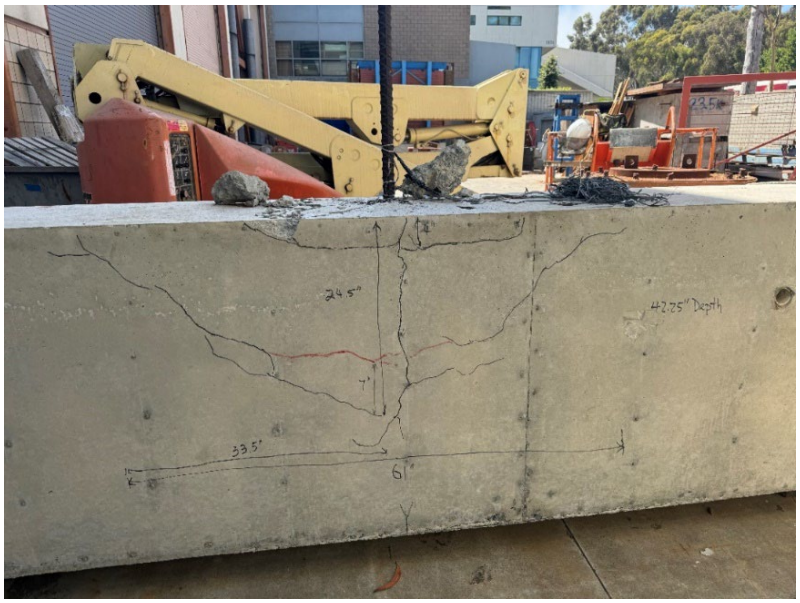

(b) Side Face 2

Figure 4.6: Breakout cracks in Specimen 2

Figure 4.7: Cracking at the top of the beam in Specimen 2

4.3.2 Test Results

Only the results from the first load test are presented here because the later tests did not yield additional information. Figure 4.8 shows the pull force applied to the headed bar plotted against

time. The bar yielded at 160 kips and the ultimate load reached was 225 kips. The ratio of the ultimate to the yield force was 1.41, which is close to the typical ratio of the tensile strength to the yield strength.

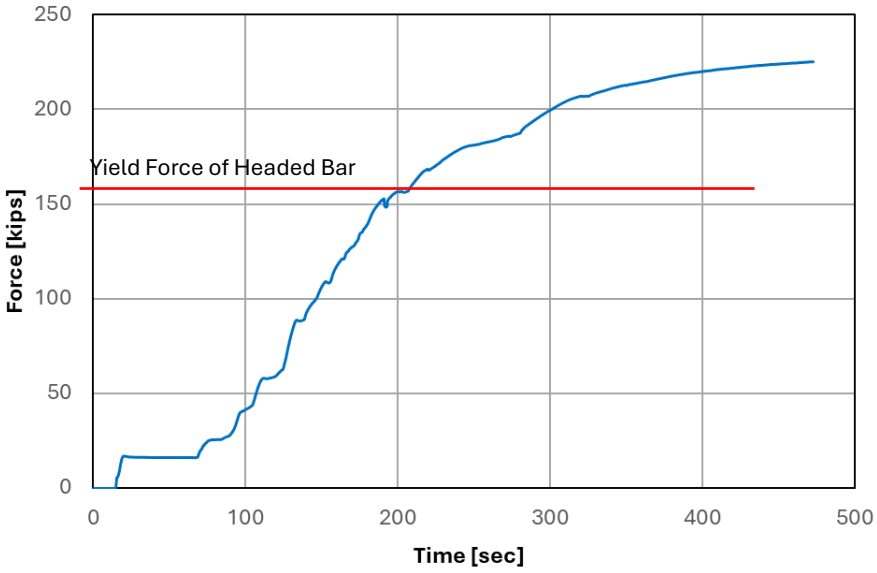

Figure 4.8: Pull force applied to the headed bar versus time for Specimen 2

Figure 4.9 shows the tensile strains developed at different locations along the headed bar over time, and Figure 4.10 and Figure 4.11 show the tensile strains in the outer and inner stirrups, respectively. They were measured by the strain gauges shown in Figures D.13 and D.14 in Appendix D. Plots of the applied force versus strains are presented in Figures D.15 through D.32 in Appendix D.

It can be observed from Figure 4.9 that the strains measured by gauges SG06 and SG05, the two uppermost gauges in the headed bar, had a rapid increase after 210 sec., at which the applied force reached 160 kips (as shown in Figure 4.8), the yield strength of the bar. However, the strain measured by Gauge SG05, which was located 4 in. below the top face of the beam, leveled off quickly probably because of gauge malfunctioning, while the strain measured by Gauge 06, which was 2 in. above the top face of the beam, continued to increase rapidly till the peak force was reached. Gauges

SG01 and SG02, both located 2 in. above the bearing surface of the T head, registered the lowest strains and stopped functioning at about 300 sec., at which the applied force was 200 kips.

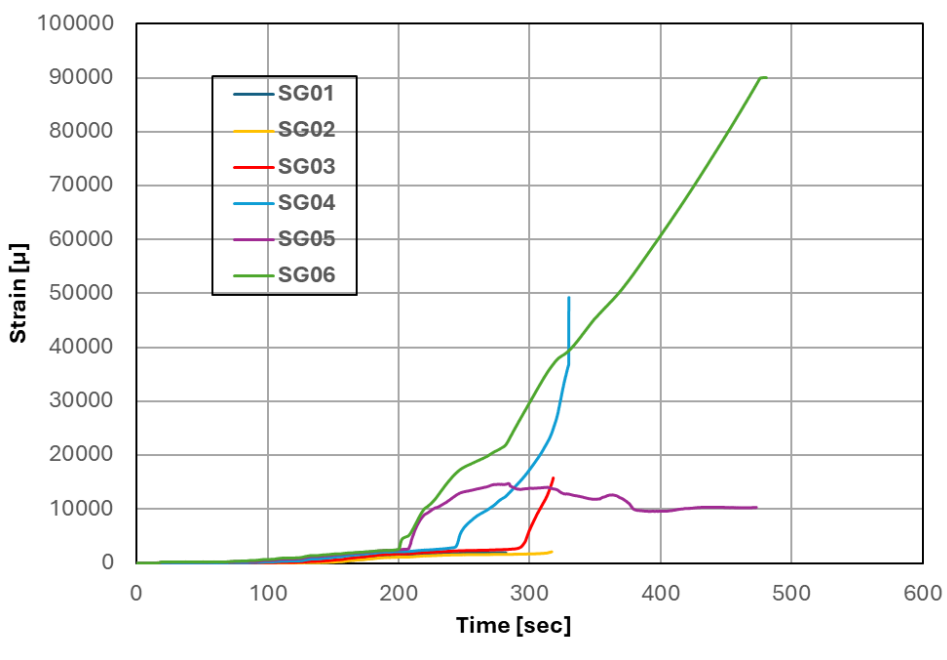

Figure 4.9: Strains along headed bar versus time for Specimen 2

As shown in Figure D.14, the outer stirrups had 8 strain gauges in total. All the gauges were functioning throughout the test. The strains registered by the gauges are plotted in Figure 4.10. A gauge with the letter "A" after the gauge number was located slightly below the potential crack plane and that without the letter was slightly above the potential crack plane. The yield and tensile strengths of the stirrups were 65.6 ksi and 91.5 ksi, respectively, and the yield strain was 0.0023. The strains registered by these gauges started to increase rapidly after the applied force reached 180 kips. The peak strain registered by Gauge SG10A was slightly shy of the yield strain of 0.0023, while the strains registered by the other gauges on the outer stirrups were below the yield value.

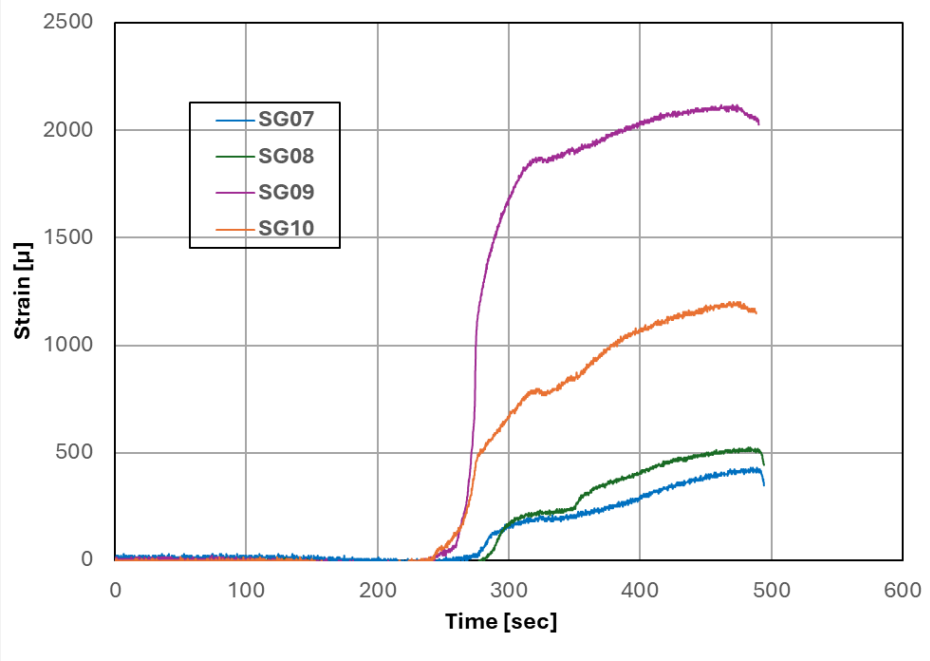

(a) Gauges above the potential crack plane

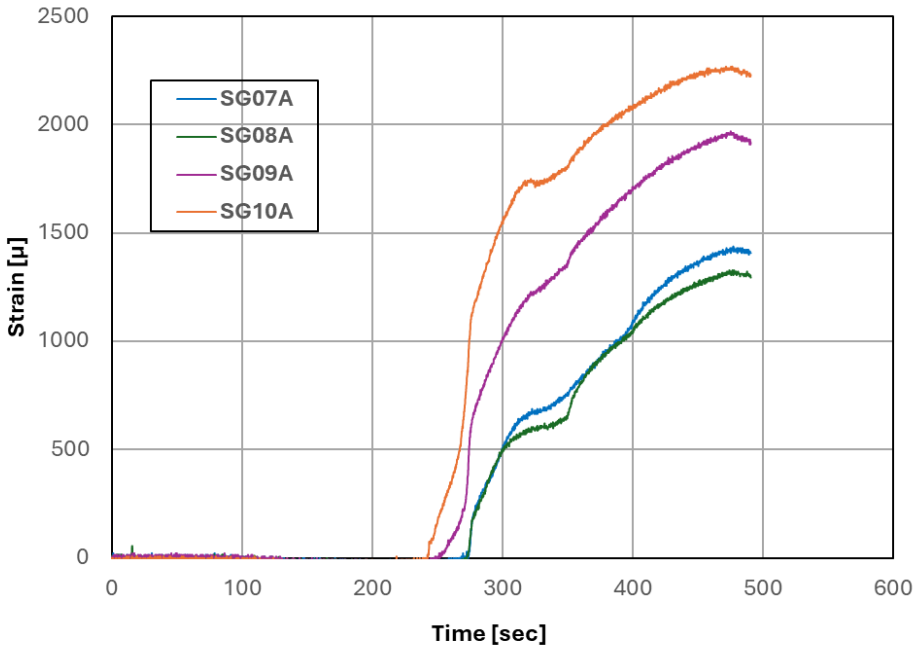

(b) Gauges below the potential crack plane

Figure 4.10: Strains in outer stirrups versus time for Specimen 2

The inner stirrups had 4 strain gauges in total. All the gauges were located slightly above the potential crack plane. The strains registered by the gauges are plotted in Figure 4.11. The inner stirrups had slightly higher strains than the outer stirrups. Two of the gauges registered strains exceeding the yield value. The strains in the inner stirrups started to increase rapidly after the applied force reached 180 kips due to the initiation of breakout cracks. Compared to Specimen 1, which had insufficient development length, Specimen 2 had breakout cracks initiated at a much higher load and had much smaller stirrups strains.

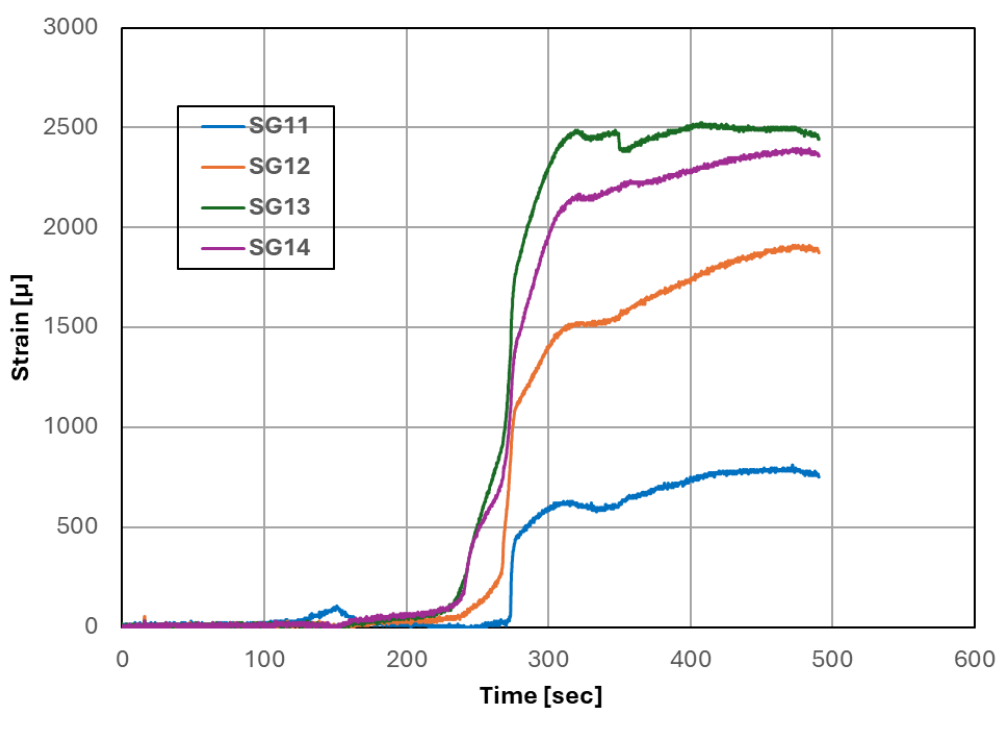

Figure 4.11: Strains in inner stirrups versus time for Specimen 2

Strains developed in the headed bar and stirrups at time instants of interest (i.e., when major strain increments occurred) are shown in Table 4.3.

Table 4.3: Strains in headed bar and stirrups at different load levels for Specimen 2

Time (sec)	Force Applied (kips)	SG01 (μstr)	SG02 (μstr)	SG03 (μstr)	SG04 (μstr)	SG05 (μstr)	SG06 (μstr)	SG07 (μstr)	SG07A (μstr)	SG08 (μstr)	SG08A (μstr)
120	60	45	15	136	378	746	948	0	0	0	0
147	100	151	136	455	953	1394	1570	0	0	0	0
182	143	963	865	1411	1878	2157	2224	0	0	0	0
209	160	1319	1161	1768	2182	3876	5652	0	0	0	0
244	180	1805	1533	2262	3238	12633	16769	0	0	0	0
279	187	1889	1601	2483	11951	14575	21412	45	227	0	207
337	210	-	-	-	-	12417	41357	197	689	228	622
471	225	-	-	-	-	10298	87931	409	1416	514	1312

Time (sec)	Force Applied (kips)	SG09 (μstr)	SG09A (μstr)	SG10 (μstr)	SG10A (μstr)	SG11 (μstr)	SG12 (μstr)	SG13 (μstr)	SG14 (μstr)
120	60	0	0	0	0	0	0	0	0
147	100	0	0	0	0	0	0	0	0
182	143	0	0	0	0	0	0	38	45
209	160	0	0	0	0	0	30	45	61
244	180	0	0	0	0	0	76	347	348
279	187	1241	678	502	1186	447	1122	1836	1462
337	210	1889	1290	813	1750	592	1524	2450	2160
471	225	2110	1955	1201	2254	781	1904	2503	2388

Table 4.3 shows that the strains developed in the stirrups were negligible when the applied force was 143 kips (69% of the yield force of the headed bar) or less. When the applied force reached 143 kips, the tensile strain in the headed bar near the T head was 0.000865, which gives a tensile force of 56.4 kips. At this stage, a significant portion of the anchorage resistance (86.6 kips) was provided by the bond. When the applied pull force was increased to 180 kips, the stirrups began to develop noticeable tensile strains. At this point, the strain in the headed bar near the T head increased to 0.001533, which corresponds to a tensile force of 100 kips, indicating that a significant portion of the anchorage force had been transferred to the T head with less contribution from the bond. At the peak load of 225 kips, most of the gauges on the headed bar stopped functioning, one

inner stirrup developed a tensile strain slightly higher than the yield value, and one outer stirrup had a strain slightly below the yield. The relatively low stirrup strains in this specimen compared to Specimen 1 are consistent with the fact that breakout failure did not here in this specimen.

4.4 Specimen 3

4.4.1 General Observations

Like Specimen 1, the headed bar in Specimen 3 had an embedment length of 16.75 in., which was 70% of the minimum required by ACI 318-19. Nevertheless, the T head in Specimen 3 was larger with a net bearing area of $9A_b$. In the test, the bar fractured at the peak load of 212.5 kips, which was slightly lower than the tensile strength of the bar. The bar was most likely weakened by the indentation caused by the lowermost gripping screw in the coupler that was used to grip the bar, and bar fracture occurred right at that location. The peak load reached was substantially higher than the peak load of 179 kips reached in Specimen 1, which had a T head with a net bearing area of $4A_b$ and had anchorage failure. This shows that the head size did affect the anchorage capacity and that the anchorage failure in Specimen 1 was most likely caused by the crushing of the concrete from the bearing force of the T head. As shown in Figure 4.12, breakout cracks developed in Specimen 3 but remained closed throughout the test. The depth of the cone-shaped breakout was measured to be about 15.5 inches. The average angle of the inclined cracks was about 33 degrees. There was also significant cracking and uplifting of concrete at the top face of the beam around the headed bar as shown by the picture in Figure 4.13.

Figure 4.12: Breakout cracks in Specimen 3

Figure 4.13: Damage in the top surface of the beam in Specimen 3

4.4.2 Test Results

Figure 4.14 shows the pull force applied to the headed bar over time. As shown in the figure, the bar was unloaded to a zero force when the applied force reached 195 kips. This was to allow the installation of a catch system, which, as shown in Figure 4.13, was intended to prevent the end piece of the bar from flying off should bar fracture occur. The bar was then reloaded to the peak load of 212.5 kips, at which the bar fractured.

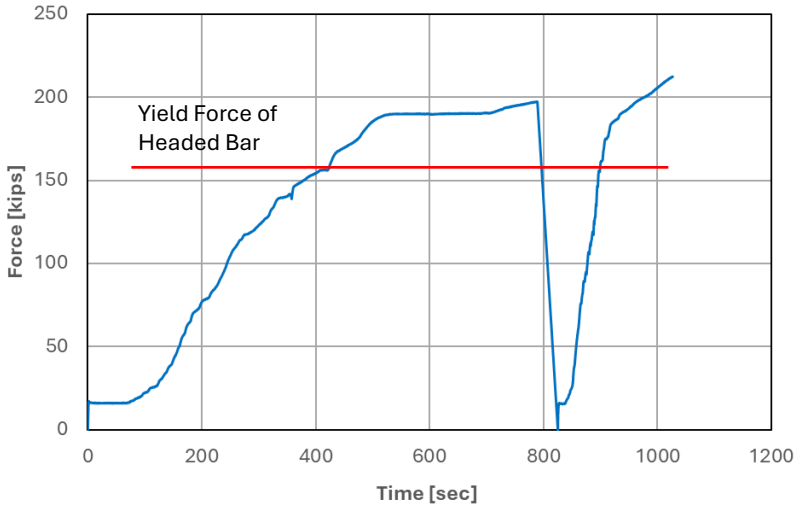

Figure 4.14: Pull force applied to the headed bar versus time for Specimen 3

Figure 4.15 shows the tensile strains developed at different locations along the headed bar over time, while Figure 4.16 and Figure 4.17 show the tensile strains in the outer and inner stirrups, respectively. The strain gauge locations and plots of the applied force versus the strains are shown Figures D.33 through D.45 in Appendix D. Data from gauges SG04 and SG08, which did not function, are not shown.

It can be observed from Figure 4.15 that the tensile strain in the headed bar near the T head (registered by gauges SG01 and SG02) were close to the yield value and started to increase rapidly soon after 500 sec., at which the applied force was 186 kips. The dips in the strains at around 800 sec. were due to the unloading of the bar. The strains dropped to the residual values before the bar was reloaded. Gauge SG03 was located 9.75 in. below the top face of the beam, while SG05 was about 2 in. above the top face. The strain registered in SG05 jumped suddenly when the applied pull force reached 160 kips due to the yielding of the bar.

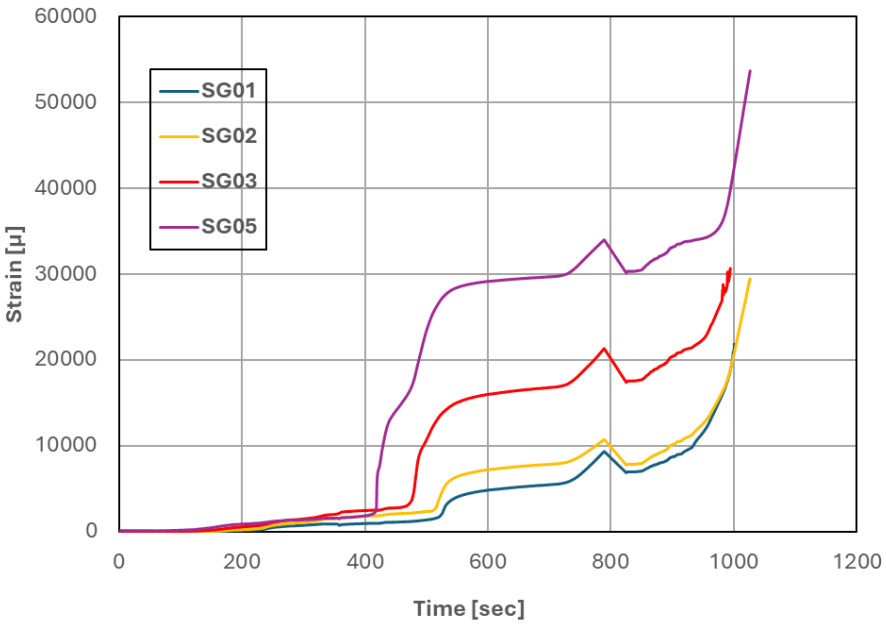

Figure 4.15: Strains along headed bar versus time for Specimen 3

The four sets of stirrups adjacent to the headed bar had 8 strain gauges in total, but one of the gauges did not function. The strains registered by the functioning gauges on the outer and inner stirrups are plotted in Figure 4.16 and Figure 4.17, respectively. The yield and tensile strengths of the stirrups were 65.6 ksi and 91.5 ksi, respectively, and the yield strain was 0.0023. The strains in the outer and inner stirrups had rapid increases soon after 350 sec., at which the applied force was 140 kips. This signifies the initiation of inclined breakout cracks. It should be noted that the breakout cracks in Specimen 1, which had the same bar embedment length but a smaller head, initiated at a slightly lower applied force of 129 kips. All the strain gauges on the outer stirrups stopped functioning before 500 seconds. After the applied force exceeded 186 kips (at 500 sec.), the inner stirrups showed significant yielding.

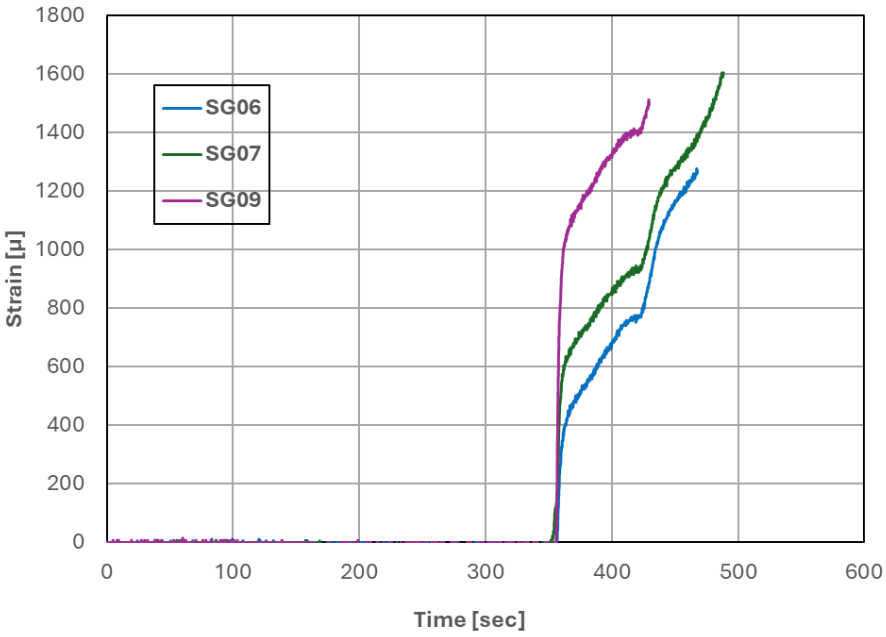

Figure 4.16: Strains in outer stirrups versus time for Specimen 3

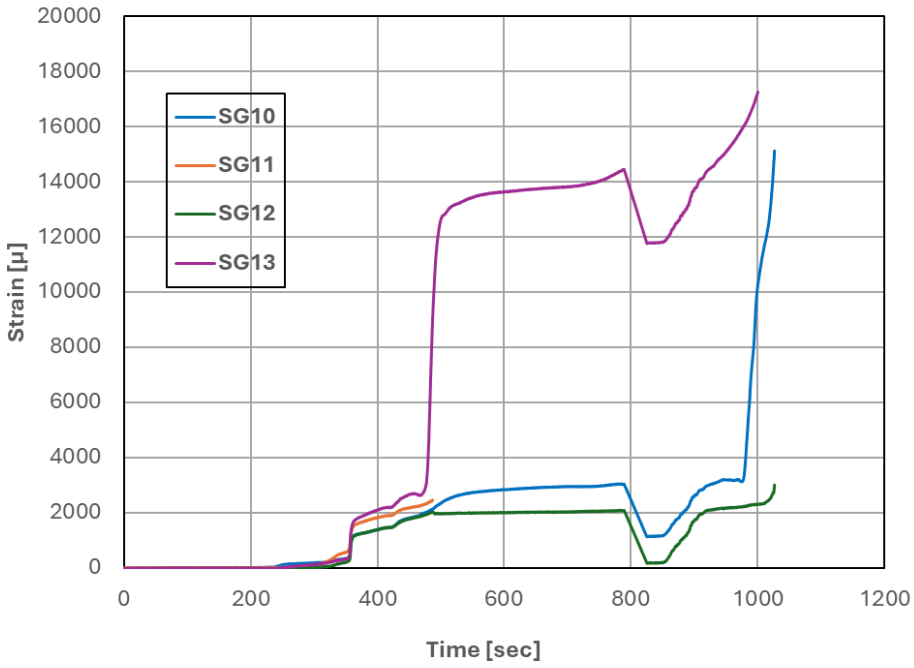

Figure 4.17: Strains in inner stirrups versus time for Specimen 3

Strains developed in the headed bar and stirrups at time instants of interest (when major strain increments occurred) are shown in Table 4.4.

Table 4.4: Strains in headed bar and stirrups at different load levels for Specimen 3

Time (sec)	Force Applied (kips)	SG01 (μstr)	SG02 (μstr)	SG03 (μstr)	SG05 (μstr)
218	83	227	347	687	1002
350	140	924	1548	2056	1606
400	154	1000	1843	2496	1893
426	160	1053	1926	2595	8747
500	186	1417	2396	10801	23538
768	195	7842	9646	19640	32538
825	0	6904	7789	17431	30149
875	94	7896	9054	19043	31879
955	195	12128	13040	22900	34293
995	204	18899	18943	31210	39928
1026	212.5	-	29375	-	53613

Time (sec)	Force Applied (kips)	SG06 (μstr)	SG07 (μstr)	SG09 (μstr)	SG10 (μstr)	SG11 (μstr)	SG12 (μstr)	SG13 (μstr)
218	83	0	0	0	0	0	0	0
350	140	0	0	0	349	561	219	333
400	154	684	847	1323	1387	1823	1390	2098
426	160	815	968	1452	1527	1945	1511	2265
500	186	-	-	-	2362	-	1973	12648
768	195	-	-	-	3017	-	2079	14209
825	0	-	-	-	1136	-	181	11773
875	94	-	-	-	1813	-	876	12594
955	195	-	-	-	3205	-	2193	15252
995	204	-	-	-	8373	-	2299	16861
1026	212.5	-	-	-	15126	-	3012	-

Table 4.4 shows that the strains developed in the inner stirrups started to increase when the applied force reached 140 kips. The inner stirrups started to yield when the applied pull force was 186 kips. The strain gauges on the outer stirrups broke at this point and could not provide more data. At 186-kip load, the average tensile strain registered in the headed bar near the T head was 0.00191,

which corresponds to a bar tensile force of 124 kips. Hence, the anchorage resistance provided by the T head was about 124 kips. Then, the remaining 62 kips of the applied force had to be carried by the bond stress along the bar. At the ultimate load of 212.5 kips, the tensile strain registered near the T head by SG02 was 0.029375, which corresponds to a bar tensile force of about 190 kips according to the bar force-vs.-strain plot shown in Figure D.38 in Appendix D. Hence, the anchorage resistance provided by the T head should be around 190 kips. The remaining 22.5 kips of the applied force must be carried by the bond stress along the bar.

4.5 Specimen 4

4.5.1 General Observations

For Specimen 4, the target concrete strength was 8,000 psi and the headed bar had an embedment of 14 in., which was equal to 70% of the minimum development length required by ACI 318-19. The maximum load reached in the test was 173 kips, at which the headed bar had anchorage failure. After that, large concrete break-off pieces at the top face of the beam were lifted as the bar was being pulled out. Although the bar did not fracture, the tensile force developed in the bar way exceeded the yield strength of 160 kips. At the end of the test, concrete break-off pieces at the top of the beam were significantly lifted as shown in Figure 4.18.

(a)

(b)

(c)

Figure 4.18: Damage in Specimen 4

Breakout cracks developed in the beam during the test and the crack patterns at the end of the test are shown in Figure 4.19. The maximum depth of the cone-shaped breakout crack was measured to be 12 in. on one face of the beam and 11 in. on the other face. The average angle of the inclined cracks was around 39 degrees. These cone-shaped breakout cracks did not open much during the test.

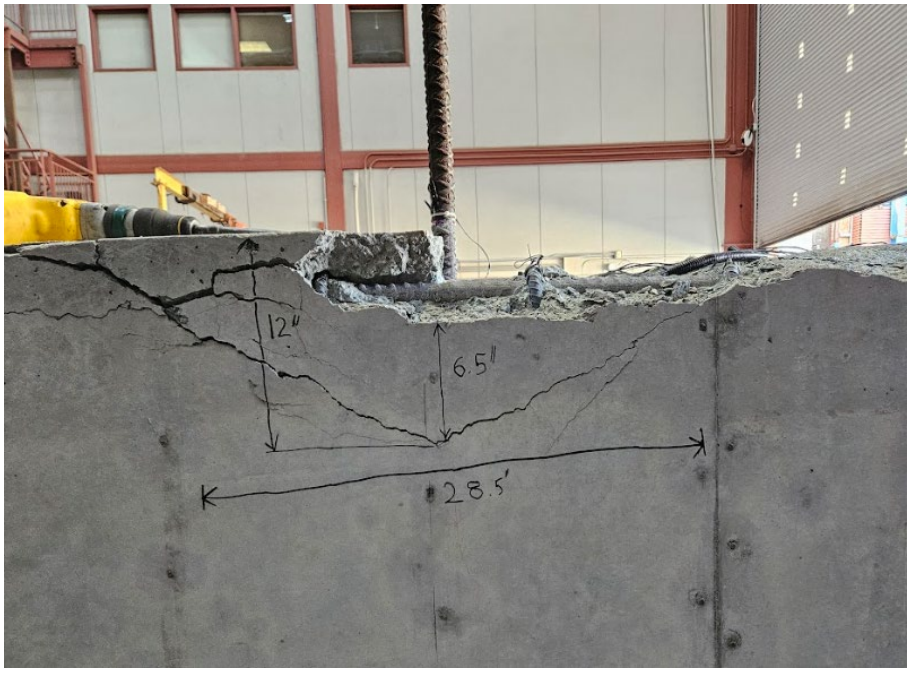

(a) Side Face 1

(b) Side Face 2

Figure 4.19: Breakout cracks in Specimen 4

After the test, broken concrete pieces at the surface of the beam were removed by hand to examine the concrete damage underneath. It can be seen in Figure 4.20 that there was concrete crushing in the vicinity of the headed bar and there was a cone-shaped concrete break-off pattern around the bar. The anchorage failure appeared to be governed by a combination of concrete breakout and concrete crushing above the T head.

(a) Crushing in the vicinity of the headed bar

(b) Cone-shaped crack surface

Figure 4.20: Damage in the vicinity of the bar after removing concrete pieces at the top in Specimen 4

4.5.2 Test Results

Figure 4.21 shows the pull force applied to the headed bar plotted against time. The ultimate load reached was 173 kips. This was less than the tensile strength but greater than the yield strength of the No. 14 headed bar.

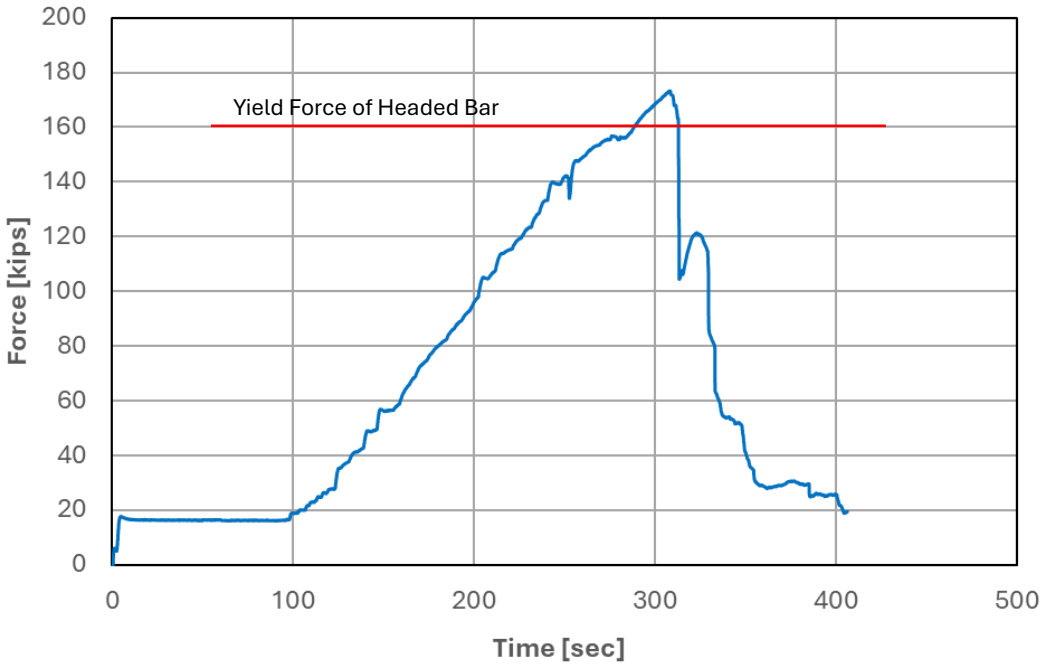

Figure 4.21: Pull force applied to the headed bar versus time for Specimen 4

Figure 4.22 shows the tensile strains developed at different locations along the headed bar over time, while Figure 4.23 and Figure 4.24 show the tensile strains in the stirrups. They were measured by the strain gauges shown in Figures D.46 and D.47 in Appendix D. Plots of the applied force versus strains are presented in Figures D.48 through D.59 in Appendix D.

It can be observed from Figure 4.22 that the tensile strains measured by gauges SG01 and SG02 reached the yield value soon after 300 seconds, which was about the same time the applied force reached the maximum of 173 kips. The dips in the strains at around 310 sec. were due to the unloading of the bar. The strains measured by gauges SG03 (located 7 in. below the top face of the

beam), SG04 (located 2 in. below the top face of the beam), and SG05 (located 1.5 in. above the top face of the beam) had a rapid increase after 280 sec., at which the applied force reached 160 kips (as shown in Figure 4.21), at which the yield strength of the bar was reached.

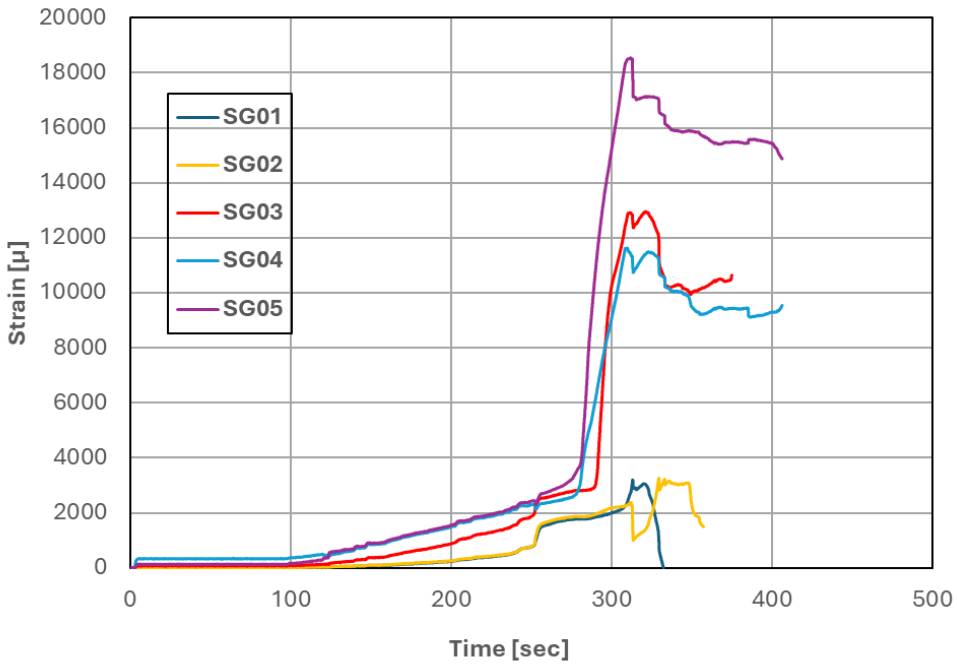

Figure 4.22: Strains along headed bar versus time for Specimen 4

The four sets of stirrups adjacent to the headed bar had 8 strain gauges in total, but one of the gauges did not function. The strains registered by the functioning gauges on the outer and inner stirrups are plotted in Figure 4.23 and Figure 4.24, respectively. The yield and tensile strengths of the stirrups were 66.2 ksi and 92.5 ksi, respectively, and the yield strain was 0.0023. The strains in the outer and inner had rapid increases at 250 sec., at which the applied force was 140 kips. This signifies the initiation of inclined breakout cracks, which were visible to the naked eye at around 158 kips during the test. The strains measured by two of the gauges on the inner stirrups increased significantly and way exceeded the yield strain right after 300 sec. when the applied load reached 170 kips, while maximum strain measured from the outer stirrups barely exceeded the yield value. The lower strains in the outer stirrups could be attributed to the fact that the upper ends of the

stirrups were close to the ends of the inclined crack planes and were thus not fully engaged to resist the pull force.

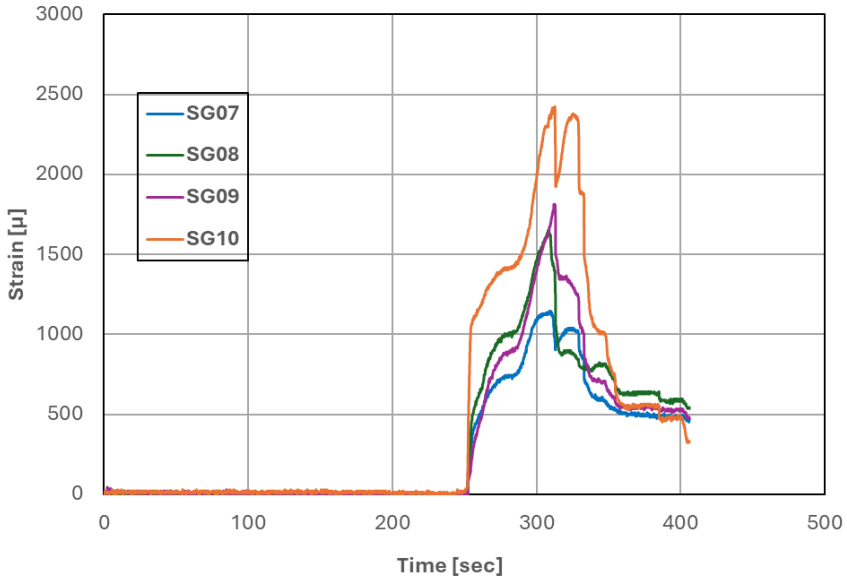

Figure 4.23: Strains in outer stirrups versus time for Specimen 4

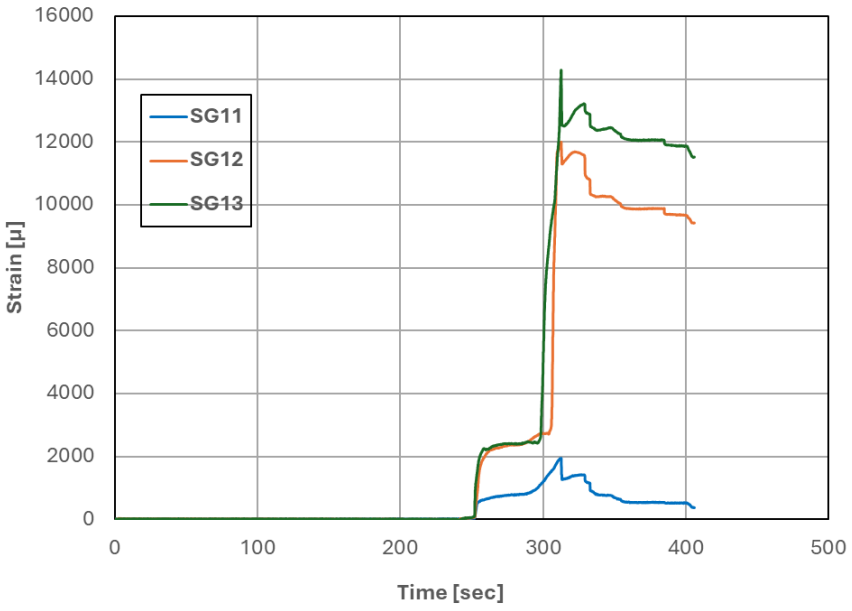

Figure 4.24: Strains in inner stirrups versus time for Specimen 4

Strains developed in the headed bar and stirrups at time instants of interest (when major strain increments occurred) are shown in Table 4.5.

Table 4.5: Strains in headed bar and stirrups at different load levels for Specimen 4

Time (sec)	Force Applied (kips)	SG01 (μstr)	SG02 (μstr)	SG03 (μstr)	SG04 (μstr)	SG05 (μstr)
152	60	83	98	376	859	910
213	112	332	353	1158	1757	1814
251	142	808	820	1941	2308	2447
252	137	944	1068	2190	2195	2364
254	141	1223	1384	2386	2225	2463
282	156	1776	1852	2816	3899	4748
289	160	1836	1927	2907	5806	10133
299	168	1988	2168	10005	8885	14964
308	173	2245	2229	12387	11582	18267

Time (sec)	Force Applied (kips)	SG07 (μstr)	SG08 (μstr)	SG09 (μstr)	SG10 (μstr)	SG11 (μstr)	SG12 (μstr)	SG13 (μstr)
152	60	0	0	0	0	0	0	0
213	112	0	0	0	0	0	0	0
251	142	0	0	0	30	38	52	78
252	137	0	0	0	60	83	81	593
254	141	196	265	128	814	489	731	1437
282	156	738	1006	898	1418	789	2364	2392
289	160	799	1075	966	1471	812	2446	2464
299	168	1078	1423	1375	1917	1151	2731	3546
308	173	1131	1651	1632	2303	1656	8751	10098

Table 4.5 shows that the strains in the inner stirrups started to increase when the applied force reached 142 kips (at 251 sec.), indicating the initiation of the inclined breakout cracks. The strain increase in the inner stirrups accelerated after 254 seconds. The outer stirrups were engaged as soon as the strain increase in the inner stirrups accelerated, indicating that the breakout cracks had fully propagated. At the ultimate load of 173 kips, the average tensile strain registered in the headed bar

near the T head was 0.00224, which corresponds to a bar tensile force of 130 kips according to the bar force-vs.-strain curve shown in Figure D.52. Hence, the maximum bearing resistance developed at the head was 130 kips.

4.6 Specimen 5

4.6.1 General Observations

Specimen 5 had the same concrete strength and embedment length as Specimen 4. The only difference between the two specimens was that Specimen 5 had four No. 4 stirrups in the concrete breakout region while Specimen 4 had No. 5 stirrups along the entire beam. The maximum load reached in the pull test was 152 kips, which corresponds to a tensile stress of 67.6 ksi. This was slightly below 160 kips, the yield strength of the bar, and a bit lower than the peak resistance of 173 kips developed in Specimen 4.

The damage in the concrete beam is shown in Figure 4.25 and Figure 4.26. Similar to Specimens 1 and 4, which had anchorage failure, cracks developed at the top of the beam and concrete pieces were lifted as the bar was being pulled out. This is shown in Figure 4.25(a). Figure 4.25(b) shows the crushing of the concrete near the headed bar with the broken concrete pieces at the top removed. As shown in Figure 4.26, breakout cracks developed and opened significantly, way more than that observed in Specimen 4. However, the wide breakout cracks appeared only in the cover concrete outside the rebar cage. At the top of the beam, it was apparent that the No. 4 stirrups had bent up more than the No. 5 stirrups in Specimen 4. The depth of the cone-shaped breakout cracks was measured to be 12 in. on one face and 13.2 in. on the other face of the beam. The average angle of the inclined cracks was about 31 degrees. The anchorage failure appeared to be caused by concrete breakout as well as concrete crushing as shown in Figure 4.25. The use of smaller stirrups

in this specimen, compared to Specimen 4, did have a significant influence on the anchorage strength.

(a) Cracking at the top of the beam

(b) After removing cracked concrete pieces at the top

Figure 4.25: Damage in the concrete beam of Specimen 5

(a) Side Face 1

(b) Side Face 2

Figure 4.26: Breakout cracks in Specimen 5

4.6.2 Test Results

Figure 4.27 shows the pull force applied to the headed bar plotted against time. The ultimate load reached was 152 kips. The load drop after the peak was caused by the initiation of breakout cracks. Figure 4.28 shows the tensile strains developed at different locations along the headed bar over time, while Figure 4.29 and Figure 4.30 show the tensile strains in the stirrups. They were measured by strain gauges, whose locations are shown in Figures D.60 and D.61 in Appendix D.

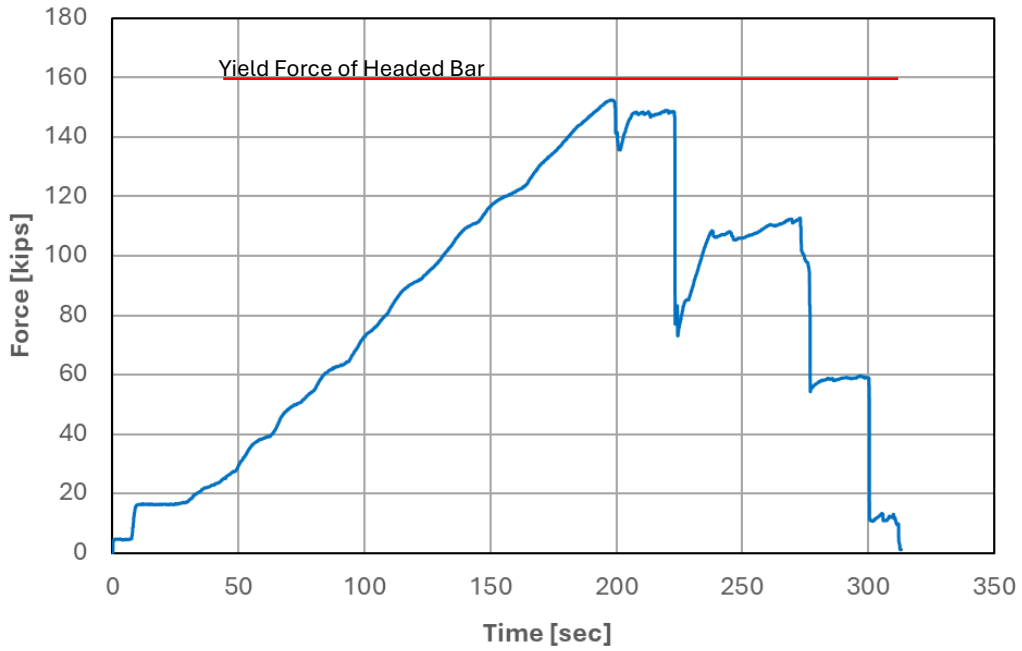

Figure 4.27: Pull force applied to the headed bar versus time for Specimen 5

It can be observed from Figure 4.28 that the strains measured by gauges SG03, SG04, SG05 and SG06 along the headed bar gradually increased until 200 seconds, at which the applied force reached the maximum value of 152 kips (as shown in Figure 4.27). Although the applied force did not reach the yield strength of the headed bar, the maximum strain measured by Gauge SG06, which was located 1.5 in. above the top face of the beam, slightly exceeded the estimated yield value of 0.0025. However, the strain measured by Gauge SG05, which was at the same location as Gauge SG06, was slightly below the yield strain. This discrepancy was likely caused by bar bending during loading. The

maximum strain measured by SG04, which was 2 in. below the top face of the beam, was a bit below the yield value. The dips in the strains right after the peak were due to bar unloading caused by the anchorage failure. However, soon after 200 seconds, the strains measured by gauges SG01 and SG02, which were located 2 in. above the T head, rapidly increased, with the strain measured by SG01 significantly beyond the yield level. The fact that the maximum strains registered by these gauges were higher than those by the gauges above is hard to explain and could be attributed to the bending of the bar near the T head caused by a non-uniform bearing force against the crushed concrete.

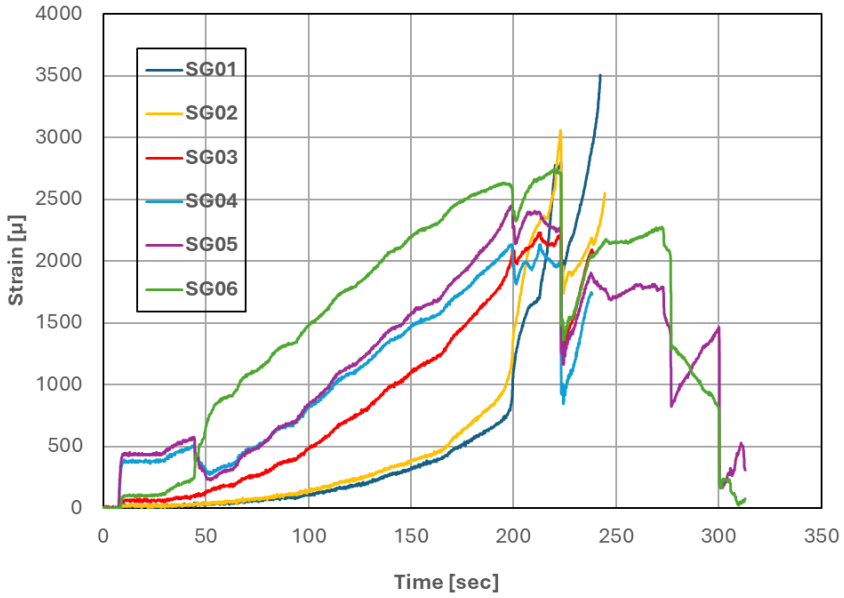

Figure 4.28: Strains along headed bar versus time for Specimen 5

The four No. 4 stirrups adjacent to the headed bar had 8 strain gauges total. All the gauges except SG13 and SG14 were functioning throughout the second test. The yield and tensile strengths of the stirrups were 66.5 ksi and 94.9 ksi, respectively, and the yield strain was 0.0023. As shown in Figure 4.29 and Figure 4.30, the strains registered by these gauges rapidly increased soon after 200 sec., at which breakout cracks initiated at the load of 152 kips. The strains in all the stirrups way exceeded the yield level at about 220 seconds.

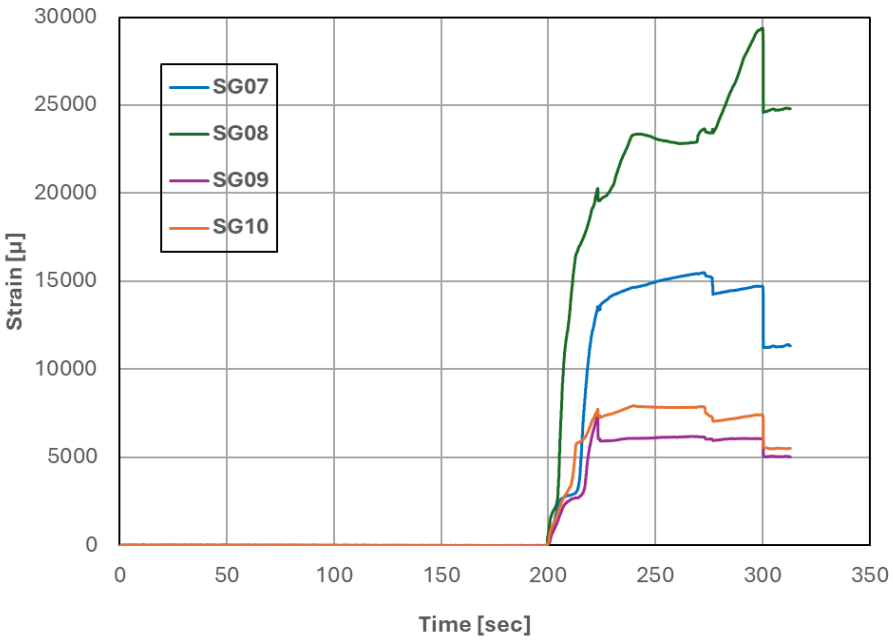

Figure 4.29: Strains in outer stirrups versus time for Specimen 5

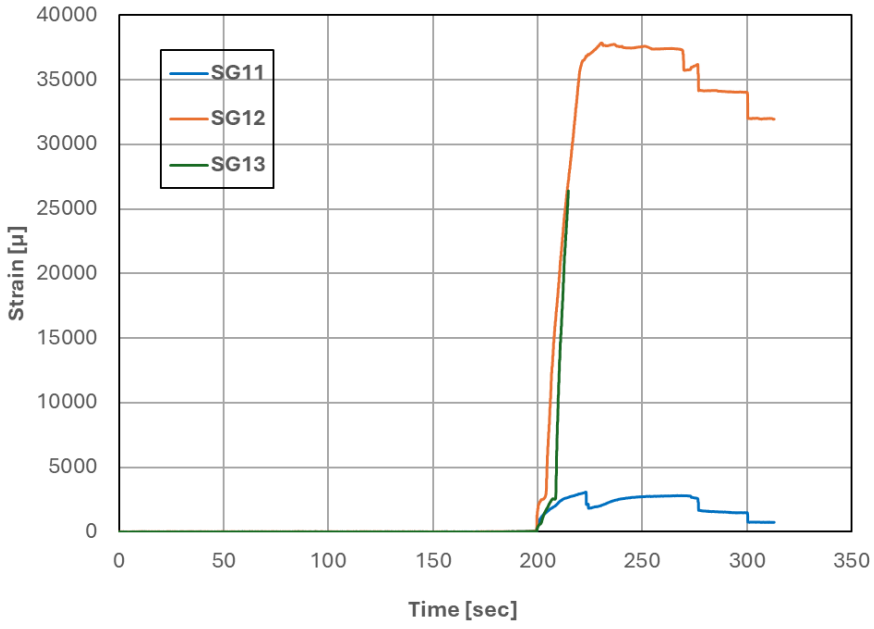

Figure 4.30: Strains in inner stirrups versus time for Specimen 5

Strains developed in the headed bar and stirrups at time instants of interest (when major strain increments occurred) are shown in Table 4.6.

Table 4.6: Strains in headed bar and stirrups at different load levels for Specimen 5

Time (sec)	Force Applied (kips)	SG01 (μstr)	SG02 (μstr)	SG03 (μstr)	SG04 (μstr)	SG05 (μstr)	SG06 (μstr)
52	32	30	45	144	295	226	768
94	65	83	121	403	703	717	1344
131	100	211	264	844	1210	1292	1921
181	140	566	718	1559	1838	2004	2534
199	152	899	1217	2054	2126	2451	2587
200	141	1058	1361	2054	1960	2269	2382
202	138	1330	1588	2009	1853	2193	2359
205	145	1496	1861	2077	1982	2307	2499
210	148	1671	2240	2161	2005	2406	2651
223	147	2800	3037	2192	1952	2231	2698
223	77	1951	1899	1277	930	1254	1484
238	109	2884	2187	2085	1747	1898	2056

Time (sec)	Force Applied (kips)	SG07 (μstr)	SG08 (μstr)	SG09 (μstr)	SG10 (μstr)	SG11 (μstr)	SG12 (μstr)	SG13 (μstr)
52	32	0	0	0	0	0	0	0
94	65	0	0	0	0	0	0	0
131	100	0	0	0	0	0	0	0
181	140	0	0	0	0	0	0	0
199	152	0	0	0	0	60	106	45
200	141	68	468	98	114	323	1291	234
202	138	965	1905	748	1145	1218	2509	945
205	145	2260	3309	1489	1935	1602	5922	1884
210	148	2855	13667	2580	3344	2333	19740	12449
223	147	13569	20275	7292	7741	3081	36841	-
223	77	13358	19584	6075	7326	2122	36809	-
238	109	14584	22972	6075	7856	2476	37605	-

Table 4.6 shows that strains developed in the inner and outer stirrups started to increase around the same time (199-200 sec.) when the applied force was 152 kips. At 152-kip load, the average tensile strain registered in the headed bar near the T head was 0.00106, which corresponds

to a bar tensile force of 69 kips. Hence, the maximum anchorage resistance provided by the T head was about 69 kips and the remaining 83 kips of the applied force was carried by the bond between the bar and the concrete. The yielding of the stirrups occurred approximately at the same time between 205 and 210 seconds. At 223 sec., the applied force dropped to 147 kips and the average strain in the headed bar near the T head increased to 0.0029, which exceeded the yield value. For this specimen, it is clear that the anchorage failure was caused by concrete breakout.

4.7 Specimen 6

4.7.1 General Observations

Specimen 6 had a target concrete strength of 8,000 psi and the headed bar had an embedment length of 20 in., which was equal to the minimum development length required by ACI 318-19. The net bearing area of the T head was $4A_b$. The maximum load reached was 212 kips, which corresponds to a tensile stress of 94.2 ksi. The bar fractured at this load. Breakout cracks developed during the test, and the cracks appeared when the applied force reached 180 kips. Figure 4.31 shows the breakout crack pattern developed in the beam at the end of the test. The maximum depth of the cone-shaped breakout crack was measured to be 17.5 in. on one face of the beam and 16.5 in. on the other face. The average angle of the inclined cracks was around 35 degrees. The breakout cracks remained fine after the load was removed at the end of the test. Additionally, there was only moderate cracking at the top surface of the beam as shown in Figure 4.32. The damage was much less severe than the first 5 specimens.

(a) Side Face 1

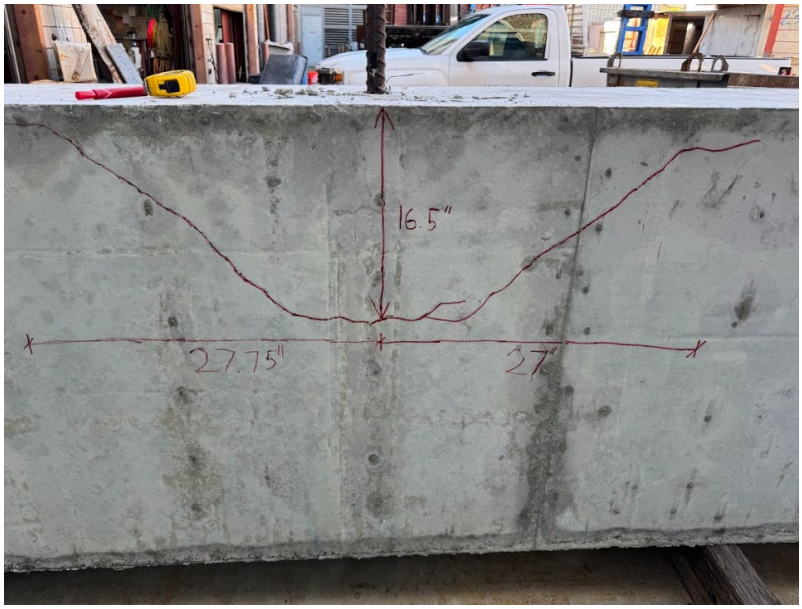

(b) Side Face 2

Figure 4.31: Breakout cracks in Specimen 6

Figure 4.32: Damage at the top surface of Specimen 6

4.7.2 Test Results

Figure 4.33 shows the pull force applied to the headed bar plotted against time. The bar yielded at 160 kips and the ultimate load reached was 212 kips. The ratio of the ultimate to the yield force is 1.33, which is a bit below the typical ratio of the tensile strength to the yield strength. This can be attributed to the fact that the bar was slightly weakened by the gripping screws in the coupler used to grip the bar. In spite of this, the peak load reached was close to 224 kips, the expected tensile strength of the bar.

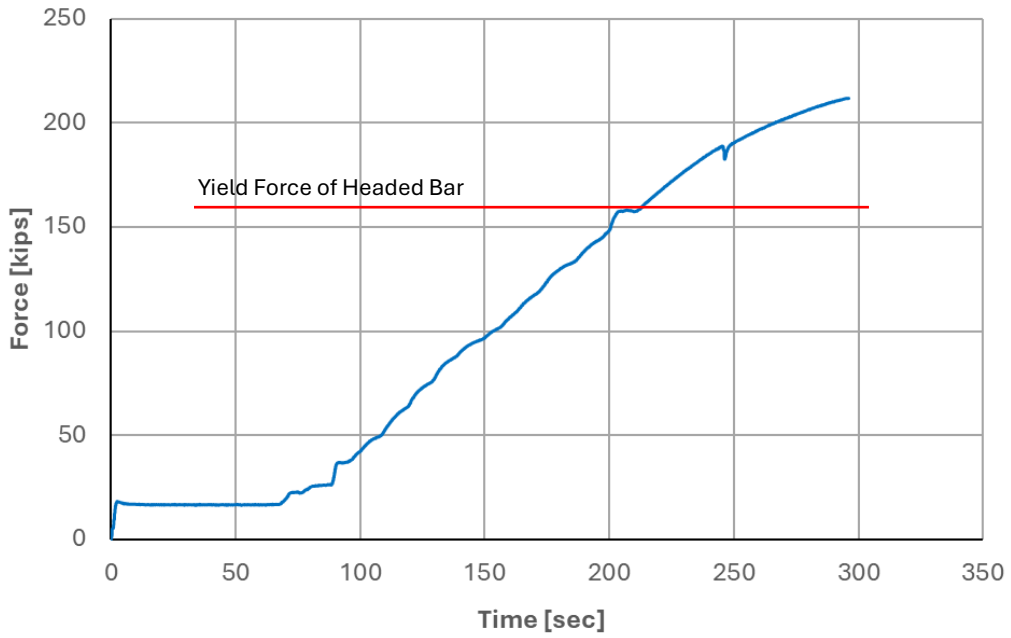

Figure 4.33: Pull force applied to the headed bar versus time for Specimen 6

Figure 4.34 shows the tensile strains developed at different locations along the headed bar over time. Figure 4.35 and Figure 4.36 show the tensile strains in the outer and inner stirrups, respectively. They were measured by strain gauges, whose locations are shown in Figures D.75 and D.76 in Appendix D. Plots of the applied force versus strains are presented in Figures D.77 through D.91.

It can be observed from Figure 4.34 that the tensile strains measured by gauges SG01 and SG02, which were located 2 in. above the T head, did not reach the yield value by the end of the test. Gauge SG03 was located 7 in. above the T head and it barely passed the yield level soon before the bar fractured. Gauge SG04 was located 12 in. above the T head, while SG05 was 17 in. above the T head. There was a rapid increase in strain at the location of SG05 at 212 sec. when the applied force reached 157 kips. The rapid increase in strain at the location of SG04 happened at 235 sec. when the applied force was about 182 kips. Gauges SG06 and SG07 were located 1.5 in. above the top surface of the beam. There was a sudden jump in strains registered by these gauges at around 205 sec. when

the applied force reached 157 kips. The strain continued to rapidly increase at this location until the bar fractured at 212 kips.

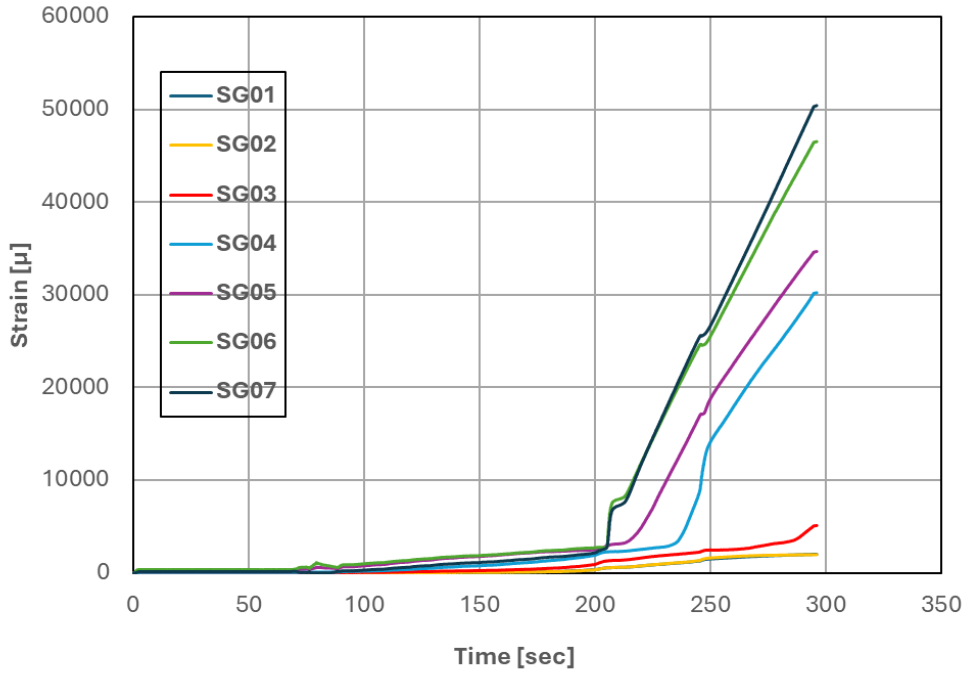

Figure 4.34: Strains along headed bar versus time for Specimen 6

The four sets of stirrups adjacent to the headed bar had 8 strain gauges in total. The strains registered by the functioning gauges on the outer and inner stirrups are plotted in Figure 4.35 and Figure 4.36, respectively. The yield and tensile strengths of the stirrups were 65.9 ksi and 90.7 ksi, respectively, and the yield strain was 0.0023. The strains in the outer and inner stirrups had rapid increases right before 250 sec., at which the applied force was about 180 kips. This signifies the initiation of the inclined breakout cracks. None of the stirrups except one outer stirrup developed strains that exceed the yield level.

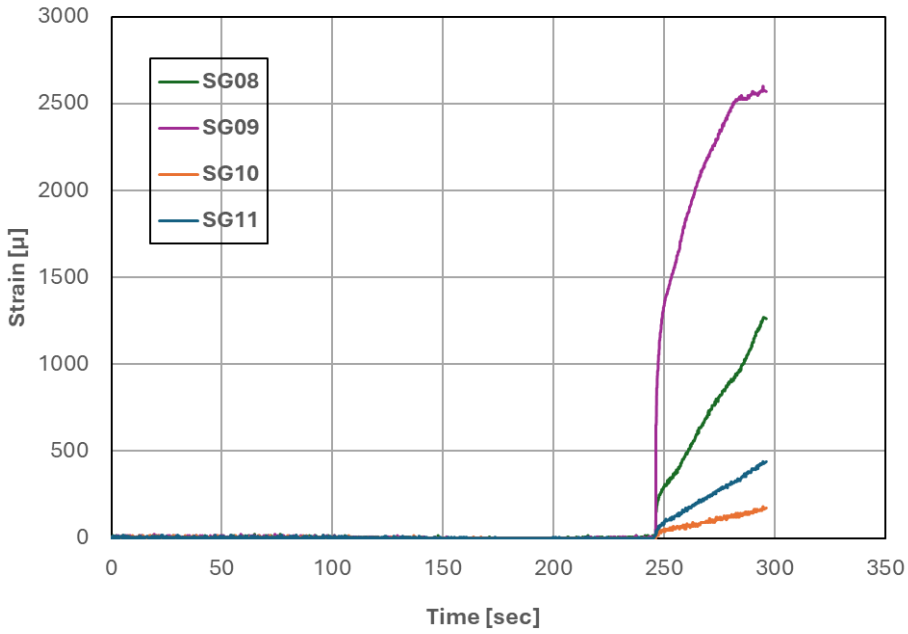

Figure 4.35: Strains in outer stirrups versus time for Specimen 6

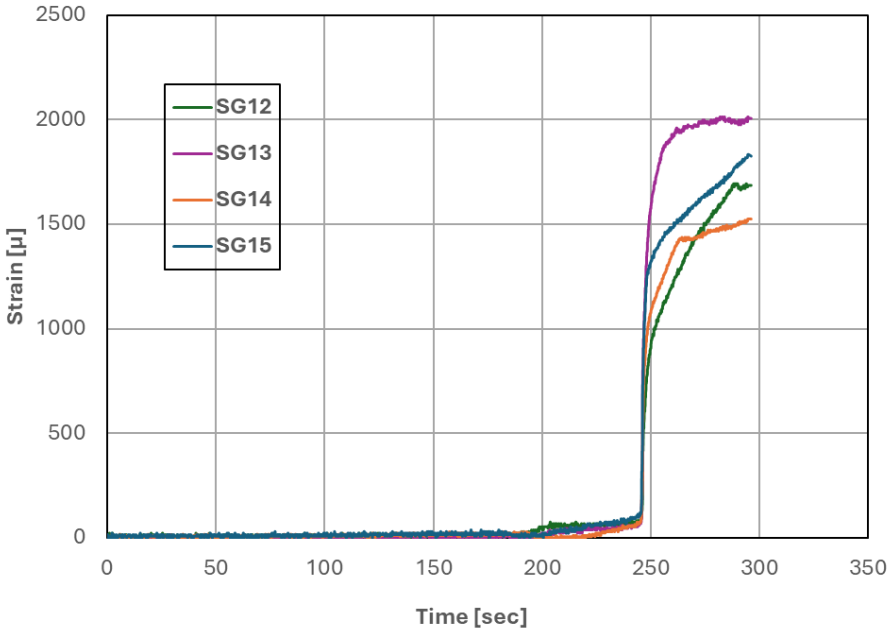

Figure 4.36: Strains in inner stirrups versus time for Specimen 6

Strains developed in the headed bar and stirrups at time instants of interest are shown in Table 4.7.

Table 4.7: Strains in headed bar and stirrups at different load levels for Specimen 6

Time (sec)	Force Applied (kips)	SG01 (μstr)	SG02 (μstr)	SG03 (μstr)	SG04 (μstr)	SG05 (μstr)	SG06 (μstr)	SG07 (μstr)
98	40	15	8	45	182	721	935	264
153	100	60	61	273	820	1824	1917	1185
173	120	98	106	410	1146	2182	2252	1503
203	156	476	469	1154	2158	2677	2748	2456
206	158	574	568	1328	2288	3013	6050	5146
213	160	612	621	1412	2356	3288	8431	7835
234	180	1036	1053	1960	3065	11325	18968	19384
246	187	1331	1402	2333	9966	17150	24657	25618
249	190	1497	1607	2462	13834	18495	25288	26413
296	212	2005	1971	5121	30237	34683	46532	50421

Time (sec)	Force Applied (kips)	SG08 (μstr)	SG09 (μstr)	SG10 (μstr)	SG11 (μstr)	SG12 (μstr)	SG13 (μstr)	SG14 (μstr)	SG15 (μstr)
98	40	0	0	0	0	0	0	0	0
153	100	0	0	0	0	0	0	0	0
173	120	0	0	0	0	0	0	0	0
203	156	0	0	0	0	0	0	0	0
206	158	0	0	0	0	0	0	0	0
213	160	0	0	0	0	68	38	6	38
234	180	0	0	0	0	68	45	41	76
246	187	8	53	0	17	158	287	273	416
249	190	287	1307	45	75	876	1543	1059	1295
296	212	1263	2571	174	441	1686	2006	1525	1826

Table 4.7 shows that the strains developed in the outer and inner stirrups were very small until the applied force reached 187 kips, after which breakout cracks initiated and the strains in the inner stirrups increased quickly until the ultimate load was reached. Strains in two of the outer stirrups increased quickly as well after that point. At the ultimate load of 212 kips, the average tensile strain registered in the headed bar near the T head was 0.00199, which corresponds to a bar tensile force of 125 kips, which was the maximum bearing resistance provided by the T head. The remaining 87 kips of the applied force was carried by the bond stress along the bar.

4.8 Specimen 7

4.8.1 General Observations

Specimen 7 had a target concrete strength of 8,000 psi and the headed bar had an embedment length of 14 in., which was equal to 70% of the minimum development length required by ACI 318-19. The net bearing area of the T head was $9A_b$. The maximum load reached was 188 kips, which corresponds to a tensile stress of 83.6 ksi. This was higher than the yield strength but below the expected tensile strength of the bar. Breakout cracks developed during the test, and the cracks appeared when the applied force was around 160 kips. Figure 4.37 shows the damage in the concrete beam. There was significant cracking and lifting of cracked concrete pieces at the top surface of the beam as shown in Figure 4.37(a). Figure 4.37(b) shows large and small concrete pieces in the vicinity of the headed bar after large cracked pieces at the top were removed. Additionally, Figure 4.38 shows the breakout crack pattern developed in the beam at the end of the test. The maximum depth of the cone-shaped breakout crack was measured to be 12 in. on one face of the beam and 11.5 in. on the other face. The average angle of the inclined cracks was around 34 degrees.

The anchorage failure mode observed for Specimen 7 was a combination of concrete breakout and crushing of the concrete above the T head. Specimen 7 had the same bar embedment length and target concrete strength as Specimen 4, except that Specimen 7 had a larger head size. Specimen 7 had anchorage failure at 188 kips while Specimen 4 had failure occurring at 173 kips.

(a) Lifting of cracked concrete pieces at the surface of the beam

(b) Crushing in the vicinity of the headed bar

Figure 4.37: Damage in the concrete beam of Specimen 7

(a) Side Face 1

(b) Side Face 2

Figure 4.38: Breakout cracks in Specimen 7

4.8.2 Test Results

Figure 4.39 shows the pull force applied to the headed bar plotted against time. The ultimate load reached was 188 kips. Figure 4.40 shows the tensile strains developed at different locations along the headed bar over time, while Figure 4.41 and Figure 4.42 show the tensile strains in the stirrups. They were measured by the strain gauges, whose locations are shown in Figures D.92 and D.93 in Appendix D.

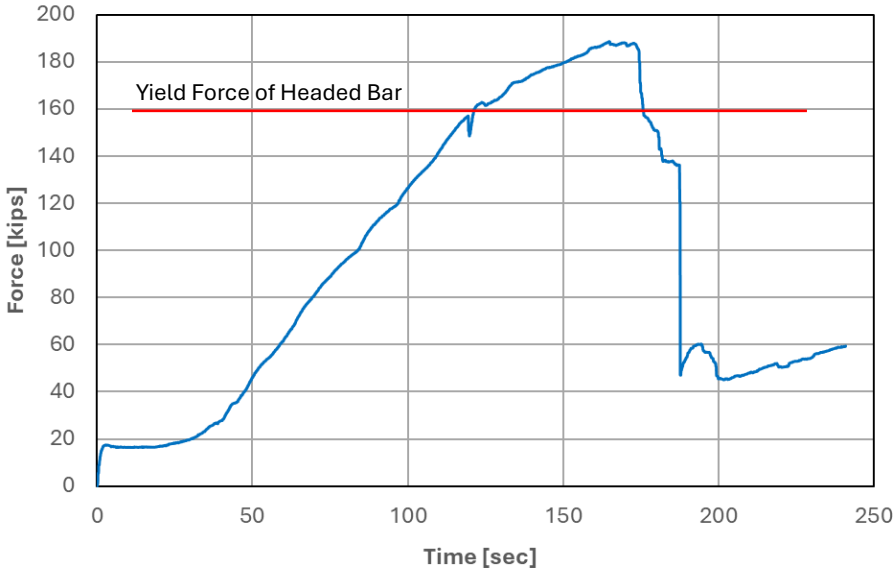

Figure 4.39: Pull force applied to the headed bar versus time for Specimen 7

It can be observed from Figure 4.40 that the strains measured by gauges SG01 and SG02 had a rapid increase at around 160 seconds when the applied force was around the ultimate load value of 188 kips. After this point, the strain in the headed bar at this location exceeded the yield value. The strains measured by the rest of the strain gauges exceeded the yield value and experienced significant plastic deformation soon after 125 seconds. Gauges SG05 and SG06, which were located 1.5 in. above the top face of the beam, registered a jump in strain at around 125 sec. when the applied force reached the yield strength of the headed bar (160 kips). The strain at this location continued to increase significantly until the applied force reached its maximum value of 188 kips. Gauge SG03,

which was located 7 in. above the T head, saw a rapid increase in strain at around 140 seconds. The applied force at this time was slightly under 180 kips. Furthermore, the dips in the strains after that are due to the unloading of the bar. The bar was then reloaded to about 60 kips, and the strains along the headed bar stayed relatively constant.

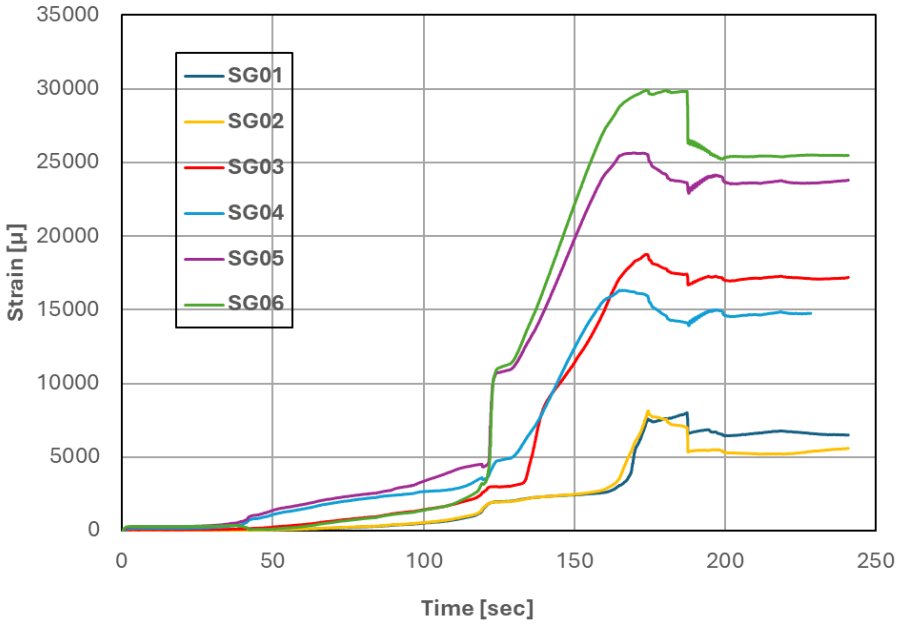

Figure 4.40: Strains along headed bar versus time for Specimen 7

The four sets of stirrups adjacent to the headed bar had 8 strain gauges in total, but one of the gauges did not function. The strains registered by the functioning gauges on the outer and inner stirrups are plotted in Figure 4.41 and Figure 4.42, respectively. The yield and tensile strengths of the stirrups were 65.9 ksi and 90.7 ksi, respectively, and the yield strain was 0.0023. The strains in the outer and inner stirrups started to increase at around 117 sec. when the applied force reached 154 kips. This indicates the initiation of inclined breakout cracks which became visible during the test. Almost all the stirrups experienced significant plastic deformation.

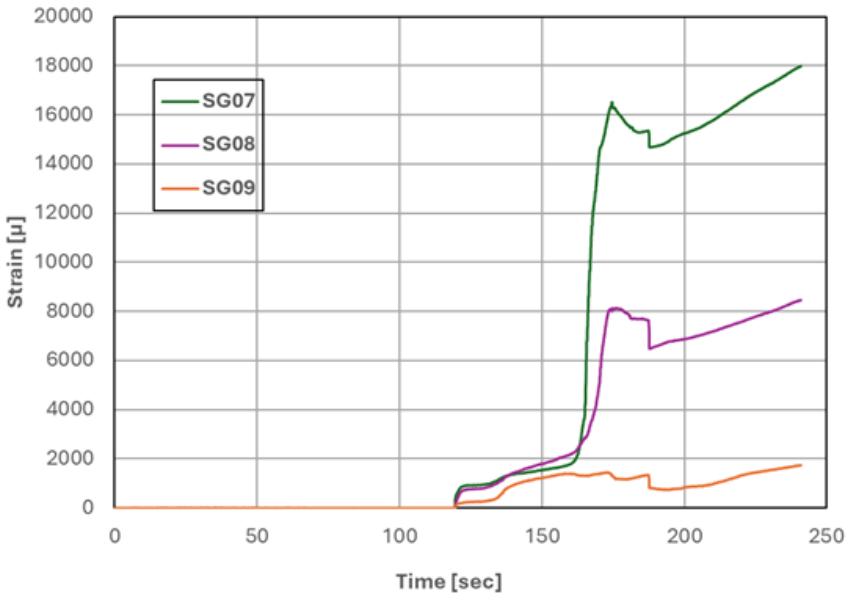

Figure 4.41: Strains in outer stirrups versus time for Specimen 7

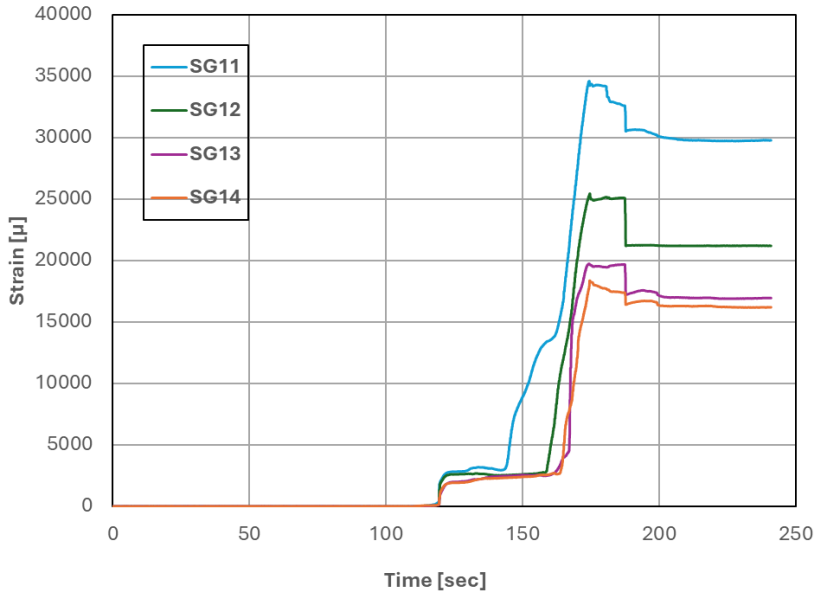

Figure 4.42: Strains in inner stirrups versus time for Specimen 7

Strains developed in the headed bar and stirrups at time instants of interest are shown in Table 4.8.

Table 4.8: Strains in headed bar and stirrups at different load levels for Specimen 7

Time (sec)	Force Applied (kips)	SG01 (μstr)	SG02 (μstr)	SG03 (μstr)	SG04 (μstr)	SG05 (μstr)	SG06 (μstr)
30	20	30	38	91	234	370	314
52	50	68	76	281	1201	1496	163
97	120	462	484	1309	2542	3095	1264
117	154	1008	1089	2178	3302	4433	2496
119	151	1426	1514	2613	3507	4357	3163
121	160	1806	1832	2912	3666	4525	3861
123	162	1927	1931	2988	4267	9445	9183
140	175	2323	2325	8671	8472	15200	16789
173	188	6702	7094	18632	16086	25643	29809

Time (sec)	Force Applied (kips)	SG07 (μstr)	SG08 (μstr)	SG09 (μstr)	SG11 (μstr)	SG12 (μstr)	SG13 (μstr)	SG14 (μstr)
30	20	0	0	0	0	0	0	0
52	50	0	0	0	0	0	0	0
97	120	0	0	0	0	0	0	8
117	154	0	0	0	121	15	68	91
119	151	390	106	68	1828	1357	659	736
121	160	838	651	204	2589	2390	1652	1710
123	162	902	726	234	2779	2565	1910	1885
140	175	1397	1454	975	3000	2535	2442	2312
173	188	15724	7720	1453	32664	23931	19010	16061

Table 4.8 shows that the strains in the inner stirrups started to increase when the applied force reached 154 kips (at 117 sec.), indicating the initiation of the inclined breakout cracks. The strains in some of the inner stirrups exceeded the yield value at around 160 kips (121 sec.). The outer stirrups were engaged right after the inner stirrups were engaged, which happened when the applied force dropped from 154 kips to 151 kips (119 sec.). This indicates that the breakout cracks had fully propagated in a very short amount of time. All the inner stirrups yielded when the applied force reached 175 kips. At the ultimate load of 188 kips, all the stirrups had significant plastic strains, and the average tensile strain registered in the headed bar near the head was 0.00690, which

corresponds to a bar tensile force of 162 kips according to the bar force-vs.-strain plot shown in Figure D.20 in Appendix D (Specimens 7 and 2 were from the same batch of No. 14 headed bars). Hence, the maximum bearing resistance provided by the T head was around 162 kips, while the remaining 27 kips of the applied force was carried by the bond stress along the bar.

4.9 Specimen 8

4.9.1 General Observations

Specimen 8 had two side-by-side No.14 headed bars spaced 8 in. apart center-to-center. The two bars are identified as bar A and bar B in the data presented below. Each headed bar had an embedment length of 24 in., which was equal to 100% of the minimum development length required by ACI 318-19. The net bearing area of the T heads was $4A_b$. On the day of the test, the compressive strength of the concrete was 4,200 psi, with the target strength equal to 4,000 psi. The maximum total pull force applied to the two bars was 469 kips, which corresponds to a tensile stress of 104 ksi in each bar assuming that the load was equally shared by the bars. This was close to the expected tensile strength of the bars and higher than the fracture strength attained by similar bars in the single-bar specimens that had been tested. Breakout cracks initiated during the test when the total applied force was around 250 kips. Figure 4.43 shows the damage on the top of the concrete beam. There were cracks radiating from the bars, and cracked concrete pieces were lifted by the bars as they were pulled.

Figure 4.44 shows the breakout crack pattern developed in the beam at the end of the test. The maximum depth of the cone-shaped breakout crack was measured to be 25 in. on one face of the beam and 23 in. on the other face. The average angle of the inclined cracks was around 36 degrees. The cracks remained fine.

Figure 4.43: Damage on top of the concrete beam of Specimen 8

(a) Side Face 1

(b) Side Face 2

Figure 4.44: Breakout cracks in Specimen 8

4.9.2 Test Results

Figure 4.45 shows the total pull force applied to the headed bars plotted against time. The ultimate load reached was 469 kips. Figure 4.46 shows the tensile strains developed at different locations along the headed bars over time. They were measured by strain gauges, whose locations are shown in Figures D.107 and D.108 in Appendix D. The letter A or B at the end of the gauge numbers for the headed bar gauges identifies the headed bar they were associated with. The letter A or B at the end of the stirrup gauges identifies the leg of each stirrup set they were associated with, as shown in Figure D.108.

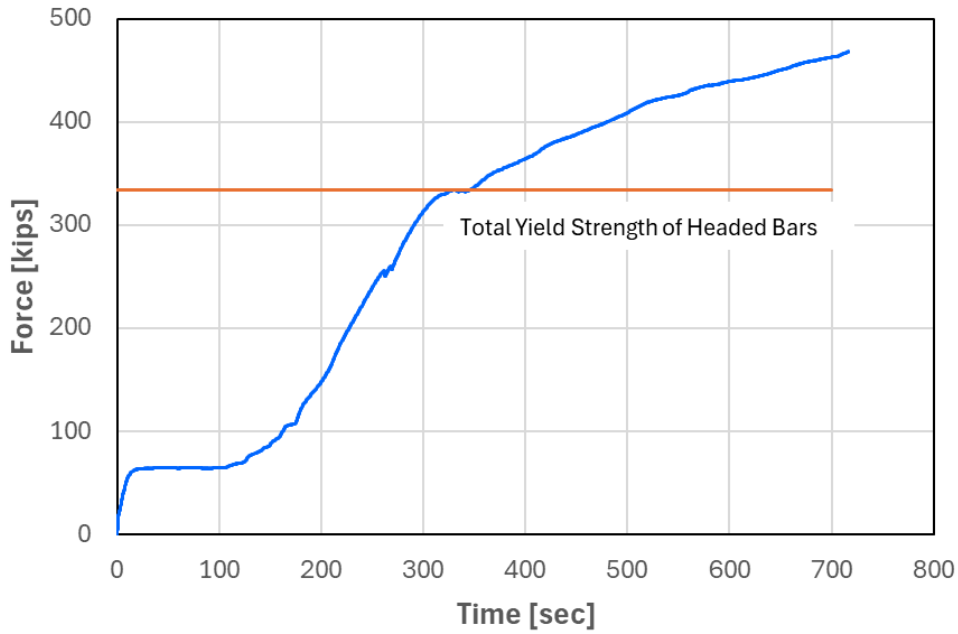

Figure 4.45: Total pull force applied to headed bars versus time for Specimen 8

It can be observed from Figure 4.46 that the strains measured by gauges SG01A, SG02A, SG01B, and SG02B, which were close to the T heads, showed a small drop at around 260 sec. when the applied load was about 250 kips, suggesting the initiation of breakout cracks in the concrete. The strain values continued to increase after the drop except for the strain registered by SG01A, which remained more or less constant and started to increase after 450 seconds. The strain registered by SG02A was higher than that by SG01A. Gauges SG02A and SG01B stopped functioning earlier than the others. The average strain value in the bars near the T heads did not exceed the yield value, but the strain measured by SG01B barely reached the yield level. As shown in Figure 4.46(b), the strains measured by the upper gauges on the two headed bars reached the yield value at about 330 seconds. Unlike the other gauge readings, SG05A showed a strain decrease after 500 seconds. This could be due to the detachment of the gauge from the bar.

Gauges SG06A, SG07A, SG06B, and SG07B, which were located on the two bars 1.0 in. above the top face of the beam, registered a jump in strains at around 330 sec. due to the initiation of bar

yielding. The strains at this location continued to increase until the total applied force reached its maximum value of 469 kips.

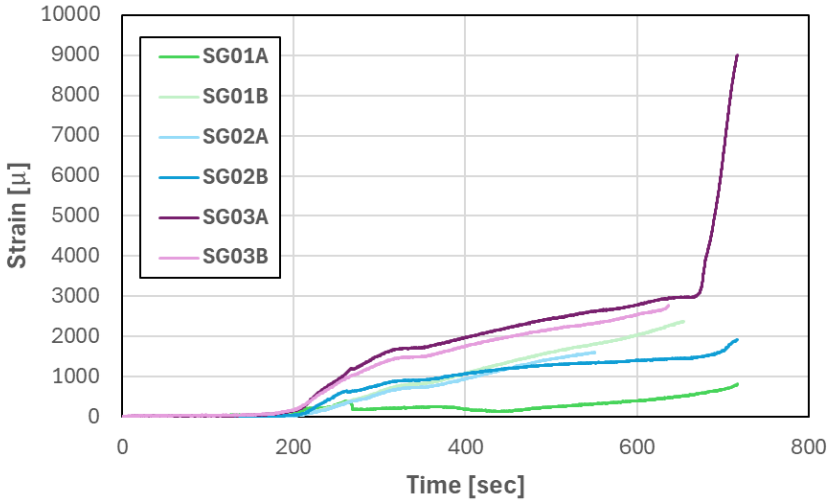

(a)

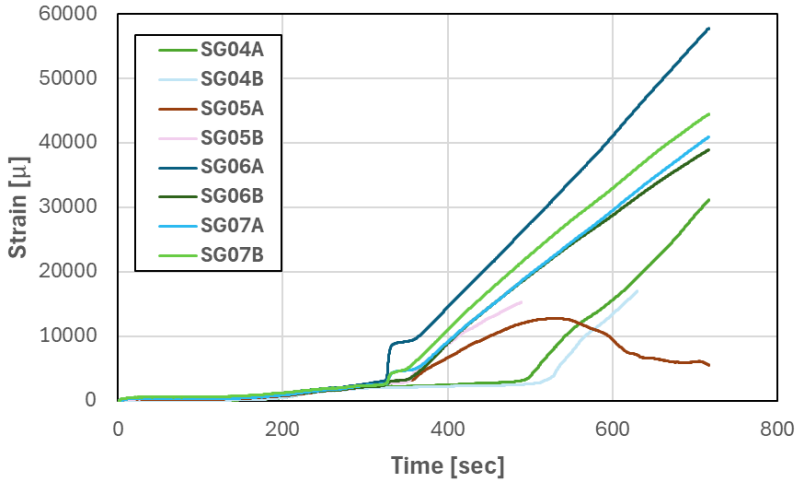

(b)

Figure 4.46: Strains along headed bars versus time for Specimen 8

For Specimen 8, stirrups were spaced at 12 in. on center. Each set of stirrups consisted of two rectangular ties (with fours legs). Strain gauges were mounted on the seven sets of stirrups closest to the two headed bars where concrete breakout cracks could develop. One set of stirrups

was located midway between the two headed bars, and it is identified as the middle set. The two sets of stirrups that were 1 ft. away from the middle set are identified as Group 1. Those that were 2 ft. and 3 ft. away from the middle set are identified as Group 2 and Group 3, respectively. For the stirrups in Gorup 1 and Group 2 and the middle set, one strain gauge was mounted on each of the two outer legs, as shown in Figure D.108. The two gauges in each set have the same identity number but are distinguished by a suffix A or B. Each set in Group 3 had only one gauge, which was mounted on one of the outer legs. Figure 4.47 through Figure 4.50 show the strains measured from the four groups of stirrups.

As shown in the figures, the strains in the stirrups showed a significant jump at 260 sec., suggesting the initiation of breakout cracks in the concrete beam. The stirrups closer to the headed bars had higher strains. The middle set yielded at about 500 sec., while the stirrups in Group 1 yielded at about 300 sec., but the highest strain attained in these stirrups did not exceed 0.0034. Stirrups in Groups 2 and 3 did not yield. Strains in Group 3 stirrups were so small that the measurements were dominated by noise. The values are practically negligible. This is consistent with the fact that concrete breakout failure did not occur.

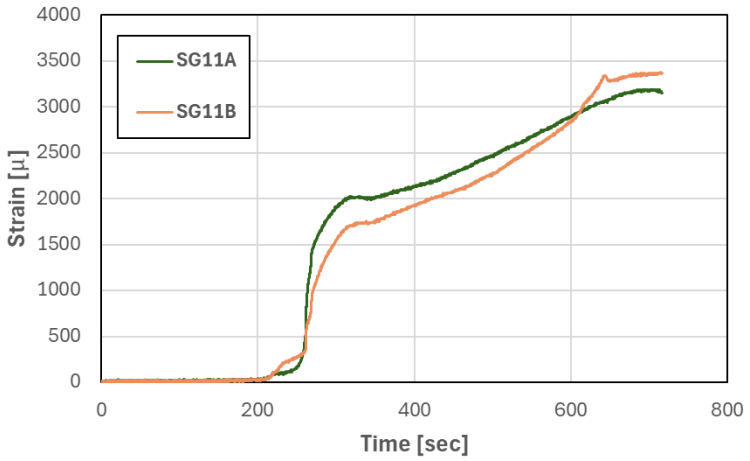

Figure 4.47: Strains in the middle stirrup set versus time for Specimen 8

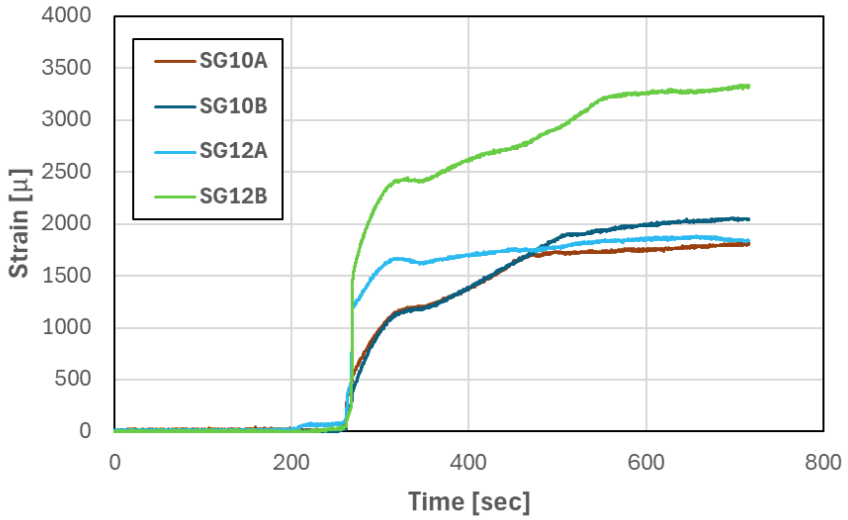

Figure 4.48: Strains in Group 1 stirrups versus time for Specimen 8

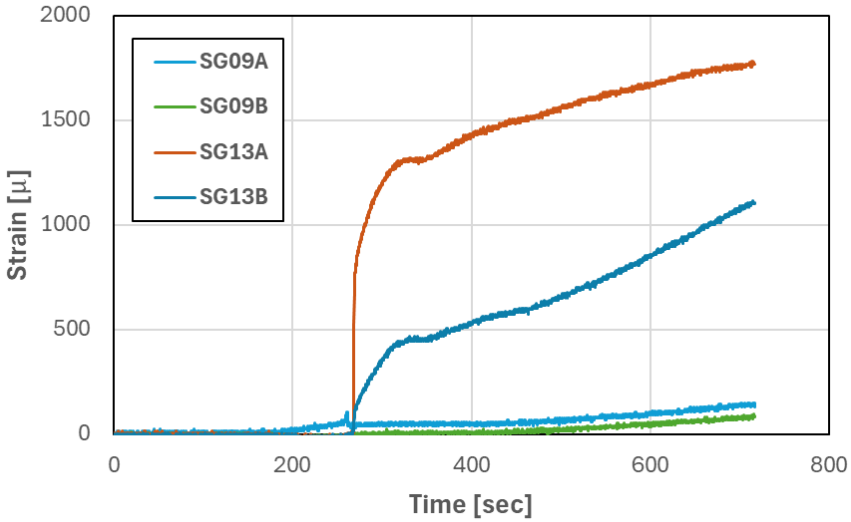

Figure 4.49: Strains in Group 2 stirrups versus time for Specimen 8

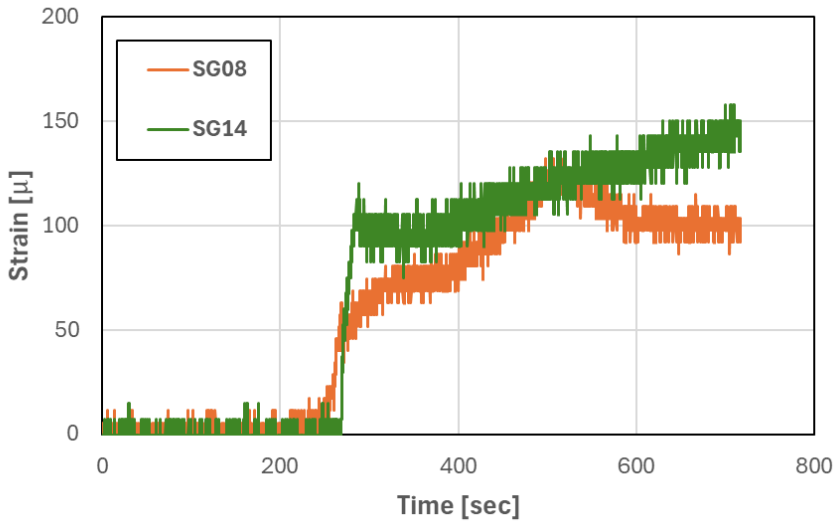

Figure 4.50: Strains in Group 3 stirrups versus time for Specimen 8

Table 4.9 shows the strains in the two headed bars, A and B, at selected time instants. At the ultimate load of 469 kips, the tensile strain registered near the head of Bar A was 0.00082 and that near the head of Bar B was 0.0019. Hence, plastic deformation did not propagate into the region adjacent to the T heads. The average bearing resistance developed by each T head was 89 kips.

Table 4.9: Strains in headed bars A and B at different load levels for Specimen 8

Time (sec)	Force Applied (kips)	Bar A						
		SG01A (μstr)	SG02A (μstr)	SG03A (μstr)	SG04A (μstr)	SG05A (μstr)	SG06A (μstr)	SG07A (μstr)
20	63	22	15	30	83	218	505	308
113	67	52	8	38	90	234	542	330
173	107	67	15	68	218	490	911	548
262	254	404	361	1116	1675	1697	1998	1798
335	333	232	722	1713	2242	2923	8817	4435
369	351	247	805	1819	2325	4441	10444	5572
498	408	239	1430	2432	3583	12285	27318	19459
524	420	284	1513	2523	7429	12741	30677	21996
680	459	613	-	3956	25730	-	52626	37496
717	469	822	-	8995	31145	-	57784	40925

Time (sec)	Force Applied (kips)	Bar B						
		SG01B (μstr)	SG02B (μstr)	SG03B (μstr)	SG04B (μstr)	SG05B (μstr)	SG06B (μstr)	SG07B (μstr)
20	63	15	23	38	83	258	324	541
113	67	15	15	45	83	302	354	579
173	107	30	15	83	234	568	595	925
262	254	384	656	995	1562	1602	1630	1949
335	333	805	920	1485	2068	2736	3106	4413
369	351	903	965	1598	2144	5666	4921	7058
498	408	1611	1297	2173	2605	-	19282	22435
524	420	1710	1327	2248	3515	-	21850	25249
680	459	-	1524	-	-	-	36009	41149
717	469	-	1917	-	-	-	38916	44464

Table 4.10 shows that the tensile strains in Group 1 and the middle stirrups started to increase rapidly when the applied force reached 254 kips (at 262 sec.), indicating the initiation of the inclined breakout cracks. The strain in the stirrup close to Bar B in Group 1 reached the yield value when the applied force was 333 kips (335 sec.). At the ultimate load of 469 kips, the strain gauges on the stirrups located on one side of the specimen in Group 1 registered higher strains than those on the other side. The middle stirrups yielded when the applied force reached 408 kips.

Table 4.10: Strains in stirrups at different load levels for Specimen 8

Time (sec)	Force Applied (kips)	Middle Stirrup Set		Group 1 Stirrups			
		SG11A (μstr)	SG11B (μstr)	SG10A (μstr)	SG10B (μstr)	SG12A (μstr)	SG12B (μstr)
20	63	15	15	15	23	15	0
113	67	23	15	30	8	15	0
173	107	15	30	30	15	15	8
262	254	708	480	166	68	158	68
335	333	2013	1737	1192	1162	1648	2426
369	351	2066	1819	1268	1260	1663	2501
498	408	2474	2256	1721	1850	1776	2909
524	420	2580	2400	1729	1903	1814	3045
680	459	3170	3351	1797	2031	1859	3295
717	469	3155	3373	1812	2054	1844	3325

Time (sec)	Force Applied (kips)	Group 2 Stirrups				Group 3 Stirrups	
		SG09 (μstr)	SG09B (μstr)	SG13A (μstr)	SG13B (μstr)	SG08 (μstr)	SG14 (μstr)
20	63	0	0	0	0	0	0
113	67	0	0	0	0	0	0
173	107	0	0	0	0	0	0
262	254	60	0	0	0	35	8
335	333	53	0	1308	460	75	98
369	351	53	11	1369	490	81	98
498	408	45	23	1550	656	115	120
524	420	75	29	1596	701	121	120
680	459	135	69	1747	1025	98	136
717	469	128	80	1770	1109	104	151

4.10 Specimen 9

4.10.1 General Observations

Similar to Specimen 8, Specimen 9 had two side-by-side No.14 bars, a concrete compressive strength of 4,200 psi, with the target strength equal to 4,000 psi, and a bar embedment length of 24 inches. The only difference compared to Specimen 8 was that the T heads had a net bearing area of $9A_b$. The maximum pull force reached was 506 kips, which corresponds to a tensile stress of 112.4 ksi in each bar assuming equal load in both bars. This was close to the tensile strength of the bars. Similar to Specimen 8, no anchorage failure occurred. Breakout cracks developed during the test when the applied force reached 253 kips. Towards the end of the test, there were cracks radiating from the headed bars on the top face of the beam, and the cracked concrete pieces were lifted as the bars extended, as shown in Figure 4.51. The cracks were a little more severe than those observed from Specimen 8 probably due to a slightly higher force reached.

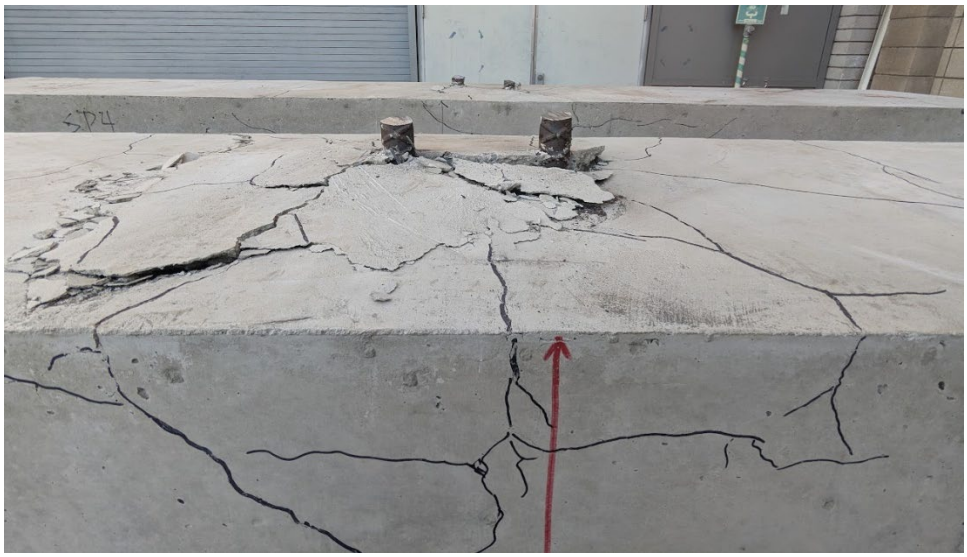

Figure 4.51: Damage on the top face of the concrete beam of Specimen 9

Figure 4.52 shows the breakout crack pattern developed on the faces of the beam at the end of the test. The maximum depth of the cone-shaped breakout crack was measured to be 26 in. on one face of the beam and 25.5 in. on the other face. The average angle of the inclined cracks was around 36 degrees.

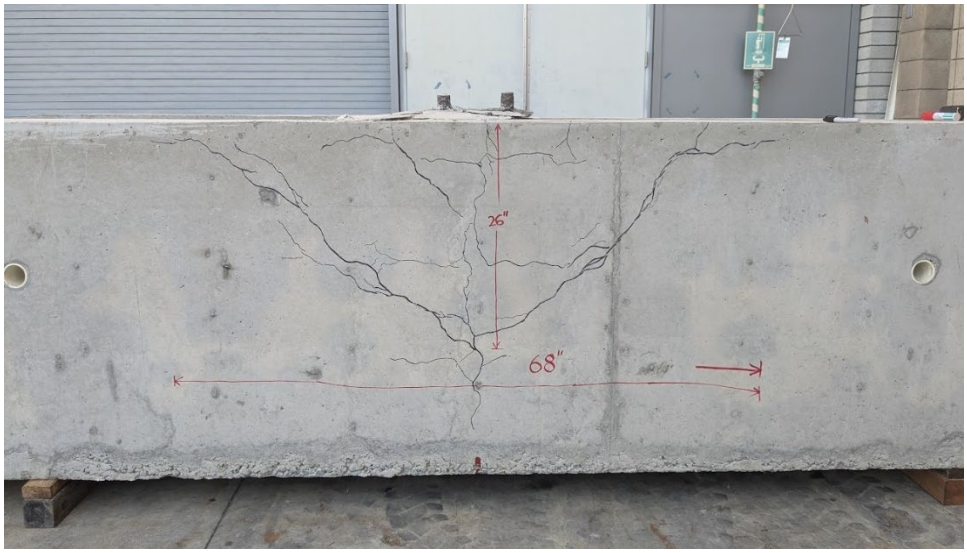

(a) Side Face 1

(b) Side Face 2

Figure 4.52: Breakout cracks in Specimen 9

4.10.2 Test Results

Figure 4.53 shows the total pull force applied to the headed bars plotted against time. The ultimate load reached was 506 kips. Figure 4.54 shows the tensile strains developed at different locations along the headed bars over time. They were measured by strain gauges, whose locations are shown in Figures D.135 and D.136 in Appendix D. The letter A or B at the end of the gauge numbers indicates the headed bar on which the gauge was mounted.

Gauges SG01A, SG01B and SG03B were damaged and did not record data during the test. Gauges SG02A and SG02B recorded strains close to the heads of the two bars up to 410 sec. during the test. It can be observed from Figure 4.54 that the strain measured by SG03A was initially higher than the strains from SG02A and SG02B, which were next to the T heads. After 162-sec. time, SG03B recorded a lower strain than gauges SG02A and SG02B. This could be caused by the initiation of cracks close to the T heads at 162 sec., which coincided with a small load drop in the force history shown in Figure 4.53. At this point, the strains in all three gauges were way lower than the yield level.

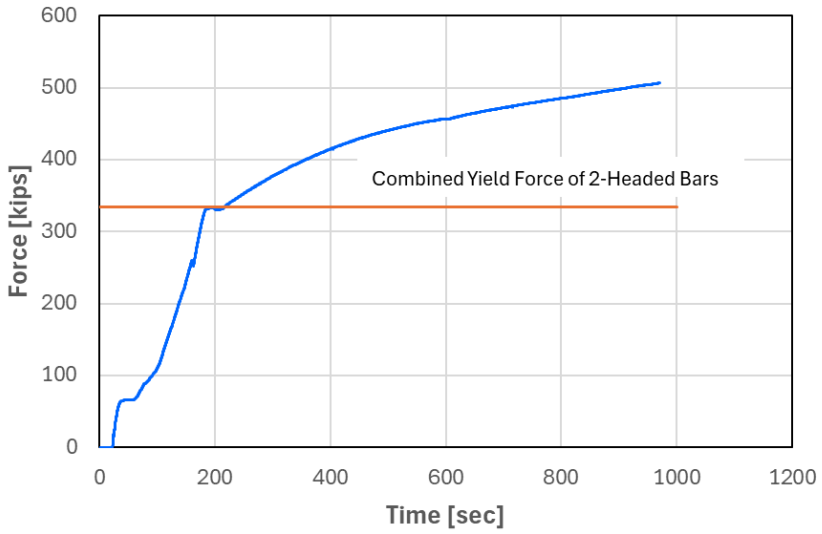

Figure 4.53: Pull force applied to the headed bar versus time for Specimen 9

Gauge SG05B did not function. Gauges SG05A, SG04A, and SG04B, registered lower strain values than gauges SG06A, SG07A, SG06B, and SG07B, which were located 1.0 in. above the top face of the beam. This indicates that the bond between the bars and the concrete remained effective at least up to 500 sec., after which gauges SG05A, SG04A, and SG04B stopped functioning. The strains registered by gauges SG06A, SG07A, SG06B, and SG07B reached the yield level at around 160 sec., and exceeded 0.1 when the peak load of 506 kips was reached. This indicates that the maximum tensile stress reached in the bars was very close to the tensile strength.

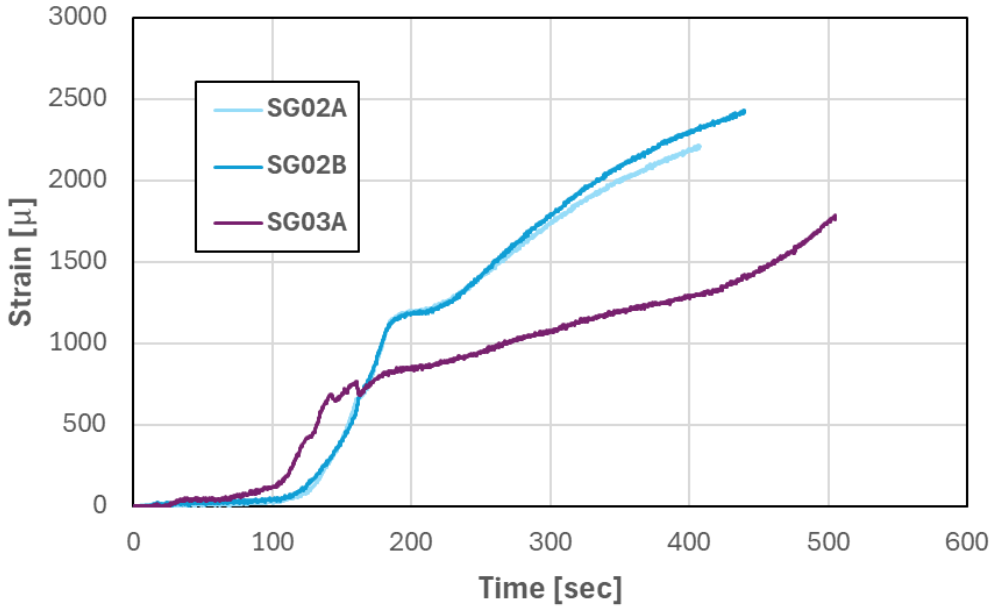

(a)

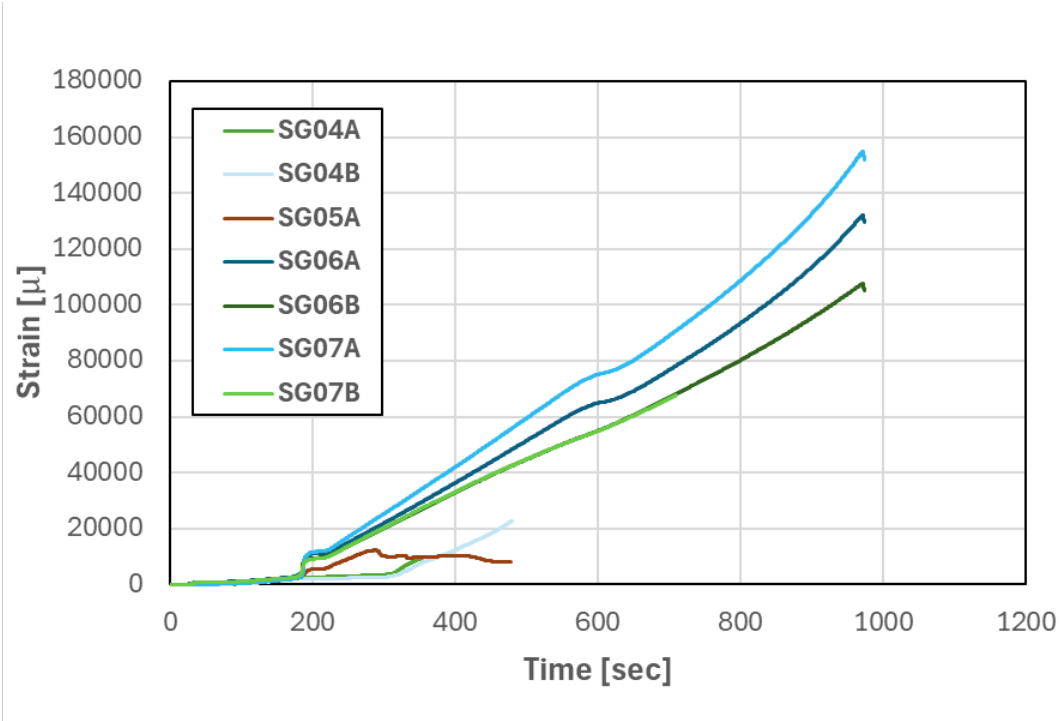

(b)

Figure 4.54: Strains along headed bars versus time for Specimen 9

Like Specimen 8, the 7 set of stirrups closest to the headed bars in Specimen 9 had strain gauges. As for Specimen 8, these stirrups are divided into four groups for the identification purpose. The middle set was between the two headed bars, the two sets 1 ft. away from the middle set belong to Group 1, the two sets 2 ft. away from the middle set belong to Group 2, and the two sets 3 ft. away from the middle set belong to Group 3. Each set had two rectangular ties (four legs), and only one of the two outer legs had a strain gauge. The locations of the gauges are shown in Figures D.135 and D.136 in Appendix D. Figure 4.55 through Figure 4.58 show the strains developed in the stirrups. At 162 sec., the time at which breakout cracks initiated, all the gauges on the stirrups recorded a jump in strain values. After the jump, the strain values increased more gradually. Only the strain values from Group 1 exceed the yield level. Similar to Specimen 8, strains in Group 3 were so small that the measurements were dominated by noise. They are practically negligible.

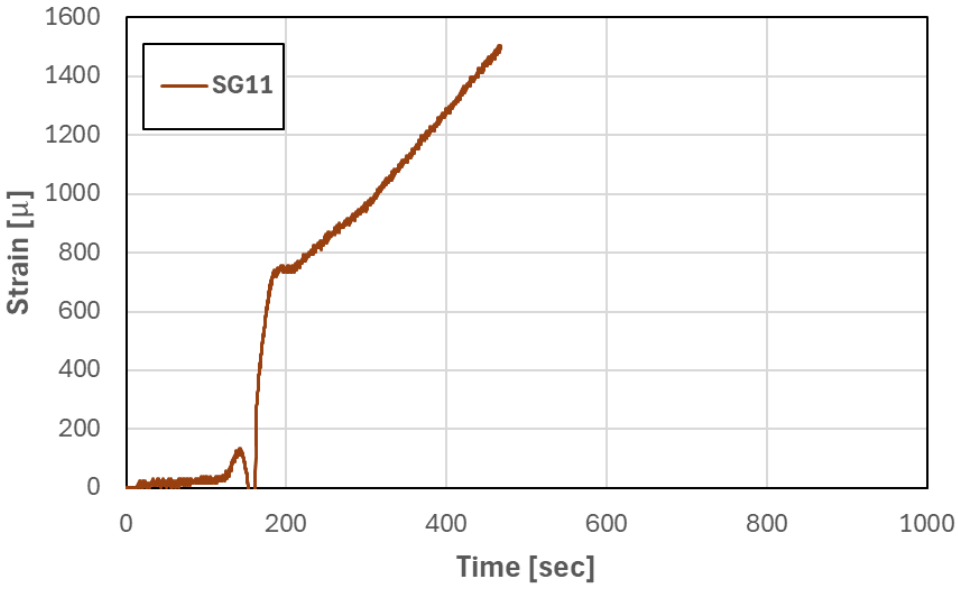

Figure 4.55: Strains in the middle stirrup set versus time for Specimen 9

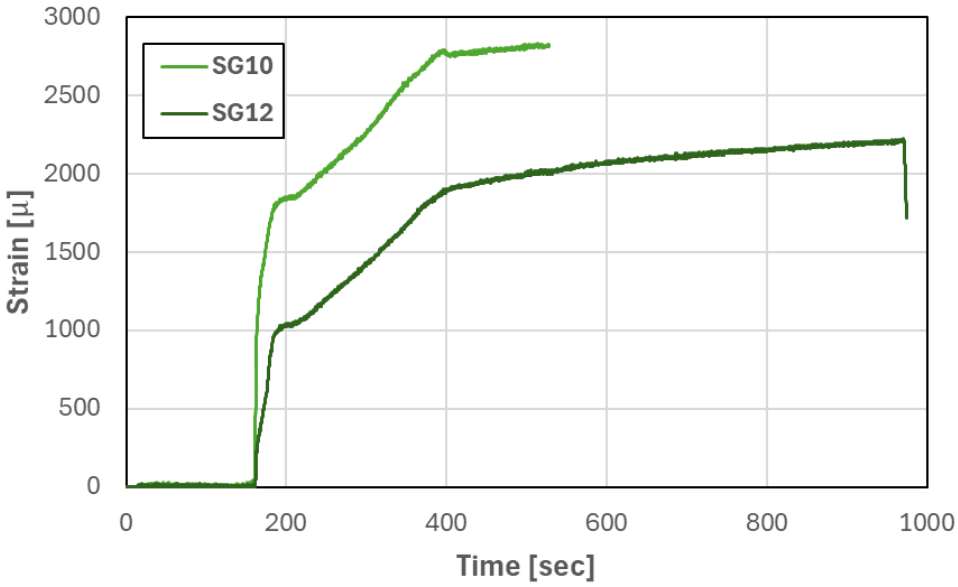

Figure 4.56: Strains in Group 1 stirrups versus time for Specimen 9

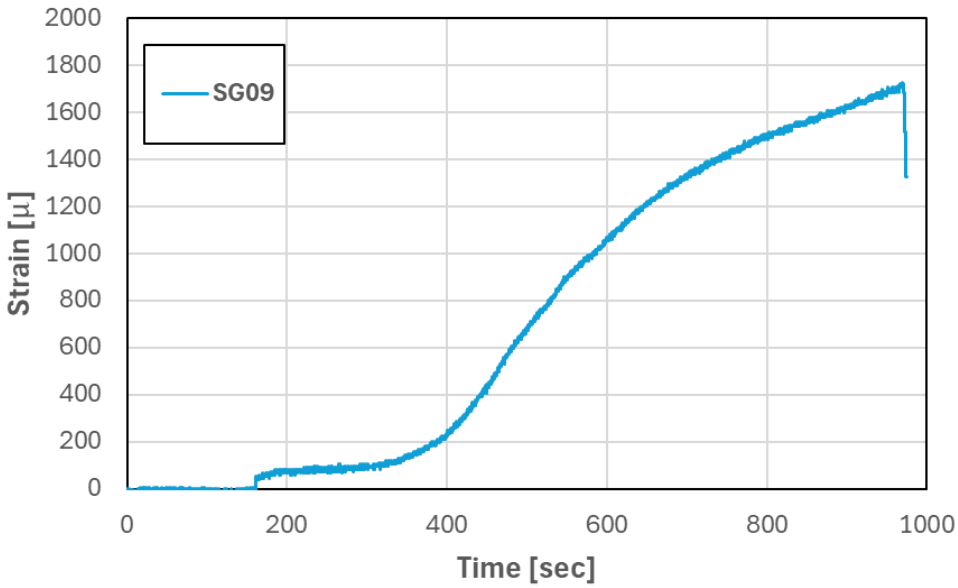

Figure 4.57: Strains in Group 2 stirrups versus time for Specimen 9

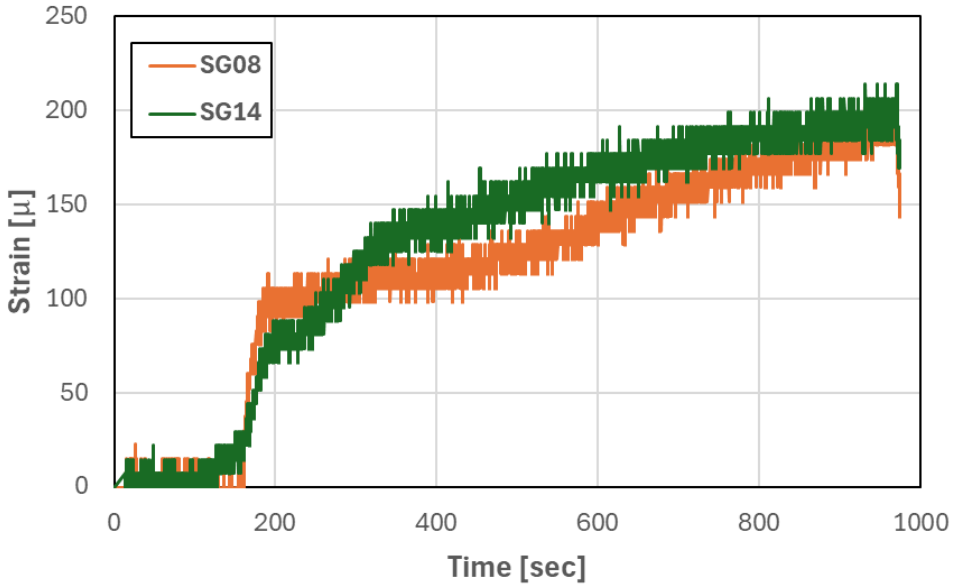

Figure 4.58: Strains in Group 3 stirrups versus time for Specimen 9

Table 4.11 shows the strain data in the two headed bars, A and B, at time instants of interest. Gauges next to the T heads, SG01A/B and SG02A/B, failed before the peak load of 506 kips were reached. At the applied force of 418 kips, the strains measured near the heads were slightly below the yield strain, while the strains in the headed bars right above the top surface of the beam way exceeded yield value. This indicates that the bond between the bars and the concrete was still effective.

Table 4.11: Strains in headed bars A and B at different load levels for Specimen 9

Time (sec)	Force Applied (kips)	Bar A						
		SG01A (μstr)	SG02A (μstr)	SG03A (μstr)	SG04A (μstr)	SG05A (μstr)	SG06A (μstr)	SG07A (μstr)
50	66	-	0	45	98	432	818	188
62	68	-	8	45	106	432	826	195
102	113	-	23	121	280	773	1281	473
162	253	-	659	689	1895	1987	2398	1670
182	328	-	1076	818	2564	2793	3853	2636
222	338	-	1250	879	2808	6223	11558	12513
283	370	-	1622	1046	3348	12137	19692	22632
410	418	-	2207	1304	-	10186	37902	43818
709	474	-	-	-	-	-	78186	90707
970	507	-	-	-	-	-	82744	96102

Time (sec)	Force Applied (kips)	Bar B						
		SG01B (μstr)	SG02B (μstr)	SG03B (μstr)	SG04B (μstr)	SG05B (μstr)	SG06B (μstr)	SG07B (μstr)
50	66	-	15	-	106	-	227	724
62	68	-	15	-	113	-	242	747
102	113	-	44	-	324	-	499	1155
162	253	-	668	-	1662	-	1681	2304
182	328	-	1091	-	2154	-	2608	3791
222	338	-	1232	-	2230	-	10408	10091
283	370	-	1671	-	2533	-	18036	18236
410	418	-	2326	-	13564	-	34193	34445
709	474	-	-	-	-	-	68130	67655
970	507	-	-	-	-	-	71848	-

Table 4.12 shows that the strains in the stirrups started to increase when the applied force reached 253 kips (at 162 sec.), indicating the initiation of breakout cracks in the beam. The strain in the middle stirrup remained below the yield value when the gauge failed at the applied force of about 433 kips (465 sec.) as shown in Figure 4.55. Only one stirrup in Group 1 reached the yield strain, which occurred when the applied load reached around 390 kips (330sec.) as shown in Figure 4.56. The

strains measured from Groups 2 and 3 did not reach the yield value at the maximum applied load of 506 kips. Strains in Group 3 were very small and negligible.

Table 4.12: Strains in stirrups at different load levels for Specimen 9

Time (sec)	Force Applied (kips)	Middle Stirrup Set	Group 1 Stirrups		Group 2 Stirrups		Group 3 Stirrups	
		SG11 (μstr)	SG10 (μstr)	SG12 (μstr)	SG09 (μstr)	SG13 (μstr)	SG08 (μstr)	SG14 (μstr)
50	66	15	0	0	0	-	0	0
62	68	23	0	0	0	-	0	0
102	113	23	0	0	0	-	8	0
162	253	205	836	121	45	-	30	22
182	328	720	1749	909	76	-	99	59
222	338	781	1906	1083	83	-	106	89
283	370	933	2183	1356	83	-	106	103
410	418	1305	2761	1910	273	-	114	133
709	474	-	-	2130	1357	-	167	177
970	507	-	-	2130	1403	-	159	184

4.11 Specimen 10

4.11.1 General Observations

Specimen 10 consisted of a single No.14 headed bar embedded in concrete that had a targeted compressive strength of 6 ksi. The embedment length of the bar was 16 in., which was 70% of the minimum required according to ACI318-19. Nevertheless, the average compressive strength of the concrete attained on the day of the bar anchorage test (51 days after casting) was 5,425 psi. The T head had a net bearing area of $4A_b$. Anchorage failure occurred in the test, and the maximum pull force reached was 179 kips, which corresponds to a tensile stress of 80 ksi. Breakout cracks initiated in the test when the applied force reached 130 kips. Figure 4.59 shows the breakout crack pattern developed on both faces of the beam at the end of the test. At the later stage of the test, the top concrete cover was lifted when the headed bar was pulled as shown in Figure 4.59 and Figure

4.60. The maximum depth of the cone-shaped breakout crack was measured to be 13 in. on one face of the beam and 14 in. on the other face. The average angle of the inclined cracks was around 34 degrees. The final anchorage failure appeared to be caused by a combination of breakout cracks and concrete crushing above the T head.

(a) Side Face 1

(b) Side Face 2

Figure 4.59: Breakout cracks in Specimen 10

Figure 4.60: Damage on the top face of the concrete beam of Specimen 10

4.11.2 Test Results

Figure 4.61 shows the pull force applied to the headed bar plotted against time. When the force reached 130 kips, a small load drop can be observed from the plot. This was caused by the initiation of breakout cracks. After that, the force continued to increase beyond the yield strength of the bar and reached the maximum load of 179 kips.

The strains in the headed bar and adjacent stirrups were measured with strain gauges whose locations are shown in Figures D.157 and D.158 in Appendix D. Figure 4.62 shows the tensile strains developed at different locations along the headed bar over time.

Strain gauges SG01 and SG02, which were close to the T head, showed a very low strain value throughout the test. However, the strain measured with SG01 was initially higher than the strains from the other gauges, which make the reading from SG01 questionable. At the peak force, the strain registered by SG01 barely reached the yield strain, while SG02 measured zero strain. Gauge SG04 did not function. At 260 sec., when the applied force reached the yield strength of the No.14 bar, the strain measured by gauge SG05 increased rapidly. At the peak force, the strain in the headed bar

outside the beam was about 10 times the yield strain but far below the strain at which the tensile strength of the bar would be reached.

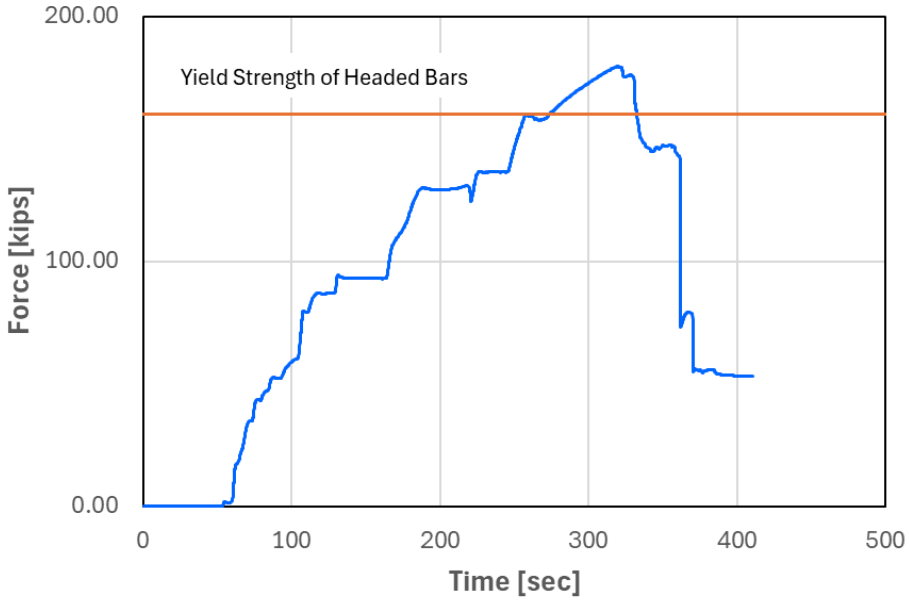

Figure 4.61: Pull force applied to the headed bar versus time for Specimen 10

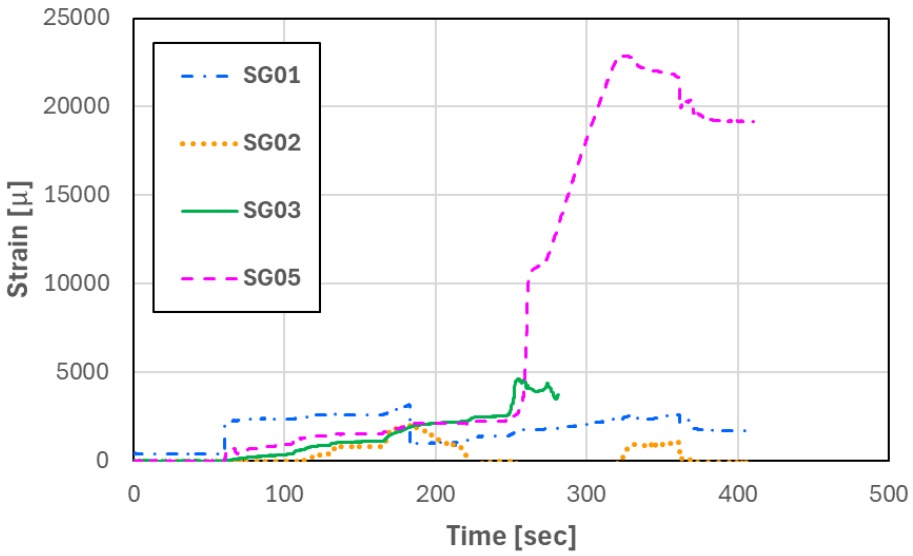

Figure 4.62: Strains along headed bars versus time for Specimen 10

Figure 4.63 and Figure 4.64 presents the strains measured with the gauges on the inner stirrups (the two stirrups closest to the headed bar) and the outer stirrups, respectively. At 220 sec. (130 kips), the strain values show a sudden jump, due to the initiation of breakout cracks, which caused a small load drop as shown in Figure 4.61. The inner stirrups developed significant yielding as the applied force approached the maximum load, while the strains in the outer stirrups were a little shy of the yield strain (with the maximum at 0.0019). The drop of the strains measured by SG09 and SG11 at the peak load could be caused by concrete crushing above the T head.

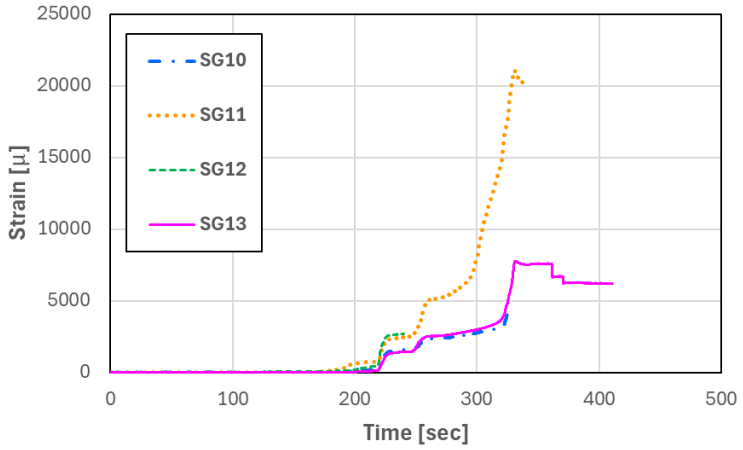

Figure 4.63: Strains in the inner stirrups versus time for Specimen 10

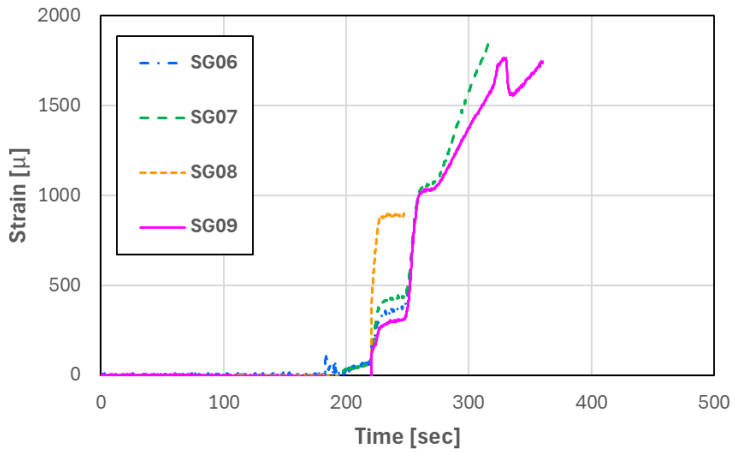

Figure 4.64: Strains in the outer stirrups versus time for Specimen 10

Table 4.13 and Table 4.14 show the strains in the headed bar and the stirrups, respectively, at time instants of interest. As shown in Table 4.13, the strain in the headed bar near the T head barely reached the yield strain. Hence, the maximum bearing resistance developed by the head was about 160 kips (the yield strength of the bar).

Table 4.13: Strains in headed bar at different load levels for Specimen 10

Time (sec)	Force Applied (kips)	SG01 (μstr)	SG02 (μstr)	SG03 (μstr)	SG04 (μstr)	SG05 (μstr)
60	3	383	0	5	-	2
80	45	2377	0	220	-	690
103	60	2353	0	372	-	948
165	97	2619	850	1136	-	1552
200	129	1029	1390	2118	-	2112
248	142	1434	-	2601	-	2349
270	158	1788	-	3957	-	11068
322	179	2398	-	-	-	22885
336	150	2342	-	-	-	22211
361	143	2628	-	-	-	21666

Table 4.14: Strains in stirrups at different load levels for Specimen 10

Time (sec)	Force Applied (kips)	SG06 (μstr)	SG07 (μstr)	SG08 (μstr)	SG09 (μstr)	SG10 (μstr)	SG11 (μstr)	SG12 (μstr)	SG13 (μstr)
60	3	6	0	0	0	0	0	0	0
80	45	6	0	0	0	0	0	10	11
103	60	2	0	0	0	0	0	12	3
165	97	4	0	0	0	0	10	49	5
200	129	9	35	0	0	98	577	164	32
248	142	397	447	934	321	1645	2611	2854	1515
270	158	-	1064	-	1034	2365	5193	-	2547
322	179	-	1967	-	1665	3267	16068	-	3966
336	150	-	-	-	1558	-	20281	-	7595
361	143	-	-	-	1749	-	-	-	7593

4.12 Specimen 11

4.12.1 General Observations

Like Specimen 10, Specimen 11 consisted of a single No.14 headed bar installed in concrete having an average compressive strength of 5,425 psi (on the day of the test) and a bar embedment length of 16 inches. However, the T head had a larger net bearing area of $9A_b$. The maximum pull force reached was 177 kips, which corresponds to a tensile stress of 79 ksi. Compared to Specimen 10, the larger bearing area of the T head did not result in a higher anchorage resistance. The crack pattern and failure mode appeared to be similar to that observed in Specimen 10. Breakout cracks initiated when the applied force reached 147 kips. The damage pattern of the specimen is shown in Figure 4.65 and Figure 4.66. The maximum depth of the cone-shaped breakout cracks was measured to be 14 in. on both faces of the beam. The average angle of the inclined cracks was about 37 degrees. Like Specimen 10, the anchorage failure mode observed for Specimen 11 was caused by a combination of concrete breakout cracks and crushing of the concrete above the T head.

(a) Side Face 1

(b) Side Face 2

Figure 4.65: Breakout cracks in Specimen 11

Figure 4.66: Damage on the top face of the concrete beam of Specimen 11

4.12.2 Test Results

Figure 4.67 shows the pull force applied to the headed bar plotted against time. The first drop in load at 147 kips was caused by the initiation of breakout cracks in the concrete. The ultimate load reached was 177 kips. After the peak load, the resistance dropped by 60%, after which the resistance

increased again gradually till it reached 96 kips. At this point, the cracked concrete cover at the top of the beam was lifted significantly.

The strains in the headed bar and adjacent stirrups were measured with strain gauges whose locations are shown in Figures D.171 and D.172 in Appendix D. Figure 4.68 shows the tensile strain developed at different locations along the headed bar over time.

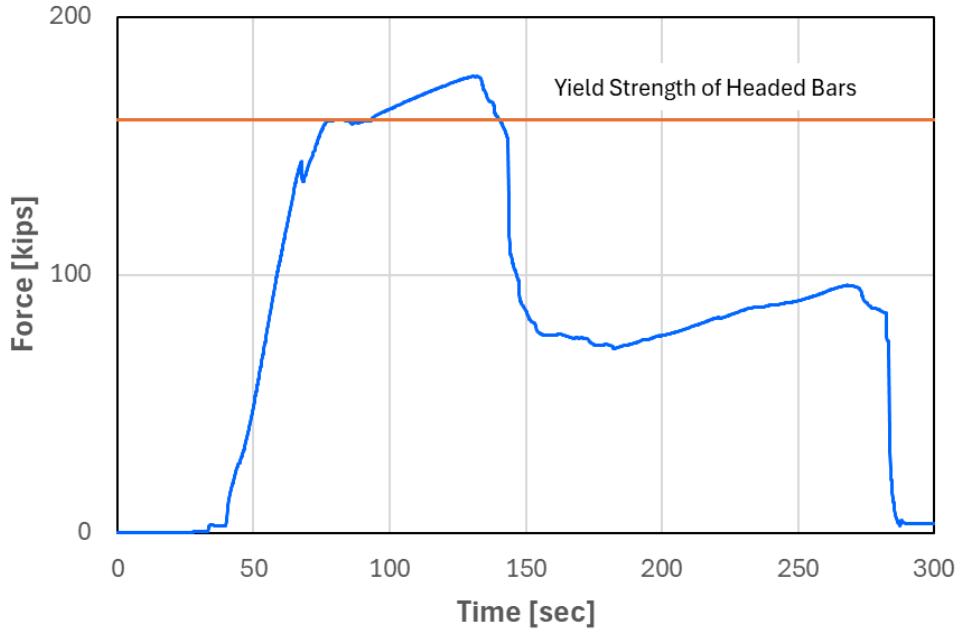

Figure 4.67: Pull force applied to the headed bar versus time for Specimen 11

Gauge SG05, which was on the headed bar outside the concrete beam, and gauges SG08 and SG13, which were on the stirrups, did not function properly. Gauge SG03, which was on the headed bar, and gauges SG10 and SG11, which were on the stirrups, got damaged early in the test soon after breakout cracks initiated. Gauge SG04, which was on the headed bar at a location slightly below the top face of the beam, registered a very high strain value of about 0.02 when the applied force reached the peak. At this point, gauges SG01 and SG02, which were close to the T head, registered strain values slightly below the yield level.

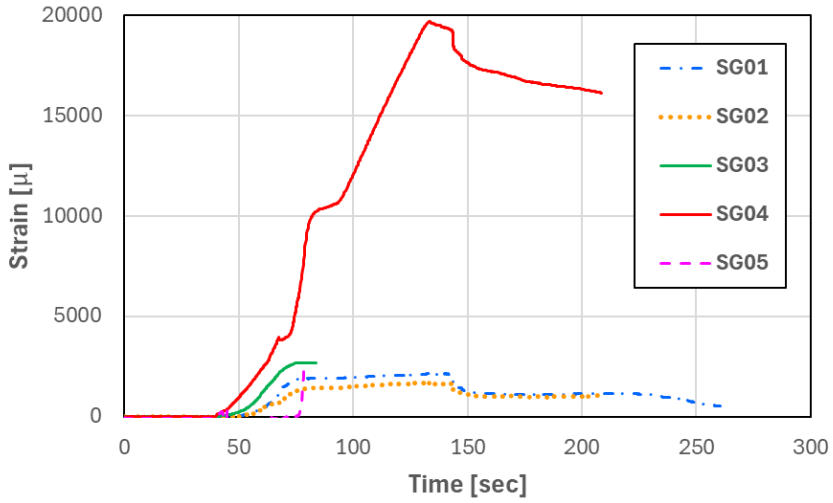

Figure 4.68: Strains along headed bars versus time for Specimen 11

Figure 4.69 and Figure 4.70 shows the strains measured in the inner and outer stirrups, respectively. Figure 4.69 shows that the strains in inner stirrups way exceeded the yield value, while Figure 4.70 shows that the maximum strain in outer stirrups was a little above the yield value when the peak force was reached.

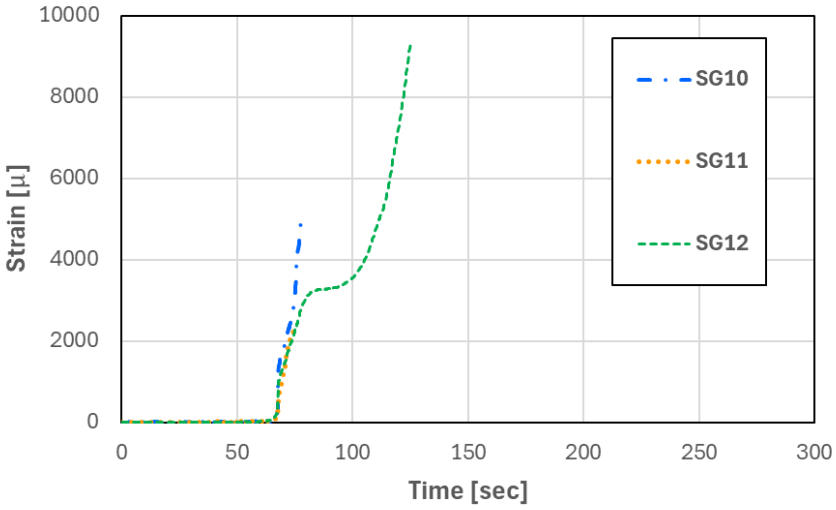

Figure 4.69: Strains in the inner stirrups versus time for Specimen 11

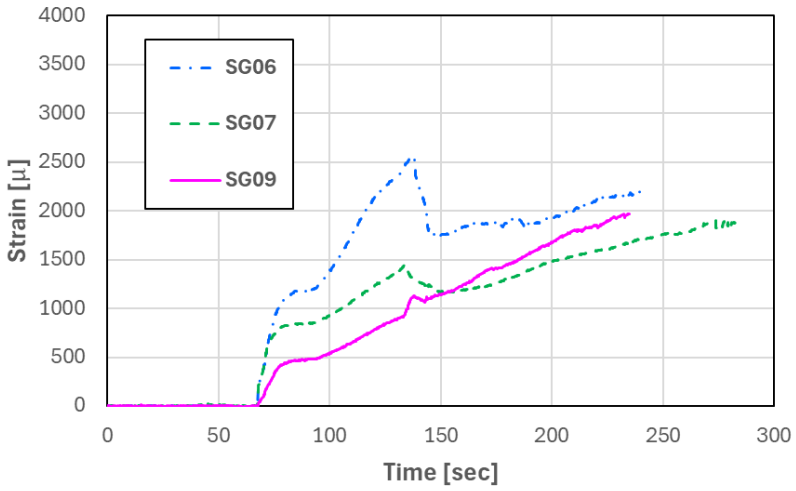

Figure 4.70: Strains in the outer stirrups versus time for Specimen 11

Table 4.15 and Table 4.16 shows the strain data in the headed bar and the stirrups at time intervals of interest. The strain in the headed bar close to the head was slightly below the yield level while the strain in the headed bars outside the beam was way above the yield value when the applied force reached the peak. This indicates that the bond between the bars and the concrete was not completely gone.

Table 4.15: Strains in headed bar at different load levels for Specimen 11

Time (sec)	Force Applied (kips)	SG01 (μstr)	SG02 (μstr)	SG03 (μstr)	SG04 (μstr)	SG05 (μstr)
41	13	7	5	31	142	-
66	137	899	673	1925	3504	-
72	147	1654	1094	2528	4037	-
82	160	1923	1424	2704	9976	-
94	161	1925	1465	2702	10728	-
100	164	1969	1505	2755	12038	-
133	177	2152	1666	-	19669	-
156	77	1180	1027	-	17315	-
182	72	1105	993	-	16608	-
271	96	371	-	-	16080	-

The strains in the stirrups had a sudden jump when the applied force reached 147 kips due to the initiation of breakout cracks.

Table 4.16: Strains in stirrups at different load levels for Specimen 11

Time (sec)	Force Applied (kips)	SG06 (μstr)	SG07 (μstr)	SG08 (μstr)	SG09 (μstr)	SG10 (μstr)	SG11 (μstr)	SG12 (μstr)	SG13 (μstr)
41	13	-2	3	-	8	5	5	4	-
66	137	-6	5	-	-2	31	63	101	-
72	147	573	586	-	188	2198	1799	1697	-
82	160	1144	837	-	465	-	-	3189	-
94	161	1210	857	-	486	-	-	3335	-
100	164	1380	929	-	541	-	-	3548	-
133	177	2429	1428	-	916	-	-	13471	-
156	77	1796	1167	-	1188	-	-	23864	-
182	72	1913	1314	-	1461	-	-	23965	-
271	96	-	1885	-	-	-	-	25225	-

4.13 Specimen 12

4.13.1 General Observations

Specimen 12 consisted of a single No.18 headed bar embedded in concrete that had a target compressive strength of 4,000 psi and an average cylinder strength of 3,935 psi (on the day of the test). The bar embedment length was 26 inches, which was 70% of the minimum required by ACI 318-19. The T head had a net bearing area of $4A_b$. The headed bar had a yield strength of 290 kips (72.5 ksi) as given by the bar force-vs.-strain curves in Figures D.193 and D.194 in Appendix D. The maximum pull force applied in the test was 369 kips, which corresponds to a tensile stress of 92 ksi. Since the force of 369 kips was close to the expected tensile strength of the bar, the test was stopped before the bar would fracture. No anchorage failure was observed. Breakout cracks developed during the test, and the cracks initiated when the force reached 290 kips, which was the yield strength of the No. 18 bar. However, the cracks did not open much throughout the test. Figure 4.71 shows the

breakout cracks on both faces of the beam at the end of the test. The maximum depth of the cone-shaped breakout crack was measured to be 24 in. on one face of the beam and 23.5 in. on the other face. The average angle of the inclined cracks was about 38 degrees. Figure 4.72 shows the damage in the concrete around the bar on the top face of the beam. The broken-off concrete piece on the top face was lifted as the headed bar developed significant plastic deformation along the embedment length. Figure 4.73 shows that the coupler, which gripped the bar and reacted against the loading beam, had a residual displacement of 2.75 in. with respect to the loading beam after the applied force had been removed. This residual displacement was mainly contributed by the plastic deformation of the headed bar with a small portion possibly contributed by the slip of the bar due to the crushing of the concrete bearing against the T head.

(a) Side Face 1

(b) Side Face 2

Figure 4.71: Breakout cracks in Specimen 12

Figure 4.72: Damage on the top face of the concrete beam of Specimen 12

Figure 4.73: Residual displacement of coupler at the end of the test for Specimen 12

4.13.2 Test Results

Figure 4.74 shows the pull force applied to the headed bar plotted against time. A small load drop can be observed at 330 sec. (290-kip force) due to the initiation of breakout cracks. The headed bar yielded at that point. The bar was unloaded at the applied force of 335 kips to correct the tilting in the loading beam. After correcting the position of the loading beam, the bar was reloaded to a load of 369 kips. This corresponds to a tensile stress of 92 ksi, which was close to the ultimate tensile strength of the bar. The test was stopped at this point to avoid large energy release that could accompany the tensile fracture of the bar.

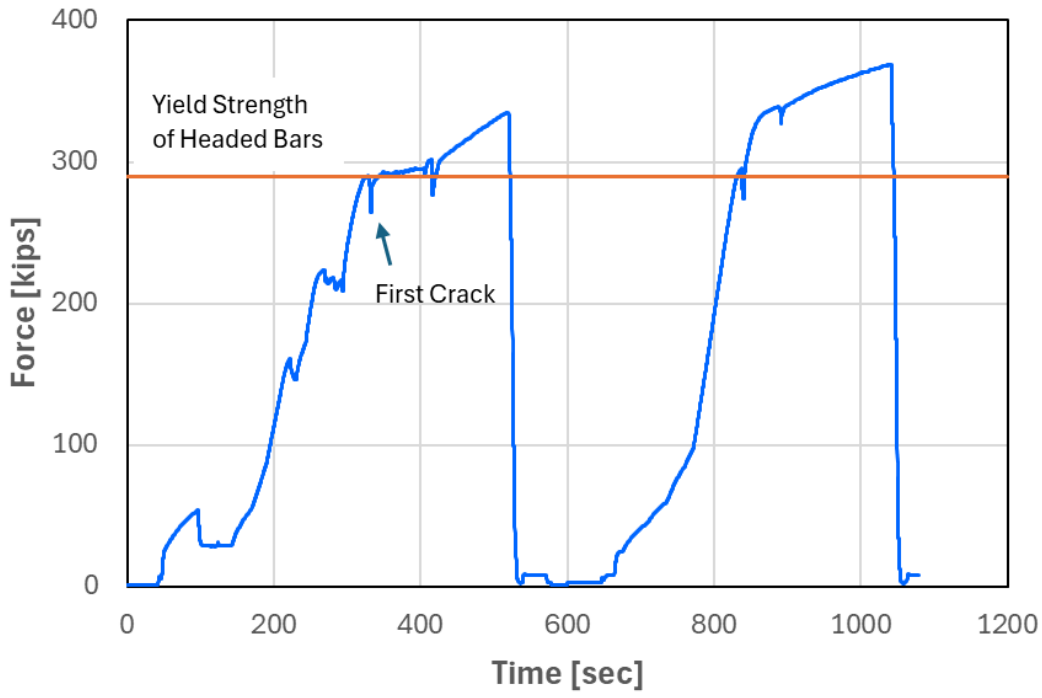

Figure 4.74: Pull force applied to the headed bar versus time for Specimen 12

Figure 4.75 shows the tensile strains developed at different locations along the headed bar over time. The strains were measured with strain gauges whose locations are shown in Figures D.185 and D.186 in Appendix D. All the gauges on the headed bar except for SG06 worked well throughout the test. At about 340 seconds, right after the headed bar had yielded, gauges SG01 and SG02, which were close to the T head, registered strains slightly lower than the yield value, suggesting some deterioration of the bond along the bar and the development of high bearing resistance at the T head. As the specimen was unloaded to correct the position of the loading beam, gauges SG04/05/07/08 registered residual strains, while the strains measured by the gauges close to the head, SG01/02/03, dropped to zero indicating no yielding at these locations. As the specimen was reloaded, the bond deterioration along the headed bar progressed deeper as SG03 showed significant strain after 900 seconds. After 1000 sec., when the specimen was loaded to the maximum load of 369 kips, the strains measured by SG01 and SG02 were more than two times the yield level.

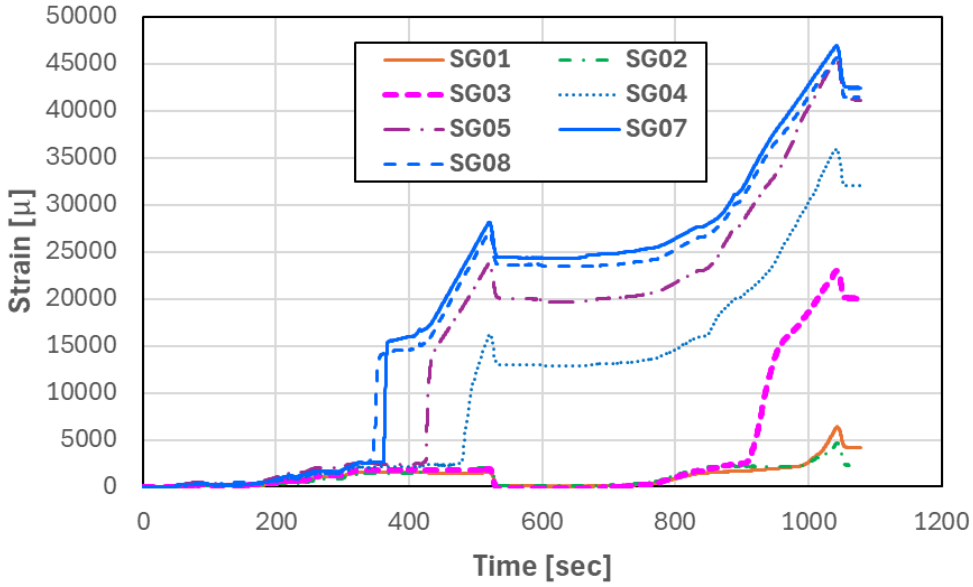

Figure 4.75: Strains along headed bars versus time for Specimen 12

Figure 4.76 through Figure 4.78 show the strains in the stirrups located 6”, 1’-6” and 2’-6” away from the headed bar on both sides. They were within the potential concrete breakout region. Gauges SG15 through SG18, which were 6” away from the headed bar, show a noticeable increase in tensile strains at about 330 sec. suggesting the initiation of breakout cracks in the beam, while all the gauges show a significant jump in strains at 426 sec. indicating the propagation of the breakout cracks. The stirrups located 2’-6” away from the headed bar did not yield while all the other stirrups yielded. However, except for the strain measured with SG12, the highest strain developed in the stirrups at the maximum load was only about two times the yield strain suggesting that the cracks did not open significantly.

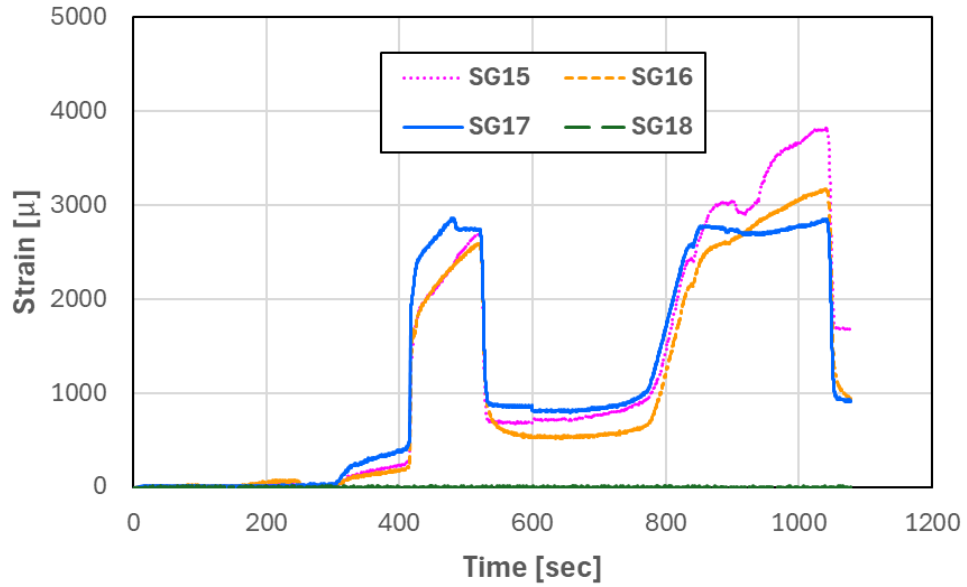

Figure 4.76: Strains in the stirrups at 6” from the bar versus time for Specimen 12

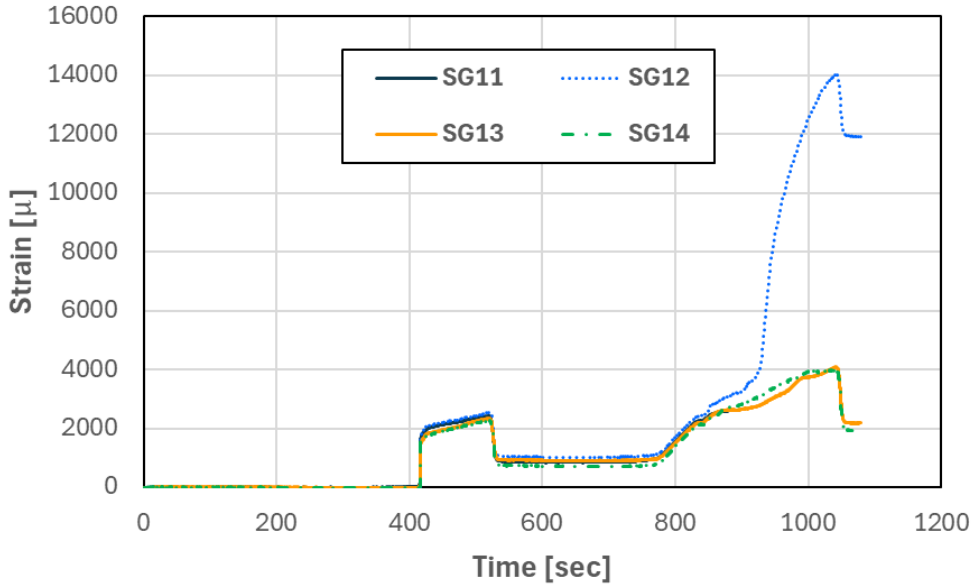

Figure 4.77: Strains in the stirrups at 1’-6” from the bar versus time for Specimen 12

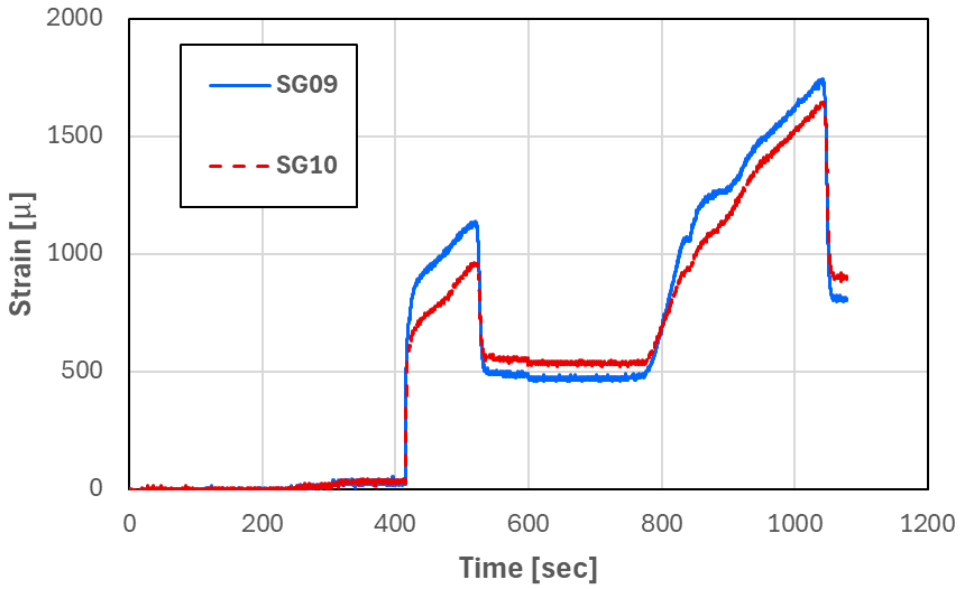

Figure 4.78: Strains in the stirrups at 2'-6" from the bar versus time for Specimen 12

Table 4.17 and Table 4.18 show the strain in the headed bar and the stirrups at time instants of interest. At the maximum applied load of 369 kips, the strain in the headed bar outside the beam was 19 times the yield value while the strains close to the head and in the stirrups were about 2 times the yield value.

Table 4.17: Strains in headed bar at different load levels for Specimen 12

Time (sec)	Force Applied (kips)	SG01 (μstr)	SG02 (μstr)	SG03 (μstr)	SG04 (μstr)	SG05 (μstr)	SG06 (μstr)	SG07 (μstr)	SG08 (μstr)
131	29	98	105	157	188	196	0	128	437
235	159	459	399	660	896	1450	0	1150	949
340	289	1498	1394	1758	2073	2473	0	2561	2650
484	324	1438	1907	1788	5591	19517	0	23687	22583
520	334	1513	2043	1871	16159	23852	0	28098	27079
680	29	68	120	-97	13028	19933	0	24687	23506
841	283	1385	1922	1683	15918	22966	0	27642	26523
893	335	1634	2179	2390	20030	27689	0	31177	30198
950	353	1913	2172	13873	23956	33142	0	37817	36624
1040	369	6088	4444	22801	35749	45399	0	46754	45436

Table 4.18: Strains in stirrups at different load levels for Specimen 12

Time (sec)	Force Applied (kips)	SG09 (μstr)	SG10 (μstr)	SG11 (μstr)	SG12 (μstr)	SG13 (μstr)	SG14 (μstr)	SG15 (μstr)	SG16 (μstr)	SG17 (μstr)	SG18 (μstr)
131	29	0	0	0	0	0	0	0	15	15	0
235	159	0	8	0	0	0	0	23	60	15	0
340	289	29	30	0	0	0	0	144	121	250	0
484	324	1031	838	2270	2366	2136	2088	2412	2378	2791	0
520	334	1134	958	2414	2555	2326	2255	2708	2606	2745	0
680	29	471	551	859	1011	897	718	750	552	835	0
841	283	1053	928	2248	2434	2197	2118	2412	2143	2562	0
893	335	1260	1132	0	3192	2621	2763	3013	2606	2722	0
950	353	1489	1382	0	8618	3068	3424	3325	2872	2707	0
1040	369	1732	1639	0	13979	4070	3964	3812	3168	2859	0

4.14 Specimen 13

4.14.1 General Observations

Specimen 13 consisted of a single No.18 headed bar embedded in concrete that had a target compressive strength of 4,000 psi and an average cylinder strength of 4,208 psi (on the day of the test). Like Specimen 12, the T head had a net bearing area of $4A_b$. However, unlike specimen 12, the bar embedment length was 37 inches, which was the minimum required by ACI 318-19. The maximum pull force applied in the test was 379 kips, which corresponds to a tensile stress of 94.8 ksi. Since the force of 379 kips was close to the expected tensile strength of the bar, the test was stopped before bar would fracture. No anchorage failure occurred. Vertical cracks developed in the beam on the two sides of the headed bar during the test, as shown in Figure 4.79. No wedge type breakout cracks were seen in the test. Figure 4.80 shows the damage in the concrete around the bar on the top face of the beam. The fine vertical cracks observed on the side faces of the beam were extensions of the radial cracks on the top face. Figure 4.81 shows that the coupler, which gripped the bar and reacted against the loading beam, had a residual displacement of 4.75 in. from the top face

of the loading beam after the applied force had been removed. Part of this residual displacement was contributed by the slip of the coupler as shown by the shiny skid mark on the bar surface. It is estimated that the plastic deformation of the headed bar contributed 4 in. to the residual displacement. This specimen had a larger residual displacement than Specimen 12. This could be due to the fact that it had a longer embedment length, which resulted in deeper plastic strain penetration.

(a) Side Face 1

(b) Side Face 2

Figure 4.79: Cracks in Specimen 13

Figure 4.80: Damage on the top face of the concrete beam of Specimen 13

Figure 4.81: Residual displacement of bar grip at the end of the test

4.14.2 Test Results

Figure 4.82 shows the pull force applied to the headed bar plotted against time. The headed bar yielded at about 460 sec. when the applied load reached 290 kips. The bar was further loaded to 379 kips before the test was terminated. This corresponds to a tensile stress of 94.8 ksi, which was close to the ultimate tensile strength of the bar. The test was stopped at this point to avoid large energy release that could be associated with the tensile fracture of the bar.

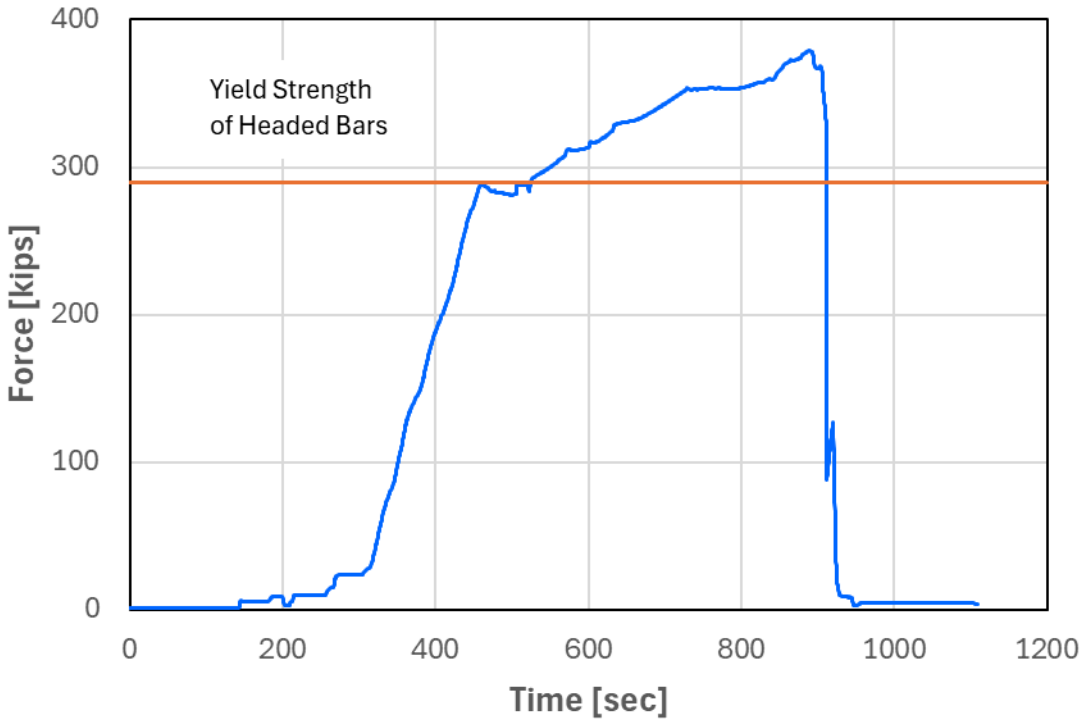

Figure 4.82: Pull force applied to the headed bar versus time for Specimen 13

Figure 4.83 shows the tensile strains developed at different locations along the headed bar over time. The strains were measured with strain gauges whose locations are shown in Figures D.205 and D.206 in Appendix D. All the gauges on the headed bar except for SG01 and SG02 worked well throughout the test. Gauges SG08 and SG09, which were above the top face of the concrete beam, showed that the bar yielded and developed a significant plastic strain after 460 seconds. At this point, gauges SG01 and SG02, which were close to the T head, and SG03 registered strains slightly lower than the yield strain, suggesting some deterioration of the bond along the bar and the development of high bearing resistance at the T head. As the load increased further, the strain measured by SG03 increased but did not reach the yield strain. Strains registered by SG05 and SG06 showed yielding at later times. Gauge SG07, which was slightly below the top face of the beam somehow registered a higher strain than SG08 and SG09.

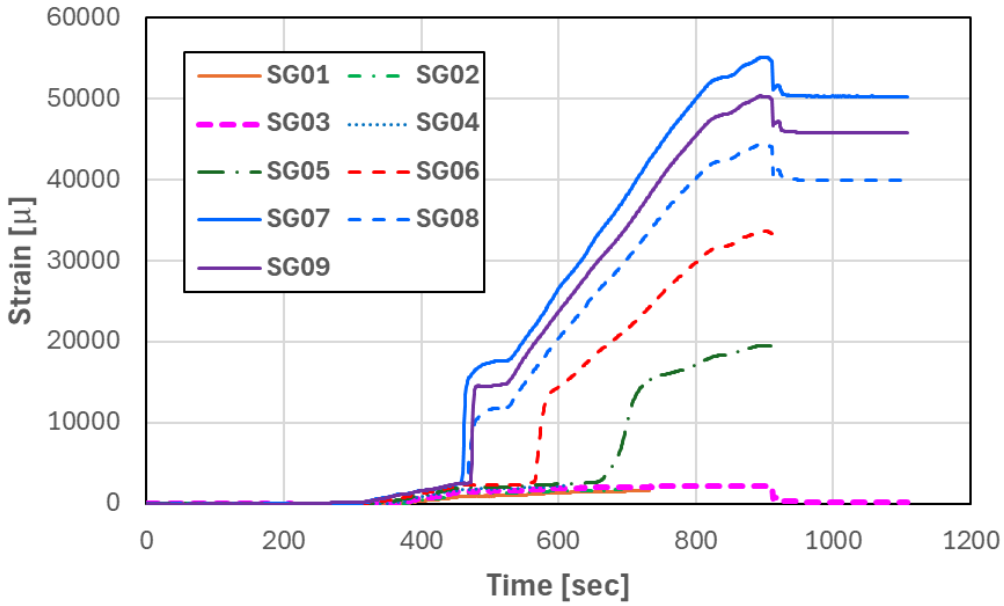

Figure 4.83: Strains along headed bars versus time for Specimen 13

Figure 4.84 though Figure 4.87 show the strains in the stirrups located 6”, 1’-6”, 2’-6” and 3’-6” away from the headed bar on both sides. They were within the potential concrete breakout region. All the gauges in the stirrups show very small strains, way below the yield level. The strains measured by these gauges were at the noise level with some negative values. This is consistent with the fact that no concrete breakout cracks occurred.

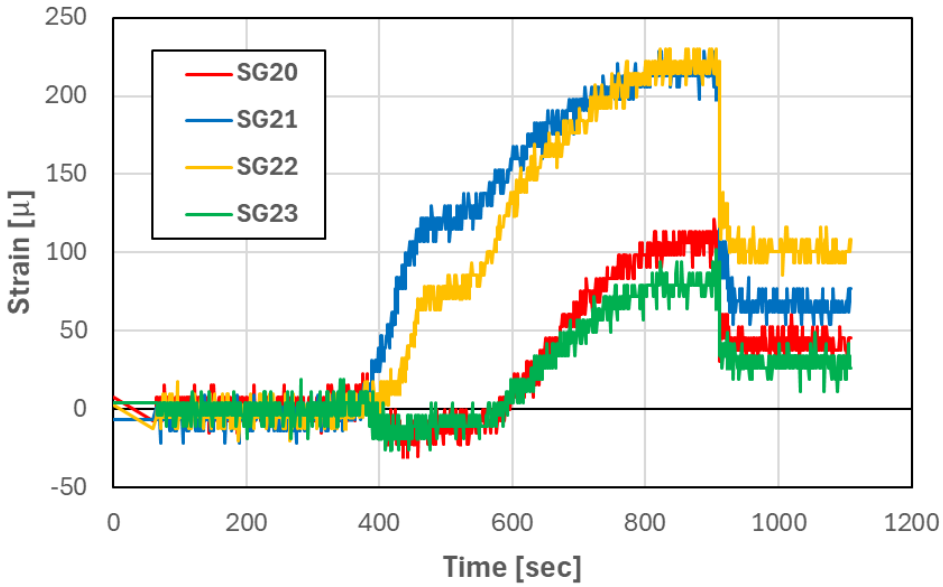

Figure 4.84: Strains in the stirrups at 6” from the bar versus time for Specimen 13

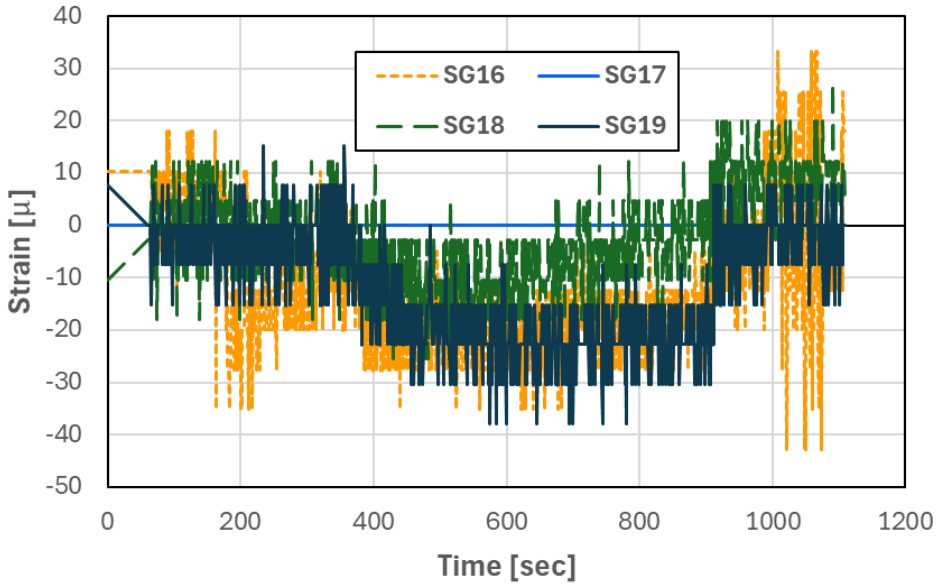

Figure 4.85: Strains in the stirrups at 1’-6” from the bar versus time for Specimen 13

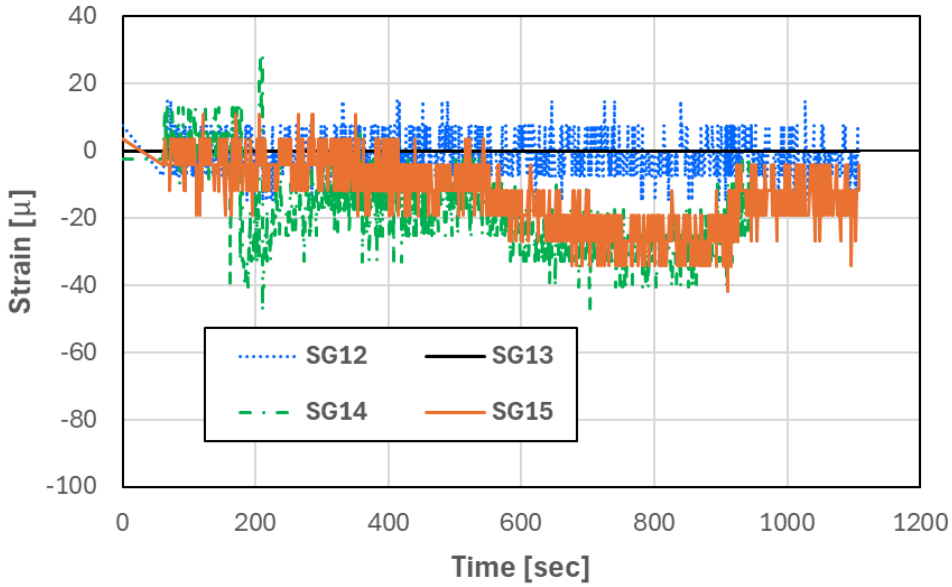

Figure 4.86: Strains in the stirrups at 2'-6" from the bar versus time for Specimen 13

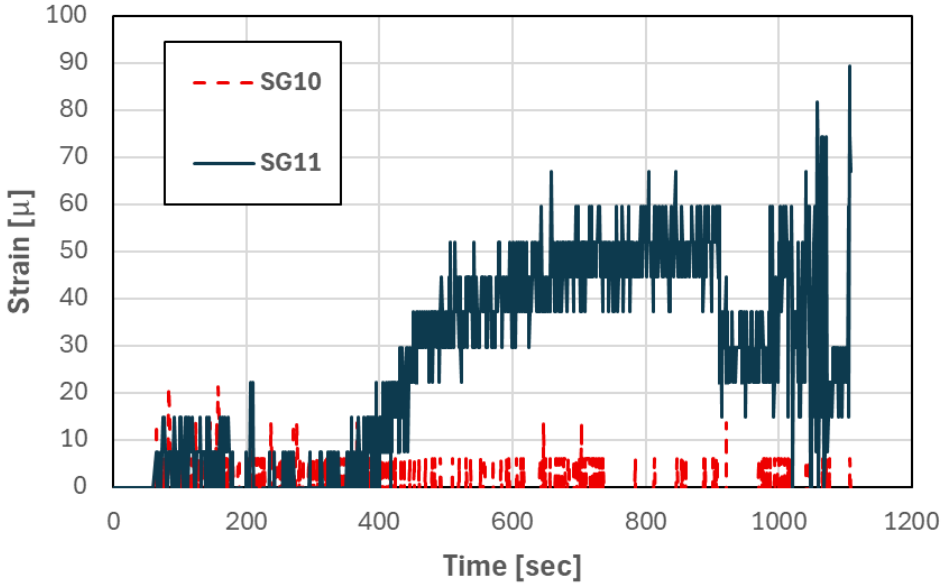

Figure 4.87: Strains in the stirrups at 3'-6" from the bar versus time for Specimen 13

Table 4.19 and Table 4.20 show the strains in the headed bar and the stirrups at time instants of interest. At the maximum applied load of 379 kips, the strain in the headed bar outside the beam was 20 times the yield strain while the strains in the stirrups were one-tenth of the yield strain. The

fact that the tensile strain registered by SG03 did not reach the yield level is an indication that the bar slip above SG03 was limited and significant bond strength remained along the bar. Similarly, the bearing resistance developed at the T head was limited.

Table 4.19: Strains in headed bar at different load levels for Specimen 13

Time (sec)	Force Applied (kips)	SG01 (μstr)	SG02 (μstr)	SG03 (μstr)	SG04 (μstr)	SG05 (μstr)	SG06 (μstr)	SG07 (μstr)	SG08 (μstr)	SG09 (μstr)
250	10	0	0	0	0	0	0	0	0	0
300	24	0	0	0	0	0	60	113	137	0
400	188	341	417	657	901	1112	1302	1605	1621	1607
460	289	961	1283	1534	1826	2053	2296	2965	2597	2519
522	285	999	1329	1571	1848	2076	2281	17625	11839	14802
570	308	1212	1496	1776	2076	2311	5244	22420	17025	20283
600	313	1356	1595	1905	2198	2448	14406	26494	20418	23685
709	346	1584	-	2109	-	12611	22251	39231	31107	35192
800	354	-	-	2208	-	17208	29771	49908	40148	45381
890	379	-	-	2253	-	19507	33590	54935	44314	50210

Table 4.20: Strains in stirrups at different load levels for Specimen 13

Time (sec)	Force Applied (kips)	SG10 (μstr)	SG11 (μstr)	SG12 (μstr)	SG13 (μstr)	SG14 (μstr)	SG15 (μstr)	SG16 (μstr)
250	10	6	0	0	0	0	0	-12
300	24	6	0	0	0	0	-4	-20
400	188	-9	0	0	0	0	4	-12
460	289	6	30	0	0	-25	-19	-20
522	285	-2	30	-7	0	-25	-12	-12
570	308	-2	37	-7	0	-25	-12	-20
600	313	-2	37	0	0	-17	-12	-28
709	346	-2	52	8	0	-25	-19	-20
800	354	-17	52	0	0	-33	-19	-20
890	379	6	60	-7	0	-33	-27	-12

Time (sec)	Force Applied (kips)	SG17 (μstr)	SG18 (μstr)	SG19 (μstr)	SG20 (μstr)	SG21 (μstr)	SG22 (μstr)	SG23 (μstr)
250	10	0	12	0	8	-14	-5	4
300	24	0	-3	-8	-7	1	3	-11
400	188	0	-3	-15	0	39	10	-11
460	289	0	-10	-15	-7	115	63	-4
522	285	0	-3	-23	0	130	71	-4
570	308	0	-10	-23	0	130	93	-11
600	313	0	-18	-38	8	160	131	4
709	346	0	-3	-23	68	190	184	49
800	354	0	-10	-15	98	221	222	79
890	379	0	5	-23	106	221	222	72

Chapter 5 Analysis of Experimental Data

5.1 Anchorage Strength of Headed Bars

As discussed in Chapter 2, the anchorage resistance of a headed bar embedded in concrete is governed by one of two possible mechanisms. One is pullout resistance, and the other is concrete breakout resistance. Pullout resistance is provided by the bonding of the bar with the surrounding concrete plus the bearing resistance of the concrete acting against the T head. Concrete breakout failure is characterized by the formation of inclined cracks radiating from the T head resulting in a cone-shaped concrete breakout. Breakout resistance depends on the tensile strength of the concrete, the surface area of the breakout cone, and the tensile strength of the tie reinforcement (stirrups) parallel to the bar crossing the inclined cracks. Figure 5.1 shows the load resisting mechanism that will develop once breakout cracks have initiated. As shown, the tensile force applied to the anchored bar is transmitted to the surrounding concrete through the bond force and the bearing force exerted by the T head, forcing the inclined cracks to open. Resistance to crack opening is provided by the tensile forces developed in the stirrups and the residual tensile and shear stresses developed along the crack planes. When the applied force exceeded the resistance, breakout failure will occur. In the following section, the aforementioned load resisting mechanisms developed in the thirteen specimens tested in this study are investigated by extracting relevant information from the strain data presented in Chapter 4.

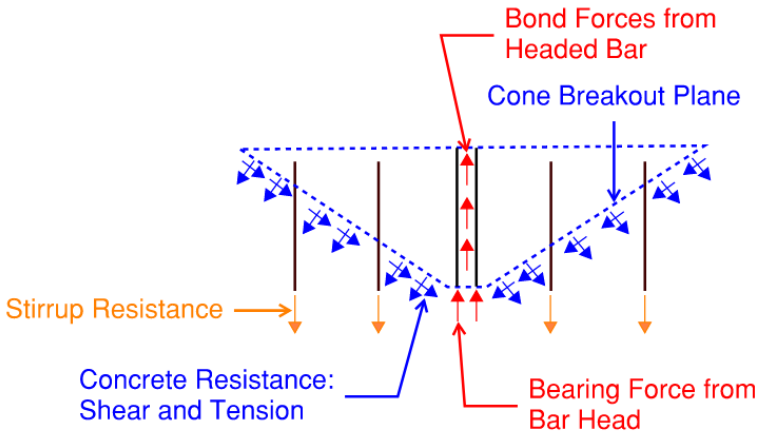

Figure 5.1: Resistance to breakout failure

5.2 Anchorage Forces Developed in Test Specimens

5.2.1 Specimen 1

Specimen 1 had one #14 headed bar with an embedment length equal to 70% of the minimum required by ACI 318-19 based on the target concrete strength of 4,000 psi. The net bearing area of the T head was $4A_b$. The average compressive strength of the concrete cylinders on the day of the anchorage test was 4,120 psi. The specimen exhibited anchorage failure. Based on the strain data presented in Table 4.2, the values of different resisting forces that contributed to the anchorage resistance in Specimen 1 have been calculated. The resisting forces include the bearing force at the T head and the bond force, which contributed to the bar pullout resistance, and the tensile forces developed in the stirrups and the resisting force developed in the concrete, which contributed to the breakout resistance. Since the bearing force at the T head should be equal to the tensile force in the bar section near the T head, the bearing force is determined with the average tensile strain measured by gauges SG01/02 located near the T head using the bar force-vs.-bar strain (measured with SG05)

relation shown in Figure D.7 in Appendix D. The bond force is then calculated by subtracting the bearing force from the applied pull force.

The tensile forces developed in the stirrups located within the breakout cone region are calculated with the average strains measured by the strain gauges located in each set of stirrups and the stress-strain relation for the steel, which are shown in Figures D.8 through D.12 in Appendix D. Four sets of stirrups (2 inner and 2 outer) were located in the breakout cone region, and the average strains measured from all the functioning gauges (which were SG06/07/08/10/12) in the stirrups are assumed to represent the strains in all the respective stirrups. The tensile and shear resistances developed along the crack planes of the concrete (see Figure 5.1) are lumped into one value termed the concrete resistance, which is calculated by subtracting the total stirrup force from the applied pull force. In reality, the concrete resistance may also include the dowel forces from the top longitudinal bars in the beam. The calculated resisting forces are shown in Table 5.1.

Table 5.1: Resisting forces at different loading phases for Specimen 1

Time (sec)	Force Applied (kips)	Head Force (kips)	Bond Force (kips)	Inner Stirrup Force (kips)	Outer Stirrup Force (kips)	Concrete Force (kips)
150	65	8	57	1	0	64
175	104	25	79	2	0	102
200	129	65	64	6	0	123
210	133	82	51	24	2	107
240	160	111	49	71	14	73
275	177	124	53	85	63	30
279	179	134	45	91	66	22

The resisting forces shown in Table 5.1 are plotted against time in Figure 5.2. It can be observed that the bearing resistance at the T head increased as the applied force increased and reached 134 kips when the applied force reached the peak value of 179 kips. The bond force reached a peak value of 79 kips when the bearing force reached 25 kips, and then it decreased as the bearing

force increased more rapidly. Eventually, the reduced bond force stabilized at about 50 kips. Forces in the stirrups started to increase rapidly when the applied force reached 129 kips due to the initiation of concrete breakout cracks. It can be observed that the bearing force at the T head also continued to increase rapidly. The tensile force in the outer stirrups increased more slowly than that in the inner stirrups. At the peak applied force of 179 kips, the inner and outer stirrups carried a total force of 157 kips, with the inner stirrups carrying 91 kips and the outer stirrups carrying 66 kips. The stirrups in the breakout region yielded before anchorage failure (as shown in Table 4.2). However, since the breakout cracks did not open very significantly and none of the stirrups fractured when the anchorage of the headed bar failed, the failure was probably caused by a combination of concrete crushing at the T head and concrete breakout.

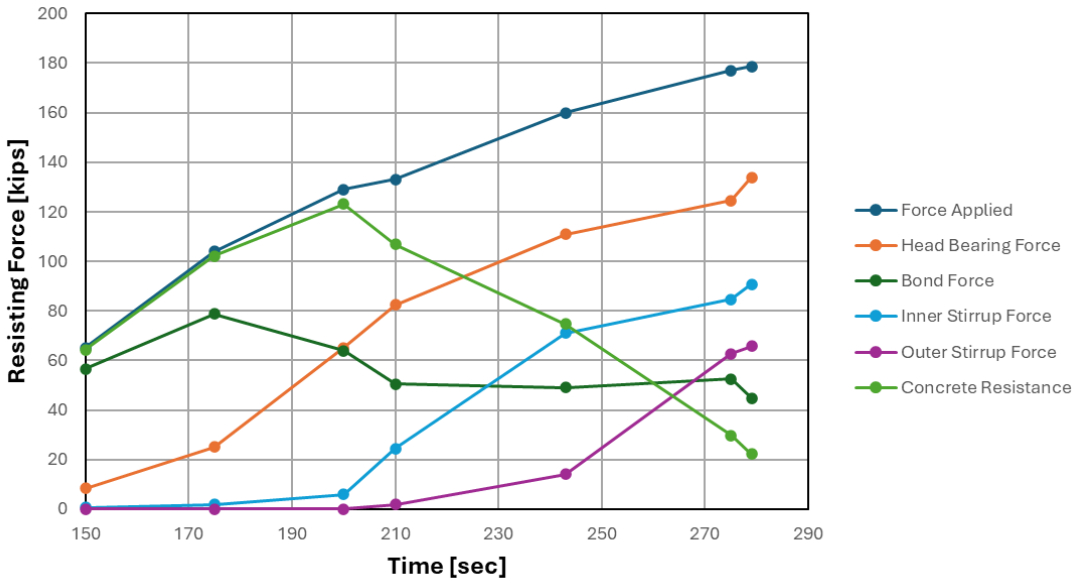

Figure 5.2: Exerted and resisting forces versus time for Specimen 1

Average bond stresses over two segments of the embedded region of the headed bar are calculated with the strain data from the bar shown in Table 4.2. Strains from gauges SG01/02/03/04 are used for the calculations. Their locations are shown in Figure D.2 in Appendix D. The strains measured by SG01/02 (which were at the same location close to the T head) are averaged. The strain

values at the three gauge locations are used to determine the tensile forces in the bar at these locations based on the bar force-vs.-bar strain (measured by SG05) relation shown in Figure D.7 in Appendix D. The average bond stress over a segment between two gauges is calculated from the bar tensile forces at the gauge locations based on the equilibrium condition of the segment. For example, the average bond stress over the segment between gauges SG03 and SG04 is calculated as follows.

$$\tau_{b,SG03-SG04} = \frac{F_{s,SG04} - F_{s,SG03}}{\pi d_b x_{SG03-SG04}} \tag{5.1}$$

in which $F_{s,SG03}$ and $F_{s,SG04}$ are the tensile forces in the bar at the respective strain gauge locations, $x_{SG03-SG04}$ is the distance between SG03 and SG04, and d_b is the nominal bar diameter. The bond stress over the segment between SG01/02 and SG03 is calculated in the same way. The average bond stresses calculated for different applied force levels are shown in Table 5.2 and plotted in Figure 5.3.

Table 5.2: Average bond stresses along headed bar for Specimen 1

Time (sec)	Force Applied (kips)	SG01 (μstr)	SG02 (μstr)	SG03 (μstr)	SG04 (μstr)	$F_{s,SG01/02}$ (kips)	$F_{s,SG03}$ (kips)	$F_{s,SG04}$ (kips)	$\tau_{b,SG01/02-SG03}$ (ksi)	$\tau_{b,SG03-SG04}$ (ksi)
150	65	106	152	473	1003	8	31	65	0.70	1.08
175	104	352	419	954	1588	25	62	104	1.16	1.30
200	129	898	1098	1571	2039	65	102	133	1.17	0.96
210	133	1132	1396	1925	2107	82	126	137	1.35	0.37
242	160	1467	1931	2324	2467	111	152	161	1.28	0.29
275	177	1656	2306	6846	13993	124	172	177	1.49	0.15
279	179	1791	2313	9746	15280	134	178	179	1.38	0.02

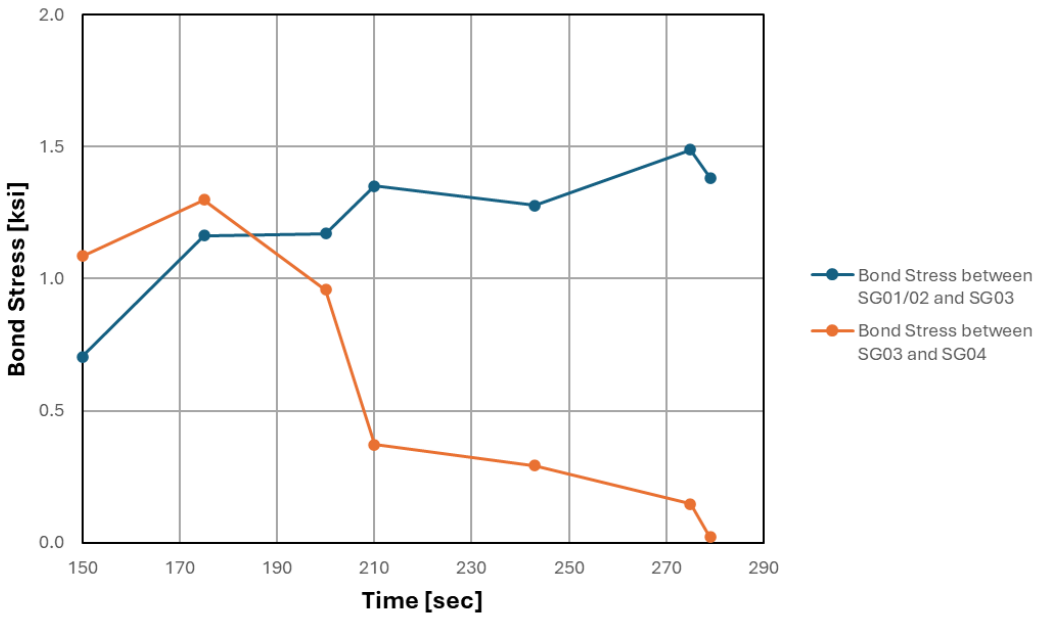

Figure 5.3: Average bond stresses along headed bar versus time for Specimen 1

Figure 5.3 shows that the bond stress in the upper region (between SG03 and SG04) of the bar was initially higher than that in the lower region due to a higher amount of slip in the upper region and the fact that the bond stress had not reached the peak bond strength. After reaching the peak value of 1.3 ksi, the bond stress in the upper region dropped rapidly. This was caused by bond deterioration as a result of increasing bar slip. The bond stress in the lower region increased continuously until it reached 1.5 ksi, after which it dropped to about 1.4 ksi when the applied force reached the maximum value. This indicates that the bar slip in the lower region was limited.

5.2.2 Specimen 2

The resisting forces calculated from the strain data for Specimen 2 are shown in Table 5.3 and plotted against time in Figure 5.4. The specimen had the same properties as Specimen 1 except that the embedment length of the headed bar was equal to the minimum required by ACI 318-19. Like Specimen 1, it can be observed that the bearing resistance at the T head increased as the applied force increased. The table shows that the maximum bearing resistance obtained from the strain gage data is 114 kips, at which the applied force is 187 kips. After that point, gauges SG01 and SG02

stopped functioning, and it is not possible to calculate the bearing resistance at the maximum applied force of 225 kips. The bond force reached a peak value of 91 kips when the bearing force reached 9 kips. The bond force slowly decreased after it reached its peak value as the bearing force rapidly increased. The reduced bond force stabilized around 70 kips. Forces in the stirrups began increasing rapidly when the applied force reached 180 kips. This indicates the initiation of the concrete breakout cracks. The resistance provided by the concrete reached its peak value of 174 kips right after the breakout cracks initiated. This is a lot higher than the peak concrete resistance of 123 kips developed in Specimen 1. At the peak applied force of 225 kips, the inner and outer stirrups carried a total force of 121 kips, with the inner stirrups carrying 63 kips and the outer stirrups carrying 58 kips. These forces were less than those from Specimen 1, and the tensile force in the stirrups also did not exceed the yield strength of the stirrups. Although there were concrete breakout cracks, the anchorage capacity was sufficient for the headed bar to develop its full tension capacity, and no anchorage failure occurred.

Table 5.3: Resisting forces at different loading phases for Specimen 2

Time (sec)	Force Applied (kips)	Head Force (kips)	Bond Force (kips)	Inner Stirrup Force (kips)	Outer Stirrup Force (kips)	Concrete Force (kips)
120	60	2	58	0	0	60
147	100	9	91	0	0	100
182	143	60	83	1	0	142
209	160	81	79	1	0	159
244	180	109	71	6	0	174
279	187	114	73	41	19	127
337	210	-	-	56	36	118
471	225	-	-	63	58	104

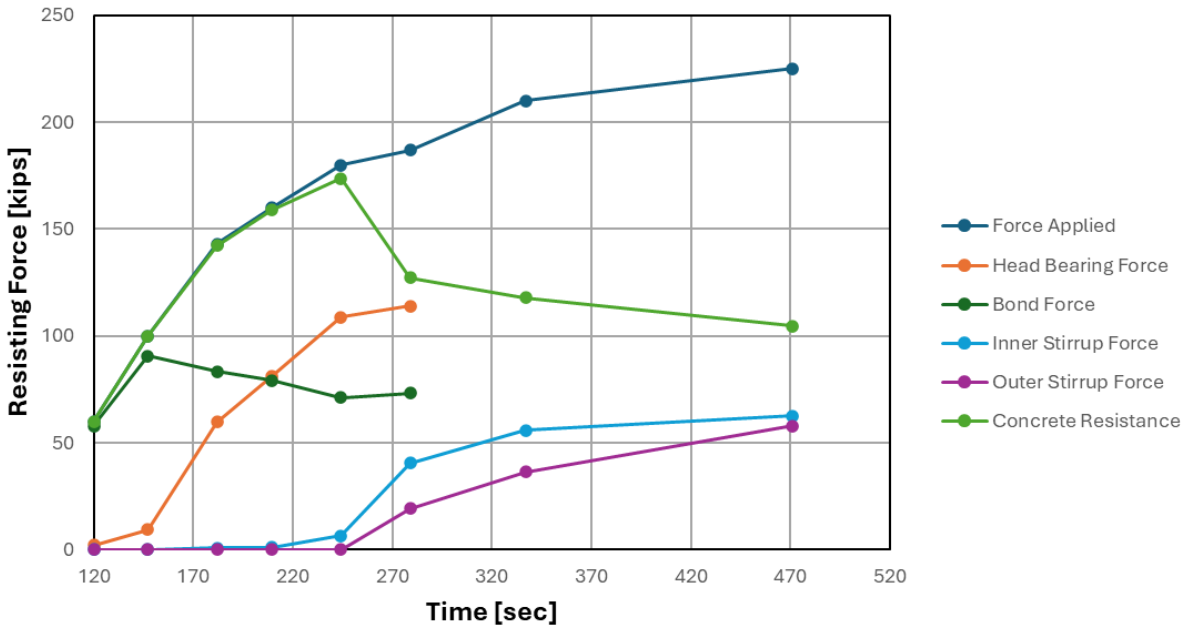

Figure 5.4: Exerted and resisting forces versus time for Specimen 2

The average bond stresses calculated for different applied force levels are shown in Table 5.4 and plotted in Figure 5.5. It can be observed that the bond stress in the upper region (between SG04 and SG05) of the bar was initially higher than that in the lower regions of the bar. After reaching a peak value of 0.9 ksi, the bond stress in the upper region dropped rapidly. The bond stress in the middle region of the bar (between SG03 and SG04) reached a peak value of about 1.0 ksi before dropping to a minimum value of 0.4 ksi. The bond stress in the lower region of the bar (between SG01/02 and SG03) increased continuously and reached 1.4 ksi at the applied force of 187 kips, after which SG01/02 stopped functioning. The bond stress variation along the headed bar in this specimen was similar to that in Specimen 1. However, the longer embedment length in this specimen did help to increase the anchorage strength.

Table 5.4: Average bond stresses along headed bar for Specimen 2

Time (sec)	Force Applied (kips)	SG01 (μstr)	SG02 (μstr)	SG03 (μstr)	SG04 (μstr)	SG05 (μstr)
120	60	45	15	136	378	746
147	100	151	136	455	953	1394
182	143	963	865	1411	1878	2157
209	160	1319	1161	1768	2182	3876
244	180	1805	1533	2262	3238	12633
279	187	1889	1601	2483	11951	14575
337	210	-	-	-	-	12417
471	225	-	-	-	-	10298

Time (sec)	Force Applied (kips)	$F_{s,SG01/02}$ (kips)	$F_{s,SG03}$ (kips)	$F_{s,SG04}$ (kips)	$F_{s,SG05}$ (kips)	$\tau_{b,SG01/02-SG03}$ (ksi)	$\tau_{b,SG03-SG04}$ (ksi)	$\tau_{b,SG04-SG05}$ (ksi)
120	60	2	9	25	49	0.22	0.49	0.75
147	100	9	30	62	91	0.64	1.02	0.90
182	143	60	92	123	141	1.02	0.96	0.57
209	160	81	115	142	156	1.08	0.85	0.43
244	180	109	148	159	173	1.21	0.36	0.44
279	187	114	157	172	177	1.35	0.47	0.16
337	210	-	-	-	-	-	-	-
471	225	-	-	-	-	-	-	-

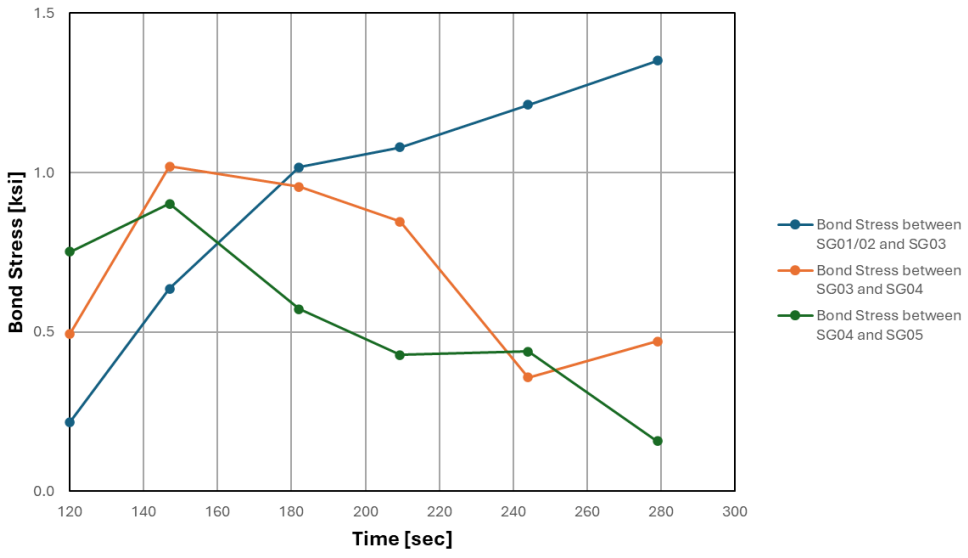

Figure 5.5: Average bond stresses along headed bar versus time for Specimen 2

5.2.3 Specimen 3

The resisting forces calculated from the strain data for Specimen 3 are shown in Table 5.5 and plotted against time in Figure 5.6. Specimen 3 had the same properties as Specimen 1 except that the net bearing area of the T head was 9 A_b. It can be observed that the bearing resistance at the T head increased as the applied force increased and reached 190 kips when the applied force reached the peak value of 213 kips, at which bar fracture occurred, while the maximum bearing resistance developed in Specimen 1 was 134 kips when anchorage failure occurred. The maximum bond force developed was 63 kips when the applied force was 83 kips, and it decreased gradually as the bearing resistance increased rapidly. After the headed bar was unloaded then reloaded, the bond force stabilized around 25 kips. The bond force developed in this specimen was comparable to that in Specimen 1 but the bearing force was a lot higher. At the peak load, most of the applied force was resisted by the bearing force at the T head. Forces in the inner stirrups started to increase rapidly when the applied force reached 140 kips due to the initiation of concrete breakout cracks, and the stirrups yielded when the applied force reached 186 kips. The outer stirrups were also engaged at around 140 kips but the forces in these stirrups were a little lower than the forces in the inner stirrups. After 426 sec., the strain gauges on the outer stirrups stopped functioning. It can be seen that the inner and outer stirrups carried a significant portion of the applied force of 160 kips at 426 seconds. The concrete resistance reached a peak value of 124 kips when the applied force reached 140 kips at 350 sec. and dropped significantly afterwards. At the end of the test, the inner stirrups carried a total force of 90 kips when bar fractured at the applied force of 213 kips.

Table 5.5: Resisting forces at different loading phases for Specimen 3

Time (sec)	Force Applied (kips)	Head Force (kips)	Bond Force (kips)	Inner Stirrup Force (kips)	Outer Stirrup Force (kips)	Concrete Force (kips)
218	83	20	63	0	0	83
350	140	85	55	12	4	124
400	154	98	56	56	40	59
418	157	100	57	59	42	56
426	160	103	57	60	44	56
500	186	140	46	74	-	-
700	191	156	35	77	-	-
768	195	160	35	78	-	-
825	0	0	0	0	-	-
875	94	74	20	24	-	-
900	160	138	22	56	-	-
955	195	167	28	74	-	-
995	204	179	25	79	-	-
1026	213	190	23	90	-	-

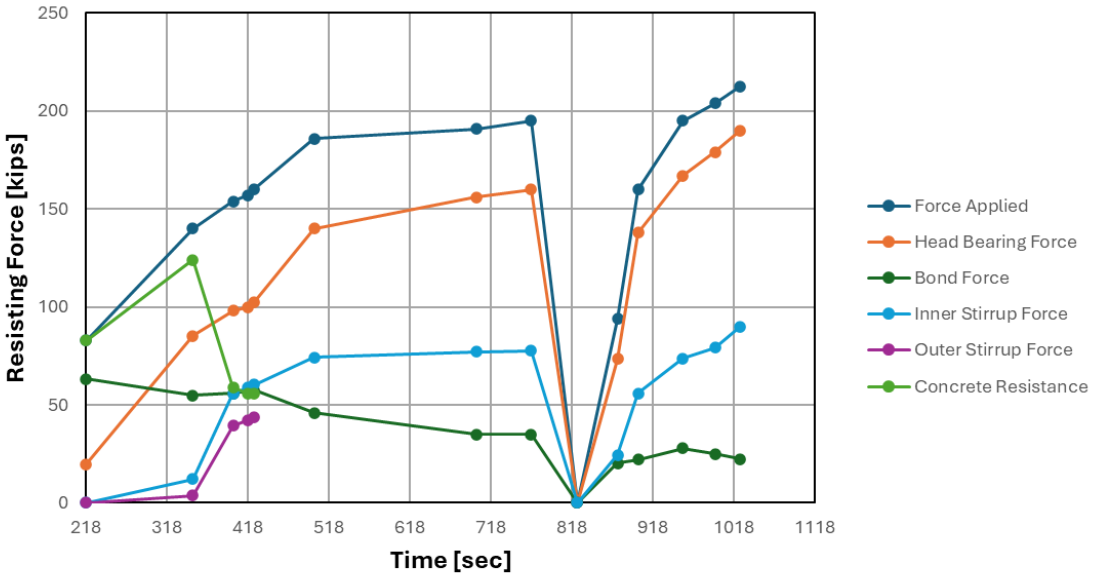

Figure 5.6: Exerted and resisting forces versus time for Specimen 3

The average bond stresses calculated for different applied force levels are shown in Table 5.6 and plotted in Figure 5.7. Gauge SG04 did not function. Hence, the bond stress in the upper region is calculated between SG03 and SG05, which was above the top face of the beam. In the calculation

of the bond stress, the distance between SG05 and top face of the beam is excluded. Table 5.6 and Figure 5.7 show that the bond stresses in the lower (between SG01/02 and SG03) and upper (between SG03 and SG05) regions were very small and close to one another at 218 seconds. After that, the bond stress in the upper region dropped to zero or negligible values, while that in the lower region increased to a peak of 1.85 ksi and then decreased to small values. This indicates severe bond deterioration along the entire embedment length and, eventually, the anchorage resistance was mainly provided by the bearing force at the T head.

Table 5.6: Average bond stresses along headed bar for Specimen 3

Time (sec)	Force Applied (kips)	SG01 (μstr)	SG02 (μstr)	SG03 (μstr)	$F_{s,SG01/02}$ (kips)	$F_{s,SG03}$ (kips)	$F_{s,SG05}$ (kips)	$\tau_{b,SG01/02-SG03}$ (ksi)	$\tau_{b,SG03-SG05}$ (ksi)
218	83	227	347	687	20	47	83	0.86	0.69
350	140	924	1548	2056	85	142	140	1.77	0*
400	154	1000	1843	2496	98	157	154	1.85	0*
418	157	1015	1888	2541	100	157	157	1.78	0
426	160	1053	1926	2595	103	157	160	1.70	0.06
500	186	1417	2396	10801	140	162	186	0.69	0.46
700	191	5510	7880	16822	156	175	191	0.60	0.31
768	195	7842	9646	19640	160	181	195	0.64	0.28
825	0	6904	7789	17431	0	0	0	0	0
875	94	7896	9054	19043	74	94	94	0.64	0
900	160	8758	10176	20457	138	160	160	0.69	0
955	195	12128	13040	22900	167	185	195	0.56	0
995	204	18899	18943	31210	179	195	204	0.50	0
1026	213	-	29375	-	190	-	213	-	-

*Since the value cannot be negative, it is assumed to be zero.

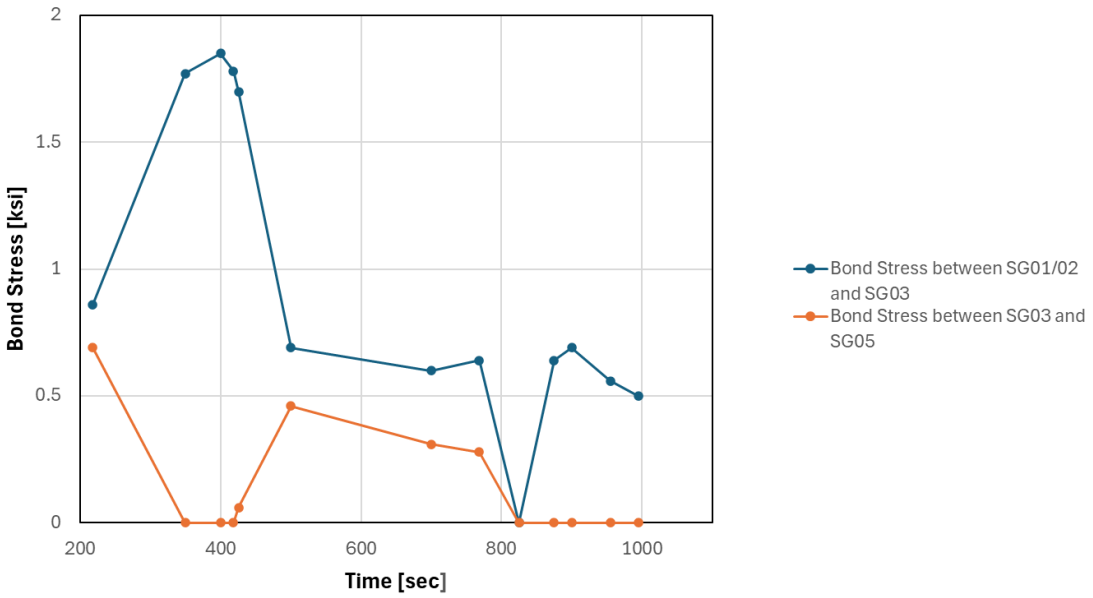

Figure 5.7: Average bond stresses along headed bar versus time for Specimen 3

5.2.4 Specimen 4

The resisting forces calculated from the strain data for Specimen 4 are shown in Table 5.7 and plotted against time in Figure 5.8. Like Specimen 1, Specimen 4 had one No. 14 headed bar with an embedment length equal to 71% of the minimum required by ACI 318-19 and a head size of $4A_b$. However, it had a concrete compressive strength of 8,000 psi. It can be observed that the bearing resistance of the T head increased as the applied force increased and reached 128 kips when the applied force reached the peak value of 173 kips. The bond force reached a peak value of 96 kips when the bearing force reached 46 kips, and then it decreased as the bearing force continued to increase. Eventually, the reduced bond force stabilized at about 50 kips. Forces in the stirrups started to increase rapidly when the applied force reached 141 kips due to the initiation of concrete breakout cracks. The tensile force in the outer stirrups was lower than that in the inner stirrups. At the peak applied force of 173 kips, the inner and outer stirrups carried a total force of 128 kips, with the inner stirrups carrying 73 kips and the outer stirrups carrying 55 kips. Anchorage failure occurred at that

point. As discussed in Section 4.5.1, a lot of concrete crushing was observed around the headed bar in the breakout cone region.

Table 5.7: Resisting forces at different loading phases for Specimen 4

Time (sec)	Force Applied (kips)	Head Force (kips)	Bond Force (kips)	Inner Stirrup Force (kips)	Outer Stirrup Force (kips)	Concrete Force (kips)
152	60	5	55	0	0	60
213	112	20	92	0	0	112
251	142	46	96	2	0	140
252	137	57	80	8	0	129
254	141	74	67	29	12	101
282	156	103	53	61	33	62
289	160	107	53	62	35	63
299	168	118	50	67	48	53
308	173	128	45	73	55	45

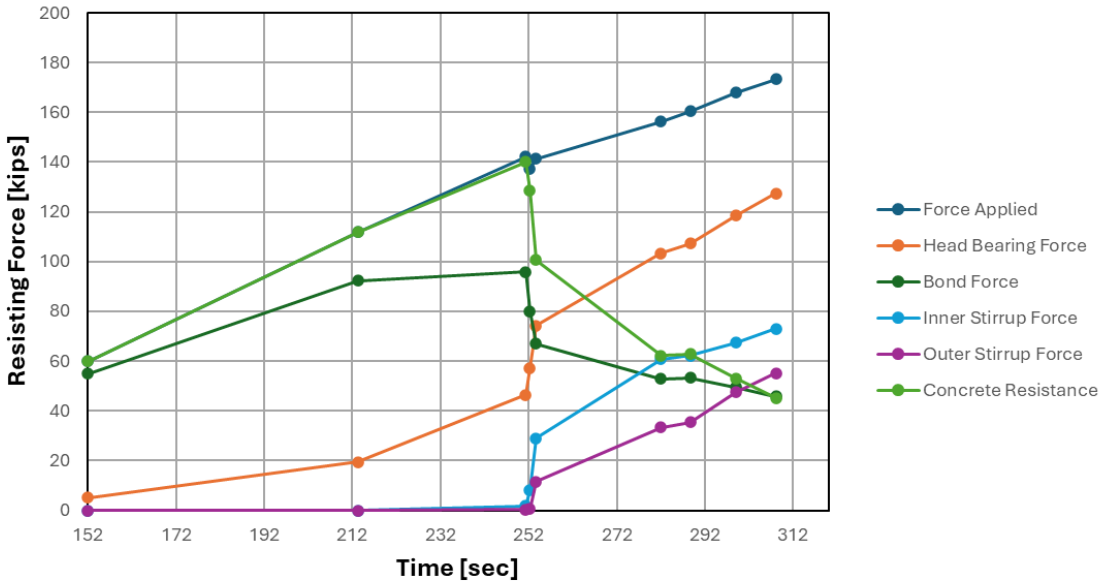

Figure 5.8: Exerted and resisting forces versus time for Specimen 4

The average bond stresses calculated for different applied force levels are shown in Table 5.8 and plotted against time in Figure 5.9. Figure 5.9 shows that the bond stress in the upper region (between SG03 and SG04) of the bar was initially higher than that in the lower region. After reaching

the peak value of 1.3 ksi, the bond stress in the upper region dropped rapidly. At later time instants, the force in the bar at the location of gauge SG04 appeared to be slightly lower than the force at gauge SG03. This could be due to strain gauge readings being influenced by slight bar bending. Because of the unreliable strain gauge readings, the bond stress in that region was taken to be zero. The bond stress in the lower region increased continuously until it reached a peak value of 2.5 ksi, after which it decreased slowly to about 1.4 ksi when the applied force reached the maximum value. The higher peak bond stress reached in this specimen was probably due to the higher concrete compressive strength of 8,000 psi. The final failure appeared to be associated with the crushing of the concrete in the breakout cone region.

Table 5.8: Average bond stresses along headed bar for Specimen 4

Time (sec)	Force Applied (kips)	SG01 (μstr)	SG02 (μstr)	SG03 (μstr)	SG04 (μstr)	$F_{s,SG01/02}$ (kips)	$F_{s,SG03}$ (kips)	$F_{s,SG04}$ (kips)	$\tau_{b,SG01/02-SG03}$ (ksi)	$\tau_{b,SG03-SG04}$ (ksi)
152	60	83	98	376	859	5	21	49	0.61	1.04
213	112	332	353	1158	1757	20	66	100	1.75	1.28
251	142	808	820	1941	2308	46	111	132	2.42	0.79
252	137	944	1068	2190	2195	57	124	125	2.51	0.04
254	141	1223	1384	2386	2225	74	136	127	2.32	0.00
282	156	1776	1852	2816	3899	103	151	156	1.77	0.21
289	160	1836	1927	2907	5806	107	152	156	1.68	0.17
299	168	1988	2168	10005	8885	118	160	158	1.56	0
308	173	2245	2229	12387	11582	128	164	163	1.36	0

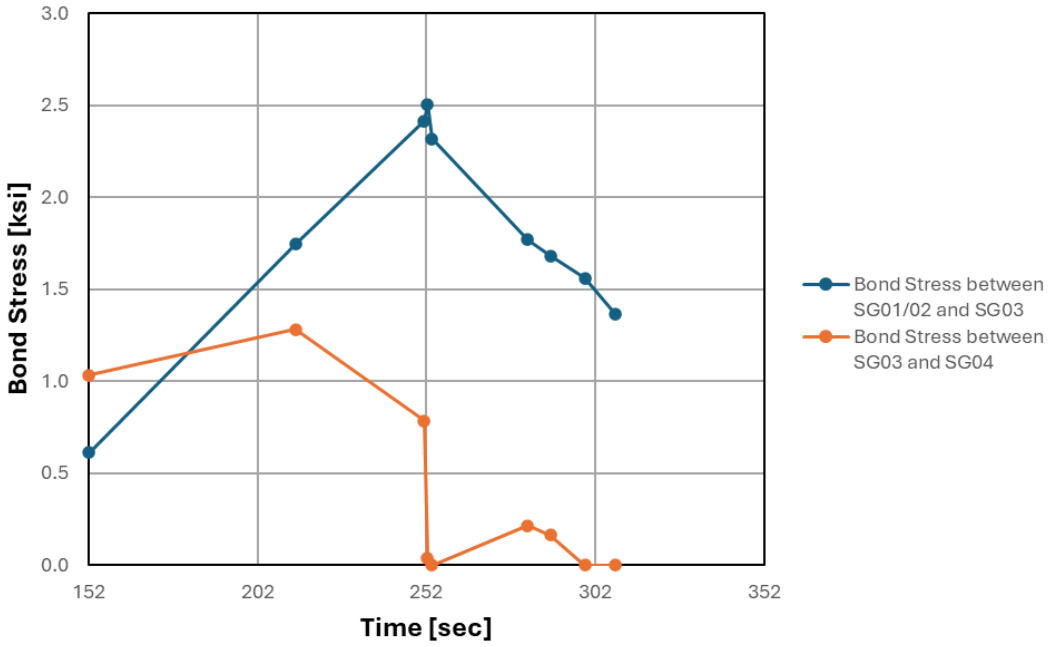

Figure 5.9: Average bond stresses along headed bar versus time for Specimen 4

5.2.5 Specimen 5

The resisting forces calculated from the strain data for Specimen 5 are shown in Table 5.9 and plotted against time in Figure 5.10. This specimen had the same properties as Specimen 4 except that it had 4 sets of No. 4 stirrups adjacent to the headed bar instead of No. 5 stirrups. It can be observed that the bearing force at the T head increased as the applied force increased and reached 65 kips when the applied force reached the peak value of 152 kips. However, the bearing force continued to increase and reached a peak value of 147 kips when the applied force dropped to 147 kips. The drop of the applied force was due to the initiation of breakout cracks. Afterwards, the bearing force remained equal to the applied force, indicating the complete loss of the bond force. The bond force reached a peak value of 100 kips when the bearing force reached 140 kips, and then it decreased as the bearing force increased. Forces in the stirrups started to increase rapidly after the applied force reached the peak value of 152 kips due to the initiation of concrete breakout cracks. As shown in Table 4.6, the strains in stirrups reached the yield value soon after that point. The tensile

forces in the inner and outer stirrups were close to each other. This shows that the diagonal breakout cracks propagated quickly. When the applied force dropped to 147 kips, the stirrups carried a total of 116 kips. Compared to Specimen 4, the anchorage capacity in this specimen was governed by the breakout cracks. Once the breakout cracks developed, the load was quickly transmitted to the stirrups, and the headed bar could not carry a higher load. Furthermore, as discussed in Section 4.6.1, the breakout cracks opened significantly in this specimen. Hence, the failure mode was clearly a concrete breakout failure.

Table 5.9: Resisting forces at different loading phases for Specimen 5

Time (sec)	Force Applied (kips)	Head Force (kips)	Bond Force (kips)	Inner Stirrup Force (kips)	Outer Stirrup Force (kips)	Concrete Force (kips)
52	32	2	30	0	0	32
94	65	6	59	0	0	65
131	100	15	85	0	0	100
181	140	40	100	0	0	140
199	152	65	87	1	0	151
200	141	75	67	12	4	126
202	138	90	48	31	24	83
205	145	104	41	41	42	63
210	148	121	27	54	54	41
223	147	147	0	60	56	31
223	77	77	0	56	56	0
238	109	109	0	59	57	0

The average bond stresses calculated for different applied force levels are shown in Table 5.10 and plotted in Figure 5.11. Figure 5.11 shows that the bond stress in the upper region (between SG03 and SG04) of the bar was initially slightly higher than that in the lower region. After reaching the peak value of 0.9 ksi, the bond stress in the upper region gradually dropped to zero when the applied force approached the maximum value of 152 kips. The bond stress in the lower region increased continuously until it reached 2.3 ksi, after which it decreased rapidly to zero. This indicates that there

was significant bond deterioration along the bar, probably caused by concrete crushing in the breakout cone region.

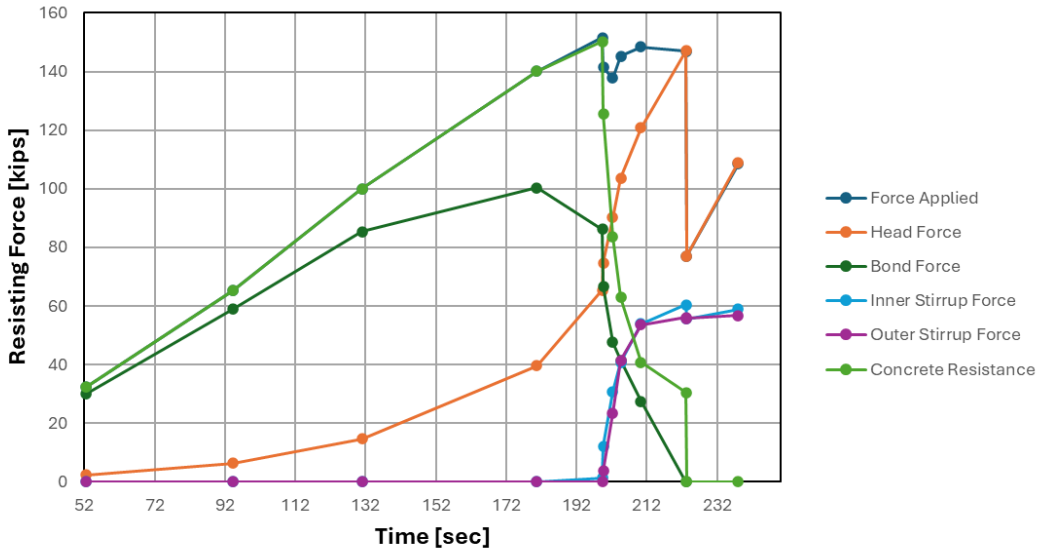

Figure 5.10: Exerted and resisting forces versus time for Specimen 5

Table 5.10: Average bond stresses along headed bar for Specimen 5

Time (sec)	Force Applied (kips)	SG01 (μstr)	SG02 (μstr)	SG03 (μstr)	SG04 (μstr)	$F_{s,SG01/02}$ (kips)	$F_{s,SG03}$ (kips)	$F_{s,SG04}$ (kips)	$\tau_{b,SG01/02\text{-}SG03}$ (ksi)	$\tau_{b,SG03\text{-}SG04}$ (ksi)
52	32	30	45	144	295	2	9	18	0.25	0.35
94	65	83	121	403	703	6	25	43	0.70	0.70
131	100	211	264	844	1210	15	52	75	1.41	0.85
181	140	566	718	1559	1838	40	96	114	2.13	0.65
199	152	899	1217	2054	2126	65	127	131	2.32	0.17
200	141	1058	1361	2054	1960	75	127	121	1.96	0
202	138	1330	1588	2009	1853	90	124	115	1.28	0
205	145	1496	1861	2077	1982	104	128	123	0.93	0
210	148	1671	2240	2161	2005	121	134	124	0.48	0
223	147	2800	3037	2192	1952	147	147	121	0	0
223	77	1951	1899	1277	930	77	77	57	0	0
238	109	2884	2187	2085	1747	109	109	108	0	0

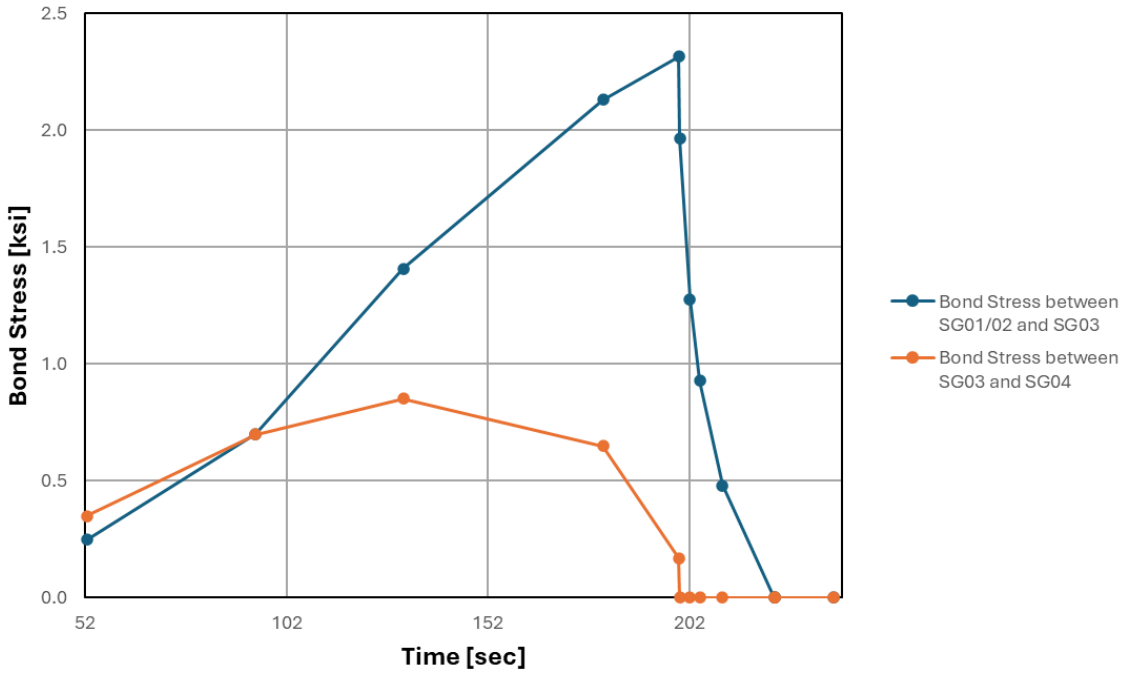

Figure 5.11: Average bond stresses along headed bar versus time for Specimen 5

5.2.6 Specimen 6

The resisting forces calculated from the strain data for Specimen 6 are shown in Table 5.11 and plotted against time in Figure 5.12. Like Specimens 4 and 5, Specimen 6 had a target concrete strength of 8,000 psi, with the average cylinder strength on the date of the anchorage test equal to 8,580 psi. The headed bar in the specimen had the full development length specified in ACI 318-19. It can be observed that the bearing resistance at the T head increased as the applied force increased and reached 125 kips when the applied force reached the peak value of 212 kips, at which the bar fractured. The bond force reached a peak value of 127 kips when the bearing force reached 30 kips, and then it decreased as the bearing force increased, dropping to 87 kips by the end of the test. Forces in the stirrups started to increase rapidly when the applied force reached 180 kips due to the initiation of the concrete breakout cracks. The tensile forces in the outer stirrups increased more slowly than that in the inner stirrups. At the peak applied force of 212 kips, the inner and outer stirrups

carried a total force of 103 kips, with the inner stirrups carrying 63 kips and the outer stirrups carrying 40 kips.

Table 5.11: Resisting forces at different loading phases for Specimen 6

Time (sec)	Force Applied (kips)	Head Force (kips)	Bond Force (kips)	Inner Stirrup Force (kips)	Outer Stirrup Force (kips)	Concrete Force (kips)
100	40	1	39	0	0	40
153	100	4	96	0	0	100
173	120	6	114	0	0	120
203	156	30	127	0	0	156
206	158	36	122	0	0	158
213	160	39	122	1	0	159
234	180	65	115	2	0	178
246	187	86	101	10	1	176
249	190	97	93	43	15	132
296	212	125	87	63	40	109

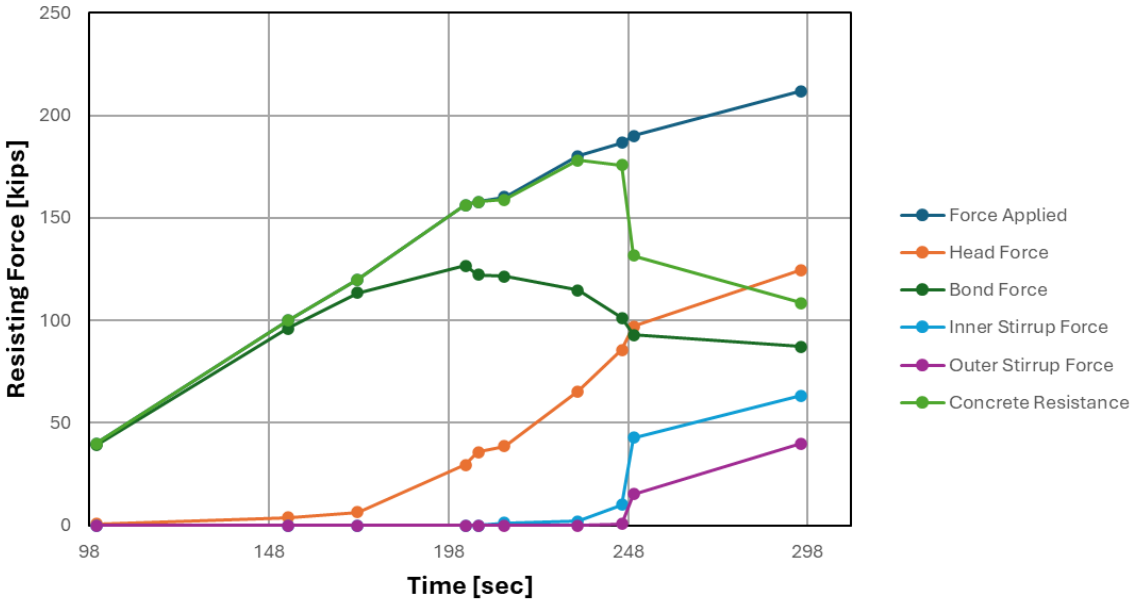

Figure 5.12: Exerted and resisting forces versus time for Specimen 6

The average bond stresses calculated for different applied force levels are shown in Table 5.12 and plotted in Figure 5.13. Figure 5.13 shows that the bond stress in the upper region (between

SG04 and SG05) of the bar was initially higher than that in the middle and lower regions. After reaching the peak value of 2.44 ksi, the bond stress in the upper region dropped rapidly. The middle region reached a peak bond stress value of 2.37 ksi a little later, after which the bond stress dropped rapidly. The bond stress in the lower region increased continuously until it reached 2.28 ksi, after which it decreased rapidly to 1.25 ksi at the maximum applied force.

Table 5.12: Average bond stresses along headed bar for Specimen 6

Time (sec)	Force Applied (kips)	SG01 (μstr)	SG02 (μstr)	SG03 (μstr)	SG04 (μstr)	SG05 (μstr)
98	40	15	8	45	182	721
153	100	60	61	273	820	1824
173	120	98	106	410	1146	2182
203	156	476	469	1154	2158	2677
206	158	574	568	1328	2288	3013
213	160	612	621	1412	2356	3288
234	180	1036	1053	1960	3065	11325
246	187	1331	1402	2333	9966	17150
249	190	1497	1607	2462	13834	18495
296	212	2005	1971	5121	30237	34683

Time (sec)	Force Applied (kips)	$F_{s,SG01/02}$ (kips)	$F_{s,SG03}$ (kips)	$F_{s,SG04}$ (kips)	$F_{s,SG05}$ (kips)	$\tau_{b,SG01/02-SG03}$ (ksi)	$\tau_{b,SG03-SG04}$ (ksi)	$\tau_{b,SG04-SG05}$ (ksi)
98	40	1	3	11	45	0.08	0.32	1.27
153	100	4	17	51	114	0.50	1.29	2.37
173	120	6	26	72	137	0.72	1.74	2.44
203	156	30	72	135	158	1.60	2.37	0.85
206	158	36	83	143	158	1.78	2.26	0.55
213	160	39	88	148	158	1.87	2.22	0.38
234	180	65	123	158	166	2.16	1.32	0.31
246	187	86	146	164	177	2.28	0.65	0.50
249	190	97	154	171	179	2.14	0.62	0.31
296	212	125	158	196	200	1.25	1.44	0.16

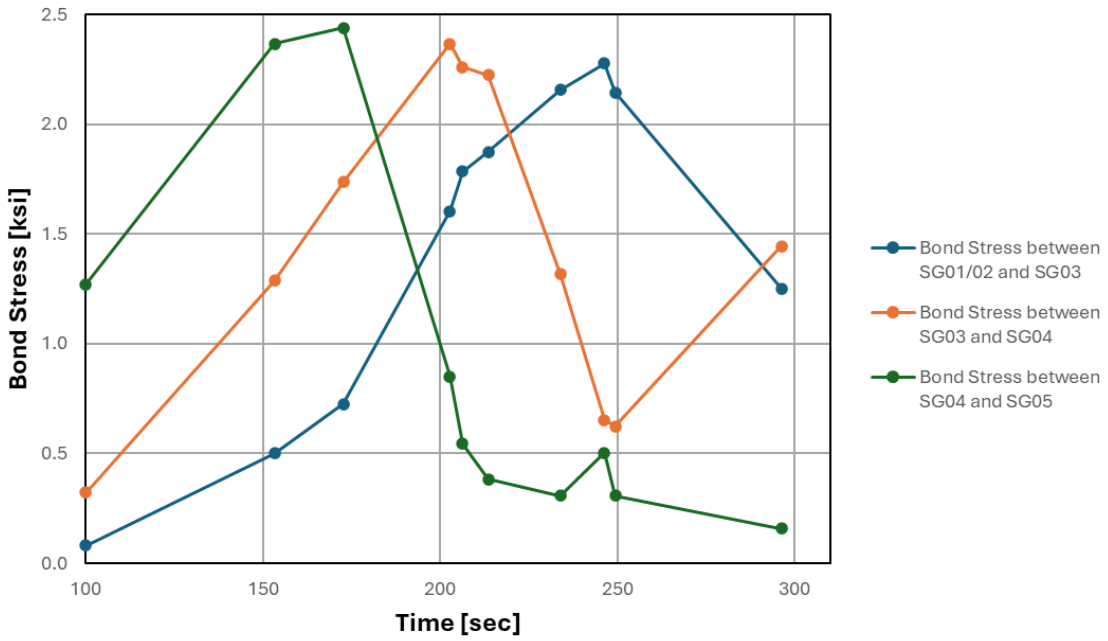

Figure 5.13: Average bond stresses along headed bar versus time for Specimen 6

5.2.7 Specimen 7

The resisting forces calculated from the strain data for Specimen 7 are shown in Table 5.13 and plotted against time in Figure 5.14. Specimen 7 had the same properties as Specimen 4 except that it had a larger T head that had a net bearing area of $9A_b$. In addition, the average concrete strength from the cylinder tests was 8,580 psi, a little higher than that for Specimen 4. Like Specimen 4, the specimen had anchorage failure. It can be observed that the bearing resistance at the T head increased as the applied force increased and reached 162 kips when the applied force reached the peak value of 188 kips. The bond force reached a peak value of 95 kips when the bearing force reached 58 kips, after which it decreased to 27 kips when the applied force reached the peak value of 188 kips. Forces in the stirrups started to increase rapidly when the applied force reached 154 kips due to the initiation of concrete breakout cracks. The tensile force in the outer stirrups increased more slowly than that in the inner stirrups. At the peak applied force of 188 kips, the inner and outer stirrups carried a total force of 188 kips, with the inner stirrups carrying 111 kips and the outer stirrups

carrying 77 kips. As shown in Table 4.8, the inner stirrups yielded earlier than the outer stirrups. As discussed in Section 4.8.1, like Specimen 4, the anchorage failure in this specimen was caused by a combination of concrete breakout and the crushing of concrete bearing against the T head. However, the bearing resistance developed in this specimen was a bit higher than that in Specimen 4 due to the larger head, resulting in slightly higher anchorage resistance.

Table 5.13: Resisting forces at different loading phases for Specimen 7

Time (sec)	Force Applied (kips)	Head Force (kips)	Bond Force (kips)	Inner Stirrup Force (kips)	Outer Stirrup Force (kips)	Concrete Force (kips)
30	20	2	18	0	0	20
52	50	4	46	0	0	50
97	120	26	94	0	0	120
117	154	58	95	3	0	151
119	151	82	69	41	7	103
121	160	101	59	75	20	65
123	162	107	55	82	22	58
140	175	129	46	92	46	37
173	188	162	26	111	77	0

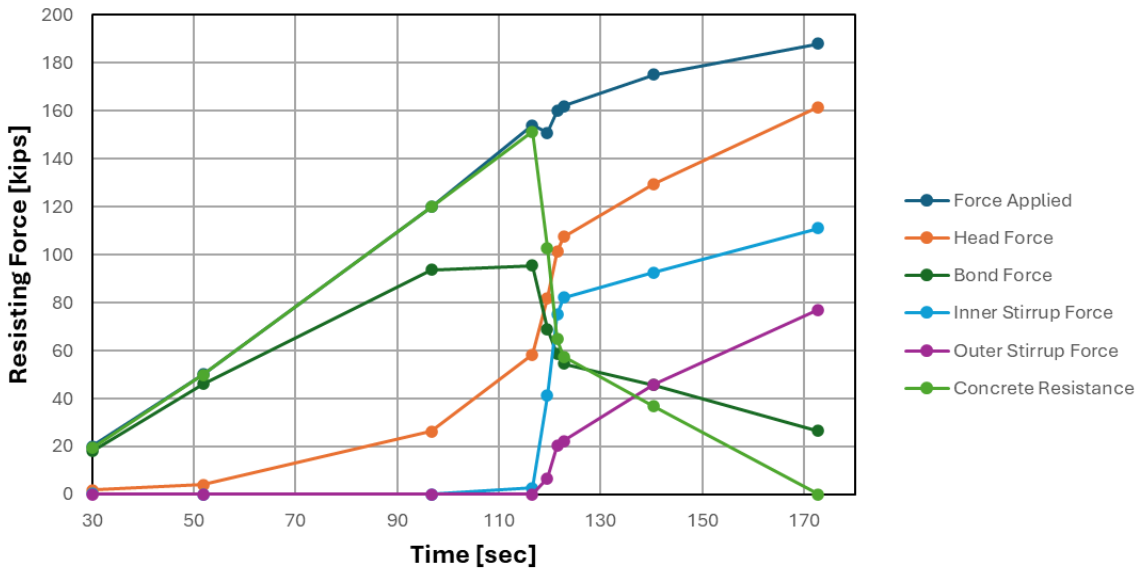

Figure 5.14: Exerted and resisting forces versus time for Specimen 7

The average bond stresses calculated for different applied force levels are shown in Table 5.14 and plotted in Figure 5.15. Figure 5.15 shows that the bond stress in the upper region (between SG03 and SG04) of the bar was initially higher than that in the lower region. After reaching the peak value of 2.6 ksi, the bond stress in the upper region dropped rapidly to zero when the applied force reached 175 kips. The bond stress in the lower region increased continuously until it reached 2.4 ksi, after which it decreased slowly to a value of 0.6 ksi at the maximum applied force. This indicates that there was significant bond deterioration.

Table 5.14: Average bond stresses along headed bar for Specimen 7

Time (sec)	Force Applied (kips)	SG01 (μstr)	SG02 (μstr)	SG03 (μstr)	SG04 (μstr)	$F_{s,SG01/02}$ (kips)	$F_{s,SG03}$ (kips)	$F_{s,SG04}$ (kips)	$\tau_{b,SG01/02-SG03}$ (ksi)	$\tau_{b,SG03-SG04}$ (ksi)
30	20	30	38	91	234	2	5	13	0.12	0.30
52	50	68	76	281	1201	4	16	67	0.44	1.93
97	120	462	484	1309	2542	26	73	142	1.75	2.58
117	154	1008	1089	2178	3302	58	121	155	2.37	1.25
119	151	1426	1514	2613	3507	82	146	158	2.40	0.46
121	160	1806	1832	2912	3666	101	157	160	2.08	0.13
123	162	1927	1931	2988	4267	107	157	161	1.85	0.15
140	175	2323	2325	8671	8472	129	162	162	1.22	0
173	188	6702	7094	18632	16086	162	178	175	0.61	0

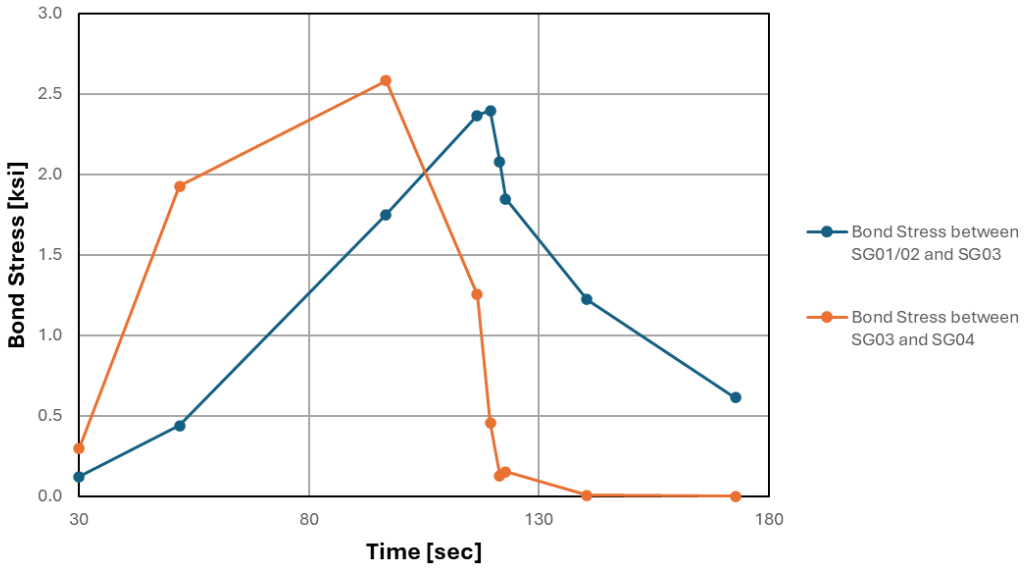

Figure 5.15: Average bond stresses along headed bar versus time for Specimen 7

5.2.8 Specimen 8

Specimen 8 had two side-by-side No. 14 headed bars spaced at 8 in. on center with T heads having a net bearing area of $4A_b$. The bars had an embedment length of 24 in., which was equal to 100% of the minimum development length required by ACI 318-19. The concrete had a target compressive strength of 4,000 psi, with the average cylinder strength on the day of the anchorage test equal to 4,350 psi. The bars were able to develop their tensile strength without anchorage failure. The resisting forces calculated from strain data are shown in Table 5.15 and plotted against time in Figure 5.16. As shown, the bearing resistance at the T heads increased as the applied force increased and reached 257 kips when the total applied force reached the peak value of 469 kips. The total bond force from the two bars reached a peak value of 234 kips when the applied force reached 351 kips, after which it decreased to 212 kips as the applied force reached 469 kips. Forces in the stirrups closer to the headed bars (middle and Group-1 stirrups) started to increase rapidly after the applied force exceeded 254 kips due to the initiation of concrete breakout cracks. The tensile forces in the stirrups further away from the headed bars increased much more slowly than those in the closer

stirrups. At the peak applied force of 469 kips, the stirrups carried a total force of 343 kips, with the stirrups in the middle and Group 1 carrying 279 kips and the remaining stirrups carrying 64 kips. The middle stirrups as well as some of Group-1 stirrups yielded, but none of the stirrups fractured. The concrete resistance attained a peak value of 222 kips when the applied force was 254 kips. It dropped to 111 kips right after and remained more or less constant.

The test was stopped when the applied force reached 469 kips because the loading beam showed tilting towards one direction. At this point, the stress in the headed bars above the RC beam was close to the peak tensile strength of the bars and the breakout cracks did not open much. Therefore, if the test were continued further, the headed bars would have fractured.

Table 5.15: Resisting forces at different loading phases for Specimen 8

Time (sec)	Force Applied (kips)	Head Force			Bond Force (kips)	Stirrup Force				Concrete Resistance (kips)
		Bar (A) (kips)	Bar (B) (kips)	Total Force (A)+(B) (kips)		Middle (kips)	Group 1 (kips)	Group 2 (kips)	Group 3 (kips)	
20	63	1	1	2	61	1	1	0	0	62
113	67	1	1	2	66	1	1	0	0	66
173	107	1	2	3	104	1	1	0	0	105
262	254	24	35	59	195	21	8	1	2	222
335	333	48	58	106	227	67	116	33	6	111
369	351	54	63	116	234	70	120	35	6	120
498	408	96	97	193	215	85	148	41	8	125
524	420	101	102	203	217	90	153	43	9	126
680	459	102*	102	204	255	117	161	54	8	119
717	469	128*	128	256	213	117	162	55	9	126

* Assumed to be the same as in Bar B because of the lack of data due to broken strain gauges.

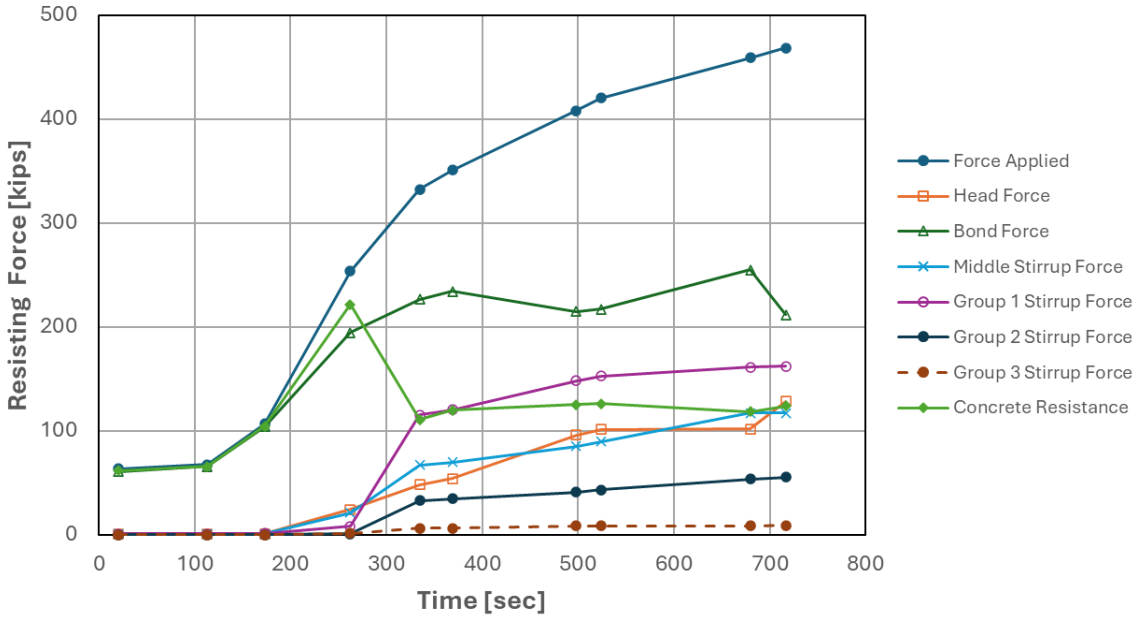

Figure 5.16: Exerted and resisting forces versus time for Specimen 8

The average bond stresses calculated for different applied force levels from the strain gauge data are shown in Table 5.16 and plotted in Figure 5.17. Figure 5.17 shows that the bond stress in the upper region (between SG04 and SG05) of both Bars A and B was initially higher than that in the lower region. At 262 sec., when concrete cracking initiated, the bond stress in the upper region dropped rapidly to zero and then rose again, while the bond stresses in the lower regions (between SG03 and SG04 and between SG01 and SG03) increased rapidly and remained higher than that in the upper region. This indicates that there was more significant bond deterioration in the uppermost region.

Table 5.16: Average bond stresses along headed bars for Specimen 8

Bar A													
Time (sec)	Force Applied Per Bar (kips)	SG01A (μstr)	SG02A (μstr)	SG03A (μstr)	SG04A (μstr)	SG05A (μstr)	$F_{s,SG01A/02A}$ (kips)	$F_{s,SG03A}$ (kips)	$F_{s,SG04A}$ (kips)	$F_{s,SG05A}$ (kips)	$\tau_{b,SG01A/02A-SG03A}$ (ksi)	$\tau_{b,SG03A-SG04A}$ (ksi)	$\tau_{b,SG04A-SG05A}$ (ksi)
20	32	22	15	30	83	218	1	2	6	15	0.0	0.1	0.3
113	34	52	8	38	90	234	1	3	6	16	0.1	0.1	0.3
173	53	67	15	68	218	490	1	5	15	33	0.1	0.3	0.6
262	127	404	361	1116	1675	1697	24	75	112	114	1.6	1.2	0.0
335	166	232	722	1713	2242	2923	48	115	150	167	2.1	1.1	0.5
369	175	247	805	1819	2325	4441	54	122	156	167	2.1	1.1	0.4
498	204	239	1430	2432	3583	12285	96	163	167	185	2.1	0.1	0.6
524	210	284	1513	2523	7429	12741	101	164	176	186	2.0	0.4	0.3
680	230	613	-	3956	25730	-	102	167	211	-	2.0	1.4	-
717	234	822	-	8995	31145	-	128	179	218	-	1.6	1.2	-

Bar B													
Time (sec)	Force Applied Per Bar (kips)	SG01B (μstr)	SG02B (μstr)	SG03B (μstr)	SG04B (μstr)	SG05B (μstr)	$F_{s,SG01B/02B}$ (kips)	$F_{s,SG03B}$ (kips)	$F_{s,SG04B}$ (kips)	$F_{s,SG05B}$ (kips)	$\tau_{b,SG01B/02B-SG03B}$ (ksi)	$\tau_{b,SG03B-SG04B}$ (ksi)	$\tau_{b,SG04B-SG05B}$ (ksi)
20	32	15	23	38	83	258	1	3	6	17	0.0	0.1	0.4
113	34	15	15	45	83	302	1	3	6	20	0.1	0.1	0.5
173	53	30	15	83	234	568	2	6	16	38	0.1	0.3	0.7
262	127	384	656	995	1562	1602	35	67	105	107	1.0	1.2	0.1
335	166	805	920	1485	2068	2736	58	99	139	166	1.3	1.2	0.9
369	175	903	965	1598	2144	5666	63	107	144	170	1.4	1.1	0.8
498	204	1611	1297	2173	2605	-	97	146	165	-	1.5	0.6	-
524	210	1710	1327	2248	3515	-	102	151	167	-	1.5	0.5	-
680	230	-	1524	-	-	-	102	-	-	-	-	-	-
717	234	-	1917	-	-	-	128	-	-	-	-		-

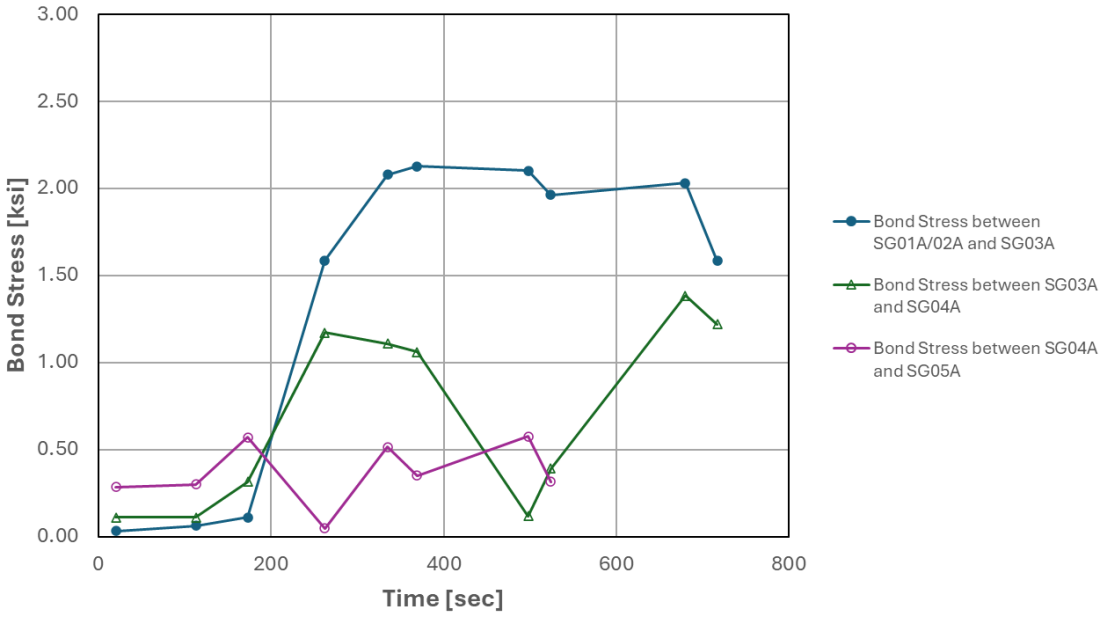

(a) Bar-A

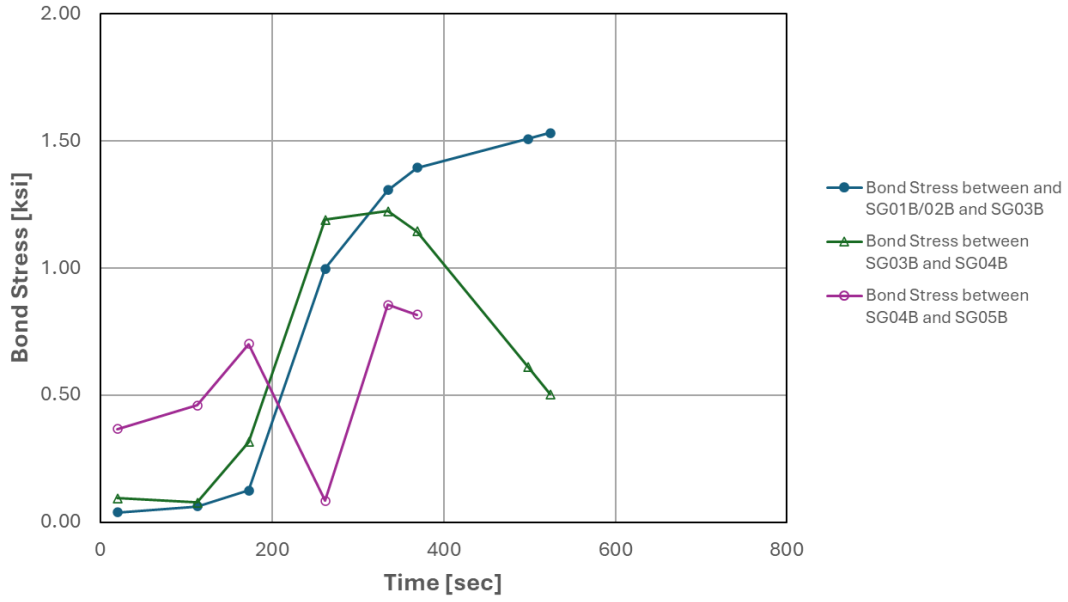

(b) Bar-B

Figure 5.17: Average bond stresses along headed bars versus time for Specimen 8

5.2.9 Specimen 9

Specimen 9 had the same design and material properties as Specimen 8, with two headed bars each having an embedment length of 24 inches, which was 100% of the minimum required by ACI 318-19. The only difference is that the T heads in Specimen 9 had a net bearing area of $9A_b$. Like Specimen 8, the bars in the specimen were able to develop their tensile strength without anchorage failure. The resisting forces calculated from strain data for Specimen 9 are shown in Table 5.17 and plotted against time in Figure 5.18. The total bearing resistance at the T heads increased as the applied force increased and reached 304 kips when the applied force reached 418 kips. The total bearing resistance at the T heads in specimen 9 was about 100 kips higher than that in Specimen 8 at the same applied force level probably due to a larger net bearing area of the T heads. Unfortunately, no reliable strain-gage data are available to calculate the bearing resistance at the heads as the applied force increased further. The bond force reached a peak value of 183 kips when the bearing force reached 145 kips, after which it decreased to 114 kips when the applied force reached 418 kips. Forces in the stirrups closer to the headed bars started to increase rapidly after the applied force reached 253 kips due to the initiation of concrete breakout cracks. This was similar to the cracking load for Specimen 8. The tensile forces in the stirrups further away from the headed bars increased more slowly. At the applied force of 418 kips, the stirrups in the four groups combined carried a total force of 244 kips, with the stirrups in the middle and Group 1 carrying 215 kips and the remaining stirrups carried 29 kips. The middle stirrup carried a much lower force compared to that in Specimen 8, while the stirrups in Group 2 carried a much higher force. The stirrups in Group 1 yielded, while the stirrups further away from the headed bars did not. The concrete resistance increased to a peak value of 206 kips when the applied force was 253 kips, and then it dropped to 195 kips and remained more or less constant when the applied force continued to increase.

The test was stopped when the applied force reached 507 kips because the hydraulic jacks reached stroke limit. At this point, the tensile stresses in the headed bars were close to the tensile strength, the breakout cracks did not open very significantly, and none of the stirrups fractured. Therefore, if the test were continued further, the headed bar would have fractured.

Table 5.17: Resisting forces at different loading phases for Specimen 9

Time (sec)	Force Applied (kips)	Head Force			Bond Force (kips)	Stirrup Force				Concrete Resistance (kips)
		Bar (A) (kips)	Bar (B) (kips)	Total Force (A)+(B) (kips)		Middle (kips)	Group 1 (kips)	Group 2 (kips)	Group 3 (kips)	
50	66	0	1	1	65	1	0	0	0	66
62	68	1	1	2	66	1	0	0	0	67
102	113	2	3	5	108	1	0	0	0	112
162	253	44	45	89	164	7	34	3	2	206
182	328	72	73	145	183	26	96	5	6	195
222	338	84	83	166	172	28	107	6	7	190
283	370	109	112	221	149	34	127	6	8	195
410	418	148	156	304	114	47	168	20	9	175
709	474	-	-	-	-	-	-	98	12	-
967	507	-	-	-	-	-	-	101	12	-

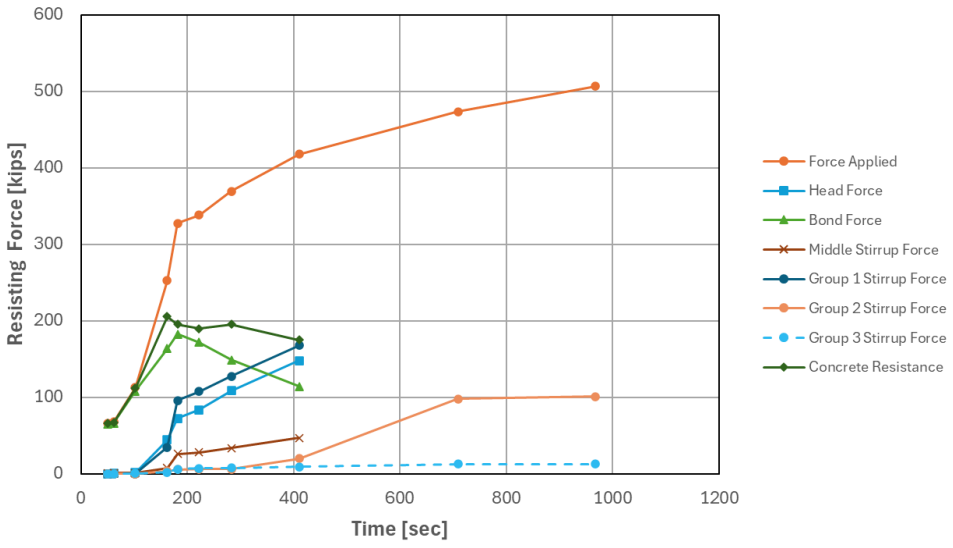

Figure 5.18: Exerted and resisting forces versus time for Specimen 9

The average bond stresses along the headed bars calculated for different applied force levels are shown in Table 5.18 and plotted in Figure 5.19. For Bar A, SG01A, one of the two gauges near the T head, did not function and only SG02A provided good data for that location. Furthermore, it is noted that the strains measured with SG03A, which was at the next level above SG02A, are lower than those with SG02A. Readings from SG03A do not appear to be reasonable. Therefore, the bond stress near the T head is calculated with data from SG02A and SG04A. For the same reason, the bond stress between SG03A and SG04A is not calculated. For Bar B, gages SG01B, SG03B, and SG05B did not function, and only SG02B and SG04B provided reliable data. Hence, the bond stress can be computed only for the region between SG02B and SG04B. Figure 5.19 shows that the bond stress in the upper region (between SG04A and SG05A) of Bar A was initially higher than that in the lower region. After 102 sec., the bond stress in the upper region dropped from its peak of 1.03 ksi to 0.19 ksi when the force applied to the bar reached 126 kips, and it remained more or less constant afterwards. The bond stress in the lower region between SG02A and SG04A reached a peak value of 1.3 ksi when the applied force reached 126 kips and dropped slowly afterwards. The bond stress computed for the region between SG02B and SG04B of Bar B is very close to that for Bar A and reached a peak value of 1.12 ksi when the applied force was 164 kips.

Table 5.18: Average bond stresses along headed bars for Specimen 9

Bar A												
Time (sec)	Force Applied Per Bar (kips)	SG01A (μstr)	SG02A (μstr)	SG03A (μstr)	SG04A (μstr)	SG05A (μstr)	$F_{s,SG02A}$ (kips)	$F_{s,SG03A}$ (kips)	$F_{s,SG04A}$ (kips)	$F_{s,SG05A}$ (kips)	$\tau_{b,SG02A-SG04A}$ (ksi)	$\tau_{b,SG04A-SG05A}$ (ksi)
50	33	-	0	45	98	432	0	3	7	29	0.10	0.70
62	34	-	8	45	106	432	1	3	7	29	0.10	0.68
102	56	-	23	121	280	773	2	8	19	52	0.27	1.03
162	126	-	659	689	1895	1987	44	46	127	133	1.30	0.19
182	164	-	1076	818	2564	2793	72	55	152	158	1.26	0.18
222	169	-	1250	879	2808	6223	84	59	158	166	1.17	0.23
283	185	-	1622	1046	3348	12137	109	70	165	171	0.88	0.21
410	209	-	2207	1304	-	10186	148	87	-	167	-	-
709	237	-	-	-	-	-	-	-	-	-	-	-
967	253	-	-	-	-	-	-	-	-	-	-	-

Bar B											
Time (sec)	Force Applied Per Bar (kips)	SG01B (μstr)	SG02B (μstr)	SG03B (μstr)	SG04B (μstr)	SG05B (μstr)	$F_{s,SG02B}$ (kips)	$F_{s,SG03B}$ (kips)	$F_{s,SG04B}$ (kips)	$F_{s,SG05B}$ (kips)	$\tau_{b,SG02B-SG04B}$ (ksi)
50	33	-	15	-	106	-	1	-	7	-	0.10
62	34	-	15	-	113	-	1	-	8	-	0.10
102	56	-	44	-	324	-	3	-	22	-	0.29
162	126	-	668	-	1662	-	45	-	111	-	1.04
182	164	-	1091	-	2154	-	73	-	144	-	1.12
222	169	-	1232	-	2230	-	83	-	149	-	1.05
283	185	-	1671	-	2533	-	112	-	152	-	0.62
410	209	-	2326	-	13564	-	156	-	174	-	0.29
709	237	-	-	-	-	-	-	-	-	-	-
970	253	-	-	-	-	-	-	-	-	-	-

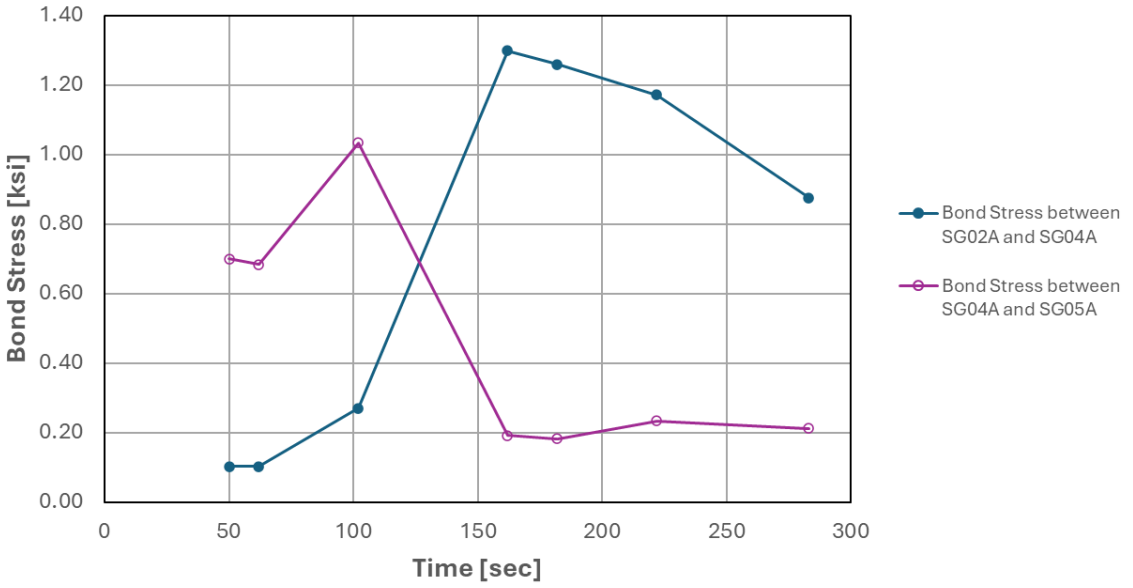

(a) Bar A

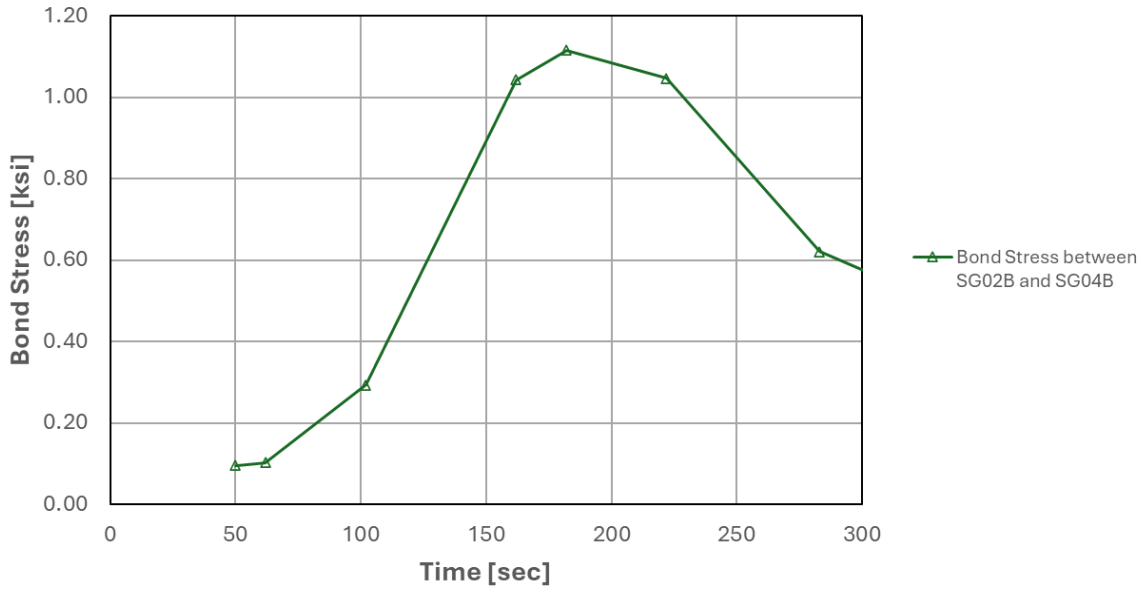

(b) Bar B

Figure 5.19: Average bond stresses along headed bars versus time for Specimen 9

5.2.10 Specimen 10

Specimen 10 consisted of a single No. 14 headed bar with a T head having a net bearing area of $4A_b$. The bar had an embedment length of 16 in., which was 70% of the minimum development required by ACI 318-19. The target compressive strength of the concrete was 6,000 psi, while the concrete cylinder strength obtained on the day of the anchorage test was 5,425 psi. The specimen had anchorage failure. The resisting forces calculated from the rebar strain data are shown in Table 5.19 and plotted against time in Figure 5.20. Readings from gauge SG01 were questionable and gauge SG02 stopped working early in the test. Hence, the bearing resistance at the T head and the bond force cannot be calculated, and only the resisting forces from the stirrups can be calculated from the strain data. Soon after 200 sec., as the applied load approached 130 kips, breakout cracks initiated, resulting in an increase in the forces carried by the stirrups and a reduction in concrete resistance. As shown in Table 4.14, when the maximum load of 179 kips was reached at 322 sec., the inner stirrups developed significant yielding while the strains in the outer stirrups were a bit below the yield value. The resisting forces of the stirrups remained more or less constant when the applied force decreased after the peak. While no data on the bearing resistance at the T head was available, the drop of the applied force could be caused by the bearing failure or the loss of the residual concrete strength along the breakout cracks. Hence, the failure of the bar anchorage could be caused by a combination of concrete breakout and concrete crushing at the T head. The low bearing resistance at the T head could be attributed to depth of the concrete breakout cone. As shown in Figure 4.59, the breakout cone was about 13 to 14 in. deep while the bearing face of the T head was 16 in. from the top face of the beam. Hence, once the breakout cone developed, the concrete cover above the T head was about 2 to 3 inches, which could not provide much bearing resistance.

Table 5.19: Resisting forces at different loading phases for Specimen 10

Time (sec)	Force Applied (kips)	Head Force (kips)	Bond Force (kips)	Inner Stirrup Force (kips)	Outer Stirrup Force (kips)	Concrete Resistance (kips)
60	3	-	-	0	0	3
80	45	-	-	0	0	44
103	60	-	-	0	0	60
165	97	-	-	1	0	96
200	129	-	-	8	0	121
248	142	-	-	57	19	66
270	158	-	-	65	37	56
322	179	-	-	65	64	50
336	150	-	-	67	55	28
361	143	-	-	65	62	16

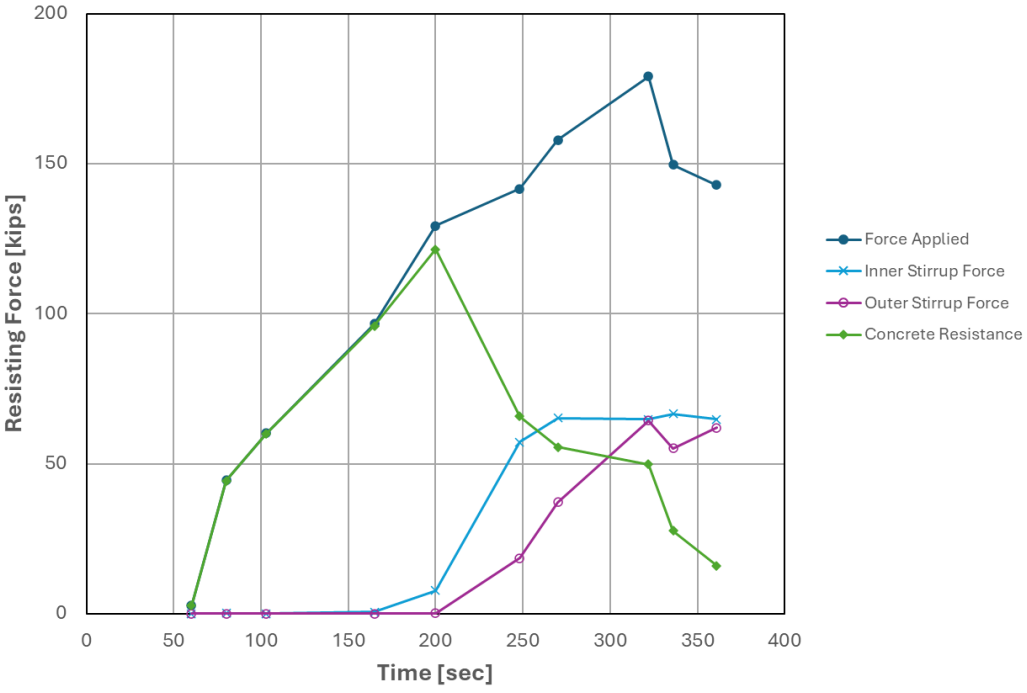

Figure 5.20: Exerted and resisting forces versus time for Specimen 10

The bond stress along the upper region of the headed bar was calculated with the data from gauges SG03 and SG05. Table 5.20 and Figure 5.21 show that the bond stress in the upper region of the bar reached a peak value of 1.05 ksi as the load reached 60 kips and dropped to 0 when the load reached 129 kips. At this point, the bond resistance in the upper portion was completely lost. Data after that point were unreliable. No data were available to calculate the bond stress along the lower region.

Table 5.20: Average bond stresses along headed bar for Specimen 10

Time (sec)	Force Applied (kips)	SG01A (µstr)	SG02A (µstr)	SG03A (µstr)	SG04A (µstr)	SG05A (µstr)	$F_{s,SG03}$ (kips)	$F_{s,SG05}$ (kips)	$\tau_{b,SG03\text{-}SG05}$ (ksi)
60	3	-	-	5	-	2	0	0	0.0
80	45	-	-	220	-	690	13	40	0.85
103	60	-	-	372	-	948	22	55	1.05
165	97	-	-	1136	-	1552	66	90	0.76
200	129	-	-	2118	-	2112	123	123	0.0
248	142	-	-	2601	-	2349	151	136	-
270	158	-	-	3957	-	11068	160	158	-
322	179	-	-	-	-	22885	-	179	-
336	150	-	-	-	-	22211	-	150	-
361	143	-	-	-	-	21666	-	143	-

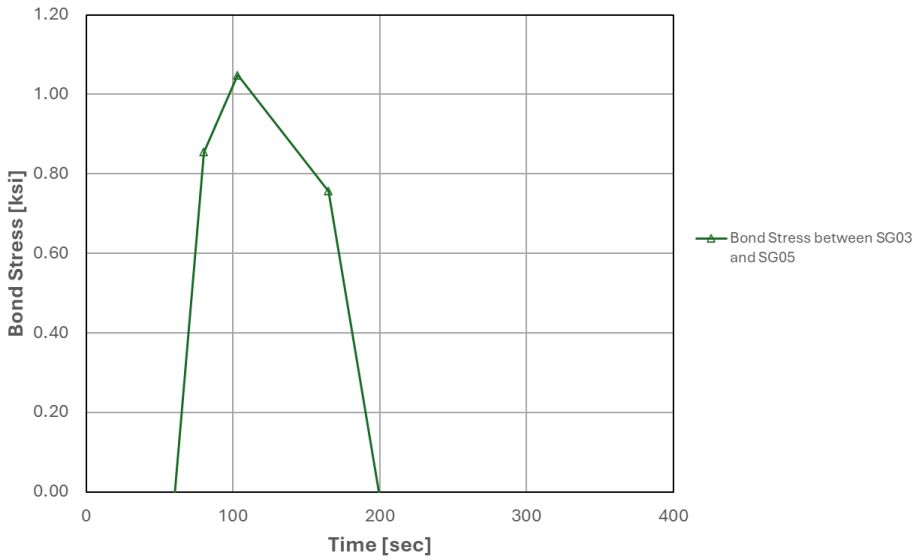

Figure 5.21: Average bond stresses along headed bar versus time for Specimen 10

5.2.11 Specimen 11

Specimen 11 had the same properties as Specimen 10, consisting of a single No. 14 headed bar with an embedment length of 16 in. (70% of the minimum required by ACI 318-19), but with a larger T head that had a net bearing area of $9A_b$. Like Specimen 10, the specimen had anchorage failure caused by a combination of concrete breakout and concrete crushing at the T head. The resisting forces calculated from the strain data are shown in Table 5.21 and plotted against time in Figure 5.22.

The maximum bearing resistance developed at the T head was 90 kips when the applied force reached the peak value of 177 kips. The tensile forces in the inner stirrups increased rapidly after the applied force reached 147 kips due to the formation of breakout cracks. As shown in Table 4.16, the inner stirrups yielded when the applied force reached 160 kips, while the strains in the outer stirrups never reached the yield value. The bond force reached a peak value of 95 kips prior to formation of breakout cracks, after which the bond force decreased gradually to 87 kips as the applied force reached 177 kips. After the formation of breakout cracks, the concrete resistance decreased from a peak value of 135 kips to 36 kips when the applied force reached 177 kips, with the stirrups carrying the remaining portion of the applied force. The data from the stirrups at 271 sec. appear to be unreliable because the concrete resistance has a negative value. The resisting forces developed by the stirrups dropped after the applied force passed the peak; so was the bearing resistance at the T head. Since the outer stirrups did not yield, like Specimen 10, the failure of the bar anchorage in this specimen was caused by a combination of concrete breakout and concrete crushing at the T head. As shown in Figure 4.65, the breakout cone was 14 in. deep while the bearing surface of the T head was 16 in. from the top face of the beam. Hence, once the breakout cracks developed, the concrete cover above the T head was no more than 2 in., which could not provide significant bearing resistance. The aforementioned failure mechanism explains why a larger T head in Specimen 11 did

not improve the anchorage capacity. When the concrete cover above the T head is thin, the bearing area is less influential.

Table 5.21: Resisting forces at different loading phases for Specimen 11

Time (sec)	Force Applied (kips)	Head Force (kips)	Bond Force (kips)	Inner Stirrup Force (kips)	Outer Stirrup Force (kips)	Concrete Resistance (kips)
41	13	0	13	0	0	12
66	137	42	95	2	0	135
72	147	67	80	67	16	64
82	160	80	80	77	29	54
94	161	82	79	77	30	54
100	164	83	81	77	34	53
133	177	90	87	85	56	36
156	77	55	22	8	41	27
182	72	53	19	12	47	14
271	96	27	69	56	67	-28

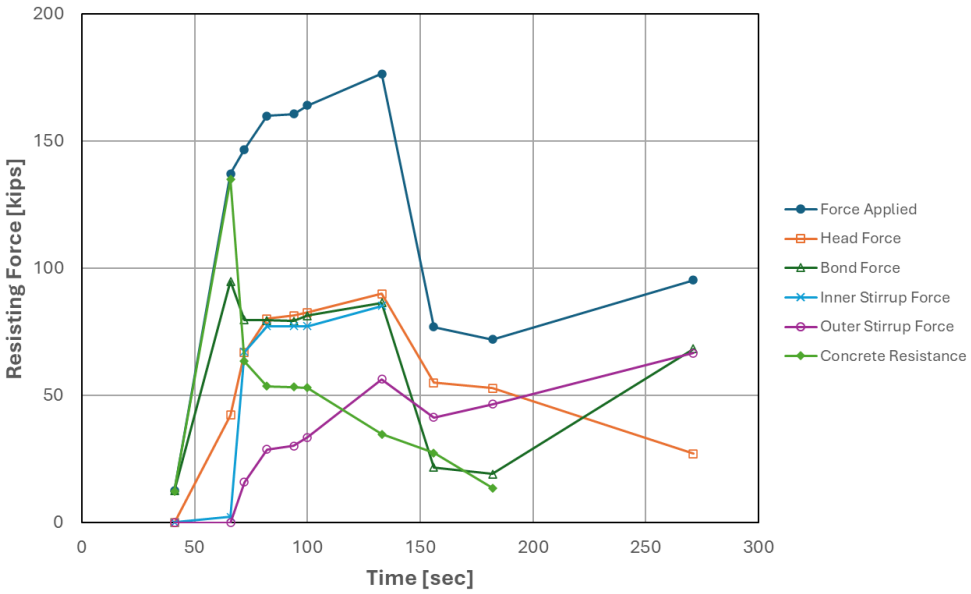

Figure 5.22: Exerted and resisting forces versus time for Specimen 11

The average bond stresses along the headed bar calculated for different applied force levels are shown in Table 5.22 and plotted in Figure 5.23. Because strain gauge SG05 did not function, the bond stress in the uppermost region cannot be calculated. Gauge SG03 stopped working after 100 seconds. Hence, the bond stresses in the lower two regions can only be computed up to 100 seconds. The bond stress in the region next to the T head, between SG01/02 and SG03, reached the maximum value of 1.53 ksi right before the formation of breakout cracks and then decreased gradually to about 1.2 ksi as the applied force increased to 164 kips. The bond stress in the region between SG03 and SG04 was very close to that in the lower region.

Table 5.22: Average bond stresses along headed bar for Specimen 11

Time (sec)	Force Applied (kips)	SG01 (μstr)	SG02 (μstr)	SG03 (μstr)	SG04 (μstr)	SG05 (μstr)	$F_{s,SG01/02}$ (kips)	$F_{s,SG03}$ (kips)	$F_{s,SG04}$ (kips)	$\tau_{b,SG01/02-SG03}$ (ksi)	$\tau_{b,SG03-SG04}$ (ksi)
41	13	7	5	31	142	-	0	0	13	0.00	0.41
66	137	899	673	1925	3504	-	42	91	137	1.53	1.45
72	147	1654	1094	2528	4037	-	67	112	147	1.41	1.10
82	160	1923	1424	2704	9976	-	80	119	160	1.21	1.29
94	161	1925	1465	2702	10728	-	82	119	161	1.17	1.31
100	164	1969	1505	2755	12038	-	83	121	164	1.20	1.35
133	177	2152	1666	-	19669	-	90	-	177	-	-
156	77	1180	1027	-	17315	-	55	-	77	-	-
182	72	1105	993	-	16608	-	53	-	72	-	-
271	96	371	-	-	16080	-	27	-	96	-	-

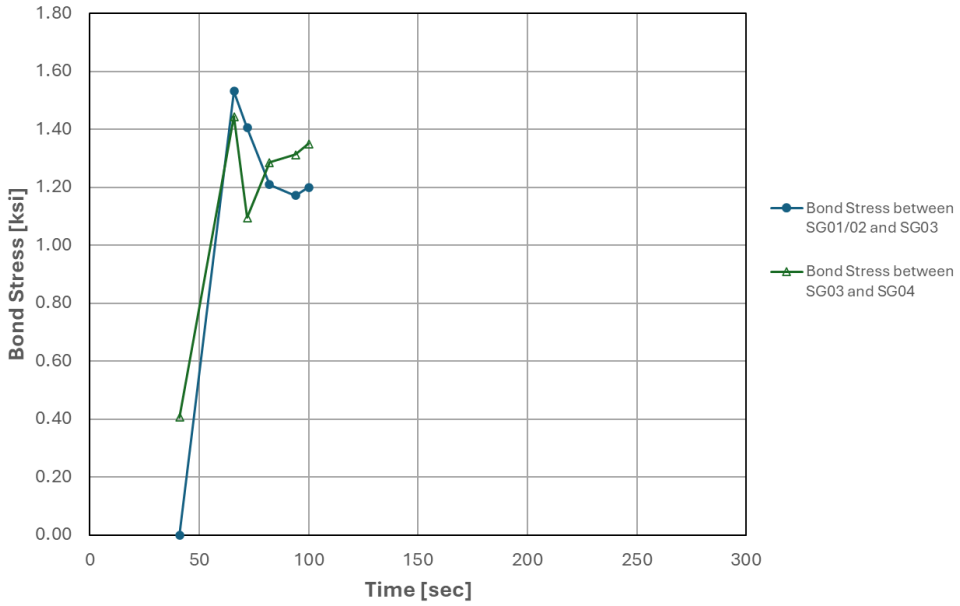

Figure 5.23: Average bond stresses along headed bar versus time for Specimen 11

5.2.12 Specimen 12

Specimen 12 had a single No. 18 headed bar with an embedment length of 26 inches, which was 70% of the minimum required by ACI 318-19 for 4,000-psi concrete. The concrete cylinders for this specimen had an average compressive strength of 3,935 psi on the day of the anchorage test. The T head had a net bearing area of $4A_b$. The specimen was able to develop the full tensile strength of the bar without anchorage failure.

The resisting forces calculated from the strain data for Specimen 12 are shown in Table 5.23 and plotted against time in Figure 5.24. In the middle of the test, the applied force was momentarily removed for reasons explained in Section 4.13. For clarity, data collected in the unloading portion of the test (between 520 and 893 sec.) are skipped here. As shown in the table and the figure, the bearing resistance at the T head increased with the increase of the applied force. At the maximum applied force of 369 kips, the bearing resistance was 291 kips, while the remaining 78 kips of the

applied force was carried by the bond force. Breakout cracks initiated when the applied force reached 290 kips. As shown in Table 5.23, after the occurrence of the breakout cracks, forces in the stirrups started to increase suddenly. The total resistance developed by the stirrups was 311 kips when the applied force reached the maximum value of 369 kips. This means that the stirrups carried 84% of the applied force. Most of the forces were carried by the four sets of stirrups that were closest to the headed bar. The low strain values of the stirrups that were 2 ft. – 6 in. away from the headed bar indicate that they still had reserve capacity to carry additional load. However, these stirrups were close to the edges of the breakout cone (whose length is shown in Figure 4.71) and were therefore not too effective in resisting breakout failure. No breakout failure was observed in the test.

Table 5.23: Resisting forces at different loading phases for Specimen 12

Time (sec)	Force Applied (kips)	Head Force (kips)	Bond Force (kips)	Stirrup Force			Concrete Resistance (kips)
				2'-6" from bar (kips)	1'-6" from bar (kips)	6" from bar (kips)	
131	29	13	16	0	0	0	29
235	159	54	105	0	0	2	157
340	289	181	108	1	0	9	279
484	324	209	115	49	110	109	57
520	334	223	111	54	109	109	62
893	335	239	96	62	109	109	55
950	353	256	97	75	111	110	58
1040	369	291	78	88	113	110	58

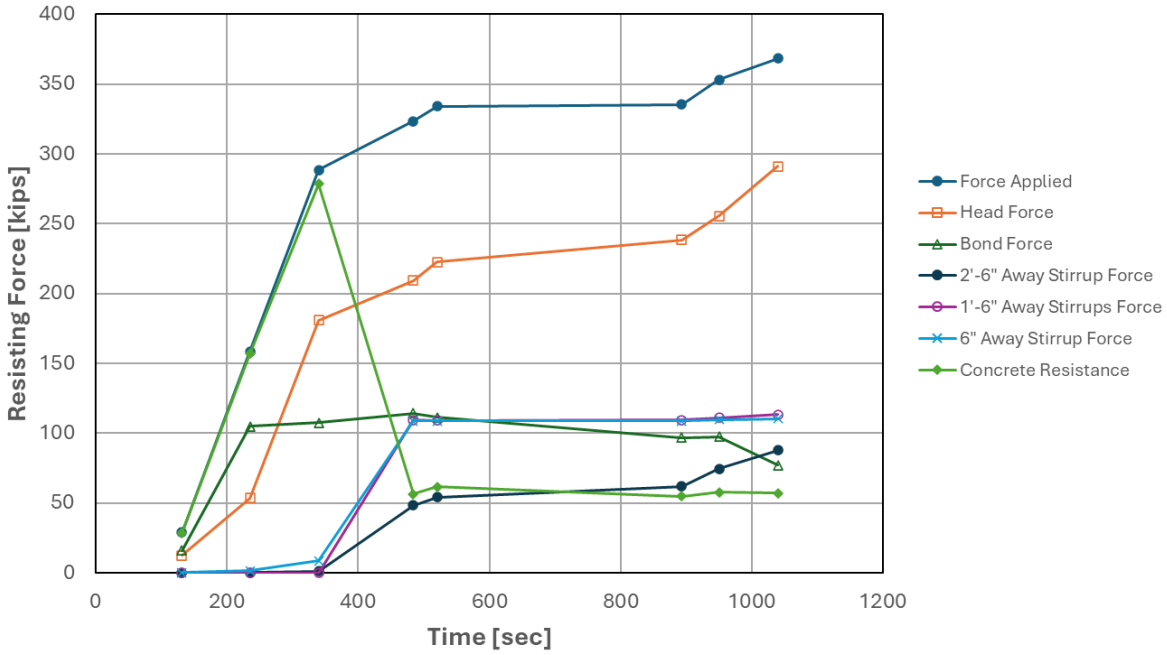

Figure 5.24: Exerted and resisting forces versus time for Specimen 12

The average bond stress along the headed bar calculated for different applied force levels are shown in Table 5.24 and plotted in Figure 5.25. As shown in Table 5.24, after the initiation of breakout cracks in the beam at 340 sec., significant yielding occurred along the upper region of the headed bar. When the applied force reached the maximum value of 369 kips, yielding propagated to the region next to the T head. The bond stress in the upper region of the bar is calculated with readings from gauges SG05 and SG07, because SG06 did not work. Since SG07 was one inch above the top face of the concrete beam, only the bonded region of the bar is considered in the calculation. Gauge SG08 was at the same elevation as SG07. However, it registered unrealistically large strain values in the early stage of the test but similar strain values as SG07 once yielding occurred (as shown in Table 4.17), it has been decided that its readings are not to be included in the calculation. Because of the severe plastic deformation of the bar in that region, significant bond deterioration occurred and the bond stress calculated is very low. The bond stress between SG04 and SG05 reached a maximum

value of 1.63 ksi at the applied force of 159 kips and then dropped to 0.56 ksi when the applied force reached 289 kips, remaining more or less constant afterwards. The bond stress between SG03 and SG04 reached a maximum value of 1.59 ksi when the applied force reached 324 kips. The bond stress close to the T head reached a maximum value of 0.96 ksi when the applied force reached 335 kips and remained more or less at that level afterwards. This indicates that the head did not slip much. It can be seen that between 484 and 520 sec., there is a significant drop of the bond stress between SG01/02 and SG03 and a significant jump in the bond stress between SG03 and SG04. This could be caused by the unusually low strain values registered by SG03 in this time interval.

Table 5.24: Average bond stresses along headed bar for Specimen 12

Time (sec)	Force Applied (kips)	SG01 (μstr)	SG02 (μstr)	SG03 (μstr)	SG04 (μstr)	SG05 (μstr)	SG07 (μstr)
131	29	98	105	157	188	196	128
235	159	459	399	660	896	1450	1150
340	289	1498	1394	1758	2073	2473	2561
484	324	1438	1907	1788	5591	19517	23687
520	334	1513	2043	1871	16159	23852	28098
893	335	1634	2179	2390	20030	27689	31177
950	353	1913	2172	13873	23956	33142	37817
1040	369	6088	4444	22801	35749	45399	46754

Time (sec)	Force Applied (kips)	$F_{s,SG01/02}$ (kips)	$F_{s,SG03}$ (kips)	$F_{s,SG04}$ (kips)	$F_{s,SG05}$ (kips)	$F_{s,SG07}$ (kips)	$\tau_{b,SG01/02-SG03}$ (ksi)	$\tau_{b,SG03-SG04}$ (ksi)	$\tau_{b,SG04-SG05}$ (ksi)	$\tau_{b,SG05-SG07}$ (ksi)
131	29	13	20	24	25	29	0.16	0.09	0.02	0.08
235	159	54	83	112	182	159	0.68	0.69	1.63	0.00
340	289	181	220	259	283	289	0.92	0.93	0.56	0.09
484	324	209	224	291	311	324	0.34	1.59	0.47	0.22
520	334	223	234	299	324	334	0.27	1.53	0.58	0.17
893	335	239	279	313	334	335	0.96	0.78	0.51	0.02
950	353	256	293	324	344	353	0.88	0.74	0.45	0.17
1040	369	291	321	349	367	369	0.70	0.66	0.41	0.03

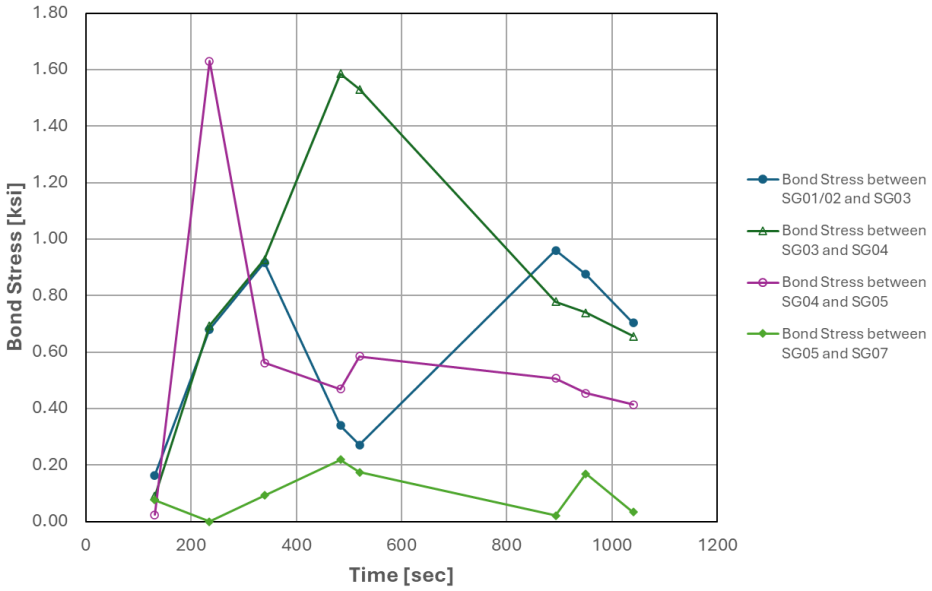

Figure 5.25: Average bond stresses along headed bar versus time for Specimen 12

5.2.13 Specimen 13

Specimen 13 had the same properties as Specimen 12. However, the No. 18 headed bar in this specimen had an embedment length of 37 inches (100% of the minimum required by ACI 318-19) instead. The T head in Specimen 13 had the same net bearing area of $4A_b$ as Specimen 12. Hence, the bar in this specimen was able to develop its tensile strength without anchorage failure as expected. Specimen 13 had much less cracks than Specimen 12. As discussed in Section 4.14, it had no breakout cracks and the cracking on the top face of the beam around the bar was much less severe.

The resisting forces calculated from the strain data for Specimen 13 are shown in Table 5.25 and plotted against time in Figure 5.26. The bearing force developed at the T head was close to zero until the applied force exceeded 24 kips. At the applied force of 188 kips, much of the applied force was resisted by the bond and only 44 kips was resisted by the T head. When the applied force

exceeded 188 kips, the bearing force at the T head had a significant increase and the bond force remained more or less at the same level. At the applied force of 346 kips, which was close to the peak force of 379 kips, the head developed a resistance of 185 kips and the bond force was 161 kips. No strain data is available beyond that point. The forces developed in the stirrups are negligible, which is consistent with the fact that no breakout cracks were observed in the test.

Table 5.25: Resisting forces at different loading phases for Specimen 13

Time (sec)	Force Applied (kips)	Head Force (kips)	Bond Force (kips)	Stirrup Force				Concrete Resistance (kips)
				3'-6" from bar (kips)	2'-6" from bar (kips)	1'-6" from bar (kips)	6" from bar (kips)	
250	10	0	10	0	0	0	0	10
300	24	0	24	0	0	0	0	24
400	188	44	144	0	0	0	0	188
460	289	131	158	0	0	0	1	288
522	285	137	148	0	0	0	1	284
570	308	159	149	0	0	0	1	307
600	313	172	141	0	0	0	2	311
709	346	185	161	1	0	0	3	345
800	354	-	-	0	0	0	4	350
890	379	-	-	1	0	0	4	375

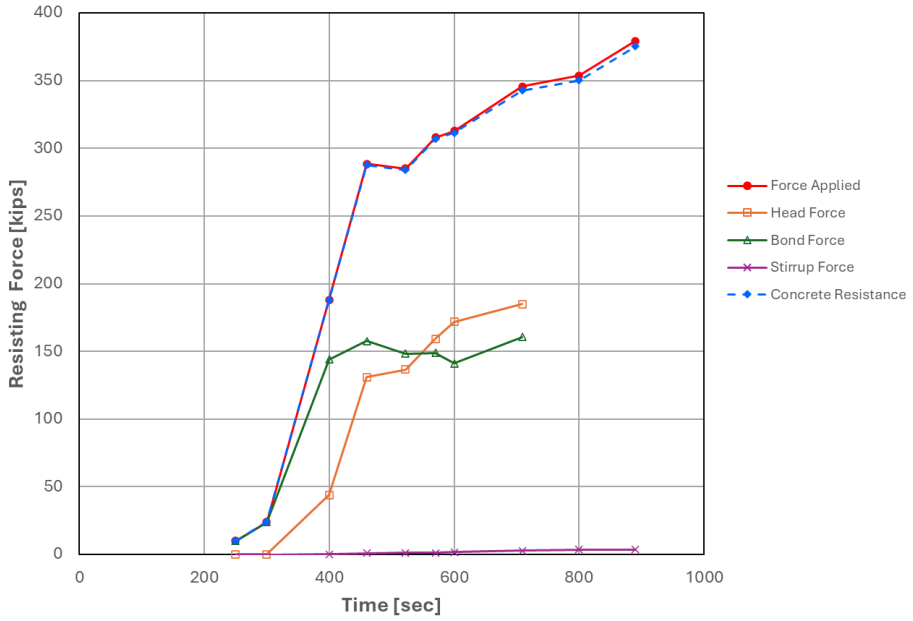

Figure 5.26: Exerted and resisting forces versus time for Specimen 13

The average bond stresses along the headed bar calculated for different applied force levels are shown in Table 5.26 and plotted in Figure 5.27. Because gauges SG01, SG02, and SG04 stopped working at or right after 600 sec., the bond stresses in the regions between SG01/02 and SG03, SG03 and SG04, and SG04 and SG05 cannot be calculated after that point. The bond stress in the region near the T head increased from 0 to 0.80 ksi when the applied force increased from 24 kips to 188 kips and continued to increase to the peak value of 1.52 ksi when the applied force reached 346 kips, indicating limited bar slip in that region. The bond stresses in the upper regions were lower and those in the two uppermost region were 0.79 and 1.12 ksi, respectively, at the end of the test.

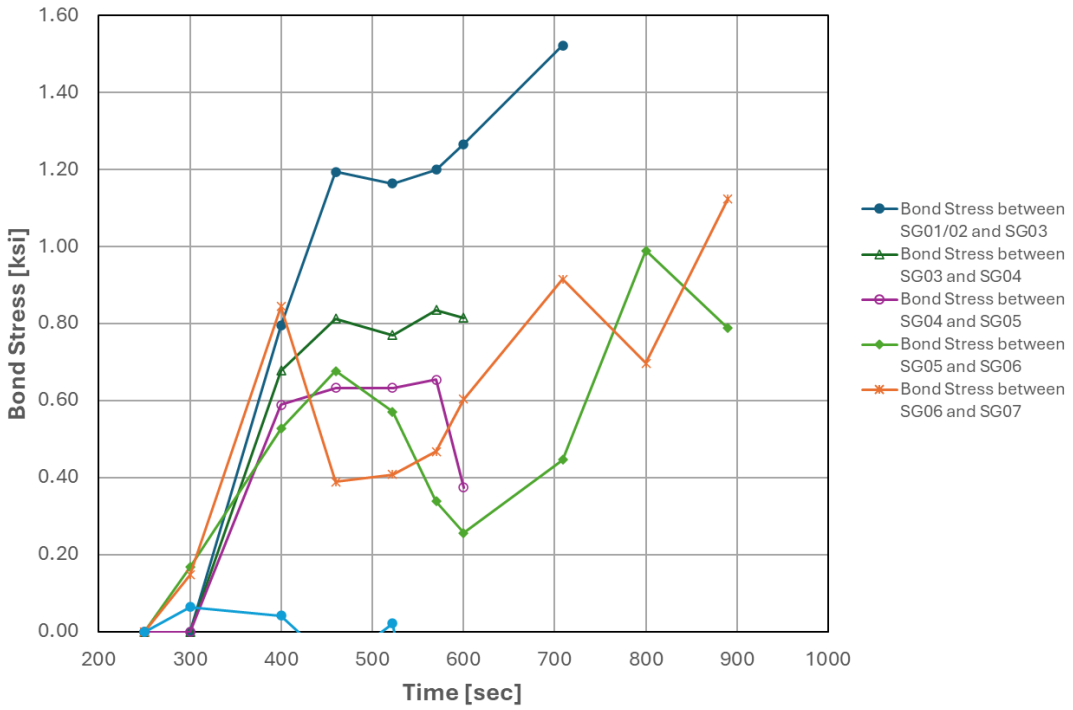

Figure 5.27: Average bond stresses along headed bar versus time for Specimen 13

Table 5.26: Average bond stresses along headed bar for Specimen 13

Time (sec)	Force Applied (kips)	SG01 (μstr)	SG02 (μstr)	SG03 (μstr)	SG04 (μstr)	SG05 (μstr)	SG06 (μstr)	SG07 (μstr)
250	10	0	0	0	0	0	0	0
300	24	0	0	0	0	0	60	113
400	188	341	417	657	901	1112	1302	1605
460	289	961	1283	1534	1826	2053	2296	2965
522	285	999	1329	1571	1848	2076	2281	17625
570	308	1212	1496	1776	2076	2311	5244	22420
600	313	1356	1595	1905	2198	2448	14406	26494
709	346	1584	-	2109	-	12611	22251	39231
800	354	-	-	2208	-	17208	29771	49908
890	379	-	-	2253	-	19507	33590	54935

Time (sec)	Force Applied (kips)	$F_{s,SG01/02}$ (kips)	$F_{s,SG03}$ (kips)	$F_{s,SG04}$ (kips)	$F_{s,SG05}$ (kips)	$F_{s,SG06}$ (kips)	$F_{s,SG07}$ (kips)	$\tau_{b,SG01/02-SG03}$ (ksi)	$\tau_{b,SG03-SG04}$ (ksi)	$\tau_{b,SG04-SG05}$ (ksi)	$\tau_{b,SG05-SG06}$ (ksi)	$\tau_{b,SG06-SG07}$ (ksi)
250	10	0	0	0	0	0	0	0.00	0.00	0.00	0.00	0.00
300	24	0	0	0	0	7	13	0.00	0.00	0.00	0.17	0.15
400	188	44	78	107	132	154	190	0.80	0.68	0.59	0.53	0.84
460	289	131	182	216	243	272	289	1.19	0.81	0.63	0.68	0.39
522	285	137	186	219	246	270	288	1.16	0.77	0.63	0.57	0.41
570	308	159	210	246	274	288	308	1.20	0.84	0.65	0.34	0.47
600	313	172	226	260	276	287	313	1.27	0.82	0.38	0.26	0.60
709	346	185	250	0	288	307	346	1.52	-	-	0.44	0.92
800	354	0	262	0	282	324	354	-	-	-	0.99	0.70
890	379	0	267	0	298	331	379	-	-	-	0.79	1.12

Chapter 6 Tension Development of Headed Bars

The test data presented in Chapter 4 have shown that the development length formula for headed bars in ACI 318-19 can be safely applied to No. 14 and No. 18 bars. Furthermore, it is a bit more conservative for No. 18 bars than No. 14 bars. However, the ACI formula is empirical and prescriptive, including the requirement for parallel tie reinforcement, which seems to be intended for beam-to-column joints in building frames rather than joints in a bridge structure, such as column-to-cap beam joints and column-to-footing joints. The test data presented in Chapter 5 have shown that parallel tie reinforcement can play a significant role in the anchorage capacity of a headed bar. Hence, it is important to have a rational way to determine the quantity of the reinforcement required for a joint region. In this chapter, a general and rational method to determine the development length required for headed bars and the quantity of parallel tie reinforcement required for the joint region is presented. It is derived from the headed anchor bolt provisions in ACI 318-19, which entail the calculation of the anchorage capacity based on probable load resisting mechanisms.

6.1 Calculation of Anchorage Strength of Headed Bars

As stated in Section 5.1, the anchorage capacity of a headed bar can be governed by the concrete breakout strength or the bar pullout strength. This is very similar to the anchorage strength of a headed anchor bolt, as discussed in Chapter 2. In this section, the experimental results presented in Section 5.2 are used to evaluate the applicability of the formulas in ACI 318-19 for calculating the breakout and pullout strengths of headed anchor bolts to the calculation of the anchorage capacity of headed bars and modify the formulas as needed to obtain a better correlation with the experimental data. In addition, a method to determine the quantity of parallel tie reinforcement needed to restrain breakout cracks is presented. The ACI anchor bolt provisions do

not provide explicit specifications for parallel tie reinforcement. The main differences between an anchor bolt and a headed bar are their diameters, surface conditions, and head size. However, a major difference is that the tensile strength of an anchor bolt can be governed by its anchorage capacity or the tensile strength of the steel while the anchorage capacity of a headed bar cannot be lower than the tensile strength of the bar.

In the following sections, the breakout resistance and pullout resistance of a headed bar are discussed in more detail, and the experimental data obtained in this study are used to understand and calibrate these load resisting mechanisms and arrive at design recommendations.

6.1.1 Breakout Resistance

As discussed in Section 5.1, the concrete breakout strength depends on the tensile strength of the concrete and the surface area of the breakout cone, which is a function of the bar embedment length. Once breakout cracks occur, stirrups (tie reinforcement) parallel to the anchored bar crossing the inclined cracks help to restrain the cracks from opening as depicted in Figure 5.1. However, the formula in ACI 318-19 for calculating the breakout strength of a headed anchor bolt does not consider the contribution of the parallel reinforcement, if any, to the anchorage capacity.

Concrete Breakout Strength

In the ACI code, the concrete breakout strength for a headed anchor bolt is given by the following formula.

$$F_{cb} = k_c \sqrt{f_c'} l_e^{1.5} \frac{A_{Nc}}{A_{Nco}} \psi_{ed,N} \tag{6.1}$$

in which F_{cb} is the concrete breakout strength in kips, f_c' is the compressive strength of the concrete in ksi, l_e is the embedment length in inches measured from the bearing surface of the head, A_{Nc} is

the projected concrete failure area for a single anchor bolt or a group of anchor bolts as defined in ACI, A_{Nco} is the projected concrete failure area for a single anchor bolt not limited by the edge distance or anchor bolt spacing, $\psi_{ed,N}$ is a factor that accounts for the proximity of the anchor bolt to the edge of the concrete member, and k_c is a factor that has a value of 0.759 for cast-in-place anchor bolts (based on the units adopted here for Equation (6.1)).

The projected failure area, A_{Nco}, for a single anchor bolt not limited by the edge distance or anchor bolt spacing and the value of the edge effect factor, $\psi_{ed,N}$, are to be calculated with the following equations specified in ACI.

$$A_{Nco} = 9l_e^2 \tag{6.2}$$

$$\psi_{ed,N} = 1.0 \text{ when } c_{a,\min} \geq 1.5l_e \tag{6.3a}$$

$$\psi_{ed,N} = 0.7 + 0.3\frac{c_{a,\min}}{1.5l_e} \text{ when } c_{a,\min} < 1.5l_e \tag{6.3b}$$

in which $c_{a,\min}$ is the minimum distance (in inches) from the center of the anchor bolt to the edge of the concrete member.

To evaluate the applicability of Equation (6.1) to headed bars, the applied forces at which breakout cracks initiated in the test specimens, which are reported in Section 5.2, are used to back calculate the value of k_c in Equation (6.1) as follows.

$$k_c = \frac{(F_{cb})_{measured}}{\sqrt{f_c'}l_e^{1.5}\frac{A_{Nc}}{A_{Nco}}\psi_{ed,N}} \tag{6.4}$$

The values of k_c calculated are shown in Table 6.1. Specimen 13 did not develop breakout cracks, and, therefore, its k_c value is not available. It can be observed from the table that the calculated values of k_c are significantly higher than 0.759, which is specified in ACI 318-19 for anchor bolts, and vary from 1.72 for Specimen 4 to 3.19 for Specimen 8. The average is 2.30 and the coefficient of variation is 0.227, which is quite large. Table 6.1 shows that the calculated value of k_c has a strong correlation with the embedment length of the headed bar in that a specimen that had a longer embedment length tends to have a larger k_c value. This can be attributed to the term $l_e^{1.5}$ in Equations (6.1) and (6.4). In theory, the concrete breakout strength is proportional to the surface area of the breakout cone if the concrete strength remains constant. Since the angle of the inclined crack surface forming a breakout cone is more or less a constant that is around 33.7 degrees (i.e., $\arctan(1/1.5)$) regardless of the embedment length, as shown in the anchorage tests conducted in this study and also assumed in the anchor bolt provisions in ACI 318-19, the surface area of a breakout cone is, therefore, proportional to l_e^2. Based on this fact, the concrete breakout strength should be proportional to l_e^2 rather than $l_e^{1.5}$. Hence, Equation (6.4) is modified as follows.

$$k_c = \frac{\left(F_{cb}\right)_{measured}}{\sqrt{f_c'} l_e^2 \frac{A_{Nc}}{A_{Nco}} \psi_{ed,N}} \tag{6.5}$$

The values of k_c calculated for the specimens with Equation (6.5) are also presented in Table 6.1. The average value of k_c is now reduced to 0.61, and the coefficient of variation is reduced to 0.136. The scatter of the calculated values has been significantly reduced. The lowest calculated k_c value is 0.50, while the highest is 0.68.

Table 6.1: Breakout resistance data from tests

Specimen	1	2	3	4	5	6	7	8	9	10	11	12	13
f'_c (ksi)	4.120	3.890	4.130	8.000	8.000	8.580	8.580	4.350	4.350	5.430	5.430	3.940	4.210
d_b (in.)	1.693	1.693	1.693	1.693	1.693	1.693	1.693	1.693	1.693	1.693	1.693	2.257	2.257
A_b (in.^{2})	2.25	2.25	2.25	2.25	2.25	2.25	2.25	2.25	2.25	2.25	2.25	4	4
A_h (in.^{2})	9.00	9.00	20.25	9.00	9.00	9.00	20.25	9.00	20.25	9.00	20.25	16	16
l_e (in.)	16.75	24.00	16.75	14.00	14.00	20.00	14.00	24	24	16.00	16.00	26	37
A_{hs} (in.^{2})	2.25	2.25	2.25	2.25	2.25	2.25	2.25	4.5	4.5	2.25	2.25	4	4
$\tilde{A}_{tt}$ (in.^{2})	2.48	3.72	2.48	2.48	1.60	3.72	2.48	8.68	8.68	2.48	2.48	5.28	8.80
$\tilde{A}_{tt}/A_{hs}$	1.10	1.65	1.10	1.10	0.71	1.65	1.10	1.93	1.93	1.10	1.10	1.32	2.20
f_{ut} (ksi)	106.6	91.5	91.5	92.5	94.7	90.7	90.7	92.7	92.7	90.6	90.6	90.0	90.0
$c_{a,min}$ (in.)	13.0	13.0	13.0	13.0	13.0	13.0	13.0	13.0	13.0	13.0	13.0	17.5	17.5
Measured F_{cb} (kips)	129	180	140	140	152	180	154	254	253	130	147	290	NA
Measured F_t (kips)	157	121	-	128	116	103	188	343	-	129	141	311	5
F_{ut} from Eq. (6.7) (kips)	264	340	227	229	152	337	225	805	805	225	225	475	792
Max. Applied Force, F_{max} (kips)	179	225	213	173	152	212	188	469[1]	507[1]	179	177	369	375
k_c from Eq. (6.4)	2.10	2.66	2.27	1.72	1.87	1.91	1.83	3.19	3.18	1.87	2.11	2.94	NA
k_c from Eq. (6.5)	0.59	0.64	0.64	0.53	0.57	0.50	0.56	0.76	0.76	0.54	0.61	0.68	NA
F_t/F_{ut}	0.594	0.355	-	0.558	0.766	0.305	0.836	0.426	-	0.574	0.628	0.654	0.006
F_t/F_{max}	0.877	0.538	-	0.740	0.763	0.486	1.000	0.731	-	0.721	0.797	0.843	0.013
Anchorage Failure	Y	N	N	Y	Y	N	Y	N	N	Y	Y	N	N

[1]Total for two bars.

Based on the above analysis, it is recommended that the concrete breakout strength for a headed bar be calculated with the following equation.

$$F_{cb} = 0.5\sqrt{f_c'}l_e^2 \frac{A_{Nc}}{A_{Nco}}\psi_{ed,N} \tag{6.6}$$

in which the value of k_c is assumed to be 0.5 to be conservative. The variables in the above equation are to be determined with Equations (6.2) and (6.3).

Equation (6.6) has been used to calculate the expected concrete breakout strength for Specimen 13, which had sufficient embedment length to prevent breakout cracks during the test. The breakout strength calculated is 352 kips, while the specimen was loaded to a peak force (F_{max}) of 375 kips without developing breakout cracks. This shows that the prediction is reasonable and conservative. If the formula is reliable, then the specimen was not far from developing breakout cracks.

Resistance of Parallel Tie Reinforcement

Once breakout cracks occur, the cracks can be restrained from opening if sufficient parallel tie reinforcement is provided in the breakout region. The breakout resistance of the parallel tie reinforcement (stirrups) is given by the following formula.

$$F_{ut} = \tilde{A}_{tt} f_{ut} \tag{6.7}$$

in which $\tilde{A}_{tt}$ is the total cross-sectional area of the parallel tie reinforcement crossing the crack planes and f_{ut} is tensile strength of the tie reinforcement. For this purpose, all the parallel tie reinforcement within the projected failure area A_{Nc} of the breakout cone can be considered. The area A_{Nc} can be determined according to the anchor bolt specifications in ACI 318-19.

In order to provide sufficient anchorage resistance to develop the tensile strength of the headed bars after the occurrence of breakout cracks, F_{ut} should be greater than $F_{hs,u}$, which is equal to $A_{hs}f_u$, where A_{hs} is the total cross-sectional of the headed bars being developed and f_u is the tensile strength of the headed bars. However, it is prudent to have the nominal tensile resistance provided by the tie reinforcement at least1.25 times that of the headed bars in consideration of the fact that the actual tensile strength of a bar can be as high as 1.25 times its nominal strength. Hence, it is recommended that the minimum tie area, $\tilde{A}_{tt}$, meet the following requirement.

$$\tilde{A}_{tt} \geq 1.25 \frac{f_y}{f_{yt}} A_{hs} \tag{6.8}$$

in which f_y and f_{yt} are the nominal yield strengths of the headed bars and tie reinforcement, respectively. The above recommendation seems adequate based on the test data presented in this report. As shown in Table 6.1, all the specimens that had anchorage failures had $\tilde{A}_{tt} / A_{hs} = 1.10$ or lower, while those with an area ratio of 1.32 or above were able to develop the full tensile strengths of the headed bars with the breakout cracks well restrained. One specimen (Specimen 3) that had $\tilde{A}_{tt} / A_{hs} = 1.10$ did not have anchorage failure. The tie reinforcement and headed bars in the specimens were all Grade 60.

Table 6.1 also shows the values of the tie resistance F_t calculated from the strains measured in the stirrups at the point when the applied force reached the peak value, $F_{\max}$, and the values of the tie capacity F_{ut} calculated with Equation (6.7) based on the measured tensile strengths of the stirrups. For Specimen 13, the value of the F_t / F_{ut} ratio is 0.006, which is extremely small because the specimen did not have breakout cracks. For the other specimens, the F_t / F_{ut} ratios vary from 0.305 to 0.836. In general, specimens that had anchorage failures have higher ratios than those

without. Specimens that had anchorage failures have an average F_t / F_{ut} ratio of 0.695, while those without (excluding Specimen 13) have an average of 0.435. It can also be observed that the $F_t / F_{\max}$ ratios vary from 0.013 to 1.0. Specimens with anchorage failures generally have higher ratios than those without. Specimens that had anchorage failures have an average $F_t / F_{\max}$ ratio of 0.816, while those without anchorage failure (excluding Specimen 13) have an average of 0.650. The reason that the $F_t / F_{\max}$ ratio is always less than one with the exception of Specimen 7, which has a ratio of one, is that part of the applied load was carried by the residual concrete resistance along the crack surfaces (as well as the dowel forces of the top longitudinal bars in the beams). The fact that specimens that had anchorage failures have the values of F_t / F_{ut} less than one is a strong indication that the anchorage failures were eventually induced by concrete crushing above the T heads when the breakout cracks opened. This is supported by the experimental observations that the breakout cracks observed from the specimens did not open much when anchorage failures occurred and none had tie fracture. In addition, severe concrete crushing was observed above the T heads in a number of specimens. Specimen 5 showed the widest breakout cracks, but these cracks appeared only in the cover concrete outside the steel cage, as shown in Figure 4.26. The specimen also had severe concrete crushing above the T head as shown in Figure 4.25.

Concluding Remarks

In theory, if headed bars have sufficient embedment length so that the concrete breakout strength F_{cb} calculated with Equation (6.6) is greater than the maximum expected tensile strength $F_{hs,u}$ of the bars, parallel ties will not be needed. If not, parallel tie reinforcement should be provided, and the total cross-sectional area $\tilde{A}_{tt}$ of the ties should satisfy Equation (6.8). However, for additional safeguard against breakout failure, it may be advisable to have a minimum amount of tie reinforcement even if it is not needed.

6.1.2 Bar Pullout Strength

The pullout resistance, F_p, of a headed bar is the sum of two components as shown in the following expression.

$$F_p = F_b + F_h \tag{6.9}$$

in which F_b is the bond resistance along the deformed bar surface and F_h is the bearing resistance at the T head. These two load resisting mechanisms are discussed below.

Bond Resistance

The total bond resistance developed by a bar that has an embedment length l_e is given by the following equation.

$$F_b = \pi d_b \int_0^{l_e} \tau_b dx \tag{6.10}$$

in which d_b is the nominal bar diameter and τ_b is the bond stress developed along the bar surface. As shown by the data presented in Section 5.2, bond stress τ_b can be highly non-uniform along the embedment length of a bar and change with the increase of the applied force. This is attributed to the non-uniform slip along the bar, with the highest slip occurring at the loaded end and the lowest slip at the T head. The bond stress-vs.-slip behavior of typical reinforcing bars is illustrated in Figure 6.1. It shows that as the slip of a bar increases, the bond stress will increase rapidly at the beginning, and it will decease quickly after passing the peak strength because of bond deterioration. Bond stress distributions along the embedment length of a well anchored reinforcing bar at different levels of loading are illustrated in Figure 6.2. The results were obtained numerically with a finite element model by Murcia-Delso et al. (2013). The figure shows the stress distributions occurring at various slip levels that were measured at the loaded end. It can be observed that as the slip at the loaded

end increased due to the increase of the applied load, bond deterioration penetrated deeper into the embedded region of the bar causing significant reduction in bond strength. At a greater depth, the bond stress became higher reaching a peak because of reduced bar slip and lesser bond deterioration. Below the peak point, the decrease in the bond stress was due to decreased bar slip.

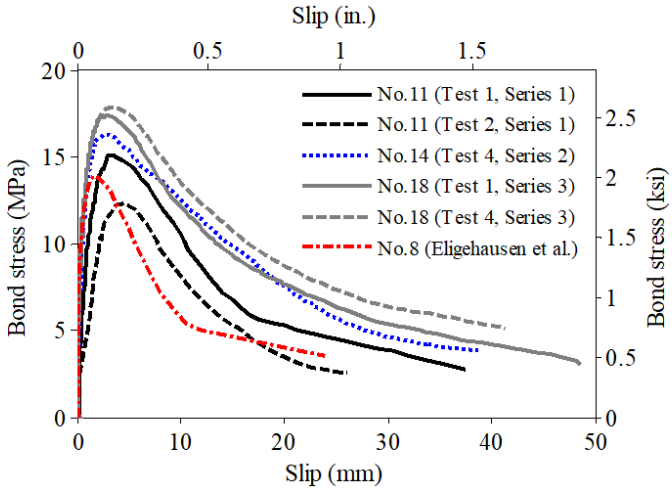

Figure 6.1: Bond-slip behavior of reinforcing bars (Murcia-Delso et al. 2013)

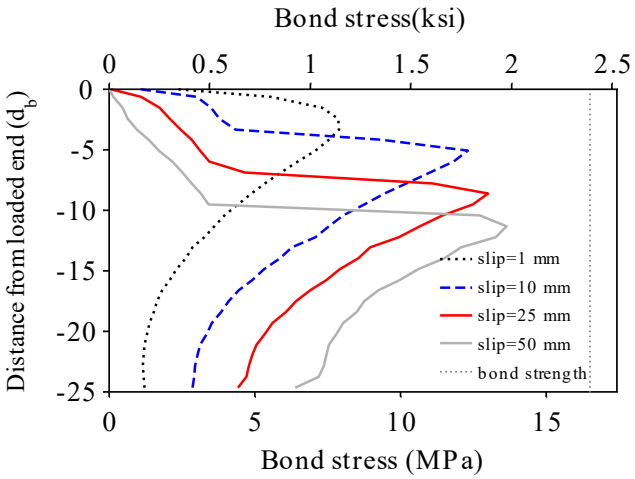

Figure 6.2: Bond stress distributions along a No. 14 reinforcing bar at different levels of bar slip at the loaded end (Murcia-Delso et al. 2013)

The variation of the bond stress with increasing bar slip, as discussed above, can be observed from the test data presented in Section 5.2. For simplicity, one may express the bond resistance in terms of an average bond stress $\overline{\tau}_b$ as follows.

$$F_b = \pi d_b l_e \overline{\tau}_b \tag{6.11}$$

The average bond stress will vary with the level of slip along the bar. For the tension development of straight deformed bars, the bond strength is often taken as the average bond stress at which pullout failure will occur. For bars embedded in well confined concrete, the bond strength has been found to be proportional to $\left(f_c'\right)^{0.75}$ in a study by Murcia-Delso et al. (2013). For headed bars, this value may vary depending on the amount of bar slip that has occurred when bearing failure initiates at the T head.

Bearing Resistance

The maximum bearing resistance at a T head can be calculated with the following equation adopted from ACI 318-19 for headed anchor bolts.

$$F_h = \alpha_c f_c' A_h \tag{6.12}$$

in which A_h is the net bearing area of the head and α_c is a factor that accounts for the increase of the compressive strength of the concrete at the T head due to the confinement effect. The concrete around a T head can be highly confined by the surrounding concrete. For headed anchor bolts, ACI 318-19 specifies the value of α_c to be 8. If this value is applied to bars that have T heads with a minimum net bearing of $4A_b$, the bearing resistance will likely exceed the tensile strength of the bar and bearing failure will not occur.

In AASHTO LRFD Bridge Design Specifications (AASHTO 2024), the formula for the bearing resistance at the T head has 0.5υ in place of α_c, where

$$0.45 \le \upsilon = 0.85 - \frac{f_c'}{20} \le 0.65 \tag{6.13}$$

in which f_c' is in ksi. Hence, the value of α_c assumed in AASHTO is effectively between 0.225 and 0.325 depending on the compressive strength of the concrete. Evidently, it is not considered as a confinement factor but rather a strength reduction factor.

It is important to note that the confinement condition for the concrete at a T head can vary significantly depending on whether the concrete in the anchorage region has cracks or not. As observed from the tests presented in this report and discussed in Section 6.1.1, concrete crushing can occur above the T head once breakout cracks develop. This is because the occurrence of breakout cracks can significantly reduce the confinement effect on the concrete.

Bond and Bearing Resistance in the Specimens

To examine the variability of the bond resistance and the bearing resistance of the concrete at the T head developed in the test specimens at the peak applied peak force, F_{max}, the values of $\overline{\tau}_b$ and α_c are calculated with Equations (6.11) and (6.12), respectively, using the values of F_b and F_h obtained at the peak applied force, which are presented in Section 5.2. The values of $\overline{\tau}_b$ and α_c calculated from the test data are shown in Table 6.2. These values do not necessarily represent the maximum bond and bearing strengths unless bar pullout failure occurred in the specimen. Furthermore, as stated previously, bond strength is a function of the compressive strength of concrete, and can be highly variable along a headed bar.

Table 6.2: Values of $\overline{\tau}_b$ and α_c deduced from test data

Specimen	1	2	3	4	5	6	7	8	9	10	11	12	13
f'_c (ksi)	4.120	3.890	4.130	8.000	8.000	8.580	8.580	4.350	4.350	5.430	5.430	3.940	4.210
d_b (in)	1.693	1.693	1.693	1.693	1.693	1.693	1.693	1.693	1.693	1.693	1.693	2.257	2.257
A_b (in^2)	2.25	2.25	2.25	2.25	2.25	2.25	2.25	2.25	2.25	2.25	2.25	4	4
A_h (in^2)	9.00	9.00	20.25	9.00	9.00	9.00	20.25	9.00	20.25	9.00	20.25	16	16
l_e (in)	16.75	24.00	16.75	14.00	14.00	20.00	14.00	24	24	16.00	16.00	26	37
Max. Applied Force, F_{max} (kips)	179	225	213	173	152	212	188	469	506	179	177	369	375
Measured F_h (kips)	134	-	190	128	65	125	162	256	-	-	90	291	-
Measured F_b (kips)	45	-	23	45	87	87	26	213	-	-	87	78	-
Calculated α_c	3.61	-	2.27	1.78	0.90	1.62	0.93	3.27	-	-	0.82	4.62	-
Calculated $\overline{\tau}_b$ (ksi)	0.505	-	0.258	0.604	1.168	0.818	0.349	0.803	-	-	1.022	0.423	-
Anchorage Failure	Y	N	N	Y	Y	N	Y	N	N	Y	Y	N	N

As discussed in Section 6.1.1, the anchorage failures observed in the tests were initiated by breakout cracks but eventually governed by concrete crushing above the T heads as the confinement effect on the concrete had been reduced by the cracks. Table 6.2 shows that the values of $\overline{\tau}_b$ vary from 0.258 to 1.168 ksi. These values appear to be consistent with the estimated bond stresses presented in Section 5.2. For the specimens that had anchorage failures, the average value is 0.730, and for those without anchorage failure, the average is 0.576. This difference could be attributed to the fact that a well anchored bar had deeper plastic strain penetration and, therefore, a larger extent of bond deterioration. Other than that, there are no distinct trends between the two groups.

The values of α_c shown in Table 6.2 vary from 0.82 to 4.62. The three specimens (5, 7, and 11) that had the values of α_c below 1.0 had anchorage failures. For the specimens that had anchorage failures, the average value of α_c is 1.61. This is significantly smaller than 8, which is specified in ACI 318-19 for headed anchor bolts. This indicates that the confinement effect on concrete was significantly diminished by the breakout cracks and was totally gone for three of the specimens. The average value of α_c for the specimens that had no anchorage failure is 2.95. However, the values of α_c calculated for these specimens do not reflect the maximum bearing strengths of the concrete since no anchorage failure occurred.

6.2 Determination of Development Lengths

Based on the information and discussion presented in the previous section, it can be concluded that the anchorage failure of a headed bar is normally initiated by concrete breakout but eventually governed by bar pullout when the bearing strength of the concrete at the T head has been weakened by the opening of breakout cracks. Without breakout cracks, pullout failure is unlikely. This provides an explanation for the observation in this study as well as other studies (e.g., Shao et al. 2016) that a larger T head would not necessarily result in a higher anchorage capacity. This can be

attributed to the fact that the size of a T head had little influence on the concrete breakout strength. Furthermore, the deterioration of the concrete bearing strength can be so rapid that size of the bearing area will make little difference. The size of a T head may affect the anchorage capacity only when the opening of the breakout cracks is not so rapid that the deterioration of the bearing strength is more gradual.

Hence, to determine the development length required for a headed bar, it is necessary to consider the breakout strength. First, one may use Equation (6.6) to determine the development length required to prevent the occurrence of concrete breakout cracks before the maximum expected tensile strength of the bar is reached, i.e., to ensure the following condition.

$$0.5\sqrt{f'_c}l_d^2\frac{A_{Nc}}{A_{Nco}}\psi_{ed,N} \geq 1.75A_b f_y \tag{6.14}$$

in which l_d is the required development length in inches, A_b is the cross-sectional area of the headed bar, and f_y is the nominal yield strength of the steel. The values of A_{Nc}, A_{Nco}, and $\psi_{ed,N}$ are to be determined according to the ACI anchor bolt provisions. The factor 1.75 is the product of 1.25 and1.40, with 1.25 representing the ratio of the expected yield strength of the steel to the nominal yield strength and 1.40 being the expected ratio of the tensile strength to the nominal yield strength. To calculate the values of A_{Nco} and $\psi_{ed,N}$, Equations (6.2) and (6.3) can be used with l_e replaced by l_d. This may entail some iteration because A_{Nc} and A_{Nco} are also functions of l_d in that the breakout cone is assumed to have a depth of l_d and the dimension of the projected failure area at the top is 3 l_d.

If the required l_d cannot be accommodated by the size of the joint, then tie reinforcement parallel to the anchored bars should be provided to prohibit the opening of breakout cracks based on

the available l_d . The total area, $\tilde{A}_{tt}$, of the tie reinforcement required for the breakout region can be determined with Equation (6.8), which is reproduced below.

$$\tilde{A}_{tt} \geq 1.25 \frac{f_y}{f_{yt}} A_{hs} \tag{6.8}$$

in which f_y and f_{yt} are the nominal yield strengths of the headed bars and tie reinforcement, respectively, and A_{hs} is the total area of the headed bars.

Chapter 7 Summary and Conclusions

7.1 Summary

Currently, there are no code standards on the development of No. 14 and No. 18 headed bars The development length requirements for headed bars in ACI 318-19 and AASHTO LRFD Bridge Design Specifications (10th Edition) limit the bar size to No. 11 or smaller. This stems from the lack of supporting experimental data for larger bar sizes. However, large-diameter bars are frequently used in bridge columns and piles. In this study, thirteen bar anchorage tests were conducted to determine the development lengths required for No. 14 and No. 18 headed bars, examining the influence of the embedment length, head size, concrete strength, parallel tie reinforcement, and bar group on the anchorage capacity, and to determine the applicability of the development length formulas in ACI and AASHTO for No. 11 or smaller headed bars to No. 14 and No. 18 headed bars. Heads with net bearing areas of $4A_b$ and $9A_b$ were considered, and anchorage tests were conducted on single bars and two side-by-side bars. The anchorage performances of bars with embedment lengths equal to 70% and 100% of the minimum calculated with the ACI 318-19 formula were compared.

7.2 Conclusions

Similar to that observed for headed anchor bolts, the anchorage capacity of a headed bar is governed by the concrete breakout strength or the bar pullout strength. Breakout cracks induced by the tensile force of a headed bar typically form a cone-shaped breakout surface. The concrete breakout resistance depends on the embedment length of the bar as well as the concrete strength. However, breakout cracks can be restrained from opening if sufficient parallel tie reinforcement (such as rectangular stirrups) is provided across the crack planes. The bar pullout resistance is provided by the bond force along the bar and the bearing strength of the concrete above the T head. The concrete bearing strength at the T head can be significantly enhanced by the confinement effect from the surrounding concrete.

The test results presented here show that the anchorage failure of a headed bar is normally initiated by concrete breakout but eventually governed by bar pullout when the bearing strength of the concrete at the T head has been weakened by the opening of breakout cracks. Without breakout cracks, pullout failure is unlikely because the concrete above the T head is normally highly confined by the surrounding concrete, which can result in a very high compressive strength. The test results

also show that the bar force at which concrete breakout occurs is approximately proportional to the square of the embedment length, rather than the embedment length to the power of 1.5 as specified in ACI 318 for embedded anchor bolts.

It may not always be practical to prevent breakout cracks. This can happen when the desired depth of the connected member is not able to accommodate the required embedment length. However, if sufficient parallel tie reinforcement is provided across the crack planes to restrain the cracks, sufficient concrete bearing strength can be retained at the T head to prevent bar pullout failure. This is supported by the test results from this study as all the specimens, except for one, had breakout cracks, and those with an adequate quantity of parallel tie reinforcement did not have anchorage failure. Hence, parallel tie reinforcement can play a significant role in providing the necessary anchorage capacity. This is recognized in ACI 318-19 and AASHTO LRFD Bridge Design Specifications (10th Edition), which allow a reduction of the required development length if sufficient parallel tie reinforcement is provided within a distance of $8d_b$ from the center of the anchored bar.

The specimens that satisfied the development length formula in ACI 318-19 performed satisfactorily. Nevertheless, two specimens that satisfied the AASHTO development length formula and had a head size of $9A_b$ had anchorage failures, while three specimens that did not meet the AASHTO requirement and had a head size of $4A_b$ did not have anchorage failure. This indicates that the AASHTO formula over-estimates the influence of the head size. The unified formula in AASHTO considers only the bond strength and the bearing resistance at the T head, and does not explicitly account for concrete breakout. It can be perceived that if anchorage failure is initiated by concrete breakout, the size of the T head will not have a significant influence on the anchorage resistance, as discussed in Section 6.2 of this report. This is supported by the data obtained in this study as well as other studies on smaller diameter bars, which have shown that the use of a head size greater than $4A_b$ will not necessarily improve the anchorage capacity and the benefit is small at best.

While the ACI formula appears to be adequate for No. 14 and No. 18 headed bars, it is empirical and prescriptive, especially with respect to the parallel tie requirement, and the formula appears to be more conservative for No. 18 than No. 14 bars. This can be attributed to the fact that ACI 318-19 has the development length proportional to the bar diameter to the power of 1.5. To address these issues, a method has been proposed in Section 6.2 of this report to determine the development lengths for headed bars and the required parallel tie reinforcement. It is based on the

anchor bolt provisions in ACI 318, which have been improved to account for the influence of the bar embedment length and the contribution of the parallel tie reinforcement in an accurate and rational manner. Even though the method has only been verified by the test data on No. 14 and No. 18 bars obtained in this study, it is believed to be applicable to smaller diameter bars as well based on the fact that it is more physics based.

The proposed method is based on data from single and double bar tests. In an actual bridge structure, there are many longitudinal bars extending from a column into a cap beam or footing for anchorage. The stress state in the column section next to the cap beam or footing is more complicated compared to the condition in the bar anchorage tests where one or two bars were subjected to tension. When bending moment is developed in the column section, part of the concrete section will be cracked in tension while the remaining area will be subjected to compression. This, in addition to the bar group effect, will affect the concrete breakout crack pattern and thereby the anchorage capacity. Hence, the proposed method needs to be further evaluated with trial applications to realistic joints that reflect the loading and reinforcement in actual bridge structures. Column-to-cap beam joints can be good candidates for such evaluations. This will entail the design and testing of large-scale column-to-cap beam assemblies.

References

AASHTO (2024). *LRFD Bridge Design Specifications (10th Edition)*. American Association of State Highway and Transportation Officials, Washington, DC.

ACI (2014/2019). *Building Code Requirements for Structural Concrete (ACI 318-14/19)*. American Concrete Institute, Farmington Hills, MI.

ASTM (2018). *Standard Specification for Headed Steel Bars for Concrete Reinforcement (A970/A970M-18)*. ASTM International, West Conshohocken, PA.

Bashandy, T.R. (1996). "Application of headed bars in concrete members." *Ph.D. Dissertation*, University of Texas at Austin, Austin, TX.

Caltrans (2016a). *Seismic Requirements for Headed Bar Reinforcement (MTD 20-21, December 2016)*. California Department of Transportation, Sacramento, CA.

Caltrans (2016b). *Seismic Design of Slab Bridges (MTD 20-7, April 2016)*. California Department of Transportation, Sacramento, CA.

Caltrans (2019). *Seismic Design Criteria (Version 2)*. California Department of Transportation, Sacramento, CA.

DeVries, R.A. (1996). "Anchorage of headed reinforcement in concrete." *Ph.D. Dissertation*, University of Texas at Austin, Austin, TX.

DeVries, R.A., Jirsa, J.O., and Bashandy, T. (1999). "Anchorage capacity in concrete of headed reinforcement with shallow embedments." *ACI Structural Journal*, Vol. 96(5).

Eligehausen, R. and Balogh, T. (1995). "Behavior of fasteners loaded in tension in cracked reinforced concrete." *ACI Structural Journal*, Vol. 92(3).

Eligehausen, R., Mallee, R., and Silva, J. (2006). *Anchorage in Concrete Construction*. Ernst & Sohn (J.T. Wiley), Berlin, Germany.

fib (2013). *fib Model Code for Concrete Structures 2010 (1st Edition)*. Ernst & Sohn, Berlin, Germany.

Fuchs, W., Eligehausen, R., and Breen, J.E. (1995). “Concrete capacity design (CCD) approach for fastening to concrete.” *ACI Structural Journal*, Vol. 92(1).

Ghimire, K., Darwin, D., and O’Reilly, M. (2018). “Anchorage of headed reinforcing bars in cocnrete.” *SM Report No. 127*, Structural Engineering and Engineering Materials, University of Kansas Center for Research, Inc., Lawrence, KS.

Ghimire, K.P., Shao, Y., Darwin, D., and O’Reilly, M. (2019a). “Conventional and high-strength headed bars – part 1: anchorage tests.” *ACI Structural Journal*, Vol. 116(3).

Ghimire, K.P., Shao, Y., Darwin, D., and O’Reilly, M. (2019b). “Conventional and high-strength headed bars – part 2: data analysis.” *ACI Structural Journal*, Vol. 116(3).

Kang, T.H.K., Ha, S.S, and Choi, D.U. (2010). “Bar pullout tests and seismic tests of small-headed bars in beam-column joints.” *ACI Structural Journal*, Vol. 107(1).

Murcia-Delso, J., Shing, P., Stavridis, A., and Liu Y. (2013). “Required embedment length of column reinforcement extended into type II shafts.” *SSRP-13/05*, Department of Structural Engineering, University of California, San Diego, CA.

Papadopoulos, V., Murcia-Delso, J., and Shing, P.B. (2015). “Development length for headed bars in slab-column joints of RC slab bridges.” *SSRP-15/10*, Department of Structural Engineering, University of California, San Diego, CA.

Shao, Y., Darwin, D., O’Reilly, M., Lequesne, R., Ghimire, K., and Hano, M. (2016). “Anchorage of conventional and high-strength headed reinforcing bars.” *SM Report No. 117*, Structural Engineering and Engineering Materials, University of Kansas Center for Research, Inc., Lawrence, KS.

Stoker, J.R., Boulware, R.L., Crozier, W.F., and Swirsky, R.A. (1974). “Anchorage devices for large diameter bars.” *CA-DOT-TL-6626-1-73-30*, Transportation Laboratory, California Division of Highways, Sacramento, CA.

Thompson, M.K., Jirsa, J.O., Breen, J.E., and Klingner, R.E. (2002). “Anchorage behavior of headed reinforcement: literature review.” *FHWA/TX-0-1855-1*, Center for Transportation Research, University of Texas at Austin, Austin, TX.

Thompson, M.K., Ziehl, M.J., Jirsa, J.O., and Breen, J.E. (2005a). “CCT nodes anchored by headed bars - Part 1: behavior of nodes.” *ACI Structural Journal*, Vol. 102(6).

Thompson, M.K., Jirsa, J.O., and Breen, J.E. (2005b). “CCT nodes anchored by headed bars - Part 2: capacity of nodes.” *ACI Structural Journal*, Vol. 102(6).

Thompson, M.K., Ledesma, A., Jirsa, J.O., and Breen, J.E. (2006a). “Lap splices anchored by headed bars.” *ACI Structural Journal*, Vol. 103(2).

Thompson, M.K., Jirsa, J.O., and Breen, J.E. (2006b). “Behavior and capacity of headed bars.” *ACI Structural Journal*, Vol. 103(4).

Wright, J. and McCabe, S.L. (1997). The development length and anchorage behavior of headed reinforcing bars.” *SM Report No. 44*, Structural Engineering and Engineering Materials, University of Kansas Center for Research, Inc., Lawrence, KS.

Zaborac, J. and Bayrak, O. (2022). “Unified approach for reinforcement development length using the partly cracked elastic stage for bond strength.” *Structural Concrete*, International Federation for Structural Concrete, Lausanne, Switzerland.

Appendix A: Design of RC Beam Specimens

Determination of Flexural Reinforcement

As discussed in Chapter 3, the beam width in each specimen was governed by the concrete side cover required for the headed bar(s) to meet a requirement in ACI 318-19 for ψ_o = 1 and to represent the minimum edge distance of a longitudinal bar extending from a bridge column into a cap beam in a typical large bent cap. The beam depth and the amount of longitudinal reinforcement in the beam were selected so that the maximum compressive stress developed in the concrete would not exceed 50% of the smallest target compressive strength of 4,000 psi, and the tensile stress in the longitudinal bars would not exceed 50% of the nominal yield strength when two side-by-side headed bars were pulled simultaneously. For the stress analysis, it was assumed that the RC beam had the two ends fixed and the span length was equal to the clear distance between the hold-down beams.

To calculate the maximum force demand, the ultimate tensile stress, f_u, that could be developed in a headed bar was considered. It was estimated with the following equation.

$$f_u = 1.4 \times 1.2 \times f_{ye} \tag{A.1}$$

in which f_{ye} is the expected yield strength, the 1.4 factor is the assumed ratio of the tensile strength to the expected yield strength, and 1.2 is a factor of safety. The expected yield strength of Grade 60 steel was assumed to be 67 ksi. This resulted in f_u = 112.6 ksi. The ultimate tensile force, P_u , that could be developed in a headed bar was then calculated as follows.

$$P_u = f_u A_b \tag{A.2}$$

in which A_b is nominal cross-sectional area of the bar. Assuming that the two ends of the beam were fixed, the maximum moment demand, M_u, that could be induced by pulling two headed bars at the same time was then conservatively estimated with the following expression.

$$M_u = \frac{P_u l}{4} \tag{A.3}$$

in which l is the clear span distance between the two steel hold-down beams at the ends. In the above expression, the tension forces from the two bars were assumed to be concentrated at the mid-span.

The maximum compressive stress, $f_{c,max}$, that could be induced in the concrete and the maximum tensile stress, $f_{s,max}$, induced in the longitudinal reinforcement were calculated with the following equations, assuming that the materials were linearly elastic.

$$f_{c.\max} = \frac{M_u c}{I_t} \tag{A.4}$$

$$f_{s,\max} = M_u \frac{d-c}{I_t} \eta \tag{A.5}$$

in which I_t is the moment of inertia of the cracked transformed section of the concrete beam, *c* is the distance of the neutral axis of bending from the extreme compression fiber, *d* is the distance of the centroid of the tension reinforcement from the extreme compression fiber, and η is ratio of the modulus of elasticity of the steel to that of the concrete. The modulus of elasticity of the steel and 4,000-psi concrete were taken to be 29,000 ksi and 3,605 ksi, respectively.

For the specimens with No. 14 headed bars, the width and depth of the specimens were determined to be 26 in. and 42 in., respectively. The clear cover at the top and bottom surfaces of the beams was 1.5 inch. The clear span distance between the two steel hold-down beams was 90

inches. Four No. 11 bars were selected for the longitudinal reinforcement at the top and the bottom of the beams, respectively. The steel in compression was ignored in the claculation. The distance of the neutral axis of bending for the elastic cracked section, c, was calculated to be 10.6 in. and the transformed moment of inertia, I_t, of the section was calculated to be 52,517 in.^4. The values of $f_{c,max}$ and $f_{s,max}$ calculated were 1,148 psi and 25 ksi, respectively.

For the specimens with No. 18 headed bars, the width and depth of the specimens were determined to be 35 in. and 48 in., respectively. The clear cover at the top and bottom surfaces of the beams was 1.5 inch. The clear span length between the two steel hold-down beams was 138 inches. Eight No. 11 bars were selected for the longitudinal reinforcement at the top and the bottom of the beams, respectively. The distance of the centroid of the longitudinal bars from the closest face was 3.2 inches. The distance of the neutral axis of bending for the elastic cracked section, c, was calculated to be 13.4 in. and the transformed moment of inertia, I_t, of the section was calculated to 126,667 in.^4. The values of $f_{c,max}$ and $f_{s,max}$ calculated were 1,643 psi and 31 ksi, respectively.

Determination of Shear Reinforcement

The amounts of stirrups serving as shear reinforcement in the beams were different depending on whether the specimens had one or two headed bars. As discussed in Chapter 3, in addition to meeting the shear demand during the tests, the cross-sectional area of the stirrups had to meet the ACI requirement that the total cross-sectional area of the parallel tie reinforcement within $8d_b$ from the center line of the headed bars shall exceed 0.3 A_{hs} , where A_{hs} is the total cross-sectional area of the headed bars being developed, for the development length modification factor ψ_p to be equal to 1.

The maximum shear demand, V_u, is equal to $0.5P_u$ for the case of one headed bar and P_u for the case of two headed bars, where P_u was calculated with Equations (A.1) and (A.2). The shear strength of the concrete was calculated with the following equation according to ACI 318-19.

$$V_c = 2bd\sqrt{f_c'} \tag{A.6}$$

in which *b* is the beam width, *d* is the effective depth, and f_c' is the compressive strength of the concrete, with all units in pounds and inches. The compressive strength of the concrete was assumed to be 4,000 psi for all the specimens regardless of the actual concrete strengths because the amount of stirrups would not change with the concrete strength. The shear resistance provided by the stirrups was calculated with the following ACI equation.

$$V_s = \frac{f_y A_v d}{s} \tag{A.7}$$

in which A_v is the total cross-sectional area of the stirrups at one location and *s* is the spacing of the stirrups. The nominal shear strength of a beam was then calculated with the following equation.

$$V_n = V_c + V_s \tag{A.8}$$

For all of the specimens, the spacing of the stirrups remained the same at 12 in. on center to reflect typical reinforcement details in the joint region of a cap beam in a bridge structure. For the specimens that had one No. 14 headed bar, the stirrups were two No. 5's at 12 in., while four No. 5's at 12 in. were selected for the specimens that had 2 No. 14 headed bars. For the specimens that had one No. 18 headed bar, the stirrups were two No. 6's at 12 inches. Table A.1 shows the maximum shear demands (V_u), shear resistance of the concrete (V_c), shear resistance of the stirrups (V_s), and the total shear strengths of the beams (V_n) calculated for the different specimens. It can be seen that the shear strengths were way beyond the shear demands.

Table A.1: Shear demands and resistances calculated for the specimens

Specimen	Stirrups	V_u (kips)	V_c (kips)	V_s (kips)	V_n (kips)
One No. 14	Two No. 5 @12”	127	130	123	253
Two No. 14	Four No. 5 @12”	253	130	246	376
One No. 18	Two No. 6 @12”	225	198	197	395

Specimen Design Drawings

The design drawings for the specimens that had 4,000-psi concrete and the full development lengths required according to ACI 318-19 are shown here. The reinforcement details for the specimens that had higher concrete strengths and 70% of the minimum development lengths required by ACI are the same.

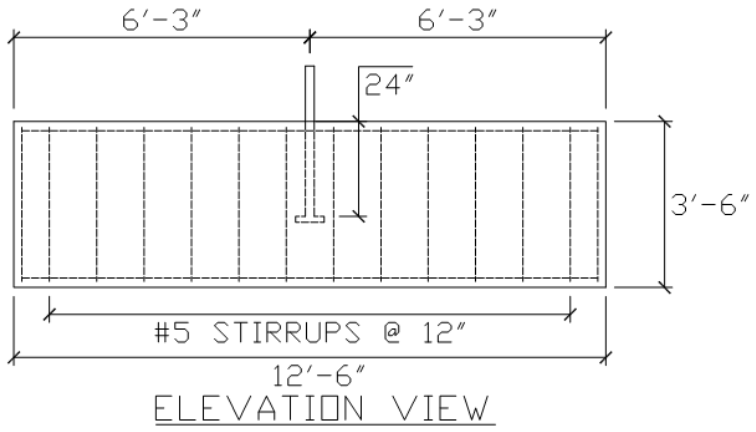

Figure A.1: Elevation view of specimens with one No. 14 headed bar

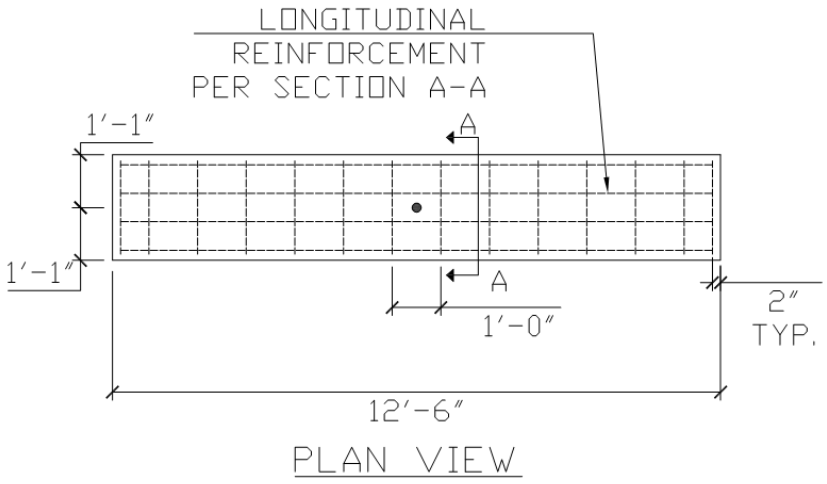

Figure A.2: Plan view of specimens with one No. 14 headed bar

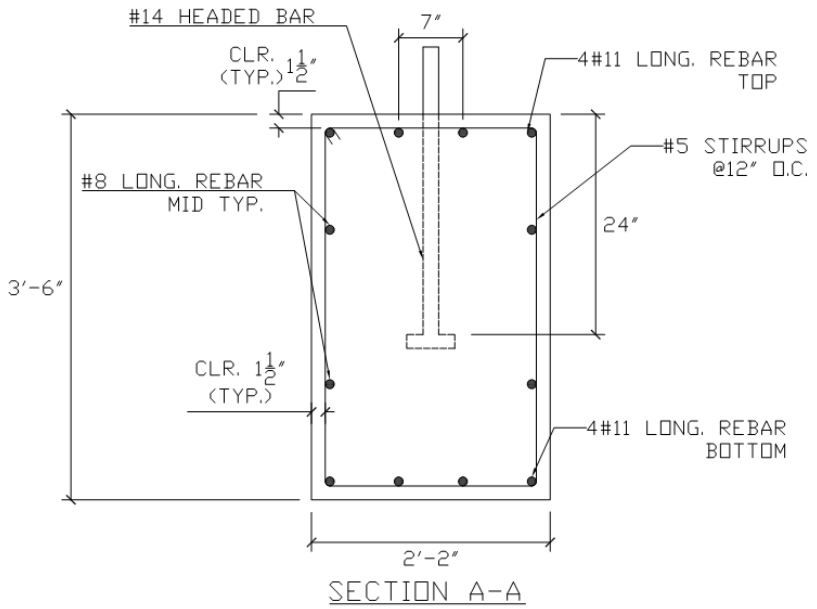

Figure A.3: Section view of specimens with one No. 14 headed bar

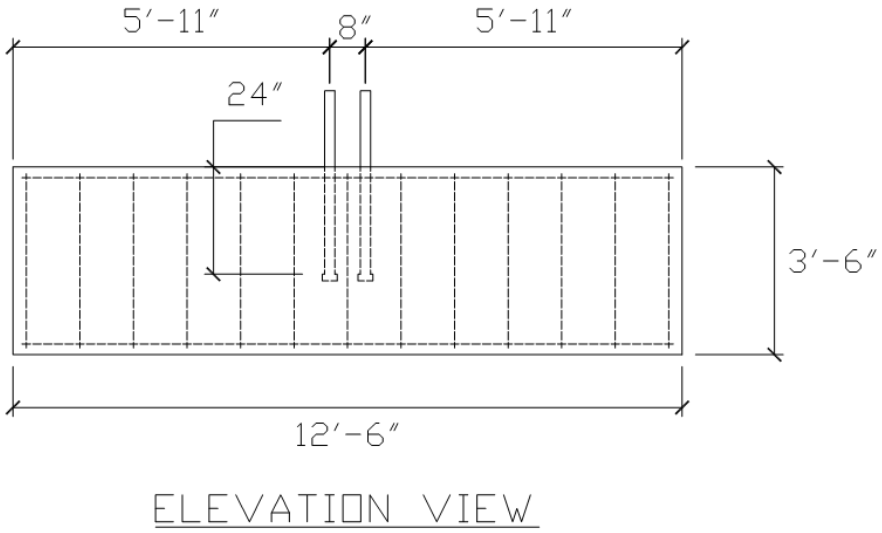

Figure A.4: Elevation view of specimens with two No. 14 headed bars

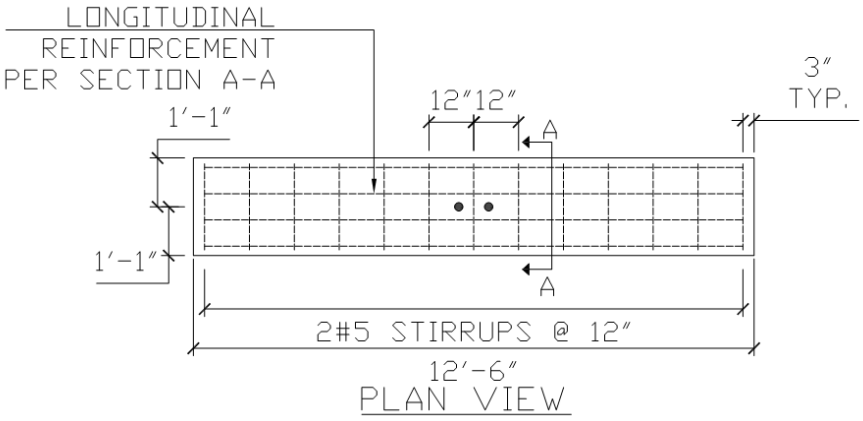

Figure A.5: Plan view of specimens with two No. 14 headed bars

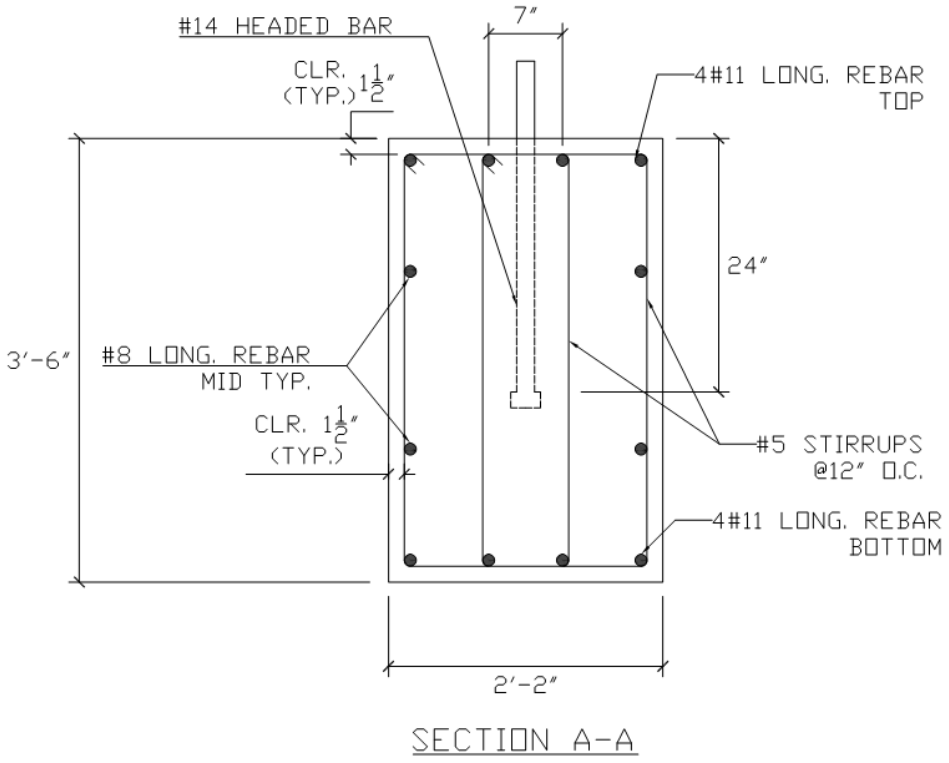

Figure A.6: Section view of specimens with two No. 14 headed bars

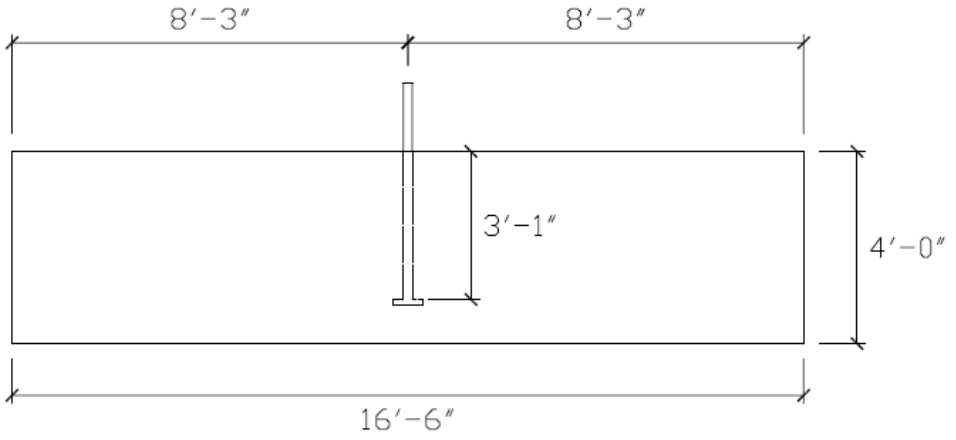

Figure A.7: Elevation view of specimens with one No. 18 headed bar

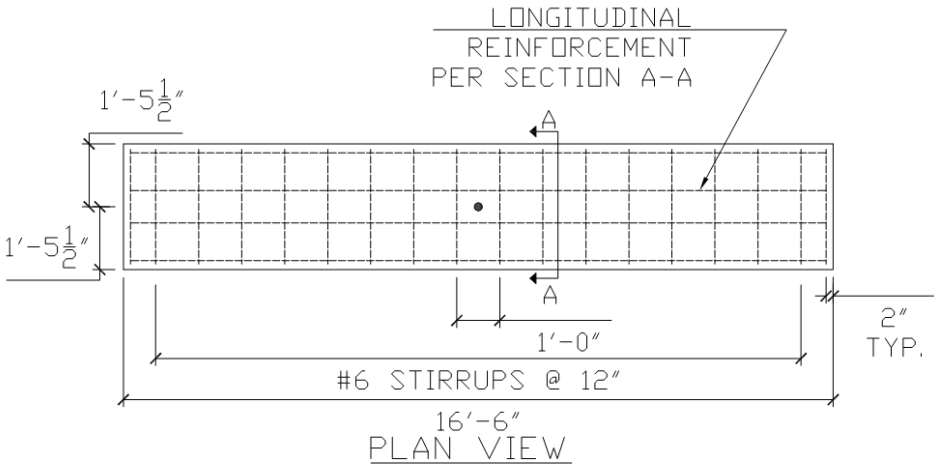

Figure A.8: Plan view of specimens with one No. 18 headed bar

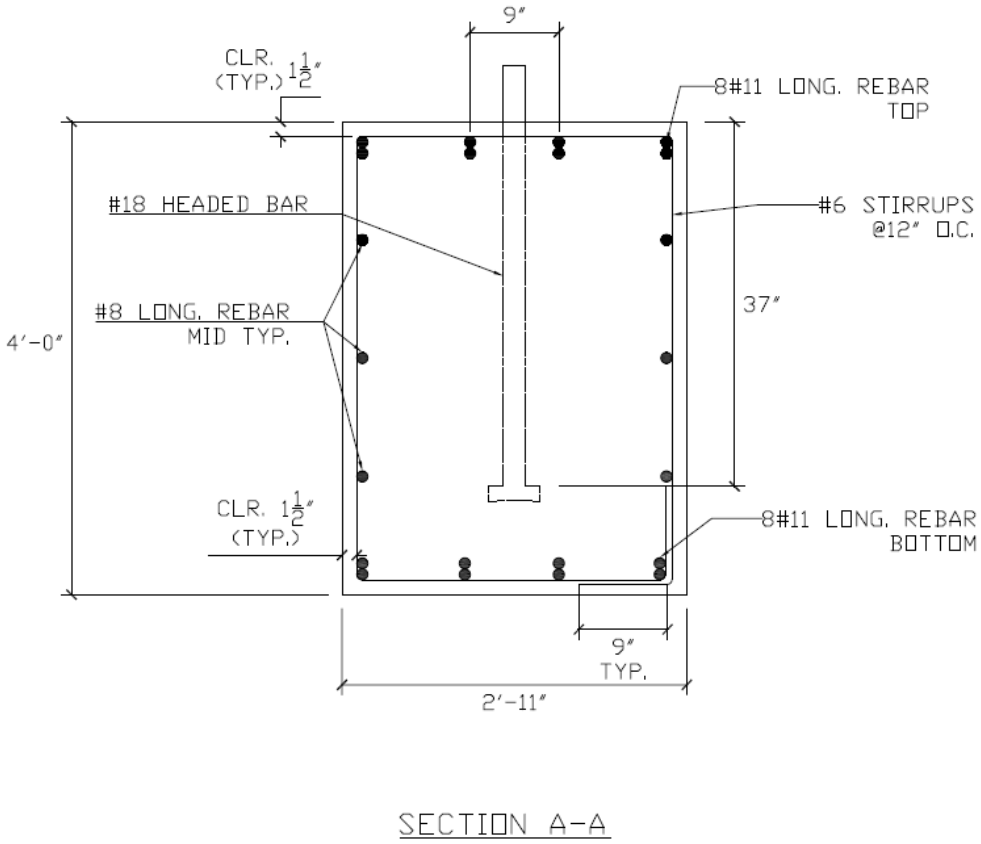

Figure A.9: Section view of specimens with one No. 18 headed bar

Appendix B: Material Properties of Stirrup Samples

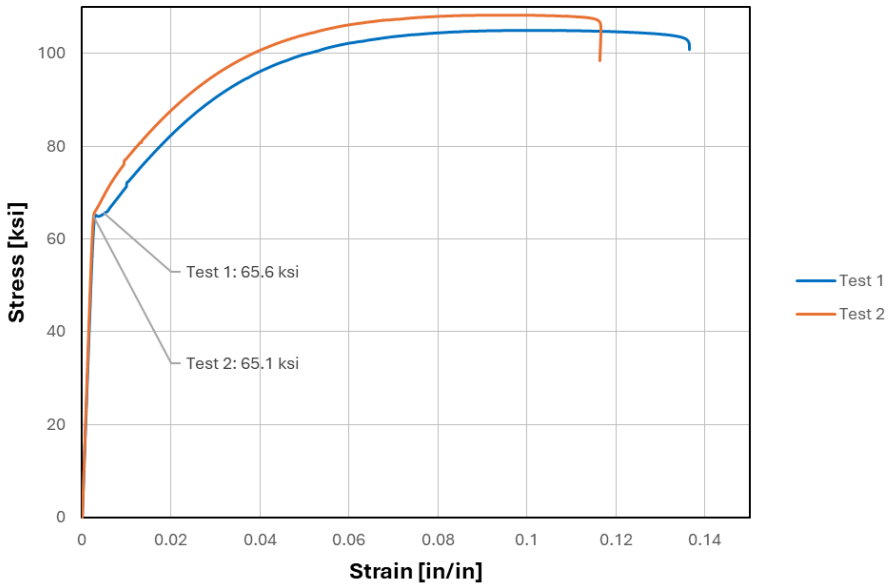

Figure B.1: Stress-vs.-strain curves for No. 5 stirrups in Specimen 1

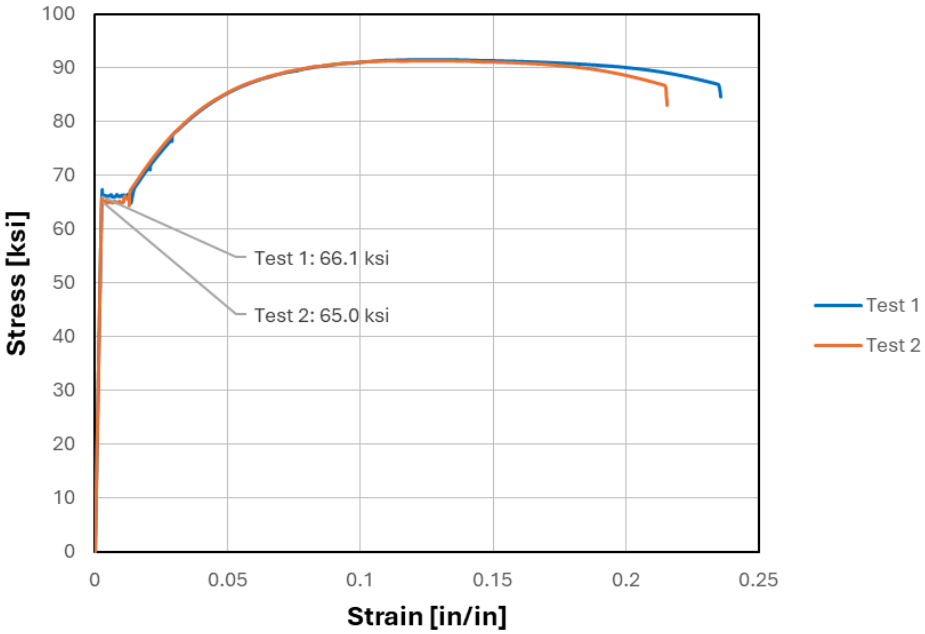

Figure B.2: Stress-vs.-strain curves for No. 5 stirrups in Specimens 2 and 3

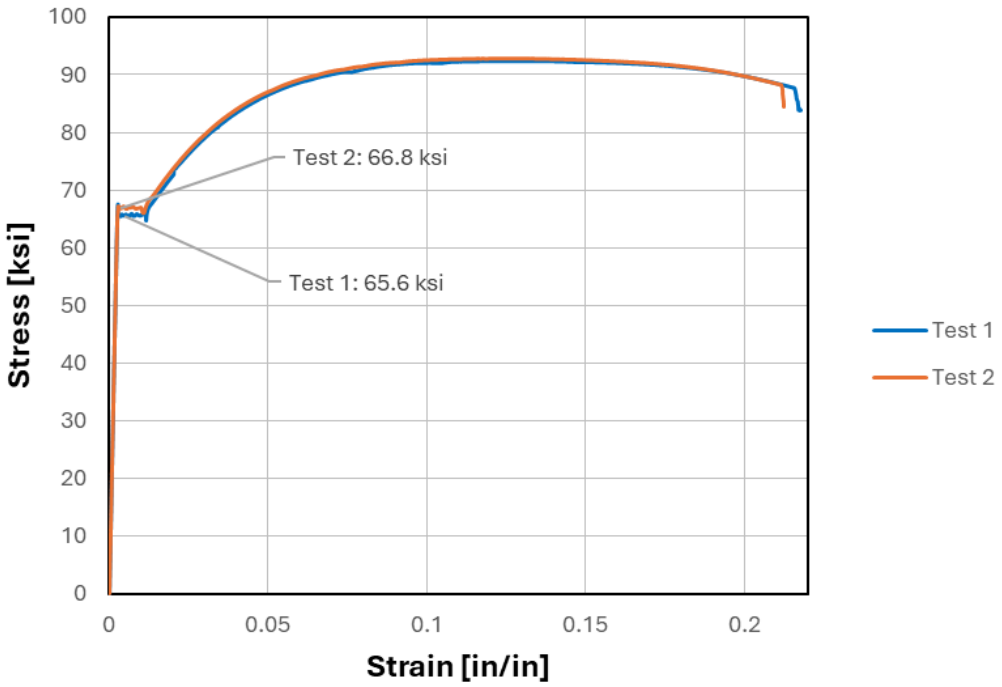

Figure B.3: Stress-vs.-strain curves for No. 5 stirrups in Specimens 4

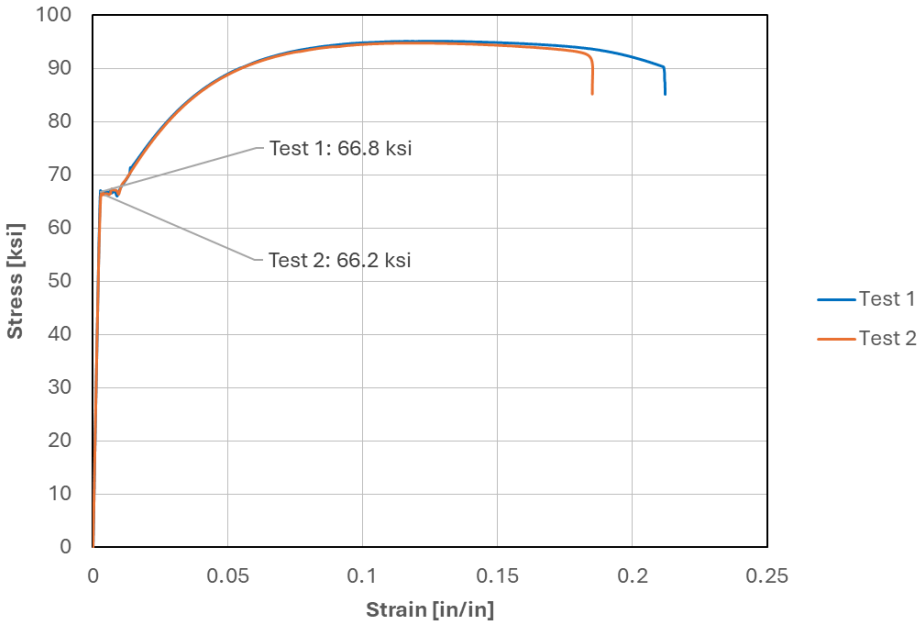

Figure B.4: Stress-vs.-strain curves for No. 4 stirrups in Specimen 5

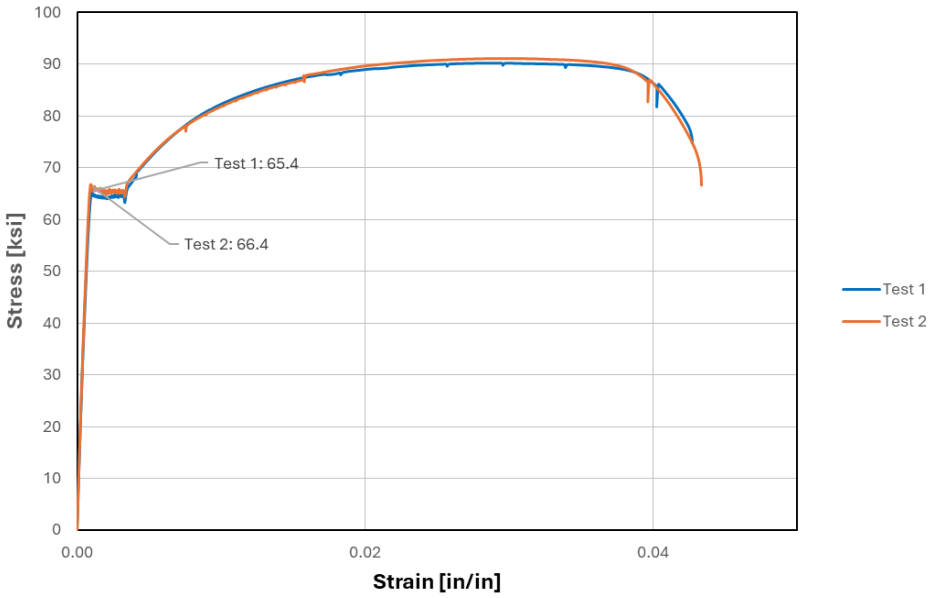

Figure B.5: Stress-vs.-strain curves for No. 5 stirrups in Specimens 6 and 7

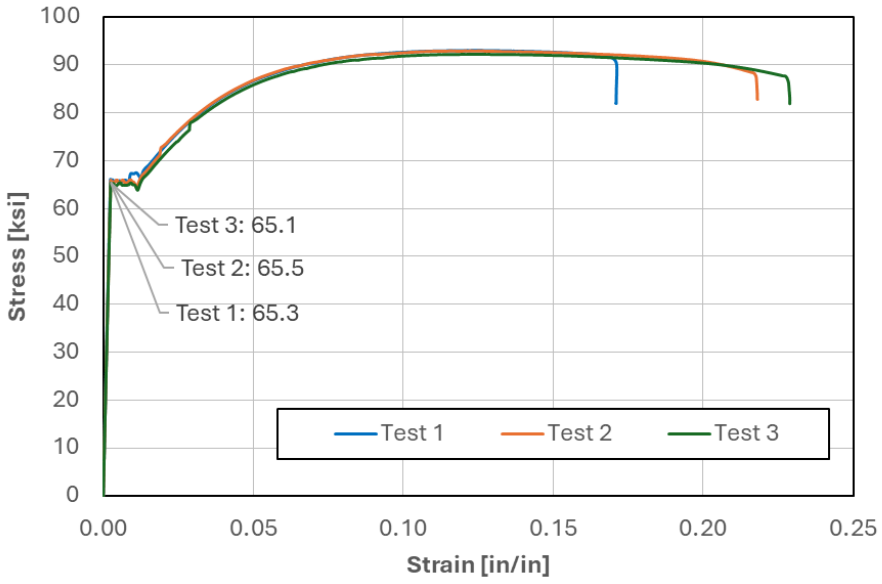

Figure B.6: Stress-vs.-strain curves for No. 5 stirrups in Specimens 8 and 9

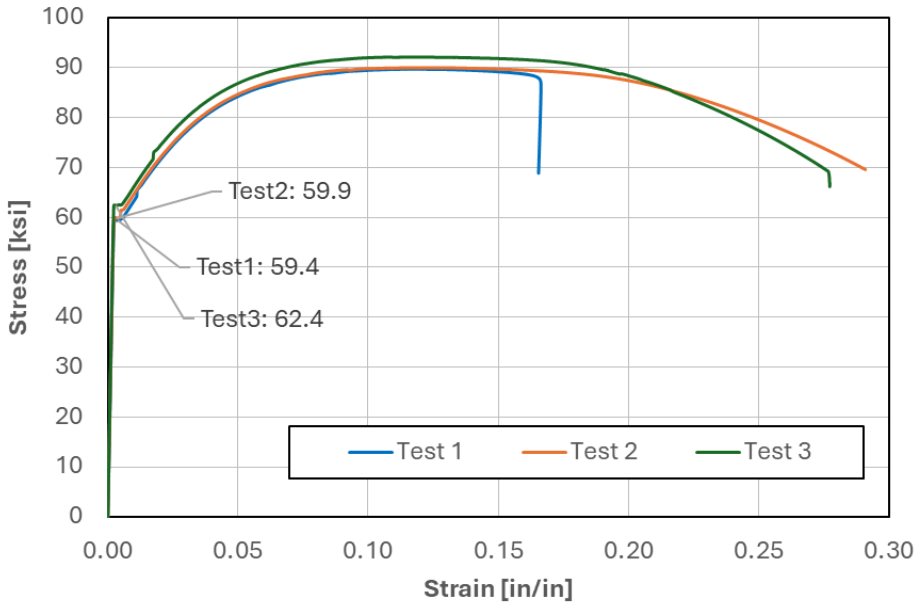

Figure B.7: Stress-vs.-strain curves for No. 5 stirrups in Specimens 10 and11

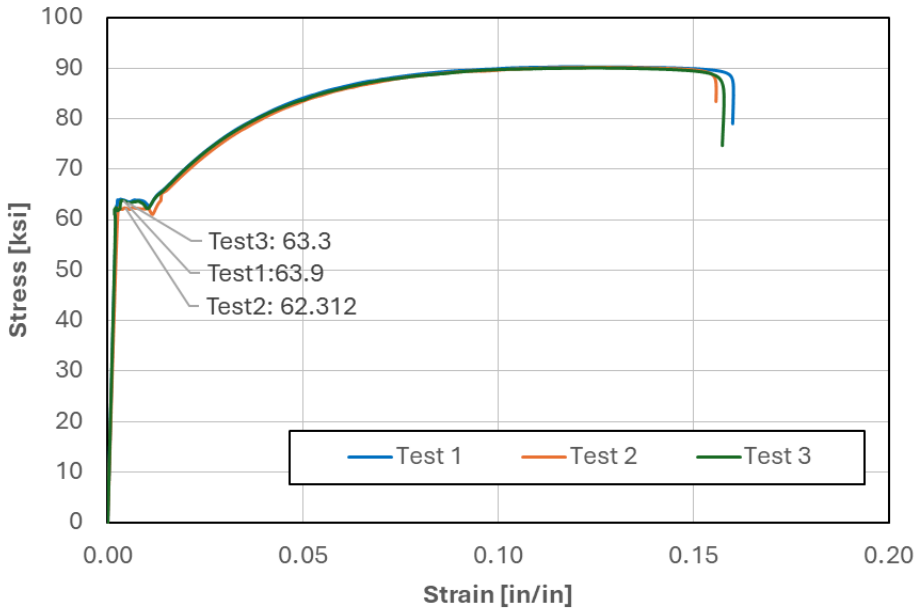

Figure B.8: Stress-vs.-strain curves for No. 6 stirrups in Specimens 12 and13

Appendix C: Drawings of Steel Load Beam

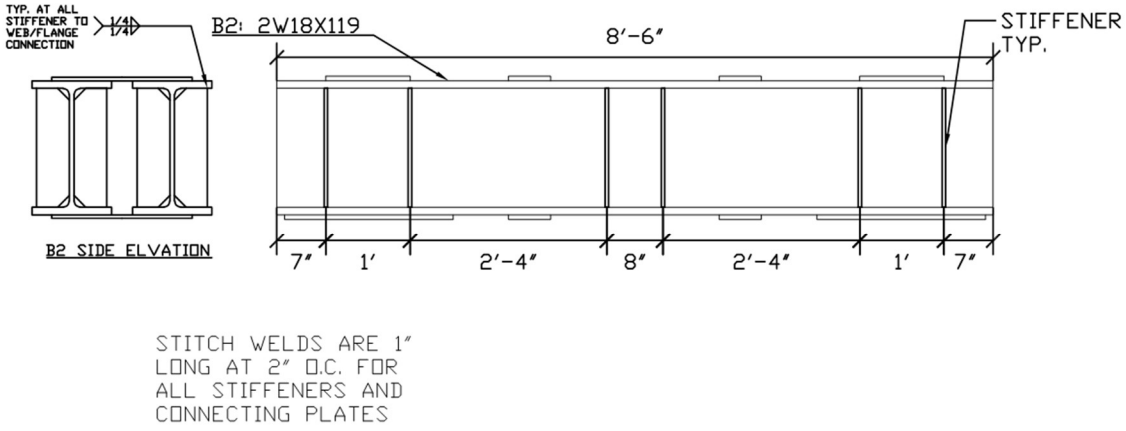

Figure C.1: Elevation view of steel load beam

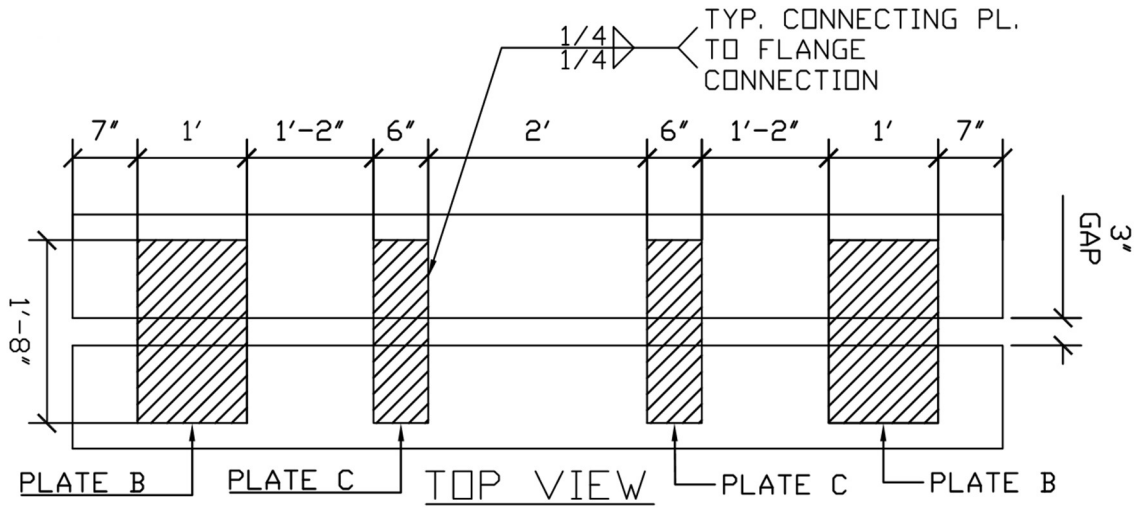

Figure C.2: Top view of steel load beam

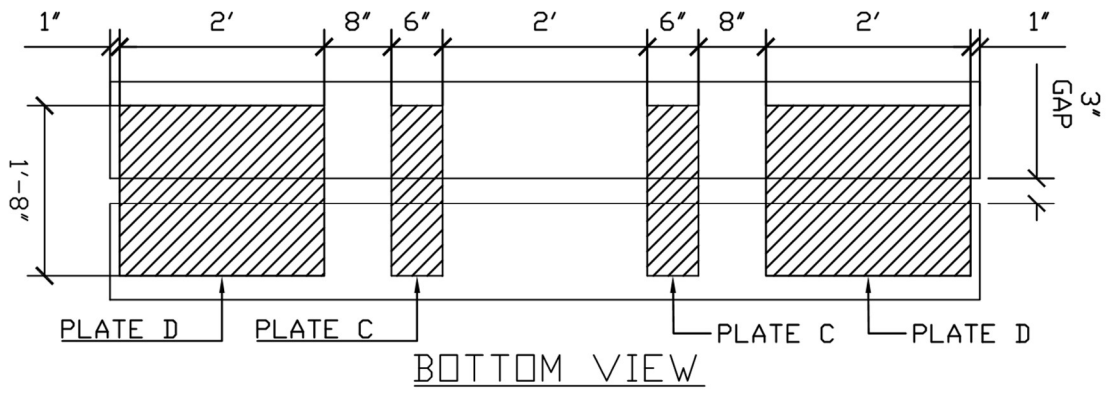

Figure C.3: Bottom view of steel load beam

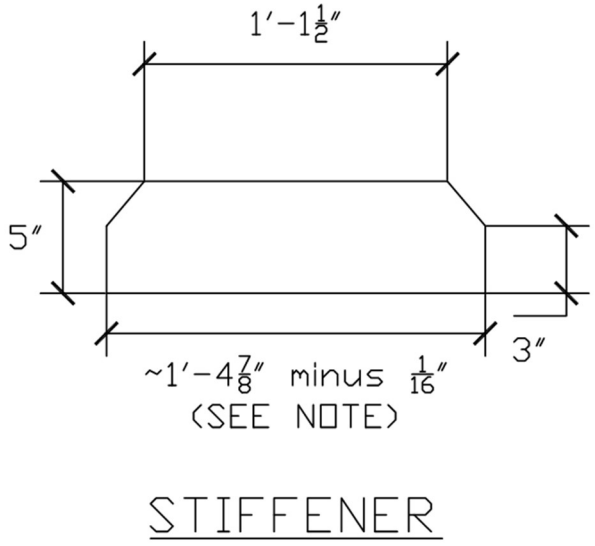

Figure C.4: Stiffener details

Appendix D: Strain Gauge Layouts & Force-Strain Curves

D.1 Specimen 1

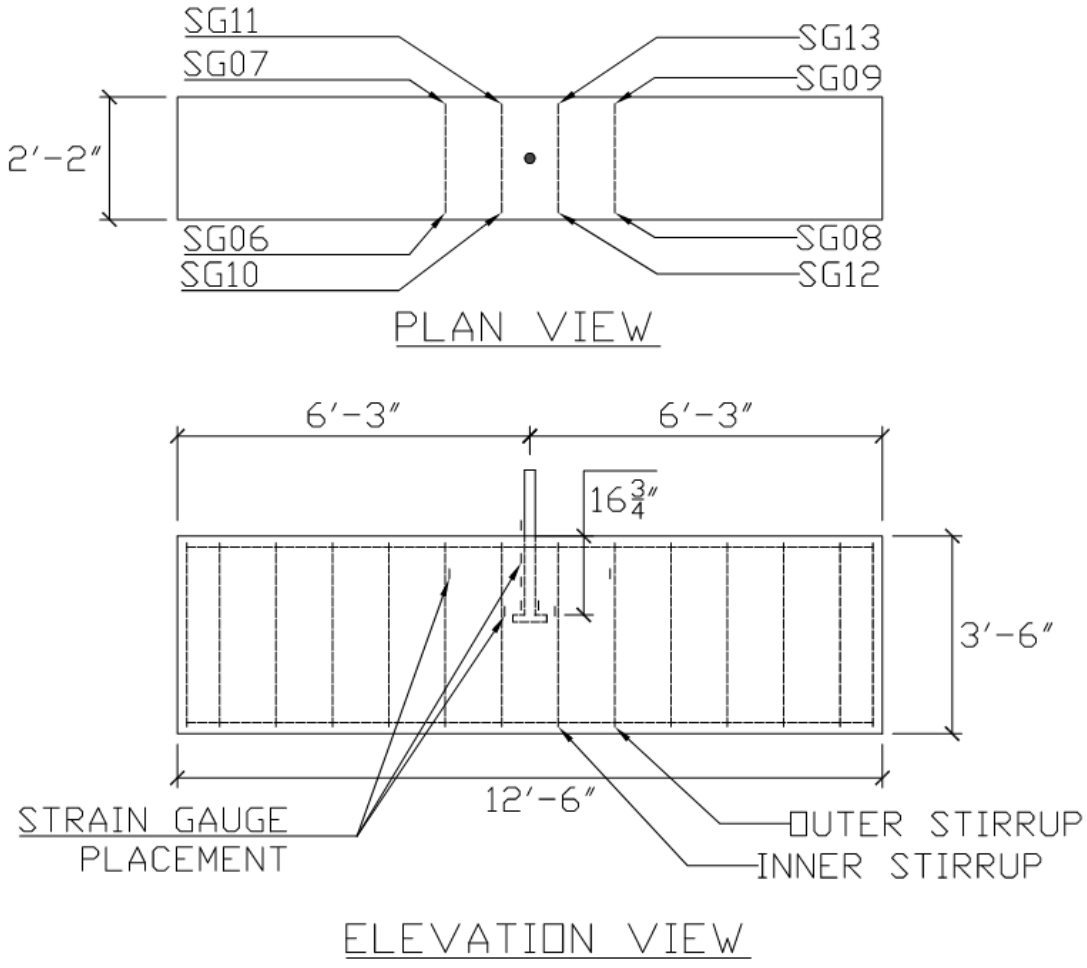

Figure D.1: Locations of strain gauges in Specimen 1

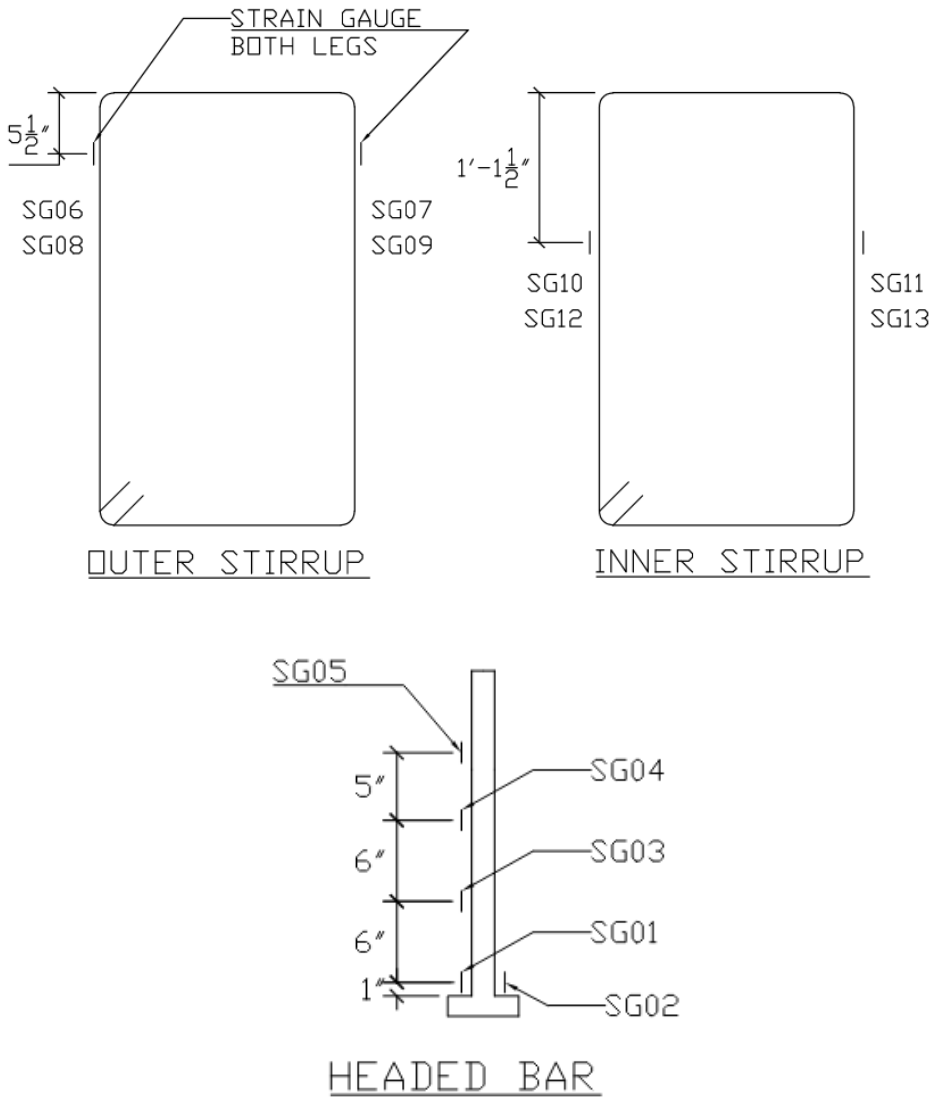

Figure D.2: Locations of stirrup and headed bar strain gauges and their labels for Specimen 1

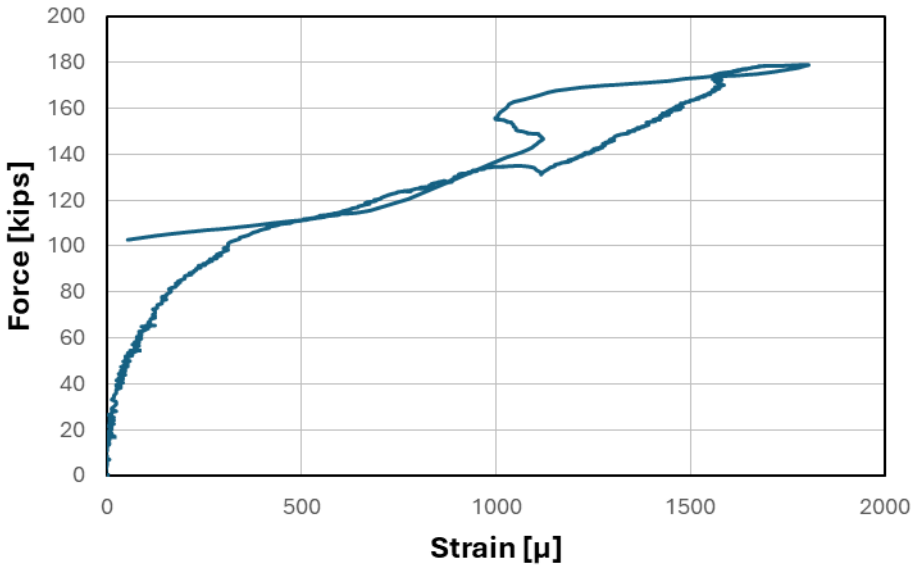

Figure D.3: Force plotted against SG01 strain for Specimen 1

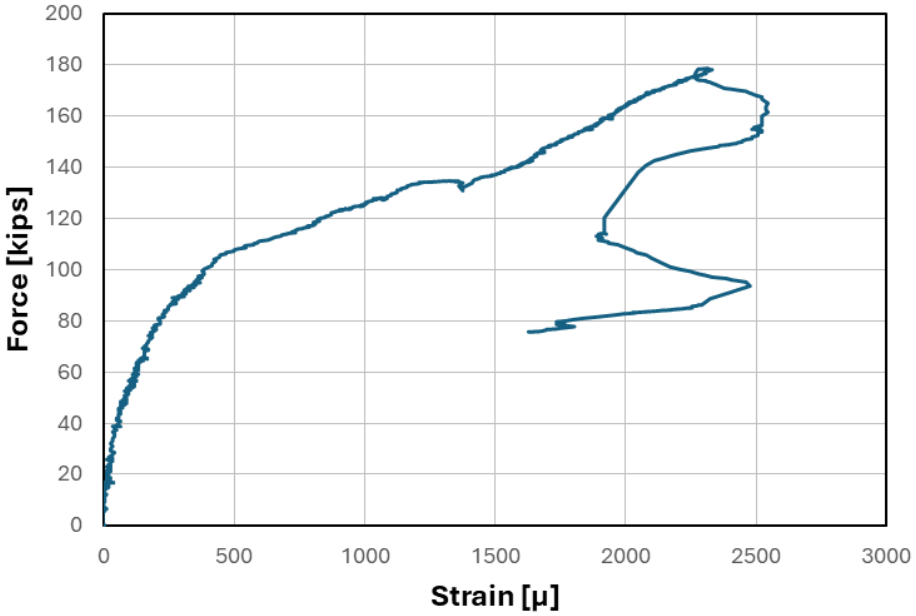

Figure D.4: Force plotted against SG02 strain for Specimen 1

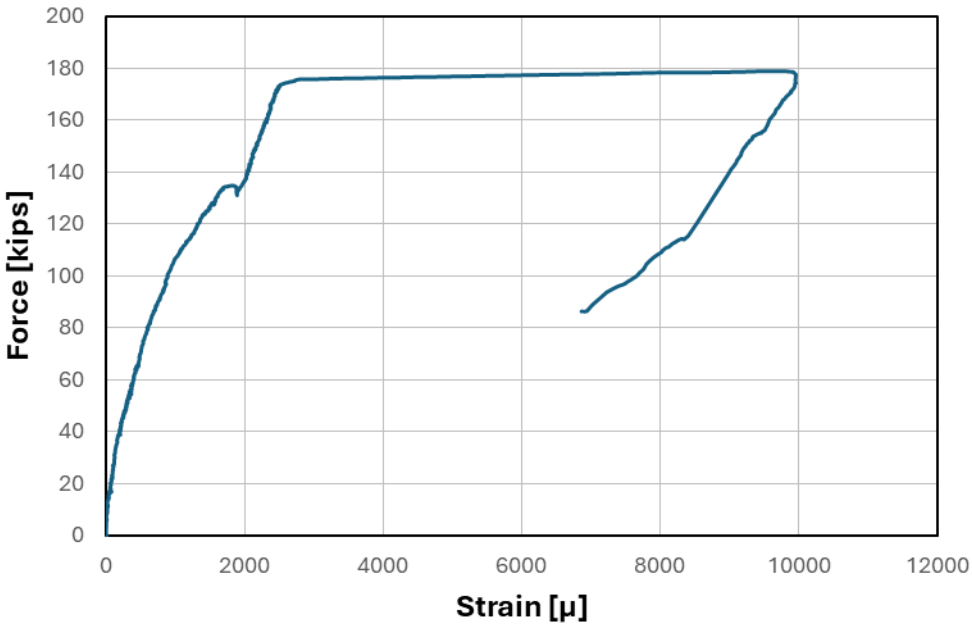

Figure D.5: Force plotted against SG03 strain for Specimen 1

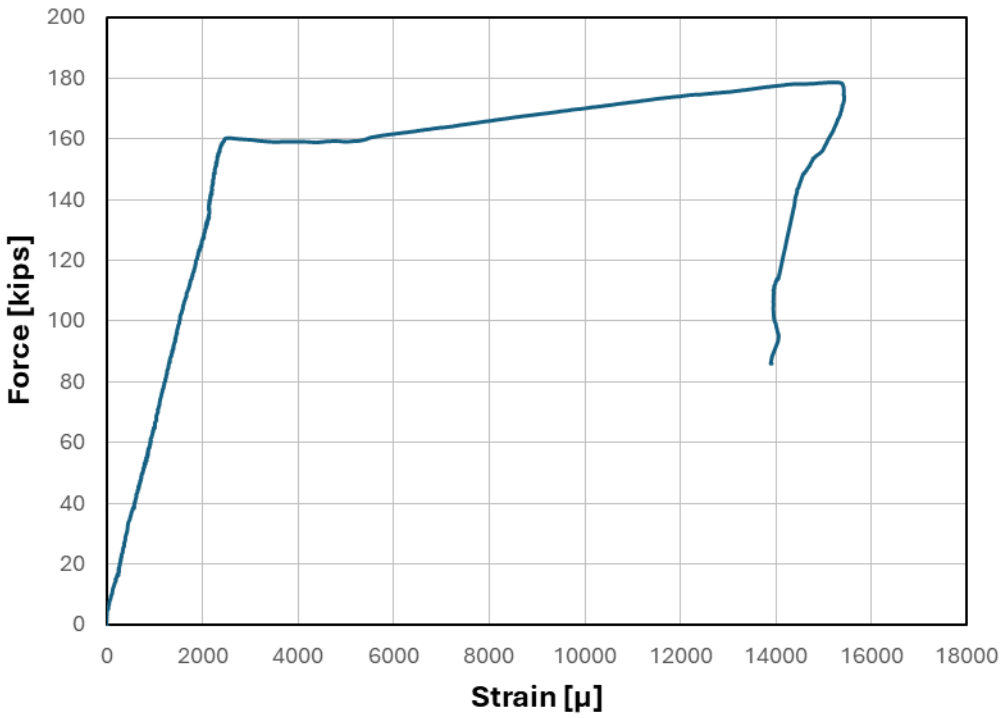

Figure D.6: Force plotted against SG04 strain for Specimen 1

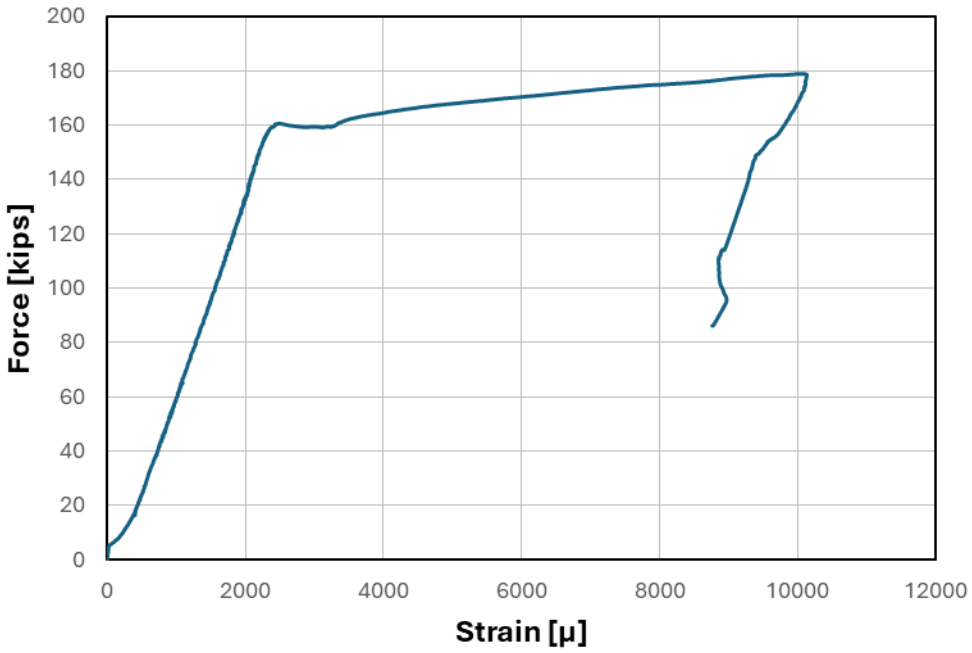

Figure D.7: Force plotted against SG05 strain in Specimen 1

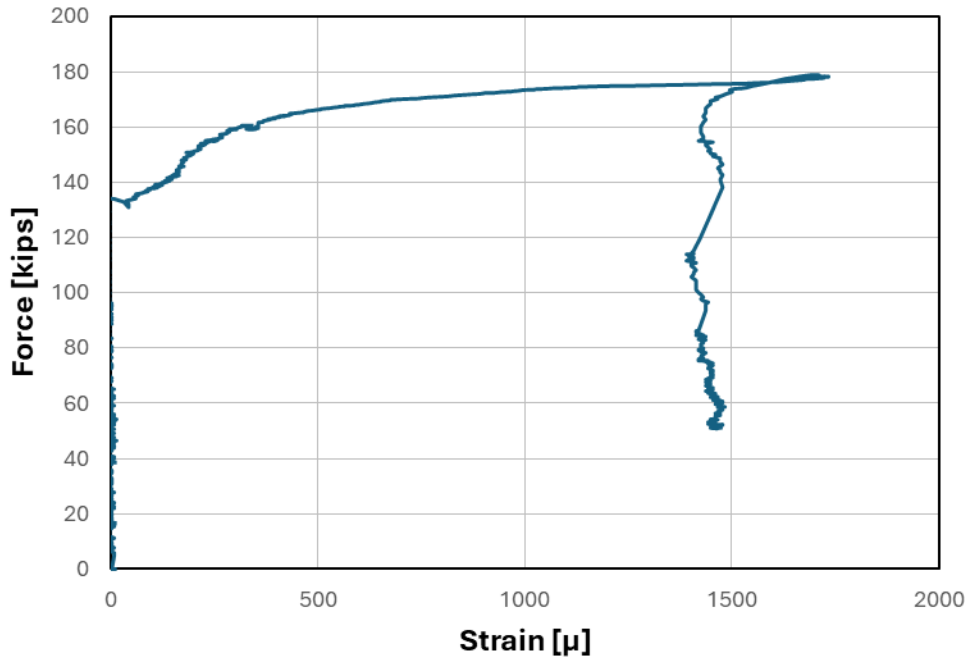

Figure D.8: Force plotted against SG06 strain for Specimen 1

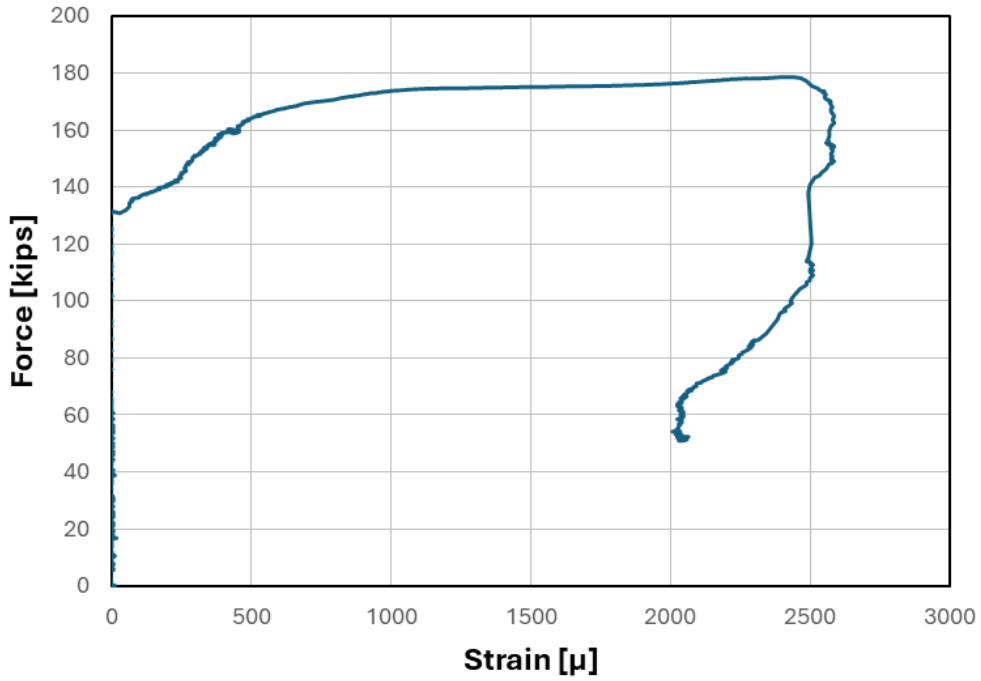

Figure D.9: Force plotted against SG07 strain for Specimen 1

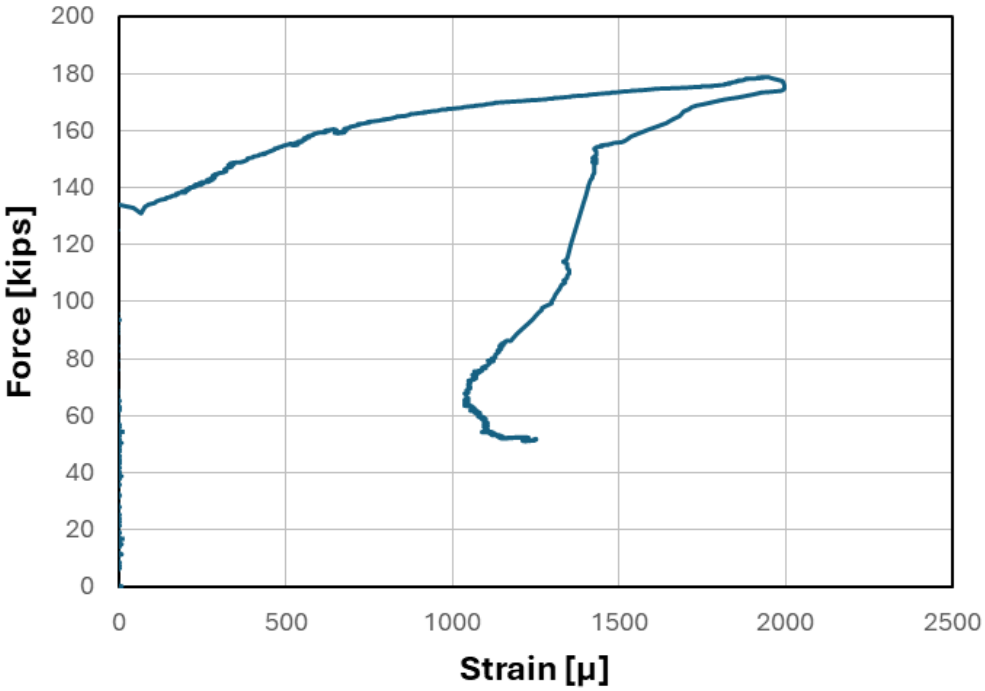

Figure D.10: Force plotted against SG08 strain for Specimen 1

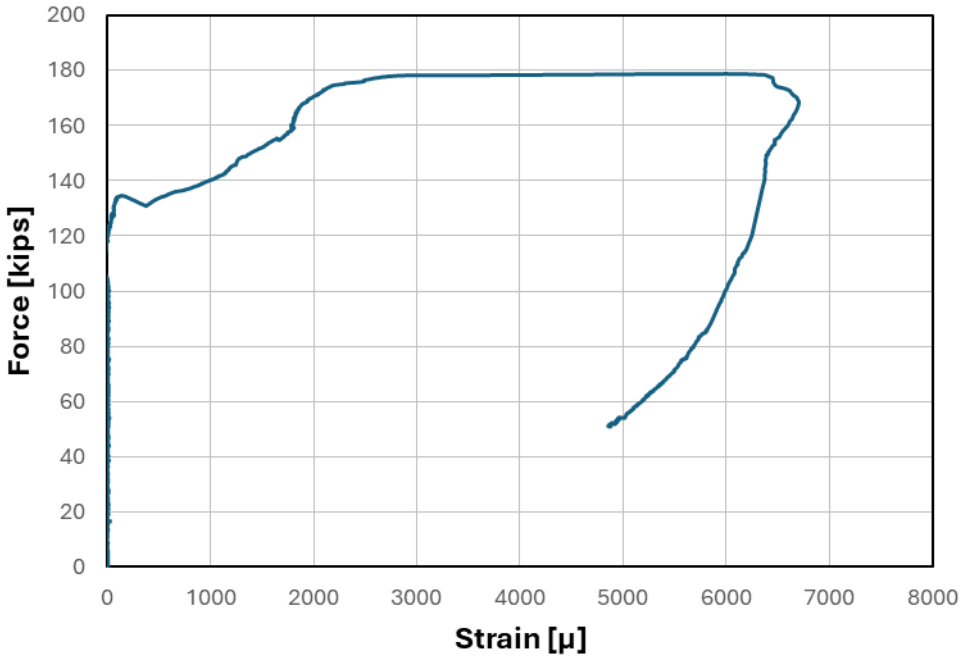

Figure D.11: Force plotted against SG10 strain for Specimen 1

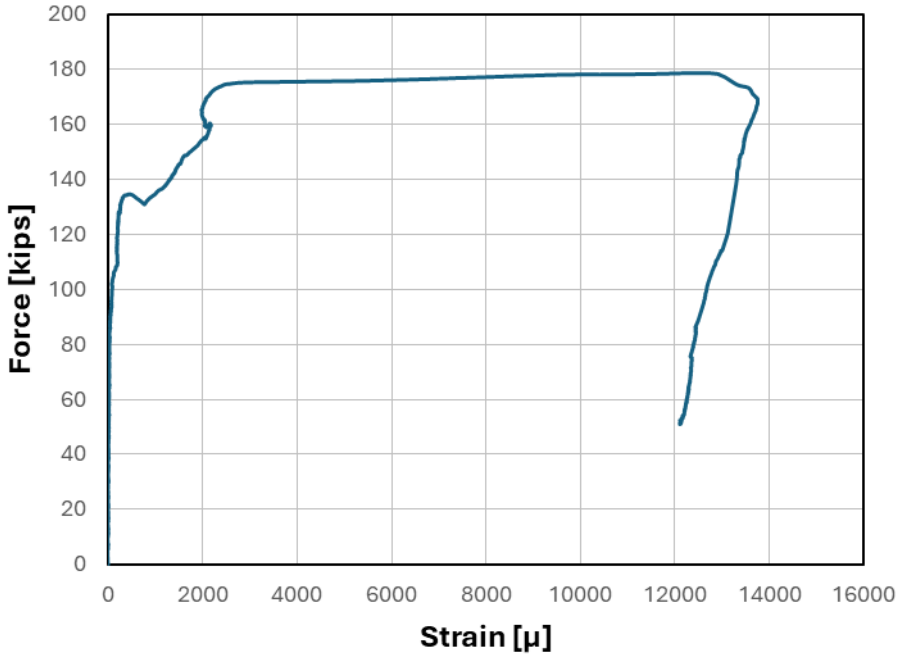

Figure D.12: Force plotted against SG12 strain for Specimen 1

D.2 Specimen 2

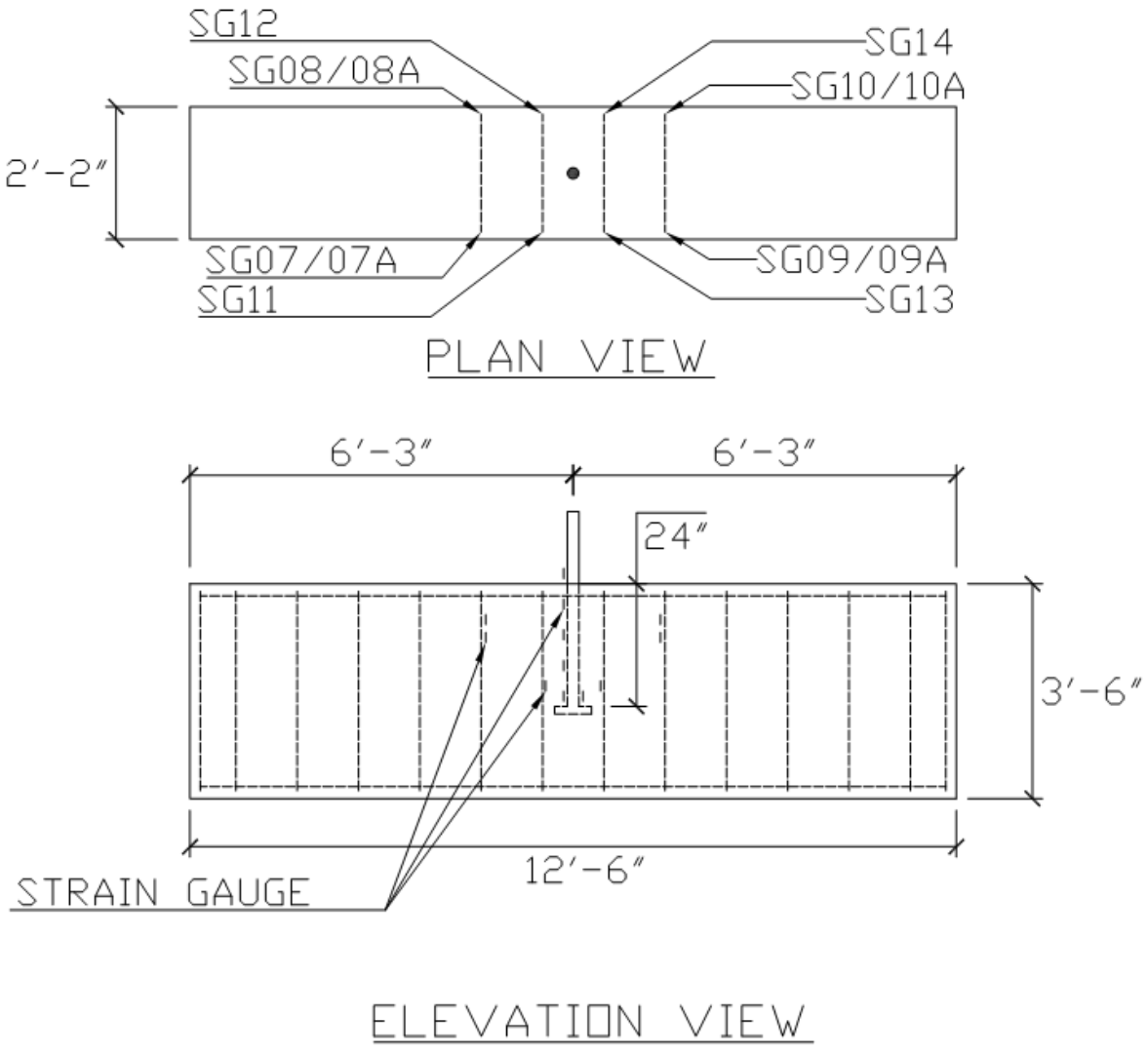

Figure D.13: Locations of strain gauges for Specimen 2

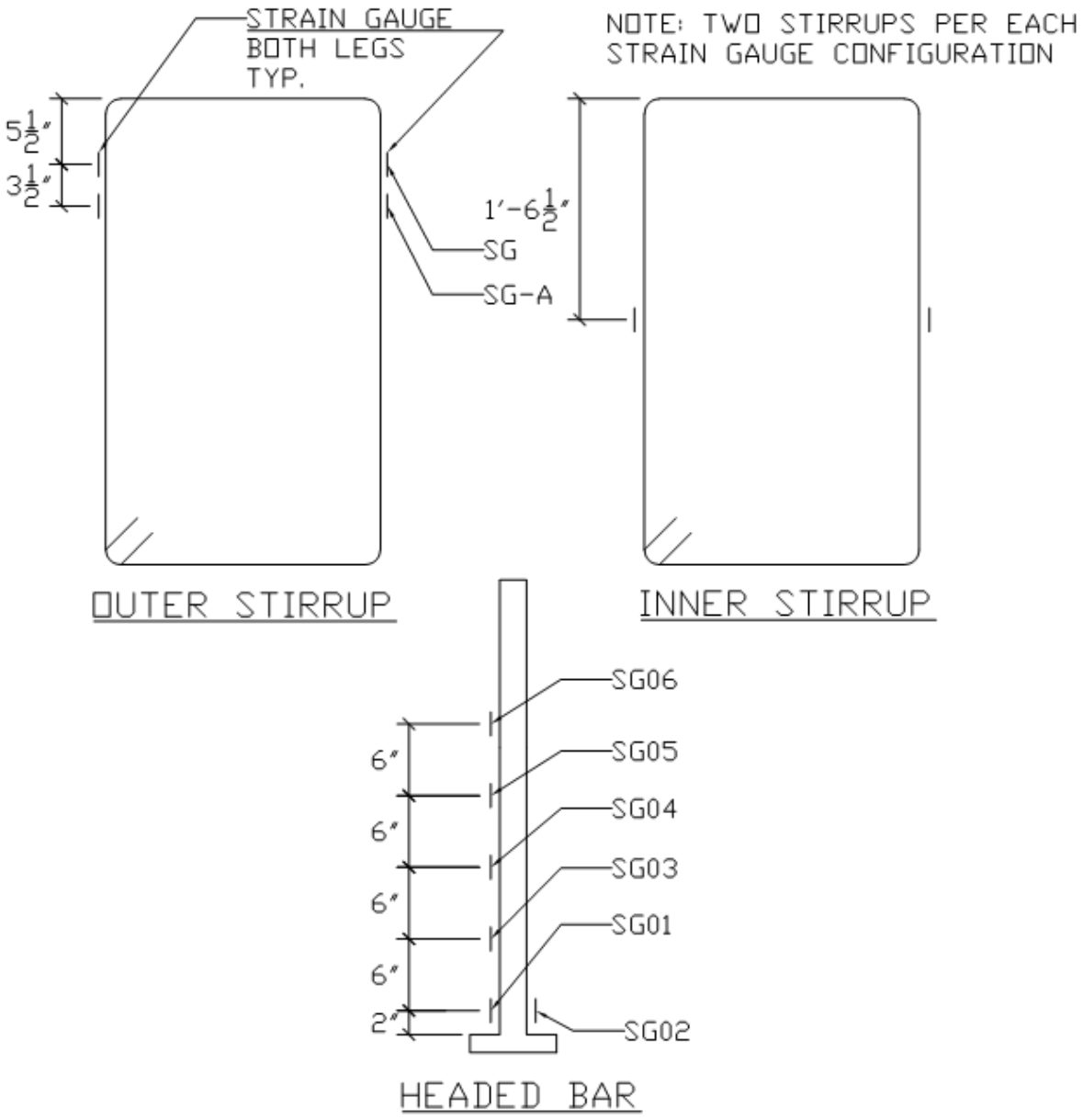

Figure D.14: Locations of stirrup and headed bar strain gauges and their labels for Specimen 2

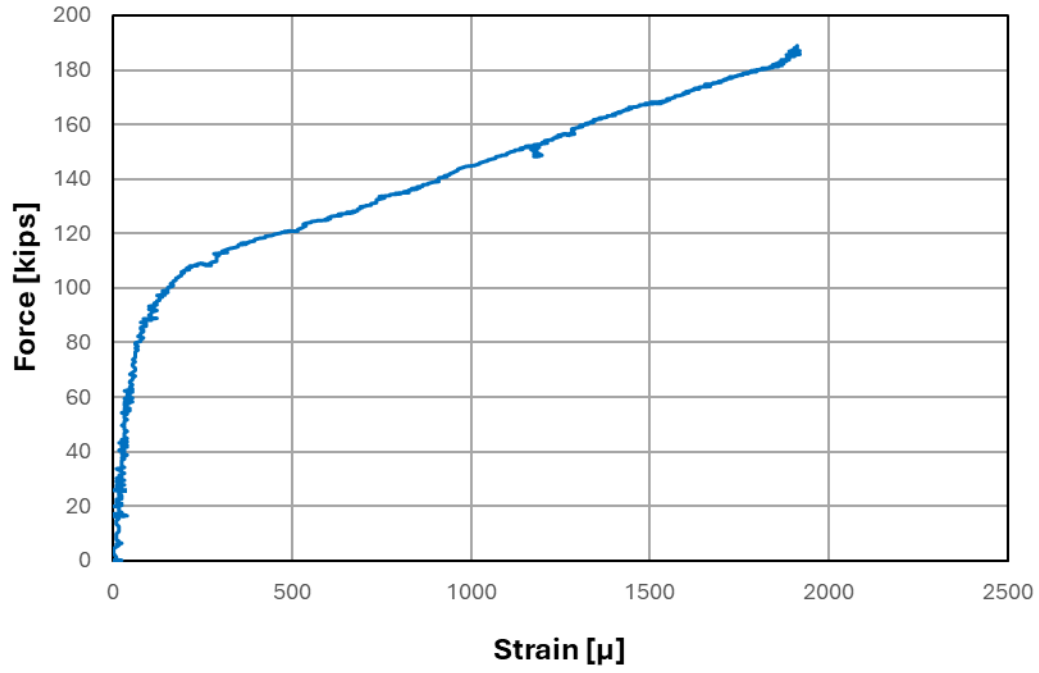

Figure D.15: Force plotted against SG01 strain for Specimen 2

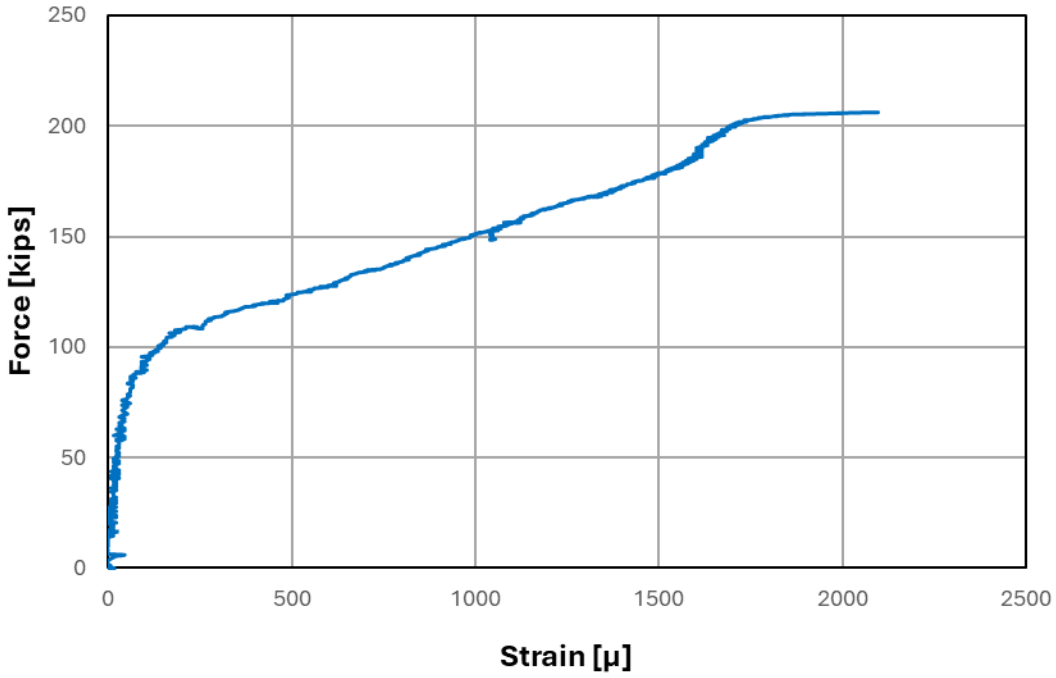

Figure D.16: Force plotted against SG02 strain for Specimen 2

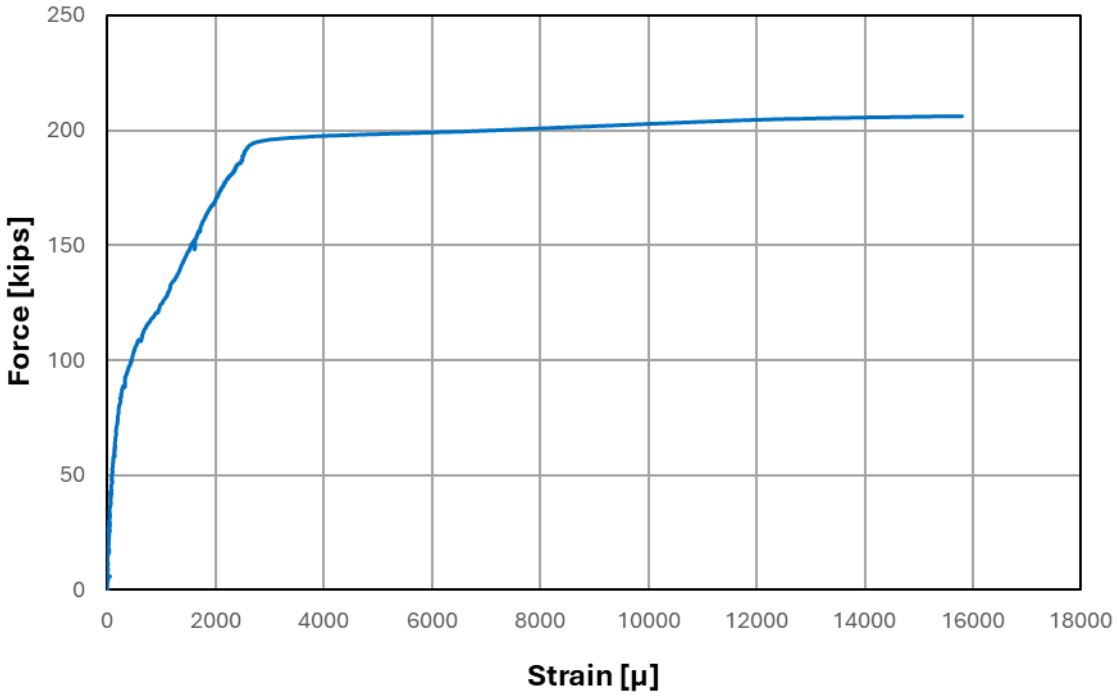

Figure D.17: Force plotted against SG03 strain for Specimen 2

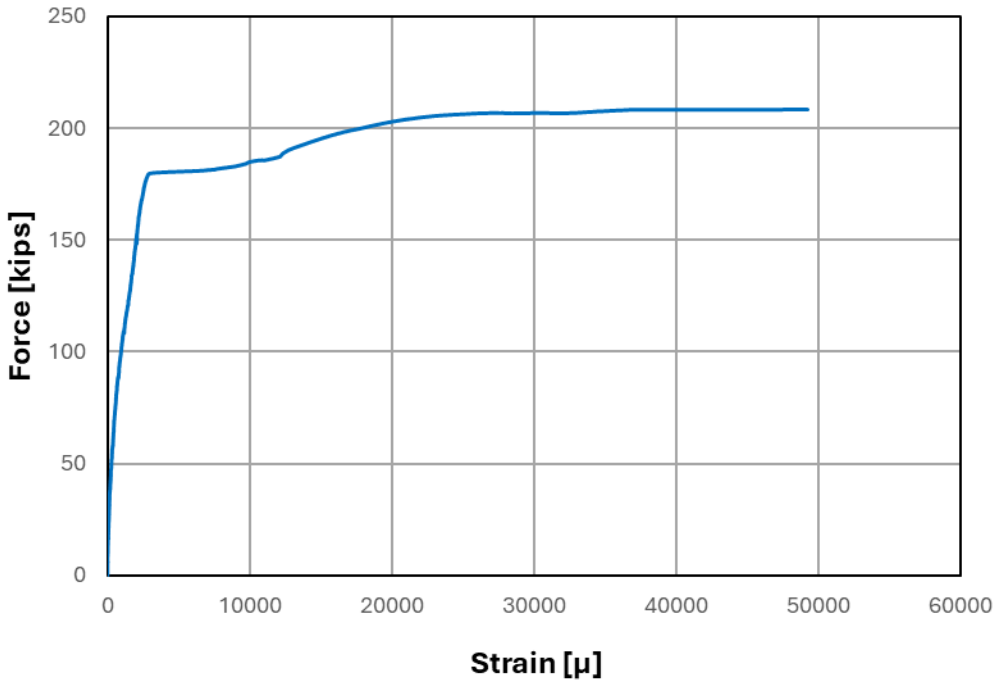

Figure D.18: Force plotted against SG04 strain for Specimen 2

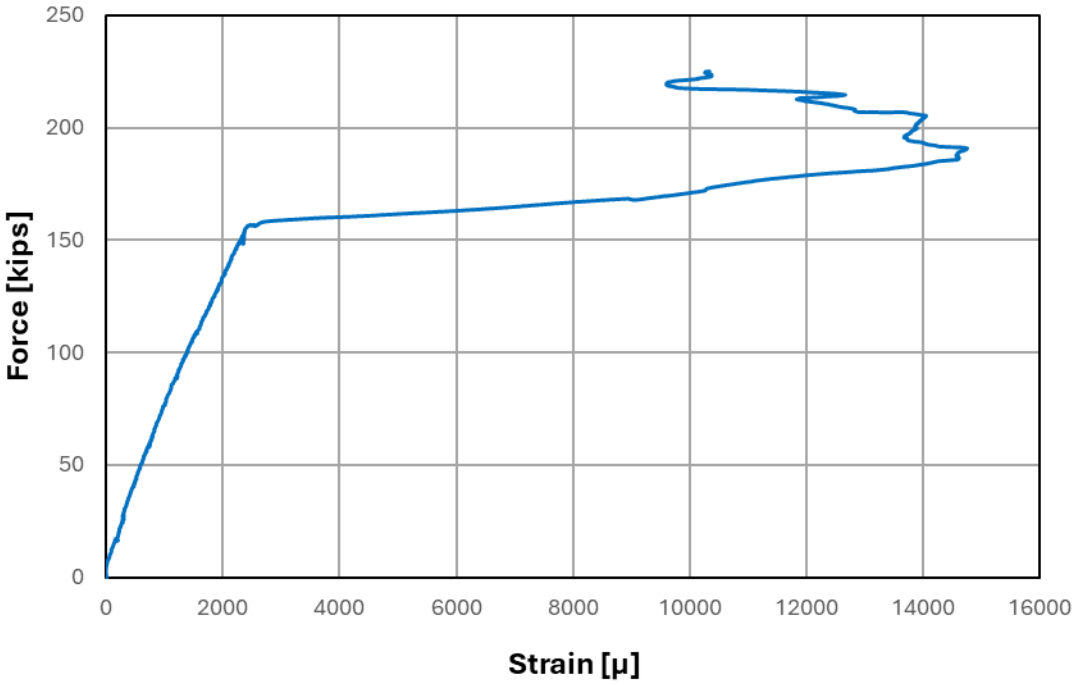

Figure D.19: Force plotted against SG05 strain for Specimen 2

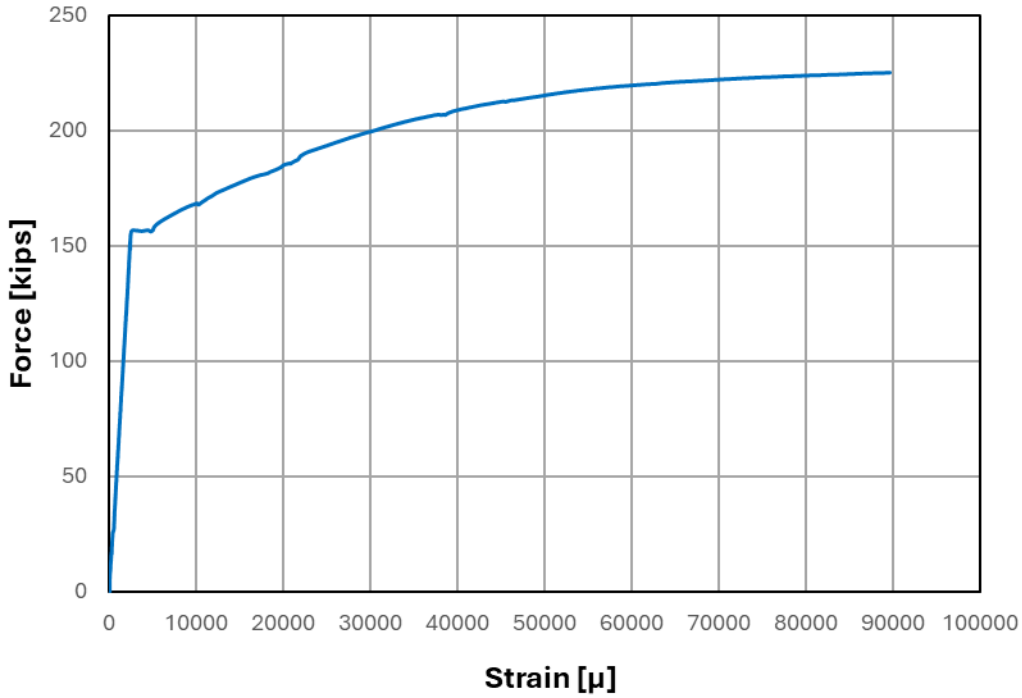

Figure D.20: Force plotted against SG06 strain for Specimen 2

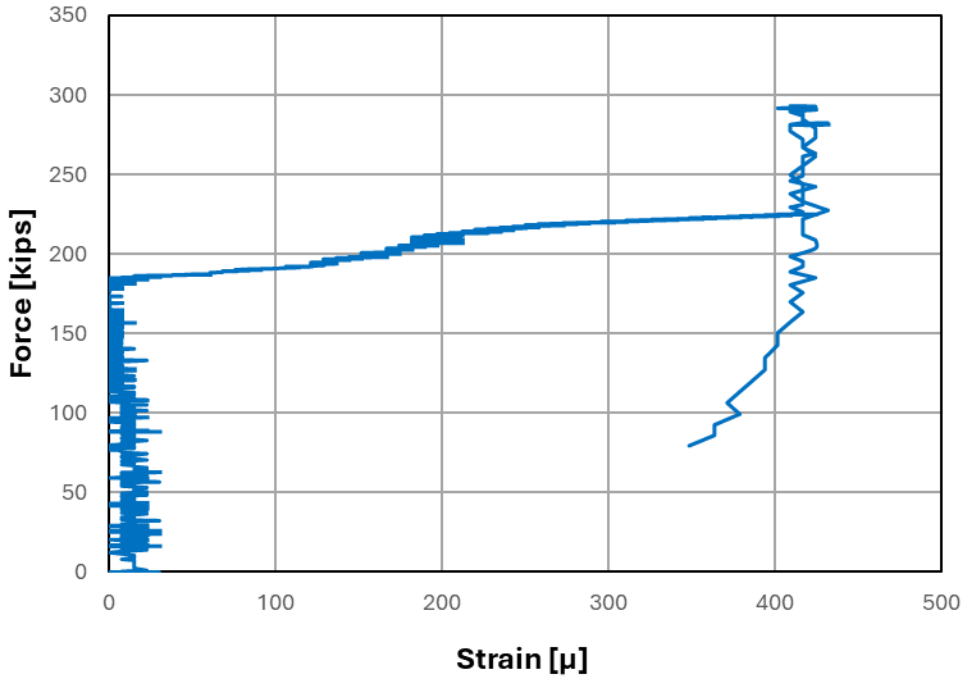

Figure D.21: Force plotted against SG07 strain for Specimen 2

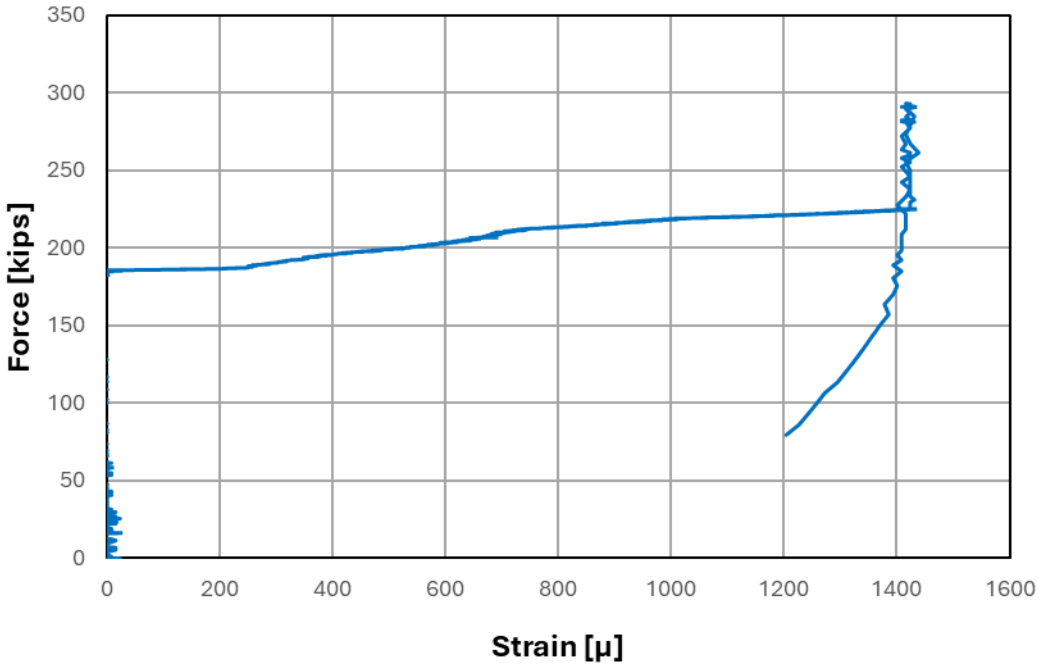

Figure D.22: Force plotted against SG07A strain for Specimen 2

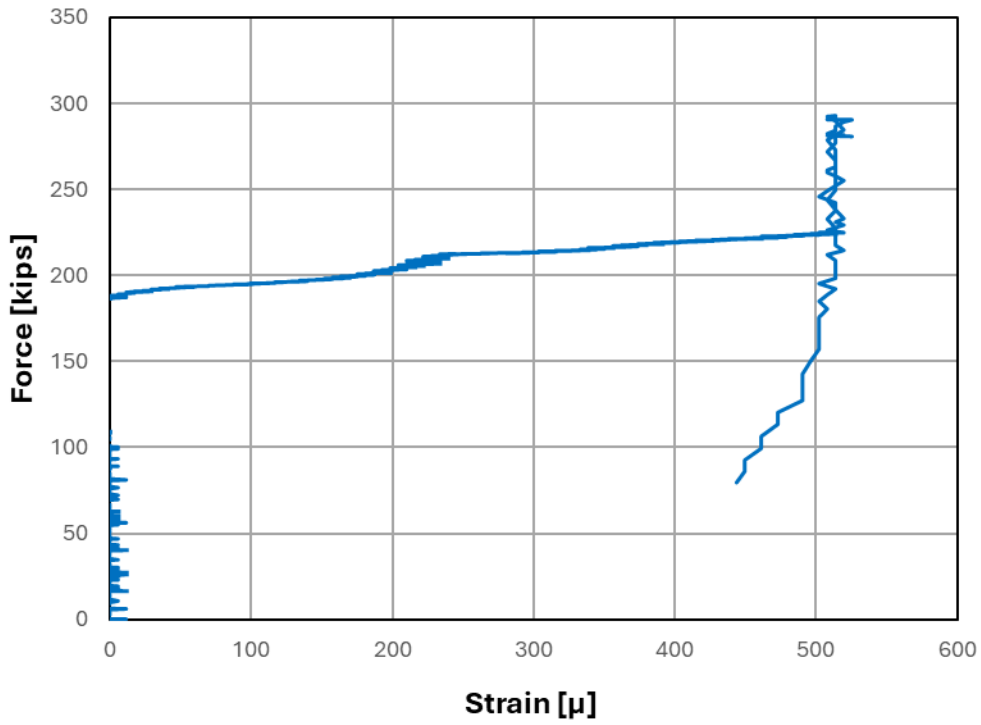

Figure D.23: Force plotted against SG08 strain for Specimen 2

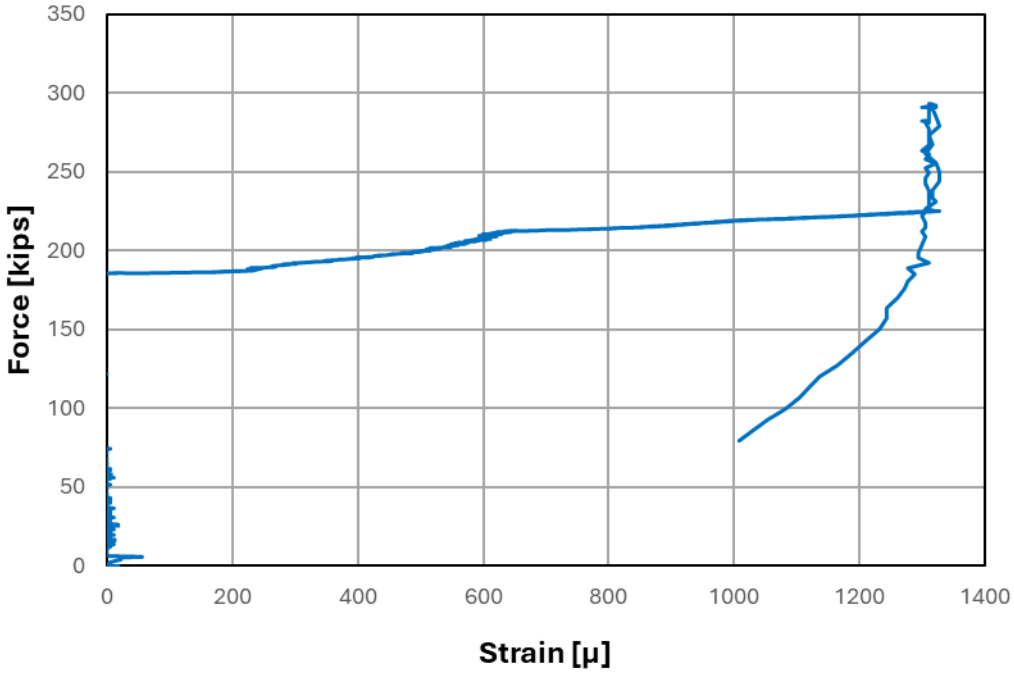

Figure D.24: Force plotted against SG08A strain for Specimen 2

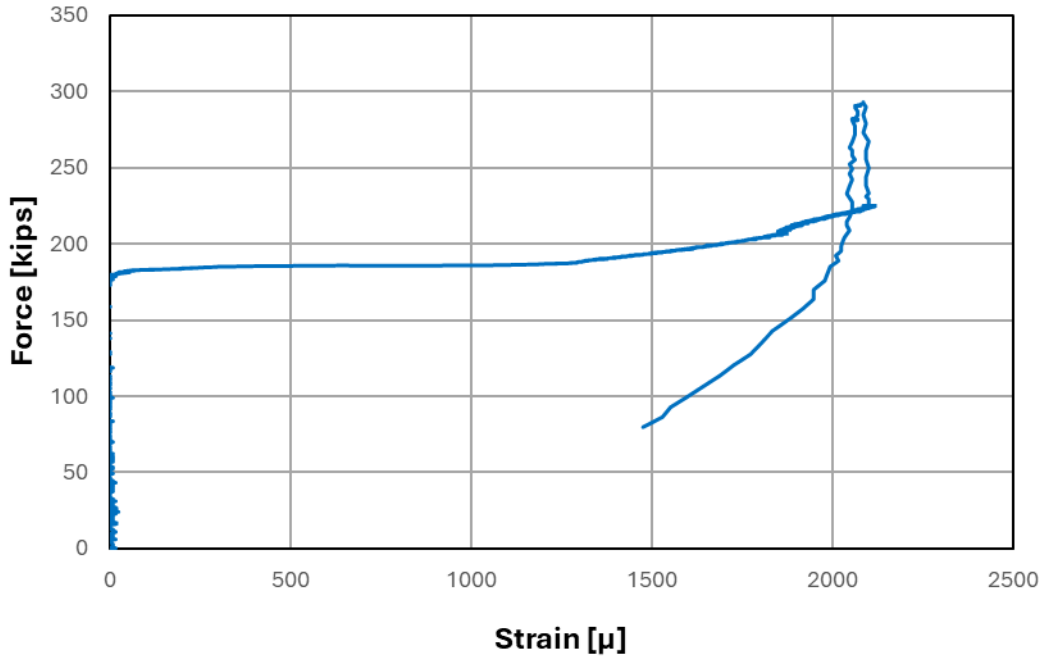

Figure D.25: Force plotted against SG09 strain for Specimen 2

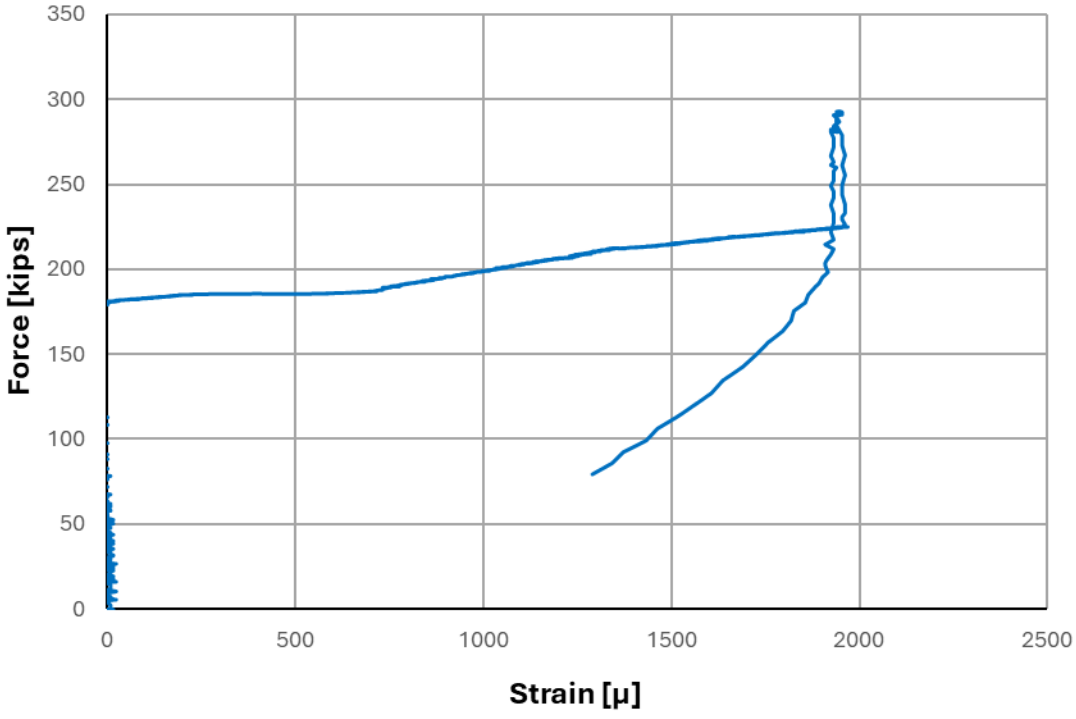

Figure D.26: Force plotted against SG09A strain for Specimen 2

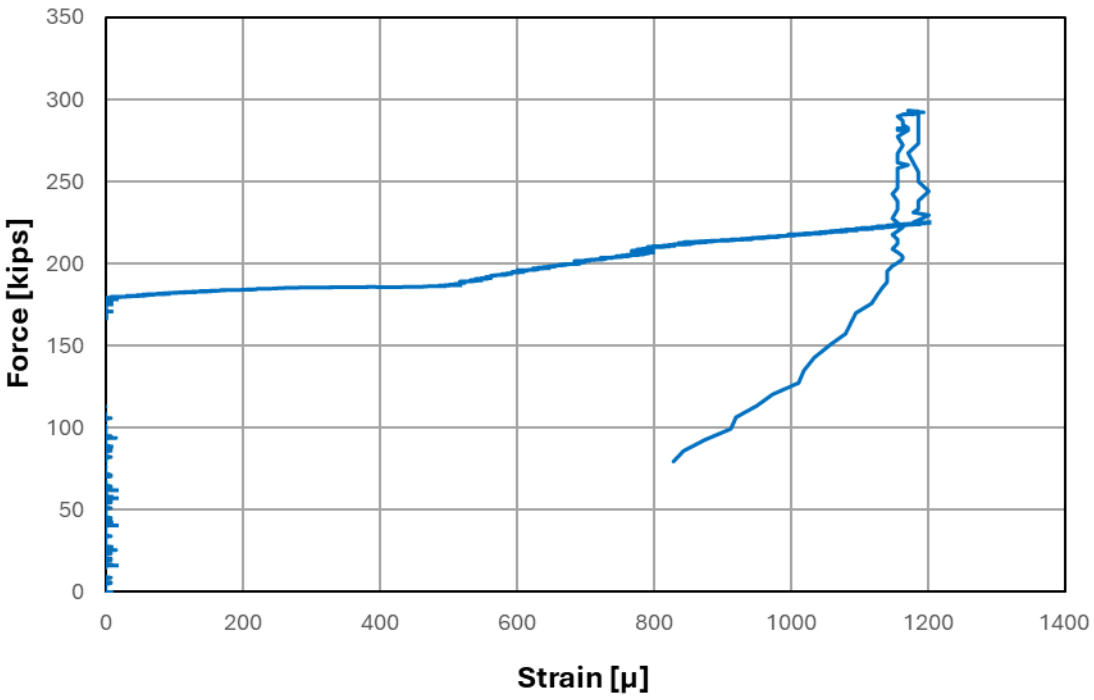

Figure D.27: Force plotted against SG10 strain for Specimen 2

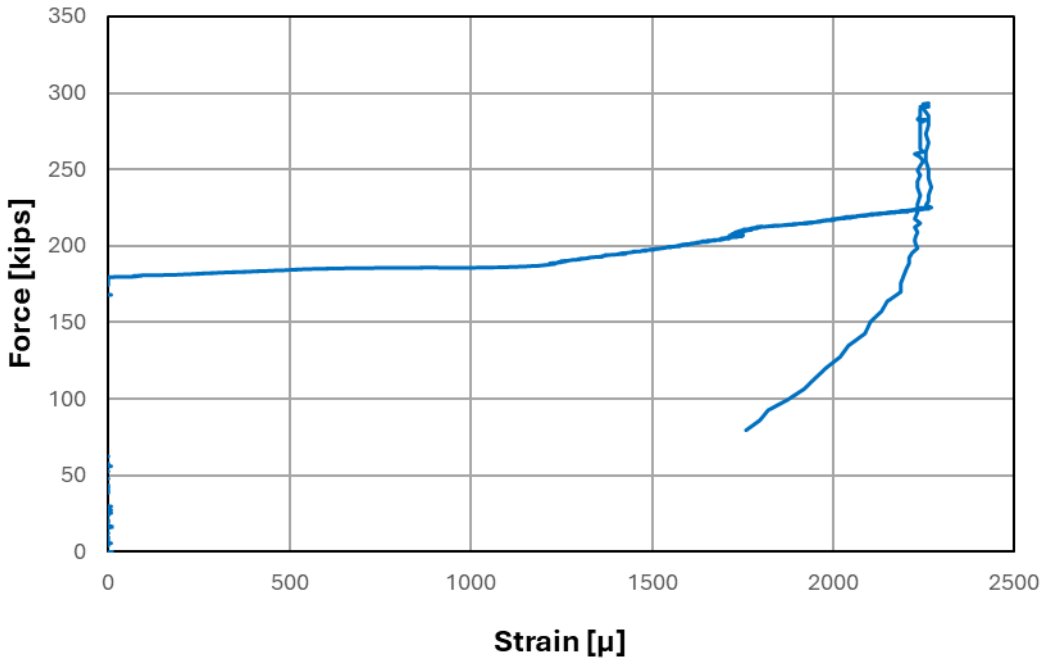

Figure D.28: Force plotted against SG10A strain for Specimen 2

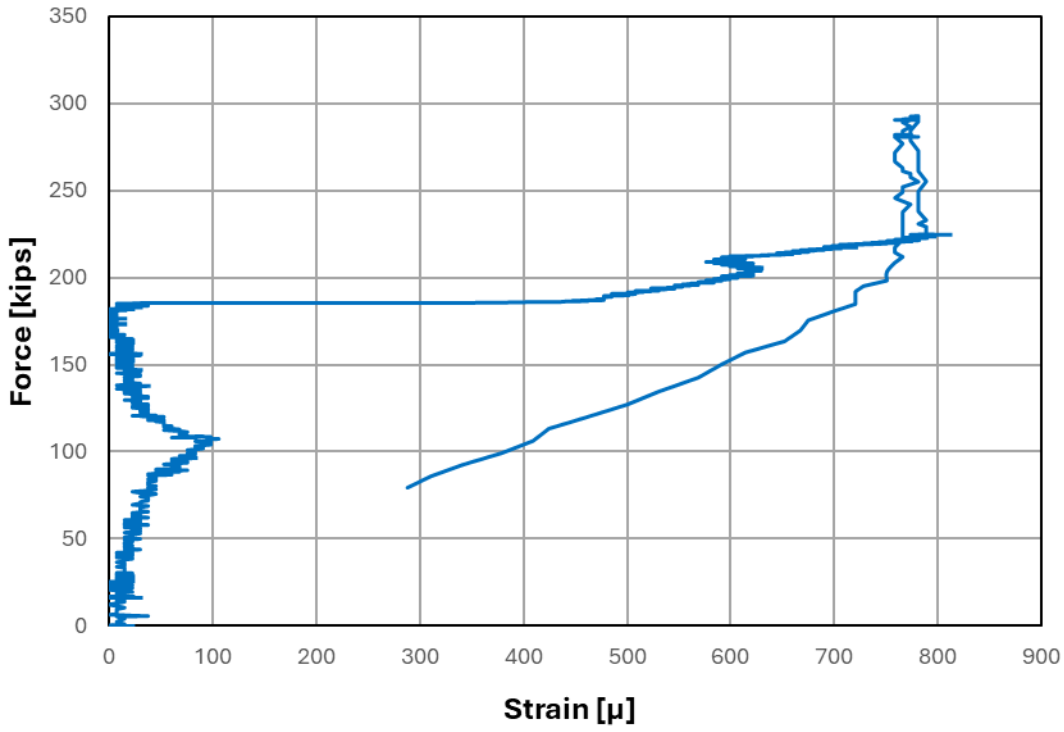

Figure D.29: Force plotted against SG11 strain for Specimen 2

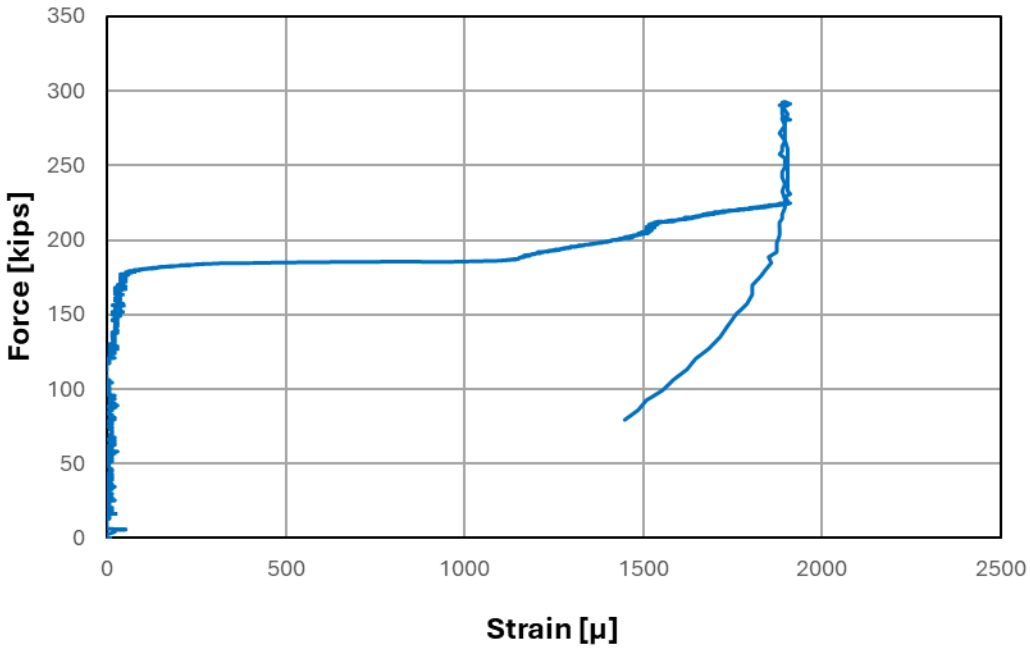

Figure D.30: Force plotted against SG12 strain for Specimen 2

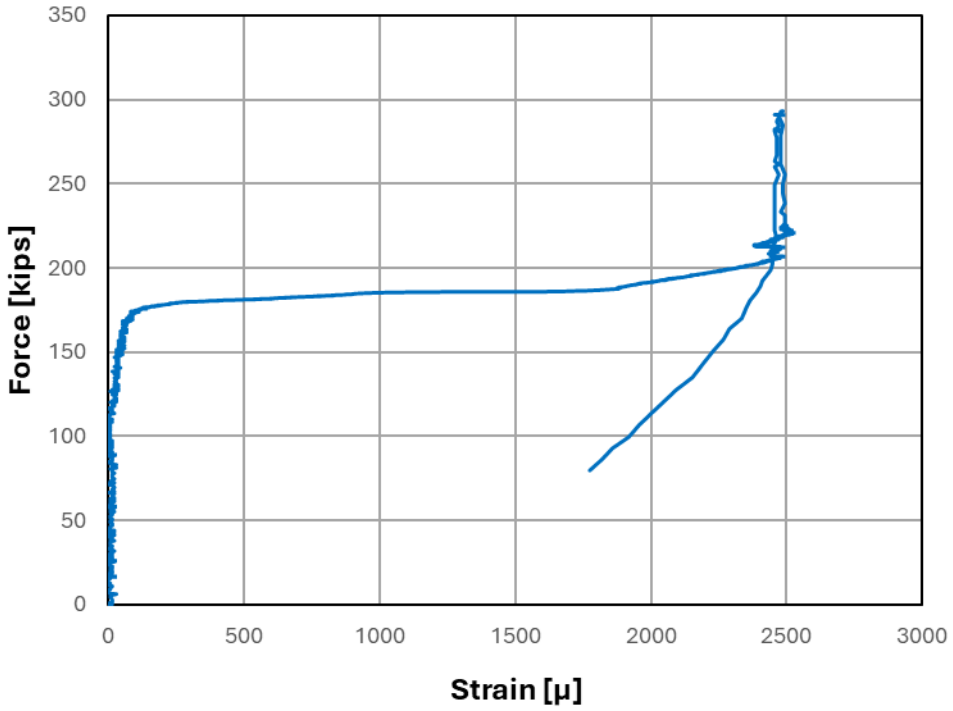

Figure D.31: Force plotted against SG13 strain for Specimen 2

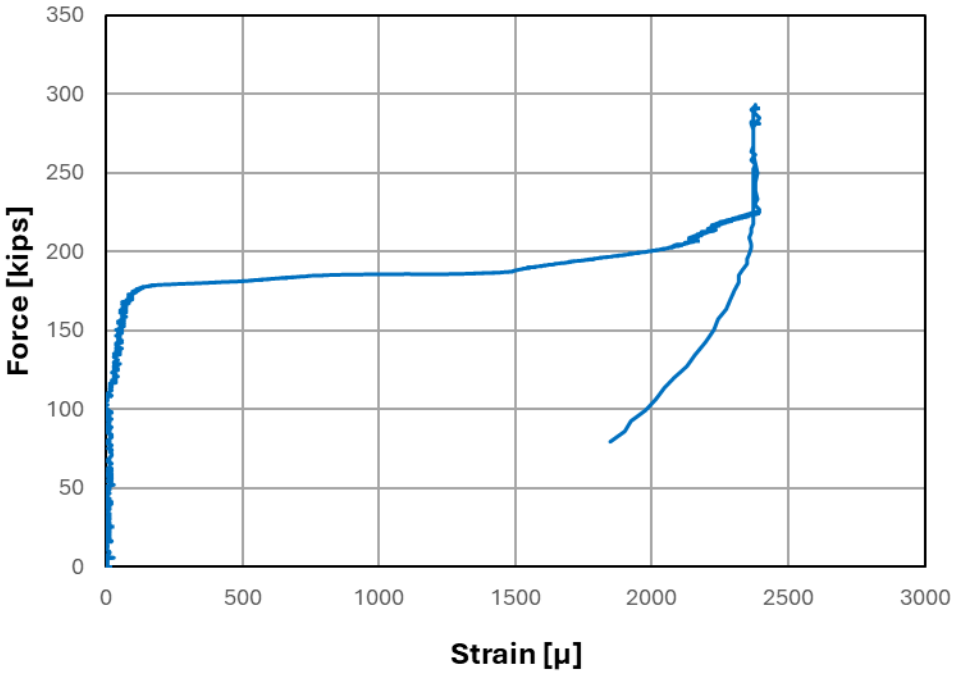

Figure D.32: Force plotted against SG14 strain for Specimen 2

D.3 Specimen 3

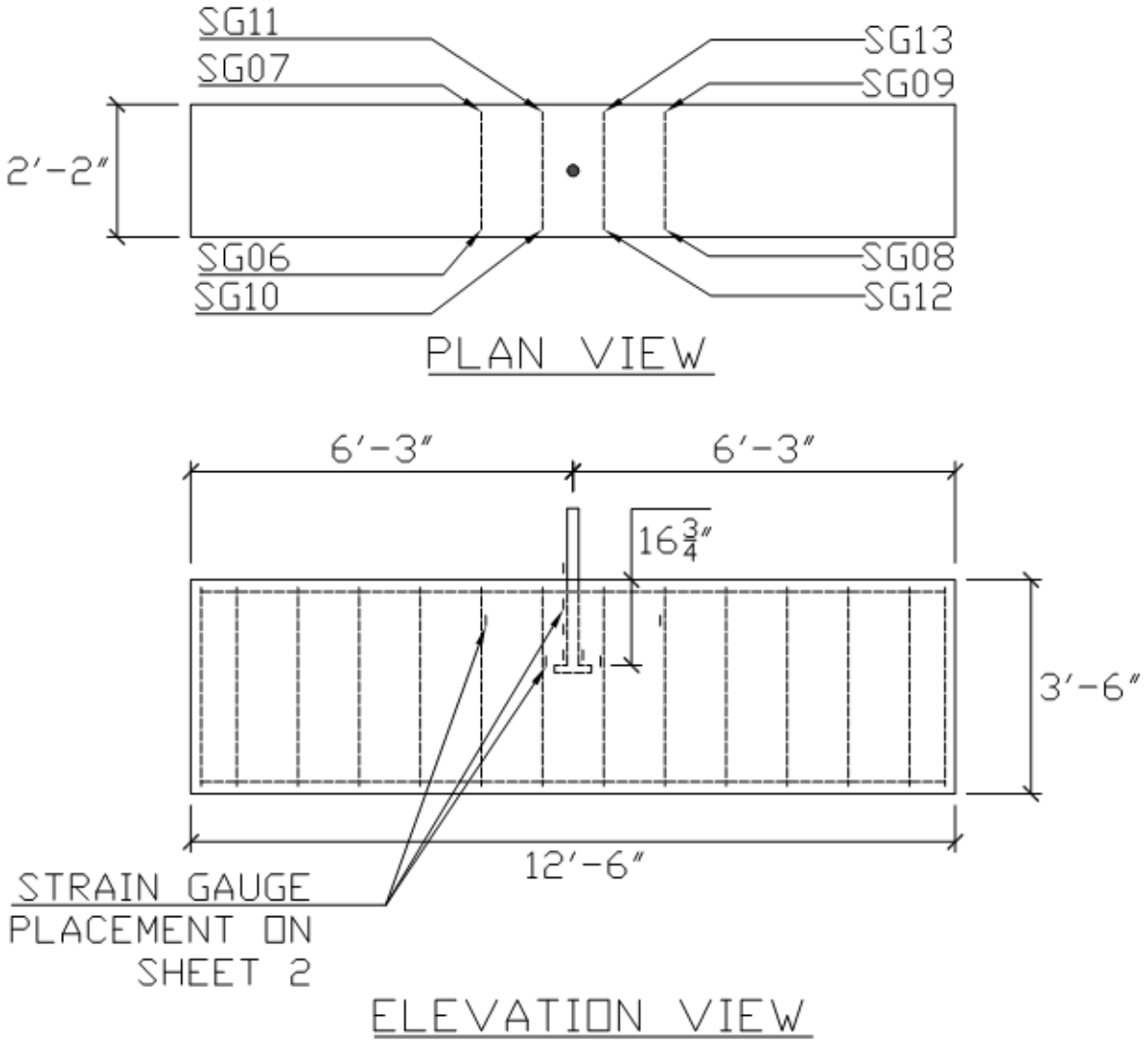

Figure D.33: Locations of strain gauges for Specimen 3

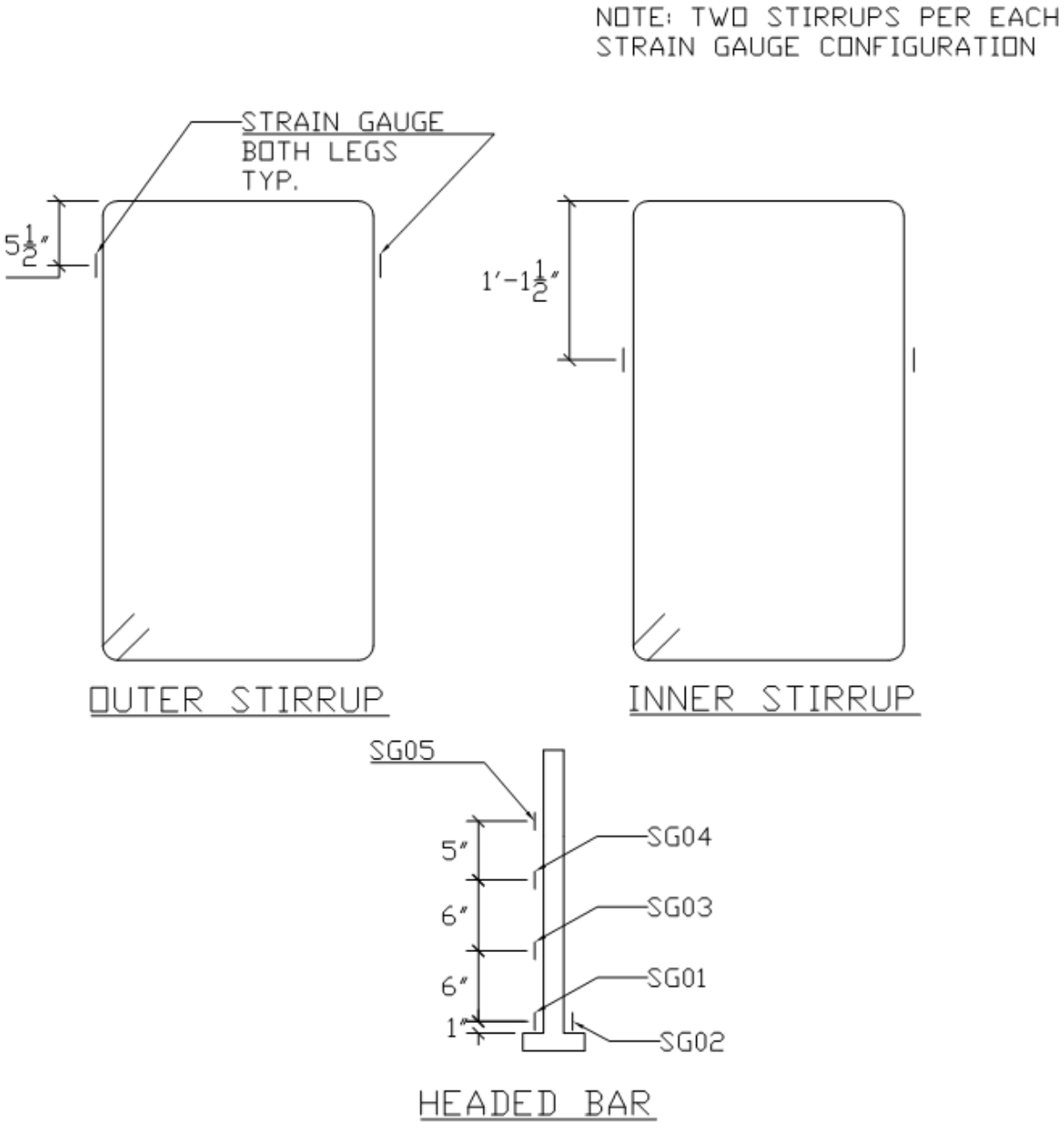

Figure D.34: Locations of stirrup and headed bar strain gauges and their labels for Specimen 3

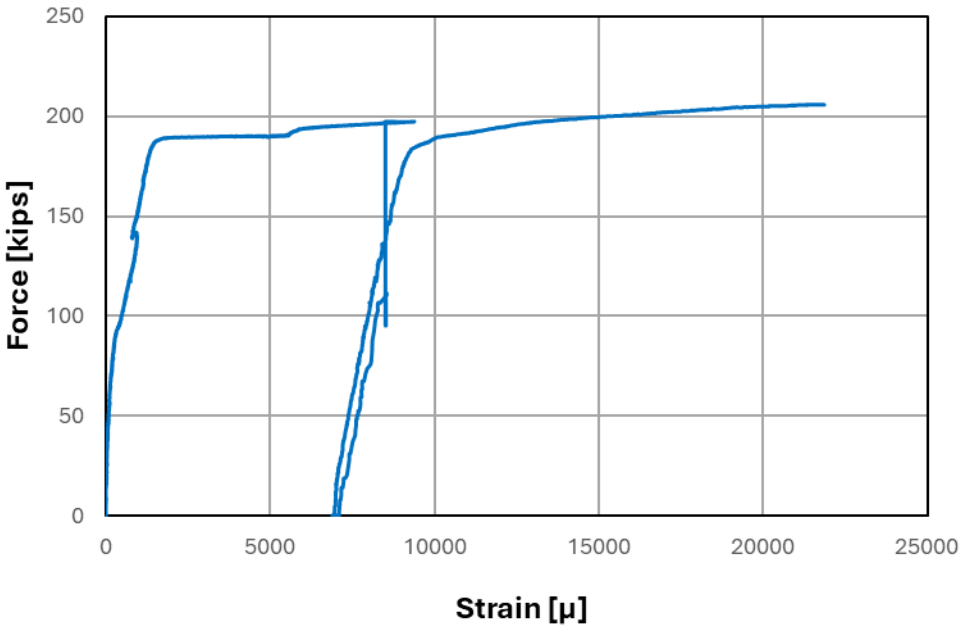

Figure D.35: Force plotted against SG01 strain for Specimen 3

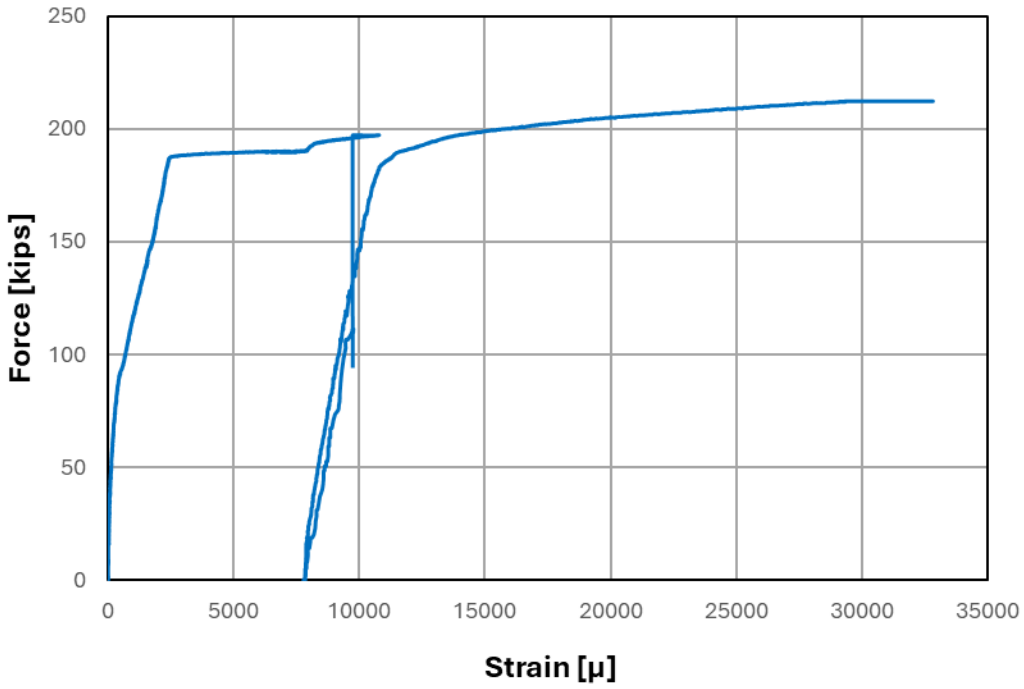

Figure D.36: Force plotted against SG02 strain for Specimen 3

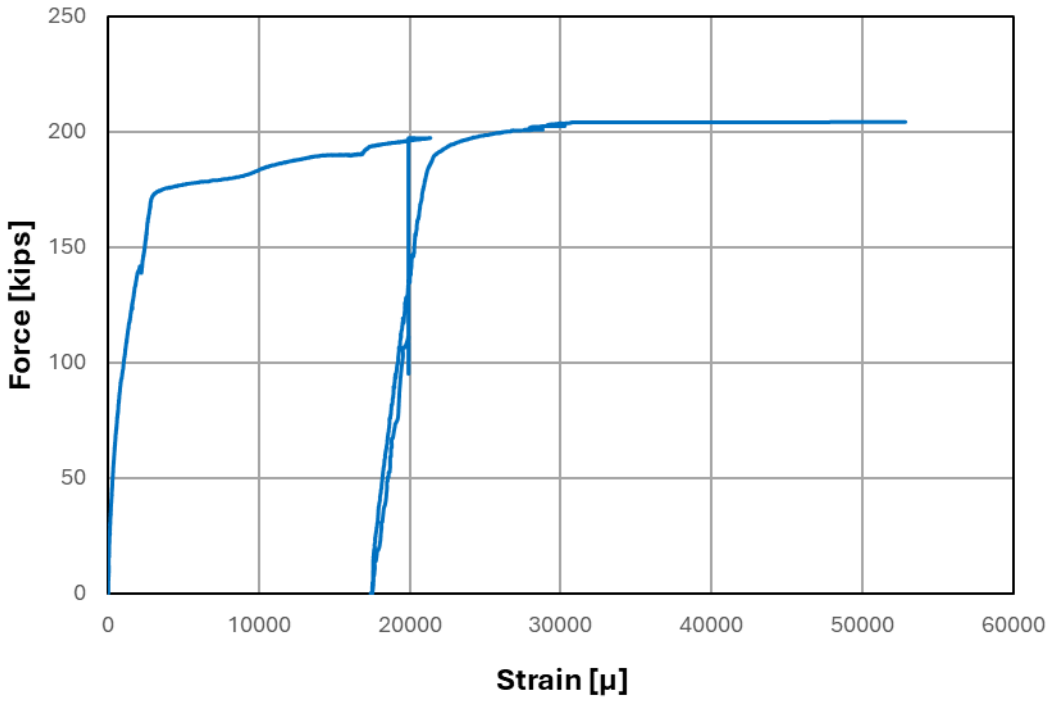

Figure D.37: Force plotted against SG03 strain for Specimen 3

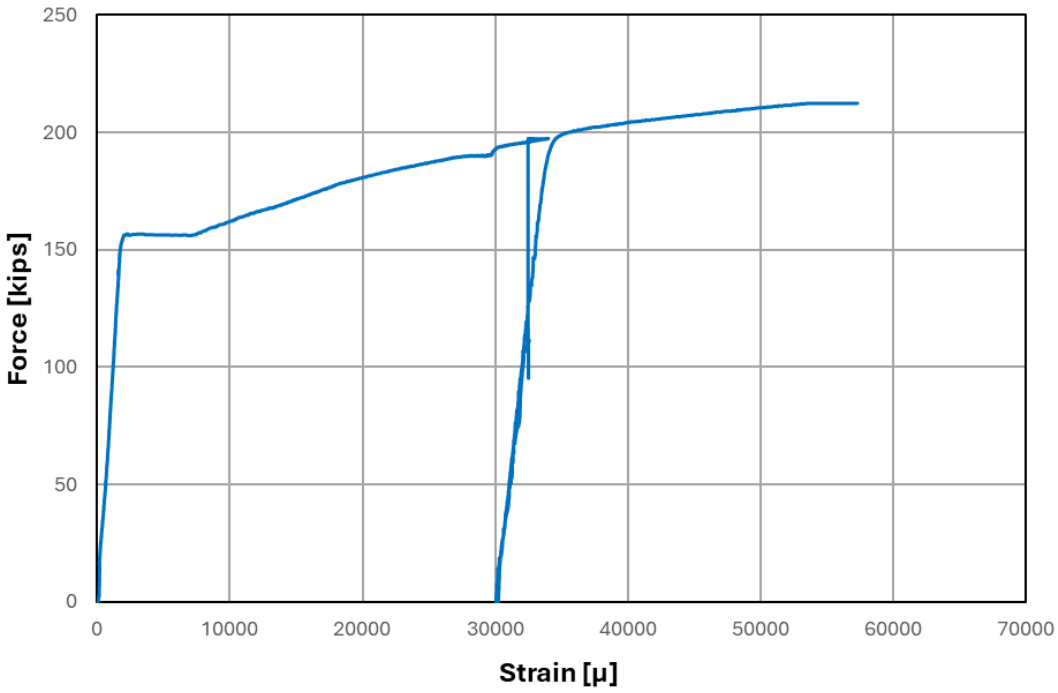

Figure D.38: Force plotted against SG05 strain for Specimen 3

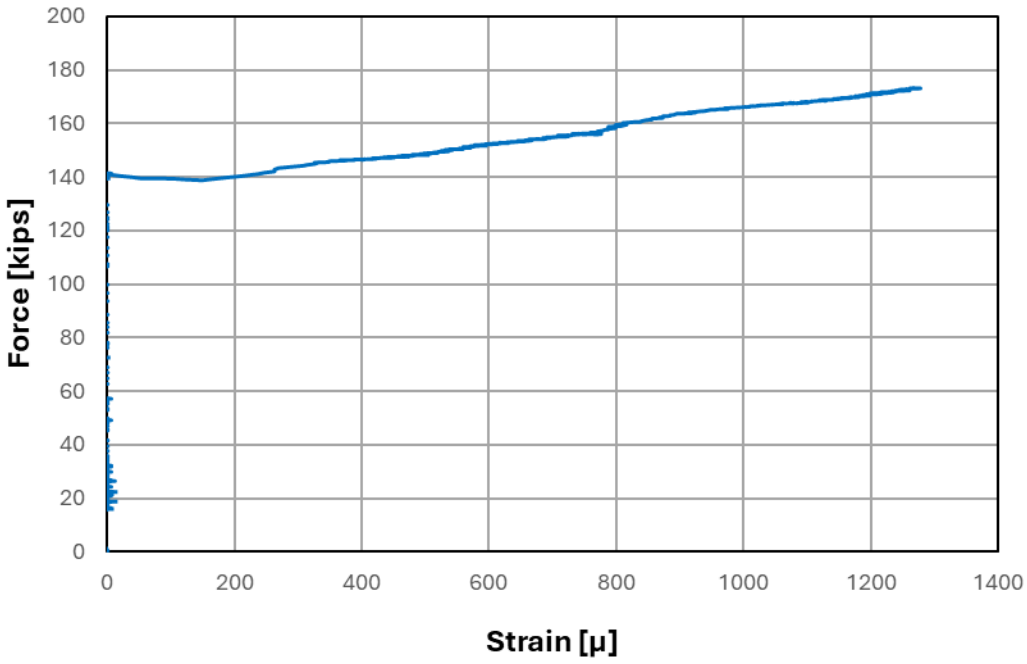

Figure D.39: Force plotted against SG06 strain for Specimen 3

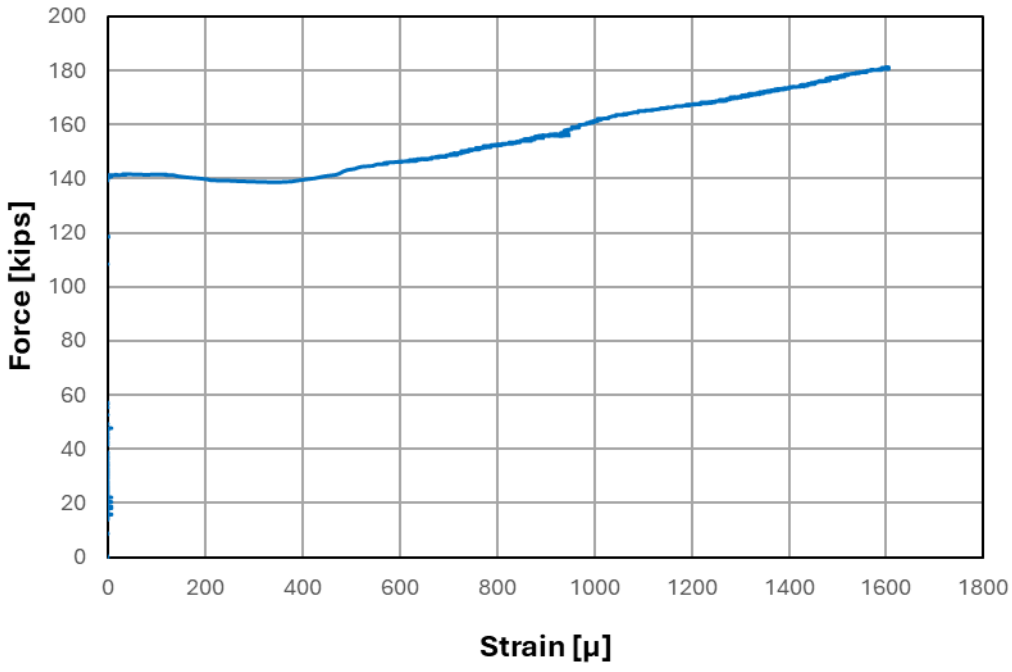

Figure D.40: Force plotted against SG07 strain for Specimen 3

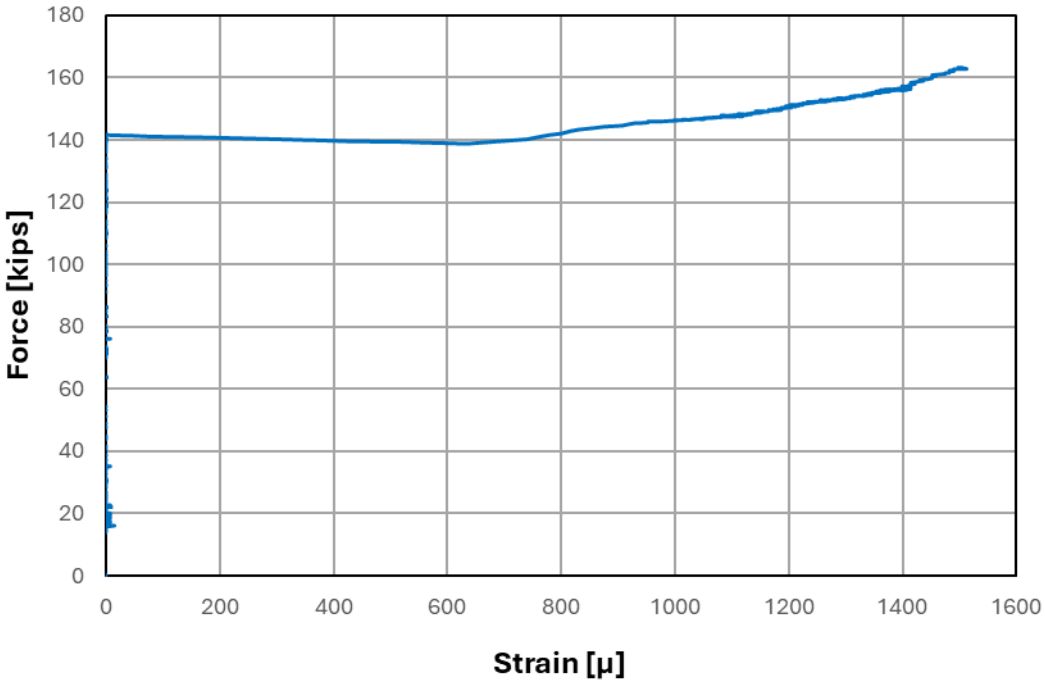

Figure D.41: Force plotted against SG09 strain for Specimen 3

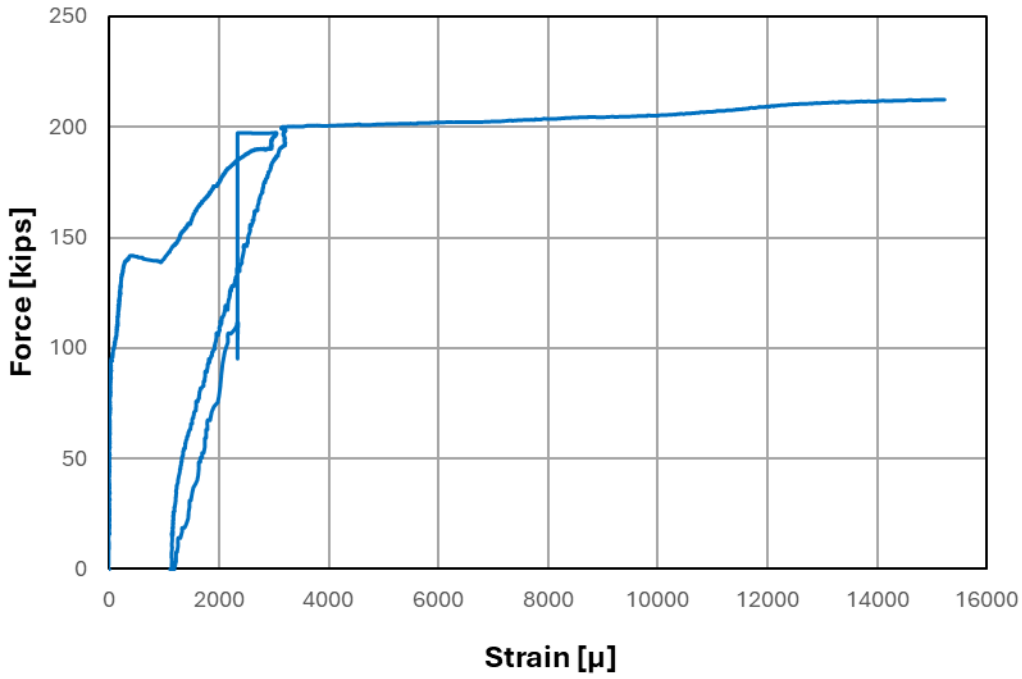

Figure D.42: Force plotted against SG10 strain for Specimen 3

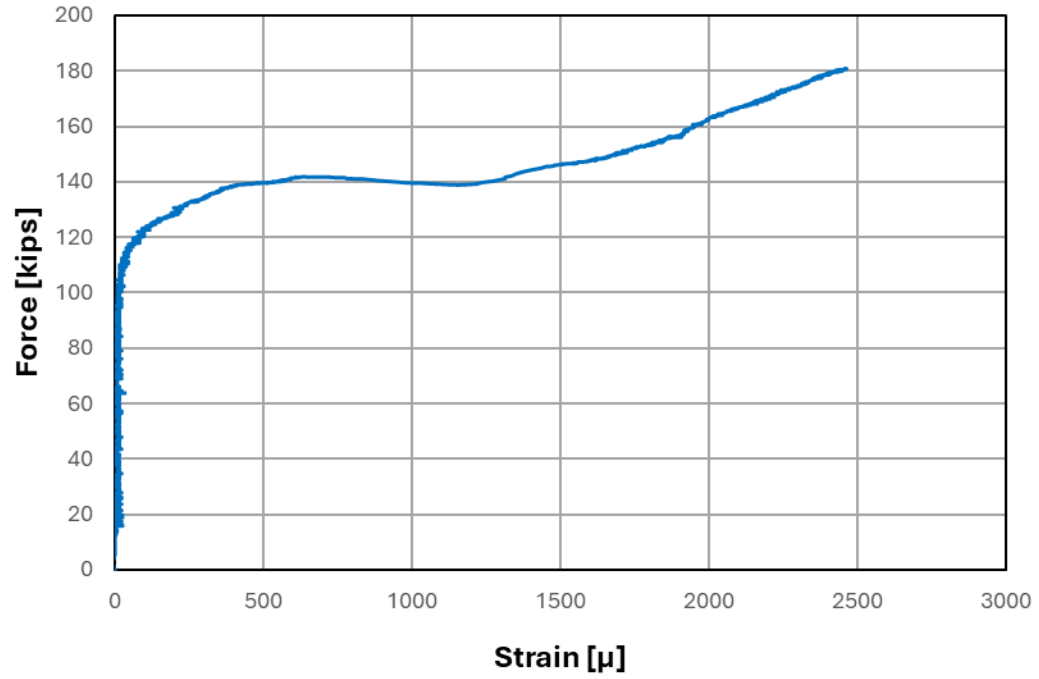

Figure D.43: Force plotted against SG11 strain for Specimen 3

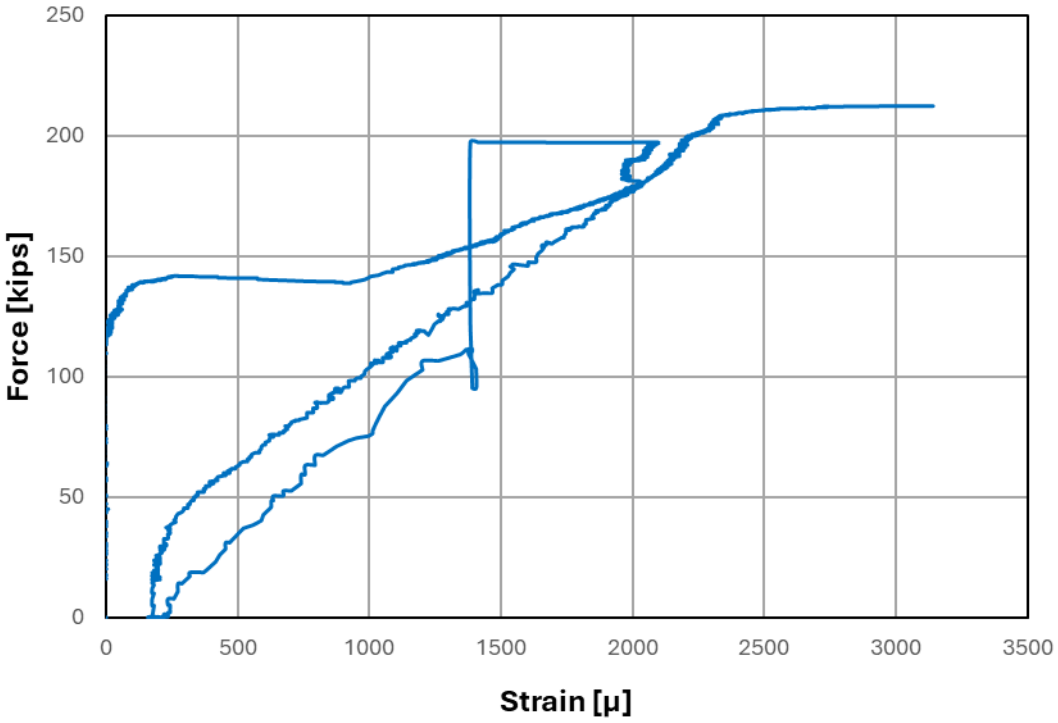

Figure D.44: Force plotted against SG12 strain for Specimen 3

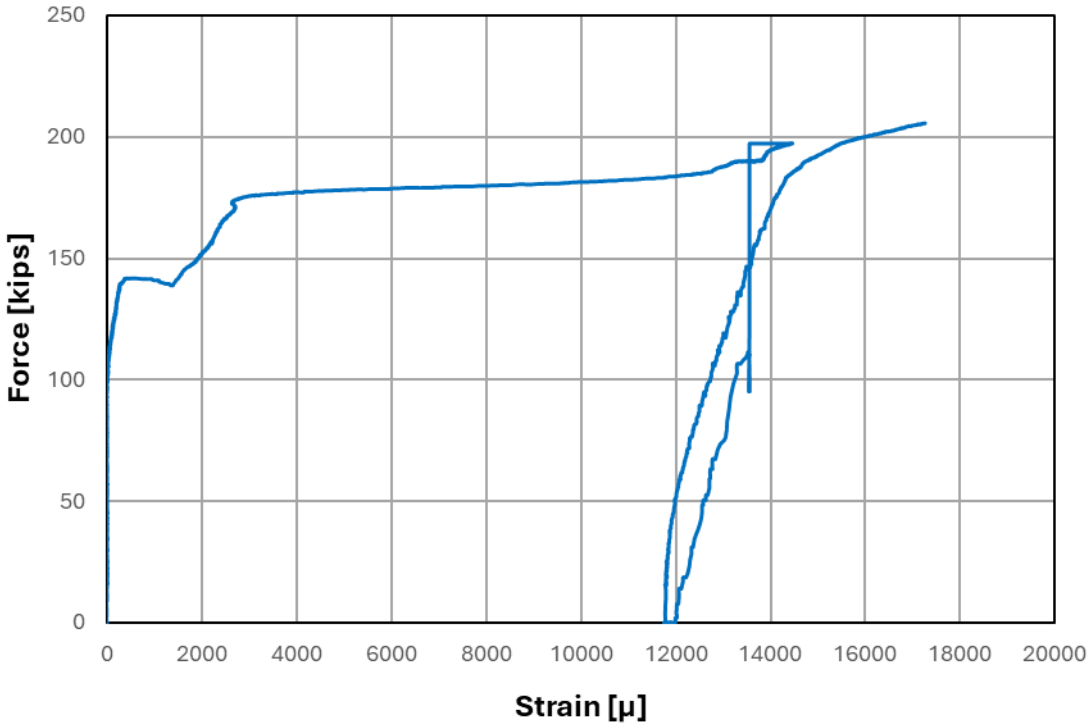

Figure D.45: Force plotted against SG13 strain for Specimen 3

D.4 Specimen 4

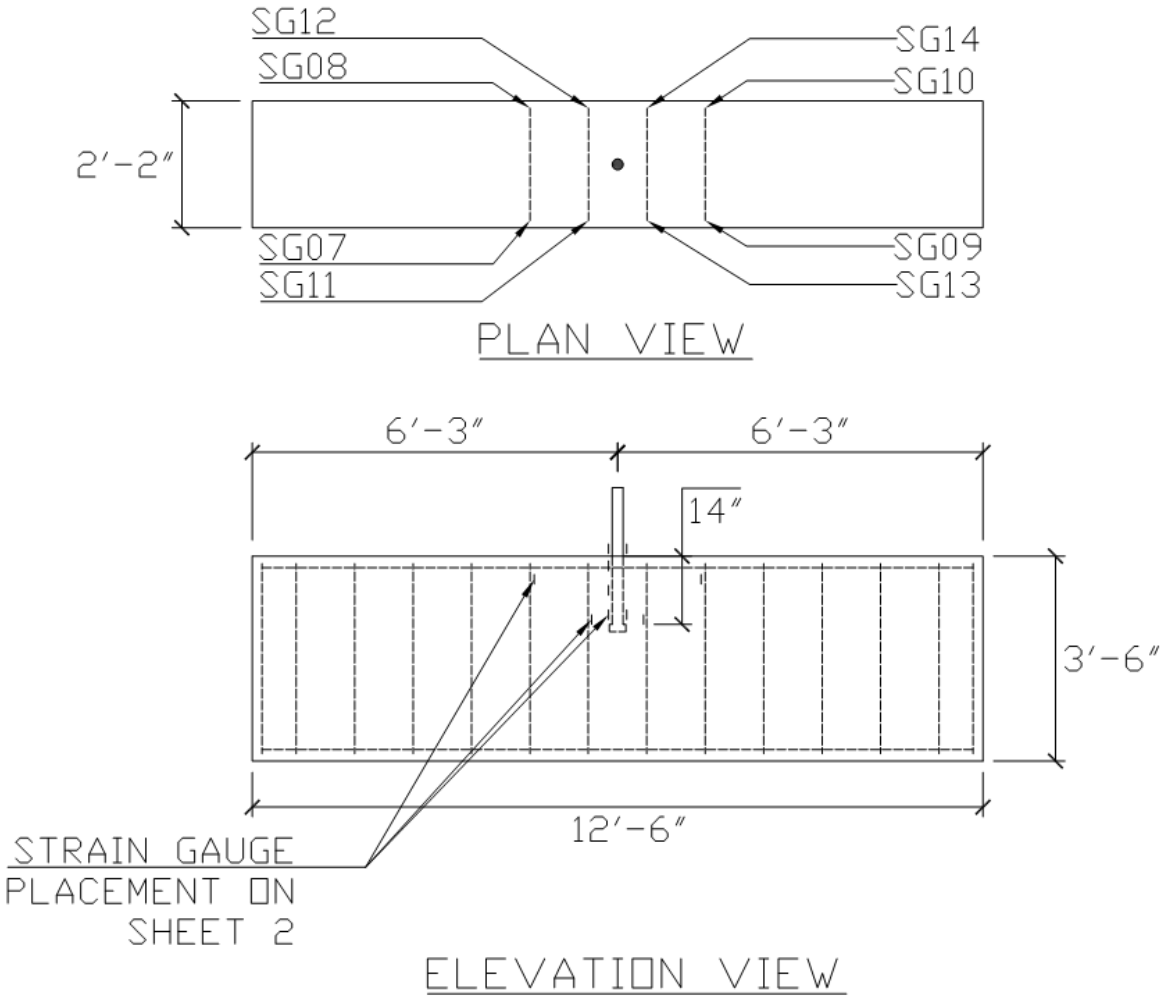

Figure D.46: Locations of strain gauges for Specimen 4

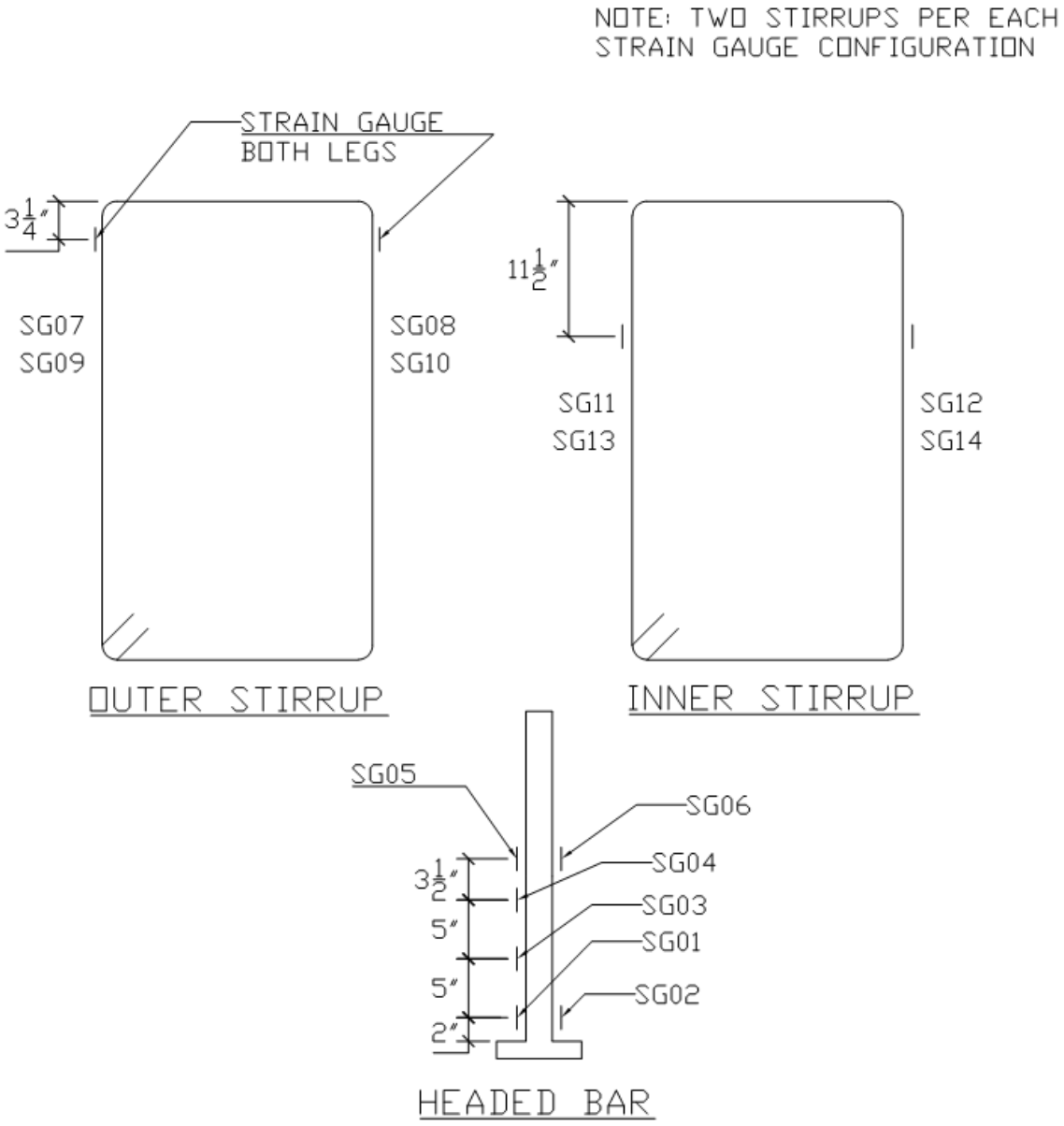

Figure D.47: Locations of stirrup and headed bar strain gauges and their labels for Specimen 4

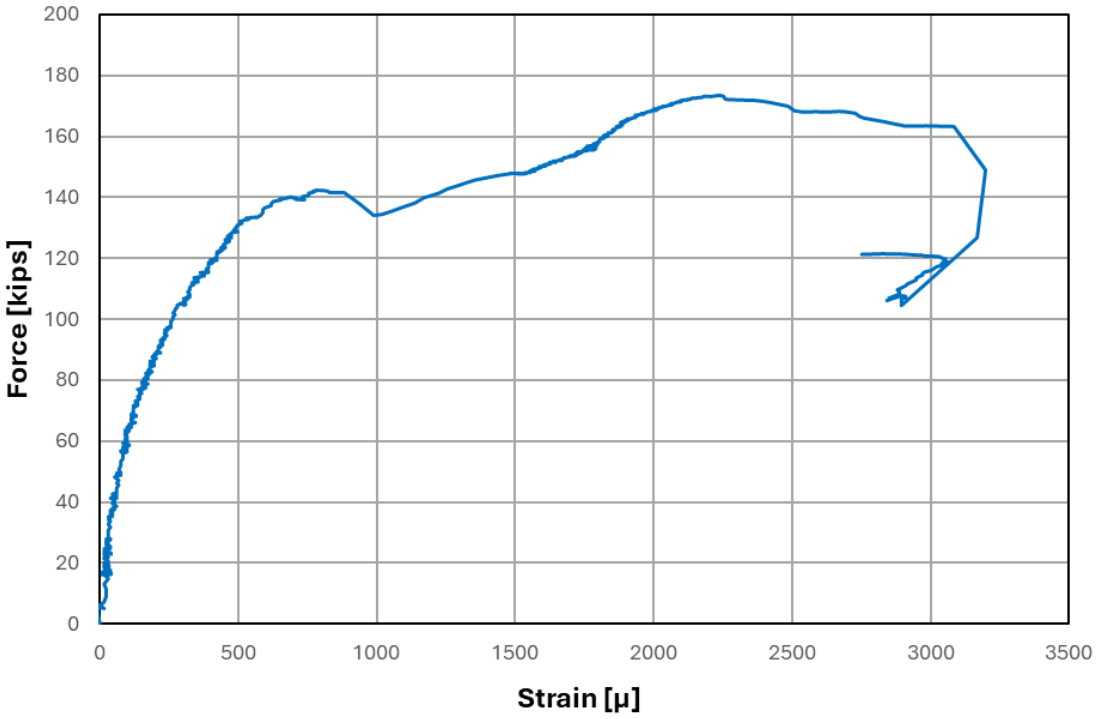

Figure D.48: Force plotted against SG01 strain for Specimen 4

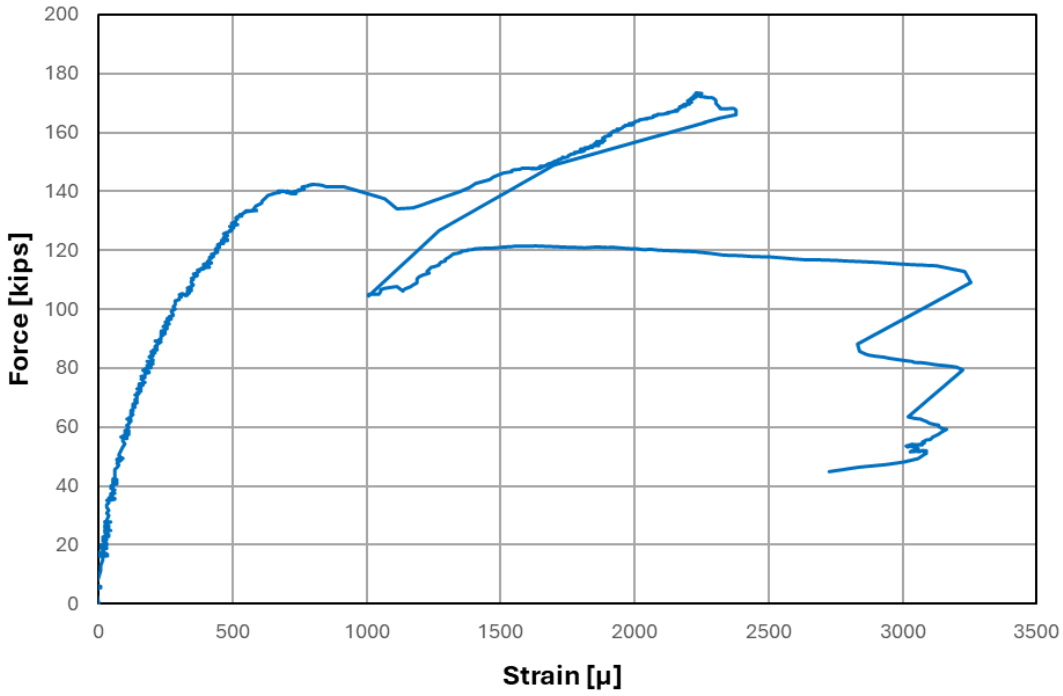

Figure D.49: Force plotted against SG02 strain for Specimen 4

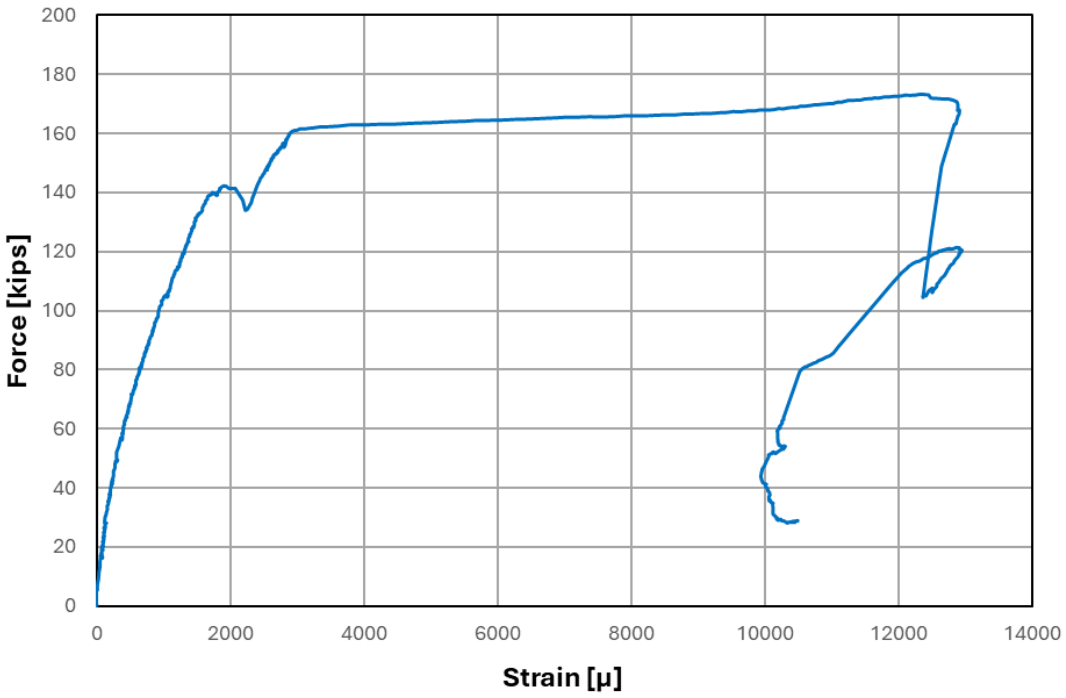

Figure D.50: Force plotted against SG03 strain for Specimen 4

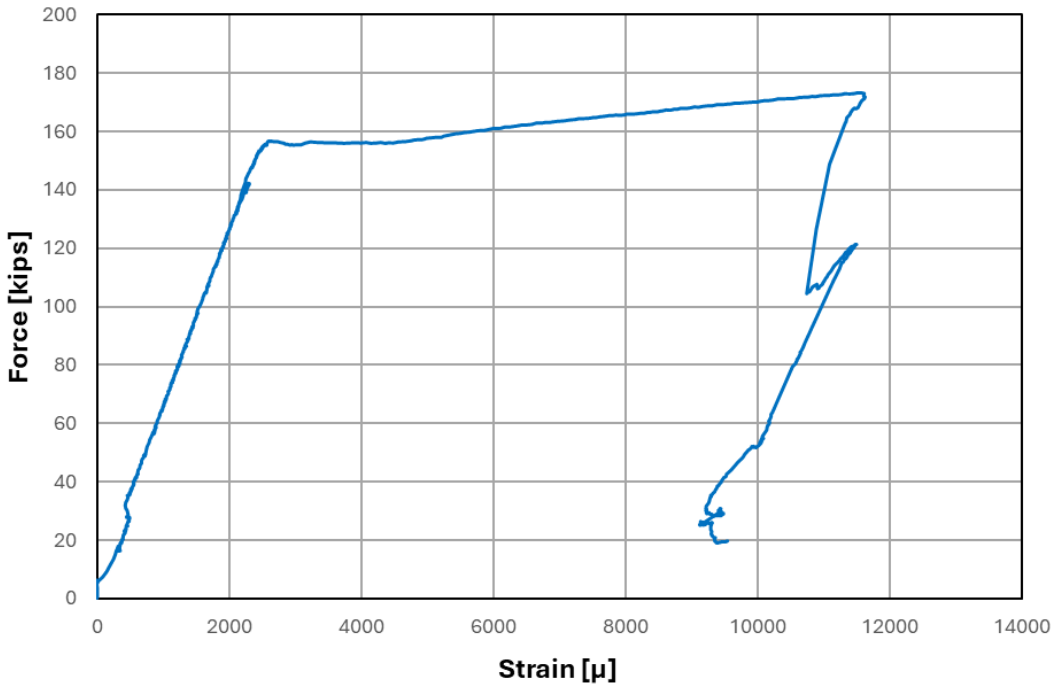

Figure D.51: Force plotted against SG04 strain for Specimen 4

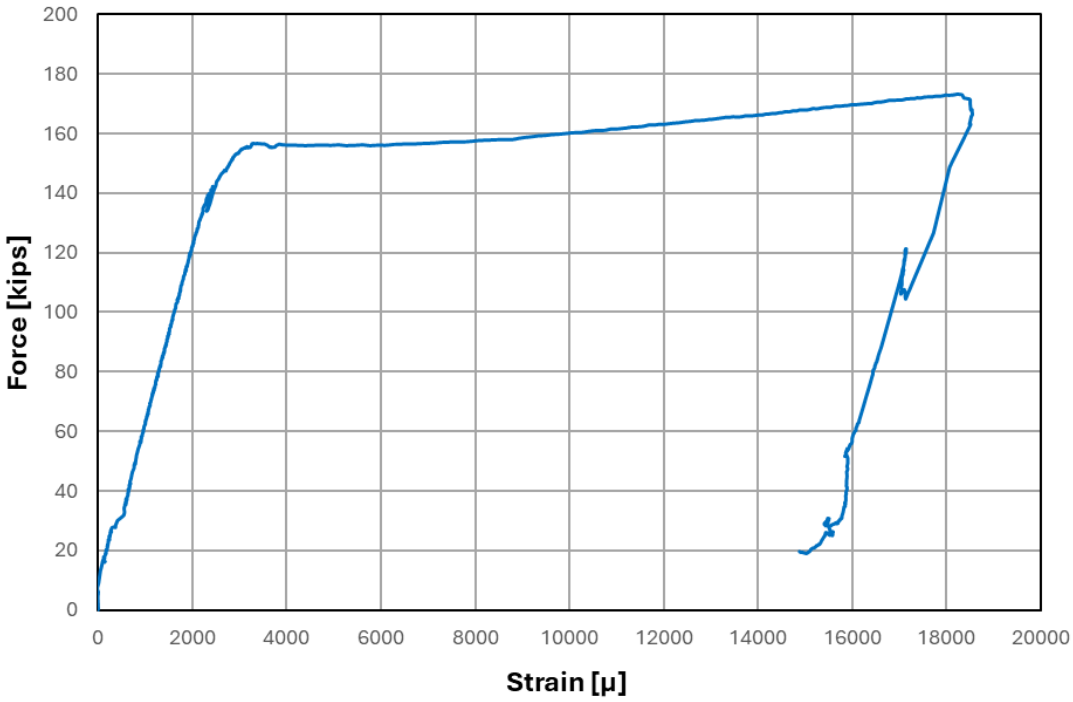

Figure D.52: Force plotted against SG05 strain for Specimen 4

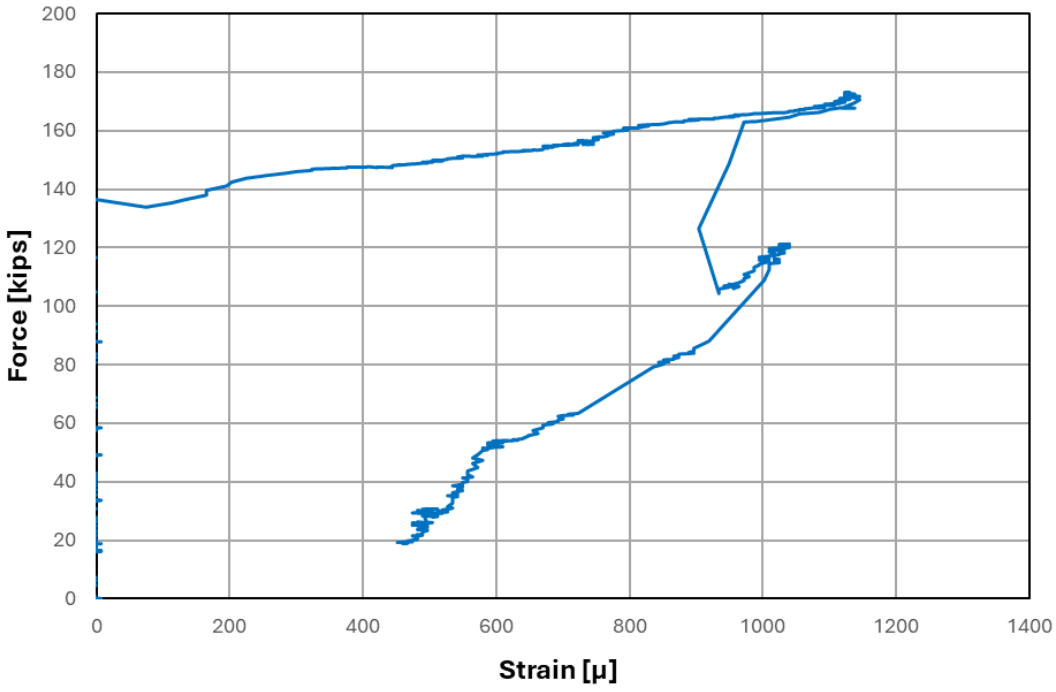

Figure D.53: Force plotted against SG07 strain for Specimen 4

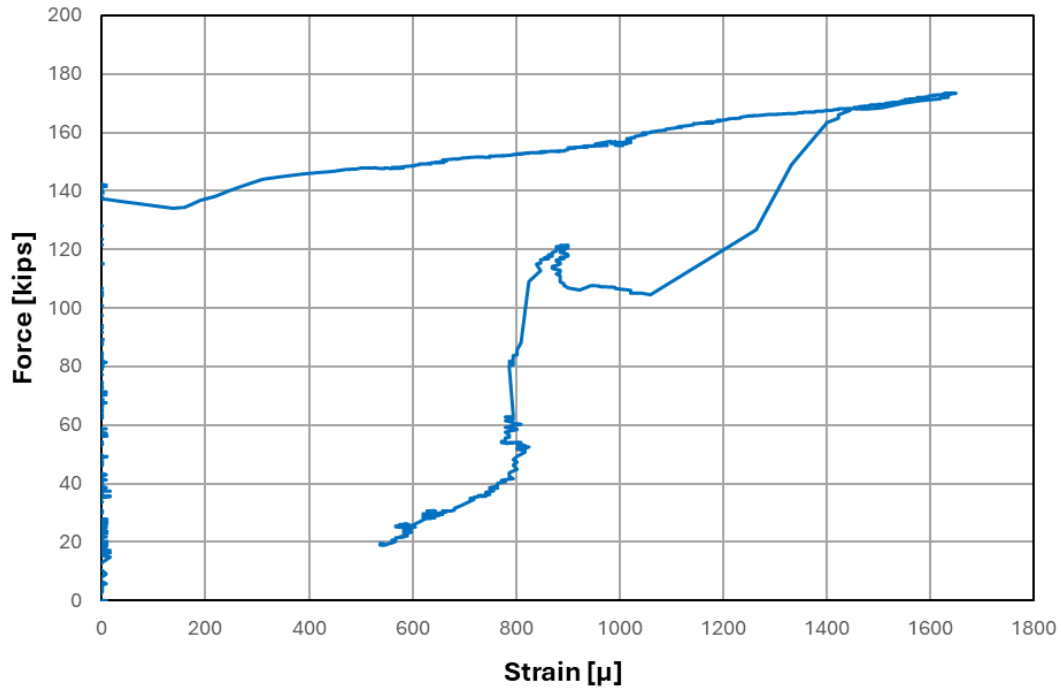

Figure D.54: Force plotted against SG08 strain for Specimen 4

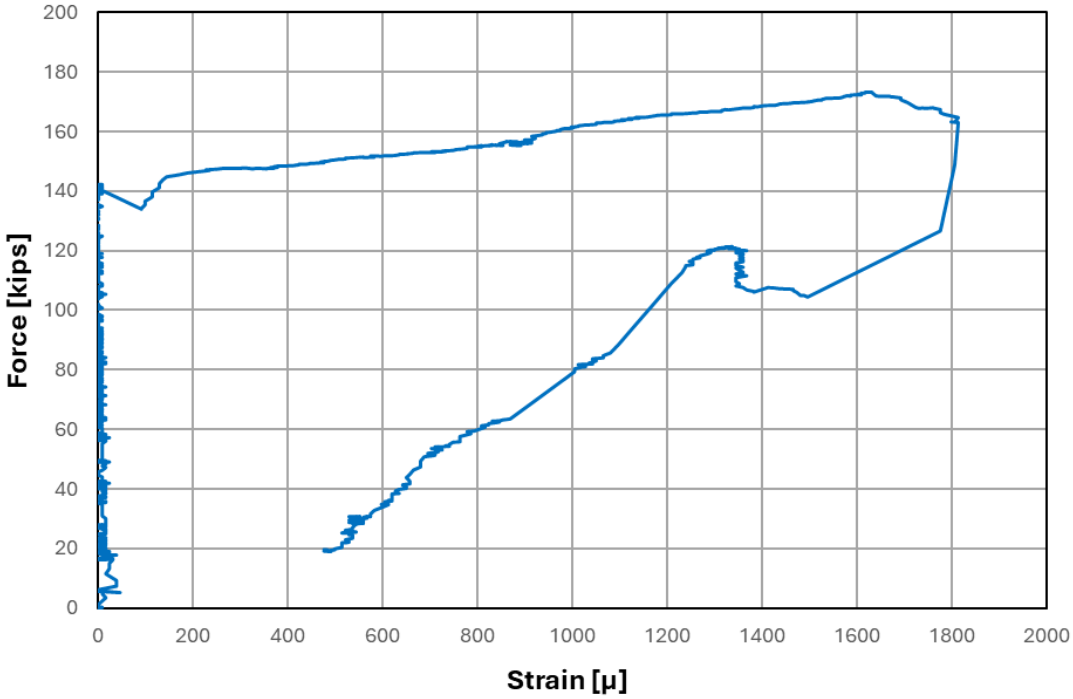

Figure D.55: Force plotted against SG09 strain for Specimen 4

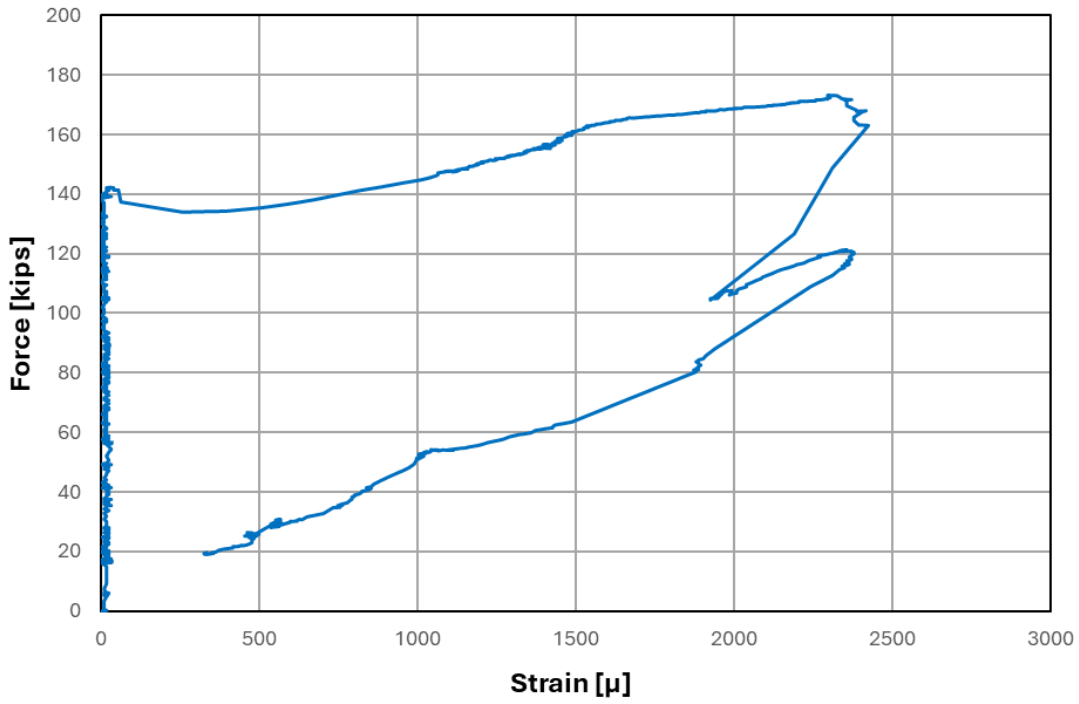

Figure D.56: Force plotted against SG10 strain for Specimen 4

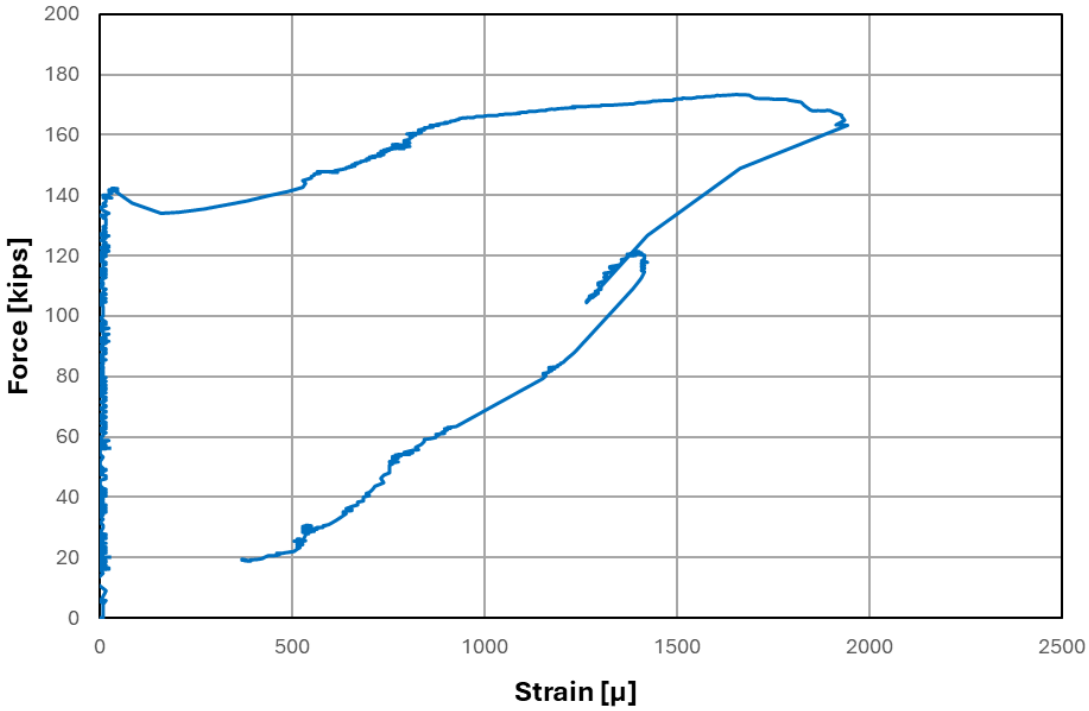

Figure D.57: Force plotted against SG11 strain for Specimen 4

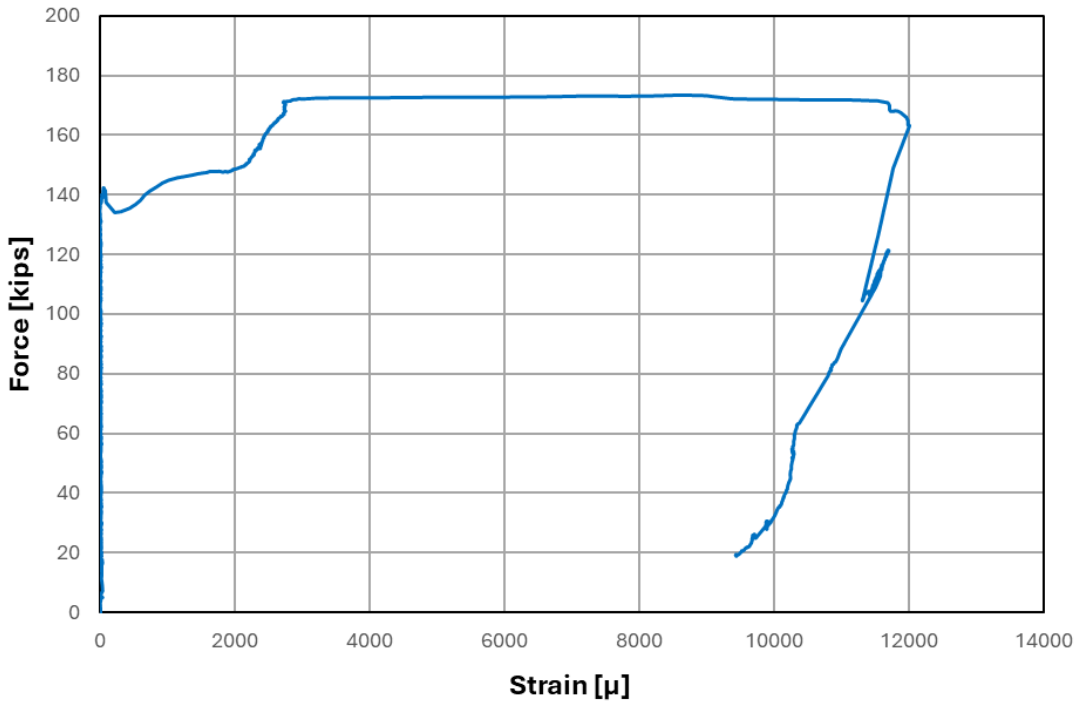

Figure D.58: Force plotted against SG12 strain for Specimen 4

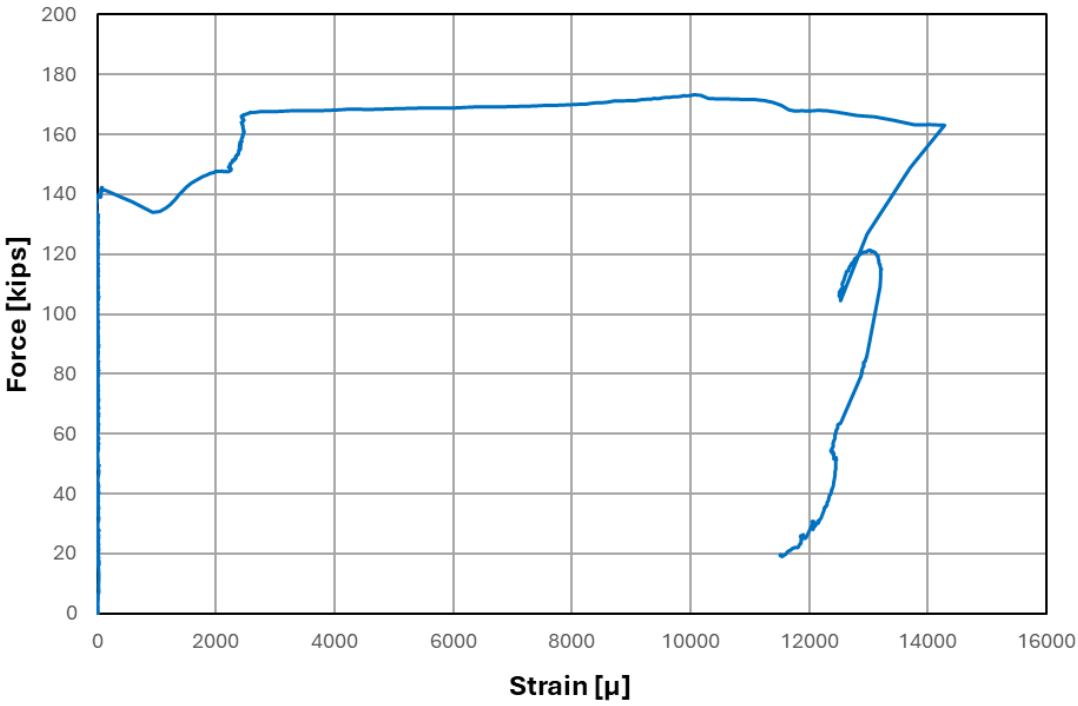

Figure D.59: Force plotted against SG13 strain for Specimen 4

D.5 Specimen 5

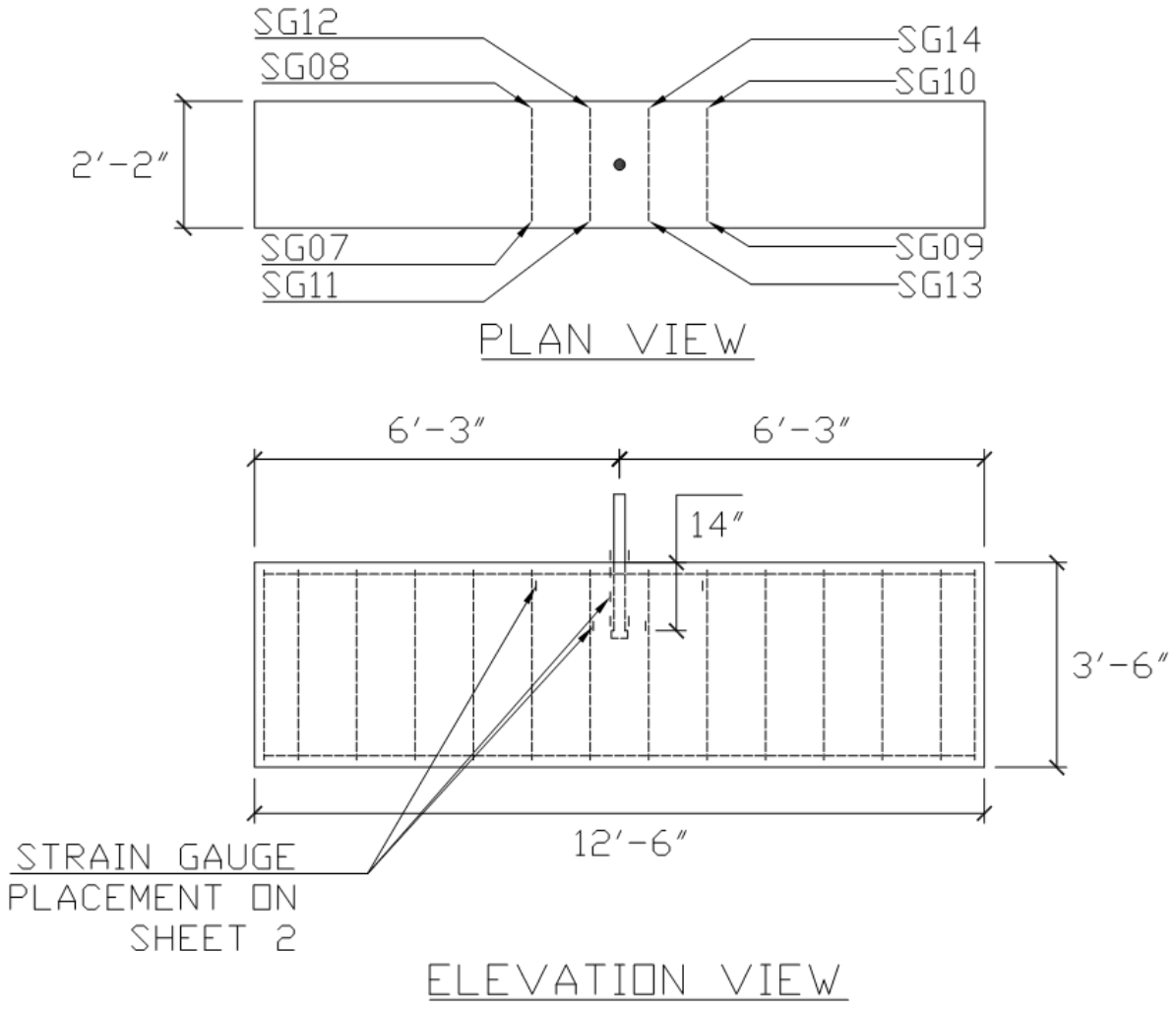

Figure D.60: Locations of strain gauges for Specimen 5

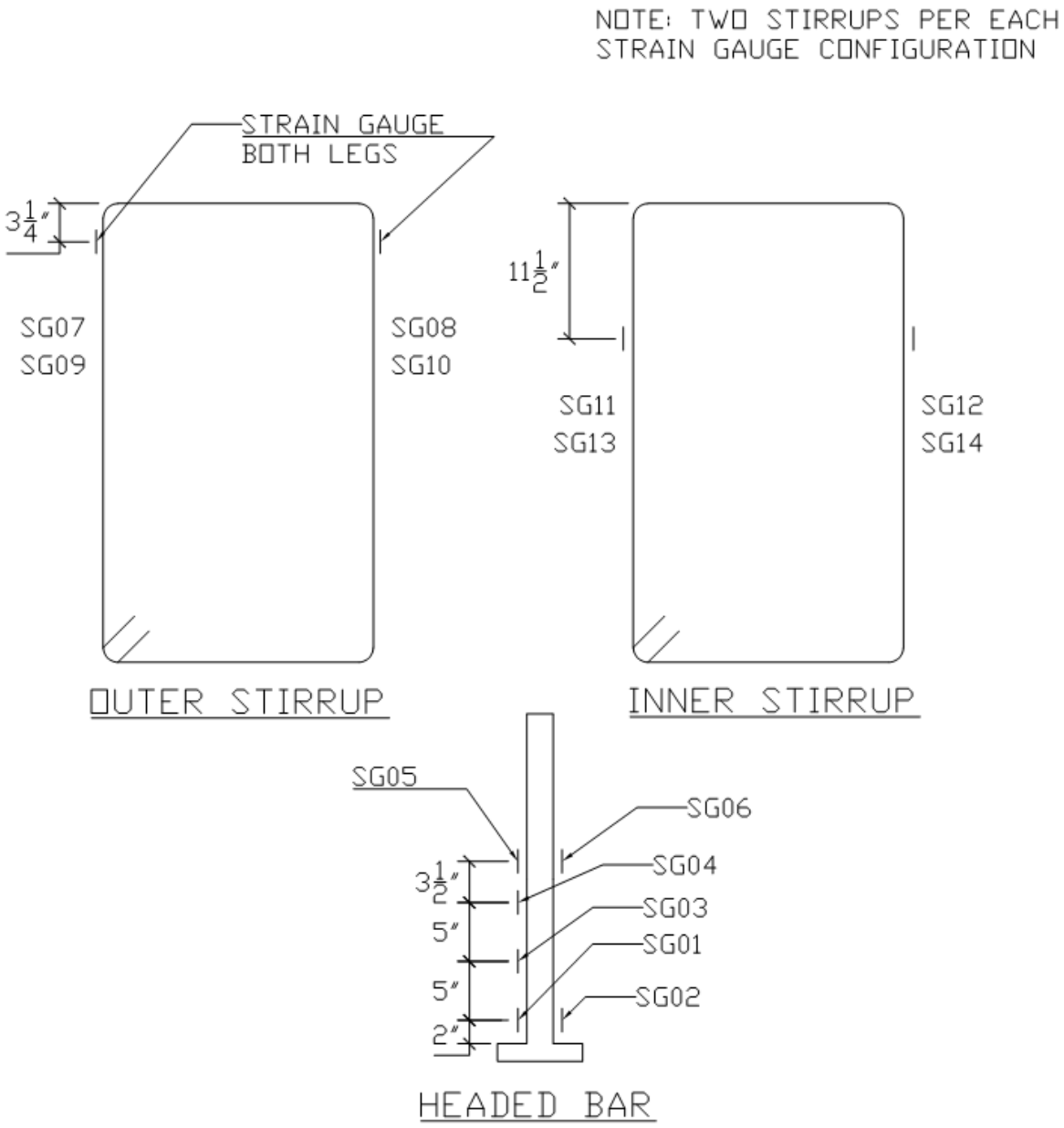

Figure D.61: Locations of stirrup and headed bar strain gauges and their labels for Specimen 5

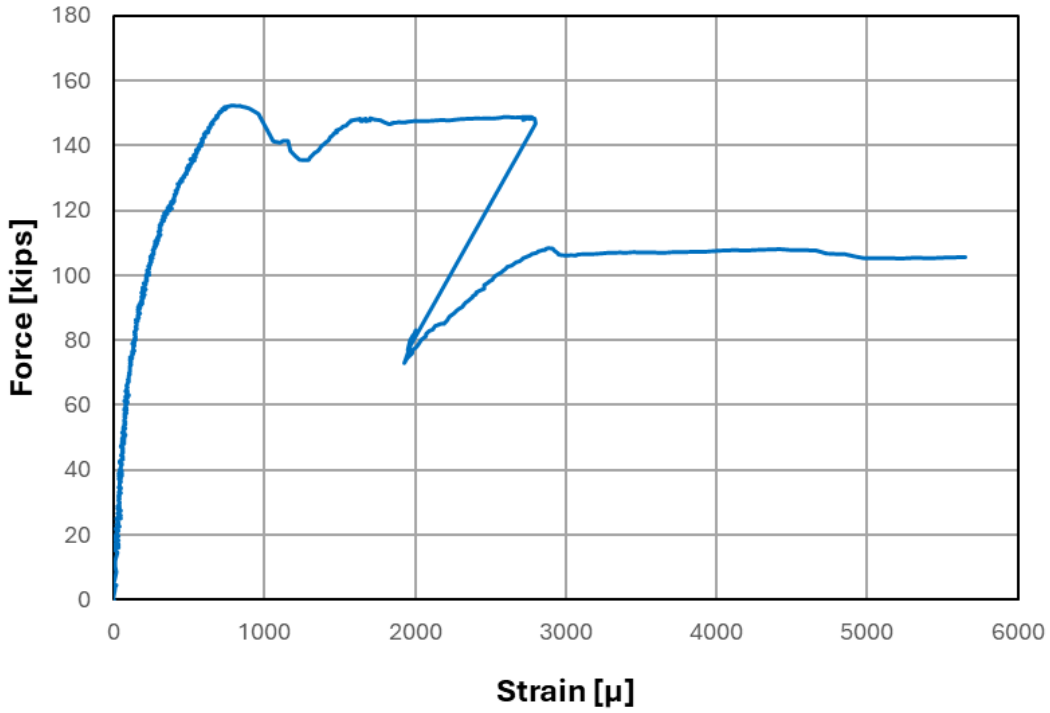

Figure D.62: Force plotted against SG01 strain for Specimen 5

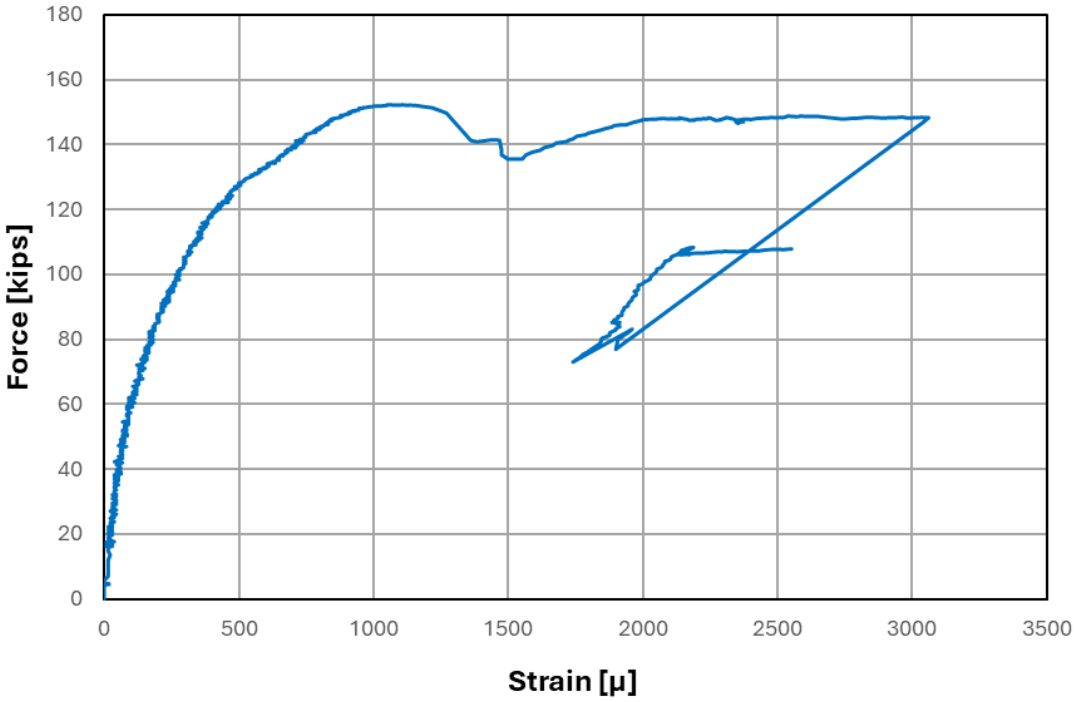

Figure D.63: Force plotted against SG02 strain for Specimen 5

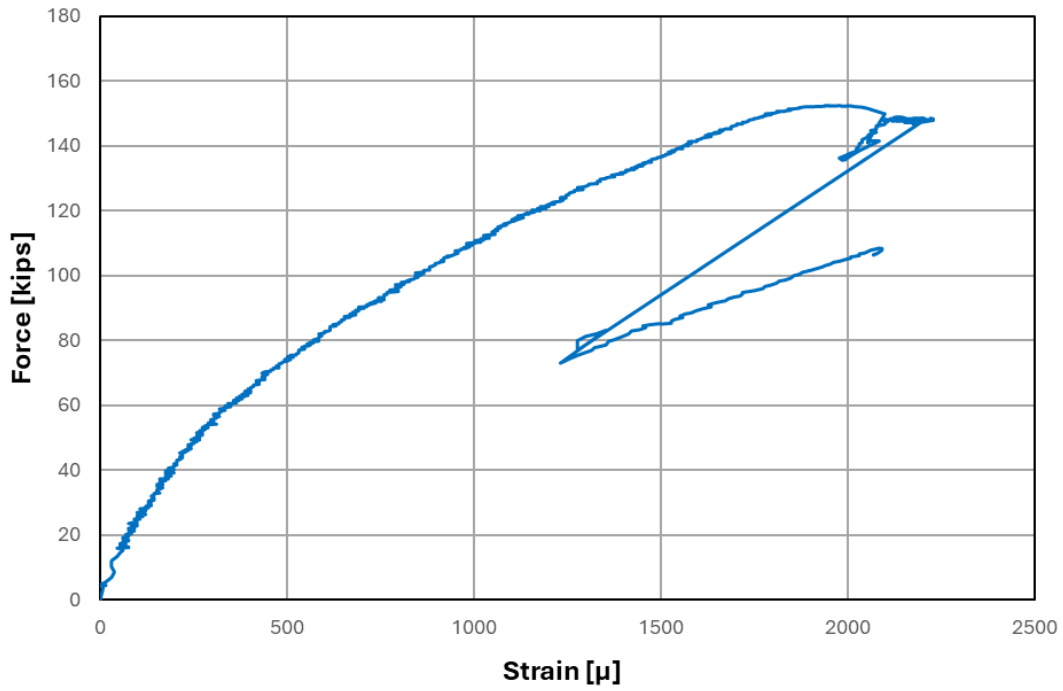

Figure D.64: Force plotted against SG03 strain for Specimen 5

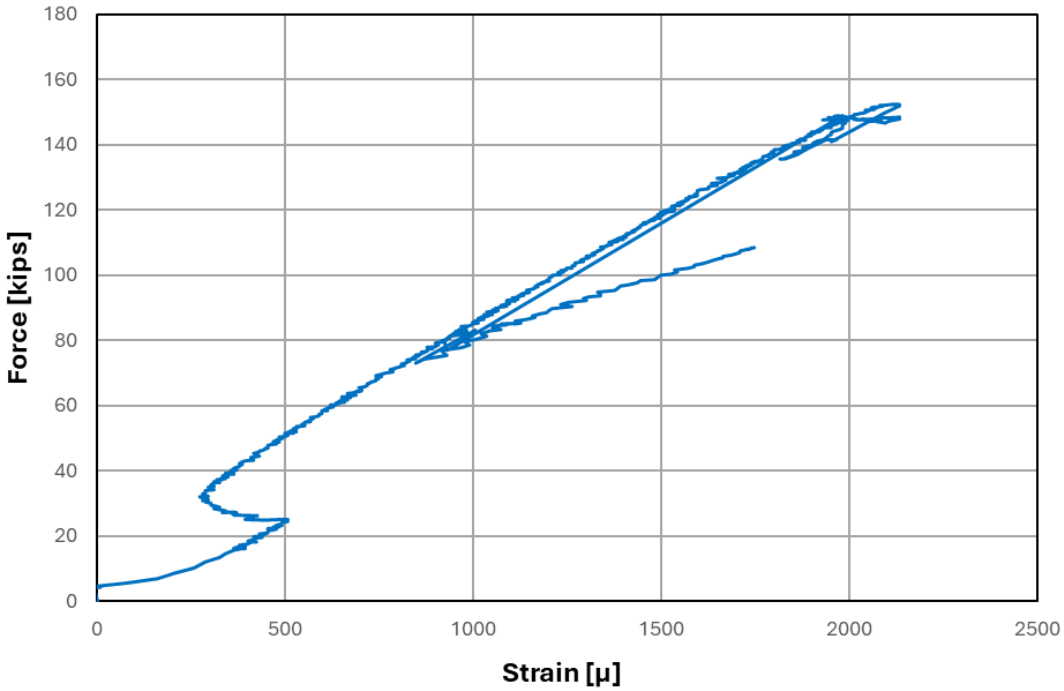

Figure D.65: Force plotted against SG04 strain for Specimen 5

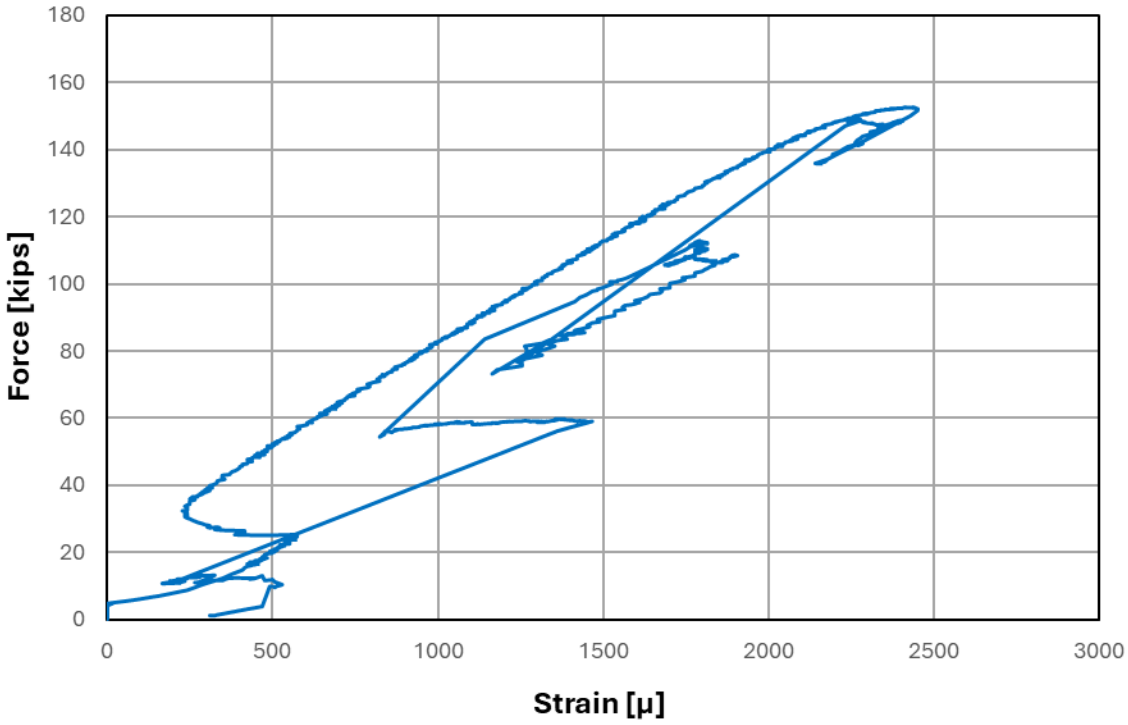

Figure D.66: Force plotted against SG05 strain for Specimen 5

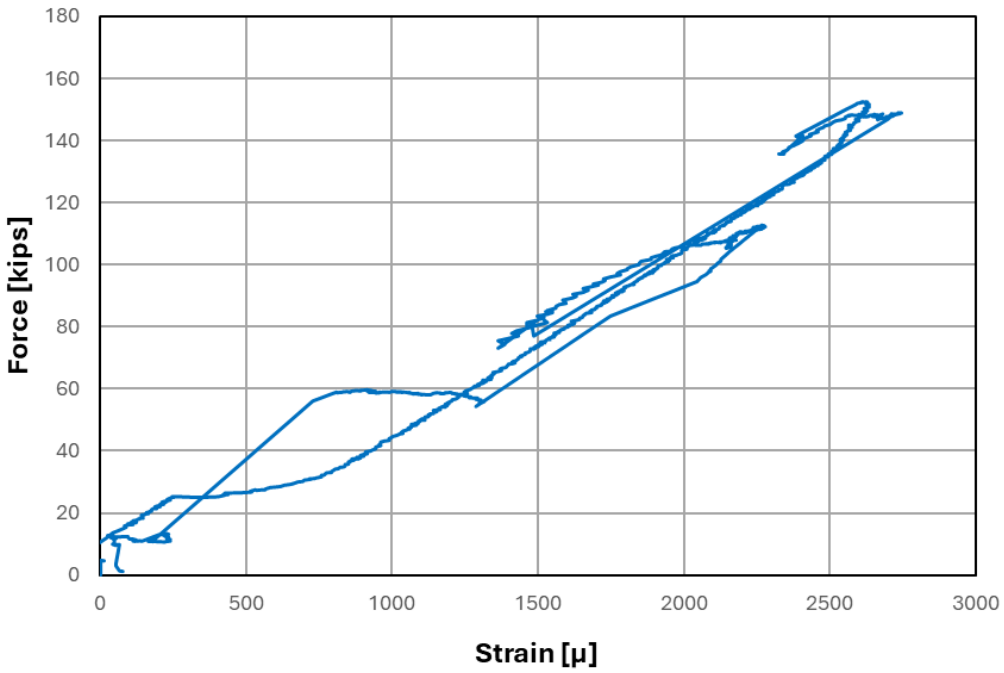

Figure D.67: Force plotted against SG06 strain for Specimen 5

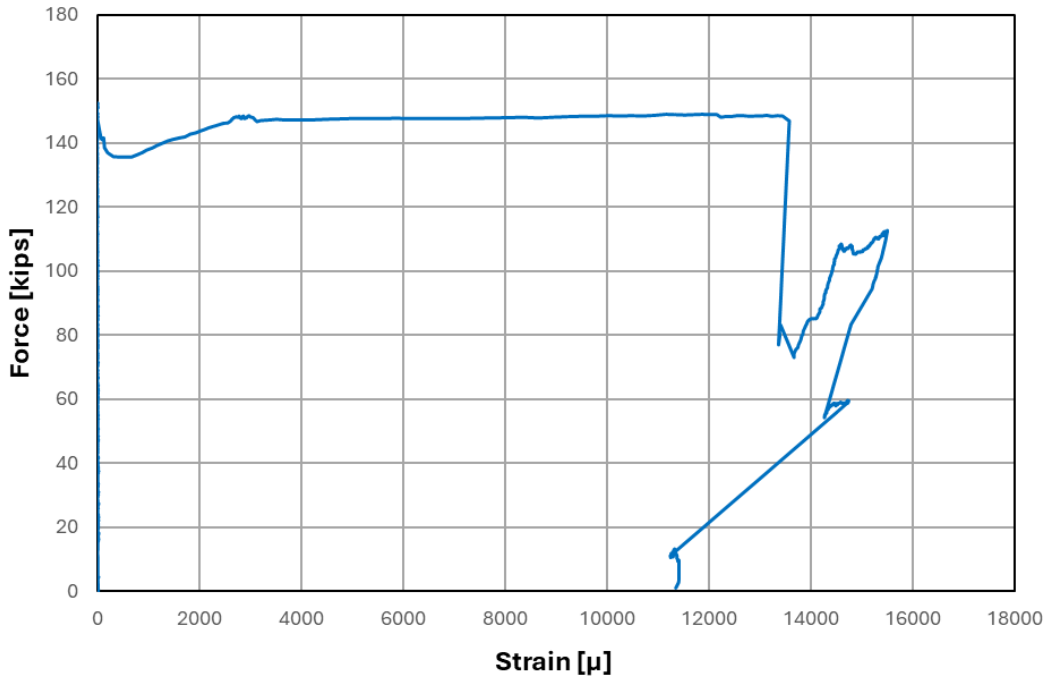

Figure D.68: Force plotted against SG07 strain for Specimen 5

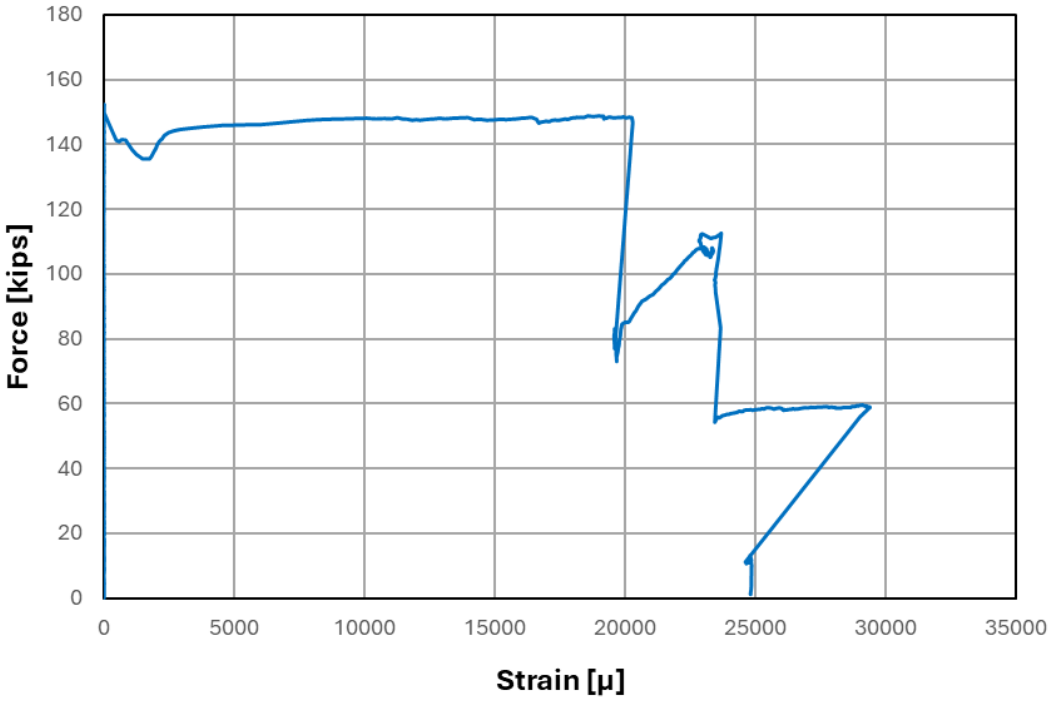

Figure D.69: Force plotted against SG08 strain for Specimen 5

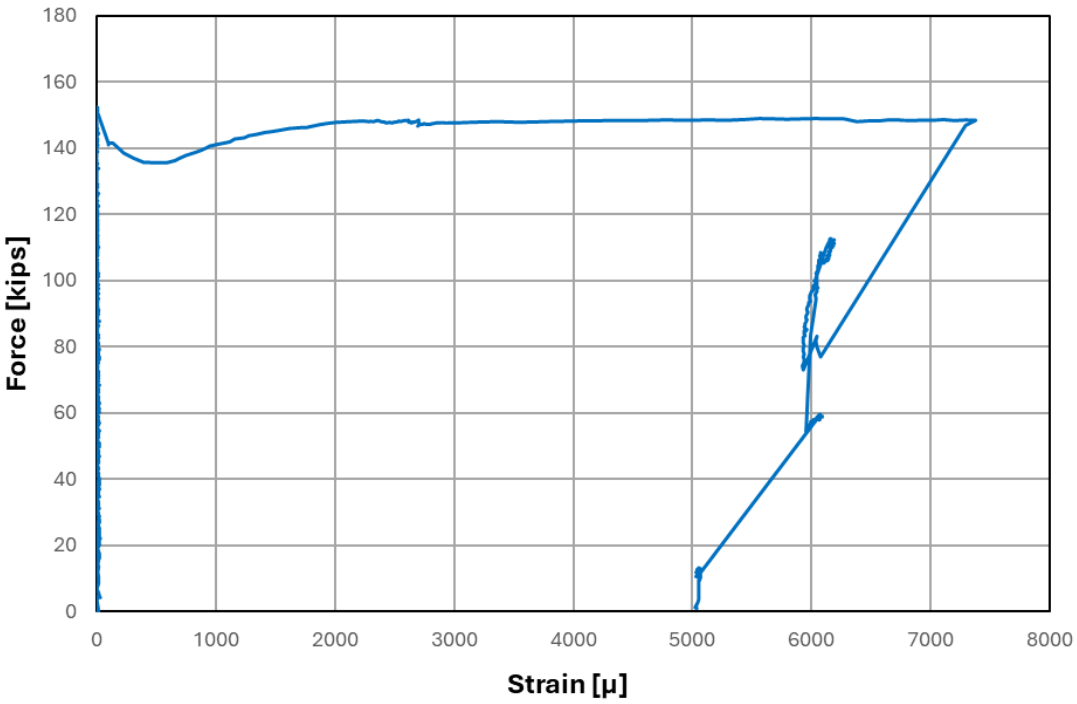

Figure D.70: Force plotted against SG09 strain for Specimen 5

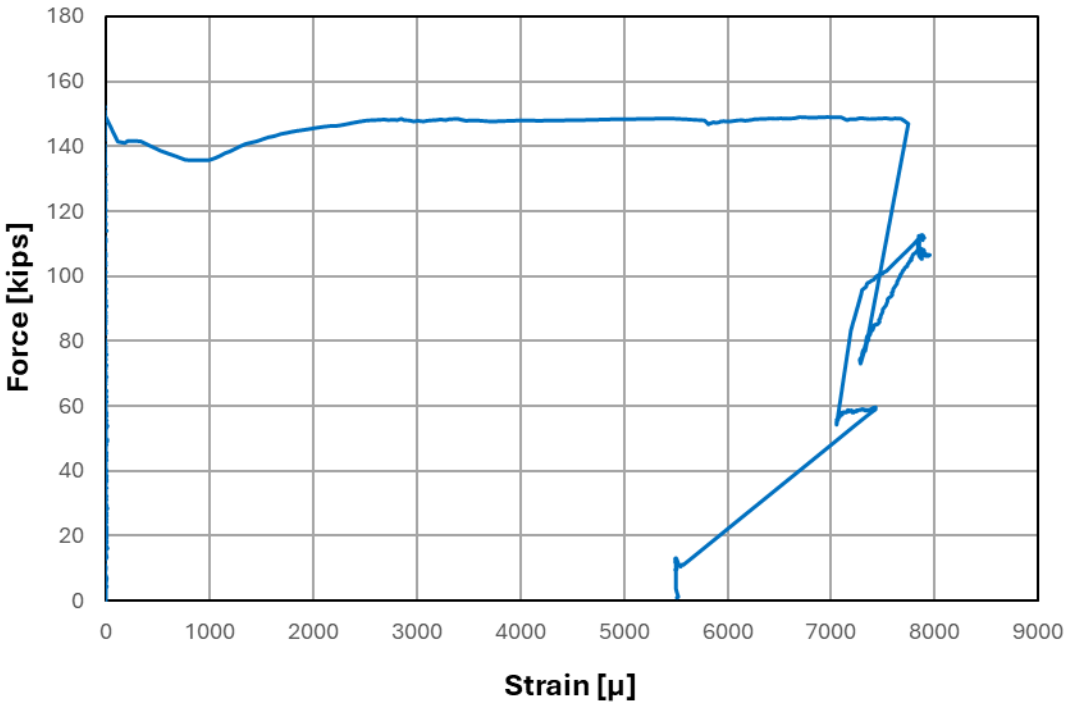

Figure D.71: Force plotted against SG10 strain for Specimen 5

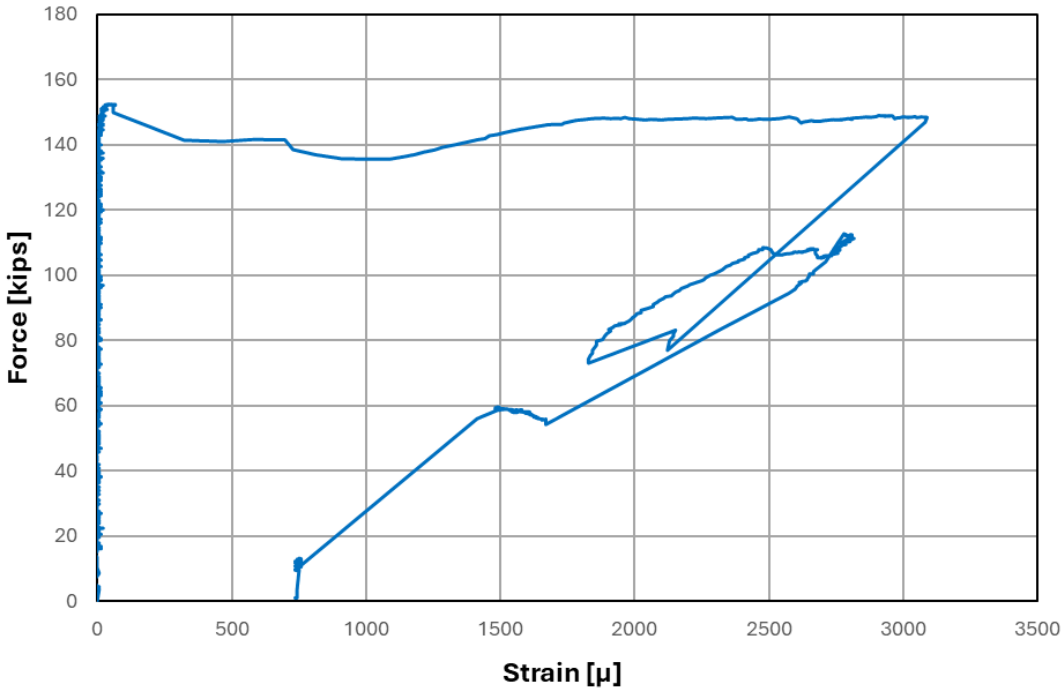

Figure D.72: Force plotted against SG11 strain for Specimen 5

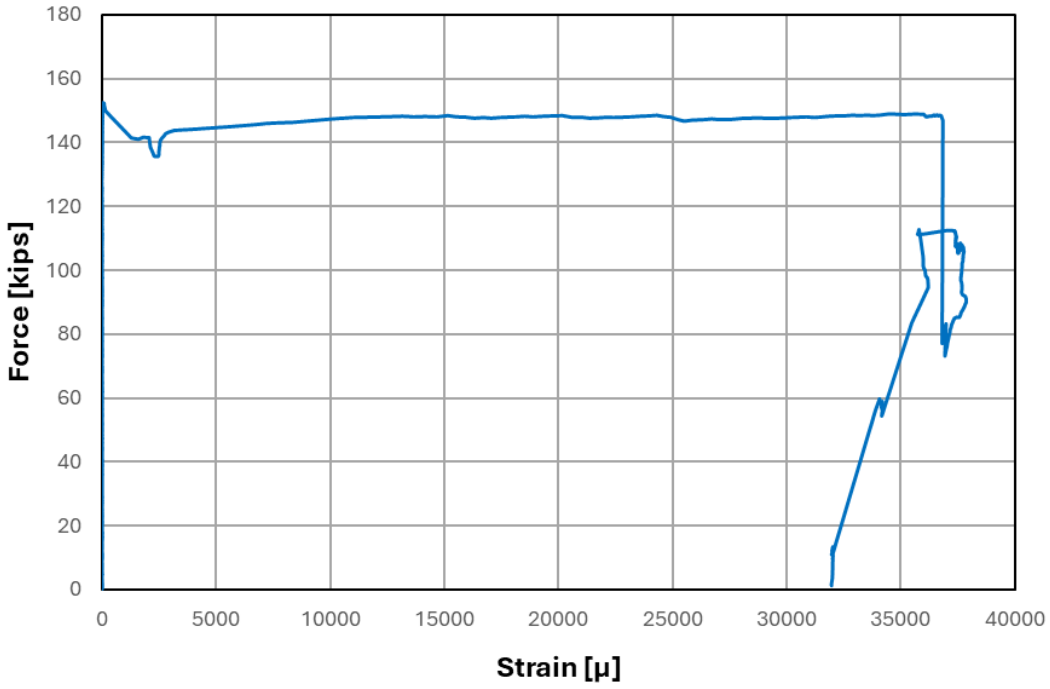

Figure D.73: Force plotted against SG12 strain for Specimen 5

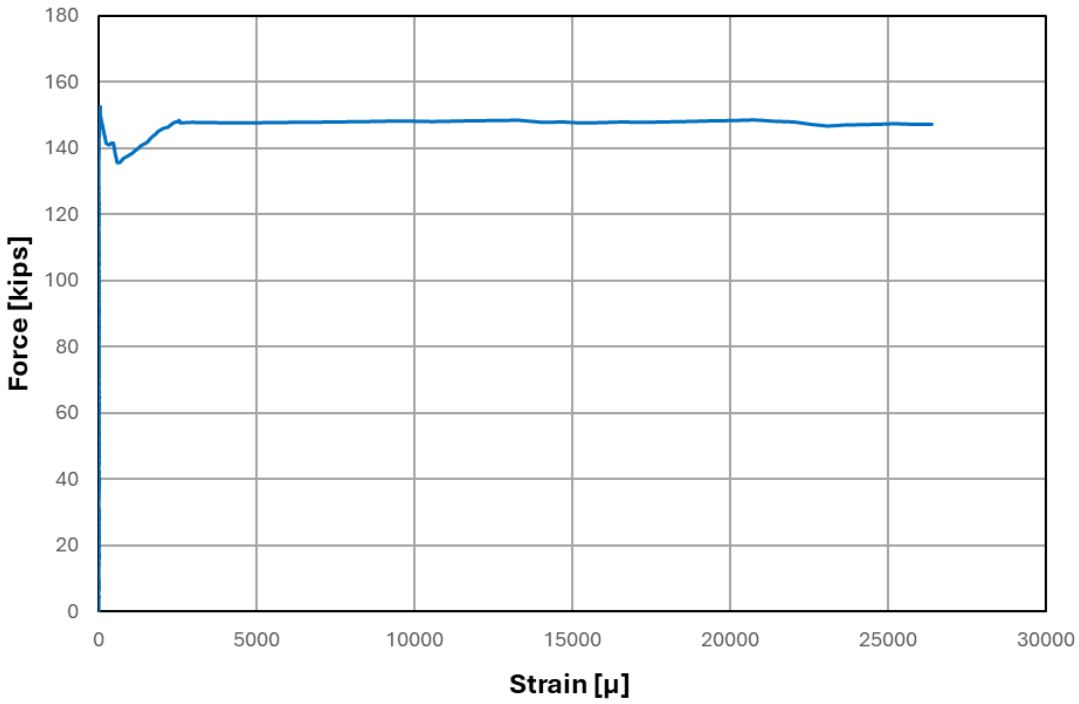

Figure D.74: Force plotted against SG13 strain for Specimen 5

D.6 Specimen 6

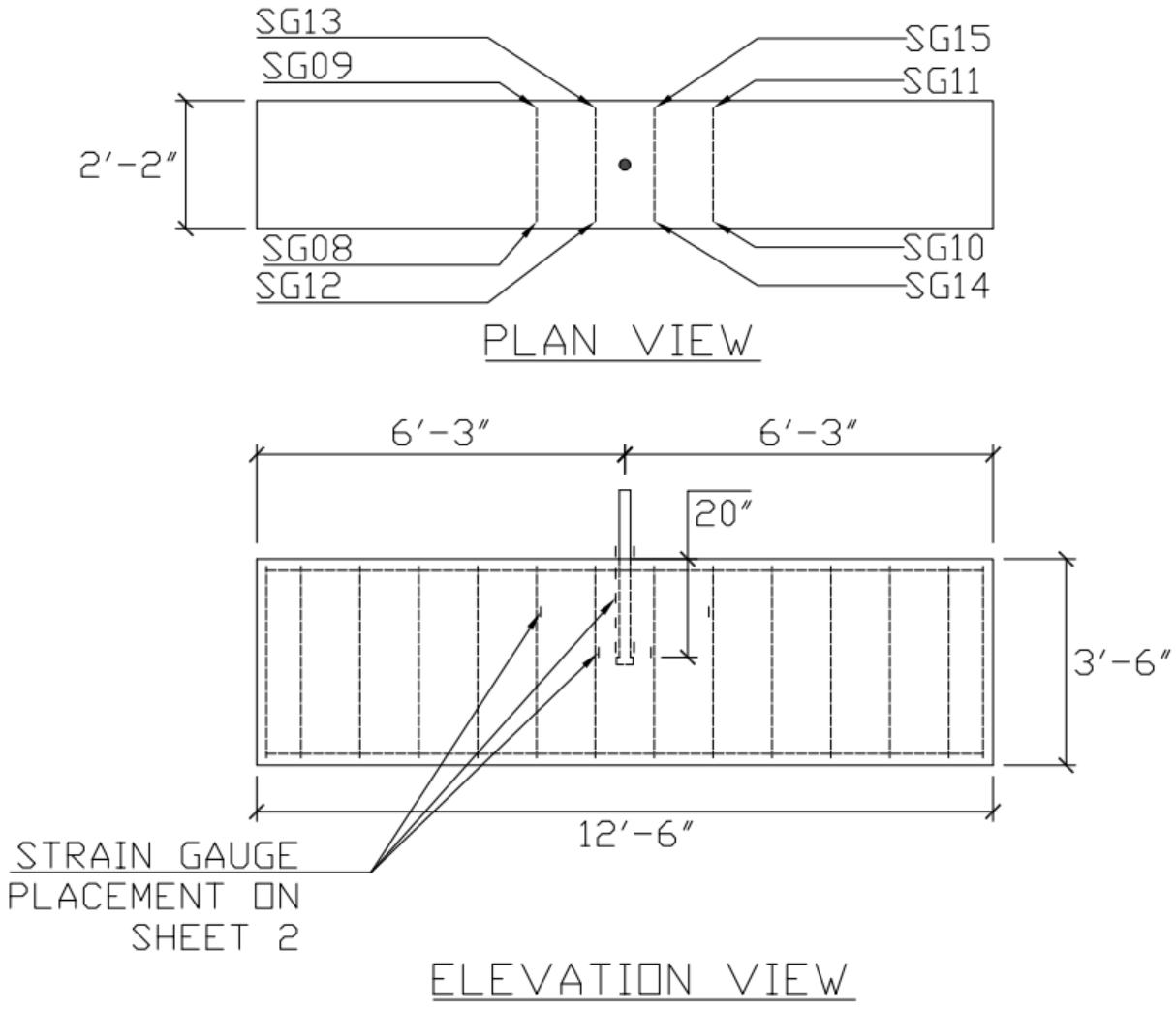

Figure D.75: Locations of strain gauges for Specimen 6

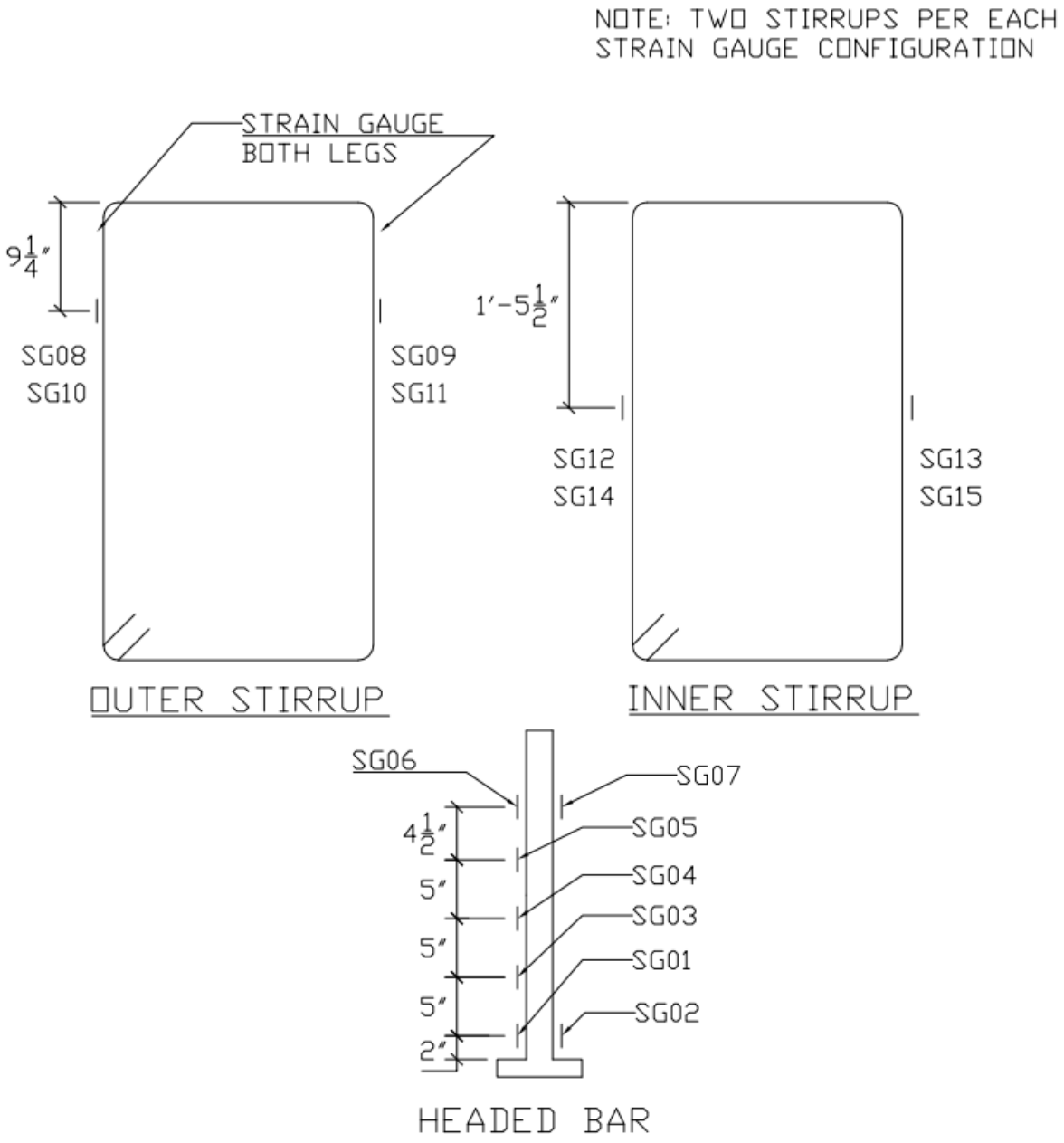

Figure D.76: Locations of stirrup and headed bar strain gauges and their labels for Specimen 6

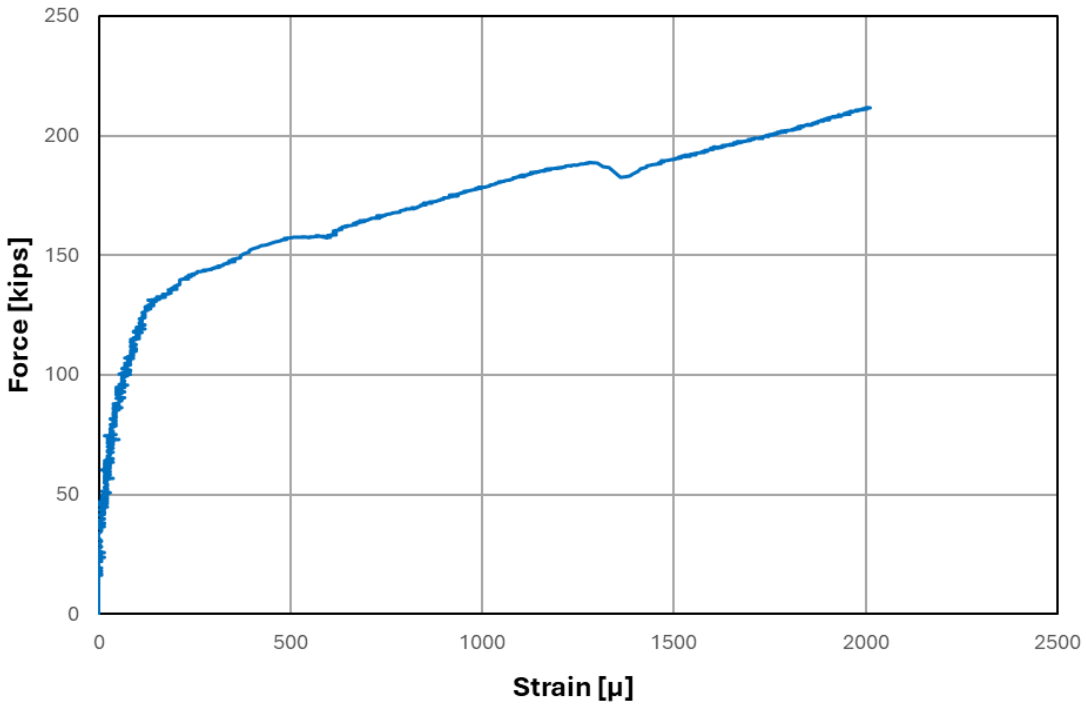

Figure D.77: Force plotted against SG01 strain for Specimen 6

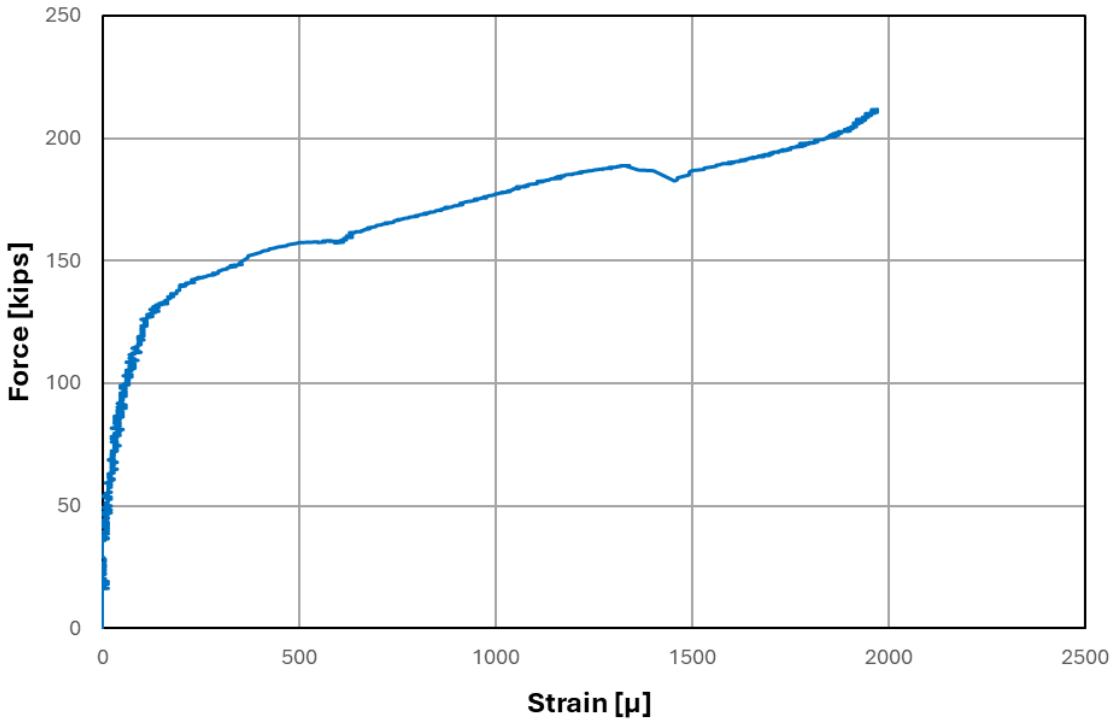

Figure D.78: Force plotted against SG02 strain for Specimen 6

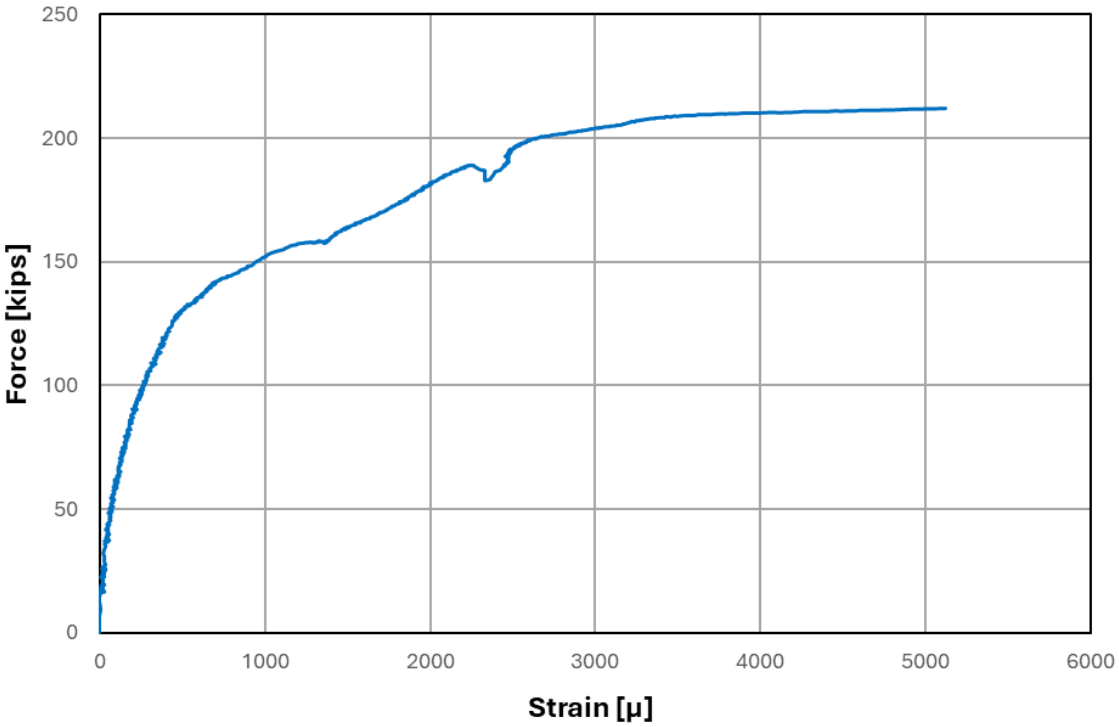

Figure D.79: Force plotted against SG03 strain for Specimen 6

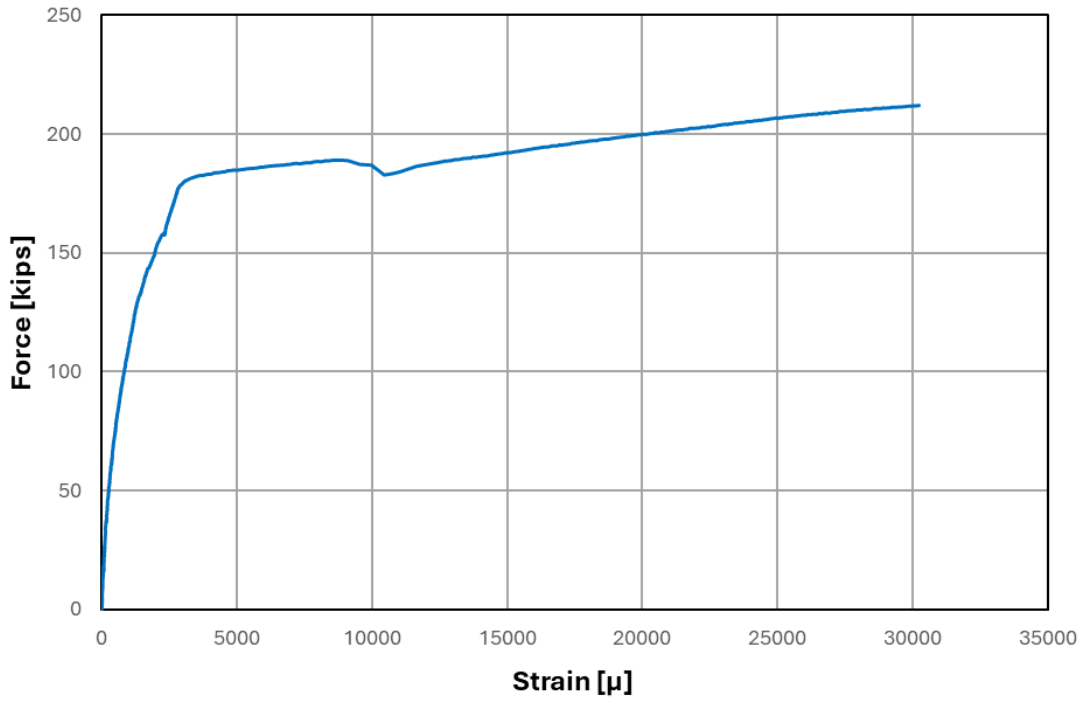

Figure D.80: Force plotted against SG04 strain for Specimen 6

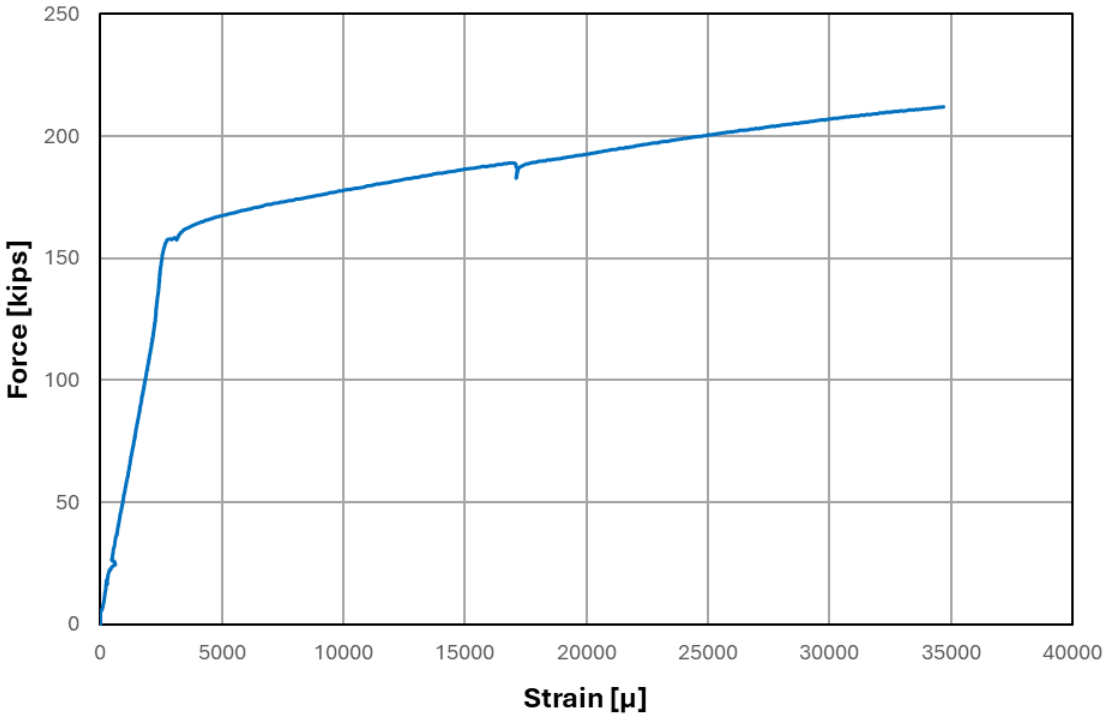

Figure D.81: Force plotted against SG05 strain for Specimen 6

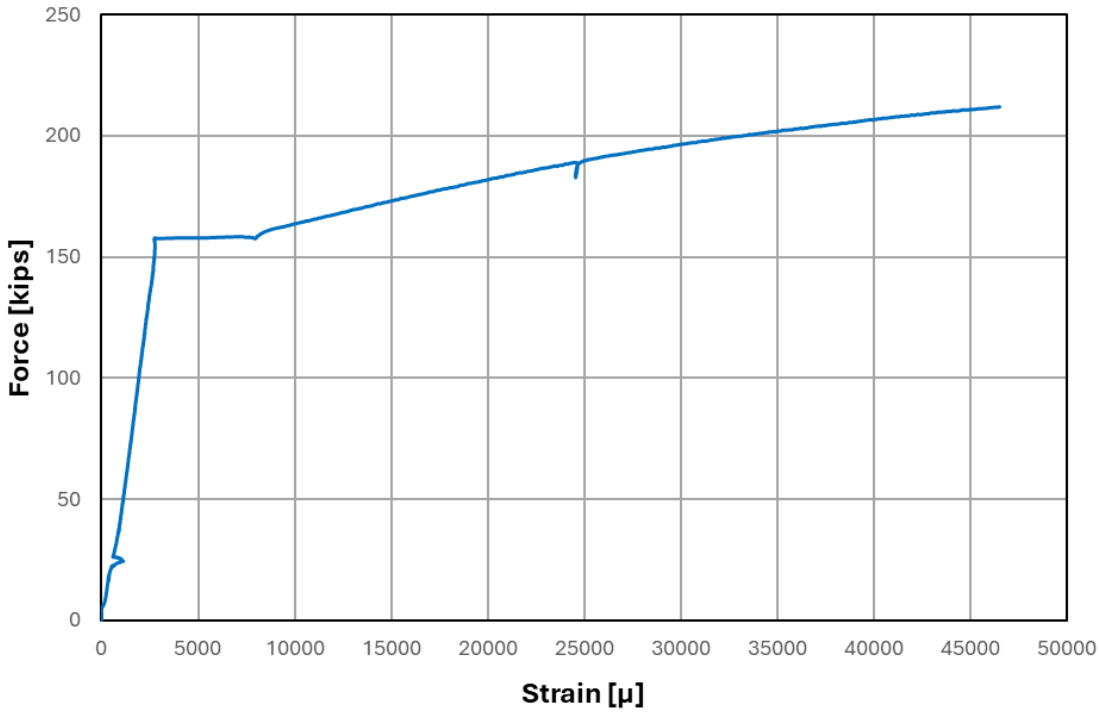

Figure D.82: Force plotted against SG06 strain for Specimen 6

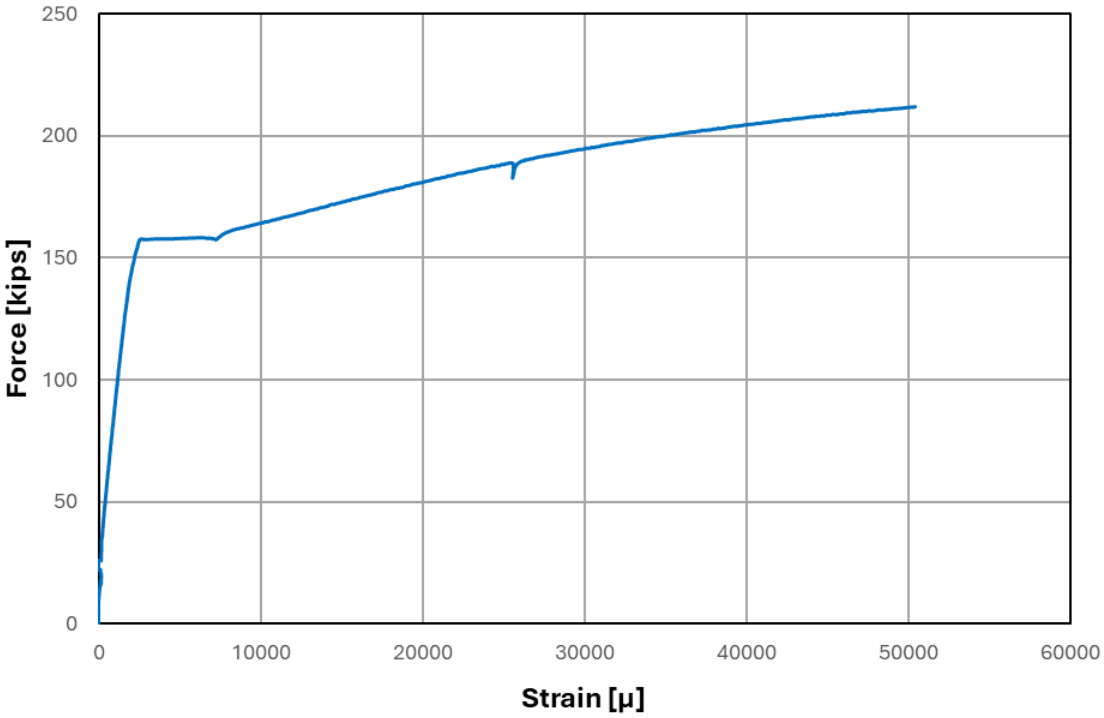

Figure D.83: Force plotted against SG07 strain for Specimen 6

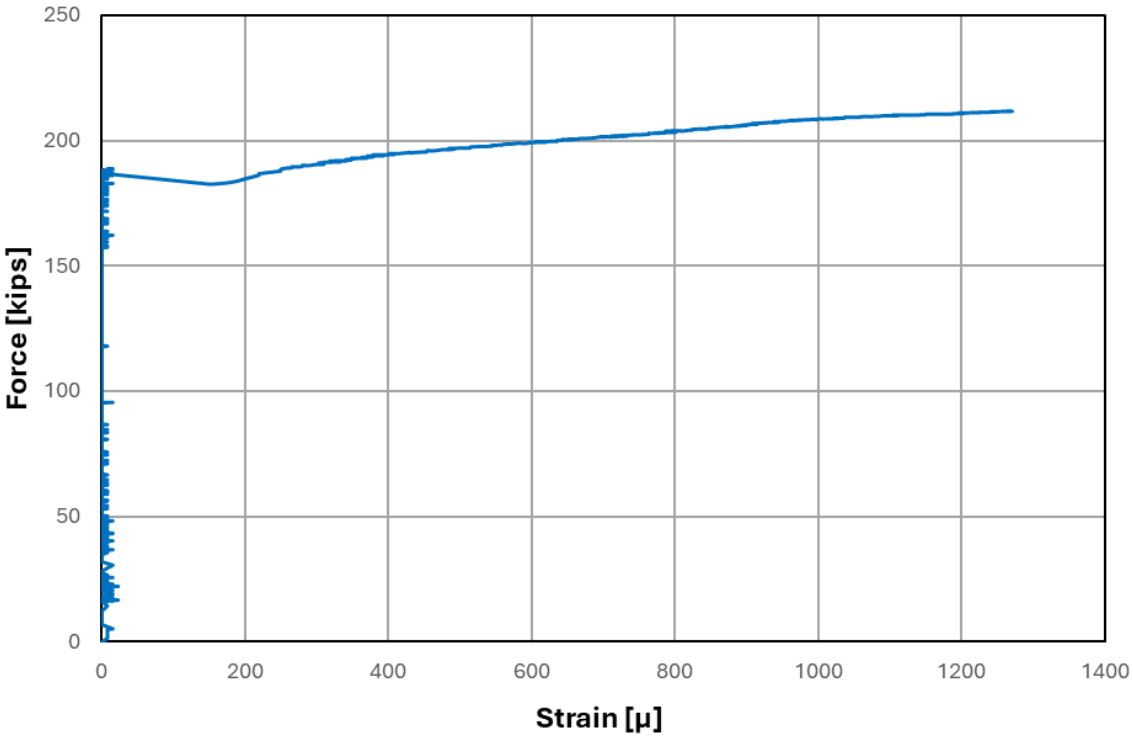

Figure D.84: Force plotted against SG08 strain for Specimen 6

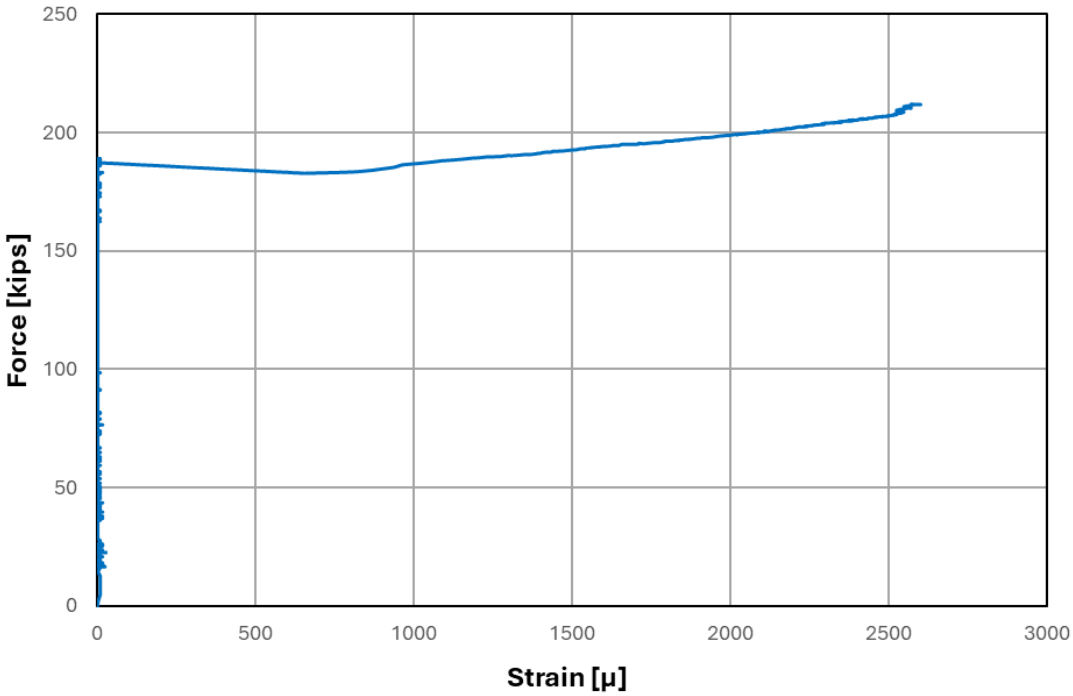

Figure D.85: Force plotted against SG09 strain for Specimen 6

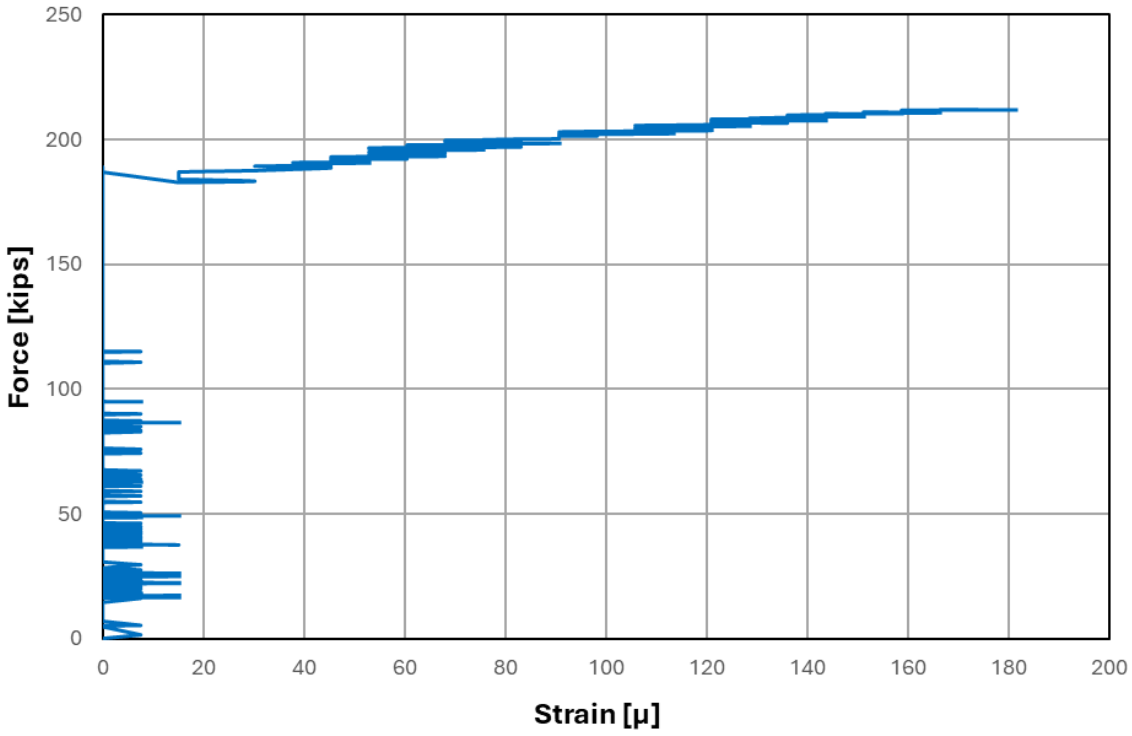

Figure D.86: Force plotted against SG10 strain for Specimen 6

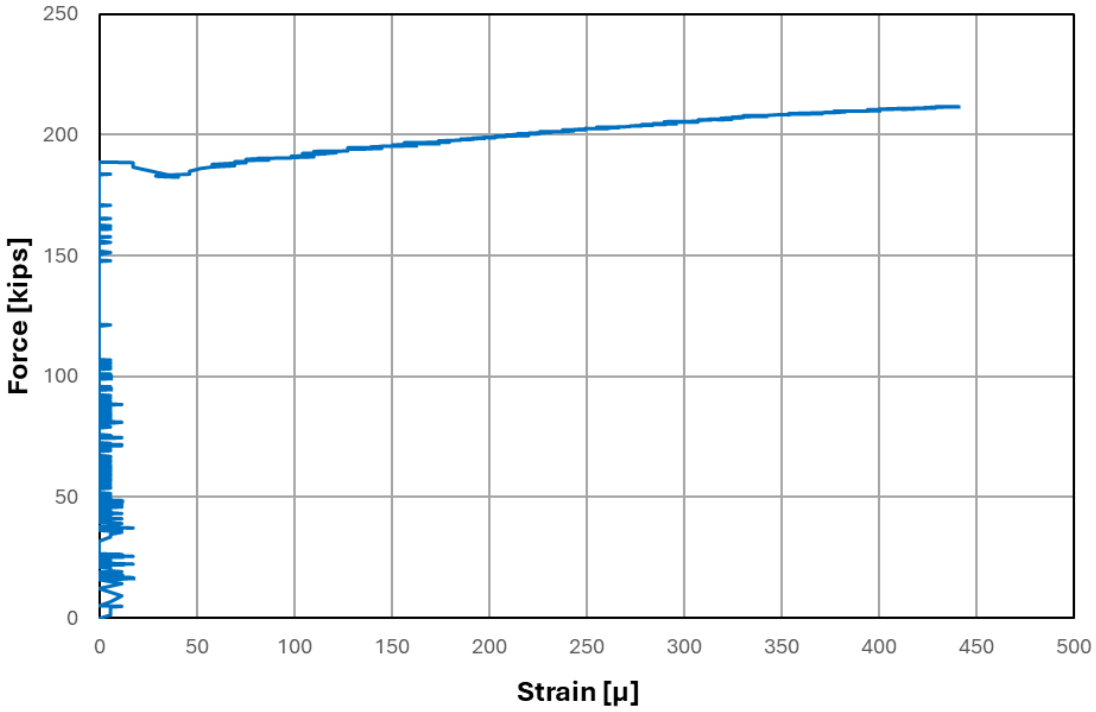

Figure D.87: Force plotted against SG11 strain for Specimen 6

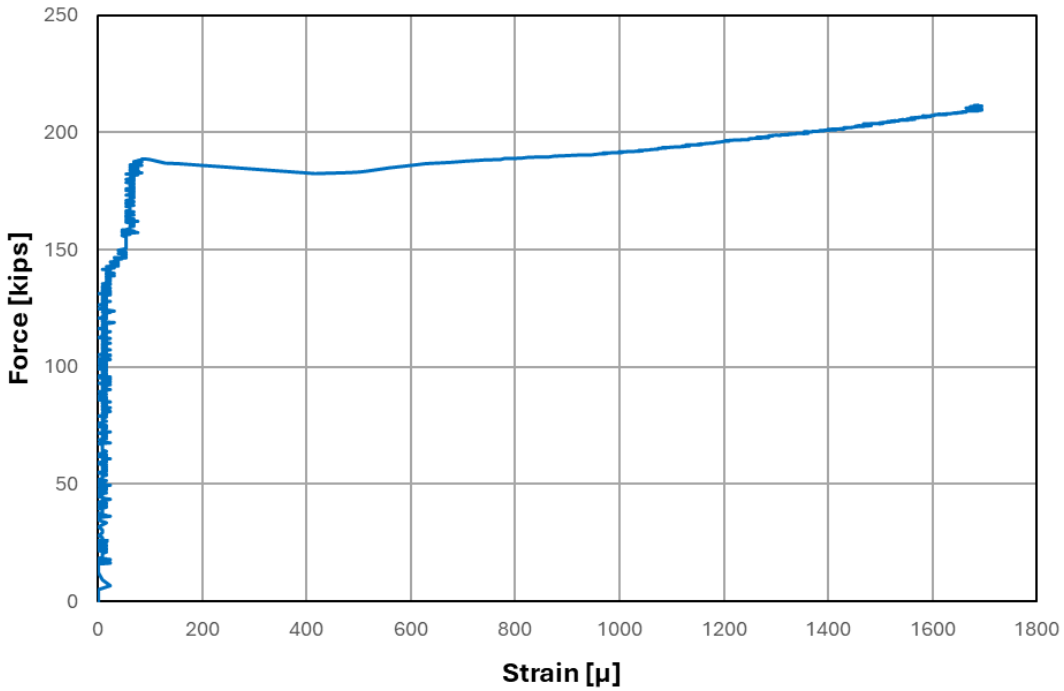

Figure D.88: Force plotted against SG12 strain for Specimen 6

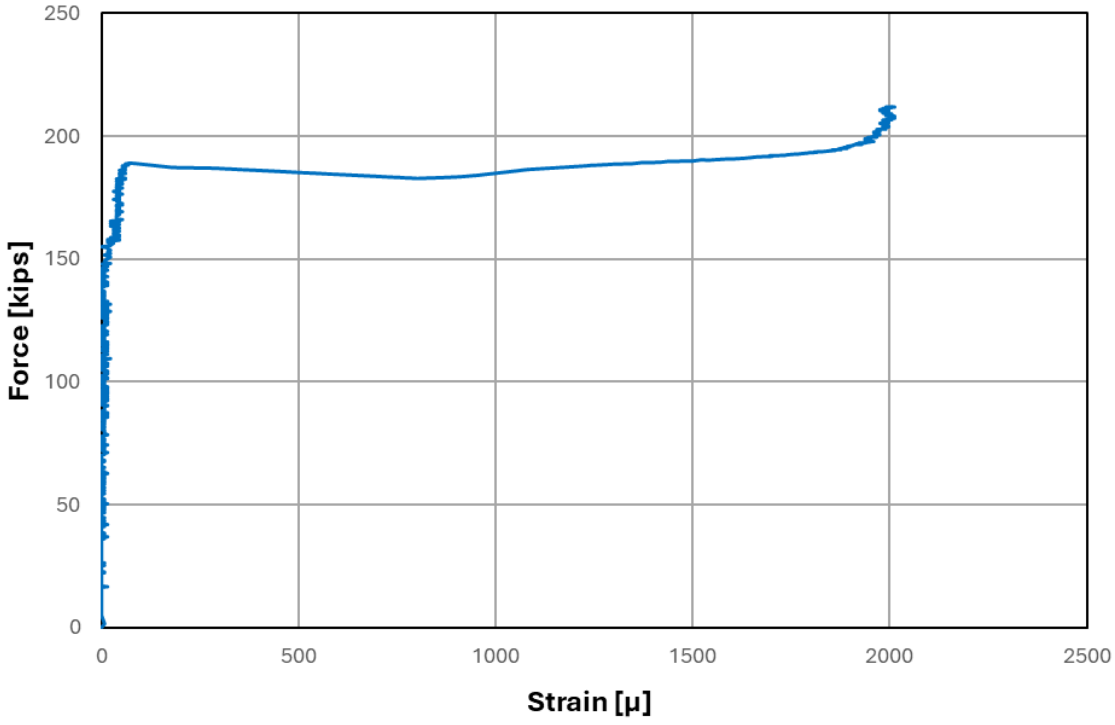

Figure D.89: Force plotted against SG13 strain for Specimen 6

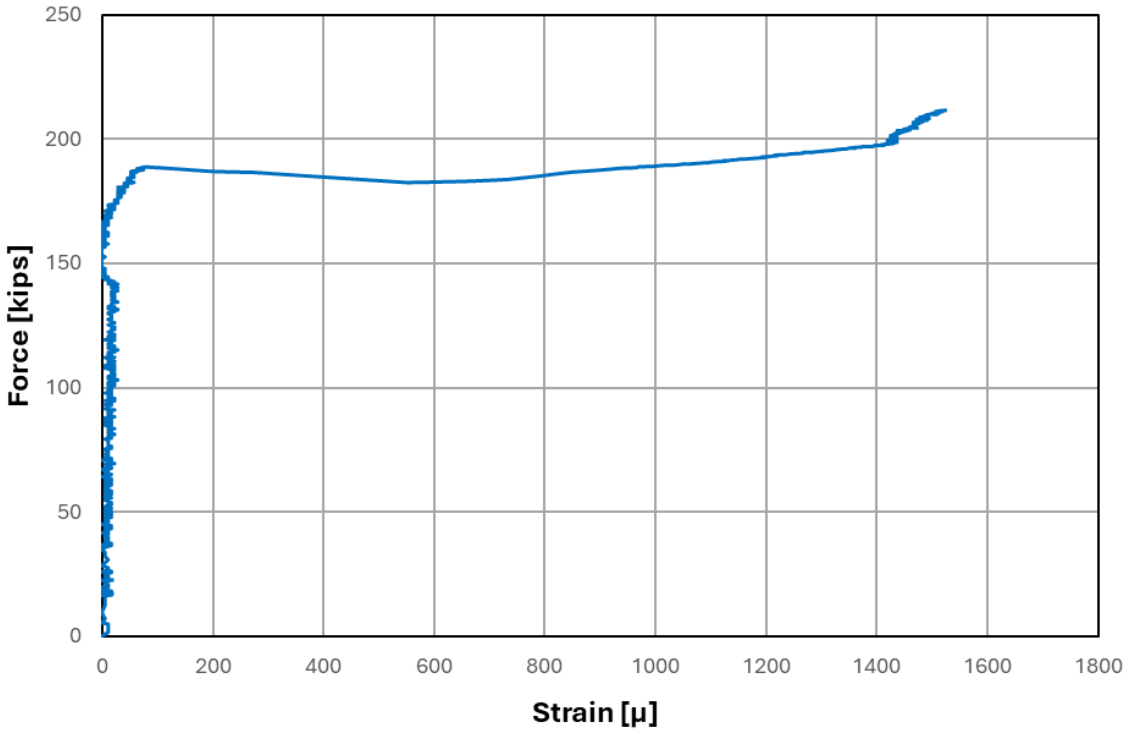

Figure D.90: Force plotted against SG14 strain for Specimen 6

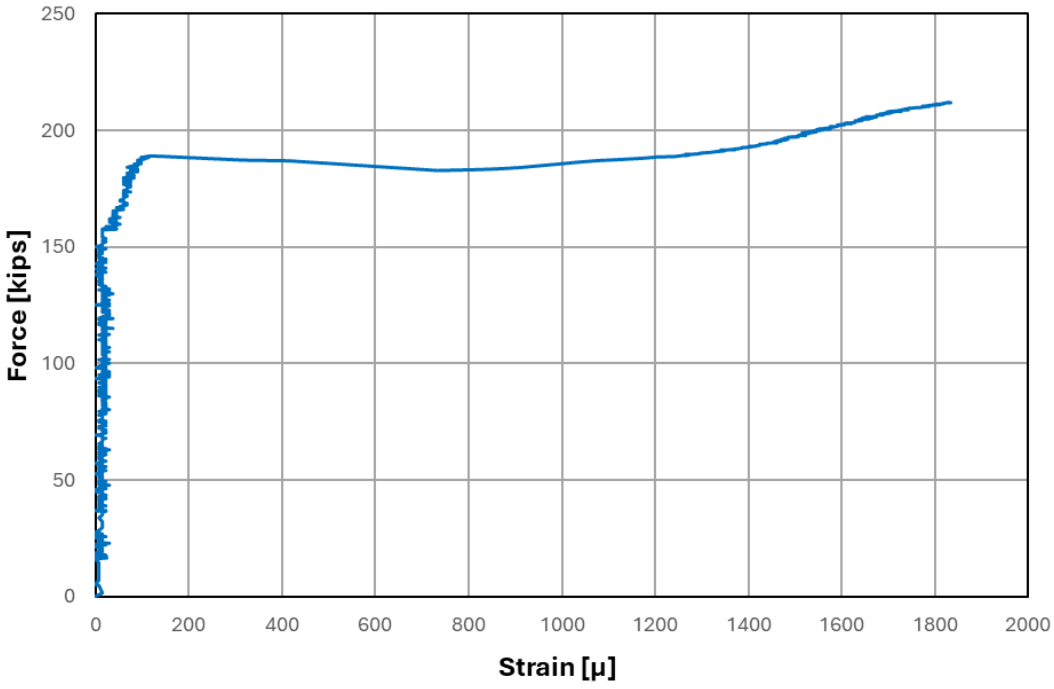

Figure D.91: Force plotted against SG15 strain for Specimen 6

D.7 Specimen 7

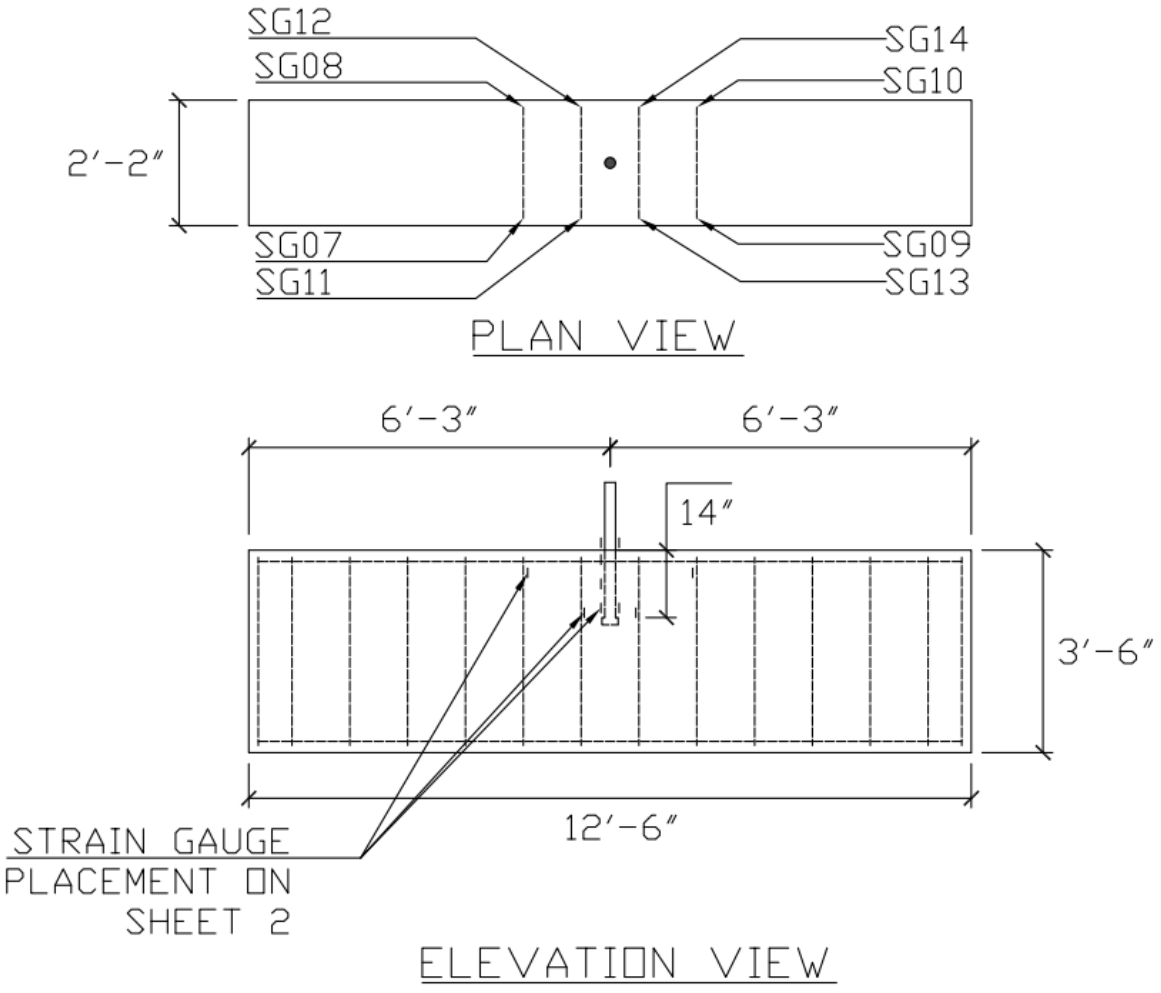

Figure D.92: Locations of strain gauges for Specimen 7

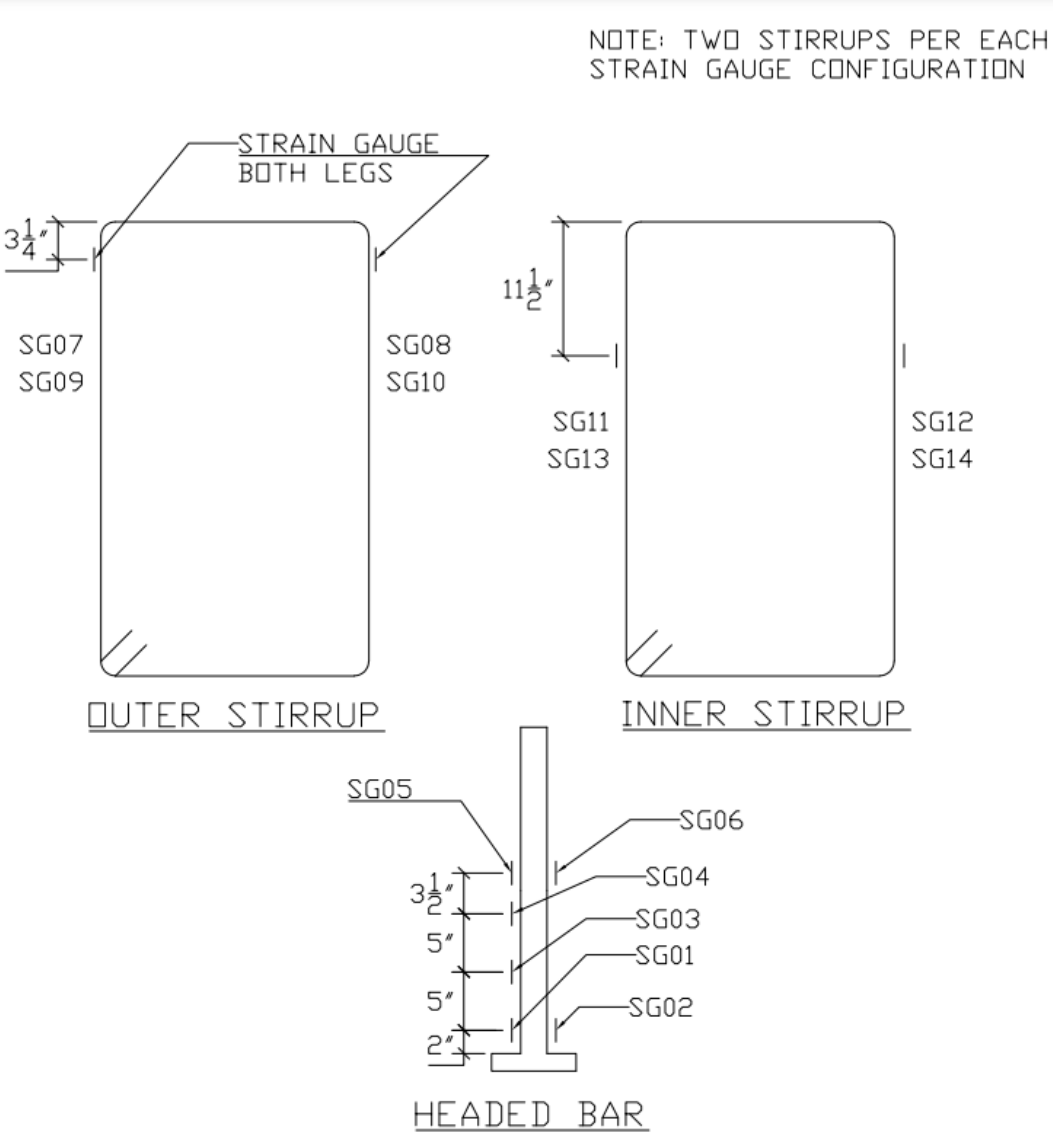

Figure D.93: Locations of stirrup and headed bar strain gauges and their labels for Specimen 7

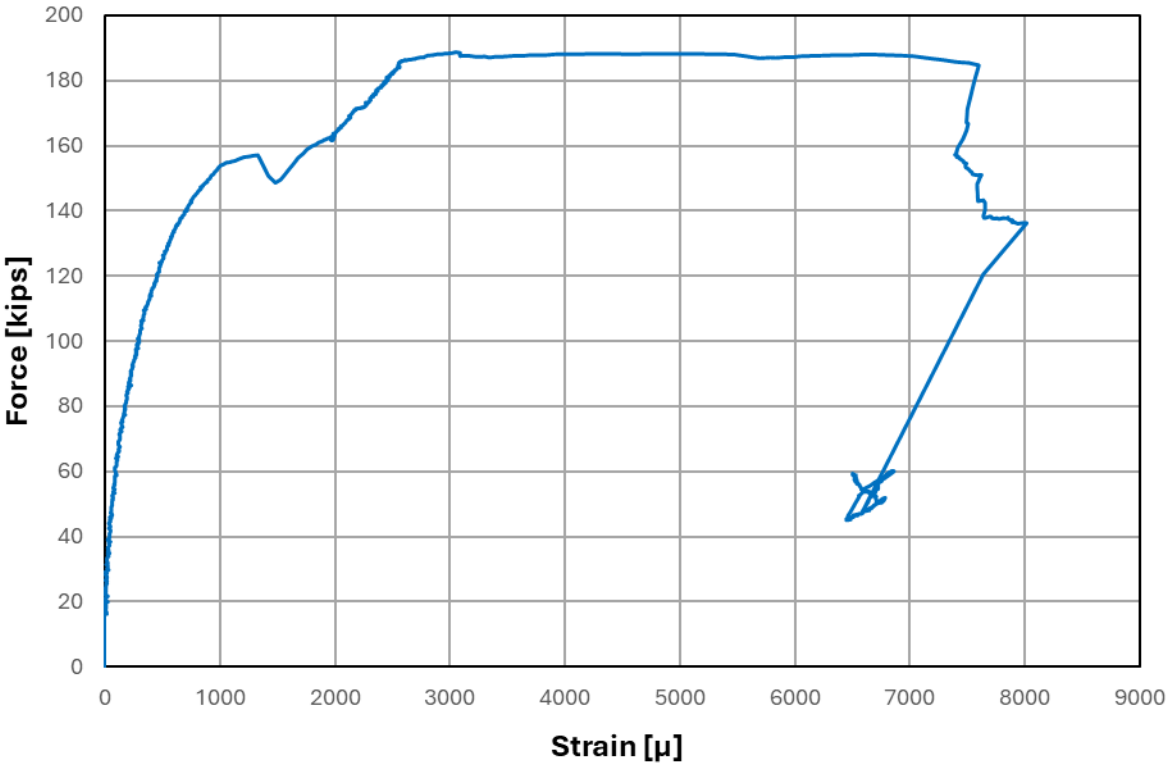

Figure D.94: Force plotted against SG01 strain for Specimen 7

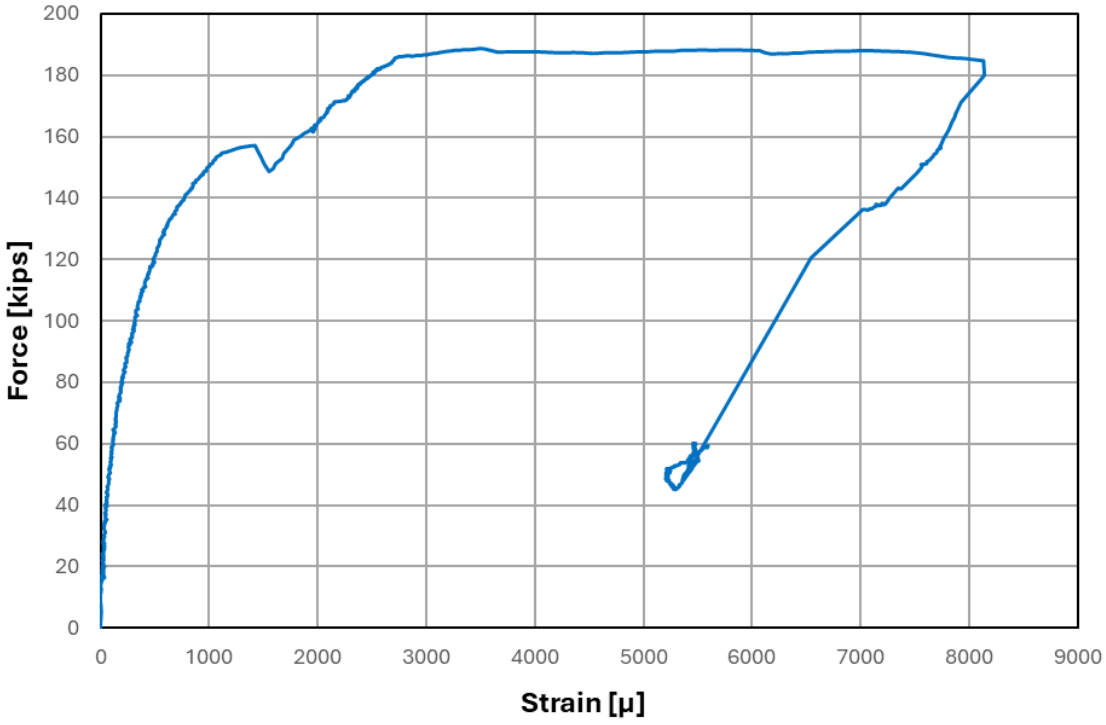

Figure D.95: Force plotted against SG02 strain for Specimen 7

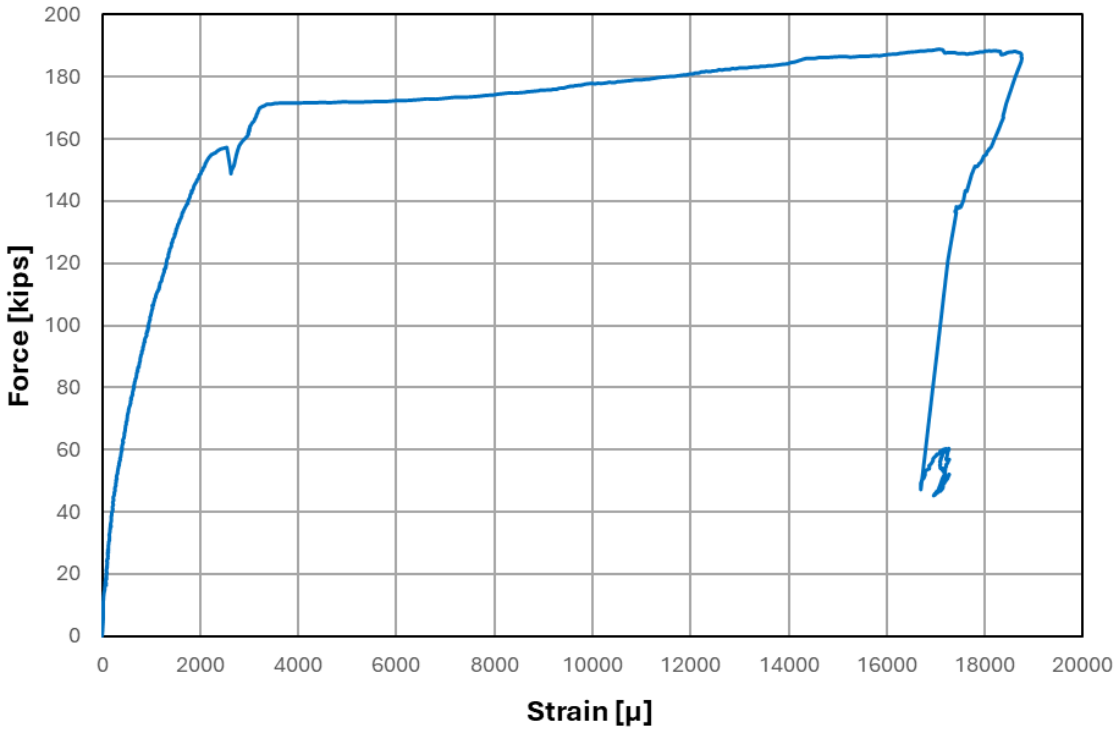

Figure D.96: Force plotted against SG03 strain for Specimen 7

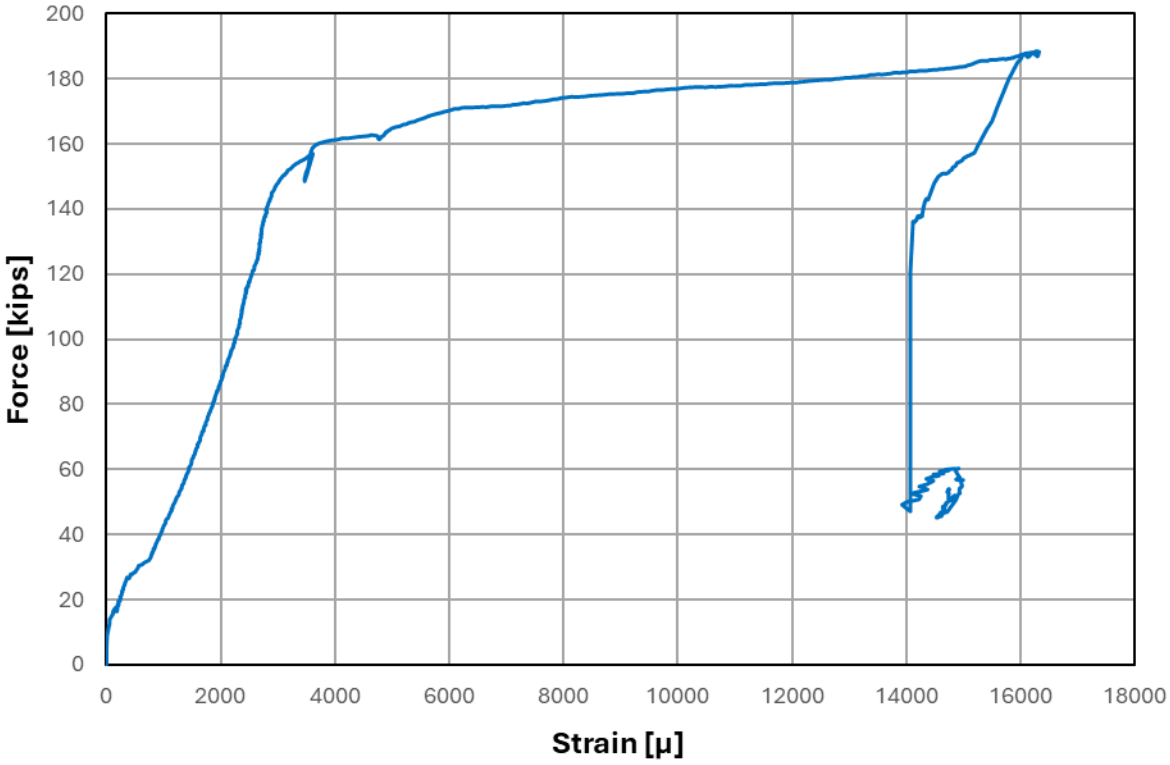

Figure D.97: Force plotted against SG04 strain for Specimen 7

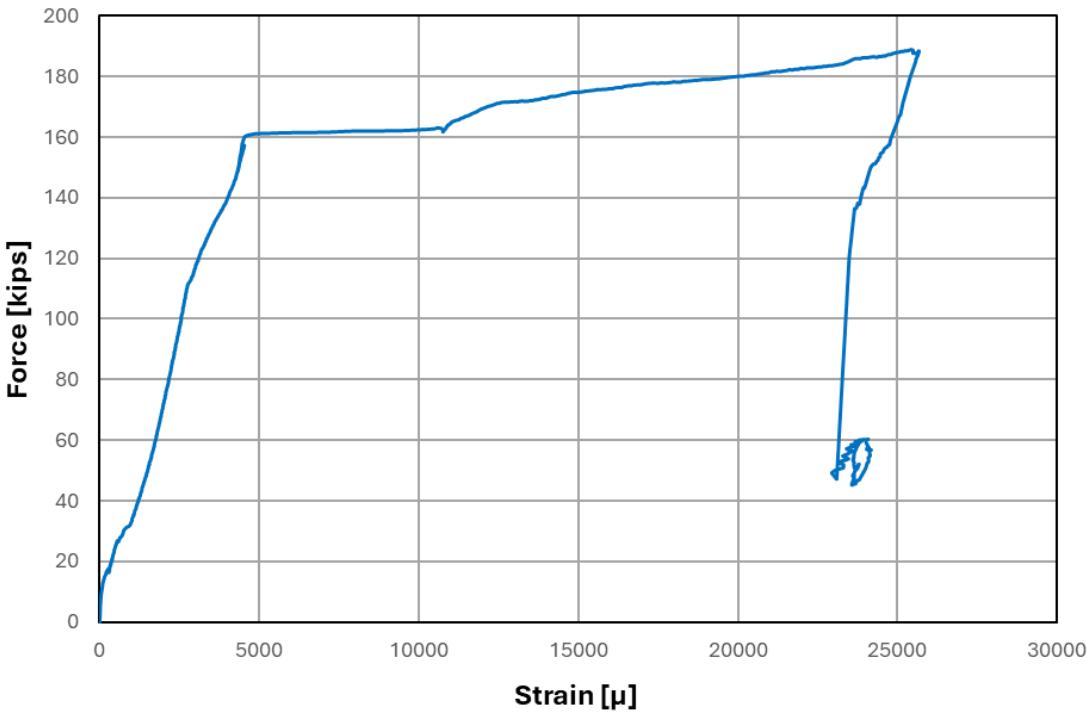

Figure D.98: Force plotted against SG05 strain for Specimen 7

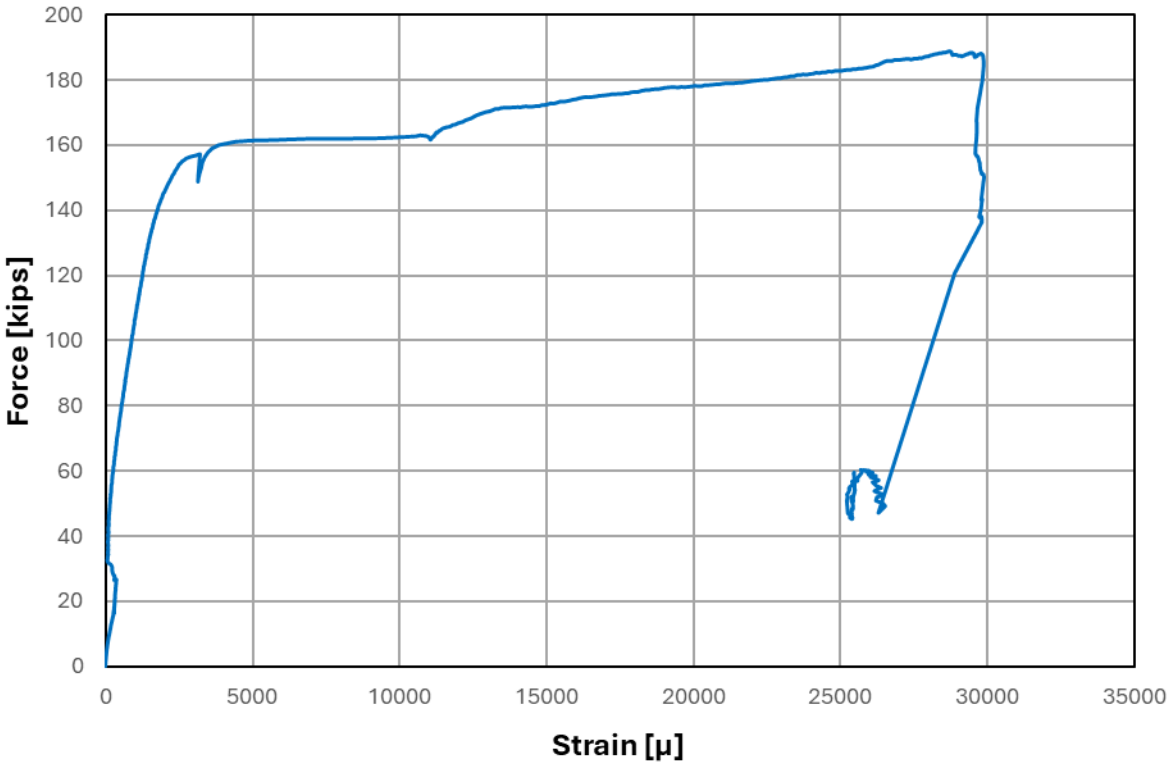

Figure D.99: Force plotted against SG06 strain for Specimen 7

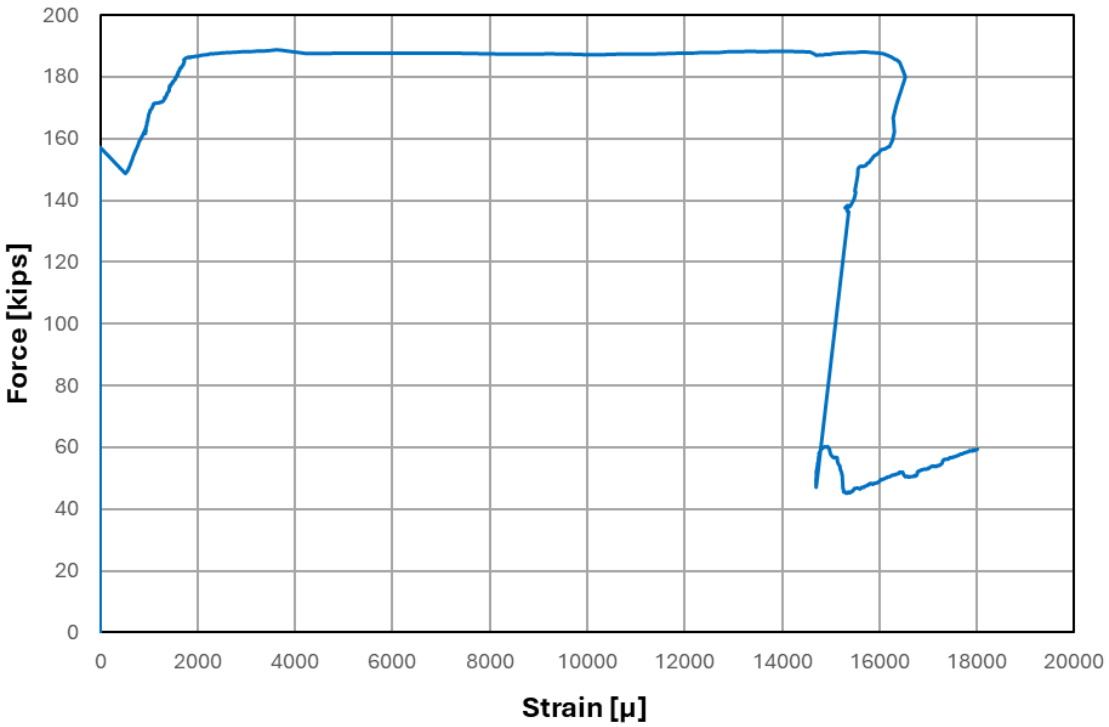

Figure D.100: Force plotted against SG07 strain for Specimen 7

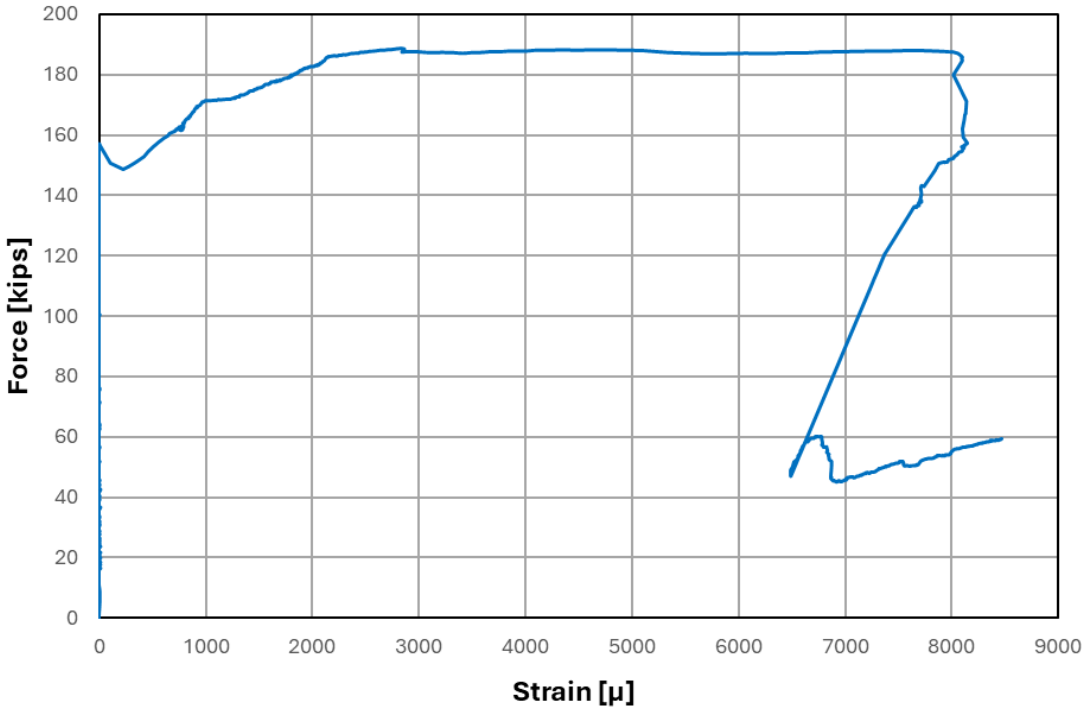

Figure D.101: Force plotted against SG08 strain for Specimen 7

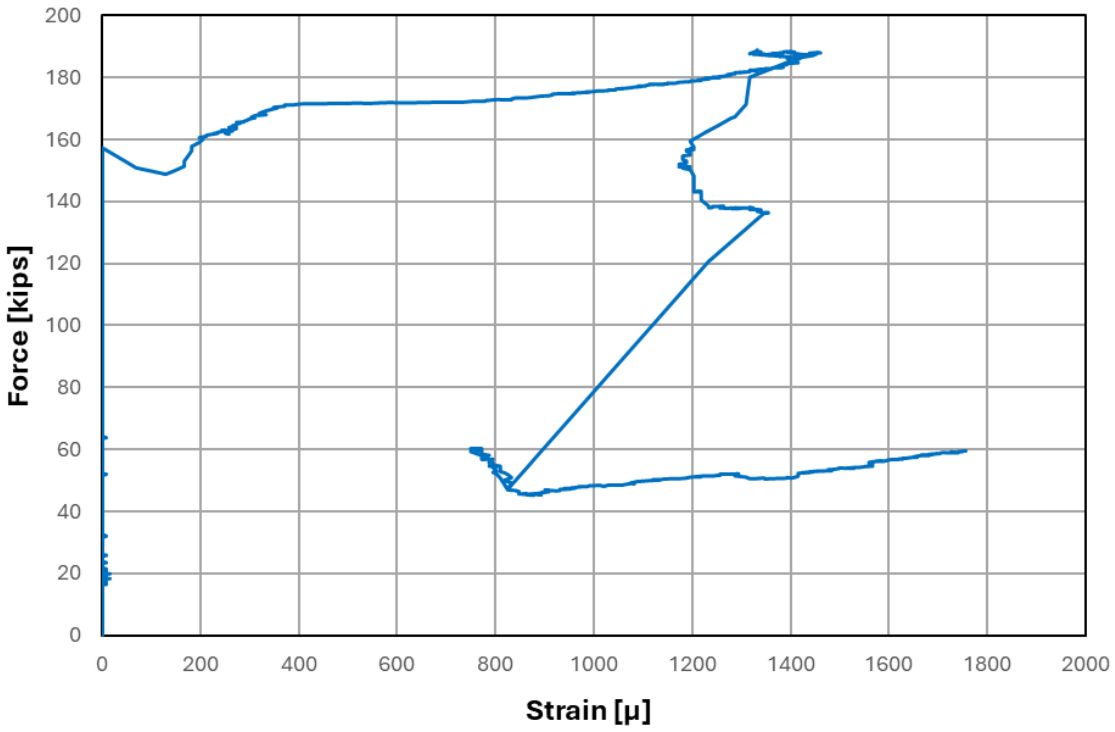

Figure D.102: Force plotted against SG09 strain for Specimen 7

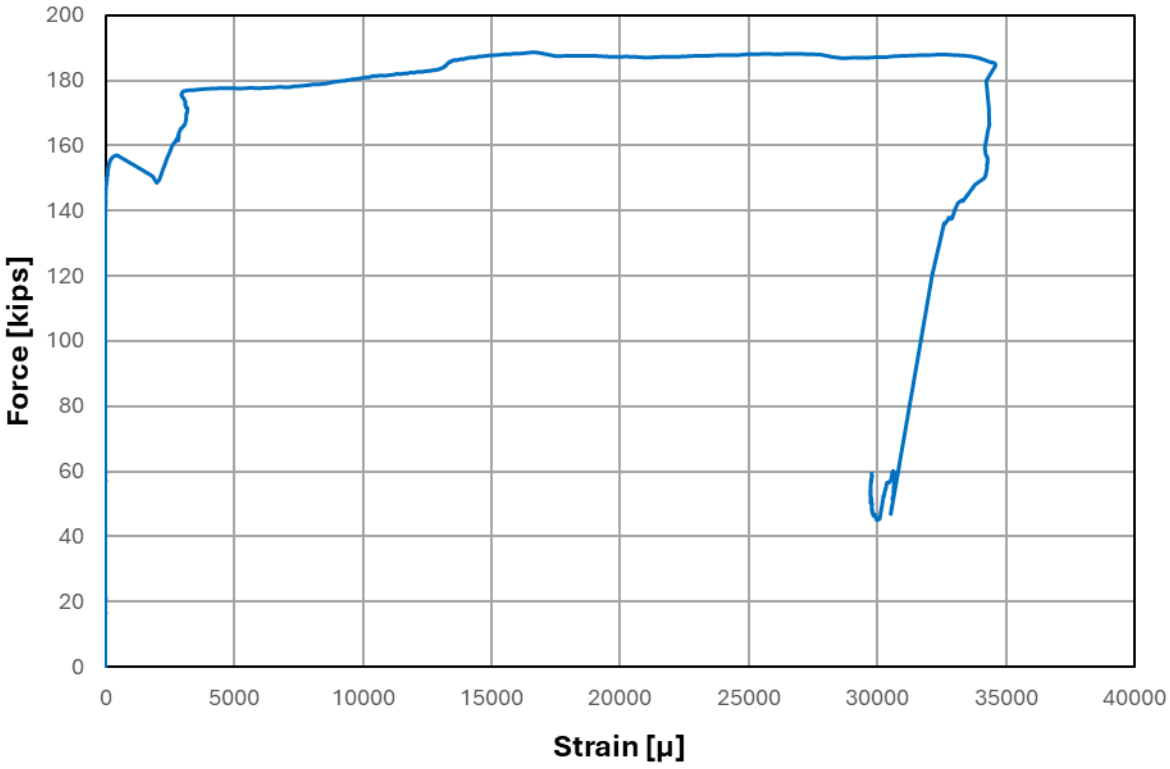

Figure D.103: Force plotted against SG11 strain for Specimen 7

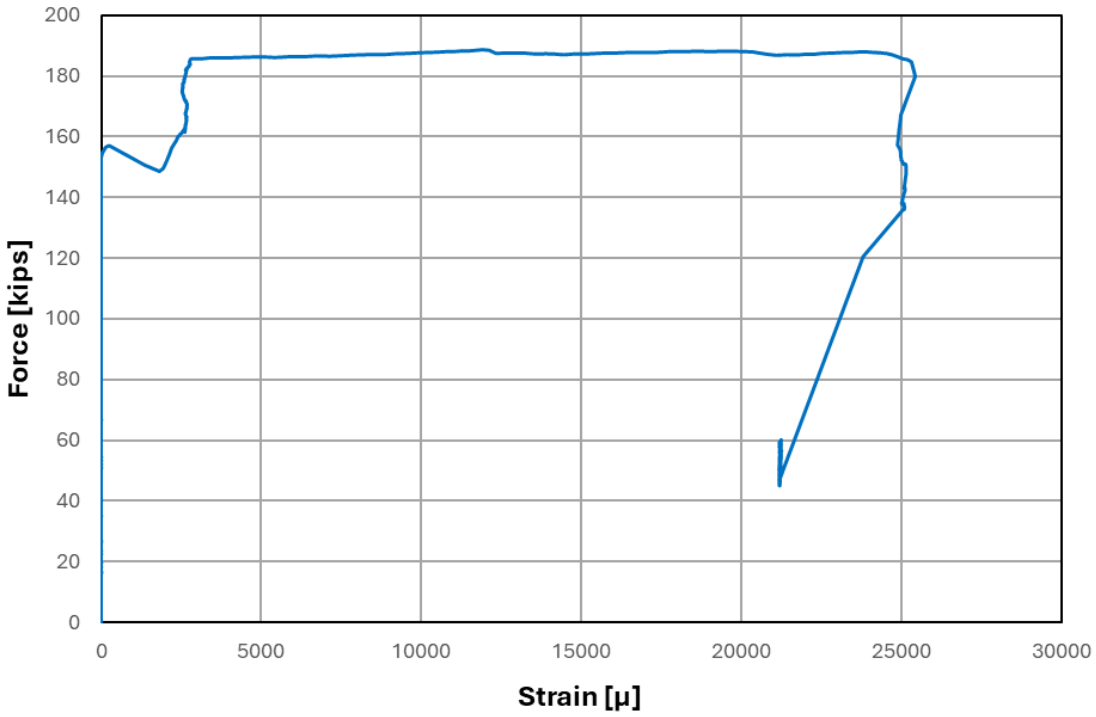

Figure D.104: Force plotted against SG12 strain for Specimen 7

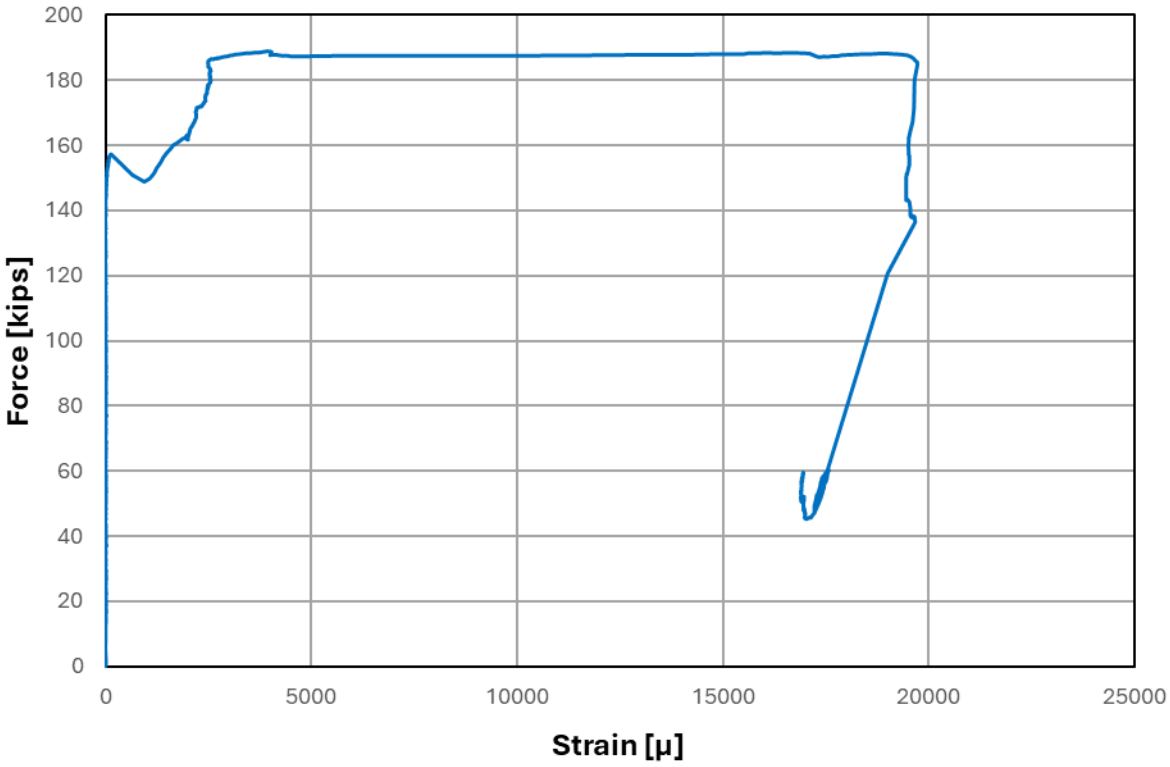

Figure D.105: Force plotted against SG13 strain for Specimen 7

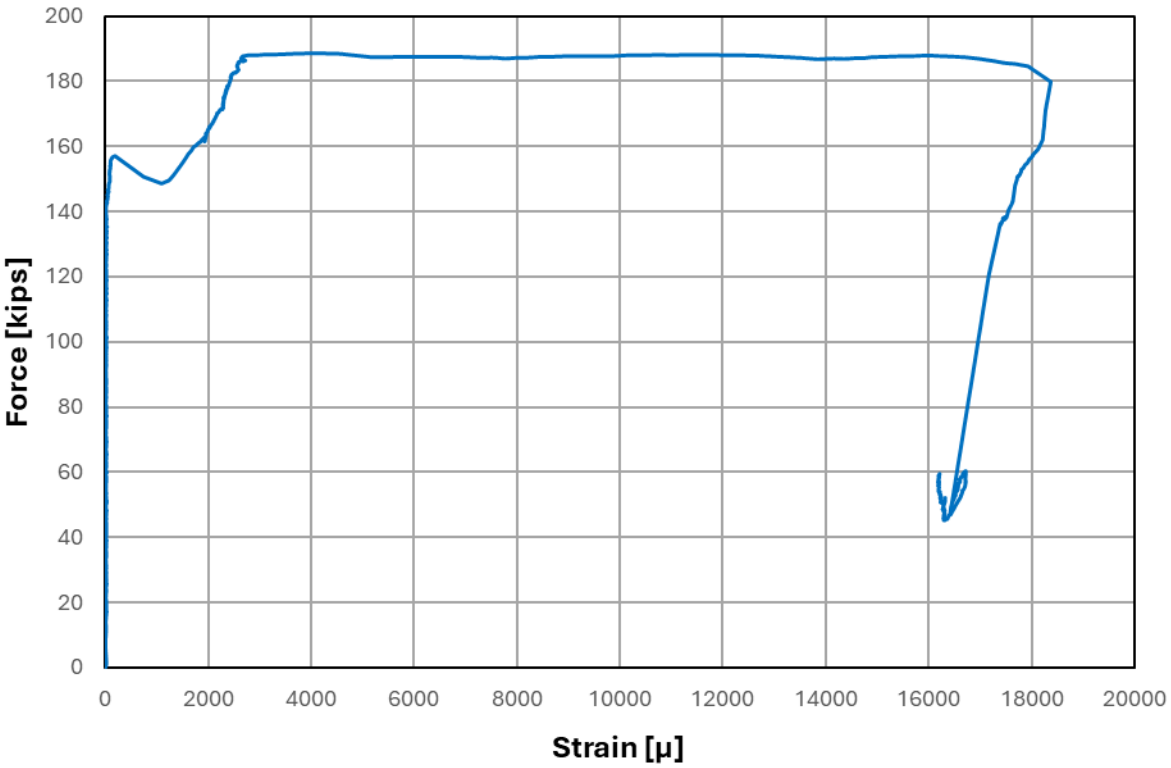

Figure D.106: Force plotted against SG14 strain for Specimen 7

D.8 Specimen 8

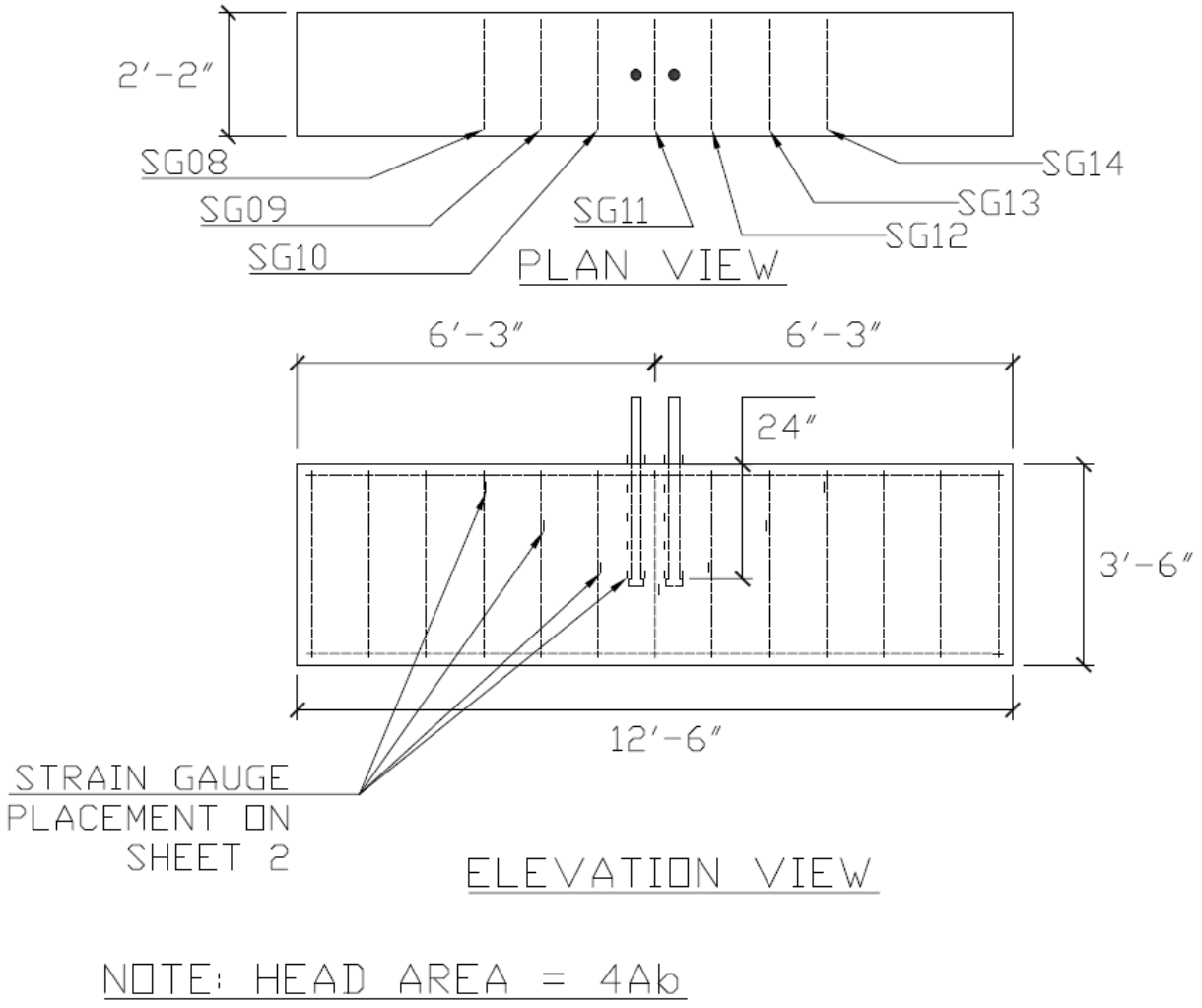

Figure D.107: Locations of strain gauges for Specimen 8

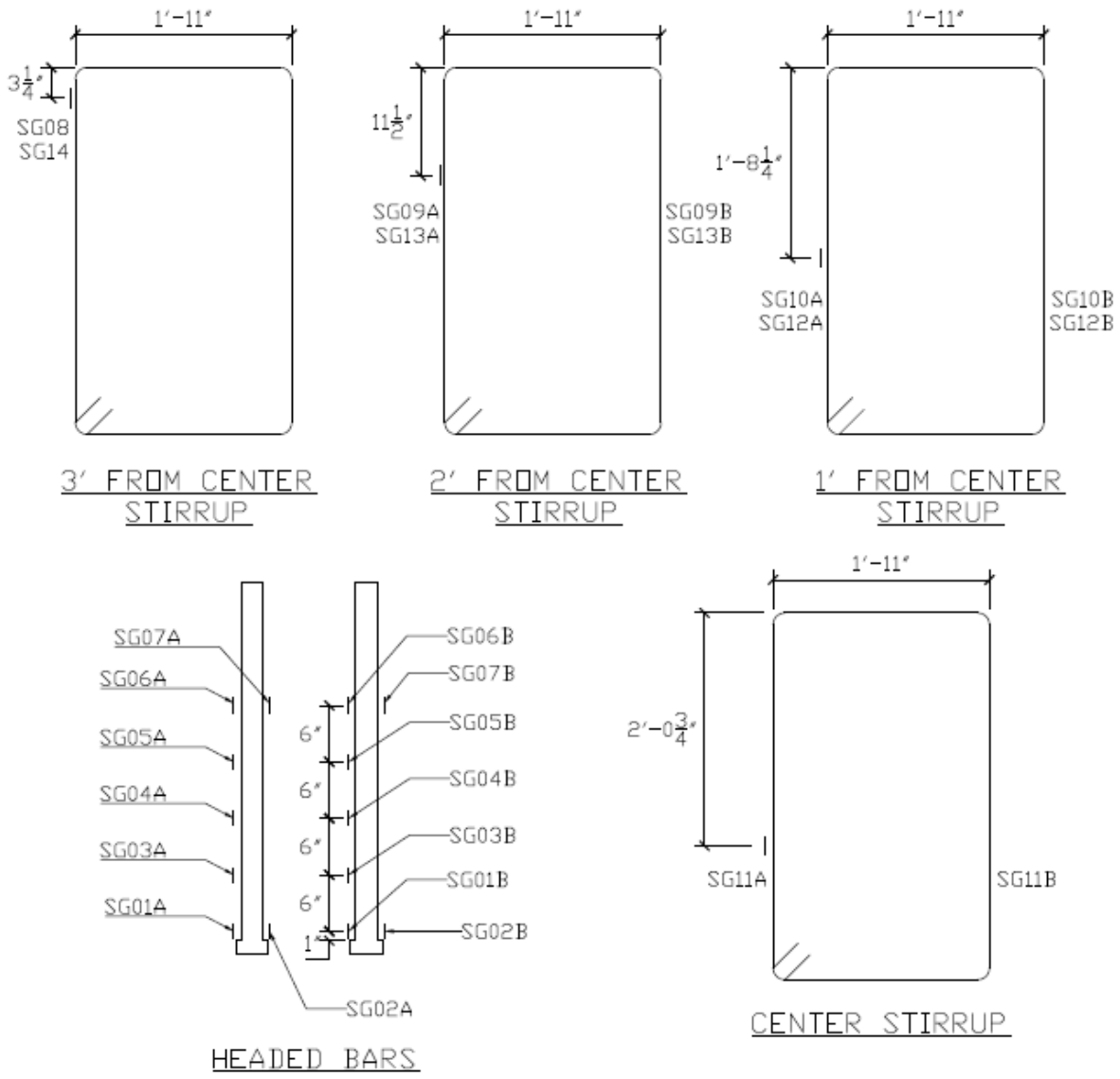

Figure D.108: Locations of stirrup and headed bar strain gauges and their labels for Specimen 8

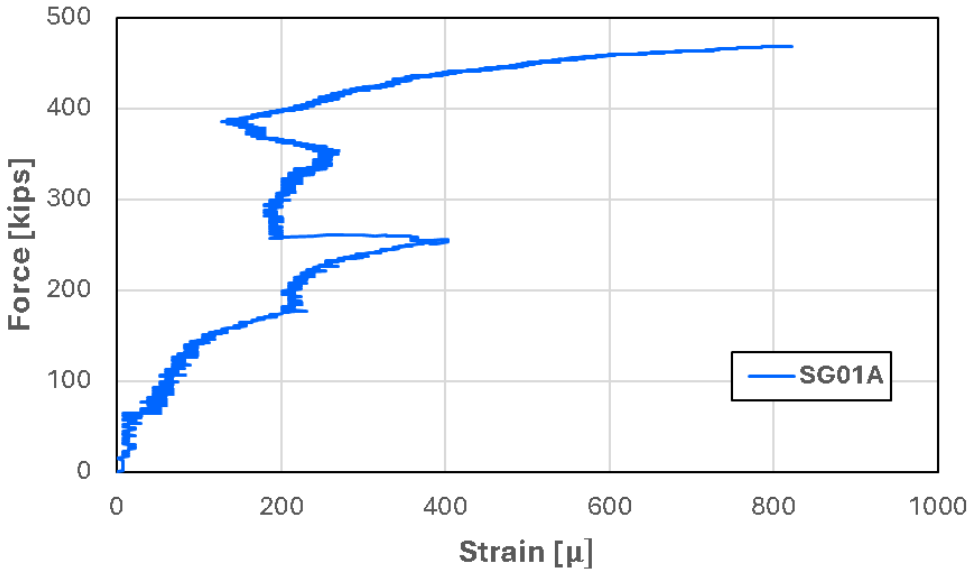

Figure D.109: Force plotted against SG1A strain for Specimen 8

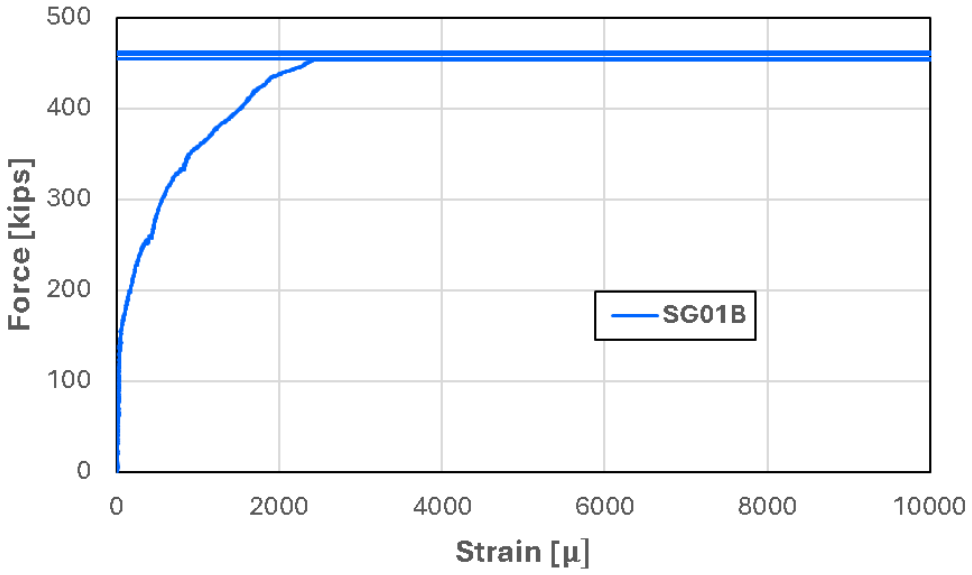

Figure D.110: Force plotted against SG1B strain for Specimen 8

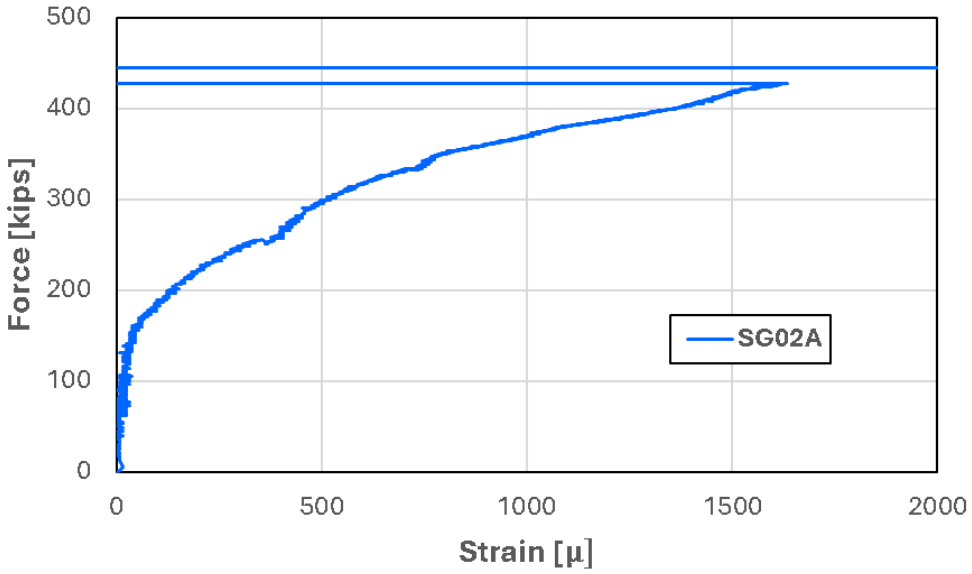

Figure D.111: Force plotted against SG2A strain for Specimen 8

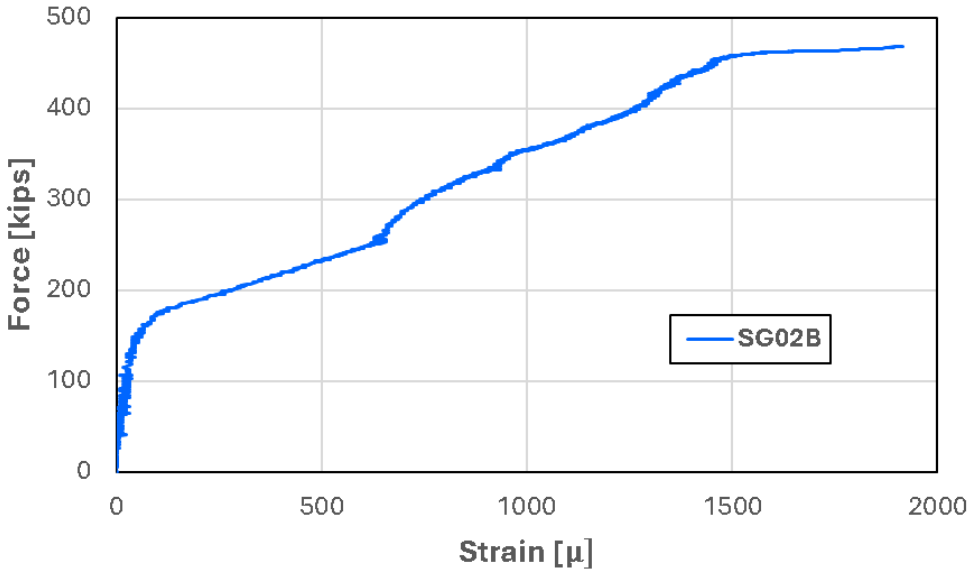

Figure D.112: Force plotted against SG2B strain for Specimen 8

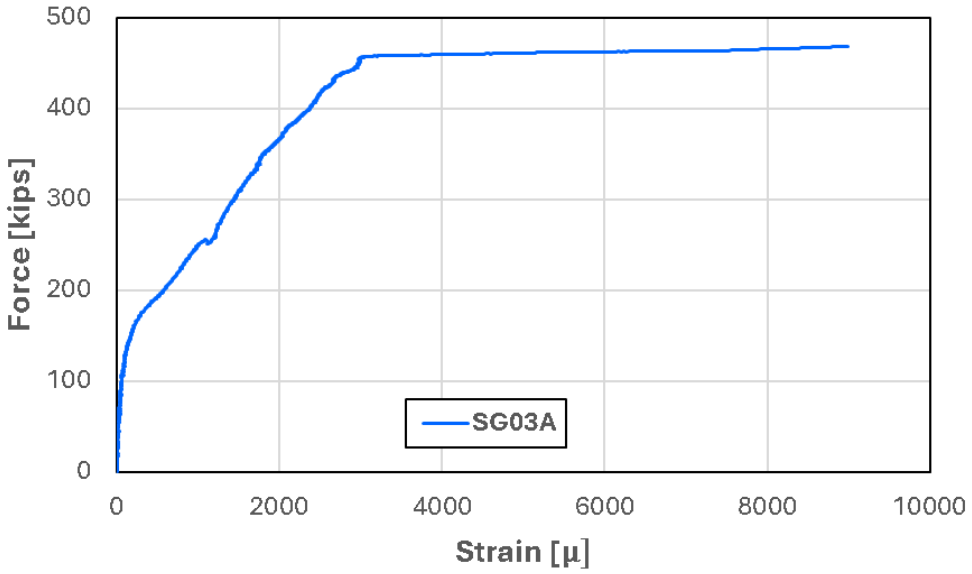

Figure D.113: Force plotted against SG3A strain for Specimen 8

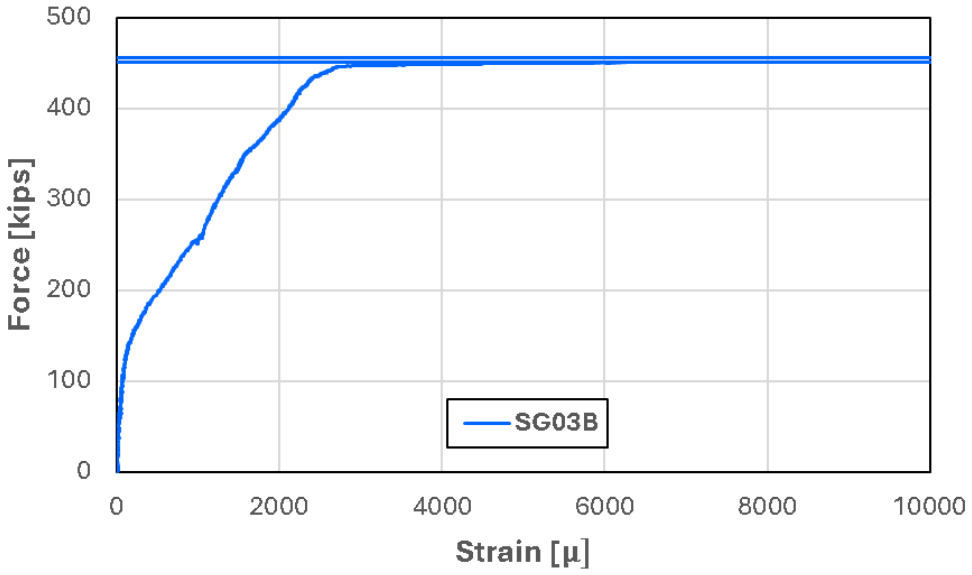

Figure D.114: Force plotted against SG3B strain for Specimen 8

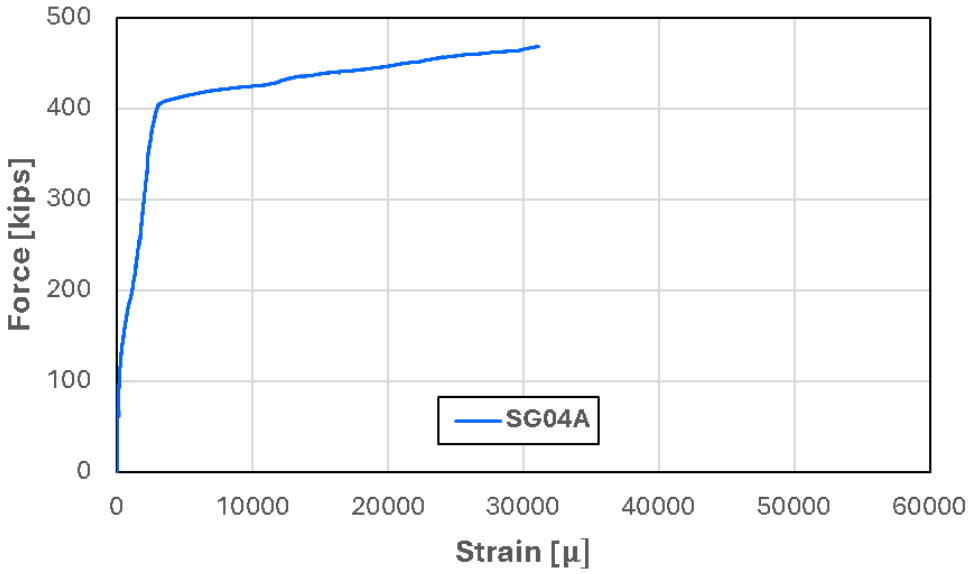

Figure D.115: Force plotted against SG4A strain for Specimen 8

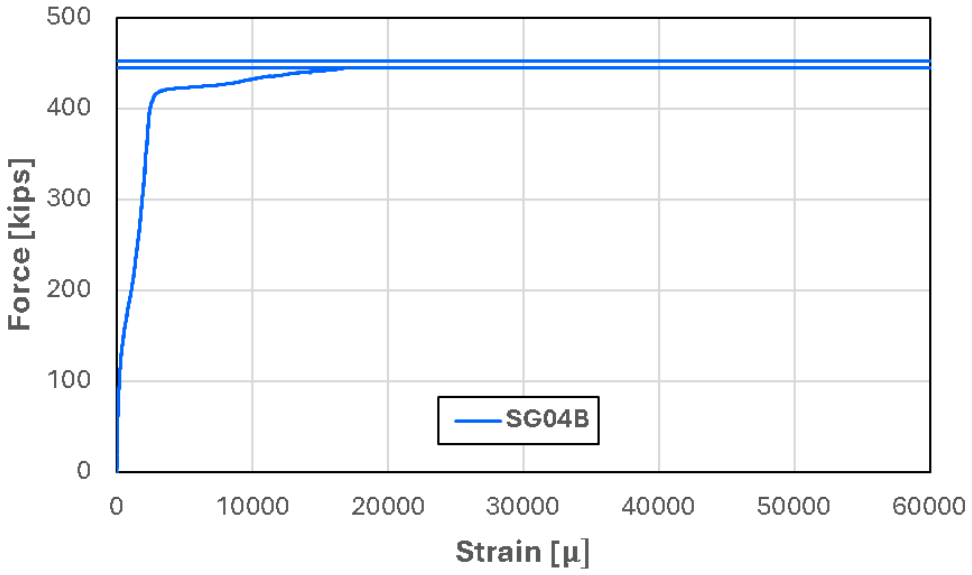

Figure D.116: Force plotted against SG4B strain for Specimen 8

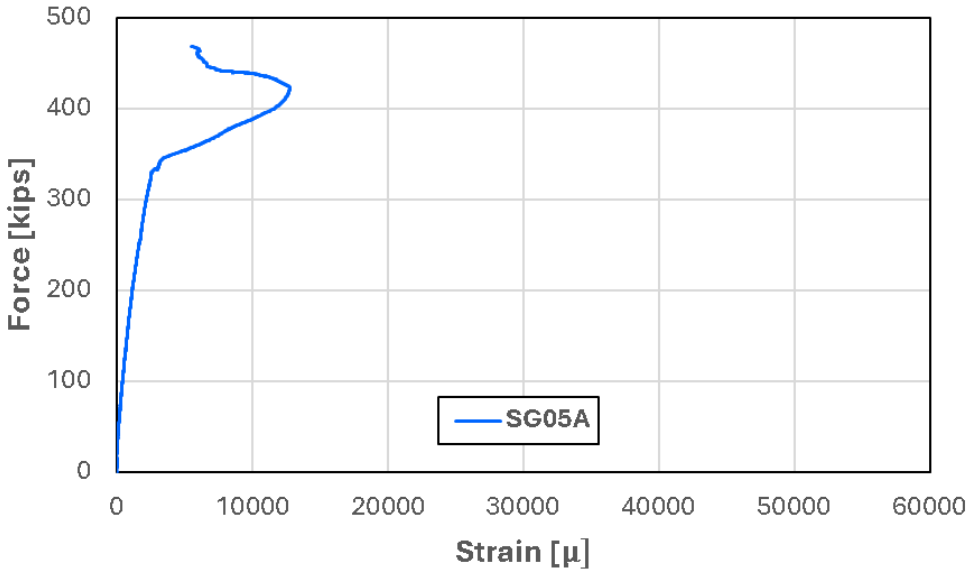

Figure D.117: Force plotted against SG5A strain for Specimen 8

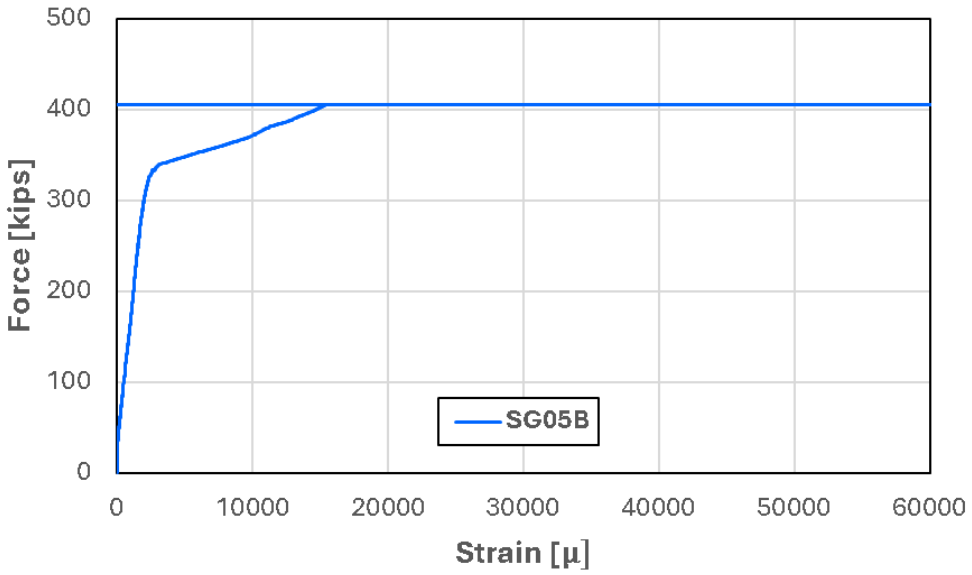

Figure D.118: Force plotted against SG5B strain for Specimen 8

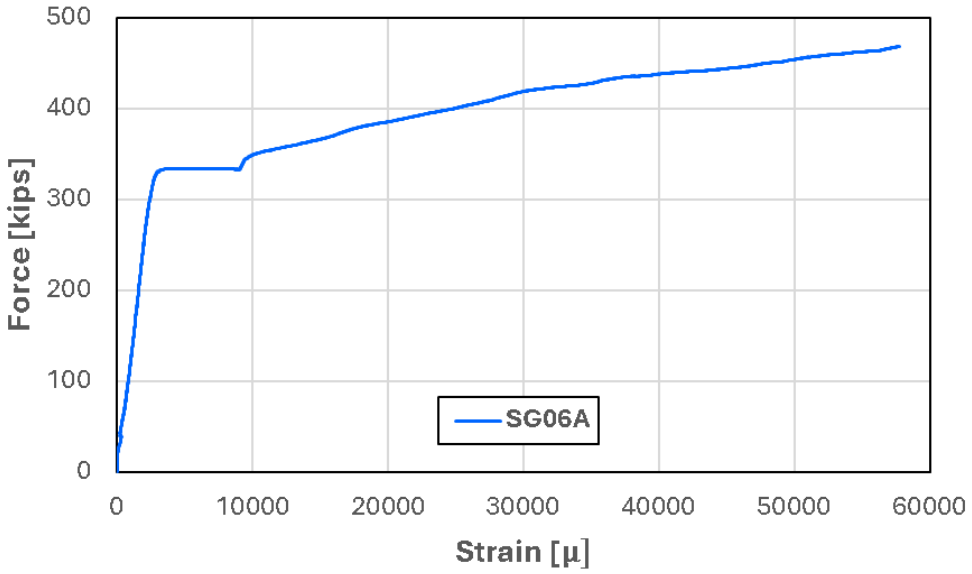

Figure D.119: Force plotted against SG6A strain for Specimen 8

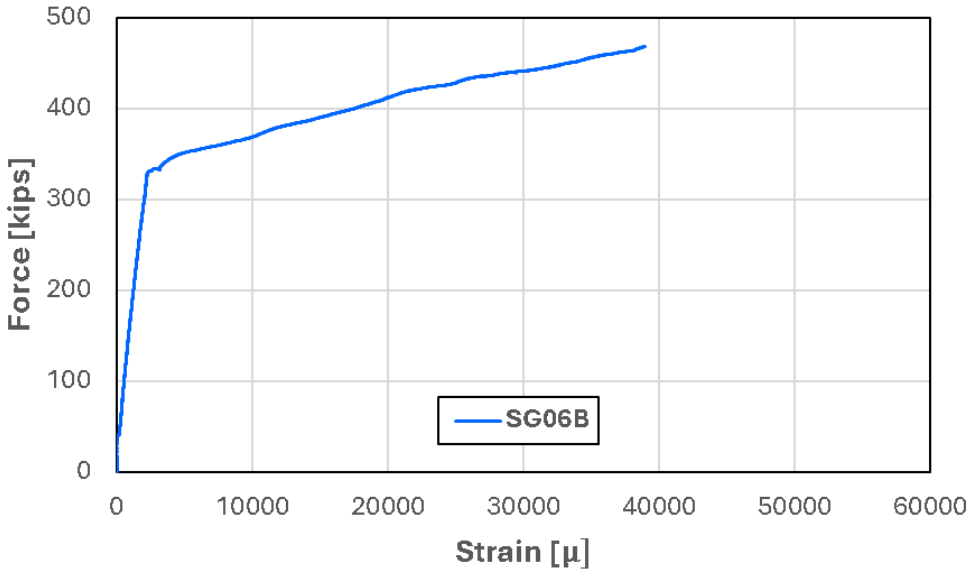

Figure D.120: Force plotted against SG6B strain for Specimen 8

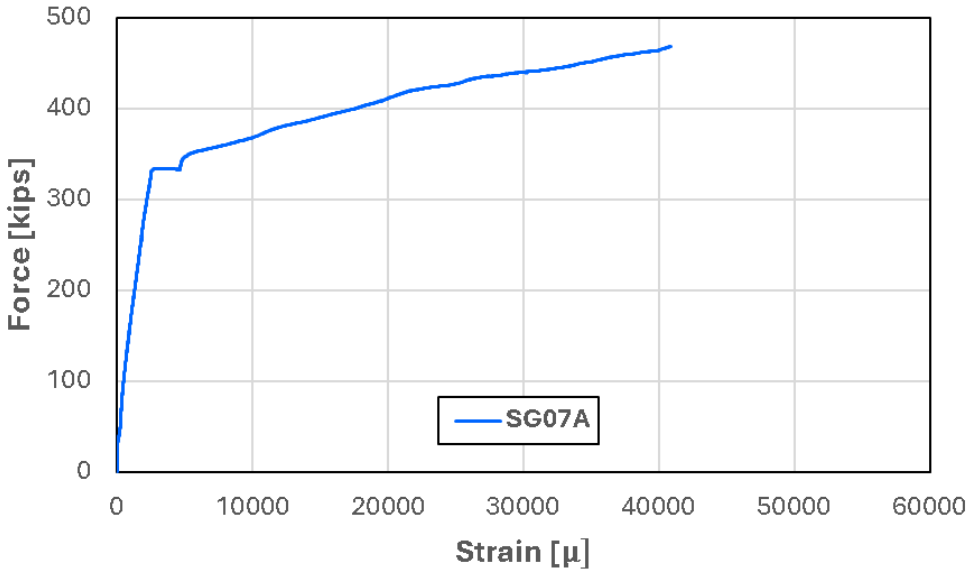

Figure D.121: Force plotted against SG7A strain for Specimen 8

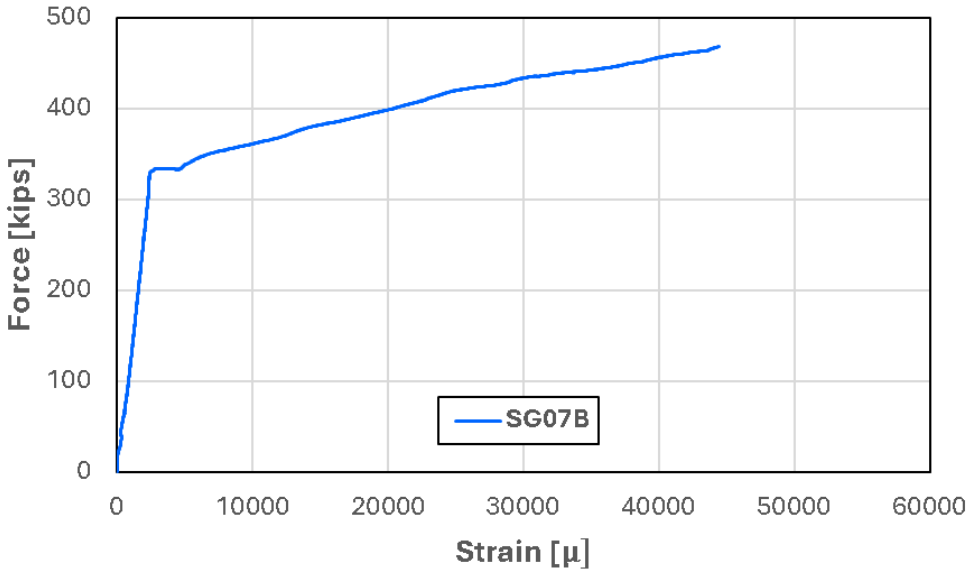

Figure D.122: Force plotted against SG7B strain for Specimen 8

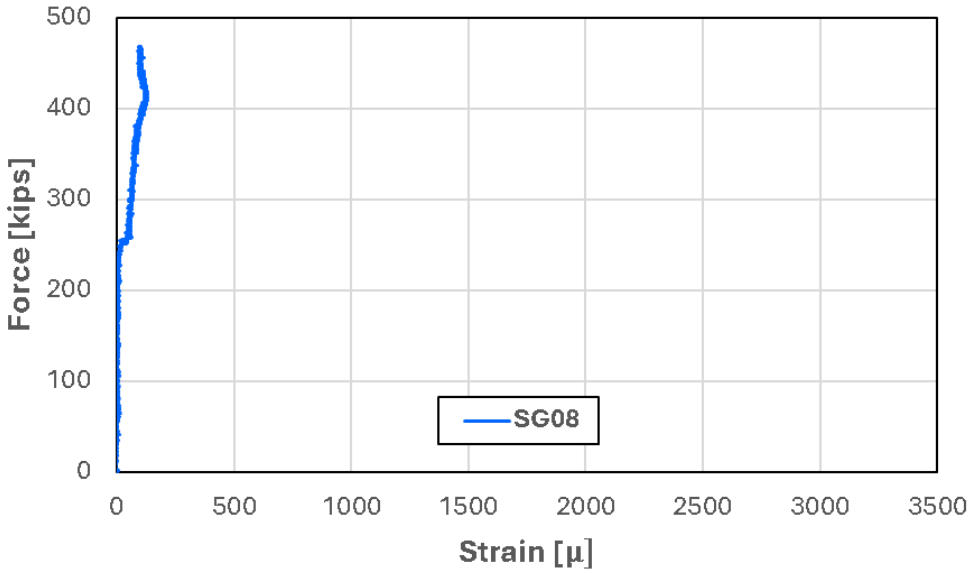

Figure D.123: Force plotted against SG8 strain for Specimen 8

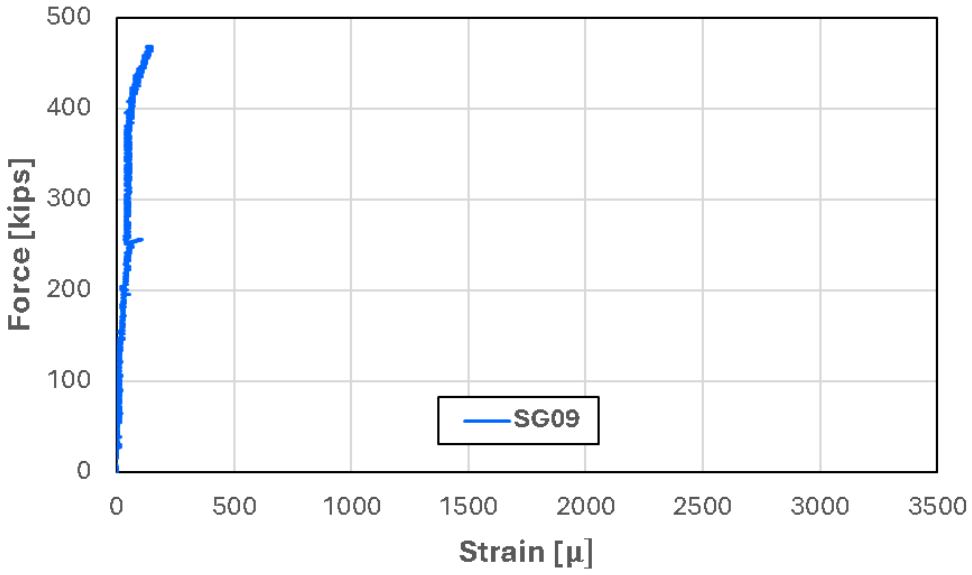

Figure D.124: Force plotted against SG9 strain for Specimen 8

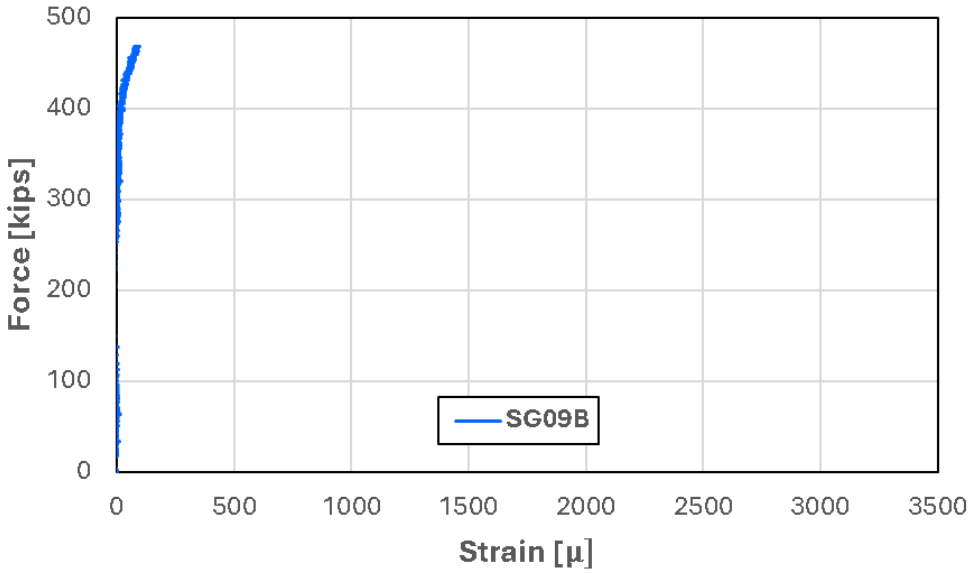

Figure D.125: Force plotted against SG9B strain for Specimen 8

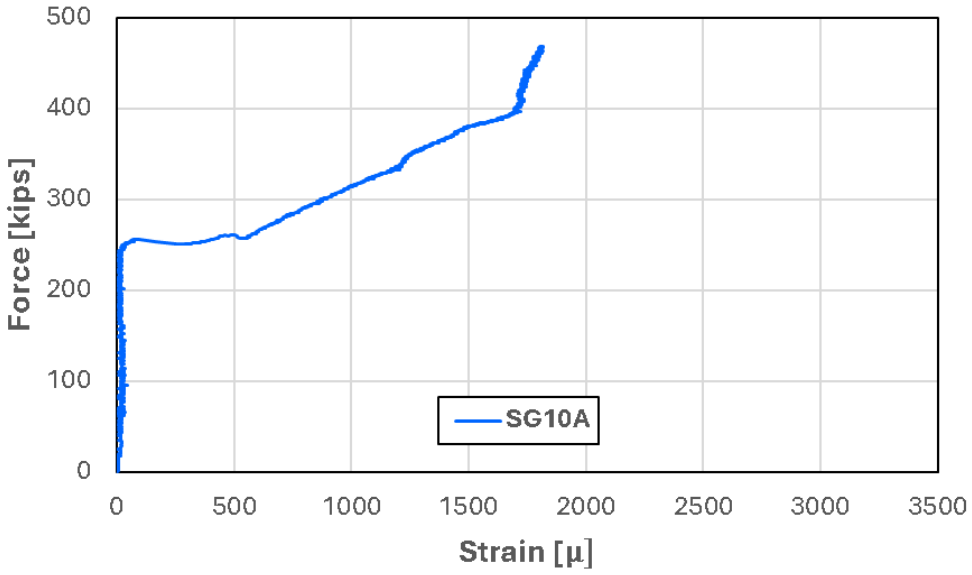

Figure D.126: Force plotted against SG10A strain for Specimen 8

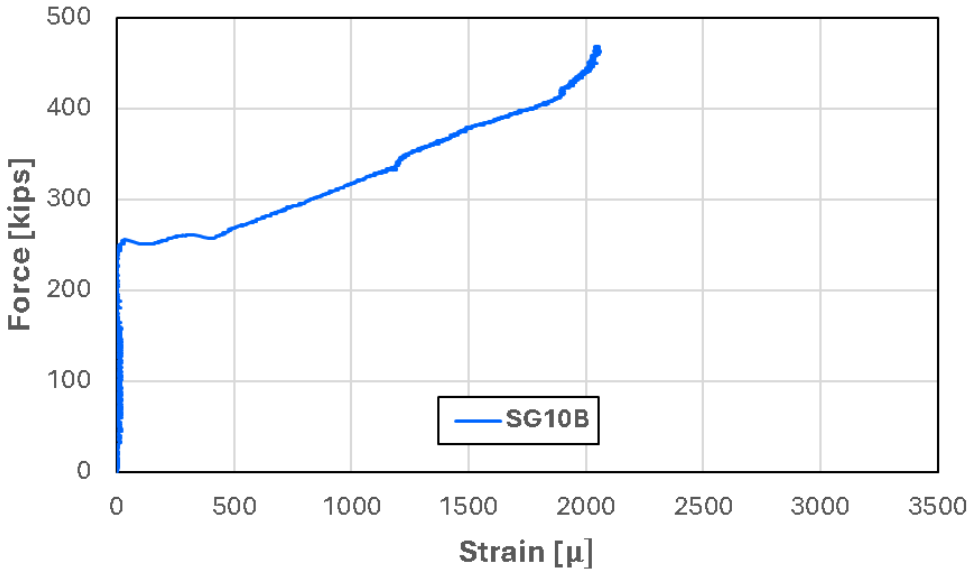

Figure D.127: Force plotted against SG10B strain for Specimen 8

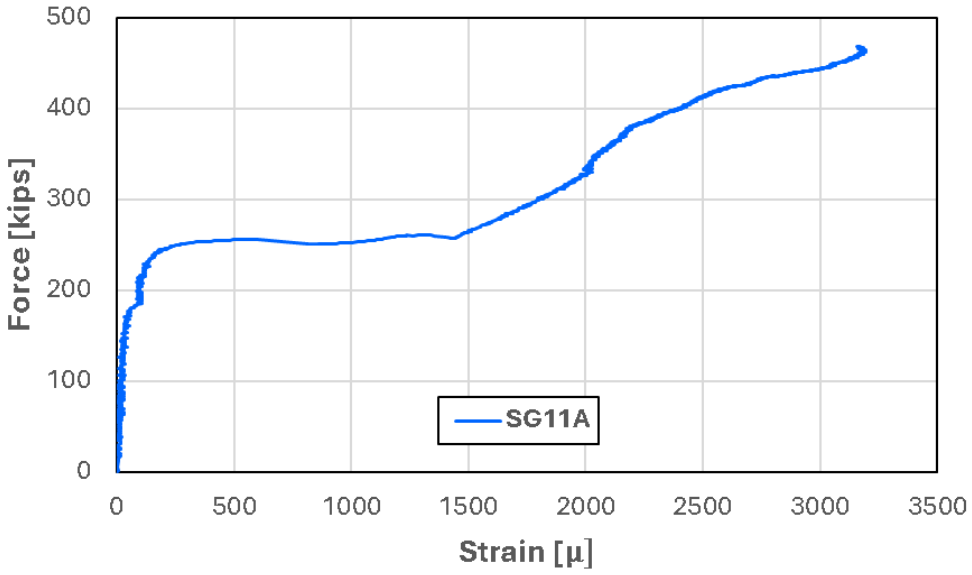

Figure D.128: Force plotted against SG11A strain for Specimen 8

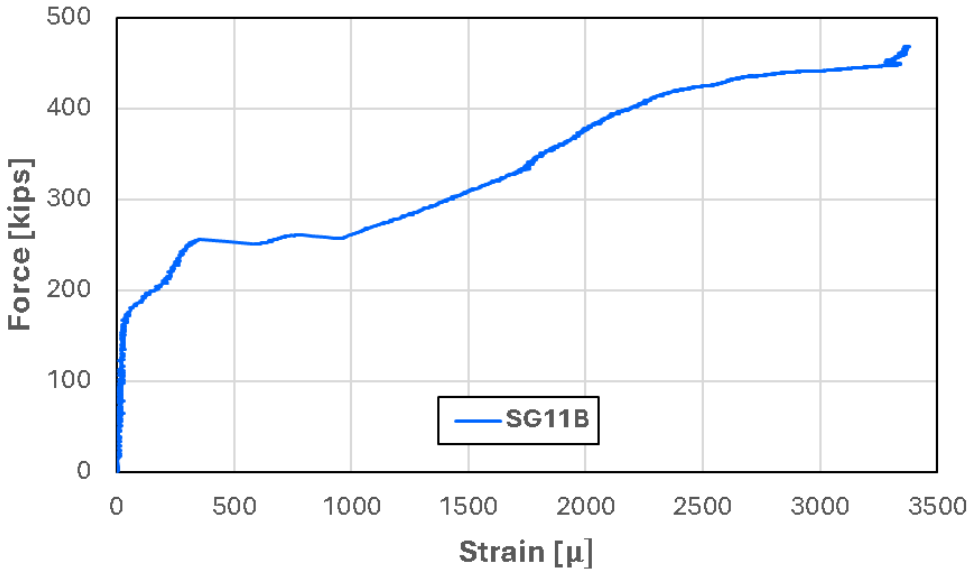

Figure D.129: Force plotted against SG11B strain for Specimen 8

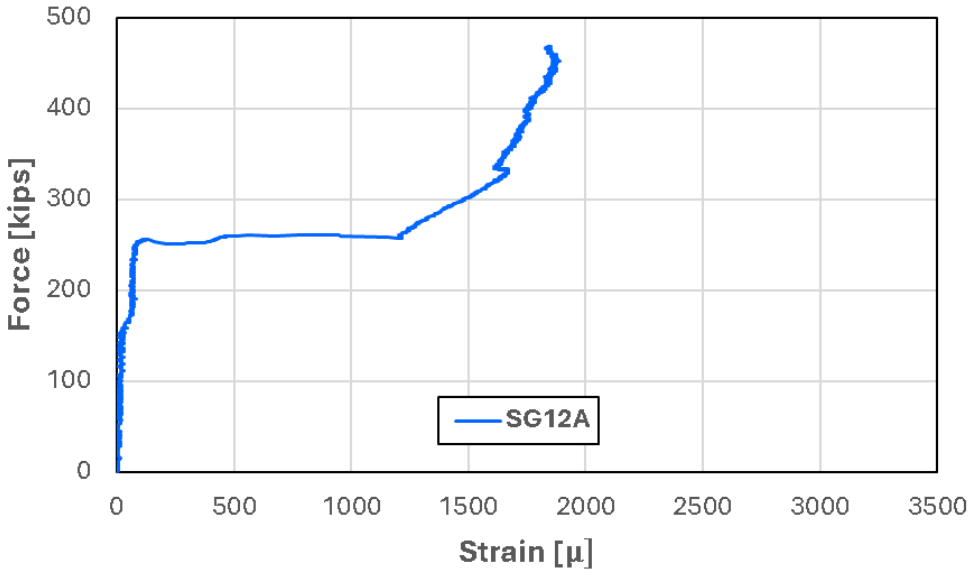

Figure D.130: Force plotted against SG12A strain for Specimen 8

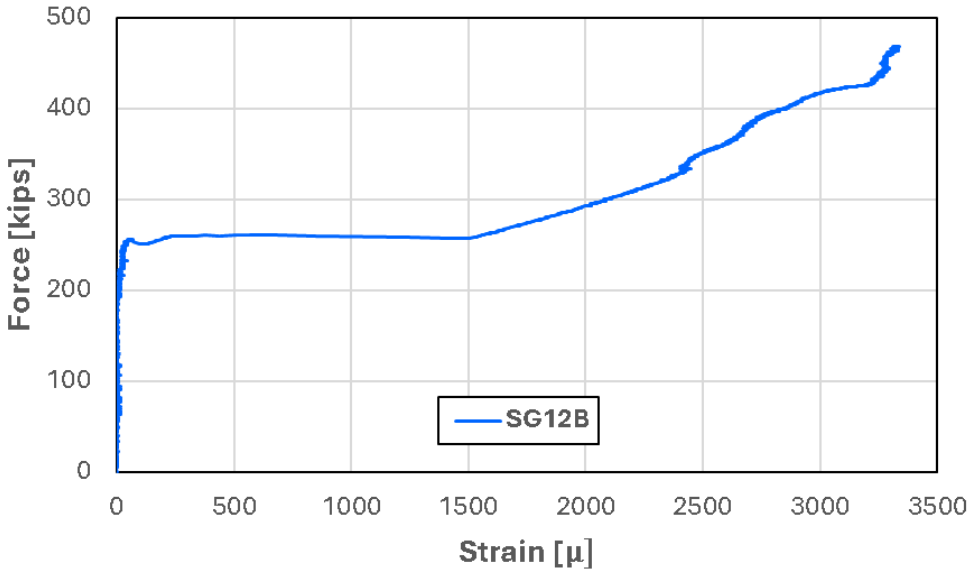

Figure D.131: Force plotted against SG12B strain for Specimen 8

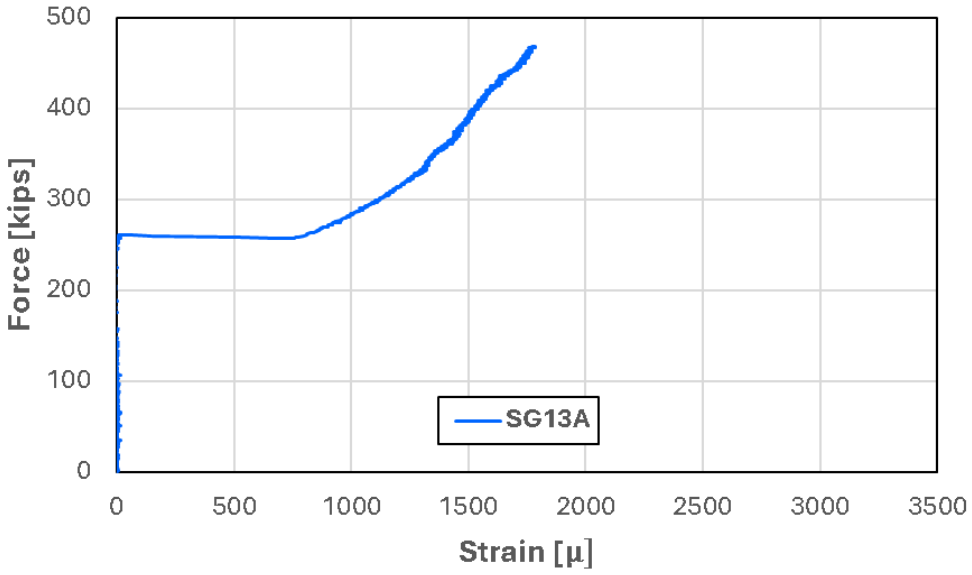

Figure D.132: Force plotted against SG13A strain for Specimen 8

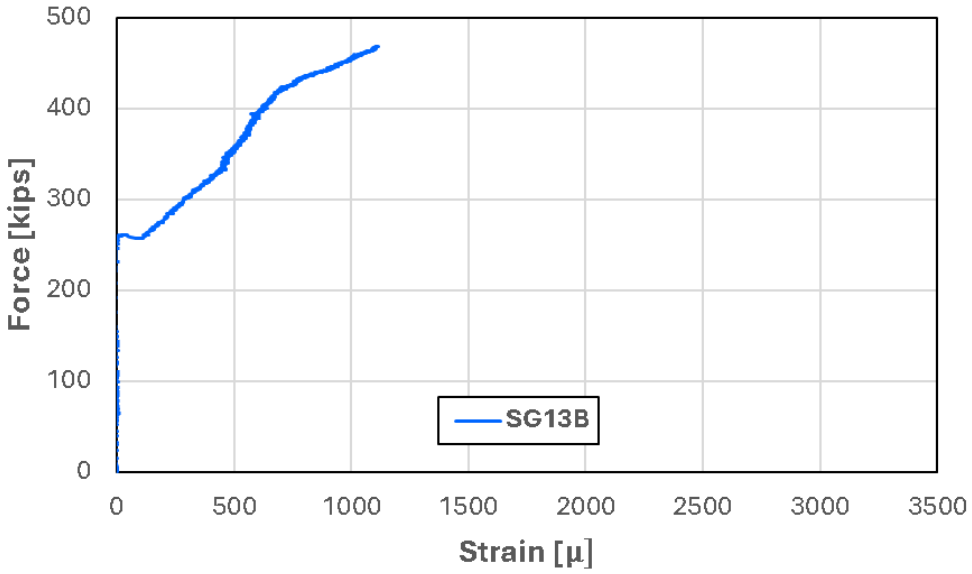

Figure D.133: Force plotted against SG13B strain for Specimen 8

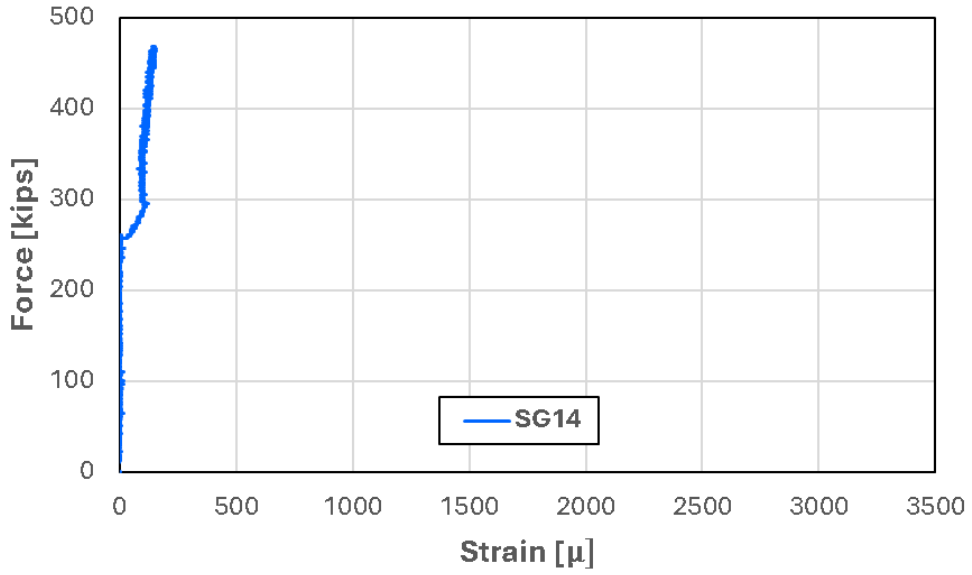

Figure D.134: Force plotted against SG14 strain for Specimen 8

D.9 Specimen 9

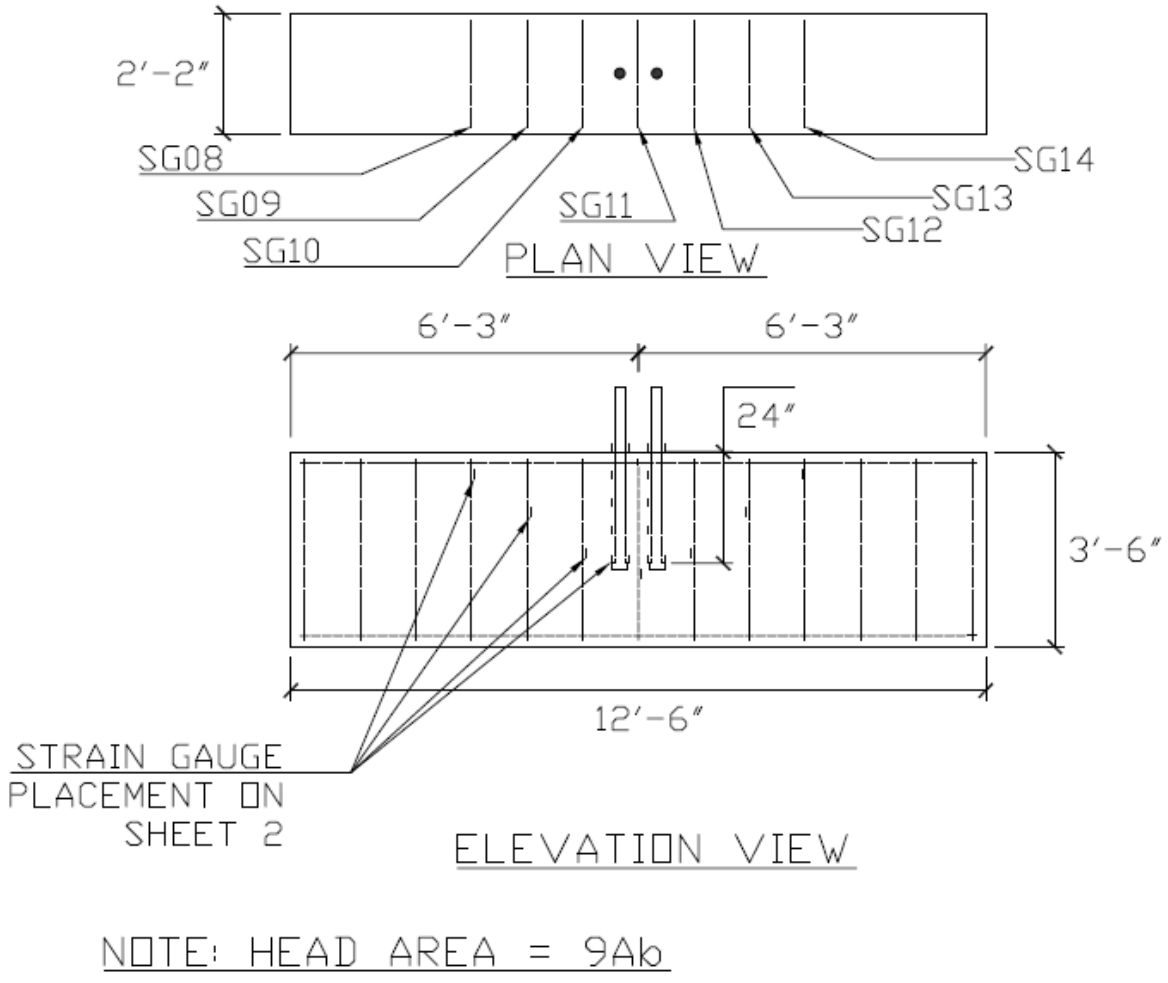

Figure D.135: Locations of strain gauges for Specimen 9

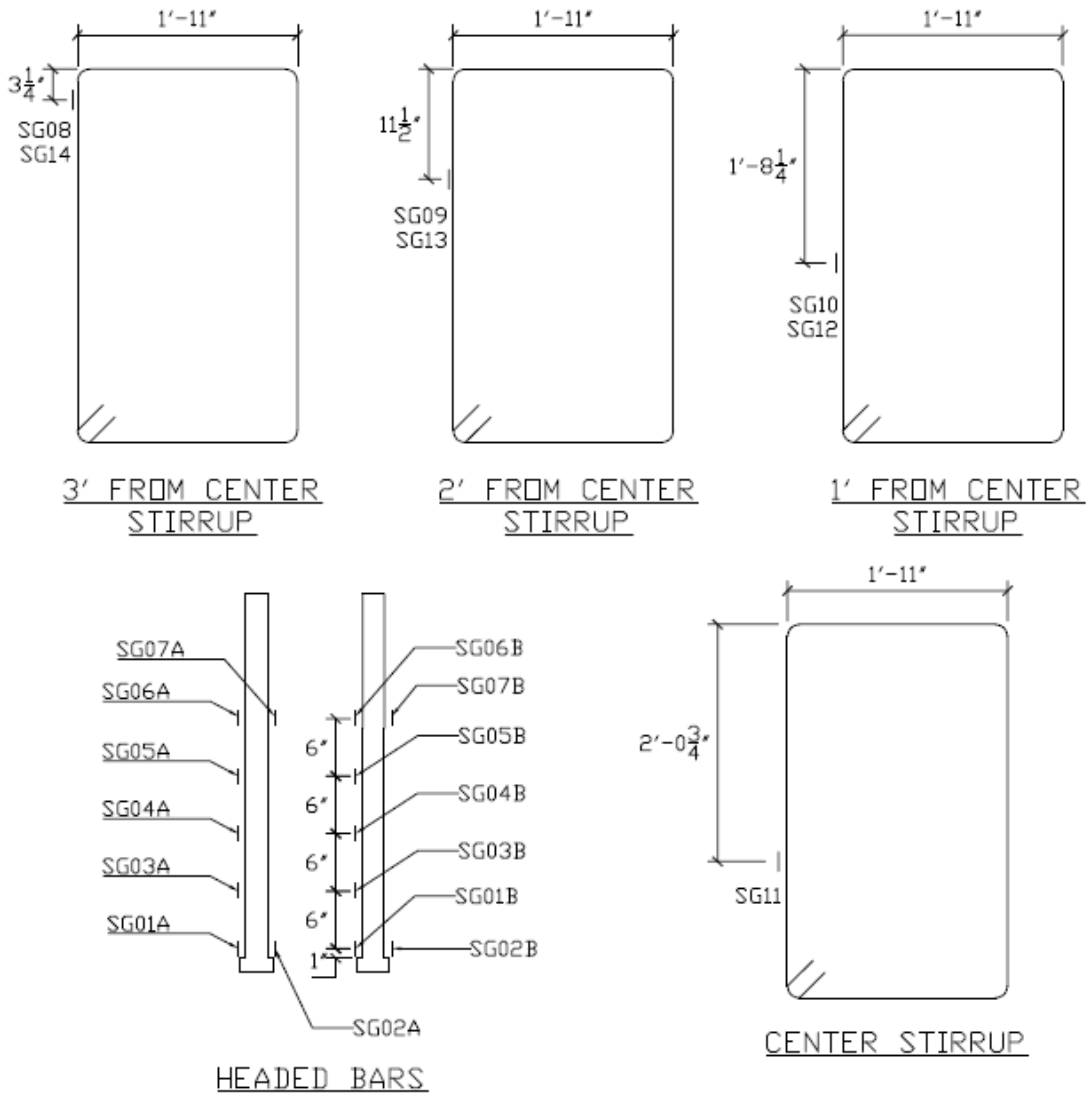

Figure D.136: Locations of stirrup and headed bar strain gauges and their labels for Specimen 9

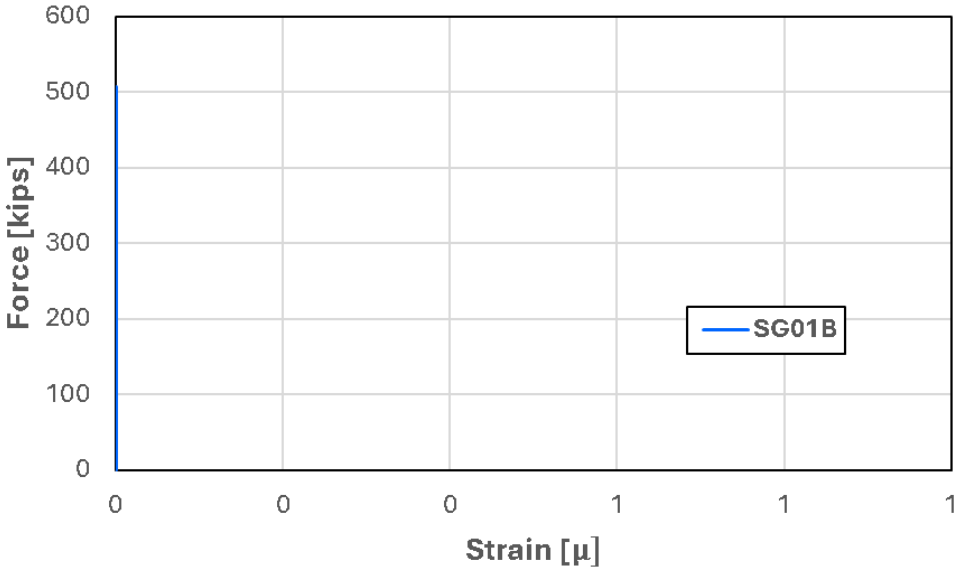

Figure D.137: Force plotted against SG01B strain for Specimen 9

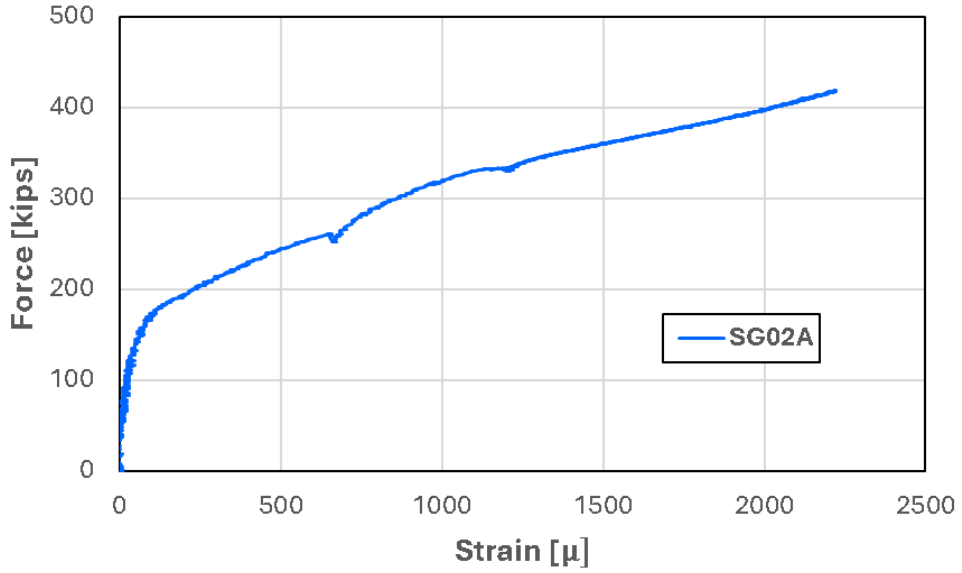

Figure D.138: Force plotted against SG02A strain for Specimen 9

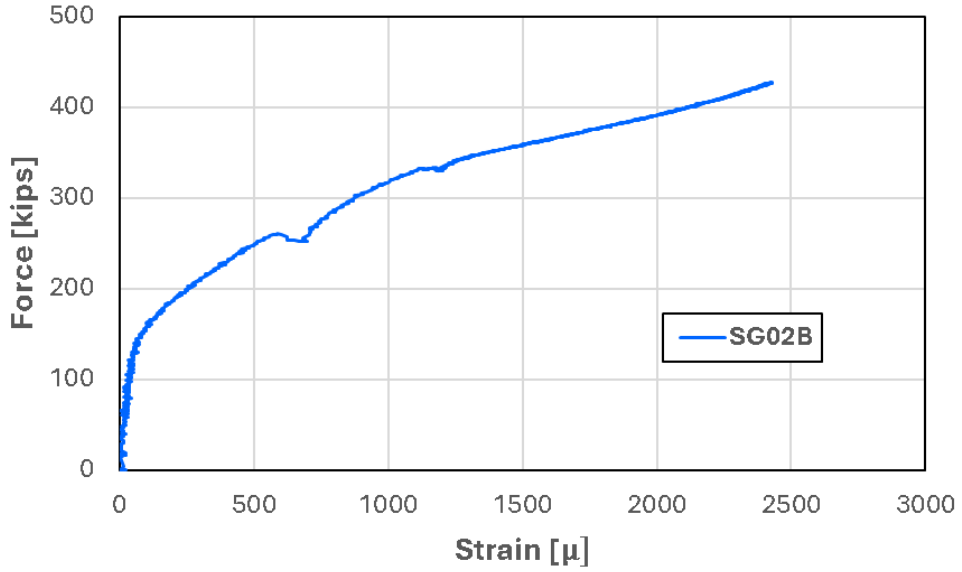

Figure D.139: Force plotted against SG02B strain for Specimen 9

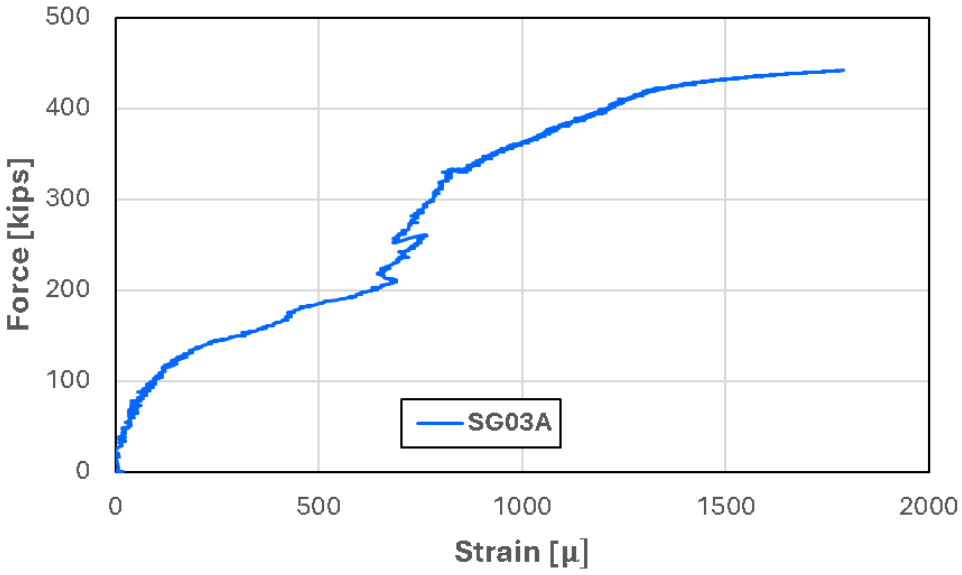

Figure D.140: Force plotted against SG03A strain for Specimen 9

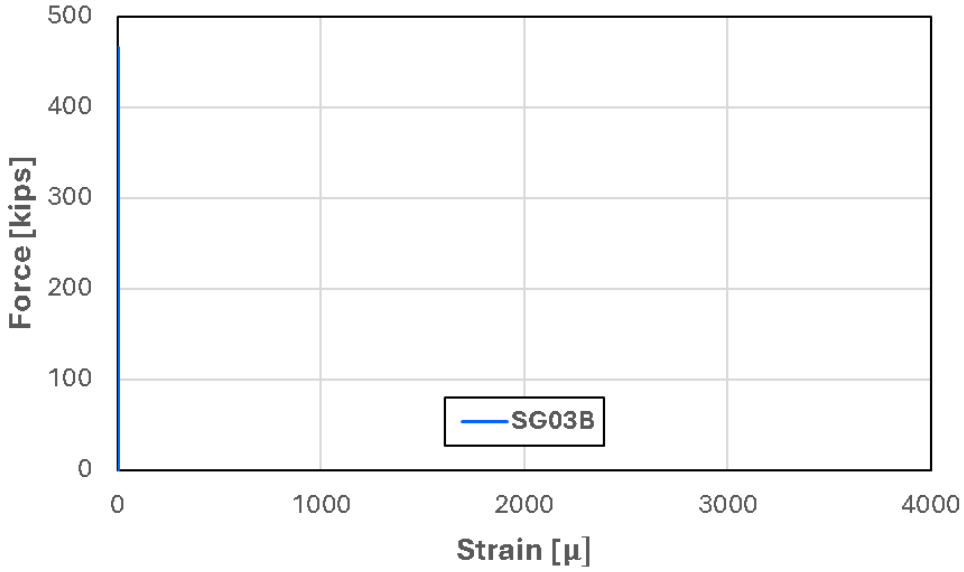

Figure D.141: Force plotted against SG03B strain for Specimen 9

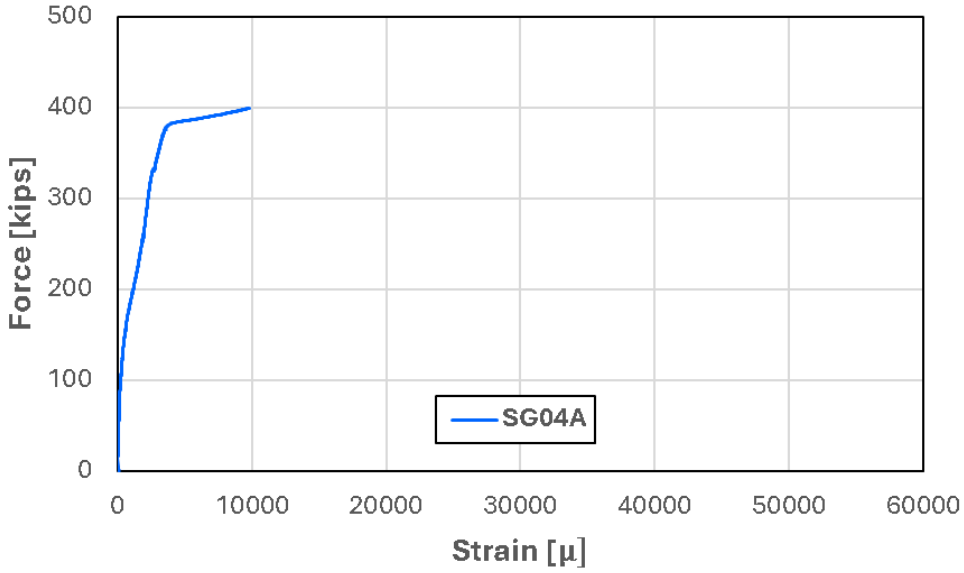

Figure D.142: Force plotted against SG04A strain for Specimen 9

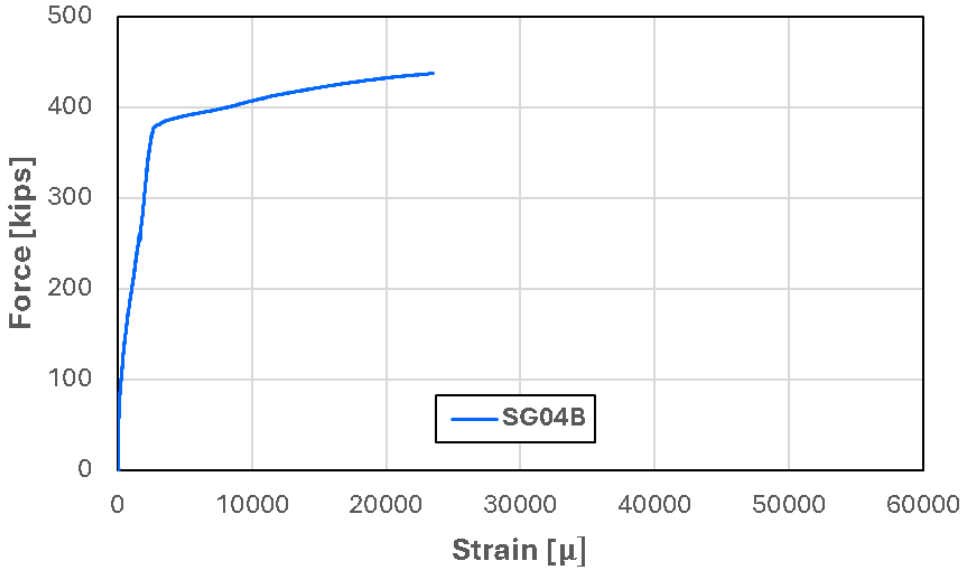

Figure D.143: Force plotted against SG04B strain for Specimen 9

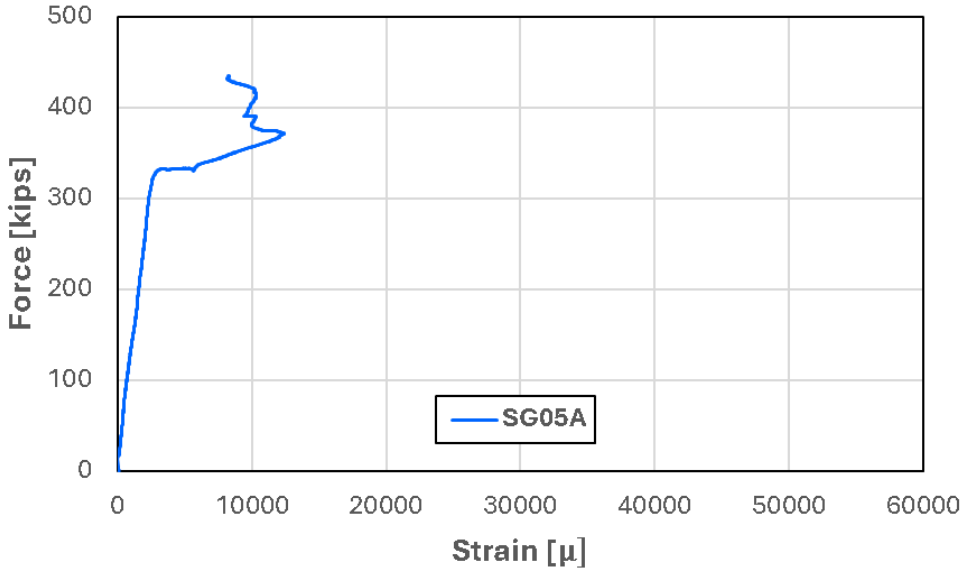

Figure D.144: Force plotted against SG05A strain for Specimen 9

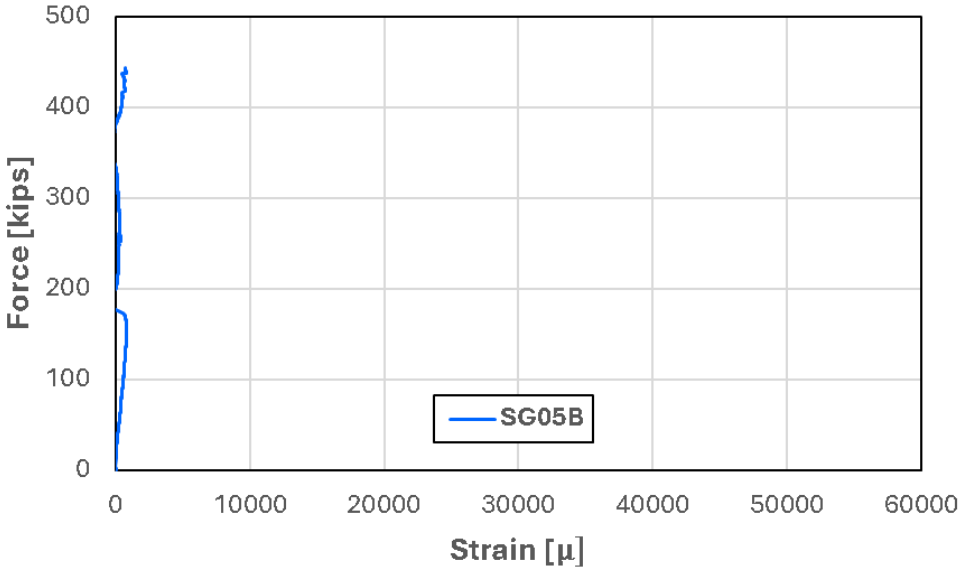

Figure D.145: Force plotted against SG05B strain for Specimen 9

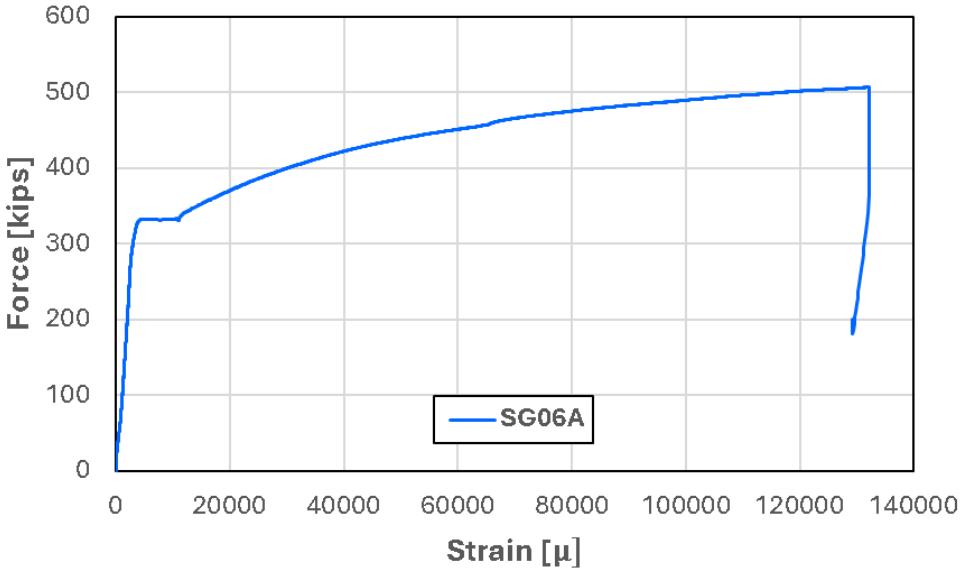

Figure D.146: Force plotted against SG06A strain for Specimen 9

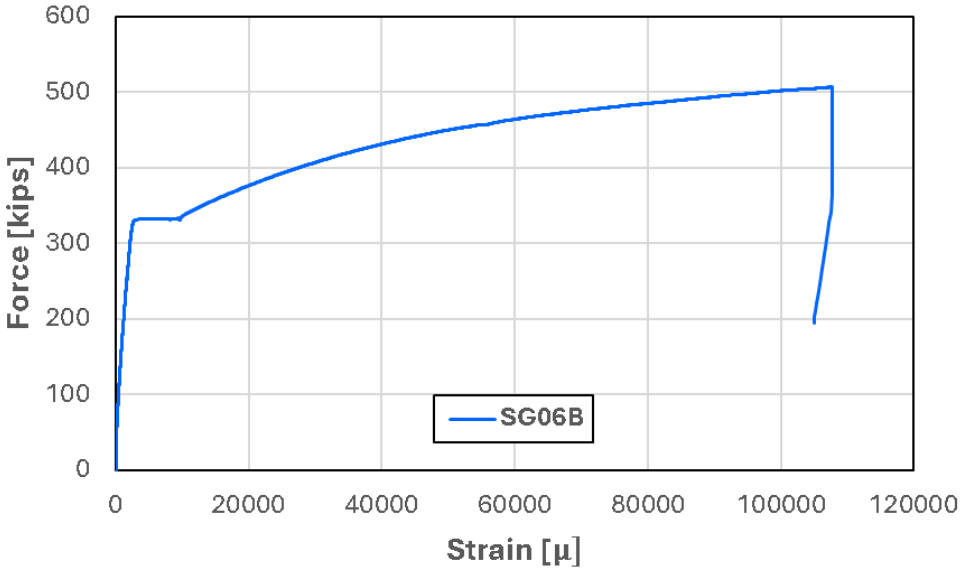

Figure D.147: Force plotted against SG06B strain for Specimen 9

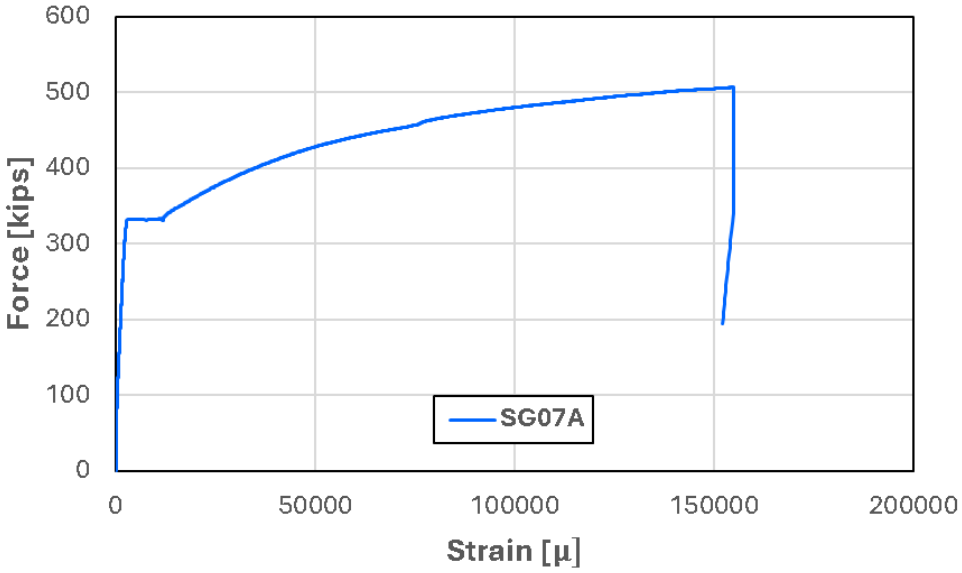

Figure D.148: Force plotted against SG07A strain for Specimen 9

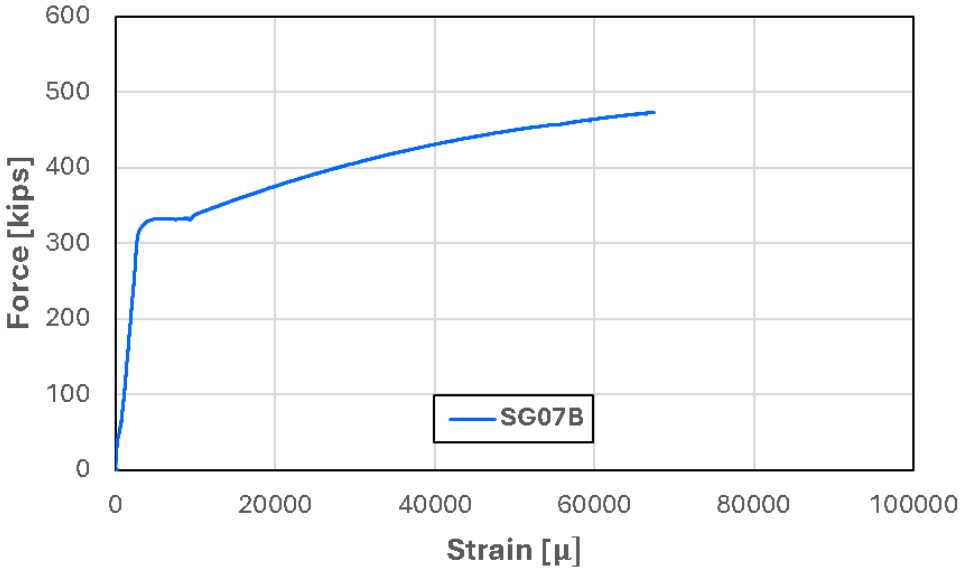

Figure D.149: Force plotted against SG07B strain for Specimen 9

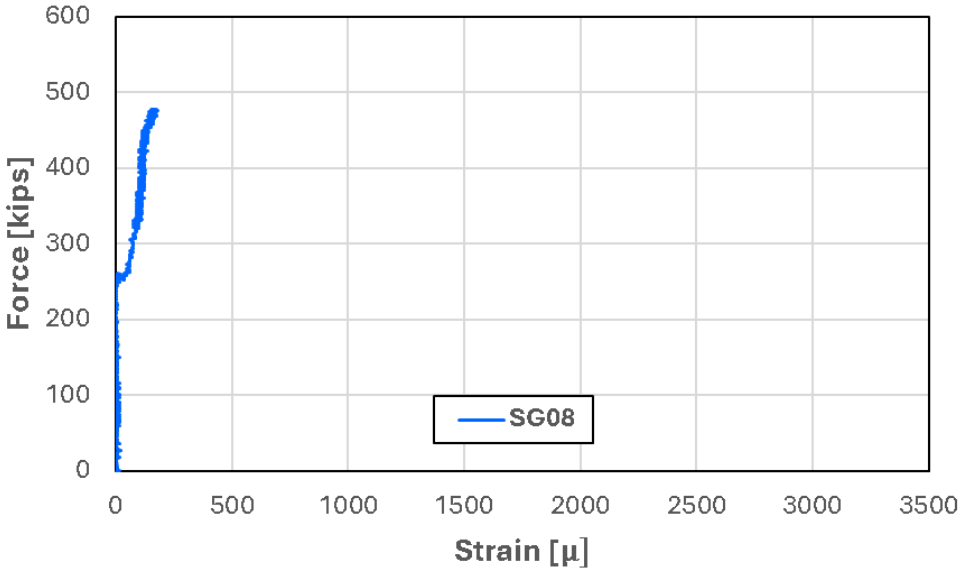

Figure D.150: Force plotted against SG08 strain for Specimen 9

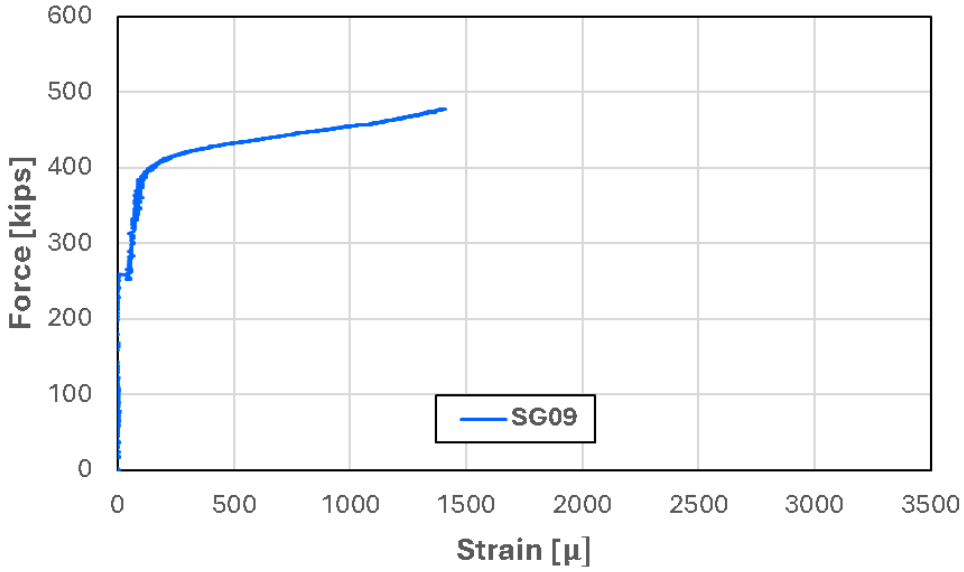

Figure D.151: Force plotted against SG09 strain for Specimen 9

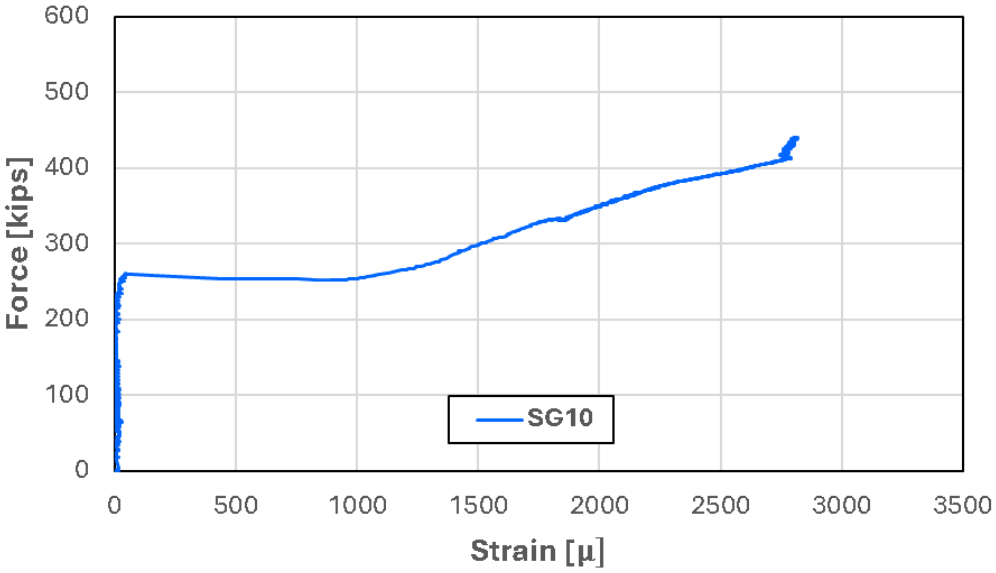

Figure D.152: Force plotted against SG10 strain for Specimen 9

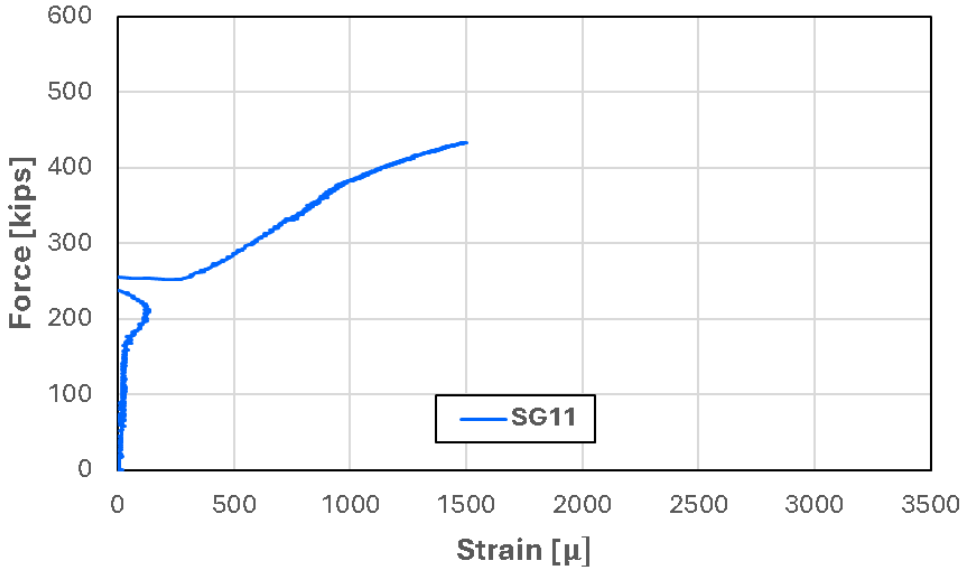

Figure D.153: Force plotted against SG11 strain for Specimen 9

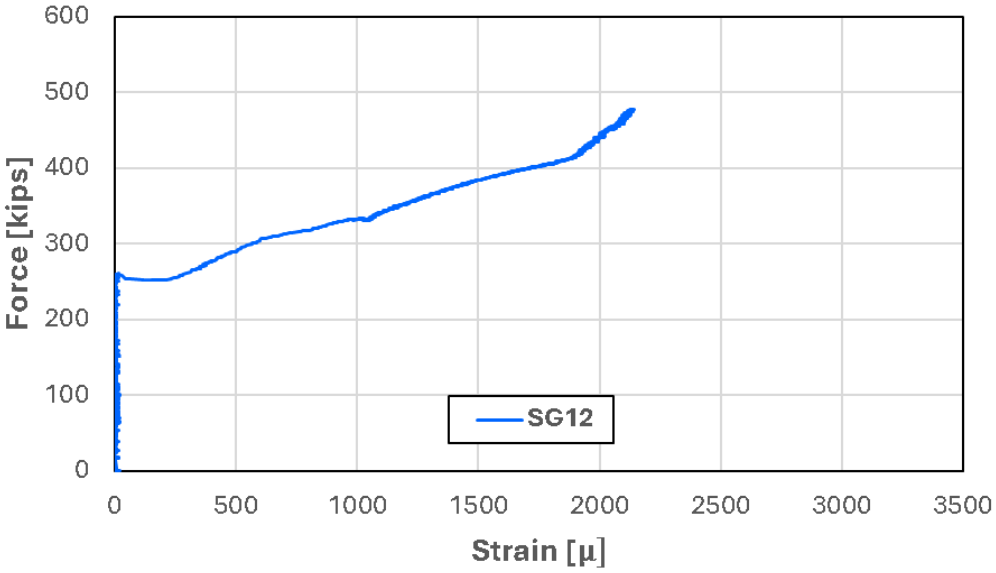

Figure D.154: Force plotted against SG12 strain for Specimen 9

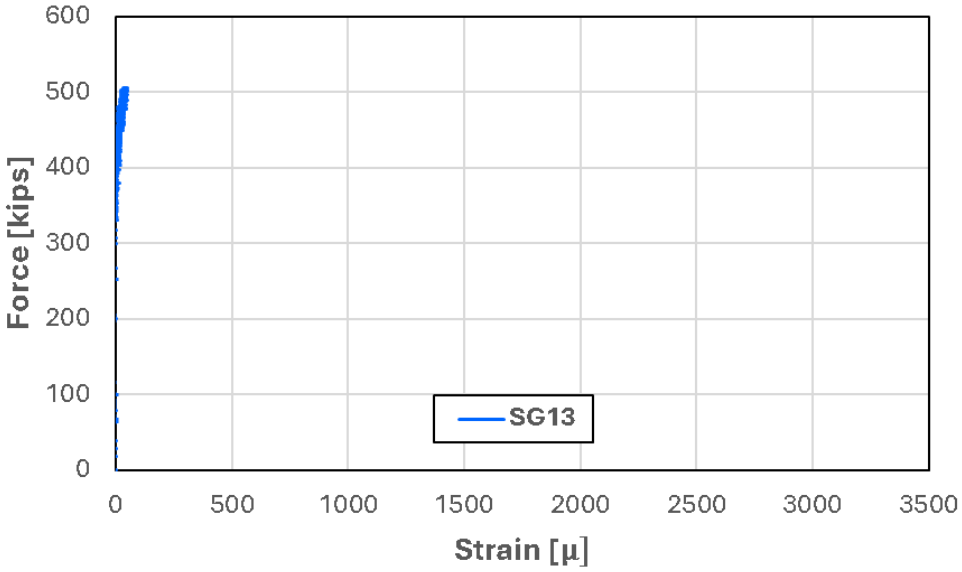

Figure D.155: Force plotted against SG13 strain for Specimen 9

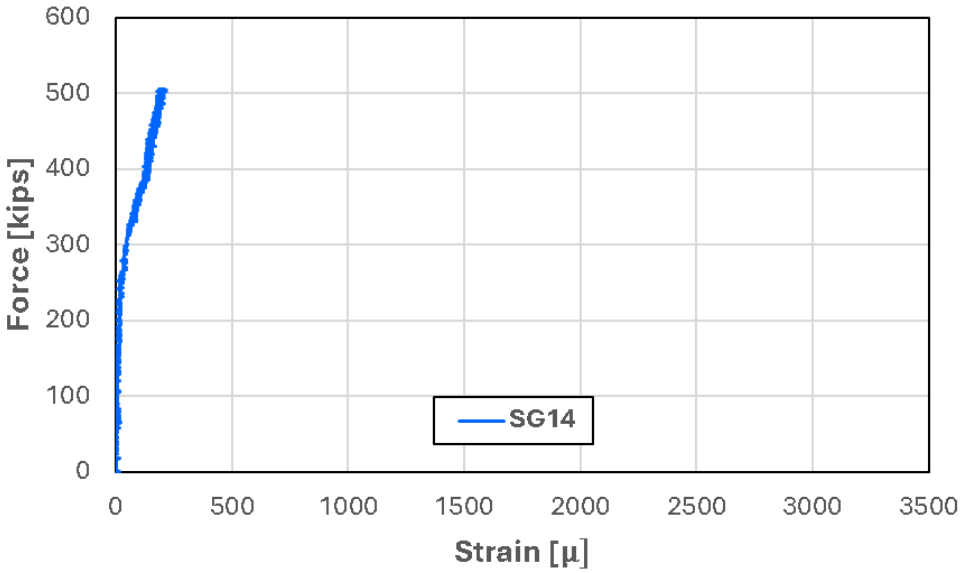

Figure D.156: Force plotted against SG14 strain for Specimen 9

D.10 Specimen 10

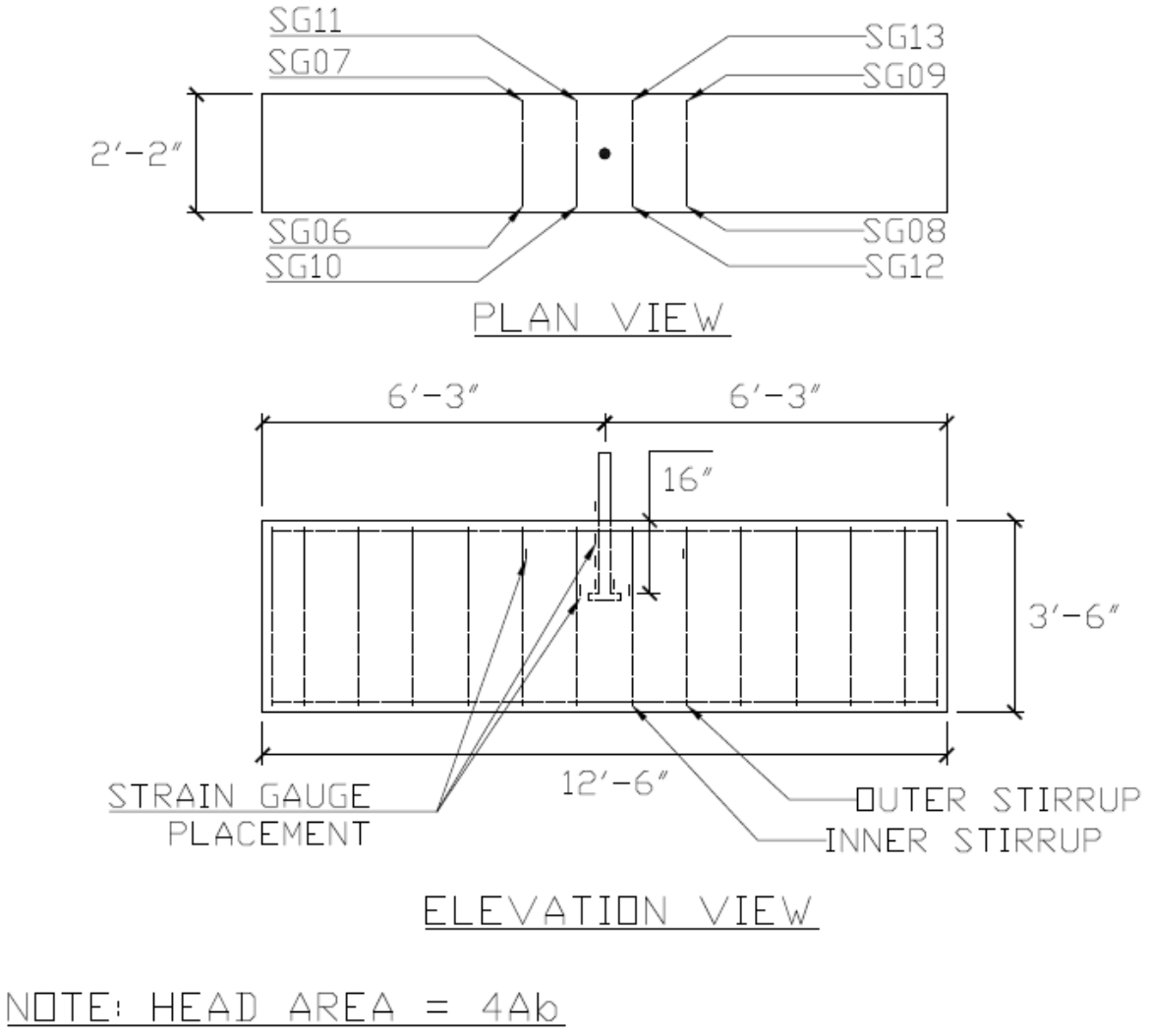

Figure D.157: Locations of strain gauges for Specimen 10

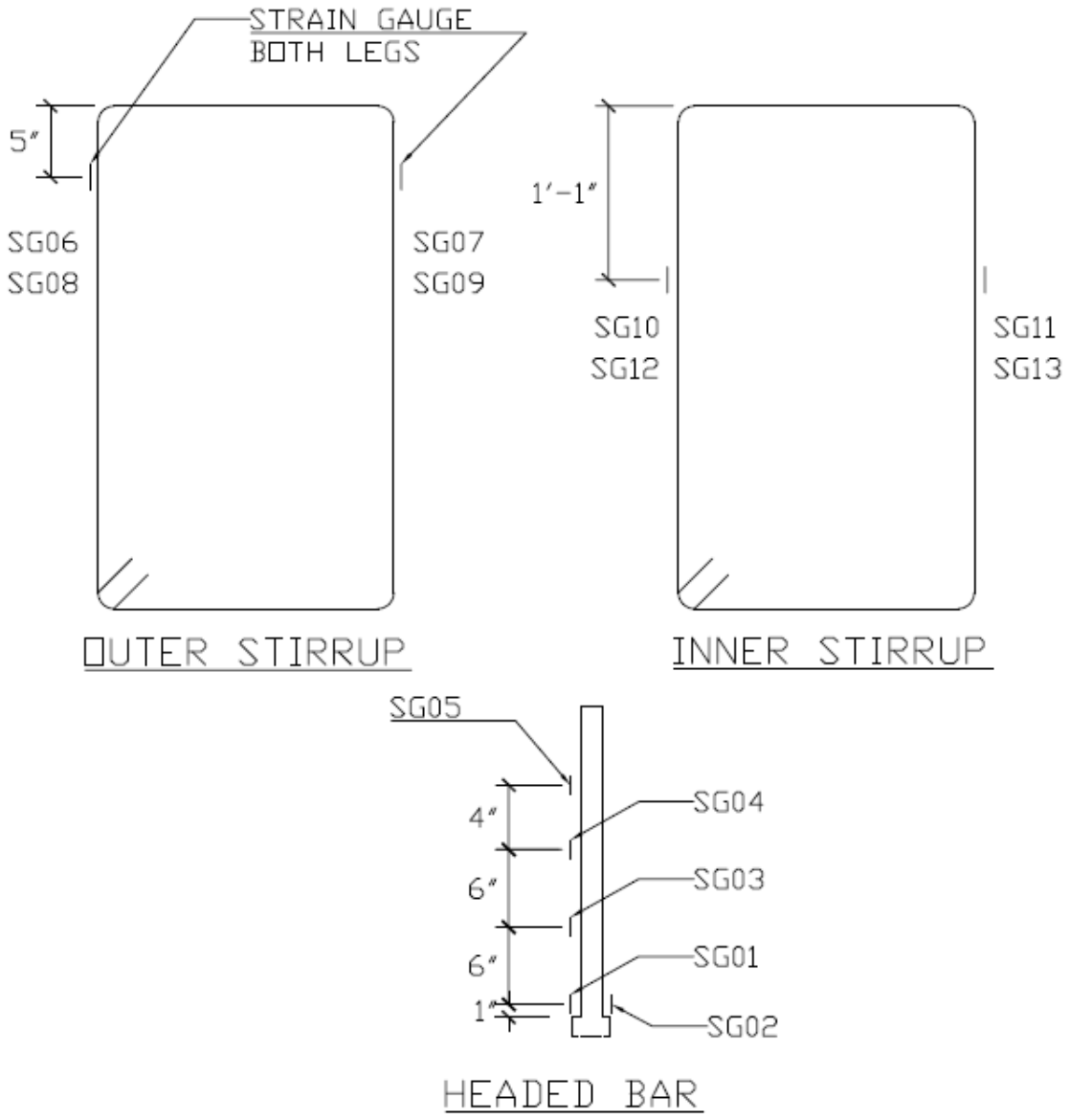

Figure D.158: Locations of stirrup and headed bar strain gauges and their labels for Specimen 10

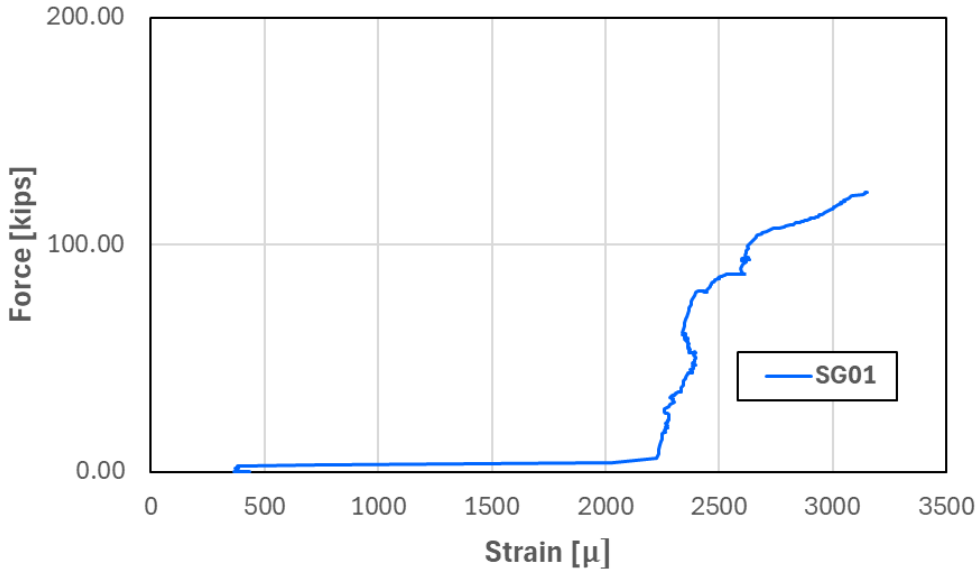

Figure D.159: Force plotted against SG01 strain for Specimen 10

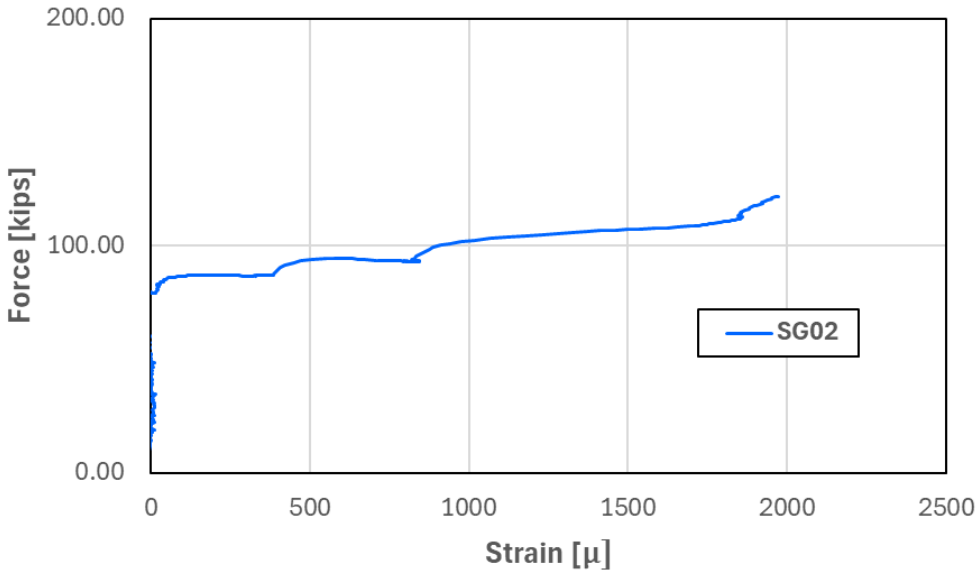

Figure D.160: Force plotted against SG02 strain for Specimen 10

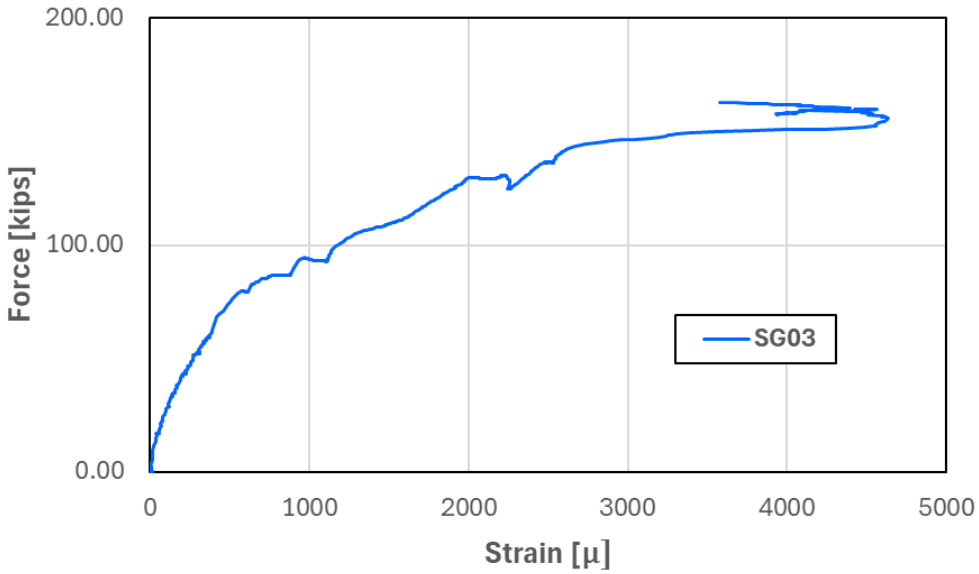

Figure D.161: Force plotted against SG03 strain for Specimen 10

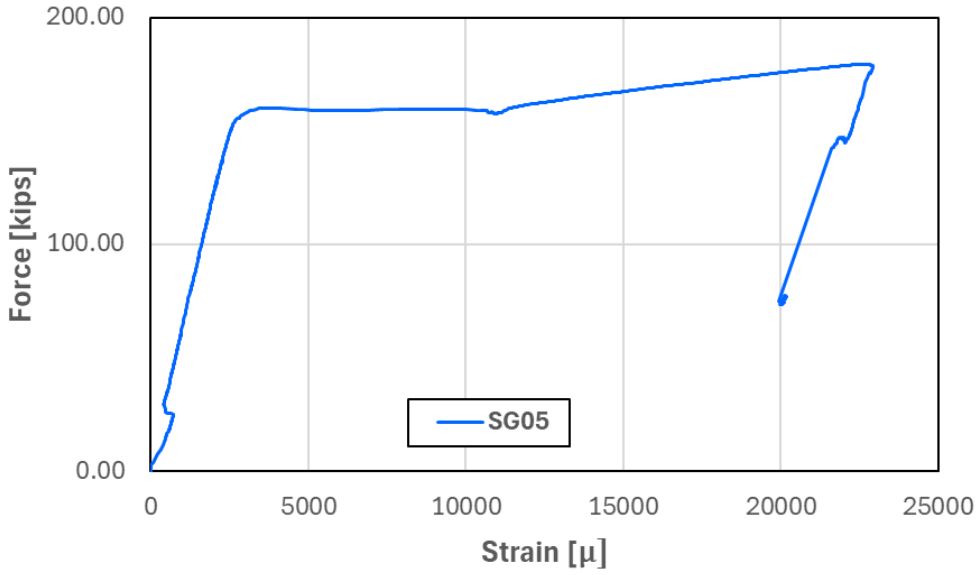

Figure D.162: Force plotted against SG05 strain for Specimen 10

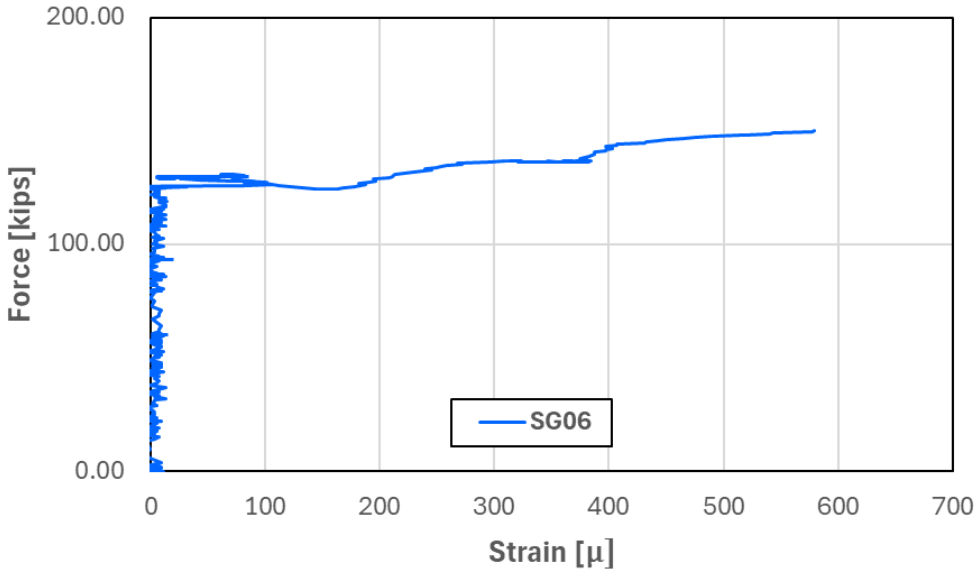

Figure D.163: Force plotted against SG06 strain for Specimen 10

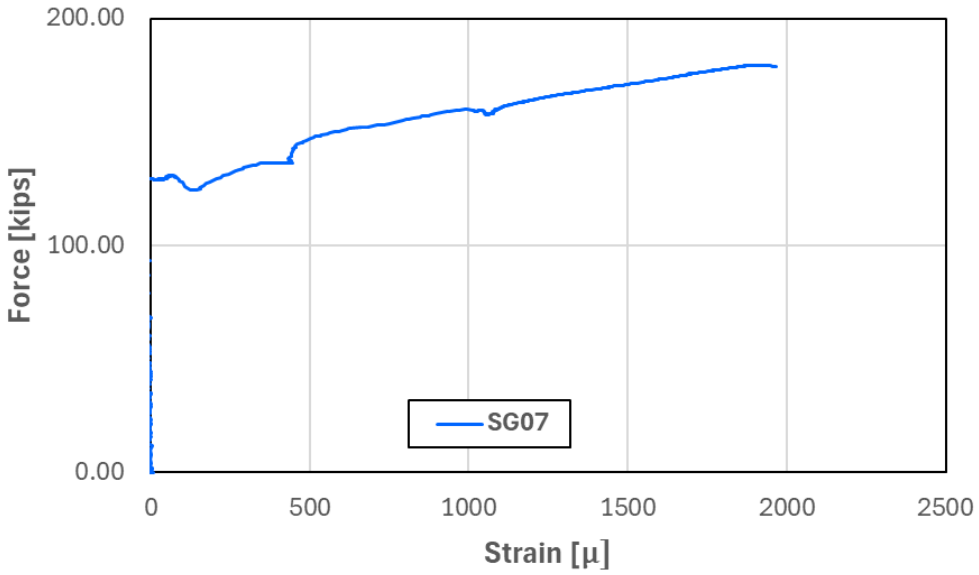

Figure D.164: Force plotted against SG07 strain for Specimen 10

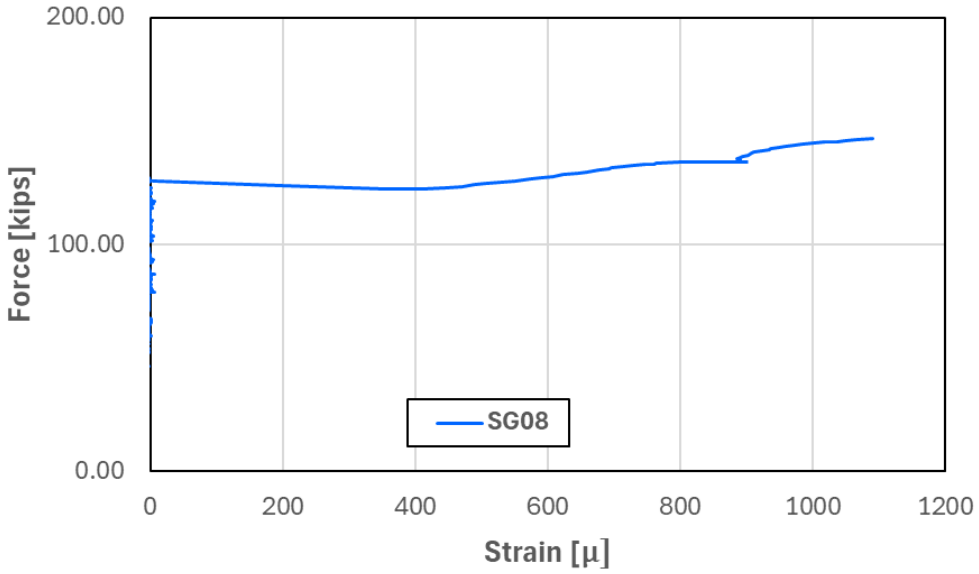

Figure D.165: Force plotted against SG08 strain for Specimen 10

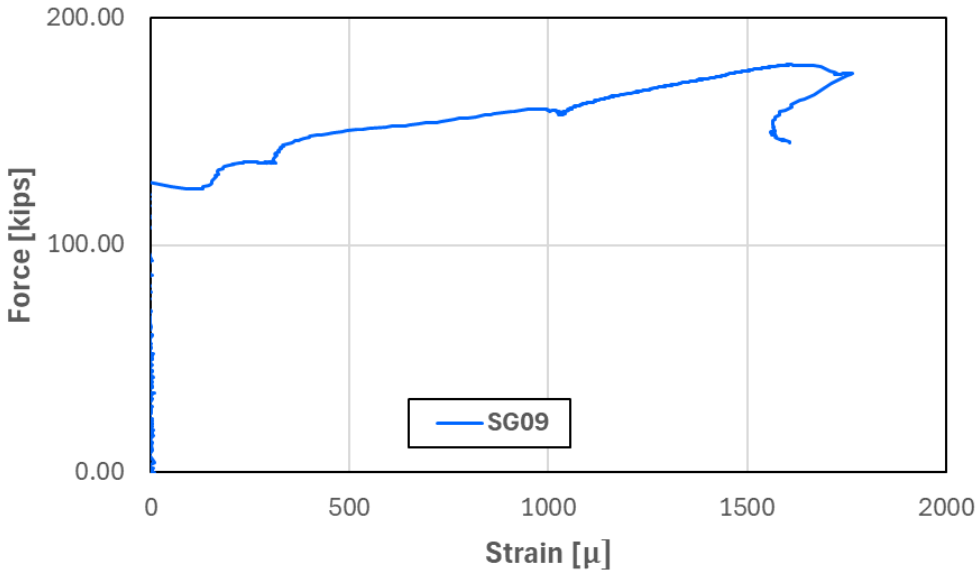

Figure D.166: Force plotted against SG09 strain for Specimen 10

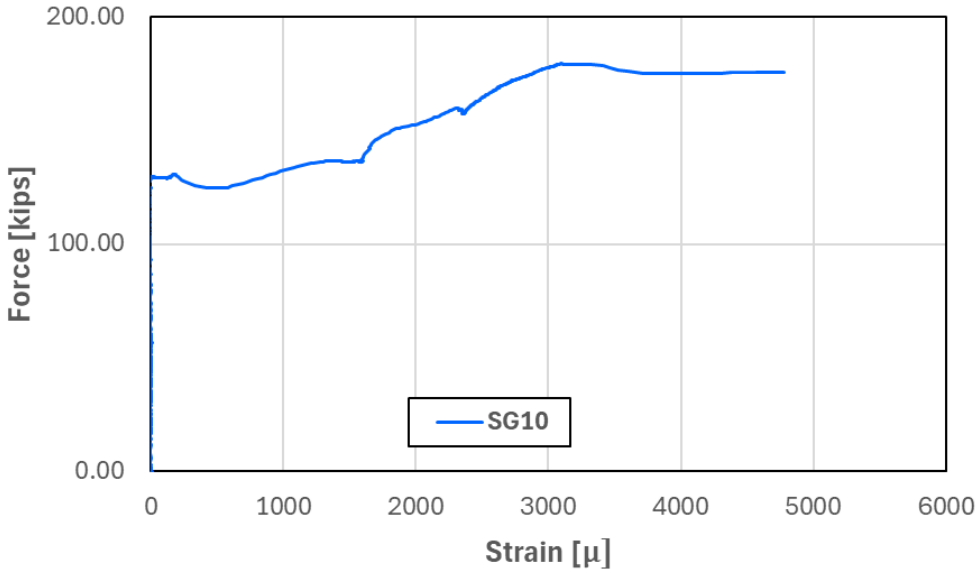

Figure D.167: Force plotted against SG10 strain for Specimen 10

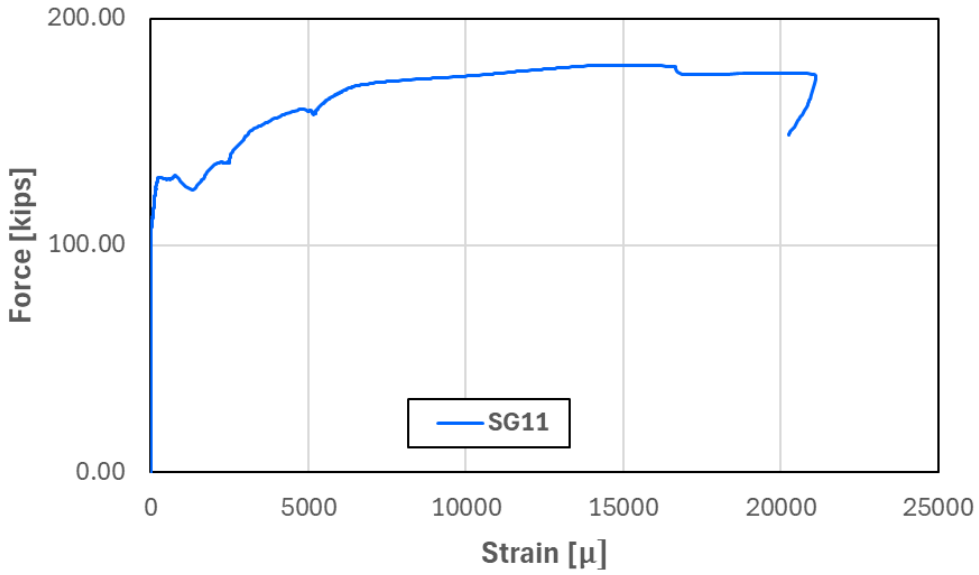

Figure D.168: Force plotted against SG11 strain for Specimen 10

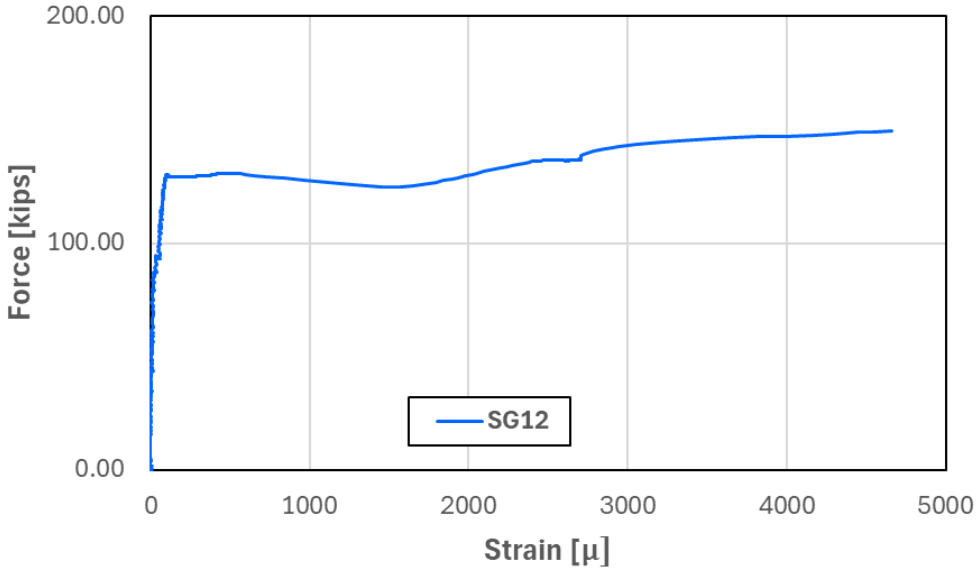

Figure D.169: Force plotted against SG12 strain for Specimen 10

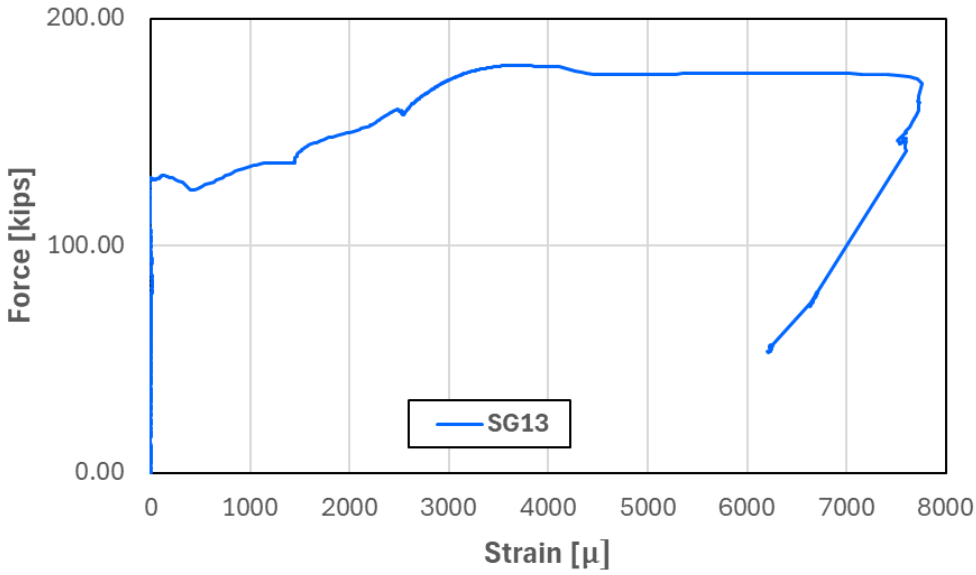

Figure D.170: Force plotted against SG13 strain for Specimen 10

D.11 Specimen 11

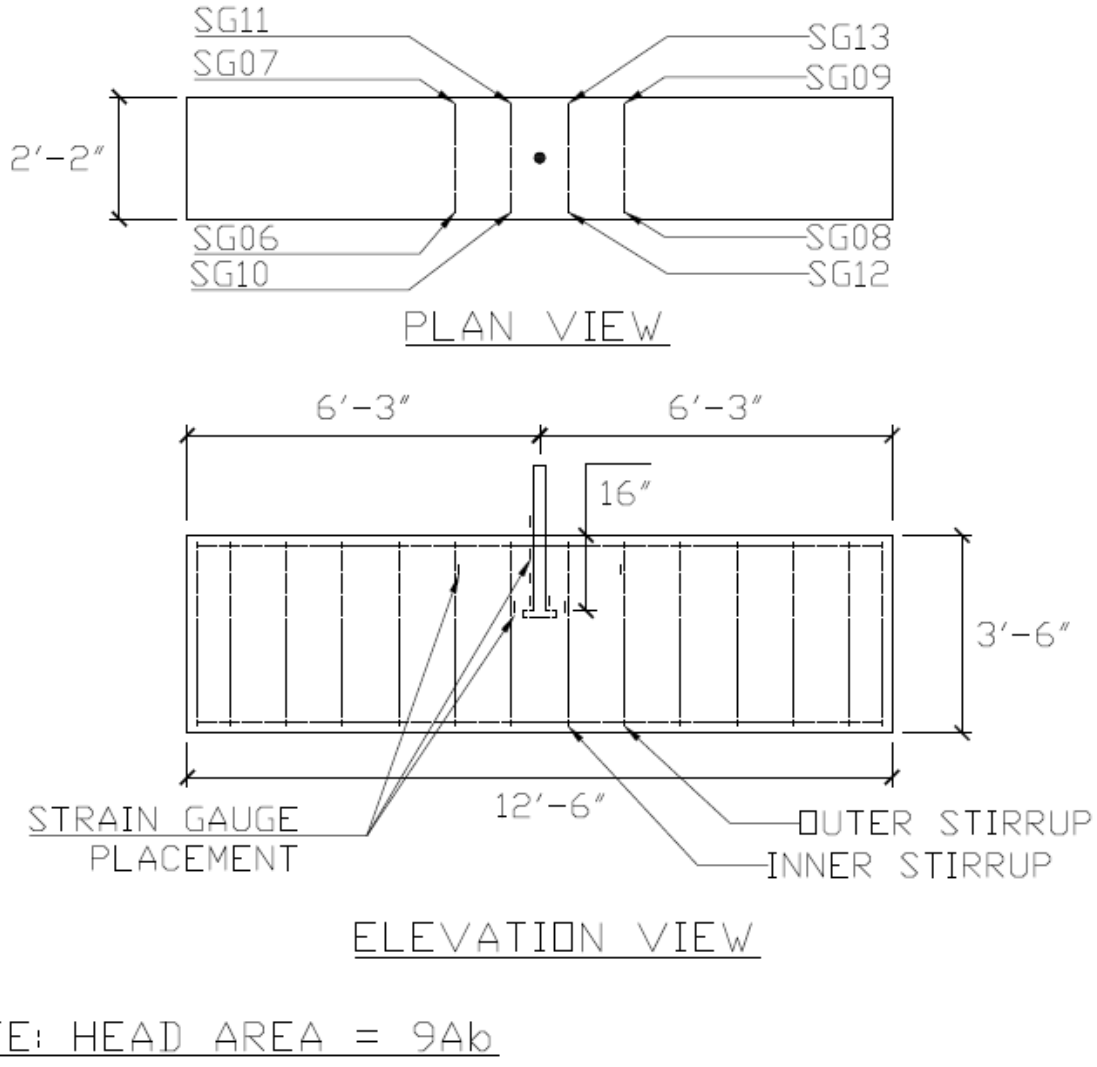

Figure D.171: Locations of strain gauges for Specimen 11

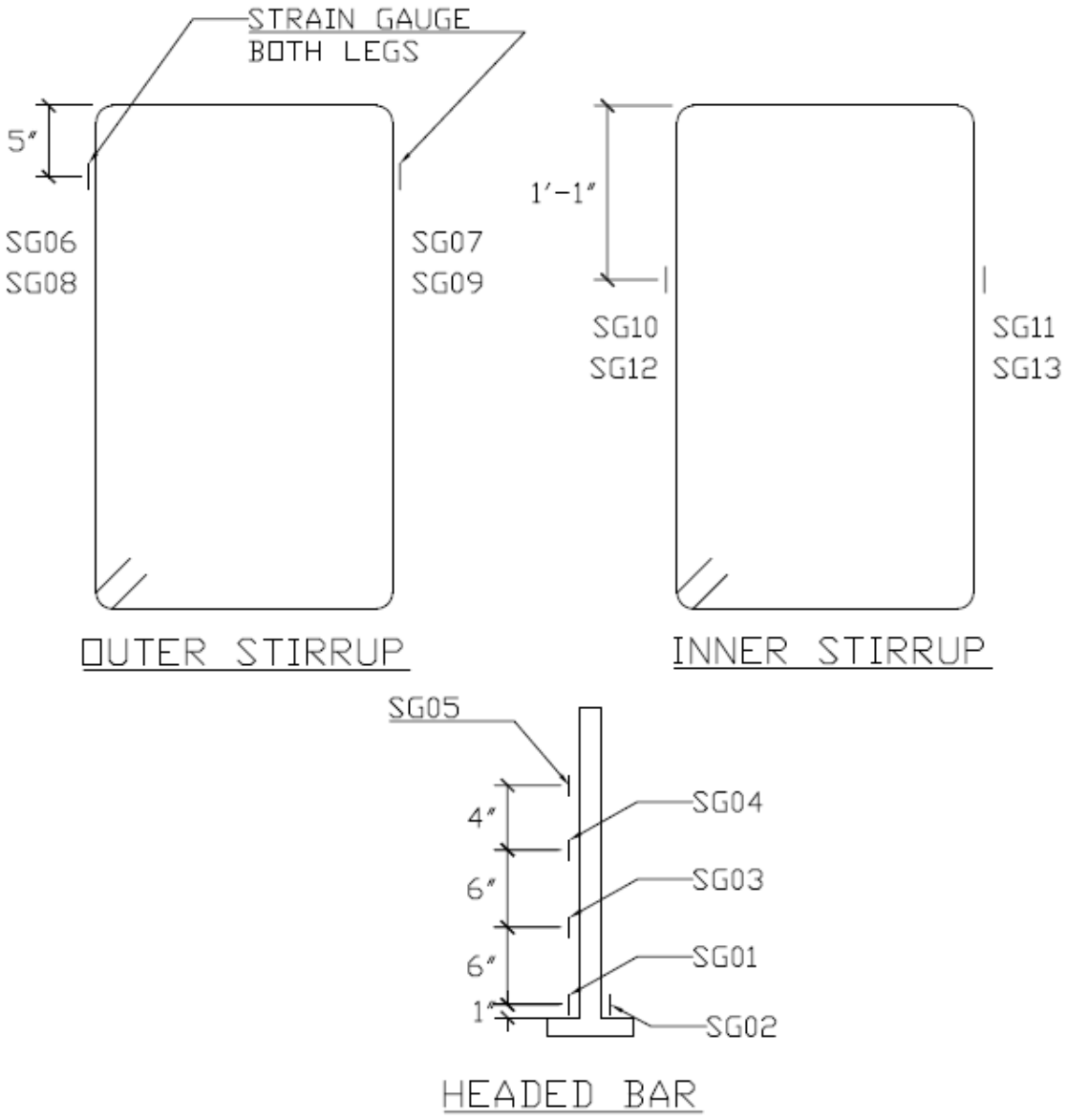

Figure D.172: Locations of stirrup and headed bar strain gauges and their labels for Specimen 11

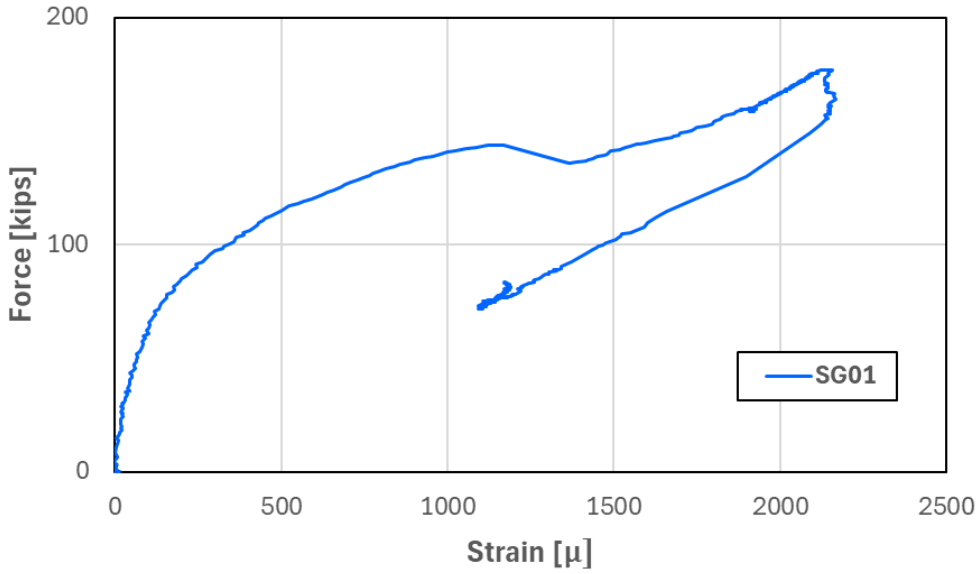

Figure D.173: Force plotted against SG01 strain for Specimen 11

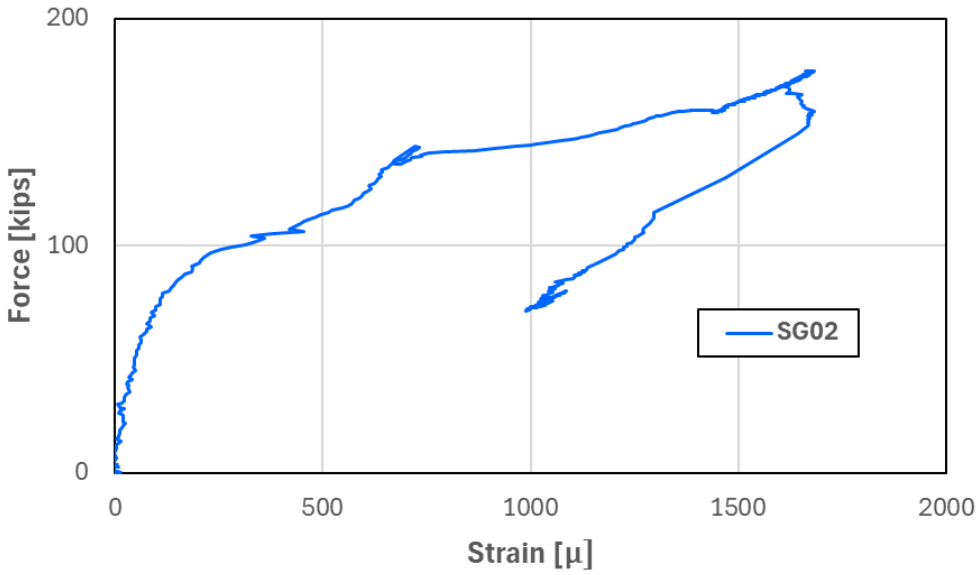

Figure D.174: Force plotted against SG02 strain for Specimen 11

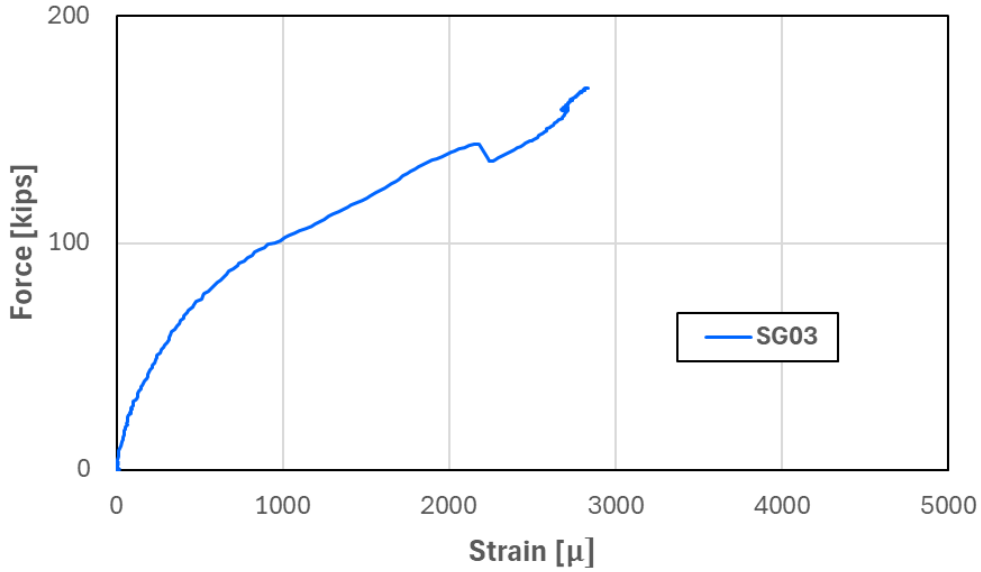

Figure D.175: Force plotted against SG03 strain for Specimen 11

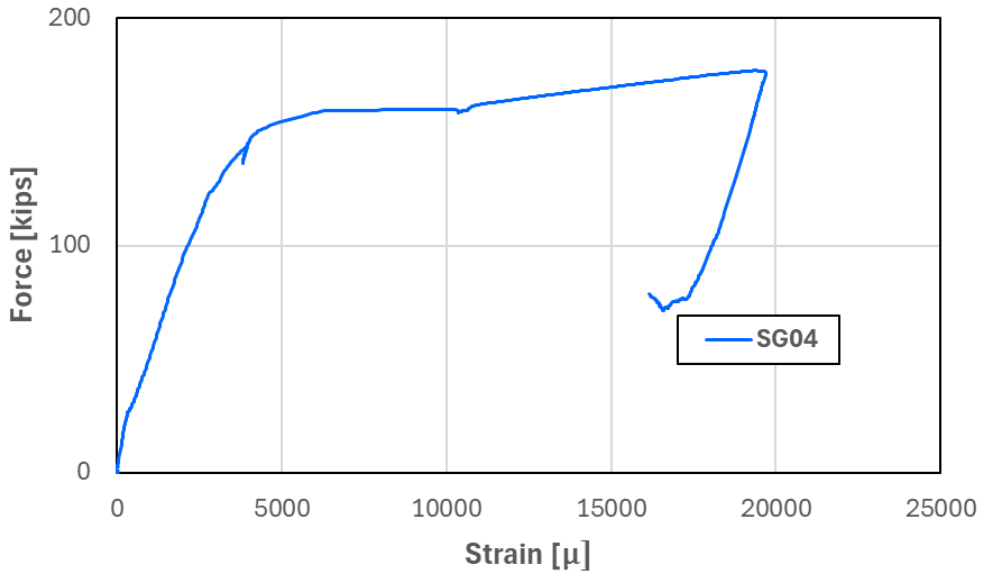

Figure D.176: Force plotted against SG04 strain for Specimen 11

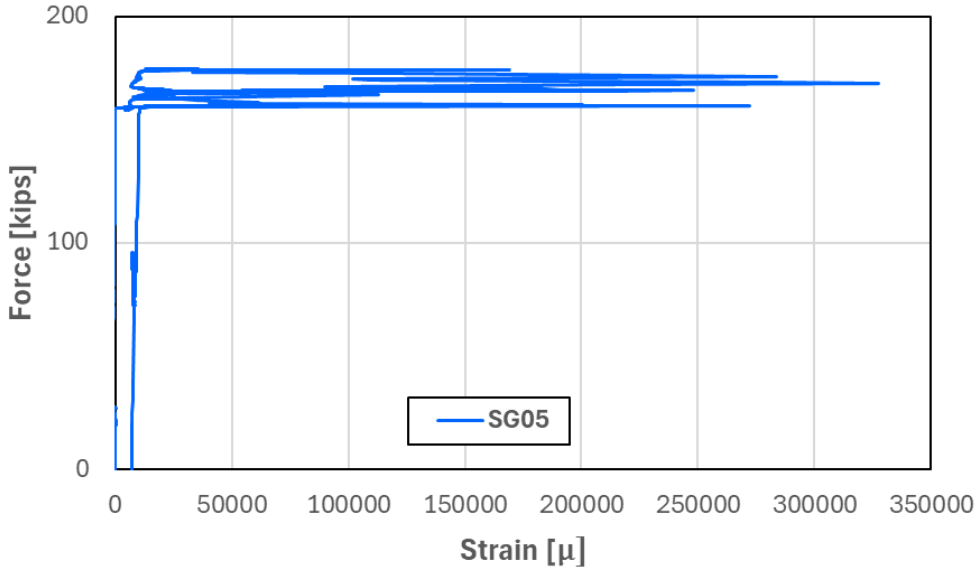

Figure D.177: Force plotted against SG05 strain for Specimen 11

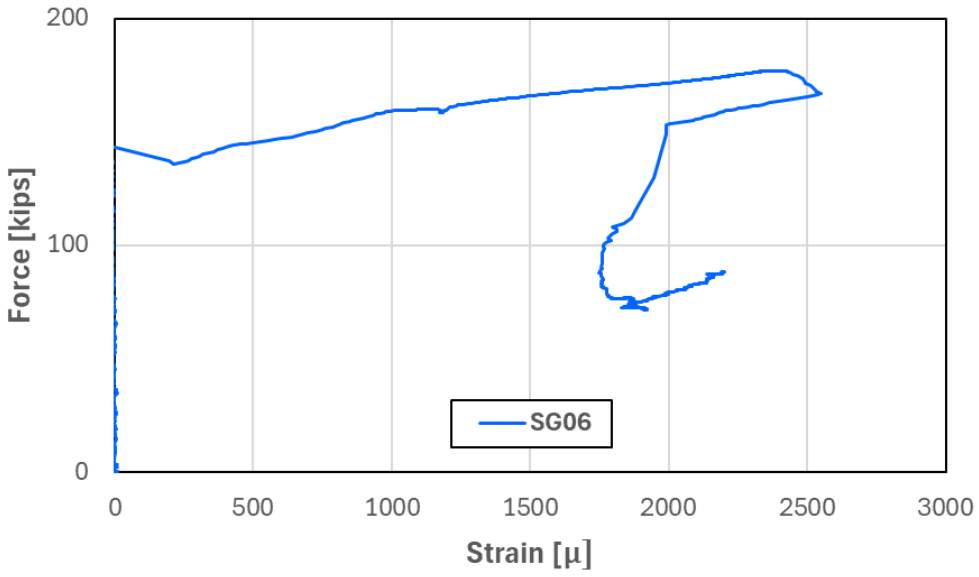

Figure D.178: Force plotted against SG06 strain for Specimen 11

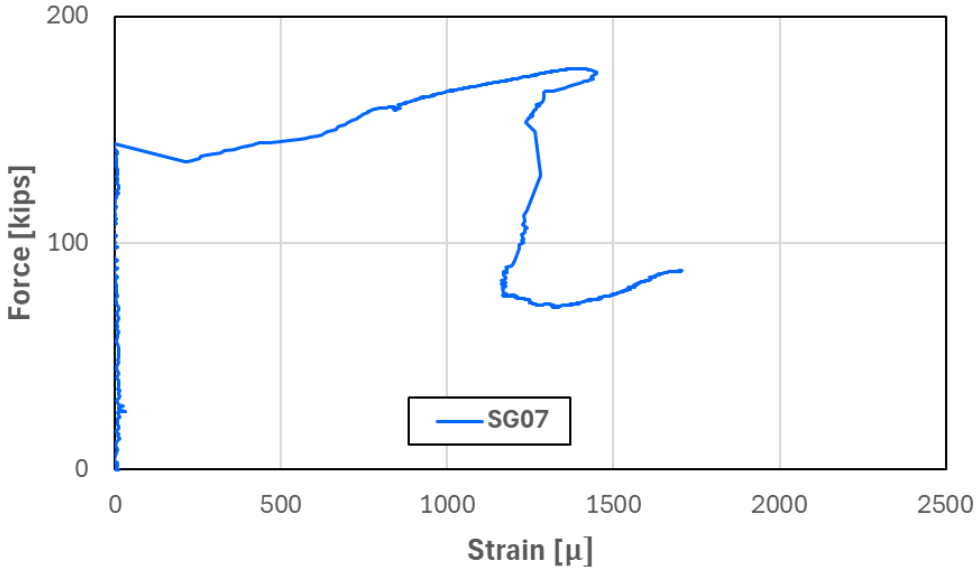

Figure D.179: Force plotted against SG07 strain for Specimen 11

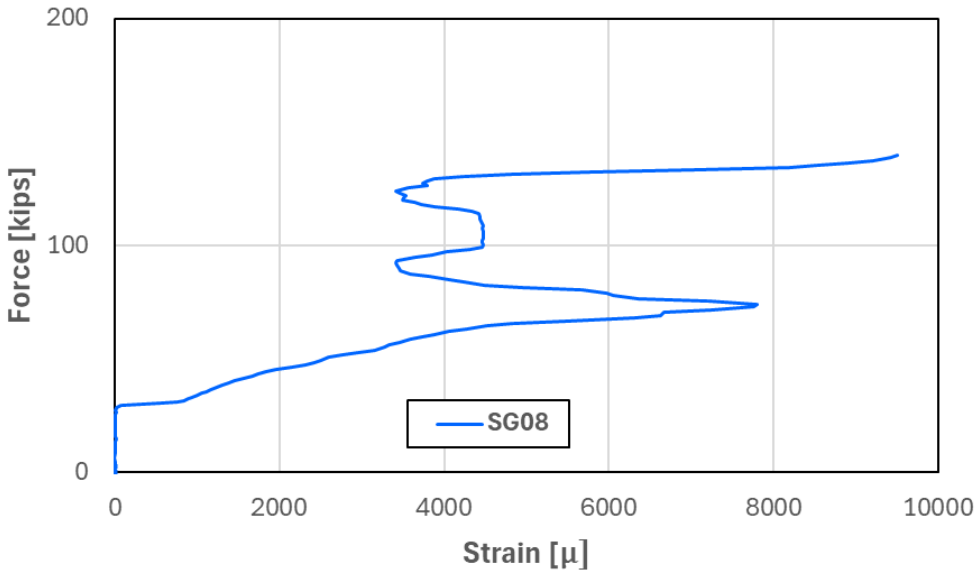

Figure D.180: Force plotted against SG08 strain for Specimen 11

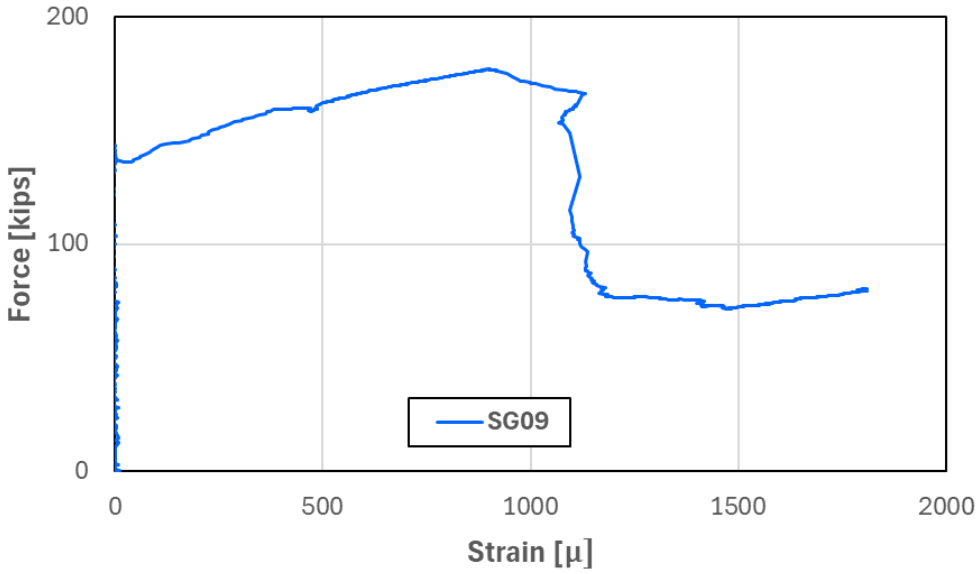

Figure D.181: Force plotted against SG09 strain for Specimen 11

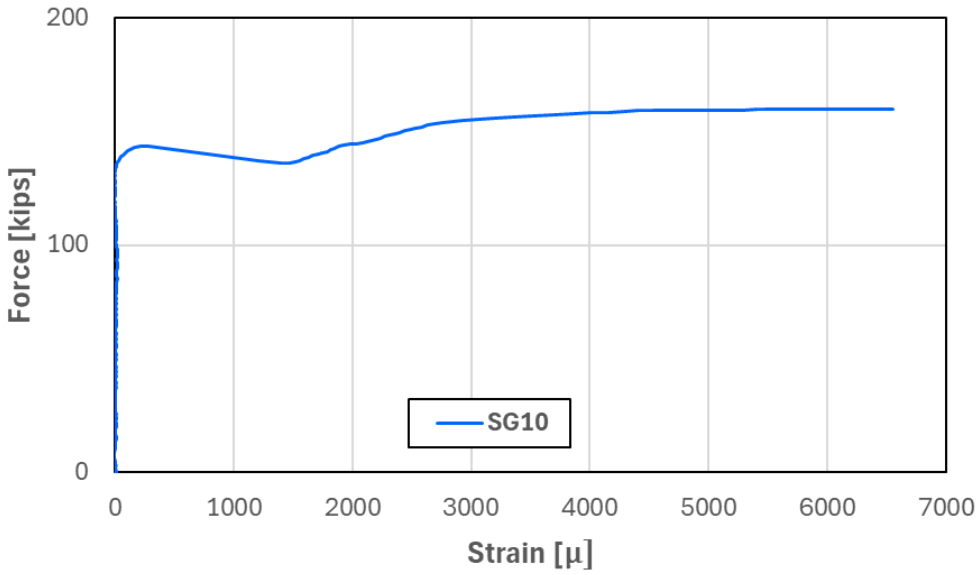

Figure D.182: Force plotted against SG10 strain for Specimen 11

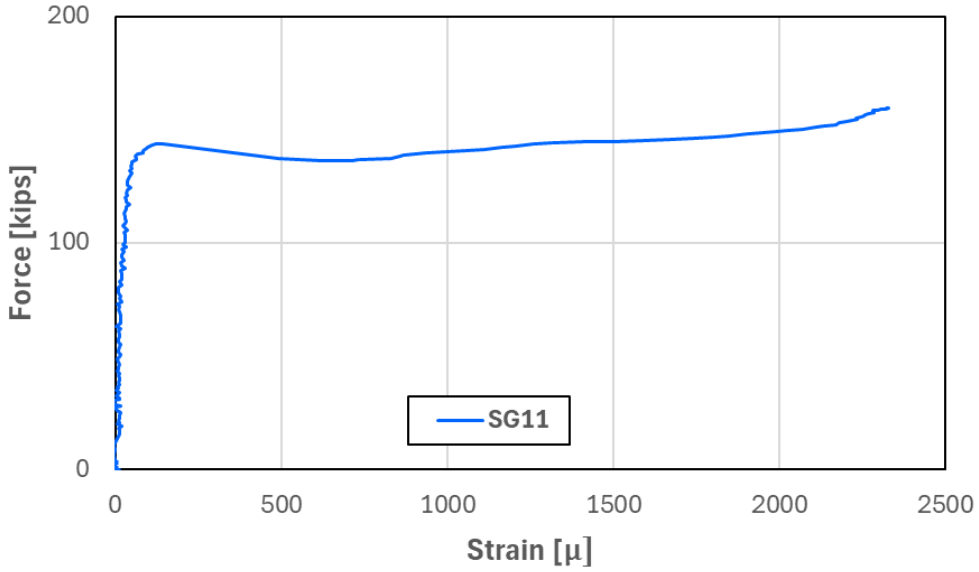

Figure D.183: Force plotted against SG11 strain for Specimen 11

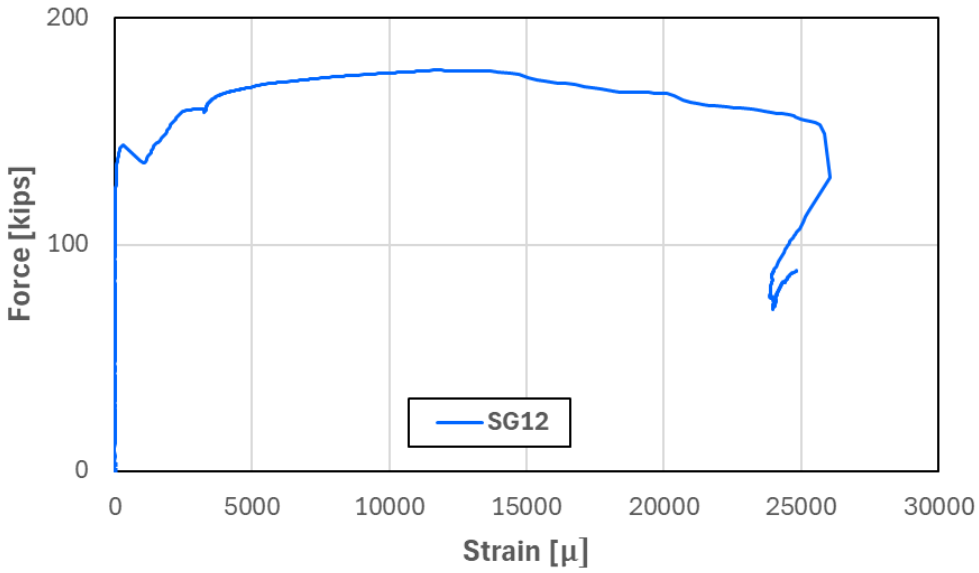

Figure D.184: Force plotted against SG12 strain for Specimen 11

D.12 Specimen 12

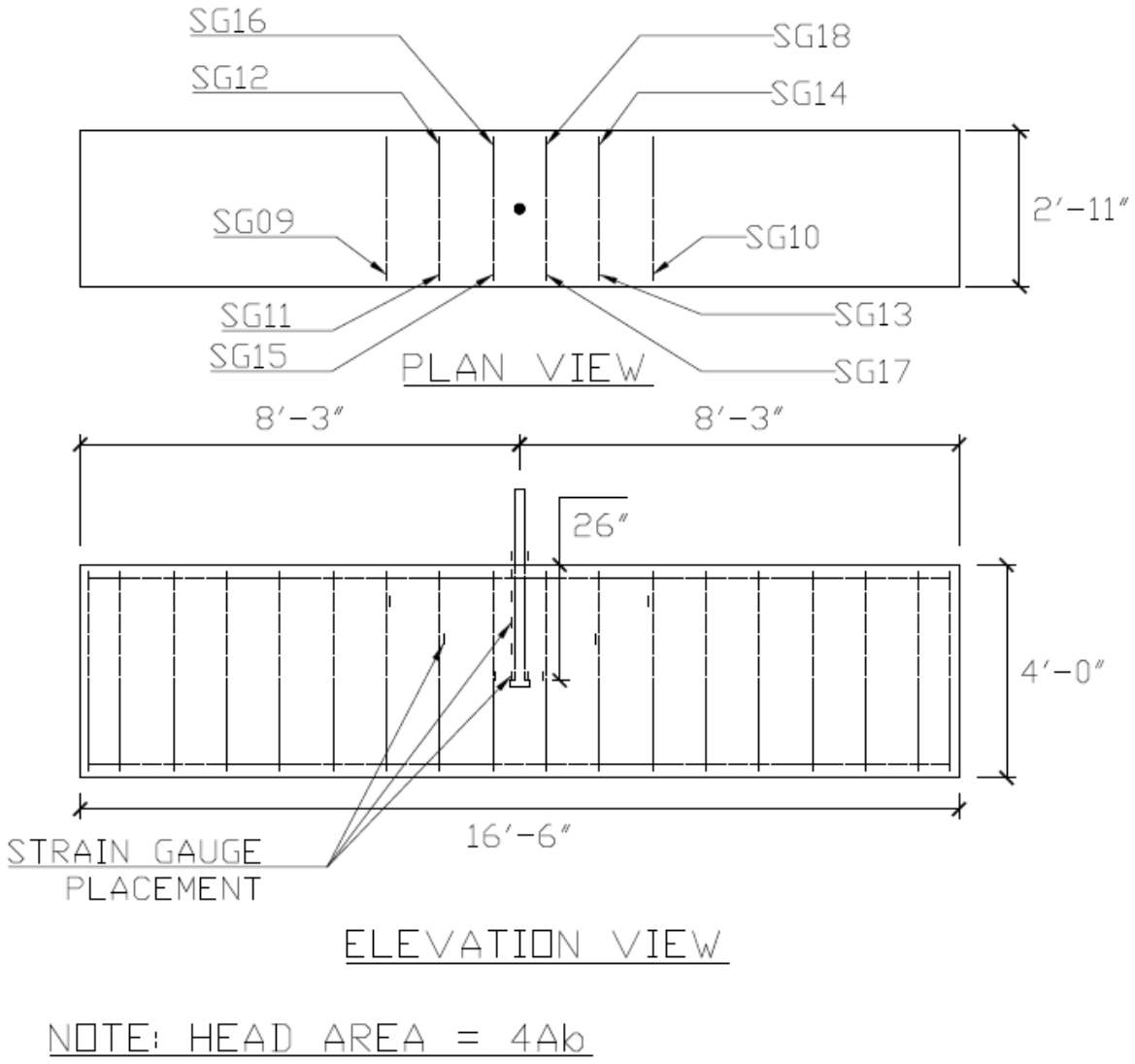

Figure D.185: Locations of strain gauges for Specimen 12

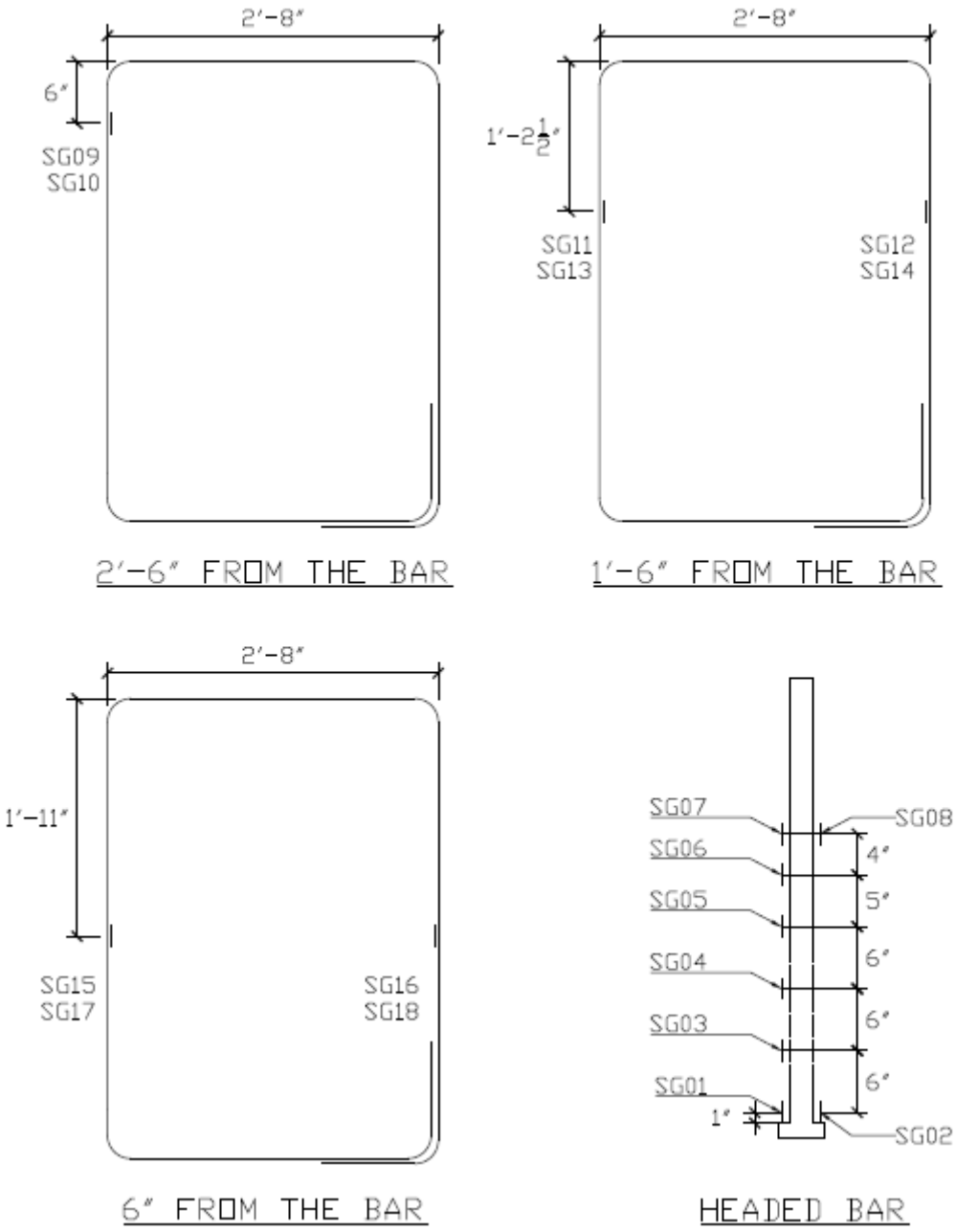

Figure D.186: Locations of stirrup and headed bar strain gauges and their labels for Specimen 12

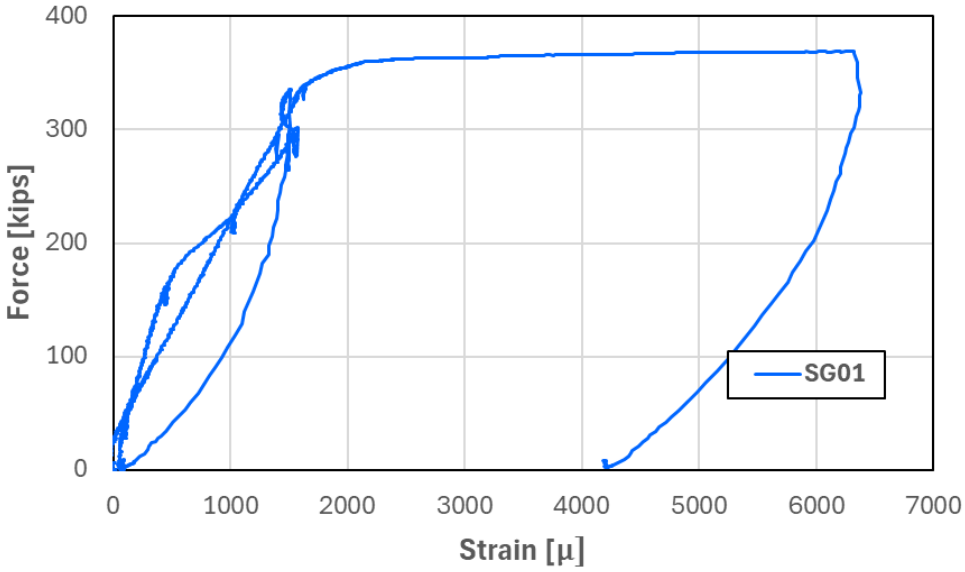

Figure D.187: Force plotted against SG01 strain for Specimen 12

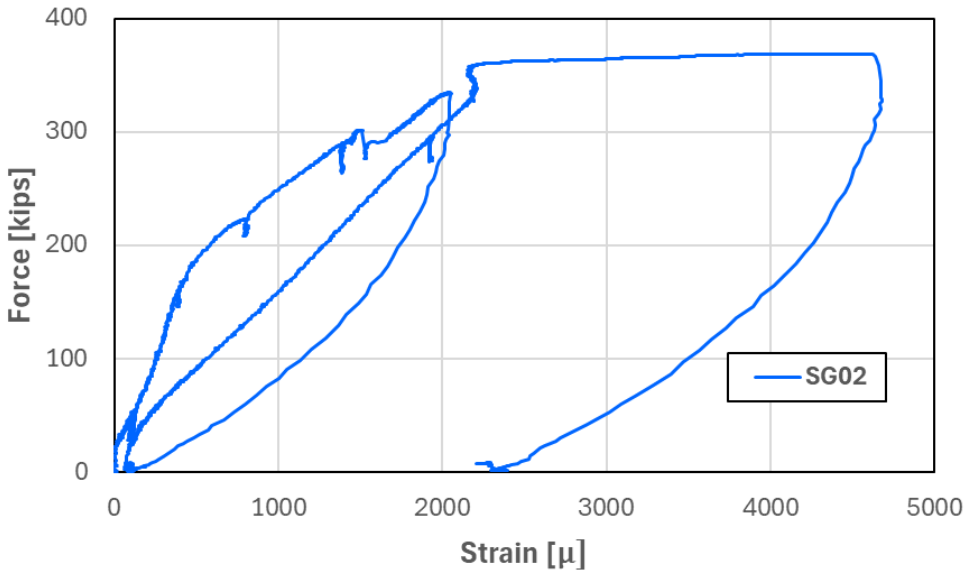

Figure D.188: Force plotted against SG02 strain for Specimen 12

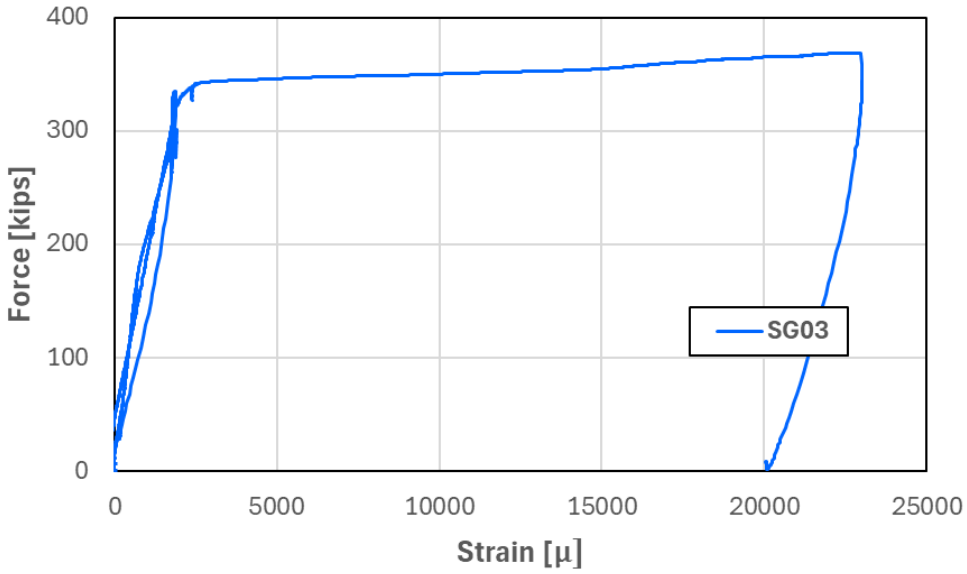

Figure D.189: Force plotted against SG03 strain for Specimen 12

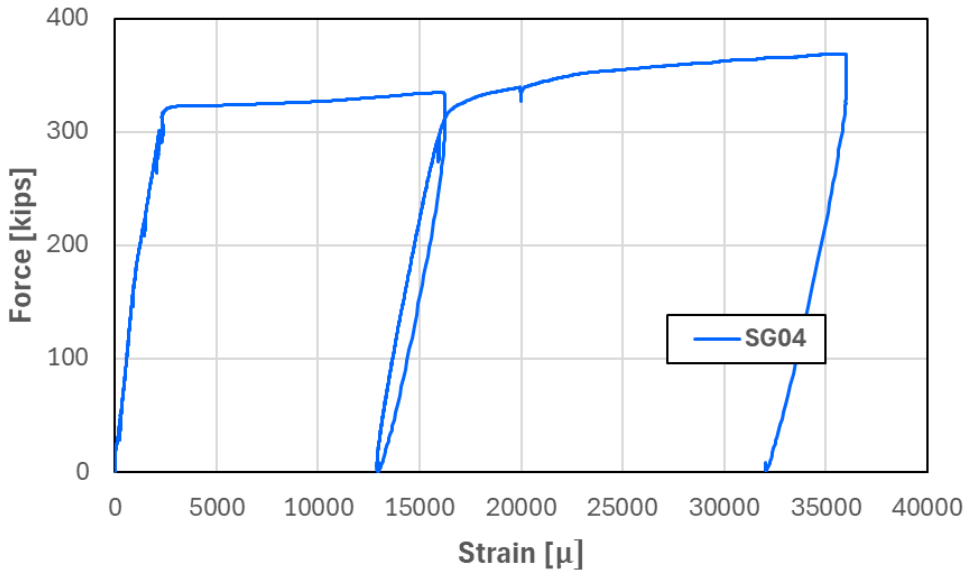

Figure D.190: Force plotted against SG04 strain for Specimen 12

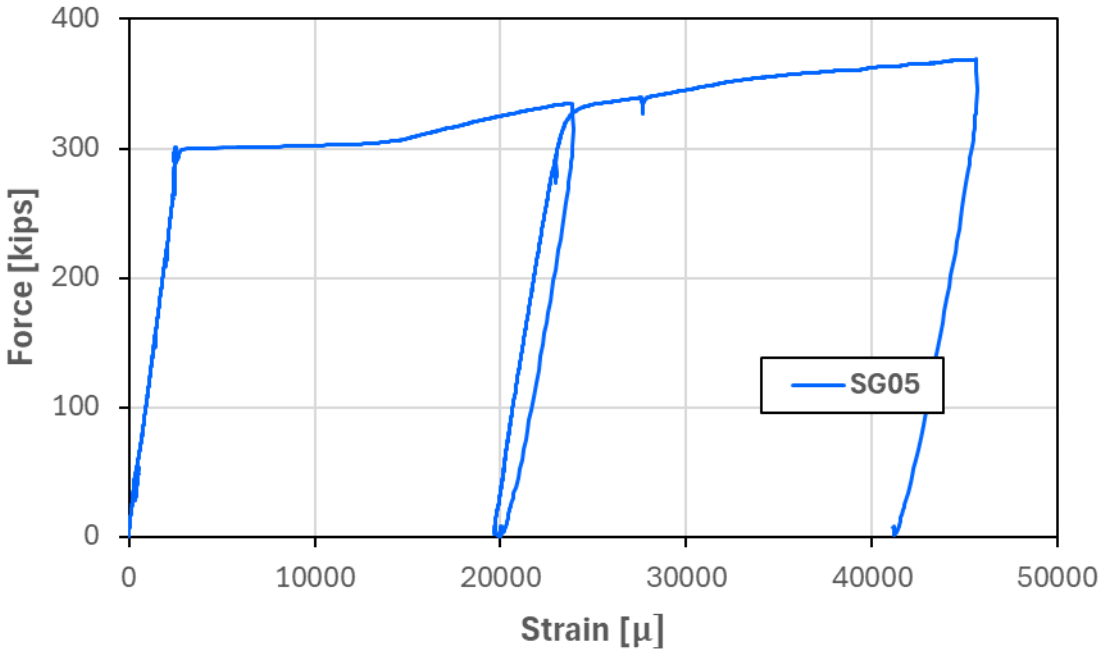

Figure D.191: Force plotted against SG05 strain for Specimen 12

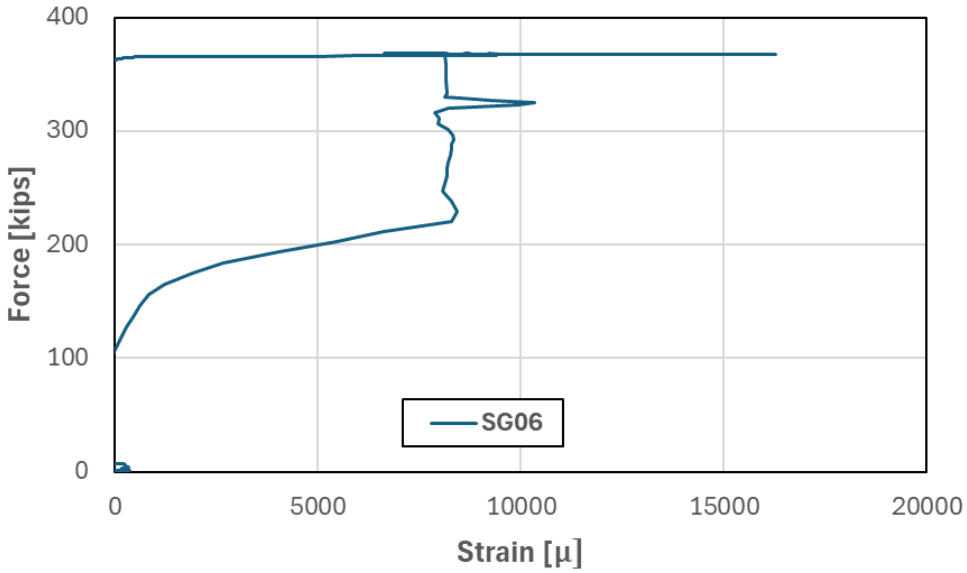

Figure D.192: Force plotted against SG06 strain for Specimen 12

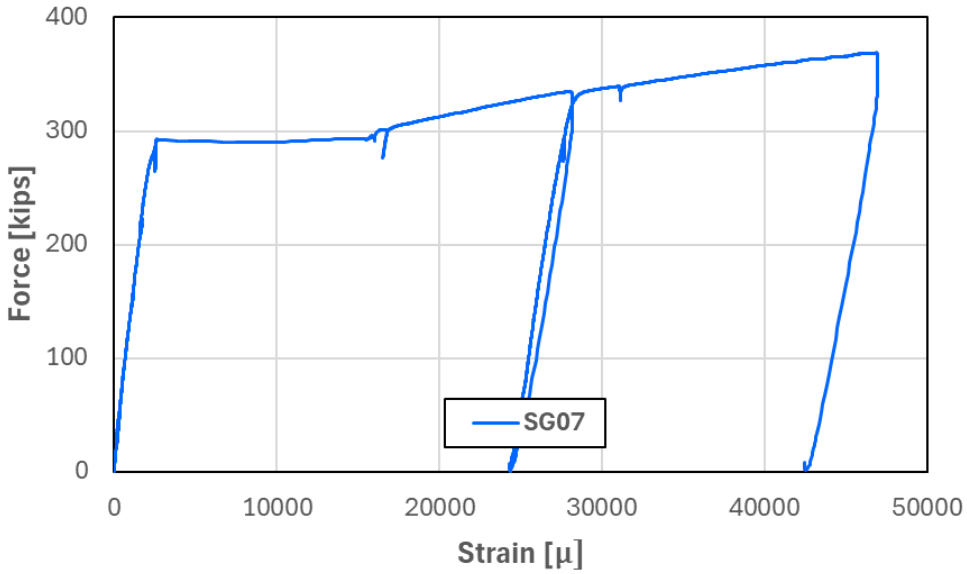

Figure D.193: Force plotted against SG07 strain for Specimen 12

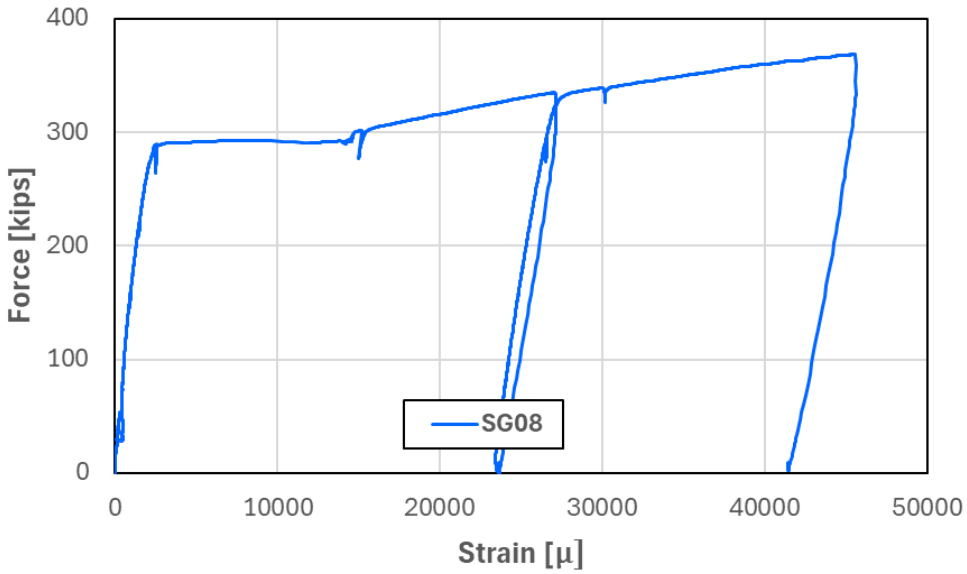

Figure D.194: Force plotted against SG08 strain for Specimen 12

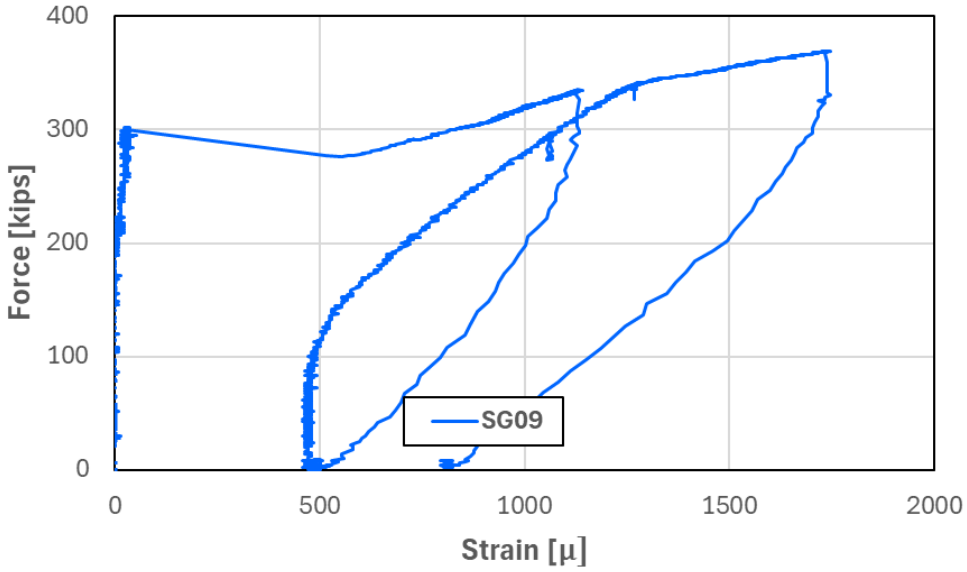

Figure D.195: Force plotted against SG09 strain for Specimen 12

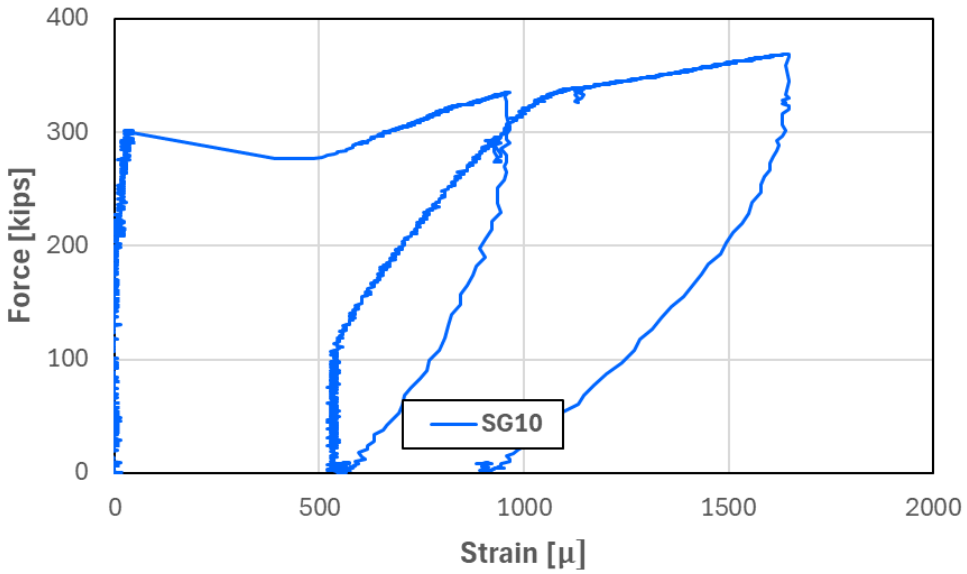

Figure D.196: Force plotted against SG10 strain for Specimen 12

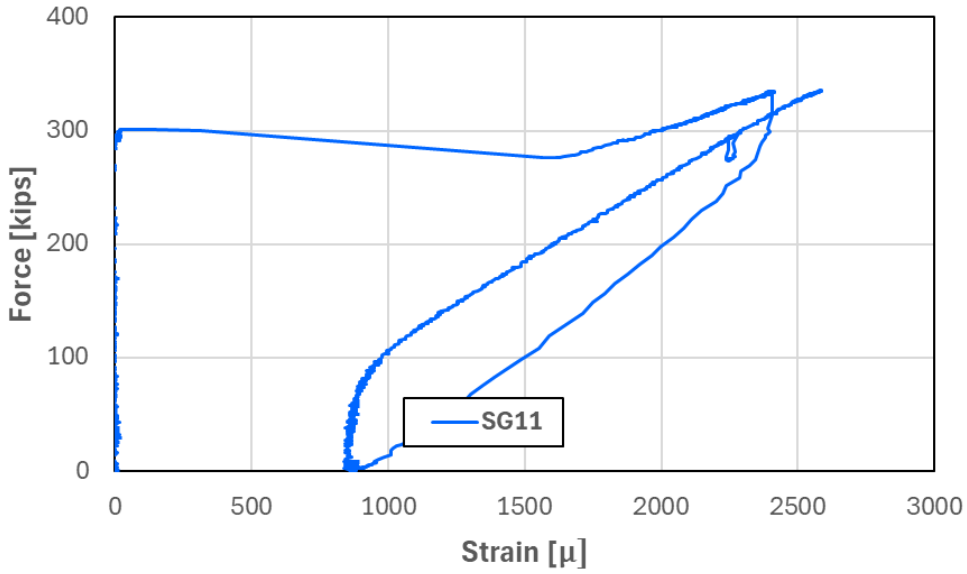

Figure D.197: Force plotted against SG11 strain for Specimen 12

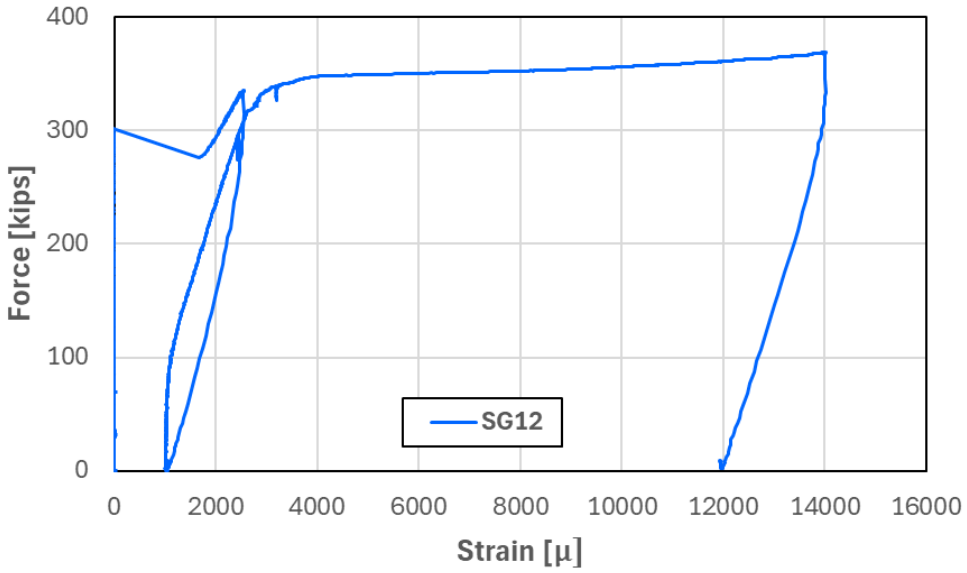

Figure D.198: Force plotted against SG12 strain for Specimen 12

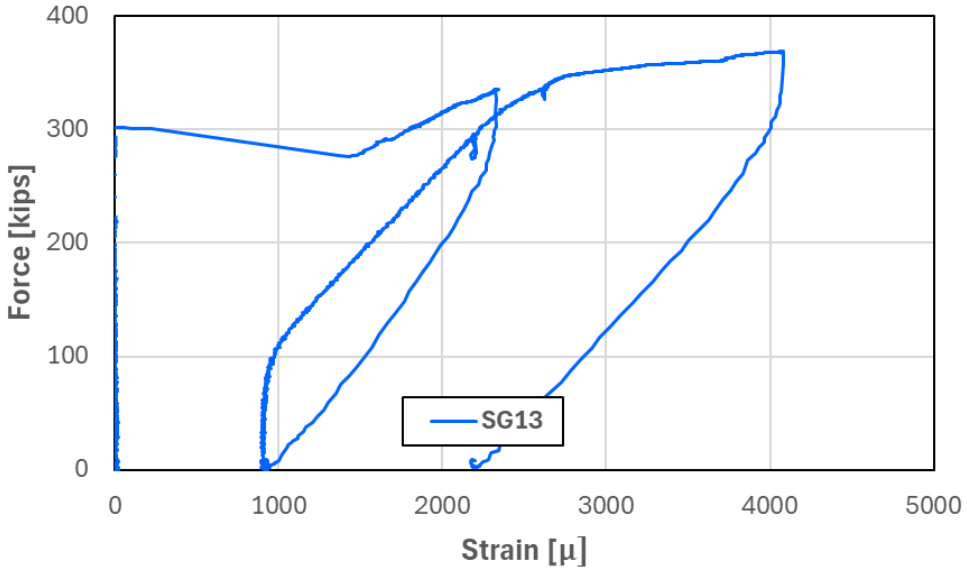

Figure D.199: Force plotted against SG13 strain for Specimen 12

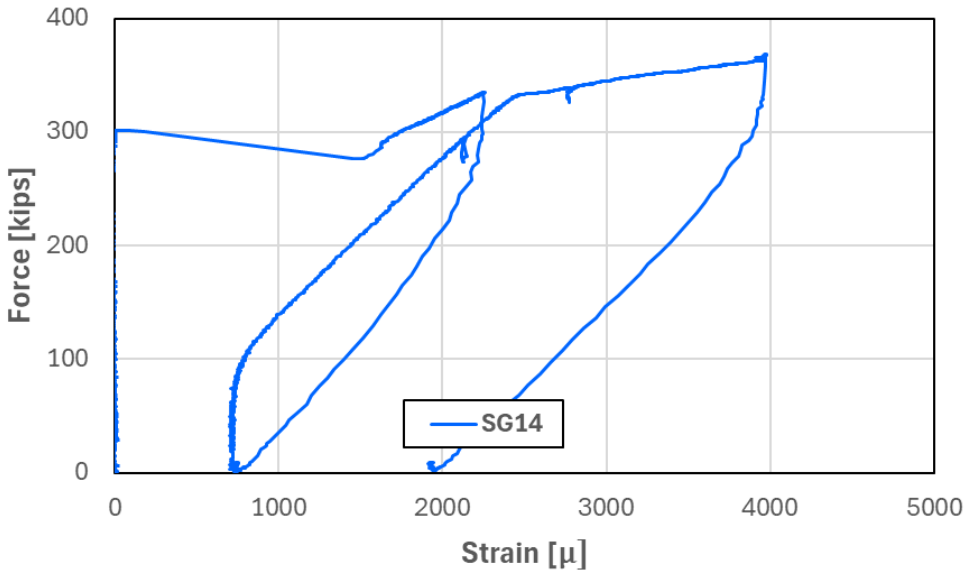

Figure D.200: Force plotted against SG14 strain for Specimen 12

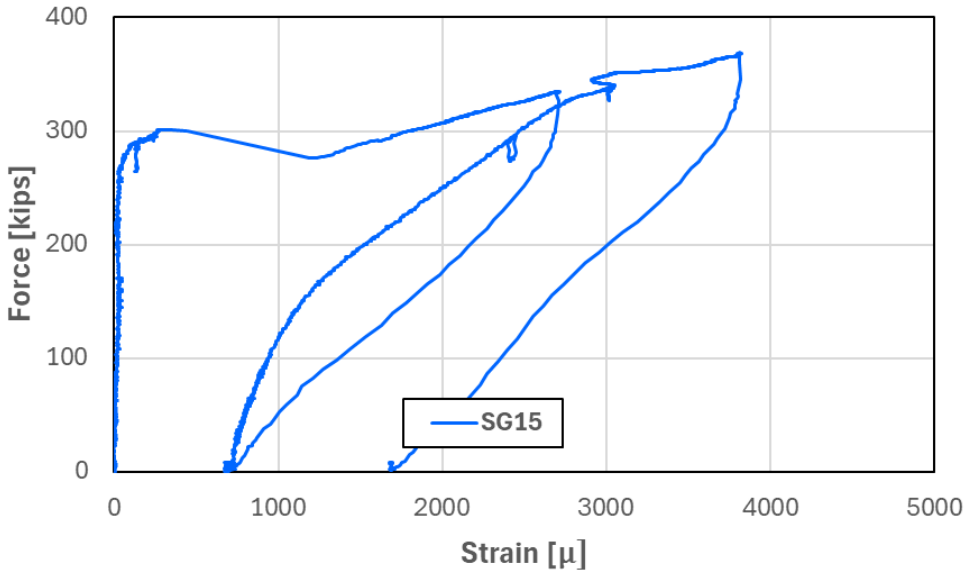

Figure D.201: Force plotted against SG15 strain for Specimen 12

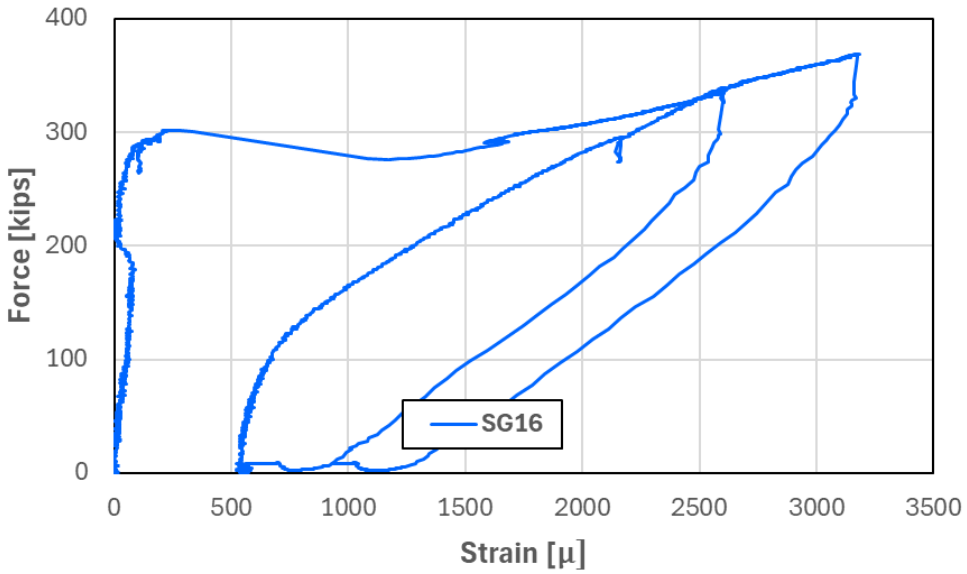

Figure D.202: Force plotted against SG16 strain for Specimen 12

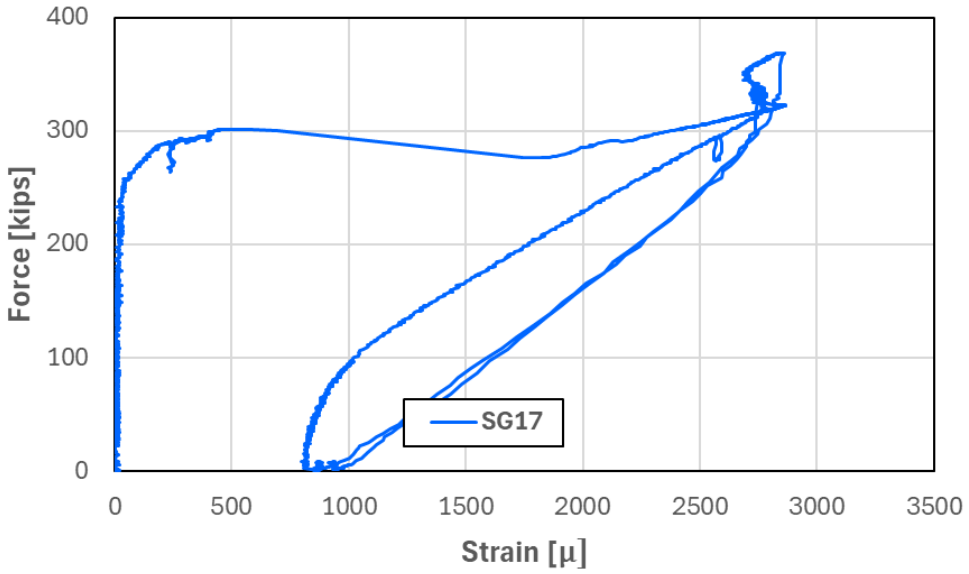

Figure D.203: Force plotted against SG17 strain for Specimen 12

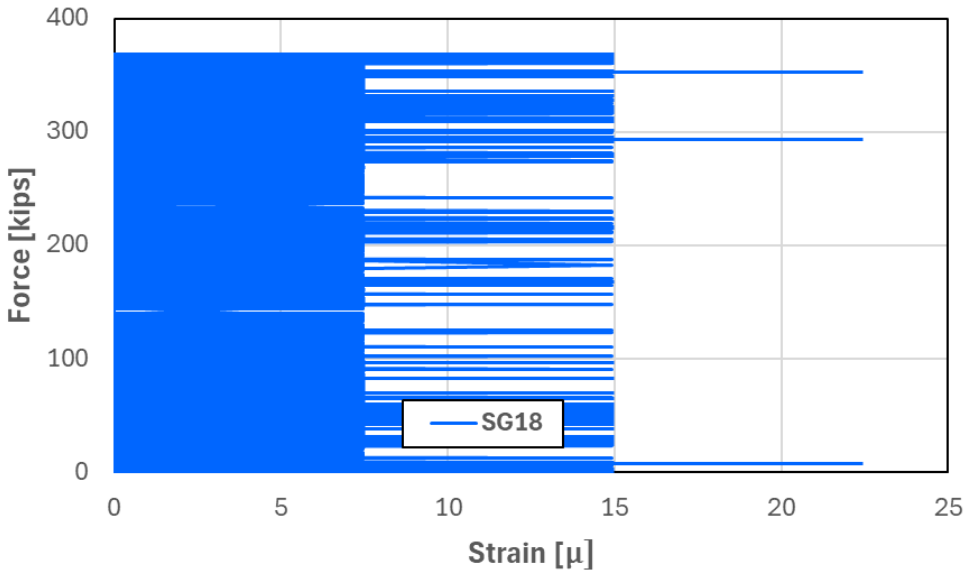

Figure D.204: Force plotted against SG18 strain for Specimen 12

D.13 Specimen 13

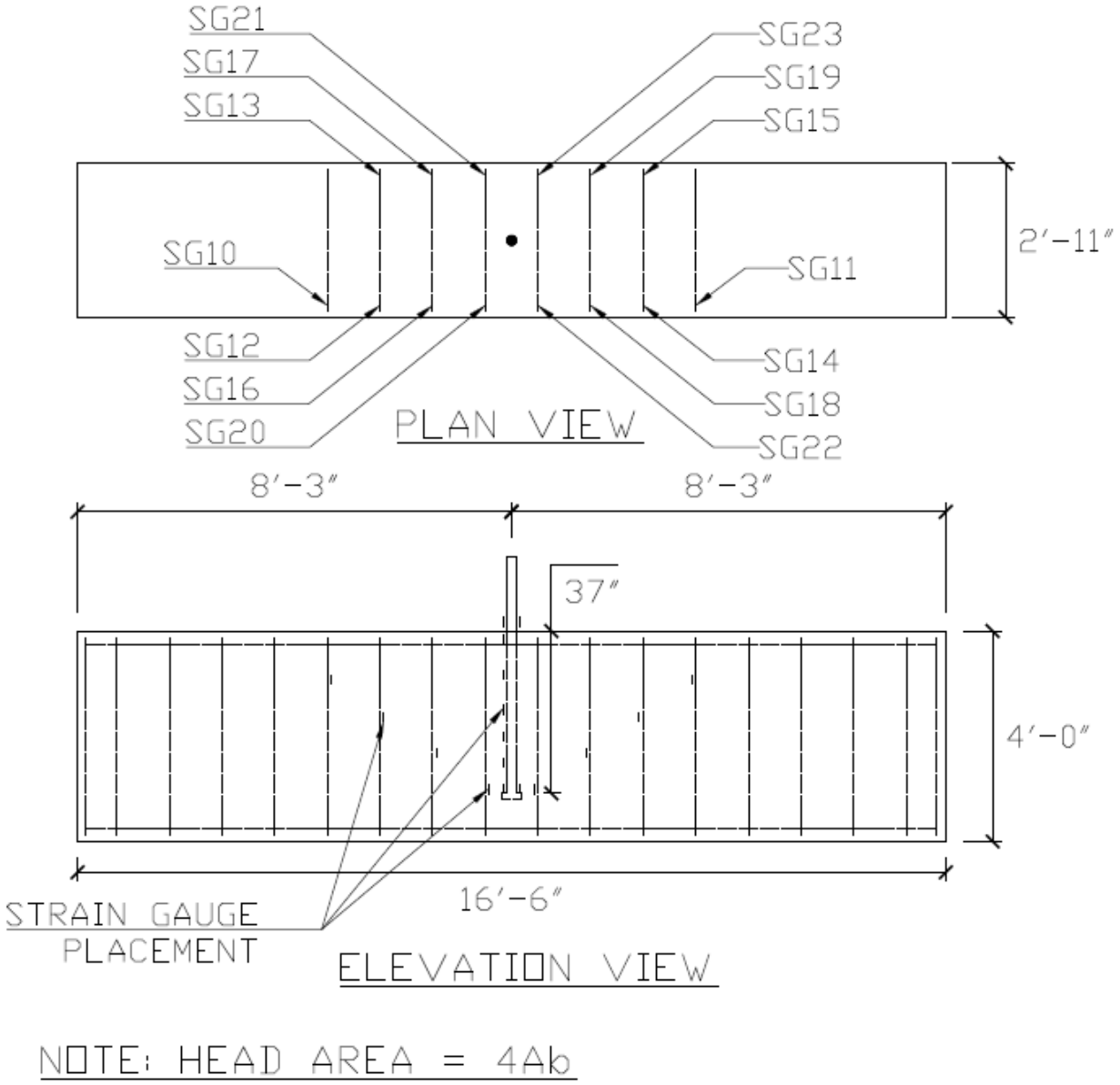

Figure D.205: Locations of strain gauges for Specimen 13

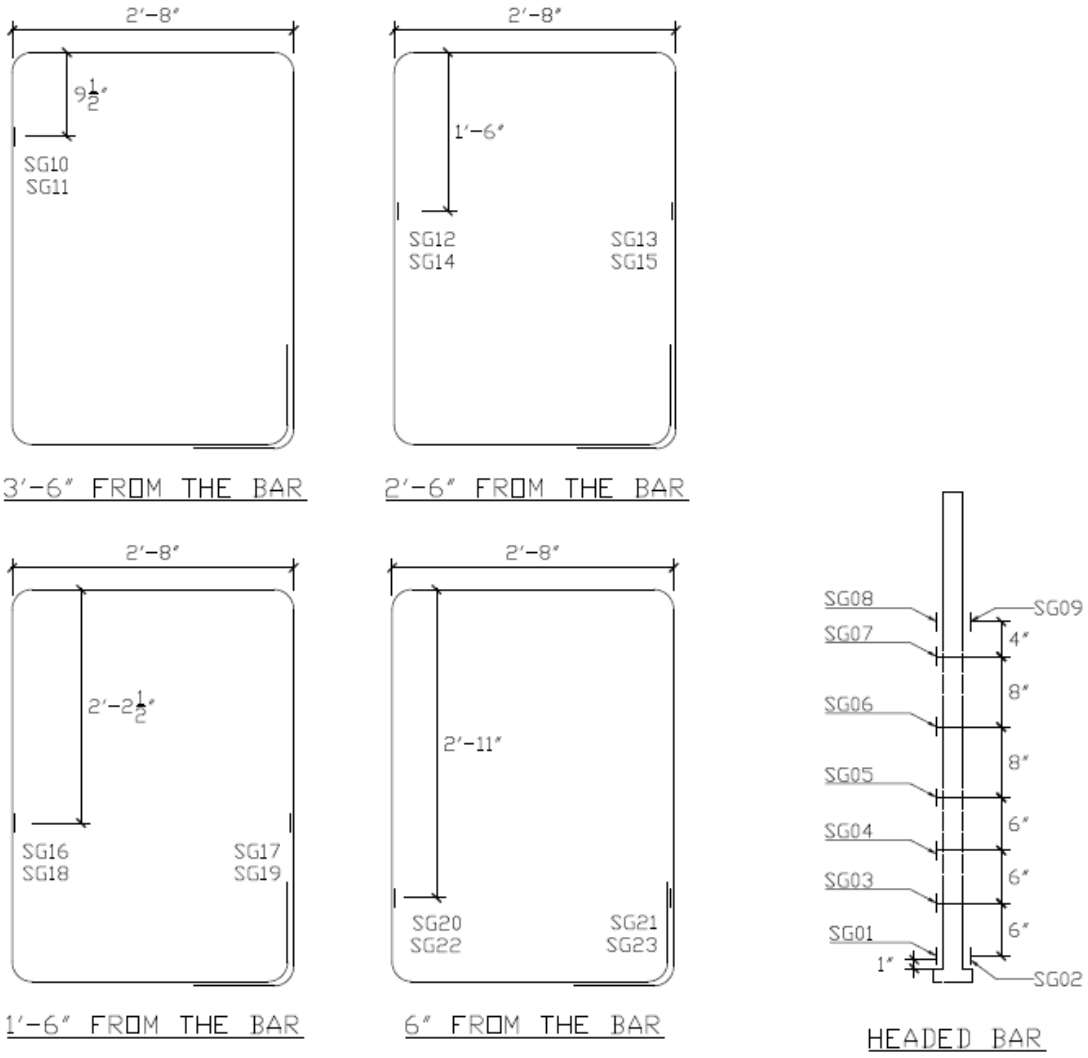

Figure D.206: Locations of stirrup and headed bar strain gauges and their labels for Specimen 13

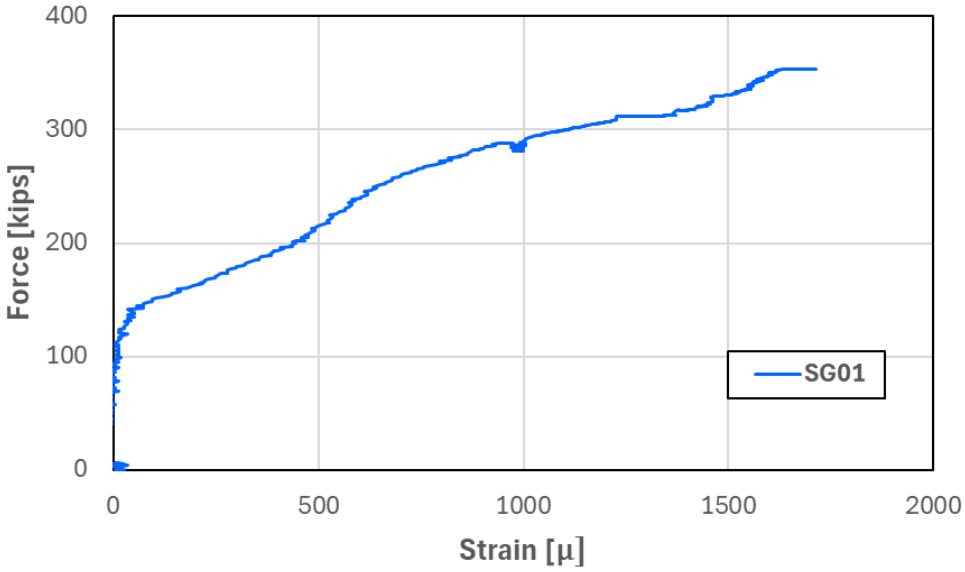

Figure D.207: Force plotted against SG01 strain for Specimen 13

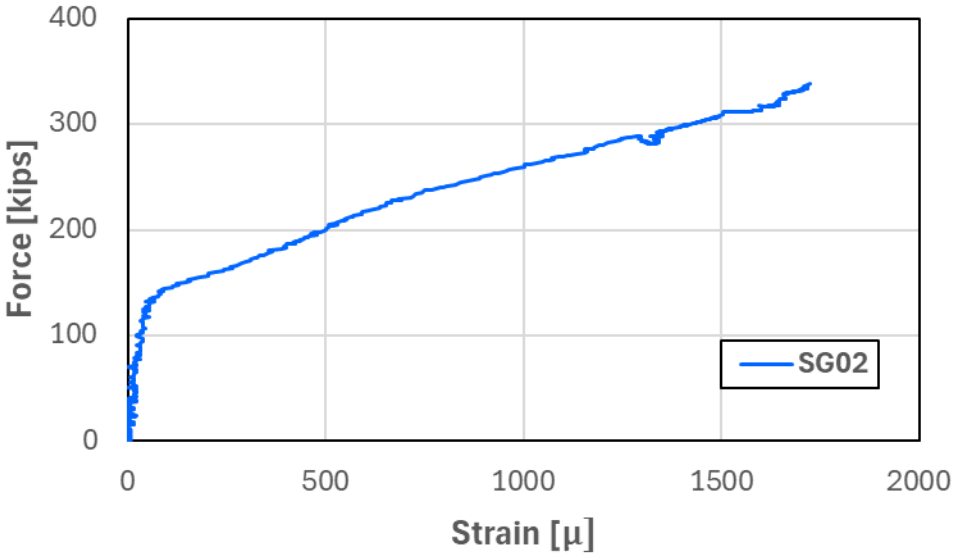

Figure D.208: Force plotted against SG02 strain for Specimen 13

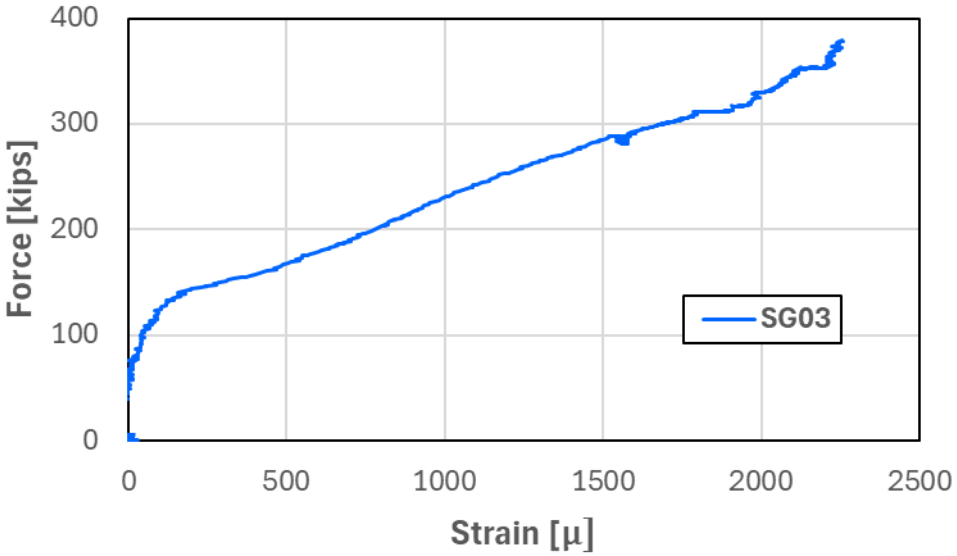

Figure D.209: Force plotted against SG03 strain for Specimen 13

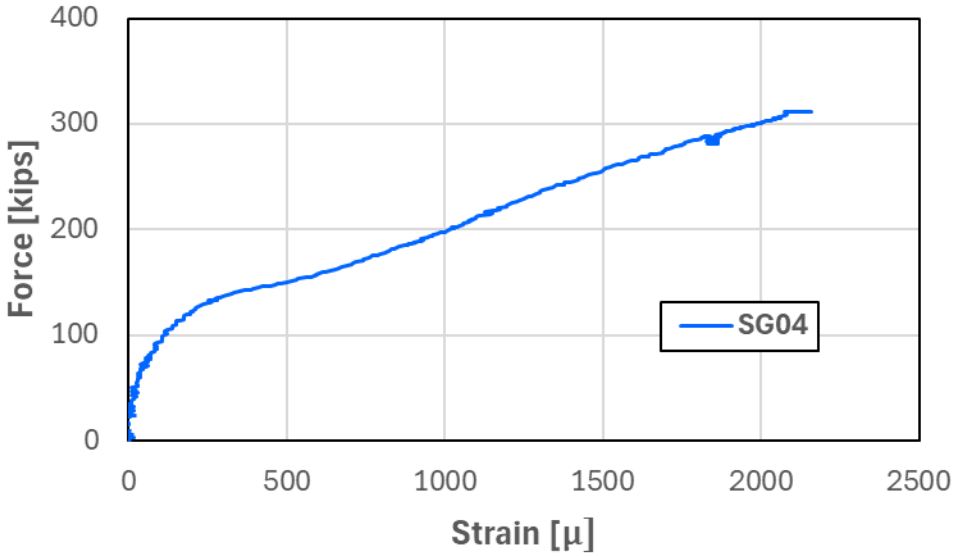

Figure D.210: Force plotted against SG04 strain for Specimen 13

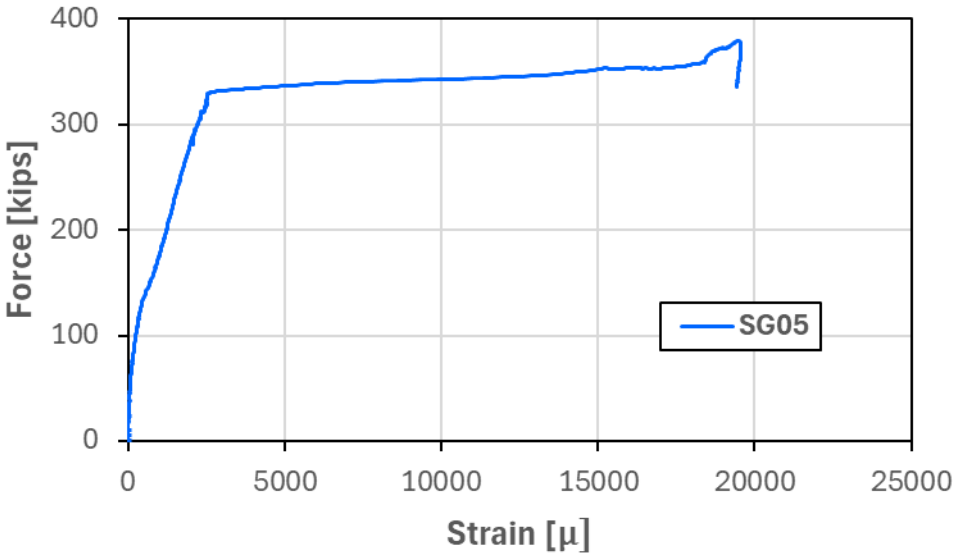

Figure D.211: Force plotted against SG05 strain for Specimen 13

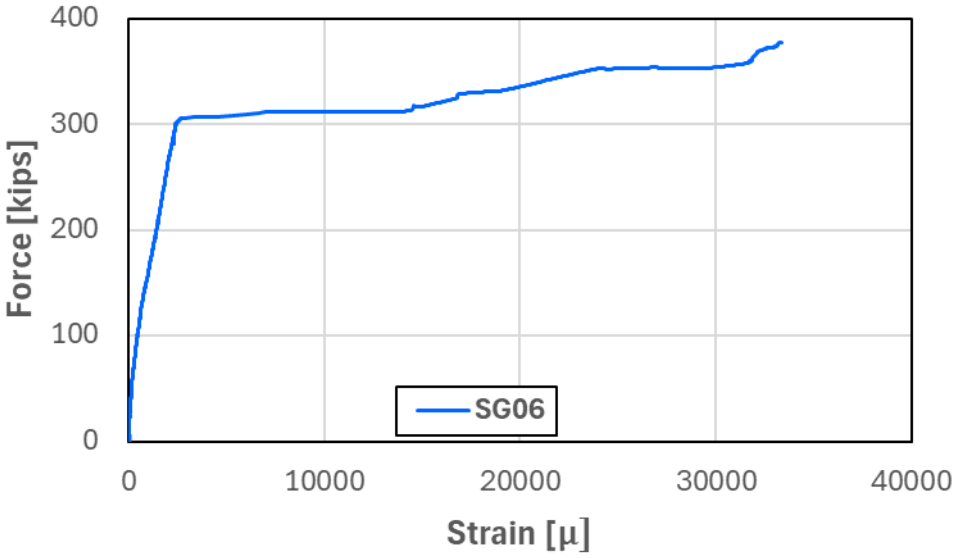

Figure D.212: Force plotted against SG06 strain for Specimen 13

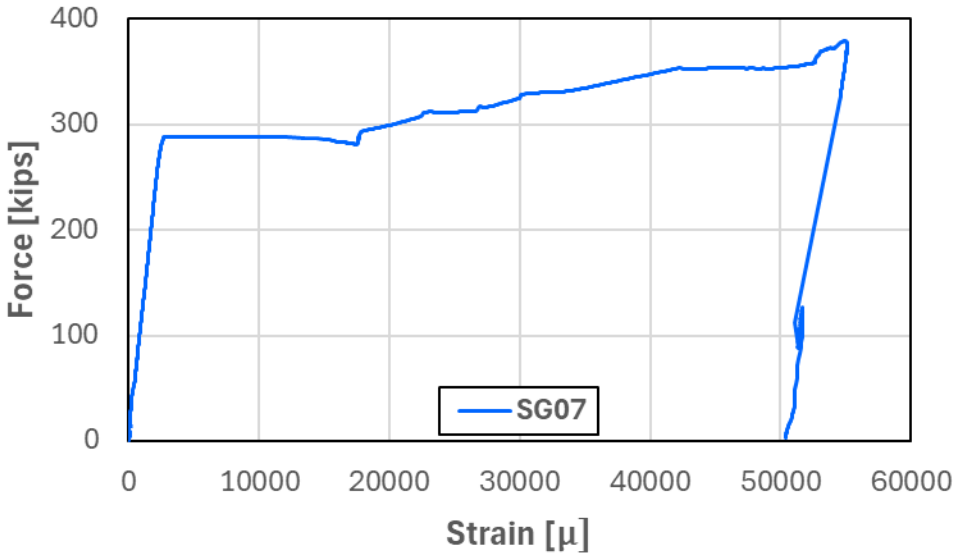

Figure D.213: Force plotted against SG07 strain for Specimen 13

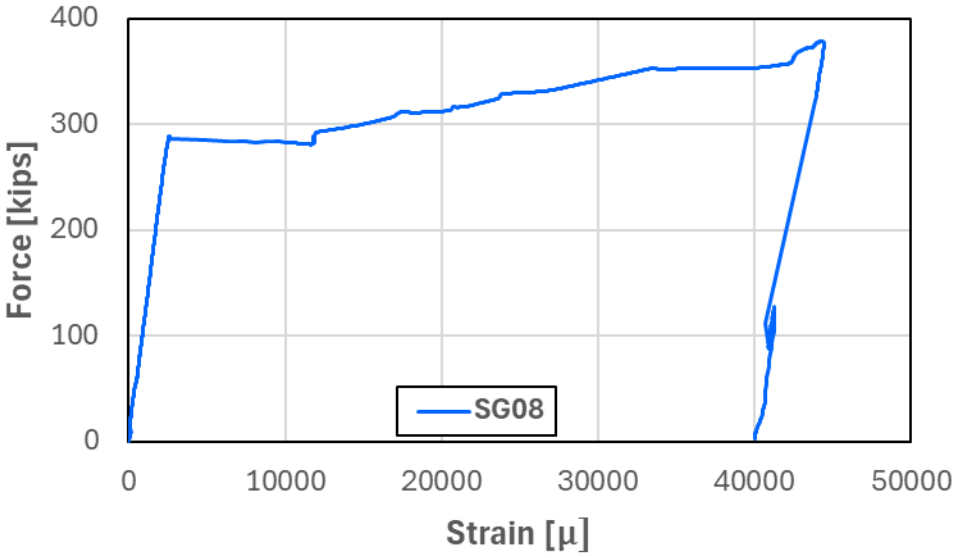

Figure D.214: Force plotted against SG08 strain for Specimen 13

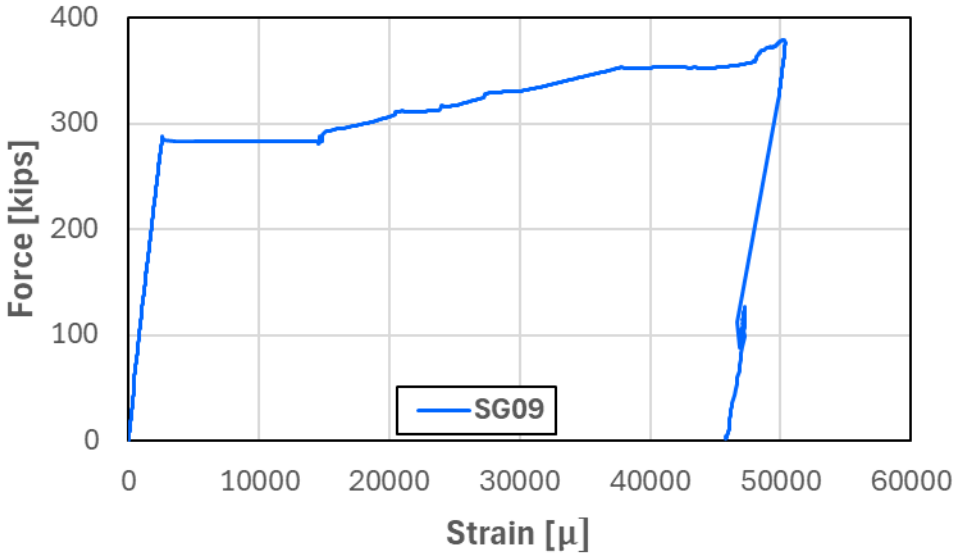

Figure D.215: Force plotted against SG09 strain for Specimen 13

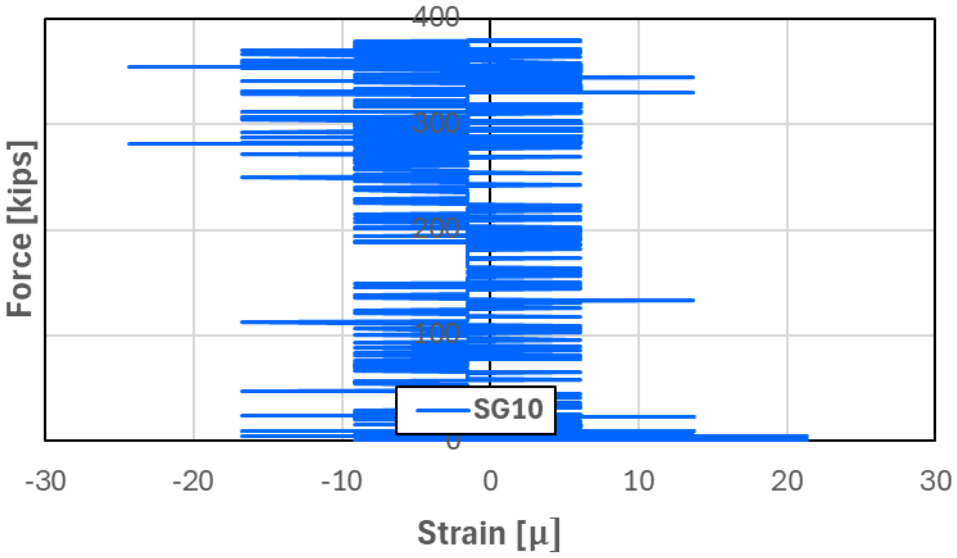

Figure D.216: Force plotted against SG10 strain for Specimen 13

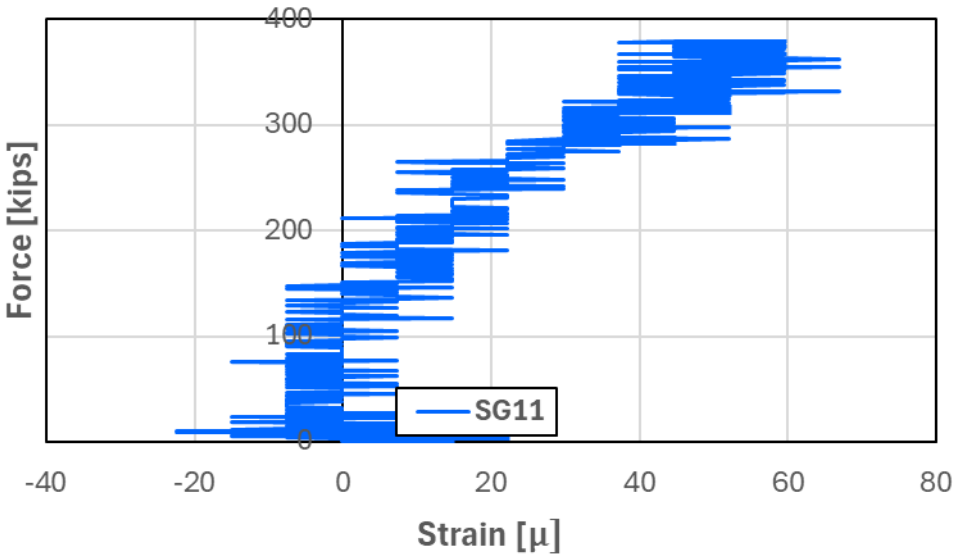

Figure D.217: Force plotted against SG11 strain for Specimen 13

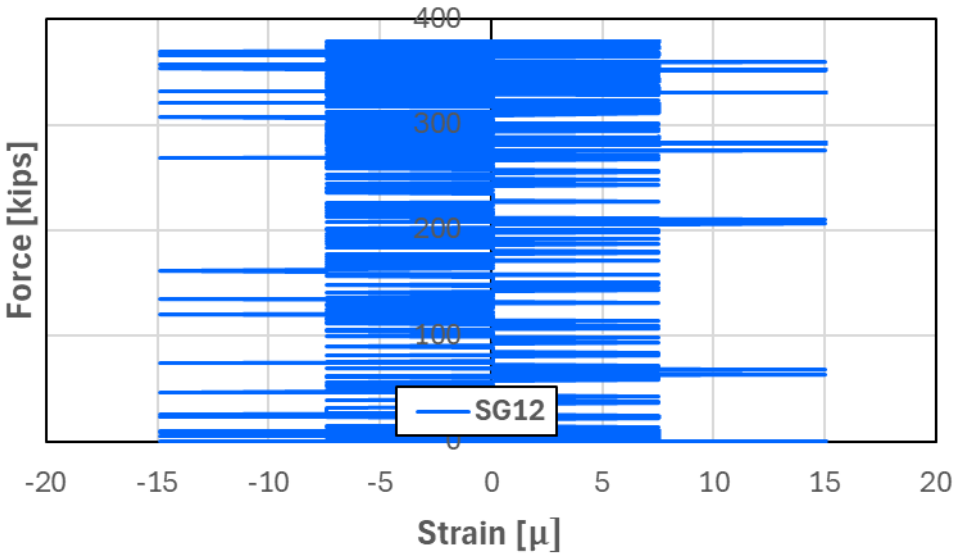

Figure D.218: Force plotted against SG12 strain for Specimen 13

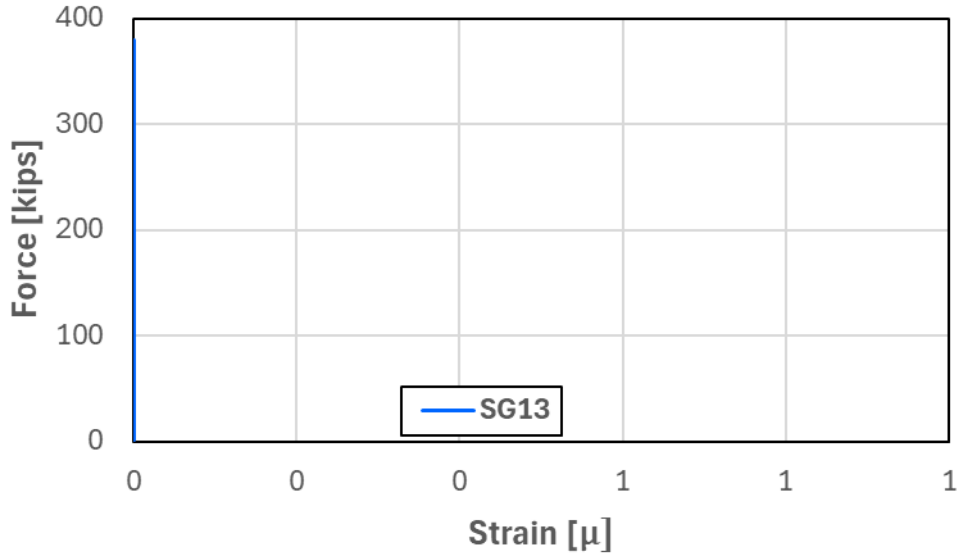

Figure D.219: Force plotted against SG13 strain for Specimen 13

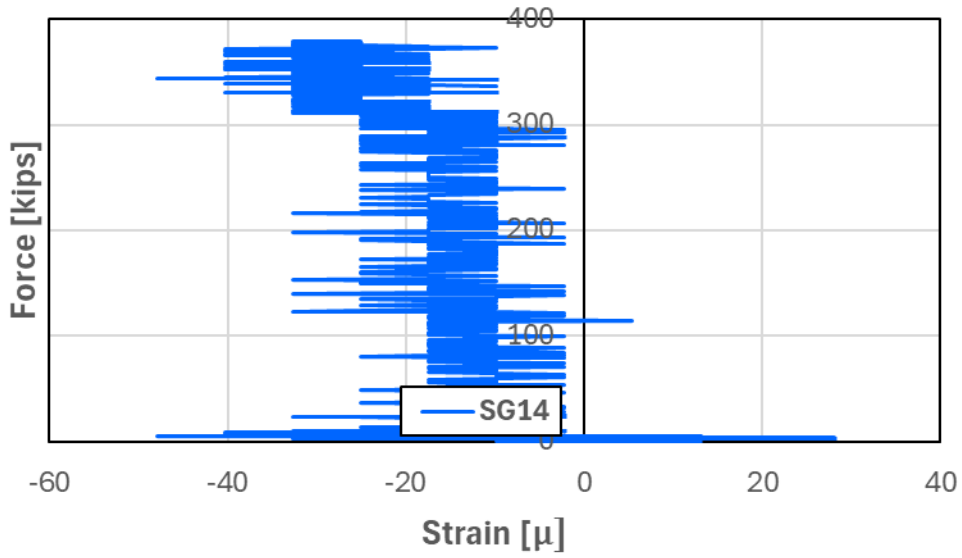

Figure D.220: Force plotted against SG14 strain for Specimen 13

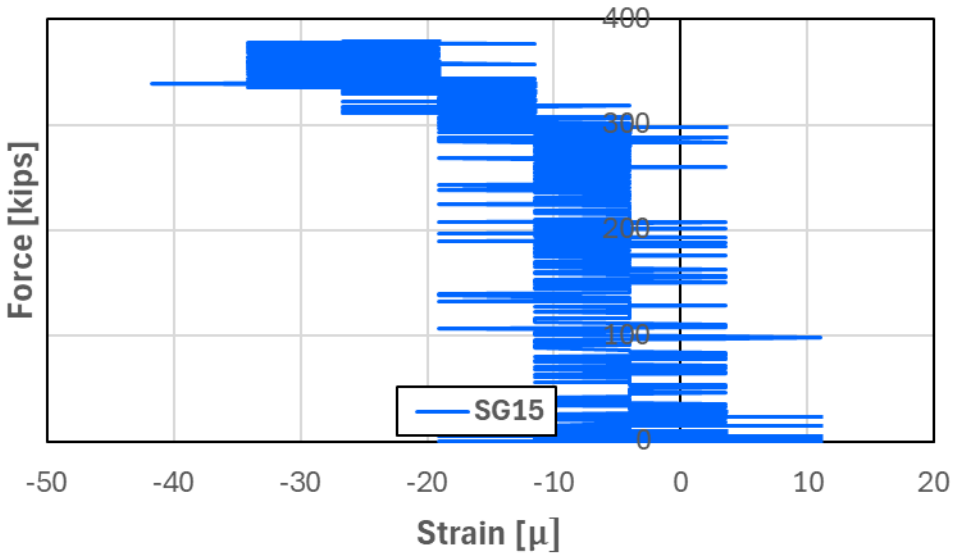

Figure D.221: Force plotted against SG15 strain for Specimen 13

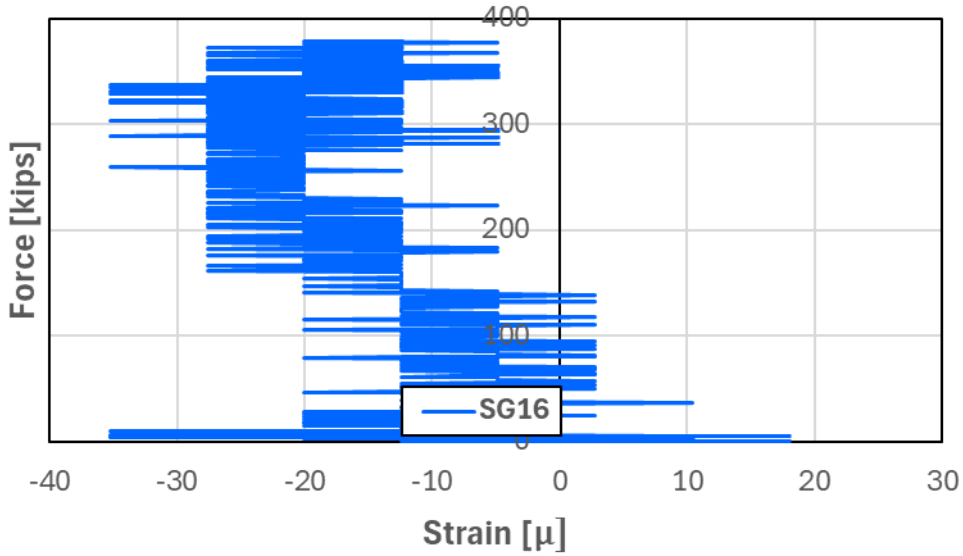

Figure D.222: Force plotted against SG16 strain for Specimen 13

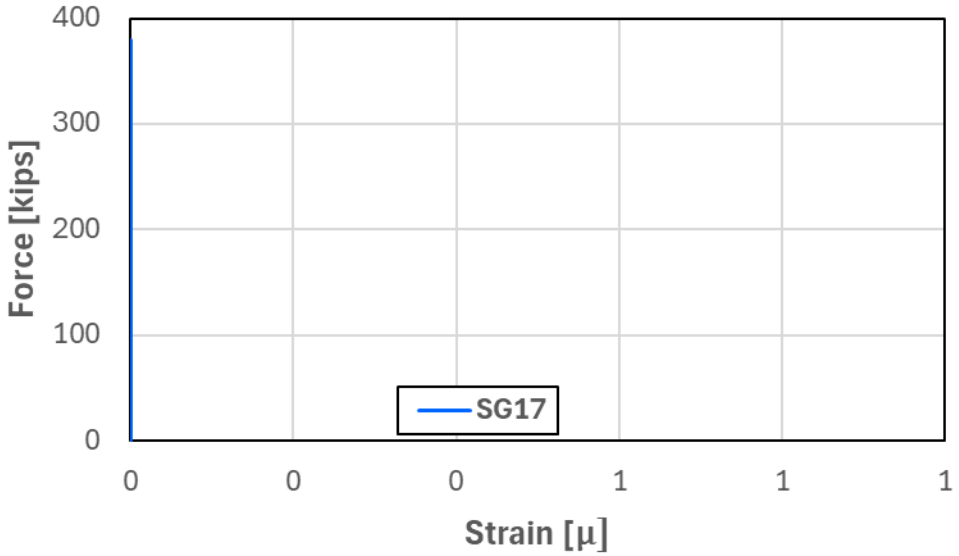

Figure D.223: Force plotted against SG17 strain for Specimen 13

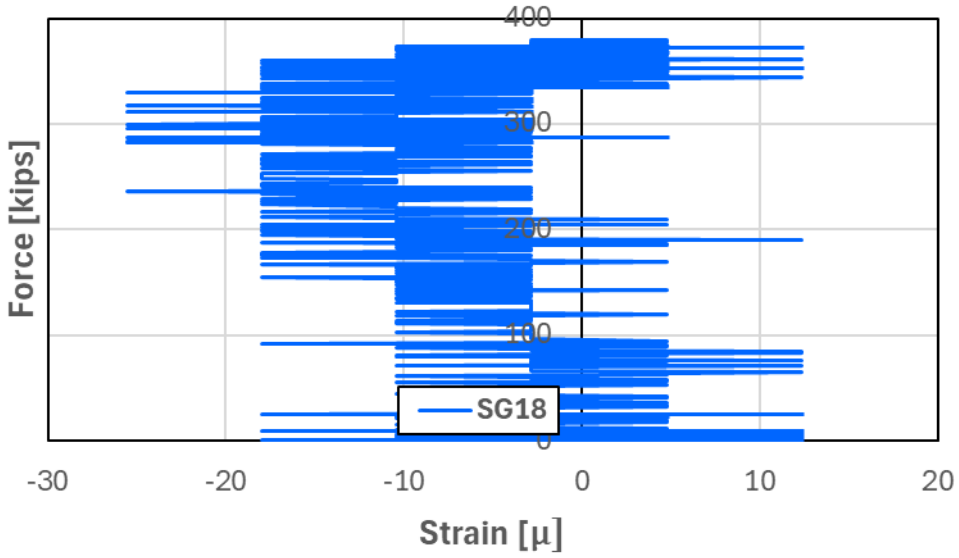

Figure D.224: Force plotted against SG18 strain for Specimen 13

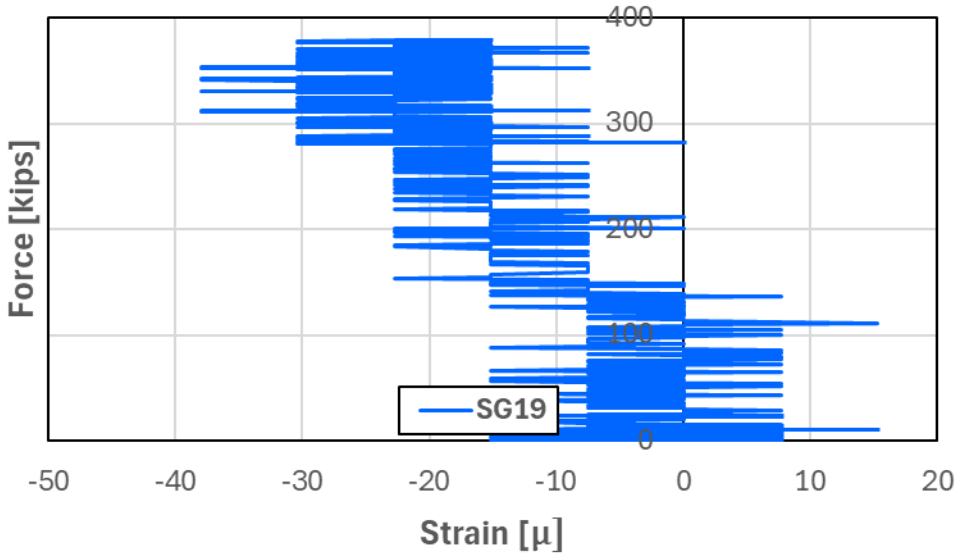

Figure D.225: Force plotted against SG19 strain for Specimen 13

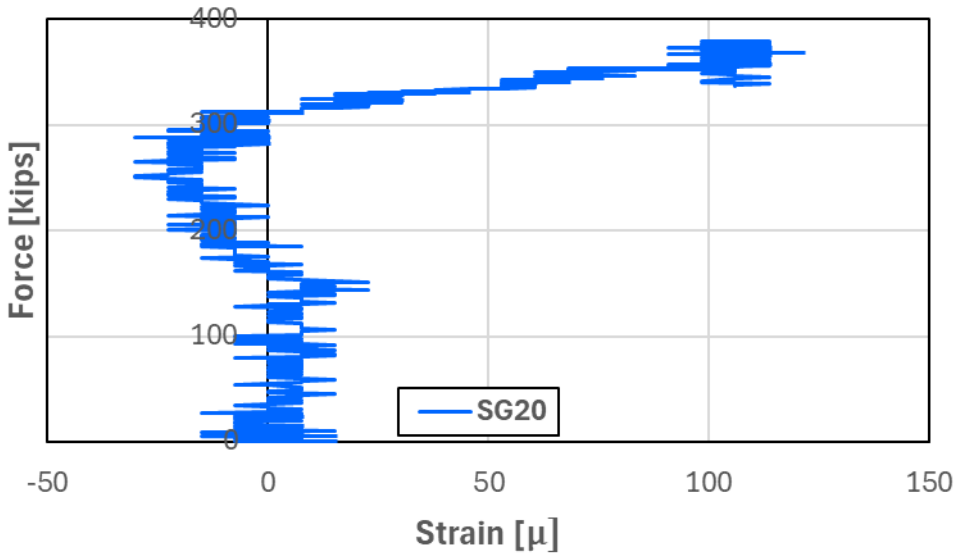

Figure D.226: Force plotted against SG20 strain for Specimen 13

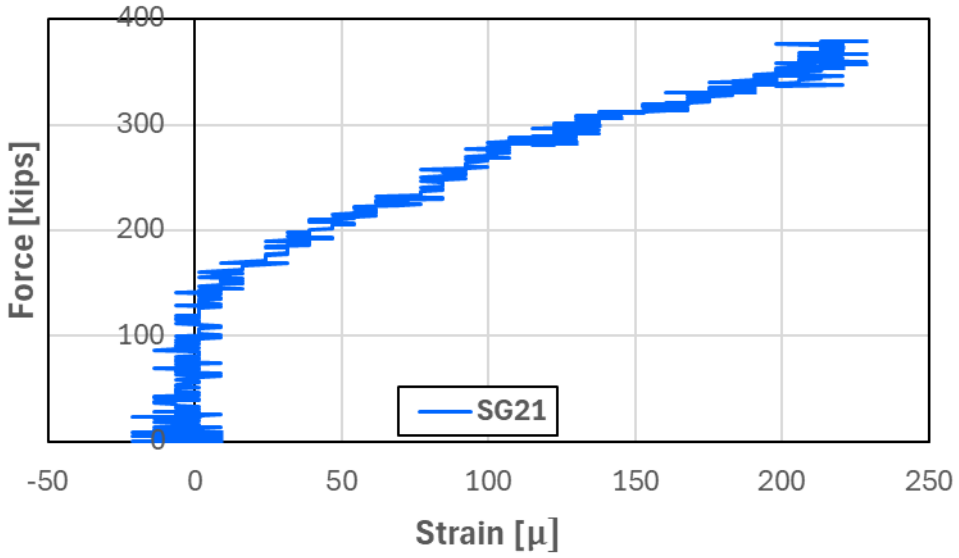

Figure D.227: Force plotted against SG21 strain for Specimen 13

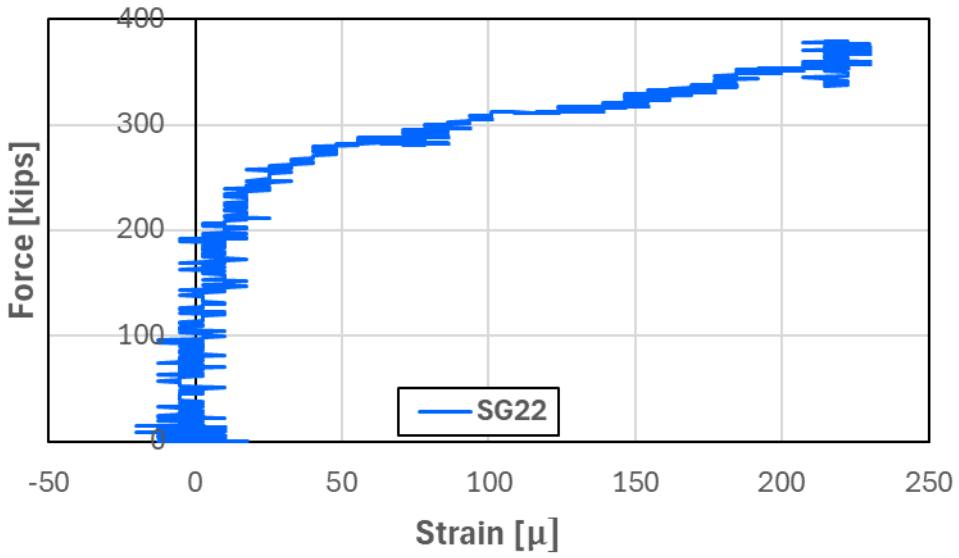

Figure D.227: Force plotted against SG22 strain for Specimen 13

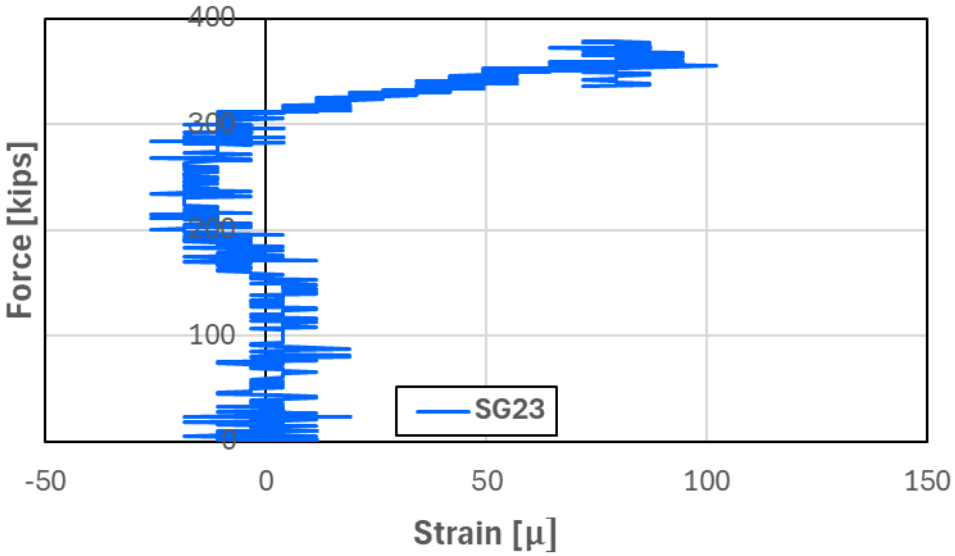

Figure D.227: Force plotted against SG23 strain for Specimen 13